Author:
Adeniran, A. O

Title:
Studies on foams and surface rheology

STUDIES ON FOAMS AND SURFACE RHEOLOGY

by

ADELEKE OLABODE ADENIRAN

A thesis submitted in partial fulfilment of the requirements
for the degree of Doctor of Philosophy

Department of Physical Chemistry
University of Bristol

December 1986

MEMORANDUM

The work presented in this thesis was carried out in the Department of Physical Chemistry of the University of Bristol and at the BP Research Centre, Sunbury-on-Thames, under the joint supervision of Dr. J.W. Goodwin and Dr. I.C. Callaghan between October 1982 and September 1985. The work is original, unless otherwise stated in the text, and no part of the work has been submitted for an award at this or any other university.

Signed: B Adamson

Date: 5.12.86

ACKNOWLEDGEMENTS

Firstly, and most importantly, I extend my sincere thanks to my supervisors, Dr. J.W. Goodwin and Dr. I. Callaghan, for their excellent guidance and advice throughout the duration of this project.

I am deeply indebted to Dr. R. Richardson for the use of the Joyce-Loebl Langmuir trough, and to Mr. M. Buhaenko for his constructive help, advice and perseverance.

I would also like to thank Dr. T. Lawrence and Dr. I. Livsey at the BP Research Centre, Sunbury-on-Thames, for useful discussions concerning the foaming experiments.

I acknowledge the co-operation of the technical staff at Bristol University BP Research Centre with the provision of laboratory services. Thanks also to David Jones for the photographs.

I am also greatly indebted to Eleanor Gibbins for her patience during the typing of this thesis, and to Mr. R. Clapperton and Mr. D. Hodge for the proof-reading.

I acknowledge the financial support of the Science and Engineering Research Council and British Petroleum plc, who made this work possible.

I would like to thank all the members of the Ottewill-Goodwin research group for making my stay in Bristol so enjoyable.

Finally, my special thanks to my parents for their continued support, both financial and otherwise, throughout my education.

ABSTRACT

This work is mainly concerned with the study of surface rheological properties of linear polydimethylsiloxane polymers when spread at the air/water interface, though some long-chain alkanoic acids have also been investigated. The alkanoic acids were chosen, in part, as a model series, which enabled the performances of the instruments used to be evaluated using well-defined insoluble monolayers.

The rheological properties studied in order to gain a better understanding of the surface monomolecular layer were: surface pressures, potentials, viscosities and elasticities of films as functions of the area available to each monomer or acid molecule on subphases. Reasonable agreement was found between the results obtained and literature values, for known alkanoic acids and similar polydimethylsiloxanes.

It has been shown that the antifoaming ability of polydimethylsiloxanes could be measured quantitatively by the simple modified Bikerman method using Offshore Magnus and Ninian crude oils and a model crude oil (containing 3% w/v aerosol OT in ethylene glycol). The synergistic effect of some mixtures of two different molecular weight-polydimethylsiloxanes was also investigated.

From the antifoaming and surface rheology results, it was possible to characterize, and partly explain, the defoaming and antifoaming ability of polydimethylsiloxane fluids.

Attempts have also been made to modify the Deer rheometer and pulsed-drop tensiometer, to measure surface rheological and dilational properties respectively.

GLOSSARY

a	width of canal
c	molar concentration
c_s	surface concentration
c_s^*	coefficient of compressibility
d	distance between parallel plates
e	electronic charge
f	shear force per cm
h	Planck's constant
k	Boltzmann's constant
k_s	compression modulus
k'	Debye-Hückel reciprocal length
ℓ	length of Wilhelmy plate
m_2	amount per unit area of film
n	degree of polymerisation
n_0	number of cations and anions per cm^3 of solution
p	pressure
p_0	total external pressure
q	reduced surface flux
q_1	number of molecules per unit volume of material
r	radius
r_2	radius of rotating element
Δs	surface flux
t	time
t_e	stress experimental time
t_m	Maxwell relaxation time
t_r	stress relaxation time

u	bond energy
v	velocity
v_m	molar volume
v_r	liquid velocity in the radial direction, r
Δv	surface potential
w	weight
x	distance
z	ionic valency
A	non-retarded Hamaker constant
C	torsion constant
D	dielectric constant
D_b	coefficient of bulk diffusion
D_e	Deborah number
D_s	coefficient of surface diffusion
E	entering coefficient
$F\phi$	resonant frequency of ring at air/water-with-monolayer interface
F	resonant frequency of ring at air/water interface
G	shear modulus
G_s	surface shear modulus
G_s^*	complex shear modulus
G_s'	elastic or storage modulus
G_s''	loss modulus
ΔG	surface free energy
H_0	surface-surface separation of planes
ΔH_R	enthalpy change
I	moment of inertia
$J(t)$	creep compliance
M	moment of the tangential frictional force

$\overline{M}_w$	weight-average molecular weight
N	Avogadro's number
N_1	number of molecules per microlitre
P	pressure
P_a	period of pendulum in air
P_G	gravitational pressure
P_H	hydrostatic pressure
$P_{\hat{\gamma}}$	capillary pressure
Q	partition function
R	universal gas constant
R_1R_2	principal radii of curvature at the border
R_e	Reynolds number
S	spreading coefficient
ΔS_R	entropy change
T	absolute temperature
T_b	time for which molecules bound
T_u	time for which molecules unbound
V	potential energy
V_A	non-retarded van der Waals energy
V_A^R	retarded attractive energy
V_G	steric interaction energy
V_K	average interaction energy (Keesom)
V_R	electrical double layer repulsion
V_T	total interaction energy
W_A	work of adhesion
W_C	work of cohesion
Y	surface Young's modulus

α	phase angle (cone and plate viscometer)
$\alpha_1\alpha_2$	molecular polarizabilities
α_C	calibration constant for cone and plate viscometer (=> shear rate)
α_D	calibration constant for rotational surface viscometer (=> shear rate)
β_C	calibration constant for cone and plate viscometer (=> stress)
β_D	calibration constant for rotational surface viscometer (=> stress)
γ	shear strain
$\dot{\gamma}$	shear rate, rate of strain
$\hat{\gamma}$	surface tension
$\Delta\hat{\gamma}$	surface tension differential
δ	distance between concentric rings (rotational surface viscometer)
$'\delta$	mean amplitude random translation
ε	surface charge density
ε_0	permittivity of free space
ε_r	relative permittivity of medium
ζ	coefficient of surface dilational viscosity
η	viscosity
η_0	viscosity of bulk subphase
η_{pl}	plastic viscosity
η_{rel}	relative surface viscosity
η_s	surface shear viscosity
η_s'	dynamic surface shear viscosity
η_{sp}	specific surface viscosity
$[\eta]$	intrinsic viscosity
η/ρ	kinematic viscosity of fluid
θ	contact angle
λ	natural logarithm
μ	chemical potential

μ_1	dipole moment
ν	Hertzian frequency
ν_0	frequency of electronic fluctuation
ρ	density
σ	surface Poisson's ratio
τ	shear stress
τ_B	Bingham yield stress
$\dot{\tau}$	time differential of stress
τ'	period of oscillation of a molecule (Eyring theory)
χ_1	dimensionless enthalpy parameter
ψ	electrostatic potential
ψ_0	electrostatic potential at the surface
ψ_d	Stern potential
ω	angular frequency
Γ	surface excess concentration
Φ	scalar quantity
π	surface pressure
π_{el}	electrostatic pressure
π_A	van der Waals interaction pressure
π_E	excess osmotic pressure
π_S	steric interaction pressure
Ω	angular rotation
gf	geometric factor
AFI	antifoaming index
FH	foam height
KO	input amplitude (oscillating ring surface rheometer)
KON	final amplitude (oscillating ring surface rheometer)
MW	molecular weight
$\propto$	proportionality
PDMS	polydimethylsiloxane

CONTENTS

CHAPTER 1

GENERAL INTRODUCTION

Surface-active or amphipathic molecules adsorb at the interface between two fluid phases because of their molecular structure. This has been illustrated by surface-active molecules possessing the ability to locate at the water/air interface by virtue of a hydrophilic portion which resists evaporation and a hydrophobic portion which reduces solubility in the aqueous phase. Provided these properties are possessed to a sufficient degree, a stable insoluble monolayer can be formed at the water/air or oil/air interface and a wide range of investigations can become possible. With surface chemical techniques[1,2] it was possible to gain information concerning such two-dimensional arrays of orientated molecules. For example, an evaluation of properties such as surface pressure, viscosity, elasticity and potential can produce a better understanding of molecular packing and of interactions between like and unlike molecules, either within a film, or between the film and subphase molecules. In addition, kinetic studies can investigate penetration into, permeation through, and reaction of bulk phase molecules with orientated films. Thus, monomolecular film studies can provide much information of value when dealing with such practical problems as lubrication, evaporation control and detergency flotation. Typical anionic surface-active molecules that have been studied in this work, at the water/air interface, are the long-chain fatty acids; where the polar, solvated head group remains in the aqueous environment and the hydrocarbon chain penetrates the gaseous phase. Such molecules stabilise both foams and emulsions by providing an electrostatic charge at the interface. The formation of the foam or emulsion is aided by the

decrease in interfacial tension produced on adsorption of the fatty acid. If the surface charge is effectively surrounded by the addition of electrolytes at a sufficiently high concentration, coalescence of the fluid particles can occur. The rate is governed not only by the collision frequency, but also by the flow properties (that is, the rheological properties) of the surface films. As a result, the study of the properties of monolayers at an interface can be of considerable importance in understanding the stability of foams and emulsions. Emulsions have been more widely used, and their stability is of major importance in such diverse areas as secondary and tertiary oil recovery, pharmaceutical creams and foodstuffs.

Plateau, in 1873, first advocated that foaming was dependent on the viscosity of adsorbed layers, but ever since this has given rise to much confusion. The early work was prejudiced by the erroneous interpretation of Plateau's experiments on the damping of moving magnetic needles (partly obscured by the Marangoni effect, and partly by surface contamination), and by the strong skin or 'pellicle' developed by the exceptional properties of the saponin solutions (used in some early experiments). The present viewpoint is that surface viscosity could never lead to film elasticity, since viscosity is only a dissipation of elastically-stored energy (cf Maxwell model, Figure 3.4) and not the generation of a net restoring force, though viscosity can be calculated from momentum transfer.

But the rheological properties of the surface layers undoubtedly do have a great influence on the rate of relaxation of stresses in lamellae. Brown *et al*[3] concluded that the most obvious effects of viscosity were the damping of any disturbances and retardation of drainage of lamellae. The rheology of surface layers is still not fully explored,

either experimentally or theoretically. Van den Tempel *et al*[4] eventually concluded that five parameters are required to characterize the behaviour of an interface completely (as long as the behaviour remains linear), namely: surface shear and dilational viscosity, surface shear and dilational elastic modulus, and the equilibrium surface tension. Of these parameters, surface shear viscosity has been fairly extensively investigated by several authors. Stuke[5] and Goodrich[6] have carried out a mathematical rheological analysis of surface flow and foaming. It is generally recognized that while some layers are freely mobile, others show shear viscosity of various magnitudes, shear elasticity with long times of relaxation, i.e. viscoelasticity, thixotropy or dilatancy. However, very few studies have been made of the properties, perhaps partly because of the experimental difficulties, but certainly largely because of the problem of interpreting any measurements that can be made on such complex systems.

The control or elimination of foam has been a major problem in many industrial processes. The search to find compounds capable of promoting antifoam action, helped by possessing the ability to form fluid films at the air/water or oil/water interface, has eventually led to the use of organo-silicon and silicone polymers.

Since the introduction of commercially-produced silicones in 1943, they have experienced a phenomenal growth in volume and types of products, and have found their way into a very large number of industries and applications - such that silicones are now sold in a multitude of forms, from minute crystal semi-conductors to fluids, emulsions, rubber, sealants and resins. Silicones are widely used as water repellents for textiles, grease, adhesives and sealants, paper-release agents, anti-foaming agents, while their surface treatments also include paper coat-

ings and moulding resins. It is also ironic that a material not present naturally on earth can be a critical material in the production of one of the earth's most desirable natural resources - crude oil. But such is the case with silicones, and their use as foam control agents in certain petroleum processes.

A comprehensive review of silicone chemistry and technology has been given by Noll[7]. To better understand silicones, it is useful to examine in greater detail the most common of the silicone products - polydimethylsiloxanes. As linear polymers, polydimethylsiloxanes are colourless fluids, available in a range of viscosities, depending on chain length, with the highest molecular weight fluid being gum-like. Polydimethylsiloxanes are also available as coatings, elastomers or resins, depending on the degree of cross-linking and the amount of filler incorporated. Foams can be controlled very efficiently with low levels of a polydimethylsiloxane fluid, and the largest single application of these antifoamers in the petroleum industry is in gas-oil separation. In its natural state, crude oil contains dissolved gases (typically 10% by weight) which are held by high reservoir pressure. When this 'live' crude oil is extracted and passed into the low-pressure environment of a gas-oil separator the dissolved gases are liberated, ideally producing a gaseous phase, comprising natural gas - which is taken from the top of the separator - and a liquid phase comprising 'stabilized' crude oil, which is taken from the bottom. Often, however, the disengagement of gas from crude oil is not clean, and a foam is formed. This may lead to the loss of crude oil via the gas stream and damage to downstream gas-processing equipment. This wasteful process can be avoided by reducing the amount of foam through the injection of an antifoamer. Silicone fluids have been used for many years to suppress foaming of

crude oil in separators, to prevent liquid carryover with the gas, and to increase capacity. In the North Sea and Gulf of Mexico, foam is controlled both to allow accurate measurements of produced oil that is sent ashore, and to prevent very large losses with gases which are burnt off. Not every crude oil foams; it must contain a critical mixture of components - either natural components or chemical additions in the well bore - before foam becomes troublesome. However, foam seems a greater problem in high-producing wells where high pressures and temperatures are encountered, such as the North Slope Alaskan oil field and the North Sea. A silicone is the only known foam control agent for gas-oil separators. The antifoam efficiency of various viscosity grades of polydimethylsiloxane was studied in gas-oil separation on Ekofisk platform in the North Sea. It was found that a polydimethylsiloxane fluid with viscosity 60,000 centipoise was four times more efficient than a 12,500 centipoise fluid; whereas a 100,000 centipoise fluid showed no improvement over 60,000 centipoise, possibly because of lower mobility and dispersability. With other factors being equal, the difference was attributed to the decreased solubility of 60,000 centipoise fluid in the crude oil, thereby providing greater efficiency.

To try and understand the nature of polydimethylsiloxanes, one must look at their structure. Polydimethylsiloxanes consist of an inorganic siloxane backbone with pendant methyl groups, and are represented by

$$CH_3Si(CH_3)_2\left[-O-Si(CH_3)_2\right]_n - Si(CH_3)_3$$

where n is the degree of polymerisation and can range from 0 to 2,500.

The principal role of the backbone in the surface activity of polydimethylsiloxanes is its ability to present the attached methyl

group at interfaces. This has led several authors[1,2,8,9,10] to conclude that polydimethylsiloxanes emerge as a favoured case of a very surface-active pendant group (the methyl group), whose activity is presented to best effect by virtue of the unique flexibility of the backbone. This high degree of flexibility is reflected in the Langmuir trough studies of spread polydimethylsiloxane monolayers on water[11,12]. Two quite different configurations account for much of the observed behaviour. The transition between one configuration (in which all siloxane bonds orientated towards the aqueous phase) and the other (a six-unit helical arrangement occurring with a very small increase in surface pressure) exemplifies the ease of reorientation possible with the polydimethylsiloxane chain. The origin of this unique flexibility is thought to be in the basic molecular geometry. The consequences of the low intermolecular forces that evolved from the molecular architecture of polydimethylsiloxane resulted in an upsurge of interest in the behaviour of spread monolayers of polydimethylsiloxanes on both aqueous and non-aqueous subphases[14,15,16,17,18,19], but little has been reported regarding their surface rheological behaviour. However, it is now believed that rheological properties such as surface and interfacial tensions and surface viscosity and elasticity are vitally important in such applications as antifoaming and de-emulsification. Polydimethylsiloxanes have the lowest recorded surface shear viscosity (less than 10^{-5}poise) - below the limit of detection of a viscometer[20]. This property is of particular interest in view of their known proficiency as defoaming and antifoaming agents[2].

In this work, the rheological properties of a number of polydimethylsiloxane monolayers were investigated. The surface viscosities were determined with a canal viscometer, which is capable of greater

sensitivity and accuracy than those methods based on the torsional behaviour of a ring or disc suspended in the interface[21,22]. The canal viscometer is satisfactory at film pressures below the characteristic 'plateaux' in the pressure-area isotherms of polydimethylsiloxane monolayers. At higher film pressures, extending into the plateau region, the adsorbed molecules on each side of the canal will have quite different orientations and compressibilities, and so it was difficult to assign an average viscosity to the film in the canal. A rotational surface viscometer was then used to try to determine the surface viscosity at the higher film pressures. An oscillating ring surface rheometer (SSE Mk 2, *S. Sciences* Enterprises) was also used to determine the surface shear elasticity of polydimethylsiloxane films at various pressures. This surface rheometer operates under surface shear conditions, and not under surface dilational conditions.

Finally, it is appropriate to give a brief outline of how the latter work reported evolved. First, fatty acids - namely myristic, stearic, nonodecanoic and arachidic acids - were used as standard substances for film-forming and compression to check on the correctness of procedures, manipulation and calibration. With these acids, a qualitative knowledge of their behaviour as surface films was needed before quantitative measurements of polydimethylsiloxane polymers could be undertaken with confidence. Some instrumental difficulties were encountered with the duralumin trough, torsional pendulum viscometer, Deer rheometer and the pulsed-drop tensiometer when used in their capacities for surface rheological study. Nevertheless, the use of a modern Joyce-Loebl Langmuir trough, and also the oscillating ring surface viscometer, ensured complete and reliable study of the fatty acid and polydimethylsiloxane monolayers.

Experiments were also conducted on non-aqueous bulk foams. The antifoaming efficiency of a number of linear polydimethylsiloxane polymers of different molecular weights, and some of their mixtures (containing various molar-proportions of two different polydimethyl-siloxanes), were measured, as a function of concentration in foams formed from offshore Magnus and Ninian crude oils; and also a 'model' crude oil (consisting of 3% w/v aerosol OT in ethylene glycol).

One of the aims of the work described in this dissertation was to be able to relate the surface rheological measurements to the unique antifoaming ability displayed by polydimethylsiloxane polymers.

CHAPTER 2

TWO-DIMENSIONAL SYSTEMS

2.1 The Interface and Interfacial Phase

Two-dimensional systems are usually regarded as being composed of a surface phase occupying an extended region of the 'interface' separating two immiscible bulk phases. The interface is the transition zone between two homogeneous bulk phases in thermodynamic equilibrium, where the compositions, structure or properties of each of the phases is modified with respect to the bulk phase. The transition zone can be regarded as being of the order of one or two molecules thick due to the immiscibility of the two bulk phases[23].

The surface or interfacial phase is, by definition, a non-bulk phase enclosed within the interfacial transition zone, between the two immiscible bulk phases. It has a different composition from that of either adjacent bulk phase, even in the case of a liquid in equilibrium with its vapour, where only a single constituent is present. Here, the laws of thermodynamics demonstrate that there exists within the interfacial transition zone an excess concentration, Γ moles cm^{-2} of the single constituent, which is given by

$$\Gamma = - \frac{\partial \hat{\gamma}}{\partial \mu} \qquad (2.1)$$

where $\hat{\gamma}$ is the surface tension of the liquid and μ is the chemical potential of the single constituent.

In the case of a system of two constituents, such as that of a solution in equilibrium with its vapour, the Gibbs equation states that

$$\Gamma_{s_1} = - \left(\frac{\partial \hat{\gamma}}{\partial \mu_{s_1}} \right)_T \qquad (2.2)$$

$$\Gamma_{s_2} = - \left(\frac{\partial \hat{\gamma}}{\partial \mu_{s_2}}\right)_T \tag{2.3}$$

where s_1 and s_2 denote the solute and solvent respectively. The signs of Γ_{s_1} and Γ_{s_2} are dependent on the nature of the components of the solution. We have also have[24]:

$$(C^B_{s_1} - C^A_{s_1})\Gamma_{s_2} + (C^B_{s_2} - C^A_{s_2})\Gamma_{s_1} = 0 \tag{2.4}$$

where $C^A_{s_1}$, $C^B_{s_1}$, $C^A_{s_2}$ and $C^B_{s_2}$ are the molar concentrations of the two components in the bulk phases A and B respectively.

It is due to the difference in composition between the interfacial region and the bulk phase that allows the transition zone to be regarded as the surface phase. However, in the case of extremely dilute solutions, we have

$$\Gamma_{s_1} = - \frac{C_{s_1}}{RT} \frac{d\hat{\gamma}}{dC_{s_1}} \tag{2.5}$$

where R is the gas constant and T is the temperature, with the difference in concentration of the solute between the bulk solution and the surface region being very large. The accumulation of molecules of s_1 at the interface constitutes an adsorbed film one molecule thick. As regards surface rheology, the monomolecular films that have been mostly studied are those of substances insoluble in water, but which have been spread on the water surface as a monolayer by means of dilution in a volatile solvent.

2.2 Amphiphilic Molecules and Monomolecular Films

It is when a substance that is insoluble in two immiscible adjacent bulk phases A or B, and possesses a strong affinity for both (i.e. it is capable of spreading at the interface, either spontaneously or otherwise, and remaining spread) that an insoluble surface phase can

arise at the interface. The free energy of the entire system must be lowered if spreading is to occur[25,26,27,28]. This is possible if the molecules are amphiphilic, possessing two sets of functional groups - one set soluble in phase A and not in phase B, and the other set soluble in phase B but not in phase A. To form a monolayer it is also necessary that the film does not dissolve in either of the two phases. For example, at the air/water interface, amphiphilic molecules possessing a hydrocarbon chain of 16 carbon atoms form stable monomolecular films when the polar groups are -OH, -COOH, -CN or $-CONH_2$, but unstable soluble films when the terminal groups are $-SO_3^-$ or $-OSO_3^-$ [29].

The monolayer in bulk form is insoluble in the subphase because of the cohesive energy of the molecules when they are in a crystal. After spreading, there is a new molecular environment for the molecules and the cohesion between the molecules can be significantly reduced, no longer offering a hindrance to solution. Lauric acid, for example, though almost insoluble in water, will not form a stable monolayer as it diffuses into the subphase[30]. At an oil/water interface, the ionised groups of an equal length of hydrocarbon chain form the most stable films because of the solubility of their hydrocarbon moeties in the oil phase[31,32].

However, in the case of high polymeric substances, formation of stable monolayers depends on there being sufficient attraction for the surface subphase to overcome bulk cohesion. A high degree of insolubility is not required, yet it is necessary that the individual monomer units have a finite free energy of adsorption from the bulk phase to the surface for a monolayer to be stable. It is then possible to obtain spread monolayers of many proteins and water-soluble polymers. The criteria of spreadability of monolayers of insoluble polymers are similar

to those of simple, non-polymeric materials, as explained in the next section.

2.3 The Spreading of One Liquid on Another

Criteria For Spreading

Some materials spread simultaneously from the pure solid or liquid phase at room temperature; others need to be heated in order to overcome the cohesive forces of the bulk phase[33]. Often, a spreading solvent is used to aid formation of the monomolecular film[29]. The solvent used should be able to disperse the film-forming molecules at the air/water interface and then evaporate. It should also be insoluble in the subphase, for if it were water-soluble some of the monolayer-forming material would be carried into the aqueous phase. The solvent must, of course, be chemically inert with respect to both the film material and the subphase. In the experiments performed in this work, petroleum ether (bp 60-80°C), chloroform (analar grade) and redistilled n-hexane were used.

Recent work has shown that the spreading solvent may alter the properties of the monolayer[33]. The presence of a high concentration of the film-forming material in the vapour phase causes the solvent molecules to adsorb on the water surface, leading to a large incresae in the film area.

If the insoluble layer applied to the subphase is of appropriate thickness (see Figure 2.1), then the layer will either spread to form a monolayer or it will remain as a duplex film. An expression can be derived to determine which of the two possibilities will occur. At constant temperature and pressure, a small change in the surface free energy, G, of the system shown in Figure 2.1 is given by the total diff-

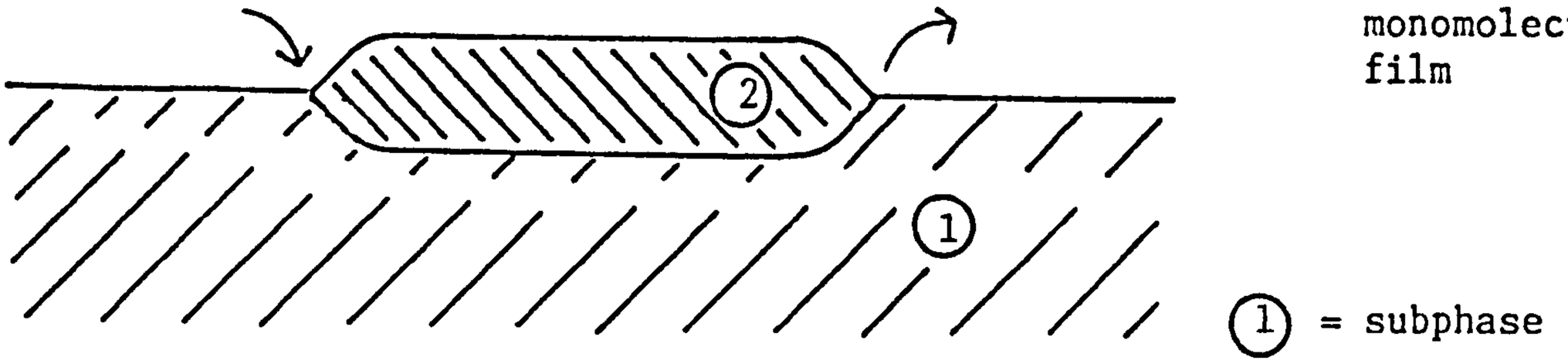

FIGURE 2.1

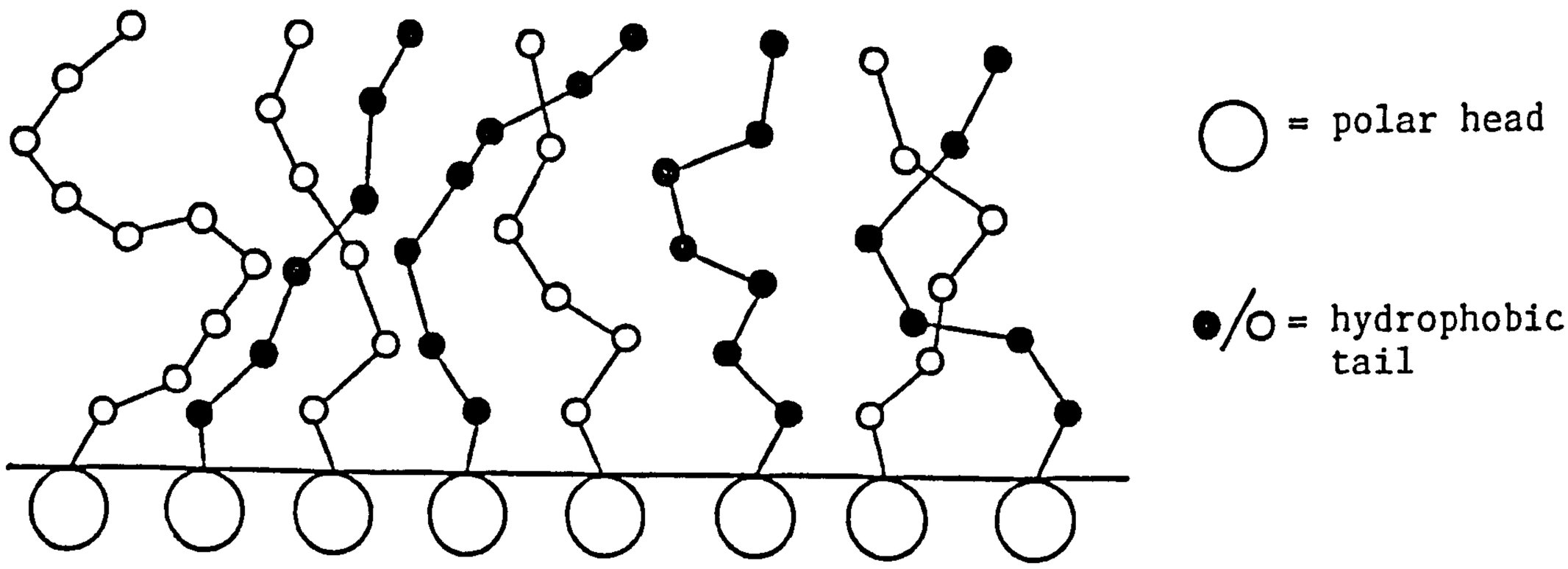

FIGURE 2.2: Schematic diagram showing the orientation of amphiphilic molecules in a monomolecular film

erential,

$$dG = \left(\frac{\partial G}{\partial A_1}\right) dA_1 + \left(\frac{\partial G}{\partial A_{12}}\right) dA_{12} + \left(\frac{\partial G}{\partial A_2}\right) \mathbf{d}A_2 \qquad (2.6)$$

but

$$dA_2 = -dA_1 = dA_{12}$$

where liquid 1 constitutes the subphase and

$(\partial G/\partial A_1) = \hat{\gamma}_1$, etc.

The coefficient $(\mathbf{d}G/\mathbf{d}A_2)_{area}$ gives the free energy for the spreading of a film of liquid 2 over liquid 1, and is called the spreading coefficient of 2 on 1. Thus

$$s_{2/1} = \hat{\gamma}_1 - \hat{\gamma}_2 - \hat{\gamma}_{12} \qquad (2.7)$$

where $s_{2/1}$ is positive if spreading is accompanied by a decrease in free energy, i.e. is spontaneous.

The work of adhesion, W_A, between two liquids 1 and 2 is given by:

$$W_A = \hat{\gamma}_1 + \hat{\gamma}_2 - \hat{\gamma}_{12} \qquad (2.8)$$

and corresponds to the work necessary to separate a unit area of interface 12 into two liquid-gas interfaces 1 and 2 respectively. Similarly, the work of cohesion, W_C, for a single liquid 1 is given by:

$$W_C = 2\hat{\gamma}_1 \qquad (2.9)$$

and corresponds to the reversible work necessary to pull apart a column of liquid. It can be seen from equations (2.7) and (2.8) that the spreading coefficient is the difference between the work of adhesion of 1 to 2 and the work of cohesion of 1,

$$s_{2/1} = W_A - W_C. \qquad (2.10)$$

When one liquid is first added to another, a thick film is formed (as in Figure 2.1) if s is positive. This occurs when a liquid of low

surface tension is placed on one of high surface tension (critical $s_{2/1}$ values are given in a paper by Harkins[34]).

Conversely, a liquid of high surface tension would not be expected to spread on a liquid of much lower surface tension. Therefore $s_{2/1}$ would be negative.

2.4 The Structure of Monomolecular Surface Films

Due to the amphiphilic nature of the molecules that make up monomolecular films at interfaces, the most favourable orientation is achieved when the polar head and the hydrophobic tail of the molecules are each in contact with the phase for which it has the greatest affinity. The long axes of the molecules are normal to the interface (see Figure 2.2). The interfacial phase is one molecule thick and can be considered as being two-dimensional, as its thickness depends only on the nature of the molecules which it comprises and the number per unit area.

2.5 The Coupling Between Film and Subphase

One of the necessary conditions for an interfacial phase to exist is that the molecules it comprises have a strong affinity for at least one of the two bulk phases. This results in a strong coupling arising between the amphiphiles and the functional groups of those molecules of the bulk phases with which they have an affinity; so when molecules of the film are displaced, they carry with them those molecules of the bulk phase with which they are in intimate contact. The molecules of the bulk phase which are in direct contact with the functional groups of the film which they solvate can be considered to be bound rigidly to the film molecules whenever the latter undergo displacements.

A kinetic unit can be defined as the smallest structural element which moves with respect to its neighbours when stress is applied to the system without undergoing internal deformations. The kinetic unit of an interfacial phase is built up from an amphiphilic molecule in addition to those molecules of the bulk phase attached to its functional groups. Therefore it is evident that the kinetic units of a system depend simultaneously on the system's nature, magnitude and the distribution of the stress applied to it. A rather more accurate rheological definition of the surface phase than that proposed in Section 2.1 would be to define the surface phase as the single layer of amphiphilic molecules in addition to those molecules of the adjacent bulk phase firmly attached to the functional groups of the film for which they have a strong affinity.

If the mean bond energy between the molecules of the bulk phase and those of the film is taken as approximately equal to that of an average hydrogen bond, then applying Frenkel's theory[35], the mean lifetime of the bond is about 10^{-9} seconds. Once broken, however, the bond will probably be reformed between the same two molecules, thus the mean lifetime of the solvation bond will be at least a microsecond. It was shown[35] that:

$$\frac{T_b}{T_u} = \frac{v.w}{kT} \geq 10^6 \qquad (2.11)$$

where T_b and T_u are time for which the molecules are bound and unbound to the subphase respectively, v is the number of subphase molecules associated with a single molecule of the film, and w is the bond energy between a subphase molecule and a molecule in the film.

The strong coupling between monomolecular films and their liquid

subphases was demonstrated for fatty acid monolayers spread on a water surface by Merigoux[36,37]. There was no detectable slip between the film and the water subphase. As a result of this coupling, there will be interference between the rheological properties of the film and those of its subphase.

2.6 States of Monomolecular Films

The presence of an amphiphilic film at an interface tends to lower the interfacial tensions. The work of Langmuir on oil films[23] enabled the effects of surface tension to be interpreted in terms of intermolecular forces. The force measured is referred to as the surface pressure, π, and is considered equal to the reduction of the pure liquid-surface tension by the film, i.e.

$$\pi = \hat{\gamma}_0 - \hat{\gamma} \qquad (2.12)$$

where $\hat{\gamma}_0$ and $\hat{\gamma}$ are the surface tensions of the pure liquid and in the presence of the monolayer respectively.

Monomolecular films can exist in many different states that are analogous to three-dimensional systems of liquids, solids and gases[29,38]. The compressional isotherms illustrated in Figure 2.3 show the presence of various physical states which represent different degrees of molecular freedom or order, resulting from intermolecular forces in the film, and between film and subphase. If no phase change occurs, then there is a change in the average molecular area of the monolayer when it is compressed, so that there is a reduction in the space occupied by each individual molecule.

From the Pressure-Area isotherms, ordinary changes of state, such as liquifaction, vaporization and sublimation are shown as plateaux in the curve. Joly[39,40] suggested that molecules in a monolayer can only

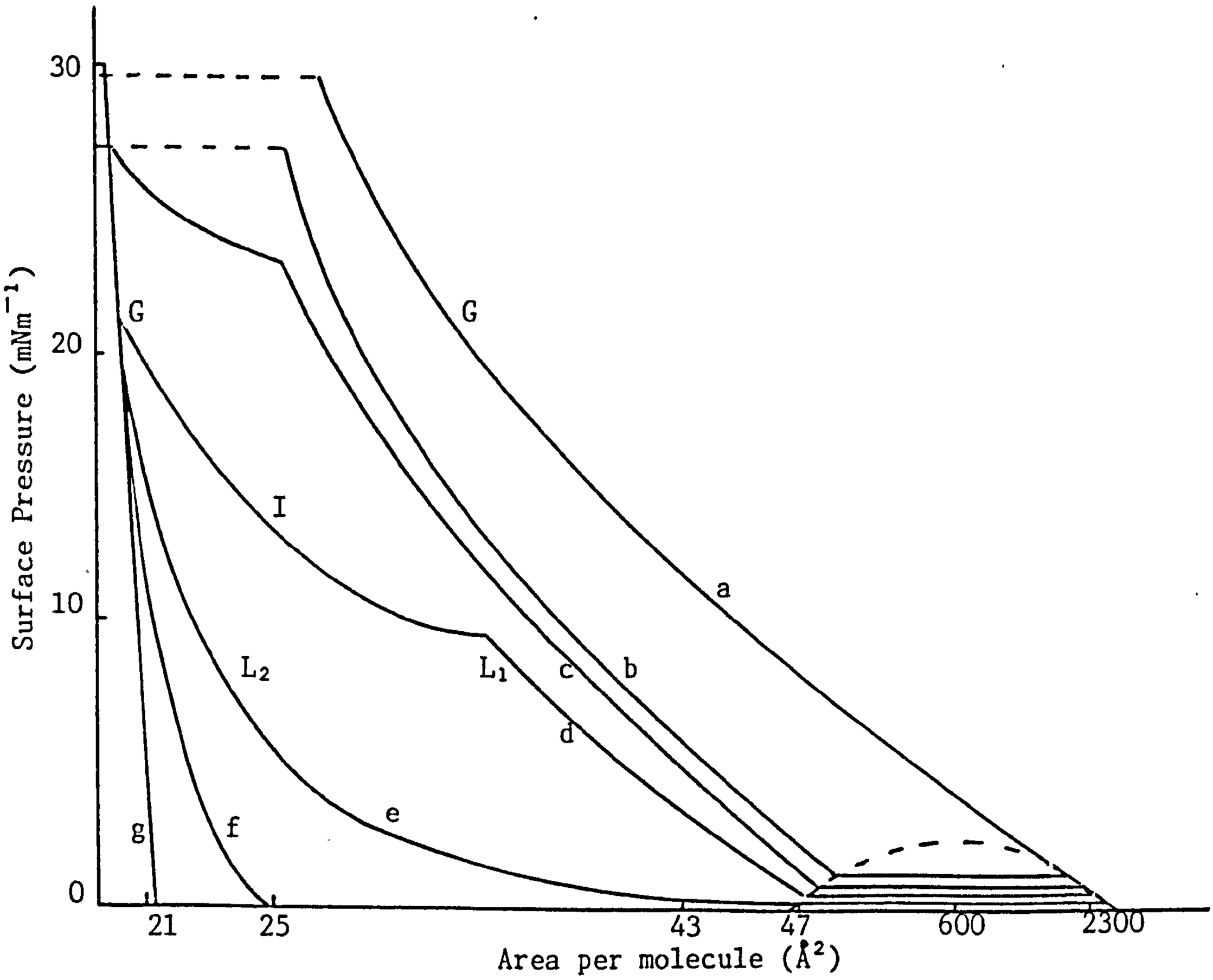

FIGURE 2.3: States of monomolecular films (schematic)

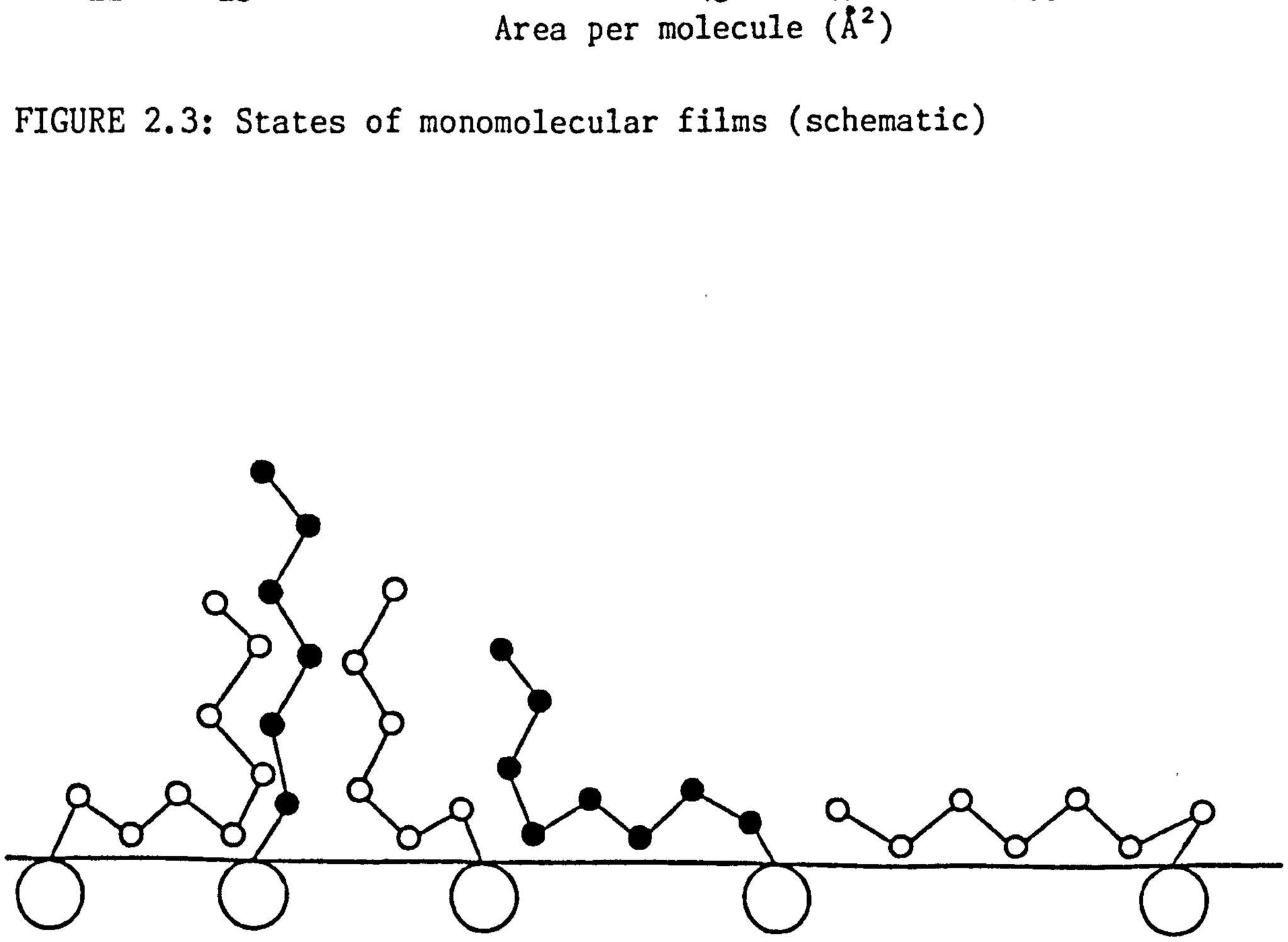

FIGURE 2.4: The liquid expanded state

occupy a certain number of equilibrium states, each corresponding to a particular stable molecular area. Phase changes occur when all the molecules are in one or another of the stable configurations. Between these points, the observed area is an average value, so that the total film area is due to a fraction of the molecules occupying a larger area, whilst the rest have taken up a configuration corresponding to the next-smallest stable molecular area. On compression, the state of a gaseous (G) film changes to that of a liquid expanded (L_1) film. This L_1-G transition is first order, there being a discontinuity in the Pressure-Area isotherm (indicated by the straight lines in the dotted region of Figure 2.3) and a lateral heat of vaporization associated with the transition. During the transition, the film consists of two different phases. For an L_1-type or G-type film, the surface potential is uniform across the film, whilst for a film in the midst of an L_1-G transition the potential undergoes an area-to-area fluctuation. Similarly, the ellipticity of reflected light fluctuates from one region to another corresponding to islands of condensed film surrounded by vapour film[41].

The usual classification of monolayer states is: gas, liquid or solid; but a number of subcategories of behaviour have also been named as one or another kind of state (see Figure 2.3).

2.6.1 Gaseous Films (G)

The concentration of surfactant at the surface may be sufficiently low to enable interactions between the amphiphilic molecules to be neglected. Under these conditions, the lowering of the surface tension will be linear with concentration, such that:

$$\hat{\gamma} = \hat{\gamma}_0 - bc \qquad (2.13)$$

where b is a constant. Therefore

$$\pi = bc \tag{2.14}$$

and

$$\frac{d\hat{Y}}{bc} = -b \tag{2.15}$$

substituting the above into equation (2.5) gives

$$\Gamma = \frac{1}{A} = \frac{\pi}{RT} \tag{2.16}$$

That is,

$$\pi A = RT \tag{2.17}$$

where A is the average area per molecule.

Hence the gaseous film obeys the equation of state of a perfect gas. The area per molecule is large compared to the actual molecular area, and the film can be expanded indefinitely without phase change. The molecules are characterized by a surface pressure which approaches zero asymptotically as the available area to the film is increased. It is probable that the molecules lie flat in the gaseous monolayer at the liquid/gas interface. This state should always be reached at sufficiently low pressures.

2.6.2 Liquid Films (L)

These films exhibit a certain degree of co-operative interaction and appear to be fluid. The Pressure-Area plot can be extrapolated to zero surface pressure at very much larger areas than the molecular cross-sectional areas, indicating a degree of looseness in the film[29,34].

2.6.2.1 Liquid Expanded Films (L_1)

L_1-type films are observed with long chain compounds having polar groups such as acids and alcohols. The Pressure-Area plots for these films extrapolate to zero surface pressure to give areas of circa 50Å^2

in the case of single chain molecules. This type of film only exists as a single phase; no islands are discernible by, for example, surface potential probing. A first order transition is observed for L_1-type films to gaseous films at low pressures, and these, when compressed, show a sharp change to a film of much higher compressibility, i.e. intermediate (I) films. The liquid expanded state is the transition from the gaseous state, in which all the molecules lie flat on the surface; and the condensed state in which the molecules are all orientated perpendicular to the surface (Figure 2.4). The equation of state[42] is obeyed by liquid expanded films and resembles the van der Waal's equation

$$(\pi - \pi_0)(A - A_0) = RT \qquad (2.18)$$

Langmuir suggested that the monolayer in the L_1 state behaved as a duplex film in which the head groups were in a state of two-dimensional kinetic agitation, whilst the attractive forces between the hydrocarbon chains kept the film together. The Pressure-Area isotherm is illustrated in Figure 2.5; above 800Å^2/molecule the film is gaseous, whilst a liquid expanded-type film is obtained when compressed to 50Å^2/molecule.

2.6.2.2 Liquid Condensed Films (L_2)

The compression of I-type films gradually led to a region of linear Pressure-Area isotherm behaviour, yet it is of low compressibility. The film in this region is known as a liquid condensed film[34] or a film with close-packed molecular head groups rearranged on compression. At low temperatures (curve e in Figure 2.3), the L_2-I-L_1 sequence has given way to an L_2-type film that either undergoes a phase transition to a gaseous film or may appear to expand indefinitely without discontinuity, as though it were above its critical temperature. Such films

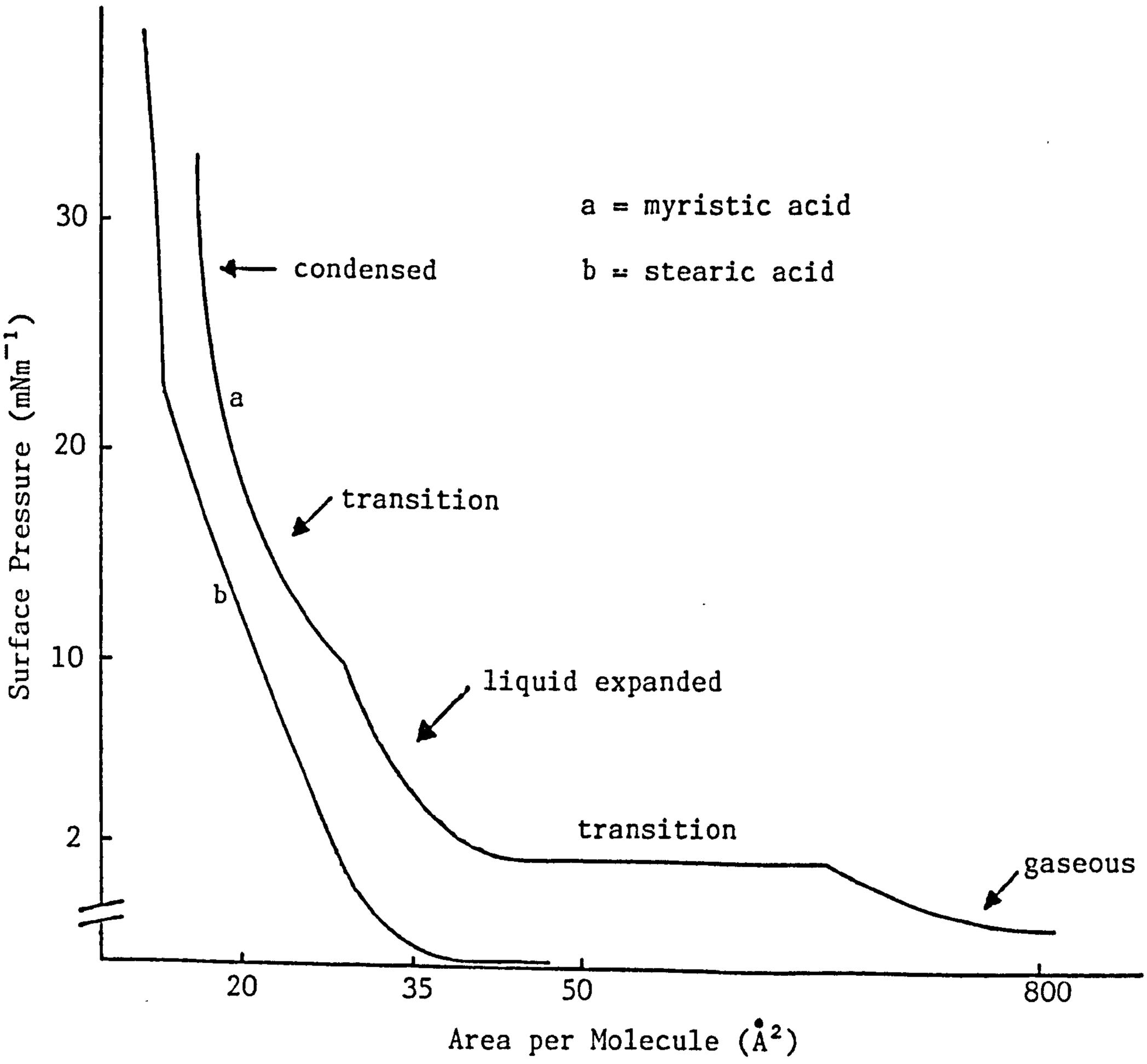

FIGURE 2.5: Schematic illustrations of the surface pressure-molecular area isotherms for myristic and stearic acids, spread on 0.01M hydrochloric acid at 14°C and 20°C respectively

may be termed vapour-expanded[29], as they expand to give a G-type rather than an L_1-type film. L_2-type films have water molecules between the polar head groups[29,43]. On compression, the water molecules are squeezed out to reduce the area and so produce a more compact solid film. In some cases as a result of compression, the monomolecular layer may rearrange with the polar heads, assuming a staggered arrangement as illustrated in Figure 2.6.

The long chain fatty acids with no less than 16 carbon atoms are examples of materials which give condensed films at room temperature. A typical example is stearic acid ($C_{17}H_{35}COOH$) and its Pressure-Area isotherm on dilute hydrochloric acid is schematically illustrated in Figure 2.5. At high film areas, the molecules of long chain fatty acids do not separate completely from one another as the cohesion between the hydrocarbon chains is strong enough to maintain the film molecules in clusters or islands on the surface, as illustrated in Figure 2.7. As a result of this strong cohesive tendency, the surface pressure remains low as the film is compressed, and then rises rapidly when the molecules become tightly packed together. Adam's observations[29] from the Pressure-Area isotherms of fatty acids indicate that the initial pressure rise occurred at circa 25Å^2/molecule, corresponding to the initial packing of the end groups. That the isotherms become very steep at circa 20.5Å^2/molecule is due to more efficient packing being achieved by the staggering of the end groups.

A limiting area of 20-22Å^2/molecule is typical for straight-chain fatty acids, irrespective of the chain length. At this point, the packing of the molecules shows a distinct similarity to that in the crystalline state. The cross-sectional area of stearic acid molecules obtained from X-ray diffraction measurements[29] was found to be circa

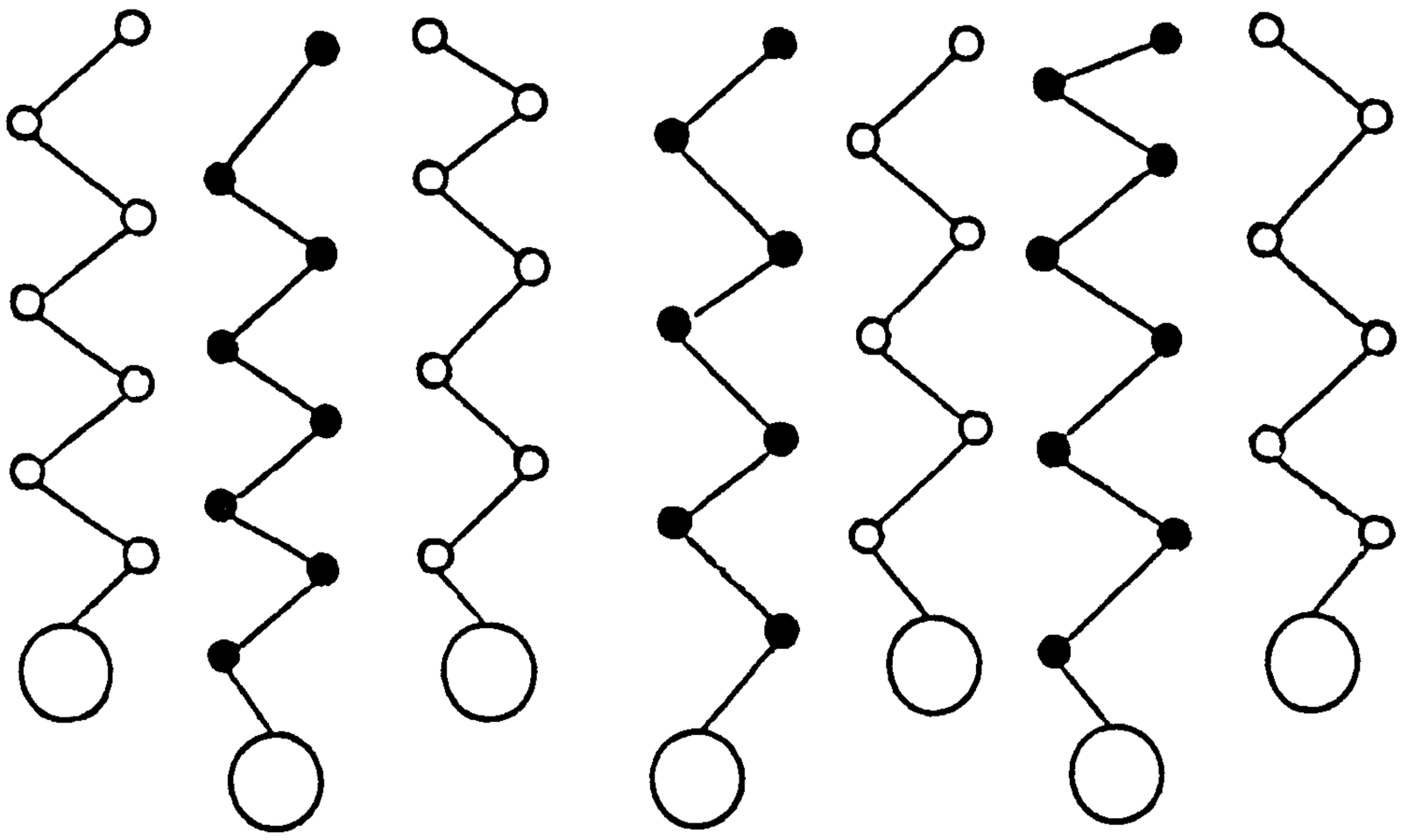

FIGURE 2.6: The staggered arrangement of the polar head groups in a condensed film

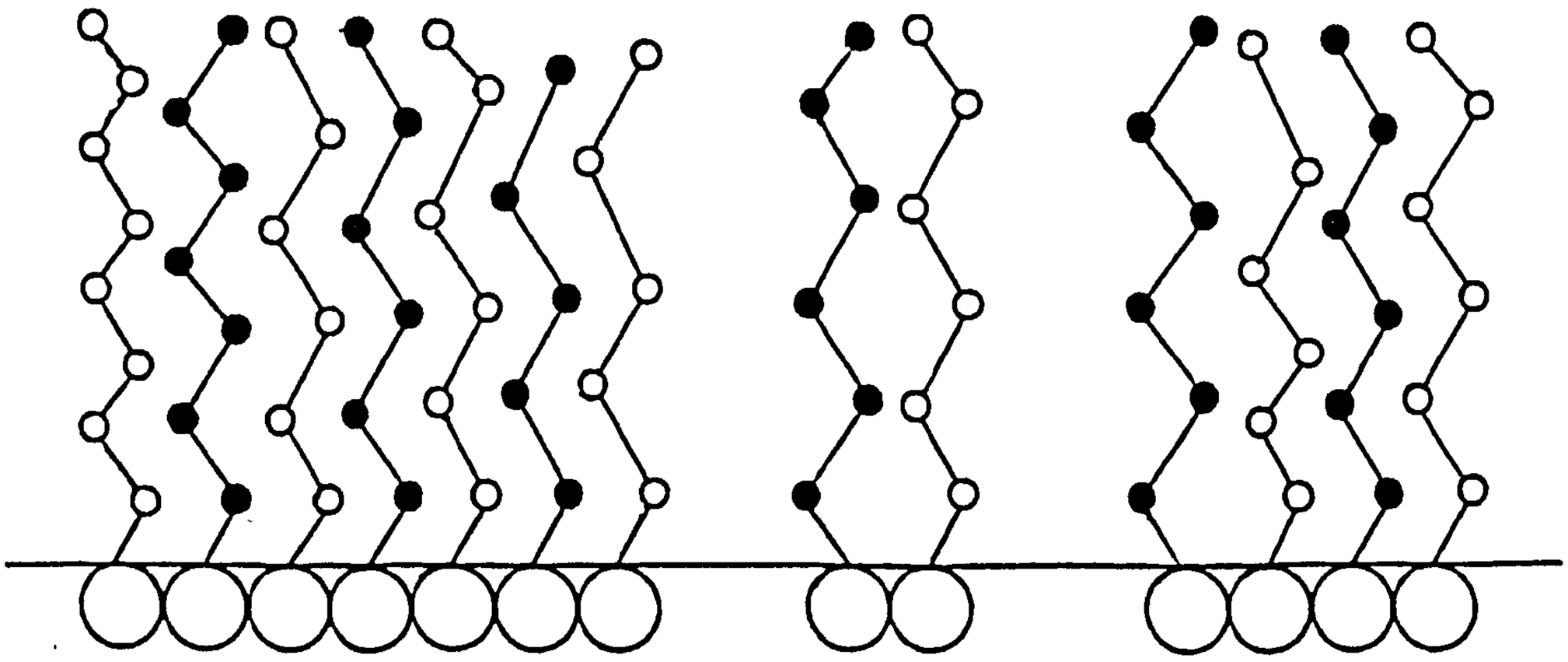

FIGURE 2.7: The staggered arrangement of the polar head groups in a condensed film at high film areas

18.5Å^2/molecule at normal temperatures. Any attempts to compress the film beyond its limiting area will only lead to the collapse of the film.

2.6.3 Solid Films (S)

According to the analysis of Harkins[44] and Dervichian[38], this phase corresponds to one of low compressibility and mostly close-packed condensed films. Most fatty acids and alcohols with long chain lengths will, at sufficiently low temperatures, exhibit this type of phase. The areas of the Pressure-Area isotherms extrapolate to circa 20.5Å^2/molecule at zero surface pressure, indicating a region of close-packed hydrocarbon chains. These films are of high rigidity and density.

2.7 Polymeric Films

The Pressure-Area isotherms for well-spread polymer or protein films on aqueous subphases are, in general, featureless in comparison to monolayers of smaller molecules. The surface pressure tends to be low at large specific areas, but increases more or less rapidly when the film is compressed to the point where the macromolecules themselves occupy most of the available surface. The isotherms tend to be moderately linear or L_2 in type at intermediate pressures. A great many polymers appear to form films having a flat molecular configuration. Thus various polyesters[45] such as poly (vinyl acetate) monolayers gave extrapolated areas of circa 60 to 70Å^2 per segment. In contrast, the behaviour of poly(vinyl benzoate) was quite different[46], giving a very compact monolayer of extrapolated area 9Å^2 per monomer unit; its compressibility was more like that of stearic acid, i.e. about 0.006m/mN, rather than the usual polymer film value of circa 0.02 to 0.1m/mN. Apparently in this case, close packing of the benzene rings occurred.

However, it must be stated that the curves were smooth and showed no distinct evidence of 'phase transformations' in the stable monolayer region. Crisp[47] suggested that the polymeric films could be separated into the condensed and expanded classes. The condensed-type films such as the monolayer of poly(ethyl methacrylate) have high viscosity or rigidity with much steeper Pressure-Area curves, whilst monolayers of the expanded type are fluid and exhibit a gradual rise in surface pressure on compression; examples of such films are those of poly(ethyl acrylate) and dimethyl siloxane polymers (see Figure 2.8). Fowkes[48] later suggested that in the expanded-type films the polymer molecules were miscible with water molecules in the surface layer, and therefore could move largely independently, as in the gaseous (or ideal surface solution) type of small molecule monolayer. Presumably, the condensed-type films have the macromolecules in contact, and are analogous to the coherent monolayers of smaller molecules.

There has been a suggestion that some spread polymer films may contain molecules arranged in coils, helices or other well-defined molecular arrangements. Fox *et al*[11] advanced one of the suggestions to account for the behaviour of poly(methyl siloxane) films at high compression, although others[49,261] had interpreted similar results in terms of simple collapse. Recent studies of wave-damping by poly (methyl siloxane) monolayers have been interpreted as supporting the concept of molecular rearrangement on compression[275].

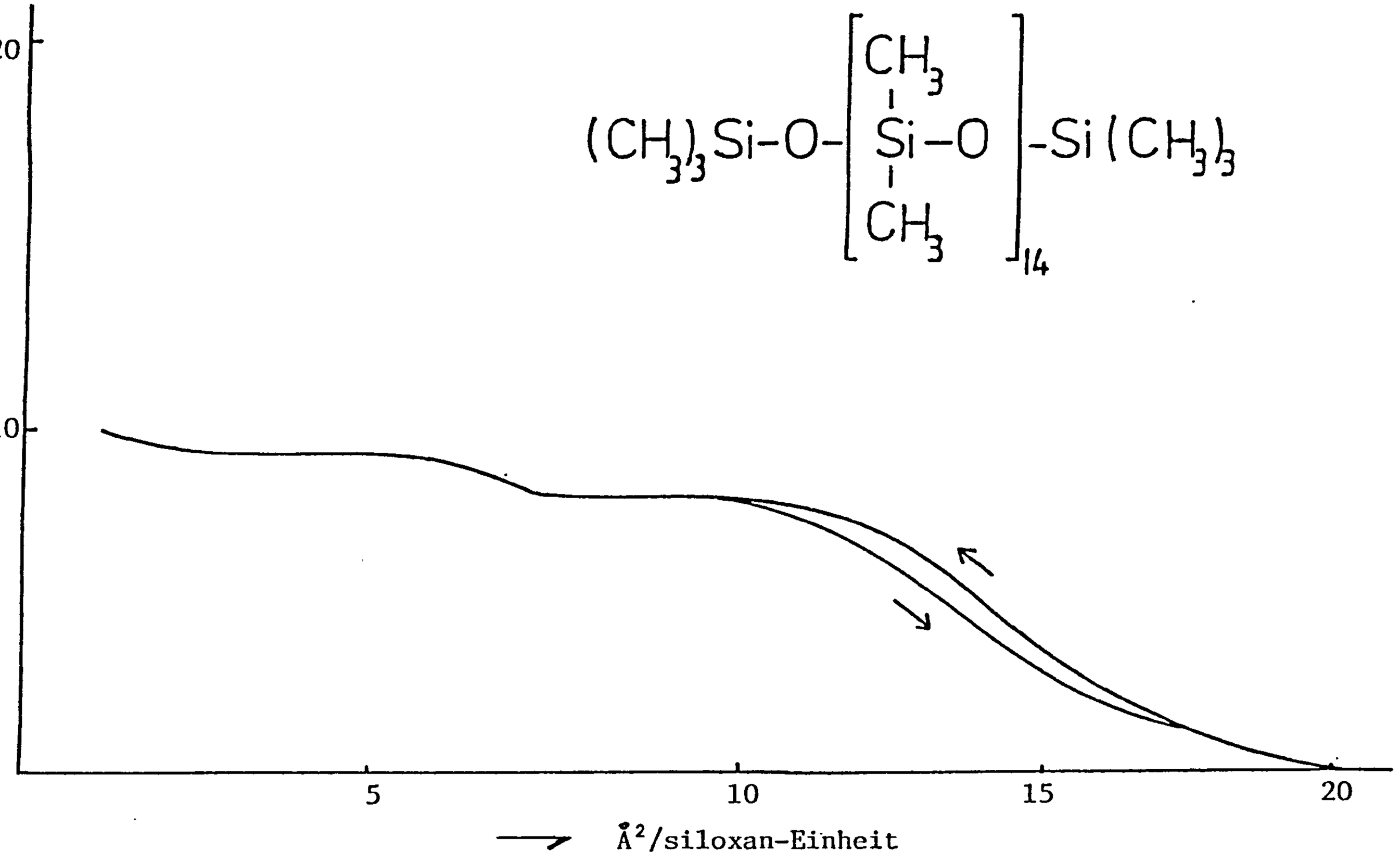

FIGURE 2.8[12]: The π(A) isotherm of a polydimethylsiloxane

CHAPTER 3

RHEOLOGY

3.1 Bulk Rheological Behaviour

The study of the science of the deformation and flow of matter[50] is known as rheology. When a stress, τ, i.e. force per unit area, is applied to a material it will deform, and the extent of the deformation relative to the original dimensions of the material is known as the strain, γ.

There are three basic types of behaviour observed in response to an applied stress, and these are illustrated in Figure 3.1. Firstly, if the deformation is reversible on removal of the stress, the material stores energy and is said to be elastic. Secondly, if the components of the material diffuse a sufficient distance during the experiment to relieve the applied stress, a viscous flow is said to have occurred, resulting in an irreversible deformation and energy is dissipated as heat. However, the response of many materials to an applied stress lies between these two extremes and is termed viscoelastic, exhibiting both viscous and elastic properties.

The classification of material is therefore governed by the decay of elastically-stored energy[51]. If the time-scale for a significant amount of decay is short compared to the duration of the experiment, the material is said to respond as a viscous fluid; and, conversely for insignificant relaxation, the material is taken to be an elastic solid. This classification is defined in terms of the Deborah number, D_e:

$$D_e = \frac{t_r}{t_e} \tag{3.1}$$

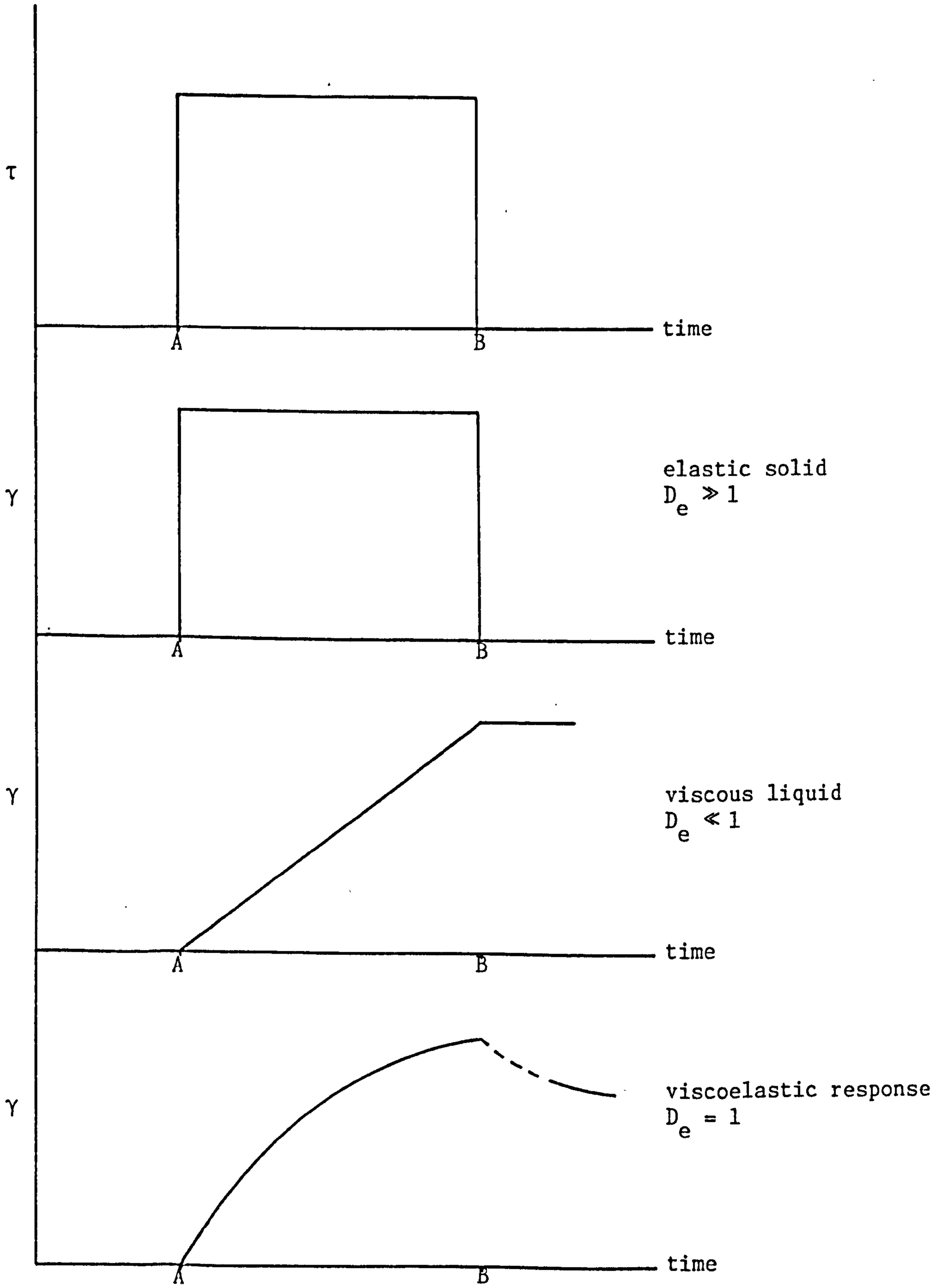

FIGURE 3.1: Elastic, viscous and viscoelastic behaviour observed in response to an applied stress

where t_r is the stress relaxation time of the material, and t_e is the experimental time, so that

$D_e \gg 1$ elastic response, solid

$D_e \ll 1$ viscous response, fluid

$D_e = 1$ viscoelastic response

The laboratory time-scale is generally of the order of $10^{-3} < t_e < 10^3$s, which is suitable for most experiments.

In order to describe viscous, elastic and viscoelastic behaviour it is necessary to find satisfactory constitutive equations relating stress, strain and time. A useful technique is to set up the equations by means of mechanical analogues which exhibit similar types of stress-strain-time behaviour as the materials under consideration.

The simplest behaviour exhibited by an elastic solid is that in accordance with Hooke's law[52]:

$$\tau = G\gamma \tag{3.2}$$

where τ is the applied shear stress, γ is the resultant shear strain, and G, the proportionality constant, is termed the shear modulus. The mechanical analogue used to represent an elastic solid is a spring, which obeys Hooke's law with the correct stress-strain proportionality constant, i.e. the shear modulus. This is illustrated in Figure 3.2(i).

The simple flow behaviour of viscous liquids is that in accordance with Newton's law:

$$\tau = \eta\dot{\gamma} \tag{3.3}$$

where τ is the shear stress, $\dot{\gamma}$ is the strain rate (a time derivative), and η, the proportionality constant, is termed the viscosity. The mechanical analogue used to represent a Newtonian fluid is a dashpot filled with a Newtonian liquid of the appropriate viscosity to generate the

(i) <u>Hookean solid</u>

G

$\tau = G\gamma$

(ii) <u>Newtonian fluid</u>

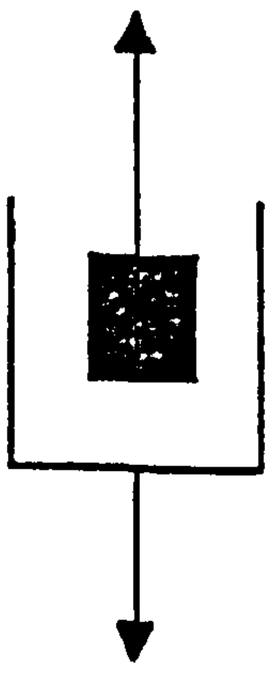

η

$\tau = \eta\dot{\gamma}$

FIGURE 3.2: Mechanical analogues and constitutive equations for a Hookean solid and a Newtonian fluid

correct stress-shear rate relationship. This is illustrated in Figure 3.2(ii). The two simple models for elastic solids and viscous liquids may be used as the building blocks for more complex responses.

3.1.1 Fluids (Newtonian and Non-Newtonian)

A material exhibits Newtonian behaviour when the shearing force per unit area, stress τ, between the two parallel plates in a liquid in relative motion is proprotional to the velocity gradient, dv/dx (shear rate), between the plates, i.e.,

$$\tau = \eta \frac{dv}{dx} \quad \text{(see Ref. (53))} \tag{3.4}$$

η is a well-defined quantity that is independent of τ and dv/dx, provided the flow is laminar.

One of the main causes of non-Newtonian flow is the formation of a structure, i.e. interparticle or intermolecular interactions, throughout the system. It is possible to characterize the non-Newtonian flow as either the steady-state phenomena or the time-dependent phenomena.

3.1.1.1 Steady-State Phenomena[50]

Pseudoplastic materials exhibit a type of behaviour which is characterized by a decrease (independent of time) in the apparent viscosity with increasing shear rate; such a shear thinning behaviour may be as a result of the breakdown of particle aggregates, leading to a reduction in the amount of solvent immobilized by the particles, thus lowering the viscosity of the system.

Plastic flow is also a shear thinning behaviour, i.e. similar to pseudoplasticity, except that the system will not flow noticeably until the shearing stress exceeds a certain minimum value (see Figure 3.3). The applied stress corresponding to a small but arbitrary chosen

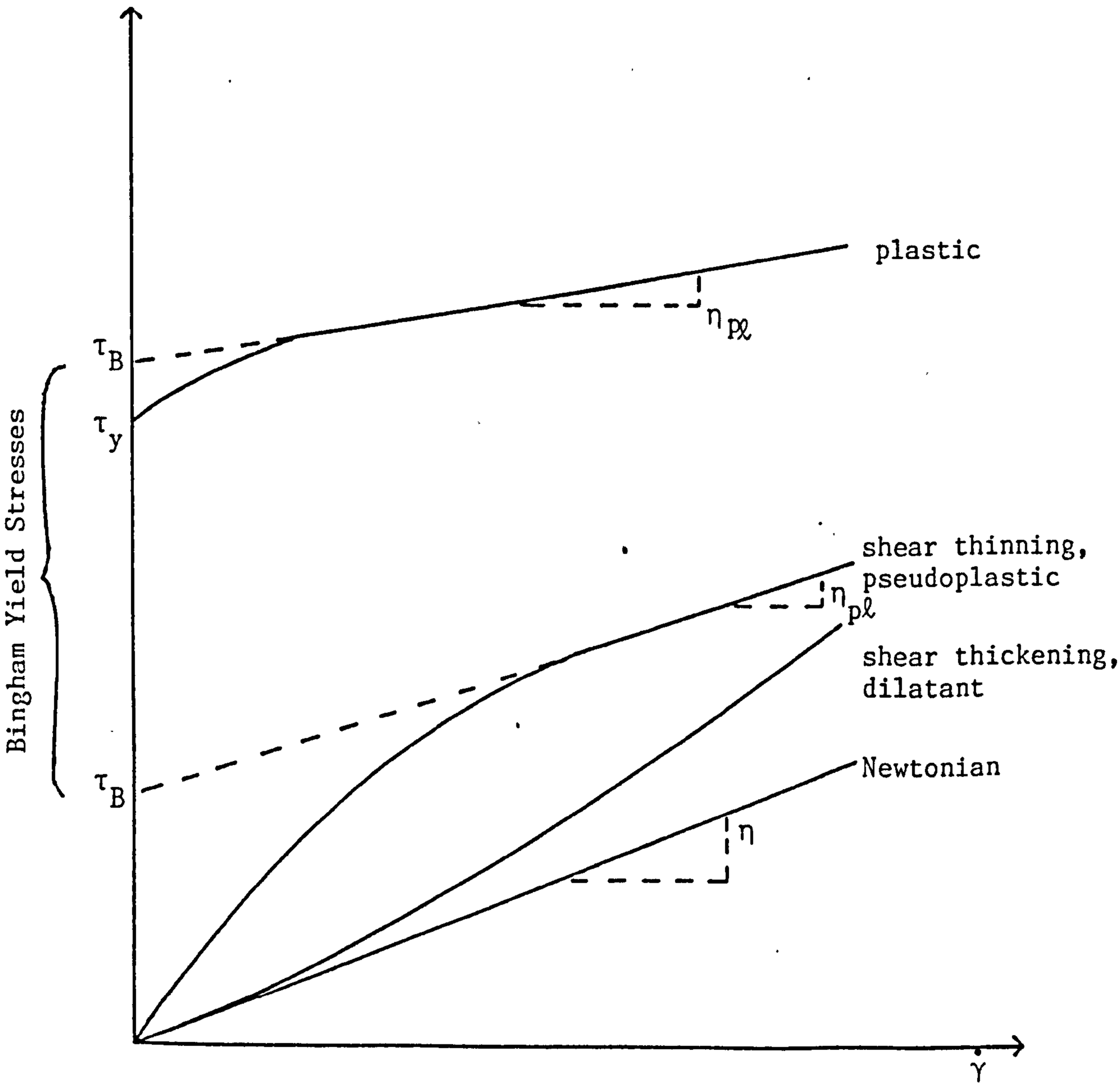

FIGURE 3.3: Stress against shear rate for Newtonian and non-Newtonian flow

rate of deformation, is known as the yield value. At high shear rates, pseudoplastic flow approximates to plastic flow and may be characterized by the equation for a Bingham body:

$$\tau = \eta_{pl}\dot{\gamma} + \tau_B \qquad (3.5)$$

where η_{pl} is the plastic viscosity, $\dot{\gamma}$ is the shear rate, and τ_B is the Bingham yield stress.

Shear thickening flow is characterized by an increase in the apparent viscosity with increasing rate of shear or deformation (see Figure 3.3). As the shear rate is increased in a densely-packed system with only sufficient fluid to fill the voids, the dense packing must be expanded to allow the particles to flow past each other. The resulting expansion leaves insufficient liquid to fill the voids and is opposed by surface tension. Volumetric dilatancy , on the other hand, is often confused with shear thickening, but strictly applies to an increase in volume caused by shear.

3.1.1.2 Time-Dependent Phenomena

When a material exhibits more resistance to flow with increasing time, while being subjected to a constant shear rate, it is then said to exhibit rheopexy.

Thixotropy is time-dependent shear thinning or plastic behaviour, and arises from somewhat similar causes. A thixotropic system becomes more fluid with increasing time, while being subjected to a constant shear rate. The viscosity decreases with time until a balance is reached between structural breakdown and reformation. If the sheared system is then allowed to stand, it eventually regains its original structure. The opposite situation of anti-thixotropy occurs with shear thickening systems.

Viscoelastic fluids cannot sustain stress for long, since the stresses are relieved by flow; whilst an extremely viscous material may exhibit elastic strain for considerable periods of time, periods which are short with respect to the time needed for appreciable flow, so that it is possible to consider a given material as an ideal elastic body for relatively short times, and as a simple viscous body for long time periods. One mechanical analogue used to represent a viscoelastic fluid is the Maxwell model, which is represented by a dashpot and spring in series, as illustrated in Figure 3.4. The spring provides the driving force for the relaxation of the stress, while the dashpot governs the rate. The stress is similar in both elements whilst the strains are additive. The following constitutive equations characterize the model:

$$\dot{\gamma} = \frac{\tau}{\eta} + \frac{\dot{\tau}}{G} \tag{3.6}$$

i.e.

$$\tau = \eta\dot{\gamma} - \frac{\dot{\tau}\eta}{G} \tag{3.7}$$

$$\frac{\eta}{G} = t_m \tag{3.8}$$

where $\dot{\tau}$ is the time differential of the stress and t_m is the Maxwell relaxation time, characteristic of a given system.

To summarize, when viscoelastic materials are stressed, some of the energy is stored elastically, with various parts of the system being deformed into new non-equilibrium positions relative to one another. The rest of the energy is dissipated as heat with various parts of the system flowing into new equilibrium positions relative to one another.

Creep compliance measurements involve the application of a constant shear stress to a sample, and the measurement of the resulting

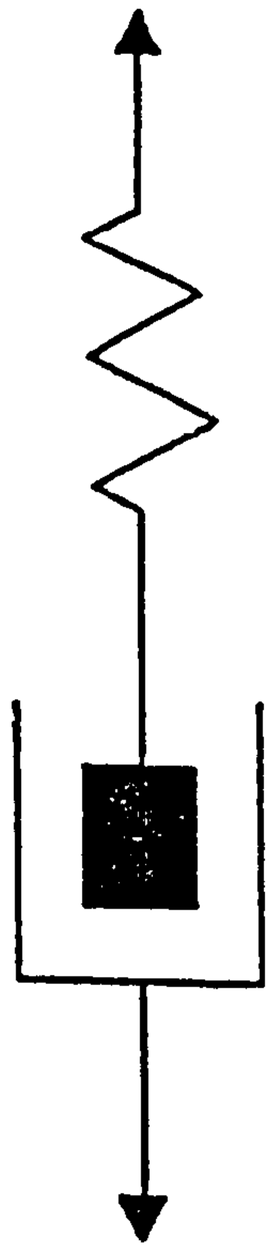

FIGURE 3.4: Mechanical analogue for a viscoelastic fluid; Maxwell model

sample deformation with time. Figure 3.5 illustrates a typical creep compliance curve and mechanical analogue for a viscoelastic fluid, indicating the four stages: instantaneous elastic response, retarded elastic response, and viscous compliance while the stress is applied, and the relaxation on removal of the stress.

The creep compliance, J, resulting from the application of a constant shearing stress is defined as

$$J(t) = \frac{\gamma(t)}{\tau} \tag{3.9}$$

where $\gamma(t)$ is the strain measured after a time t has elapsed.

3.2 Surface Rheological Behaviour

The behaviour of films on a surface can be represented by three element models. The more complicated the system, the more models are needed to exhibit their behaviour.

These models are constructed as mentioned above, by having a spring in series or in parallel with a dashpot, and are invariably termed the Maxwell or Voight models respectively. It is also possible to have both the Maxwell and Voight models in series, and this is termed the Burger body, representative of the creep phenomena and well illustrated in Figure 3.5.

3.2.1 Dilational, Compressional and Extensional Strains

These problems are exhibited when the compression or expansion of the surface phase is caused by the stress applied. This type of deformation is observed, for example, when there is either a growth or diminution of the area occupied by a monomolecular film containing a fixed number of molecules. By varying the area occupied, the compression

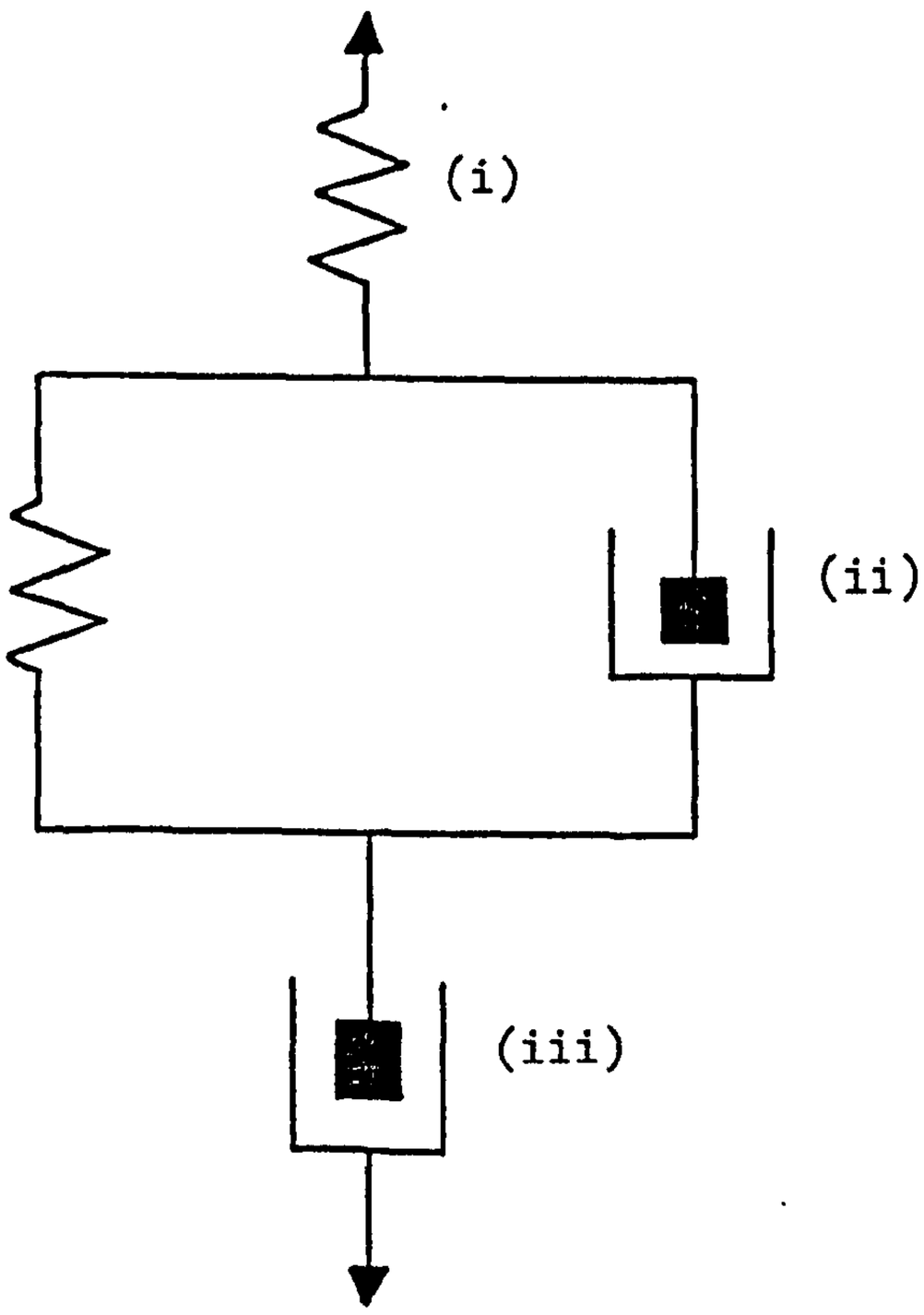

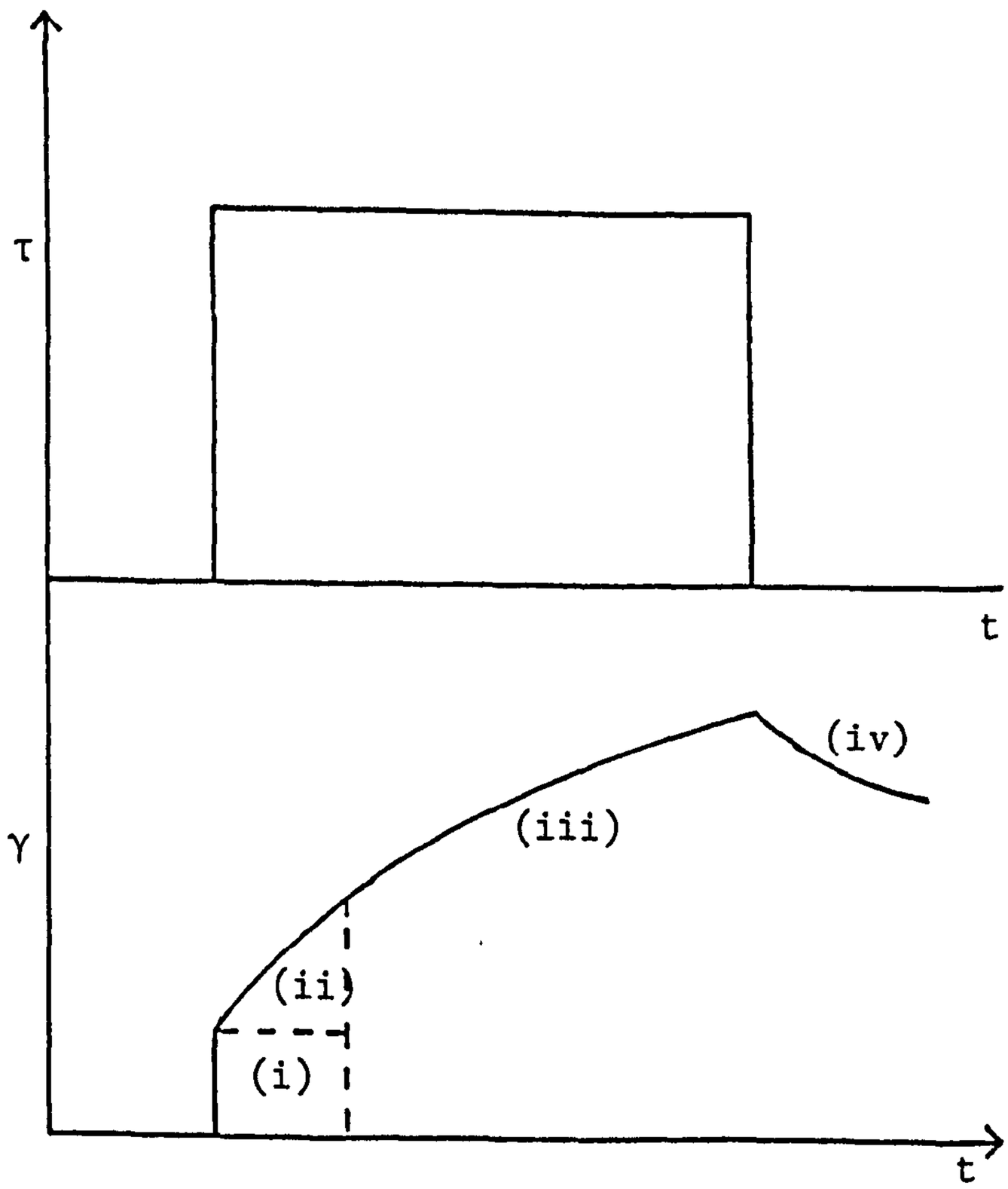

(i) instantaneous elastic response

(ii) retarded elastic response

(iii) viscous compliance

(iv) stress relaxation

FIGURE 3.5: Creep compliance curve and analogue for a viscoelastic fluid

or expansion of the films can be conveniently studied and, with shear strains being negligible, isotherms $\pi = f(A)$ can be obtained.

For insoluble films, the compression modulus, k_s, also known as the surface compressional or area modulus, is defined as the reciprocal of compressibility,

$$k_s = - A\left(\frac{\partial \pi}{\partial A}\right)_T \qquad (3.10)$$

This definition is valid for both solid and liquid film, and has units of surface pressure (mNm^{-1}). It is usually obtained from the compression isotherm $\pi = f(A)$, and varies according to the physical state of the film and the molecular packing. For example, a stearic acid film spread on 0.01M hydrochloric acid at $20^{o}C$, with molecular area $0.19nm^2$, has a compression modulus of $750mNm^{-1}$. For a mesomorphic film with a molecular area of $0.20nm^2$, the value is $140mNm^{-1}$. For a film in a single phase, the compression modulus decreases with molecular area[55]. Scheider *et al*[56] found that for aliphatic compounds, the compression modulus increased with the length of the chain and the number, location and stereochemistry of the double bonds in the chain.

If a rectangular sample of solid film is subjected to a tension, ΔF, directed along the longer edge, then an elasticity coefficient or surface Young's modulus, E, may be defined as

$$\Delta F = E \times \frac{\Delta L}{L} \qquad (3.11)$$

where $\Delta L/L$ is the relative extension. The surface Young's modulus has dimensions of Nm^{-1}, in contrast to that of the bulk, Nm^{-2}. Similarly, as in the three-dimensional model, the extension of the film is accompanied by a lateral contraction, $\Delta \ell/\ell$, related to the extension by the Poisson's ratio, σ[57],

$$\sigma = - \frac{\Delta \ell}{\ell} \frac{L}{\Delta L} \qquad (3.12)$$

Due to the fact that a film cannot be manipulated without enclosing it within a framework, it is impossible to obtain experimental measurement of E and σ. The parameters do, however, play an active role in the description of the rheological behaviour of an arbitrary interfacial phase.

In an insoluble film (for deformation without shear) a coefficient of surface dilational viscosity may be defined as

$$\Delta \hat{\gamma} = \zeta \frac{1}{A} \frac{\partial A}{\partial t} = \zeta \frac{d \ \ell n \ A}{dt} \qquad (3.13)$$

where $\Delta \hat{\gamma}$ is the surface tension differential $\hat{\gamma}_2 - \hat{\gamma}_1$, and A is the area per molecule. The dilational viscosity can be studied from the changes in the $\pi(A)$ behaviour on compression or hysteresis. It is rather difficult to measure this viscosity, since the advancement of the film also needs to be monitored. The study of true dilational viscosity is limited to insoluble films because the dilational viscosity of soluble films would require the replacement of ζ by a pair of parameters, ζ_1 and ζ_2, corresponding to the re-establishment of uniform molecular concentration in the film and the exchange of matter between film and subphase. The experimental separation of these two parameters does not appear to be possible.

3.2.2 Shear Strains and Surface Shear Viscosity

Some films exhibit Newtonian behaviour, where the surface viscosity is independent of shear rate, or non-Newtonian behaviour, where the viscosity is dependent on the shear rate. However, some films, as with solids, can deform elastically. This kind of behaviour can be characterized by a set of elastic moduli. These include the surface

dilational modulus, k_s (defined earlier), and the surface shear modulus, G_s.

For deformations that occur without appreciable change in the area occupied by the stressed film, the simple shear in the plane of an insoluble film, the elastic modulus or shear modulus is defined as:

$$G_s = \frac{\partial f_x}{\partial y} \left(\frac{\partial u_x}{\partial y}\right)^{-1} \qquad (3.14)$$

i.e. the ratio between the increment of stress $\partial f_x/\partial y\ dy$ and the increment of strain $\partial u_x/\partial y\ dy$ between two parallel rows of kinetic units orientated along the direction of slip and separated by a distance, dy.

A similarity to the three-dimensional systems also exists here, where simple relations can be obtained between the compression, shear and Young's moduli, and also Poisson's ratio for two-dimensional systems[58]:

$$k_s = \frac{Y}{2(1-\sigma)},\ G_s = \frac{Y}{2(1+\sigma)},\ E = \frac{4k_sG_s}{k_s + G_s},\ \sigma = \frac{k_s - G_s}{k_s + G_s}$$

These equations cannot be verified experimentally, due to reasons discussed in Section 3.2.4.

The coefficient of viscosity, η, is the proportionality factor relating shear force to the flow rate or shear rate. It is possible to generalize in the case of a fluid surface plane flowing in the x-direction with a uniform velocity, $V_x(y)$, driven by a surface pressure head, $FmNm^{-1}$, then

$$\frac{\partial F}{\partial y} = \eta_s \frac{\partial V_x}{\partial y} \qquad (3.15)$$

where η_s is the surface shear viscosity with units of surface poise.

For very dilute monomolecular films, it is possible to define a

relative surface viscosity[59] as:

$$\eta_{rel} = \frac{\eta}{\eta_0} \tag{3.16}$$

where η_0 is the viscosity of the pure subphase and is equal to η in the absence of a film;

specific surface viscosity as:

$$\eta_{sp} = \frac{\eta - \eta_0}{\eta_0} \tag{3.17}$$

reduced surface viscosity as:

$$\eta_{red} = \frac{\eta - \eta_0}{c_f \eta_0} \tag{3.18}$$

where c_f is the surface concentration of the monomolecular film;

and finally, intrinsic viscosity as:

$$|\eta| = \lim_{c \to 0} \eta_{red} \tag{3.19}$$

Surface phases frequently display viscoelastic behaviour. A complex surface modulus[60] G_s^* can be defined, and the film may be modelled by a Maxwell body

$$G_s^* = G_s' + j\omega\eta_s' \tag{3.20}$$

where G_s' and $G_s''(\omega\eta_s')$ are the real (elastic) and imaginary (viscous) components of the surface modulus, G_s^*, ω is the frequency of periodic or oscillatory straining of a film, and $j = \sqrt{-1}$. The real component of the complex modulus, G_s', the ratio of the stress in phase with the strain to the strain, is termed the storage modulus because of the association with the storage and release of elastic energy during periodic deformation. The imaginary component G_s'', the ratio of the stress 90^o out of phase with the strain to the strain, is called the loss modulus because of the association with the dissipation of energy as heat by viscous flow. Hence

$$G_s'' = \frac{G_s'}{\cos \delta} = \frac{2\pi\eta_s'}{T \sin \delta} \tag{3.21}$$

and

$$\delta = \tan^{-1} \frac{2\pi\eta_s'}{TG_s'} \tag{3.22}$$

in which T is the period of oscillations in the presence of a film and δ is the phase angle between stress and strain. For purely viscous systems, $\delta = \pi/2$, $G_s^* = \omega\eta_s'$, and for elastic systems, $\delta = 0$, $G_s^* = G_s'$.

It must be emphasized that all the coefficients that have been defined above are properties of ensembles of kinetic units. The experimental values of k_s, E and G_s become the properties of the films alone, with negligible subphase contribution if only small strains are studied. However, for fluid films, and for large strains which are compared with molecular dimensions, the subphase contribution to the dilational or shear viscosity is dominant.

The relationship between bulk and the surface shear viscosity is

$$\eta = \frac{\eta_s}{d} \tag{3.23}$$

where d is the thickness of the film or 'surface phase' (approximately $0.25nm^2$ for most monolayers), η_s is usually of the order of 10^{-3}-1 surface poise. With the thickness of the monolayers taken into account in three-dimensional surface viscosity, the resulting viscosity is often far greater than the liquid viscosity for the same substance and molecular volume, due largely to the contribution from the bound substrate molecules to the surface viscosity. Subtracting this contribution, however, leads to a reduced viscosity in comparison to the liquid viscosity, indicating that the film molecules are statistically orientated with respect to the direction of flow.

3.2.3 Measurement of Surface Viscosity

The two types of surface viscosity generally referred to are the dilational and the shear. The surface dilational viscosity is often more important in films and surfaces than surface shear viscosity, due to the fact that interfaces are more often subjected to dilational than to shear stresses.

In general, three-dimensional rheological methods have been adapted and modified for the measurement of surface viscosity at the air/water an oil/water interface. However, it appears that only a limited number of techniques have been advanced in measuring surface dilational viscosity compared to the number available for surface shear viscosity measurements. The design and operation of surface rheological equipment have been reviewed by Davies and Rideal[256].

Van den Tempel *et al*[61] have measured the surface dilational viscosity, ζ, by extending the film surface by means of two barriers moving apart at such a velocity that the relative rate of extension, $d\ell nA/dt$, is constant. A related measurement has been performed by Ter-Minassian-Saraga *et al*[62], who measured the contact potential change following a change in surface area, i.e. the rate of change of surface dipole orientation.

The measurement of the surface shear viscosity, η_s, can be made in a manner entirely analogous to the Poiseuille or Ostwald[63] methods for liquids by determining the rate of flow of a film through a narrow canal under a surface pressure gradient. It is evident that this method, which depends upon the maintenance of a steady surface pressure gradient, can be used only for surface films that are insoluble in both of the contiguous bulk phases. Two techniques which have been used depend on

whether the flow is generated by maintaining a constant surface pressure difference between both ends of the canal[20,21,64,65,66,67,68,225], or whether it is generated by bulk flow in the subphase[20,64,69,70]. For the first type, the depth of the canal is very small[65,66], and the viscous flow in the canal can be derived as follows (see Figure 3.6).

Consider a surface element dxdy of the film moving with velocity v, then

$$\text{velocity gradient} = \frac{d^2v}{dy^2}; \tag{3.25}$$

therefore the viscous drag due to neighbouring elements is equal to

$$\eta\left(\frac{\partial^2 v}{\partial y^2}\right)_{z=0} dxdy \tag{3.26}$$

the difference in surface pressure between the ends of the canal is:

$$\frac{\Delta\pi}{\ell} dxdy. \tag{3.27}$$

At steady state,

$$\eta\left(\frac{\partial^2 v}{\partial y^2}\right)_{z=0} - \eta_0\left(\frac{\partial v}{\partial z}\right)_{z=0} + \frac{\Delta\pi}{\ell} = 0 \tag{3.28}$$

Within the interior of the subphase, the Navier-Stokes equation reduces to

$$\frac{\partial^2 v}{\partial y^2} + \frac{\partial^2 v}{\partial z^2} = o \tag{3.29}$$

If $h \ll 2a$, where h is the depth of the canal and 2a is the width, then the boundary conditions are

$$v = 0 \text{ for } z = 0 \qquad |y| \geq a$$

and

$$v = 0 \text{ for } y = \pm\infty \text{ and } z = +\infty$$

The steady state cannot be solved[71], yet an approximation solution can be derived by replacing $(\partial v/\partial v)_{z=0}$ with Av, i.e. the first term

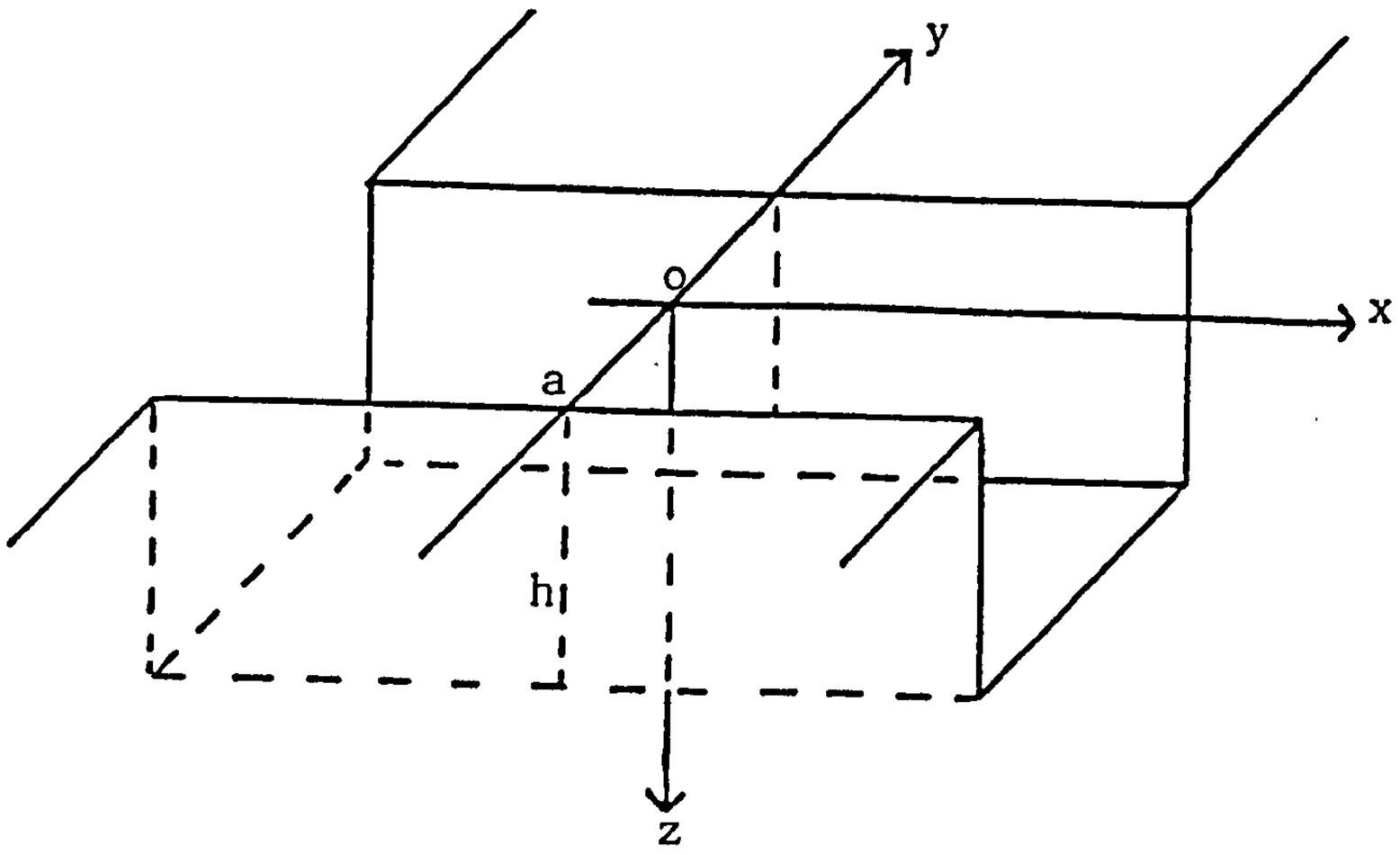

FIGURE 3.6: Flow in a surface canal

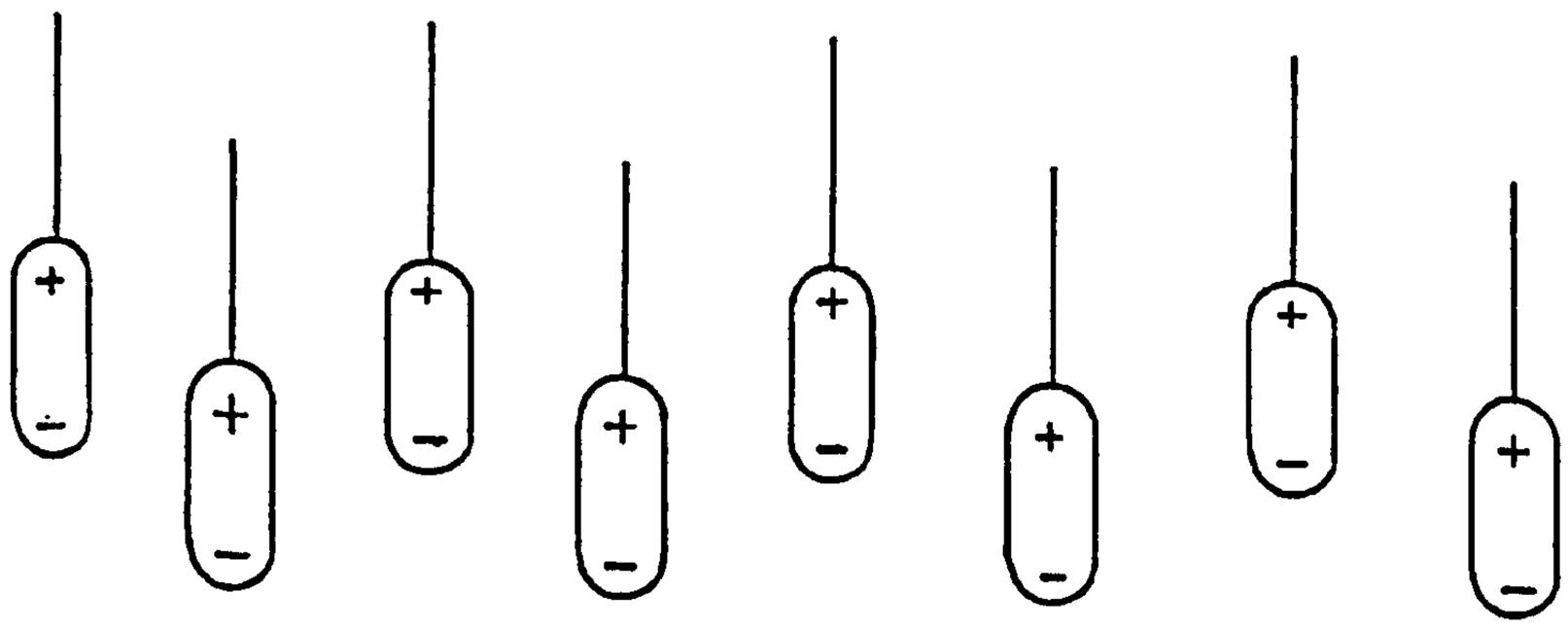

FIGURE 3.7[72]: A possible orientation of molecular dipoles in a monolayer which would reduce the repulsion between molecules

of its series development where A is a constant. The equation of motion of the film then reduces to

$$\eta \frac{d^2v}{dy^2} - A\eta_0 v + \frac{\Delta\pi}{\ell} = 0 \qquad (3.30)$$

Integrating

$$v = \frac{\Delta\pi}{A\ell\eta_0}\left[1 - \left(\cosh\sqrt{\frac{\eta_0 A}{\eta}}\, y\right)\left(\cosh\sqrt{\frac{\eta_0 A}{\eta}}\, a\right)^{-1}\right] \qquad (3.31)$$

Therefore

$$q = \frac{2}{A\eta_0}\left[a - \sqrt{\frac{\eta}{\eta_0 A}}\tanh\sqrt{\frac{\eta_0 A}{\eta}}\, a\right] \qquad (3.32)$$

in which q is the reduced flux = $\left(\frac{\Delta s}{\Delta\pi}\right)\ell$, and Δs is the quantity of film passing through the canal each second. For very wide canals, equation (3.32) reduces to

$$q = \frac{2a}{\eta_0 A} - \sqrt[2]{\frac{\eta}{\eta_0^3 A^3}} \qquad (3.33)$$

A simple approximation for very narrow canals is

$$q = \frac{2a^3}{3\eta} \qquad (3.34)$$

In the second variation, the canal depth is no longer negligible with respect to width[20,21,64]. This method is less sensitive than the preceding one, due to the resistance to flow of the larger subphase contribution. The partial differential equations are the same as those for the canal of negligible depths, but with different boundary conditions:

$v = 0$ for $y = 0$ and $z > 0$

and

$v = 0$ for $z = h$.

For a canal depth n, the reduced surface flux is[225]:

$$q = \frac{64a^3}{\pi^4\eta}\sum_{n=0}^{\infty}(2n+1)^{-4}\left[1 + \frac{2a\eta_0}{(2n+1)\pi\eta}\coth\frac{(2n+1)}{2a}\pi h\right]^{-1} \qquad (3.35)$$

or approximately

$$q = \frac{2\pi a^3}{3(\pi\eta + 2a\eta_0)} \tag{3.36}$$

If $a\eta_0 \ll \eta$, then equation (3.36) becomes identical to equation (3.34), i.e.,

$$q = \frac{2a^3}{3\eta}$$

This method cannot be used for films of high fluidity because if $a\eta_0 \gg \eta$ then equation (3.36) becomes

$$q = \frac{\pi^2 h}{6\eta_0} \tag{3.37}$$

with the reduced flux becoming independent of the surface viscosity. However, if $h \gg 2a$ (see Appendix A), then

$$q = \frac{2a^3}{3\eta}\left[1 + \frac{2a\eta_0}{\pi\eta}\coth\frac{\pi h}{2a}\right]^{-1} \tag{3.38}$$

If $h/a = \gg 1$, and $a\eta_0 \ll \eta$, then $q = 2a^3/3\eta$, analogous to the Poiseuille formula in two-dimensional surface rheology.

The canal viscometer gives absolute viscosities and the effect of subphase drag can be analysed theoretically, but the measurement cannot be made at a single film pressure, as a gradient is needed; nor is the shear rate constant. Also, it is unsuitable for the measurement of surface elasticity. A second basic method involves the determination of the damping of oscillations of a torsion pendulum, disc or ring[72]. Gaines[72] gives the equations

$$\eta_s = \frac{\sqrt{CI}}{2\pi}\left(\frac{1}{r_1^2} - \frac{1}{r_2^2}\right)\left[\frac{\lambda}{\sqrt{4\pi^2 + \lambda^2}} - \frac{\lambda_0}{\sqrt{4\pi^2 + \lambda_0^2}}\right] \tag{3.39}$$

$$G_s = \frac{I}{4\pi}\left(\frac{1}{r_1^2} - \frac{1}{r_2^2}\right)\left[\frac{4\pi^2 + \lambda^2}{T^2} - \frac{4\pi^2 + \lambda_0^2}{T_0^2}\right] \tag{3.40}$$

where r_1 is the radius of disc or ring, r_2 is the radius of the (cicular) film covered area, λ and λ_0 are the natural logarithms of the ratio of successive amplitudes in the presence and absence of a film, T and T_0

are the periods of (complete) oscillations in the presence and absence of a film, and I is the moment of inertia. The torsion constant, c, is given by

$$c = \frac{4\pi^2 I}{P_a} \tag{3.41}$$

where P_a is the period of the pendulum in air. Tschoegl[73] has made a detailed analysis of torsion pendulum methods, including the difficult theoretical treatment of subphase drag.

The viscous traction viscometer corresponds more closely than any other apparatus to the idealizations demanded by the hydrodynamic analysis. In this instrument the film is spread in a circular annular canal formed by concentric cylinders[74]. The problem of subphase drag is greatly reduced in the case of a rotating ring making a knife-edge contact with the air/water or oil/water interface[75,76]. The shear gradient is mainly confined to the outer region of the circularly-confined film, with the inner region rotating as a uniform island. A simple equation that works well is

$$\eta_s = 0.5631 \frac{\Omega}{\omega} \eta a \tag{3.42}$$

where Ω is the rotational speed of the central island and ω is that of the knife-edge ring; a is the radius of the outer cylinder contained (and of the knife-edge ring). This instrument has the great advantage of being applicable to both soluble and insoluble films at either the air/water or oil/water interface. Its only disadvantage is the fact that it can be usefully applied only to films which are neither too viscous nor too fluid[74]. However, Wasan *et al*[77] have made an exhaustive study of the sources of error in this viscometer. Three major approximations were identified:

(i) a cylindrical canal had been approximated by a linear channel;

(ii) the gap width, d, between the fixed walls of the canal and the moving floor had been idealized to d = 0;

(iii) the contact angle at the intersection of the interface with the walls of the canal had been idealized to 90^{o} so that the interface was rigorously flat.

3.2.4 Theoretical Interpretation of the Viscosity of Monomolecular Films

Except for highly-condensed films, adsorbed amphiphilic molecules are usually in a state less compact than in the case for three-dimensional liquids. Attempts have been made[78] to interpret the viscosity of these films in the same way as for the viscosity of gases, by studying momentum transfer by intermolecular collisions, taking account of only the forces of intermolecular interaction which contribute to the $\pi = f(A)$ isotherm and neglecting the interaction between the film and its subphase. Obviously, this model is incapable of accounting for surface viscosity because, apart from the intermolecular interaction between molecules, the interaction with the subphase has a significant role in the mechanism of surface rheology. However, the use of the theory of liquids has been successful in interpreting surface rheology.

Eyring's Theory

Eyring has developed a theory of viscosity by considering flow as a particular case of an activated reaction[79] and applying this theory to monolayers[80]. In a liquid, each molecule can be pictured as residing in a potential well, each well corresponding to a possible equilibrium position of the molecule. Thermal agitation can be thought of as consisting of oscillation around equilibrium positions, which are themselves subject to disordered transitions[81]. The mean life-time

of a molecule in one of its equilibrium positions is

$$\tau' = \tau_0 \, e^{u/kT} \tag{3.43}$$

where τ' is the period of oscillation (approximately 10^{-13}s), and u is the activation energy for a transition from one equilibrium position to another (several $kJmol^{-1}$). The self-diffusion coefficient, D, is given by

$$D = \frac{'\delta^2}{\sigma\tau'} = \frac{\delta^2}{\sigma\tau_0} \, e^{-u/kT} \tag{3.44}$$

where $'\delta$ is the mean amplitude random translation, k is the Boltzmann's constant, T is the temperature, and σ is the surface Poisson's ratio. And the viscosity is

$$\eta = \frac{k\tau_0}{\pi'\delta^2 r} \, e^{u/kT} \tag{3.45}$$

Here it has been assumed that the molecular radius, r, is the same order of magnitude as $'\delta$, and that Stoke's law is valid, even on a molecular scale.

Applying this analysis to a two-dimensional liquid, the surface viscosity becomes[80,82],

$$\eta = c \, e^{\Delta F/kT} \tag{3.46}$$

in which c and ΔF are practically independent of temperature. ΔF is regarded as the free energy of activation, with $c = hN/V_m$, where h, N and V_m are Planck's constant, Avogadro number and the molar volume respectively.

During flow, the kinetic units pass from one potential well to the next by surmounting potential barriers; the flow mechanism is therefore an activation process. For surface flow of the Couette type, if λ_1 and λ_2 are the distances between the kinetic units measured perpendicular and parallel to the streamlines respectively, then the coefficient

of surface shear viscosity is

$$\eta_s = \frac{f}{\dot{\gamma}} = \frac{f\lambda}{\Delta u} \tag{3.47}$$

where f is the shear force per cm, $\dot{\gamma}$ is the shear rate, and Δu is the increment of velocity between streamlines.

Setting λ equal to the distance between two potential wells and assuming the barrier is symmetrical on each side of its maximum, then the maximum occurs at a distance $\lambda/2$ from each well. The shear force acting on a kinetic unit is $f\lambda_2$ and the energy acquired by the kinetic unit is its motion through the distance $\lambda/2$, which is $\frac{1}{2}f\lambda_2$. The effect of the force producing the flow is thus to reduce the height of the barrier by $\frac{1}{2}f\lambda\lambda_2$ in the flow direction and to increase it by $\frac{1}{2}f\lambda\lambda_2$ in the opposite direction.

If E is the activation energy for transport over the potential barrier then in the absence of shear stresses, the number of kinetic units transported per second in either direction is

$$K = \frac{kT}{h}\frac{Q_+^+}{Q}e^{-E/kT} \tag{3.48}$$

where Q and Q_+^+ are the partition functions of the kinetic units in the initial and activated states respectively.

Under the action of a shear stress, the rate of transport over the barrier in the direction of force is

$$K_1 = ke^{f\lambda\lambda_2/2kT} \tag{3.49}$$

and the rate in the opposite direction is

$$K_2 = ke^{-f\lambda\lambda_2/2kT} \tag{3.50}$$

But $\Delta u = \lambda(K_1 - K_2)$

therefore

$$\Delta u = 2\lambda K \sinh \frac{f\lambda\lambda_2}{2kT} \tag{3.51}$$

and

$$\eta = \frac{f\lambda_1}{2\lambda K \sinh \frac{f\lambda\lambda_2}{2kT}} \tag{3.52}$$

If ΔF is the activation free energy for flow

$$\frac{Q_+^+}{Q} e^{-E/kT} = e^{-\Delta F/kT} \tag{3.53}$$

so

$$\eta = \frac{f\lambda_1 h e^{\Delta F/kT}}{2\lambda kT \sinh \frac{f\lambda\lambda_2}{2kT}} \tag{3.54}$$

Replacing f by $\eta\dot{\gamma}$,

$$2\lambda kT \sinh \frac{\eta\dot{\gamma}\lambda\lambda_2}{2kT} = \dot{\gamma}\lambda_1 h e^{\Delta F/kT} \tag{3.55}$$

Also if $\lambda \simeq \lambda_1$ and $\lambda\lambda_2 \simeq A_1$, the area occupied by a kinetic unit, the final result is

$$\sinh \frac{\eta\dot{\gamma}A}{2kT} = \dot{\gamma} h e^{\Delta F/kT} \tag{3.56}$$

If $\eta\dot{\gamma}A \ll 2kT$, the monolayer flow remains Newtonian and equation (3.56) becomes

$$\eta = \frac{h}{A} e^{\Delta F/kT} \tag{3.57}$$

For monomolecular layers $Q_+^+/Q \simeq A_+^+/A$, (where A_+^+ is the area occupied by a kinetic unit in the activated state) and in addition, for sufficiently condensed states of the film, $A_+^+/A \simeq 1$. Therefore

$$\ln \eta = \frac{\Delta E}{kT} - \ln A + \ln h \tag{3.58}$$

The Activation Energy for Flow

The water molecules in immediate contact with the polar groups of the amphiphilic molecules in the film are bound to them and are trans-

ported with similar velocity. Therefore the activation energy for flow of the kinetic units can be divided into two terms, characteristic of the amphiphilic molecule and the bound water respectively.

$$\Delta E = \Delta E_c + \Delta E_s \tag{3.59}$$

Therefore, equation (3.58) becomes

$$\ell n\ \eta = \frac{\Delta E_c + \Delta E_s}{kT} - \ell n\ A + \ell n\ h \tag{3.60}$$

Without the participation of this water in the subphase, $\Delta E = \Delta E_c$ and the viscous film contribution would be

$$\ell n\ \eta = \ell n\ \eta - \frac{\Delta E_s}{kT} \tag{3.61}$$

If η_0 is the contribution to the surface viscosity of the water bound to the polar groups in the film, then the subphase contribution is obtained from

$$\ell n\ \eta_0 = \frac{\Delta E_s}{kT} - \ell n\ A + \ell n\ h \tag{3.62}$$

The activation energy of flow can be divided into two parts[83]:

1. the energy required to create a hole in the film, into which an activated neighbouring molecule may be moved;
2. the energy necessary to cause a molecule to pass from one equilibrium position to a free neighbouring position; this energy consists of:
   (i) the energy necessary for the translation of the molecule;
   (ii) the energy corresponding to the local deformation of the network during this translation; and
   (iii) the energy of the change of equilibrium stable form of the molecules during their displacement.

Moore and Eyring[80] modified the equation for the fluidity of

liquid based on the reaction rate theory of viscous flow to interpret the data for liquid films. The free energy of activation for viscous flow was found to be about twice that for the flow in the bulk liquid. This was explained by the occurrence of various types of association in the liquid films such as lateral association between the surface molecules and vertical association of the surface molecules with those of the subphase. Equations were given for the pressure and temperature effect on surface viscosity. Knowledge of these effects may be used to interpret the structure of the film and to separate and evaluate the constants to the free energy of activation due to lateral association, solvation and hydrogen-bonds.

3.2.5 Surface Potentials

The surface potential, ΔV, is due to the molecular orientation in the monolayer when spread on a polar liquid, such as water. Since the molecules are themselves dipoles, this uniform alignment will produce an electric field near the surface. Hence any effect causing a change in the molecular orientation will alter the ΔV, enabling the study of the nature, orientation and effects of pH to be carried out.

The potential, V, of a point in free space is the work required to bring a unit charge from infinity to that point, and the potential difference, ΔV, is the difference in two points in a potential field. The Galvani potential, which is the potential across an interface (i.e. defining ΔV across an interface) cannot be determined experimentally. This is because the imaginary unit charge does not exist, and so the movement of an electron, ion or a proton from one phase to another complements another component of work besides physical work, and results in 'chemical work', e.g. van der Waal's, which is due to the differences

in chemical environment in the two phases. However, it is possible to measure a potential difference known as the Volta potential; this is the potential or work required to bring a unit charge from infinity to just up to the phase boundary, but not into it. The Volta potential difference at a phase boundary is then the difference in the Volta potentials of the two phases. It is also known as the contact potential; typically, it is used to denote the change in potential of a surface on the spreading of a film. Adam[84] has suggested that the Volta potential is the potential at a distance 10^{-3}mm from the surface. However, it must be noted that an insoluble monolayer will set up an electrical double layer just below the surface, which contributes to the potential difference measured. Davies and Rideal[85] have presented arguments as to why the measured surface potential, ΔV, is exactly equal to the Volta potential difference.

The surface potential, ΔV, of a monolayer is then the measured potential difference between the clean and the film-covered surface. Any change in the area available to a monolayer results in a change in surface potential likewise; this is expected, due to the change in concentration of polar molecules forming the monolayer. Simply, to take account of this variation of dipoles in compression, consider $\Delta V/n$, in which n is the number of film molecules per unit area of the film, when $\Delta V/n$ is constant (apparent for many films), which occurs over regions of no change in monolayer state, then the contribution of each film-forming molecule to the surface potential is largely independent of concentration.

If the film is compared to an ordinary parallel plate condenser, then $\Delta V = Qd/A\varepsilon$, therefore

$$\Delta V = \frac{4\pi\epsilon d}{D} \tag{3.63}$$

where ϵ is the surface charge density, d is the distance between the plates, and D is the dielectric constant. By using the analogy (very imperfect), the film is assumed to be an array of dipoles whose effective dipole moments in the perpendicular direction, $\mu_\perp$, produce similar effects as the surface charge and spacing; and taking the dielectric constant, D (unit area) as unity,

$$\Delta V = 4\pi n\mu_\perp \tag{3.64}$$

This expression appears to have been introduced by Schulman and Rideal[84]. If the value of ΔV or $\mu_\perp$ is little changed by being compressed, as observed by some authors, then the effective perpendicular moment is due to an intrinsic moment, $\bar{\mu}$, making an angle of inclination θ with the vertical, therefore

$$\Delta V = 4\pi n\bar{\mu} \cos\theta \tag{3.65}$$

This equation has severe limitations, such as the reorientation of subphase molecules and that the $\mu_\perp$ value obtained is generally one-third to one-tenth of that of the intrinsic dipole moment.

The surface dipole moment for an un-ionized monolayer is given by

$$\mu_\perp = \left(\frac{1}{4\pi}\right)\left(\frac{\Delta V}{n}\right) \tag{3.66}$$

If A is molecular area in $\text{Å}^2\text{mol}^{-1}$ and ΔV is in mV, then equation (3.66) becomes

$$\mu_\perp = \frac{A\Delta V}{12\pi} \tag{3.67}$$

since $\Delta V = 4\pi n\mu_\perp$ (see Appendix B for conversion of cgs to SI units). Then

$$\Delta V = \frac{4\pi n\mu_\perp}{4\pi\epsilon_0} = \frac{n\mu_\perp}{\epsilon_0} \tag{3.68}$$

therefore

$$\mu_{\perp} = \frac{\varepsilon_0 \Delta V}{n} \tag{3.69}$$

Most film-forming molecules have positive ΔV, hence $+\mu_{\perp}$, the positive end of the dipole is uppermost. $\mu_{\perp}$ has units of millidebye (mD).

However, no equation has been proposed that accounts for induced polarization within the monolayer itself, even though close packing of the polar molecules should lead to the same effect. It is likely that 'staggering' of the film-forming molecules occurs on compression, as illustrated in Figure 3.7.

So far, only the behaviour of monolayers composed of neutral molecules has been considered. Ionized monolayers are formed by metal soaps, protonated amines ($-NH_2+H^+ \rightarrow NH_3^+$) etc. The properties of ionized monolayers are governed analogously to un-ionized monolayers by the interactions with other film-forming molecules and interactions with subphase molecules. This balance is further upset by two other forces, i.e. the interactions (non-dispersive forces) with other film molecules and interactions with cations and anions present in the subphase. The last application sets up an ionic double layer at the surface. This ionic charge leads to solubility problems, which are enhanced by their removal to the region of lower potential and increased polarity of the molecule. Davis[87] suggested that ionized straight-chain compounds must have at least 24 carbon atoms to avoid solubility. Schulman and Hughes[88] pointed out that allowance should be made for the potential due to the electrical double layer. Hence, the surface potential is altered due to ionized molecules, so

$$\Delta V = 4\pi n\mu_{\perp} + \psi_{AB} \tag{3.70}$$

where ψ_{AB} represents the difference in potential between the surface and

the bulk of the subphase. ΔV changes by kT/e or ~60mV for each ten-fold change in univalent ion concentration. In fact, the most comprehensive treatment of properties of ionized monolayers has been done by Davies[87].

The characterization of the surface potential of a monolayer is usually carried out simultaneously with the measurement of area, A, and surface potential, ΔV, as the spread film is compressed.

The measurement of surface potential of a liquid/gas interface can be performed using two different procedures. The first, referred to as the Ionizing Electrode method[86,89,90], involves the ionization of the gas above the monolayer, so that it becomes conducting. Hence it is possible to measure the direct potential difference between the two electrodes, one in the aqueous subphase and the other in the air above the subphase. In the second, referred to as the vibrating plate method[91,92,93], the electrode in the air is moved with respect to the water surface, with the resulting change in the capacity of the air gap leading to a current flow in the external circuit. The magnitude of the current is proportional to the potential difference across the gap.

Generally, either method is accomplished by a null method, whereby a potentiometer is incorporated into the circuit to oppose the Volta potential and the voltages required to prevent current flow are measured. ΔV is taken directly as the difference of the null values, with or without the monolayer. Figure 3.8 shows the principle of both measuring methods. In the experiments performed, the Ionizing Electrode procedure was employed.

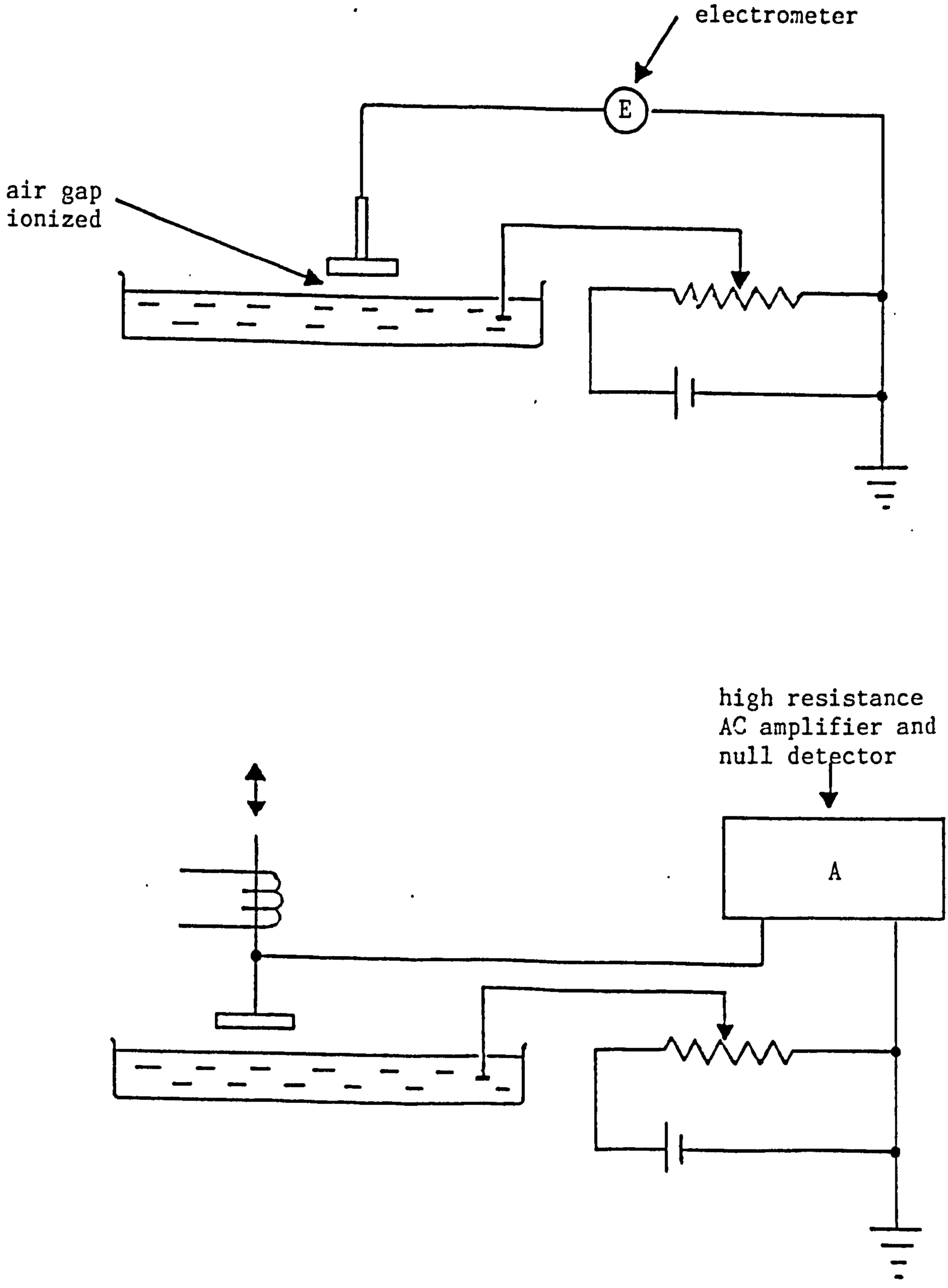

FIGURE 3.8[72]: Arrangement for measuring surface potentials by the ionizing electrode and vibrating plate methods

CHAPTER 4

NON-AQUEOUS BULK FOAMS

4.1 Types of Non-Aqueous Foaming System

In a systematic investigation of the type of non-aqueous system that would foam, King[94] found that the bulk viscosity and vapour pressure of the system were not important parameters in the initial production of foam, but could affect the stability of a foam once produced. The time for a foam (which was produced by shaking a known volume of liquid in a measuring cylinder) to collapse completely was taken as a measure of the stability of the foam. Foaming systems usually exhibited a surface tension lowering; for example, a 5% solution of aerosol AY in ethylene dichloride. However, solutions which exhibited a surface lowering did not necessarily foam; for example, a 5% solution of aerosol AY in ethylene glycol. Yet a 3% solution fo aerosol OT in ethylene glycol was considered to be a good foaming system. Teitelbaum[95] investigated the lifetime of a foam, τ, as measured by the time for a foam produced in a sealed ampoule to collapse to the last bubble, as a function of concentration of mesitylene in methanol; the maximum lifetime, τ_m, decreased on increasing the concentration. Robinson and Woods[96] found that a mixture of an aliphatic and aromatic hydrocarbon produced a more stable foam than a mixture of two aliphatic or aromatic hydrocarbons, where the foam lifetime was measured in a similar way to that described by Teitelbaum[95].

4.2 The Stability of Crude Oil Foams

The stability and breaking of non-aqueous foams is a subject of great importance to industry, as such foams occur, for example, in the

production and refining of crude oil and polymer latex production. The stability of both crude oil emulsions and foams is governed by the properties of the film formed at the oil/water and oil/air interfaces respectively, so the breaking of such emulsions and foams is a process of major significance to the oil industry. In particular, a reliable method of assessing the foamability of crude oil is highly desirable, as the potential handling problems that occur can be anticipated at an early stage.

A number of researchers[97,98,99,100,101,102,103,104] have worked specifically with non-aqueous systems and highlighted certain factors as being important in non-aqueous foam stability; these are: bulk viscosity, interfacial viscosity and surface tension. For example, Brady and Ross[97], in studying a series of engine and mechanical grade paraffin oils, found that foam stability increased linearly with the kinematic viscosity of the oil. This dependence of stability with viscosity was confirmed by McBain and Robinson[98], who showed that a high viscosity both in the bulk and surface was often associated with the high foam stability. They attributed the high surface viscosities they had observed to the formation of plastic films at the gas/liquid interface. Callaghan and Neustadter[103] also concluded that surface rheological properties such as shear and dilation viscosities had a pronounced effect on oil foam stability. Callaghan *et al*[104] later found that the dilational rheology of crude oil/air systems is markedly affected by the addition of antifoam. Surface tension has been shown to play a major role in non-aqueous foam stability, but this is a minor role compared to the preceding factors[98,102].

A notable characteristic of stable films is their resistance to mechanical disturbance. Gibbs[106] considered the important property

to be the elasticity of the film, ε,

$$\varepsilon = \frac{2d\hat{\gamma}}{d\ell nA} \tag{4.1}$$

where $\hat{\gamma}$ is the surface tension and A is the area of the film. For a two-component system, equation (4.1) can be put in the form

$$\varepsilon = 4(\Gamma_2^1)^2 \frac{d\mu_2}{dm^2} \tag{4.2}$$

Here Γ_2^1 is the surface excess of component 2, μ_2 is the chemical potential of that component, and m_2 is its amount per unit area of film. Qualitatively, ε gives a measure of the ability of a film to adjust its surface tension in an instant of stress. If the surface should be extended, the surface concentration of the surfactant drops and the local surface tension rises accordingly; the film is thus protected against rupture. For pure liquids, ε as given would be zero, and this is in accord with the observation that pure liquids do not give a stable form.

The foregoing is an equilibrium or reversible concept, and some transient effects have also been suggested as important to film resilience. Consider a bubble wall with surfactant at the interface, as shown in Figure 4.1. The bubble wall (film) is a dynamic system, constantly stretching and contracting; the thinner film section after stretching contains less surfactant and has a higher surface tension. The surfactant migrates along the bubble wall from a low to a high surface tension region to restore equilibrium, and carries with it relatively thick layers of underlying fluid which restores film thickness and gives a stable film. This ability to resist film thinning is referred to as the Marangoni effect[105] or the 'self-heal' process. The surfactant concentration may alternatively be equalized by a second mechanism shown in Figure 4.1. However, the surfactant molecule may migrate from the bulk liquid to the bubble wall. If this happens faster

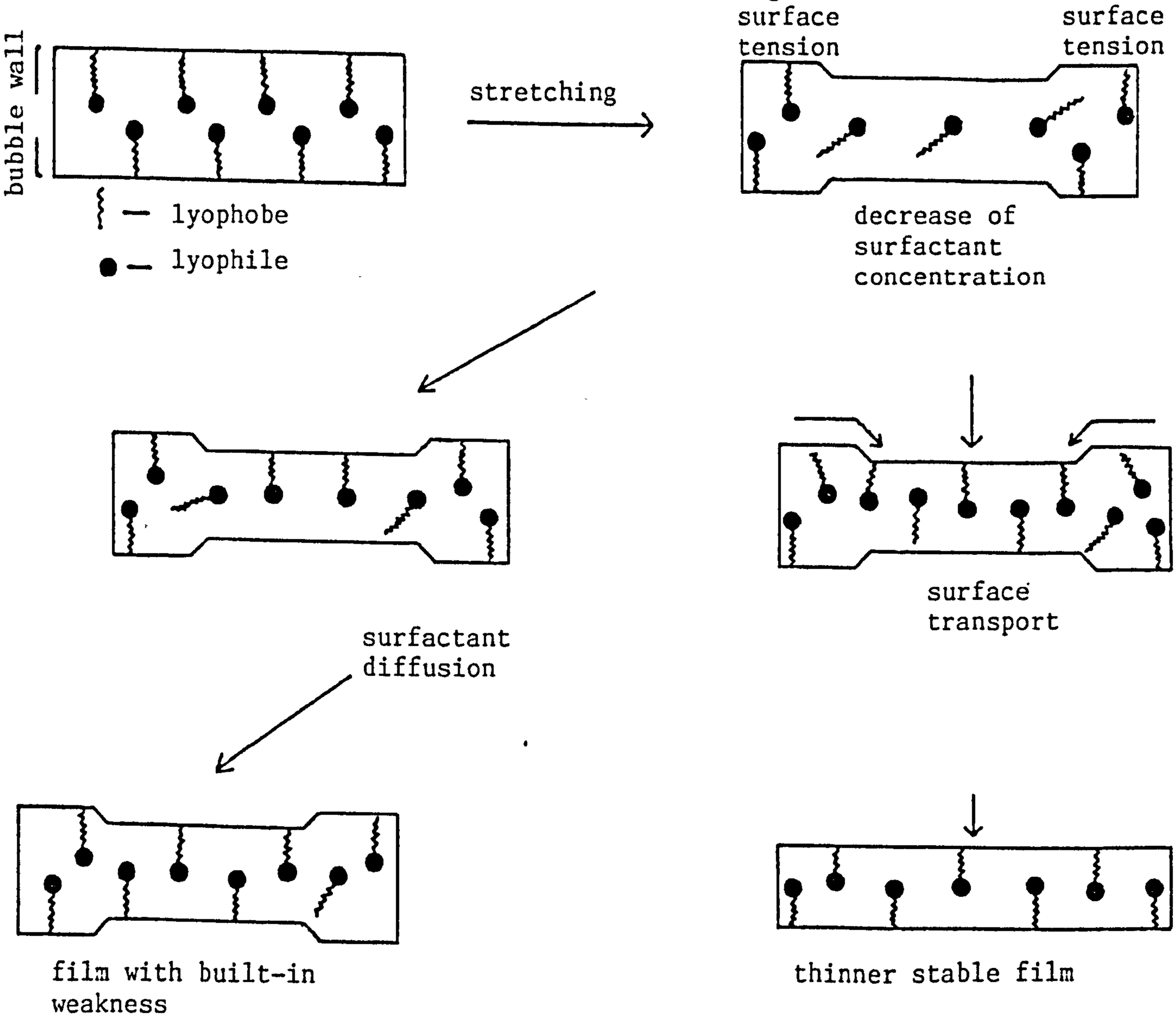

FIGURE 4.1: Film elasticity (Marangoni effect)

than surfactant migration at the surface, the thinned spot will not heal, with the film being mechanically weak and unstable for a while.

In addition to high elasticity and resilience as properties giving stability to foams, high surface viscosity appears also to be important. The surface viscosity results from the interaction between neighbouring surfactant molecules at the liquid surface by hydrogen bonding and dipole-dipole interaction forces. This intermolecular interaction may cause the formation of a quasi-polymer network at the surface to increase surface viscosity, inhibit drainage at the bubble wall and stabilize the foam.

According to this analysis, it is important that a foam-stabilizing agent be surface adsorbed only slowly (on a millisecond time-scale). With anionic or cationic surfactants, the thinning of the bubble wall proceeds until the charged groups at the interface become sufficiently close to cause electrical repulsion and prevent further thinning. This effect operates only in very thin films and does nto operate with non-ionic surfactants[108].

4.3 Foam Control

Methods involving ways of preventing or disrupting the foam stabilizing influences described previously are necessary in controlling foam.

The physical-chemical processes associated with the making and breaking of foams are complicated, and not fully understood. Two methods that have been adopted are:

1. physical or mechanical methods; usage of heating elements, temperature change or centrifugal forces etc.;

2. chemical methods; addition of anti-foaming agents.

The latter is very important, but often not well understood. There has to be a distinction between antifoams (chemicals added before the foam has formed, to inihibit foam formation) and defoamers (chemicals added after foam has formed, to break down the foam). An antifoam is usually a good defoamer; it functions in the bulk liquid to control foam as the bubbles are nucleating, but will also act on the bubble surface to destroy foam. However, some defoamers are not good anti-foamers; they are effective when dispersed on the foam surface, but are poor foam-preventers. With the development of excellent silicone anti-foamers, the chemical method has mostly been applied. Silicones have been found useful in a wide variety of foaming problems where the collapse of the foam can be brought about by very small concentrations of silicone, usually in the order of a few parts per million.

The performance of an antifoamer or foam-preventer is divided into the film-breaking action and the foam-preventing action. In this work, the effectiveness of the anti-foamer has been examined using a modified version of the Bikerman[109-111] method amongst the many industrial methods such as the Ross-Miller[112] method, the Ross-Mcbain[105] pop test and the Okasaki and Sasaki[113] tests. These are described briefly later in this chapter.

4.4 The Mode of Action of Particulate Silicone Antifoaming Agents

Different theories[114,107] have been proposed to explain the mode of action of silicone antifoaming agents. The size of the particle seemed to be an important factor, otherwise they acted as profoamers.

Antifoam theory in the simplest sense suggests that an antifoam must meet four basic requirements to achieve maximum effectiveness:

1. insolubility in the foaming liquid;

2. lower surface tension than the foaming liquid;

3. rapid dispersion; and

4. chemical inertness.

According to Ross[107], two modes of antifoam action are possible: that the antifoam enters the liquid/gas interface and spreads spontaneously over the surface, thereby causing bubble rupture; or that spreading is limited and a mixed monolayer of surfactant and antifoam molecules of altered surface properties and reduced stability is produced.

The antifoam's ability to enter the liquid/gas interface and spread in a developing foam system was determined by a combination of surface and interfacial tensions. An entering coefficient, E[115], and a spreading coefficient, S[116], have been defined by the equations below:

$$E = \hat{\gamma}_m + \hat{\gamma}_{ma} - \hat{\gamma}_a \qquad (4.3)$$

and

$$S = \hat{\gamma}_m - \hat{\gamma}_{ma} - \hat{\gamma}_a \qquad (4.4)$$

where $\hat{\gamma}_m$, $\hat{\gamma}_a$ are the surface tensions of the foaming liquid and antifoam, and $\hat{\gamma}_{ma}$ is the interfacial tension between the liquid and the antifoam. Both E and S must have positive values before an antifoam will enter and spread in a foam system on a molecular level. When an antifoam spreads, it carries along a quantity of liquid of considerable thickness[117] to increase film drainage, disrupt the 'self-heal' effect and cause foam rupture[118]. This mechanism is shown in Figure 4.2.

Trautman's[119] observation that silicone antifoamers were effective only when present in concentrations exceeding their solubility was

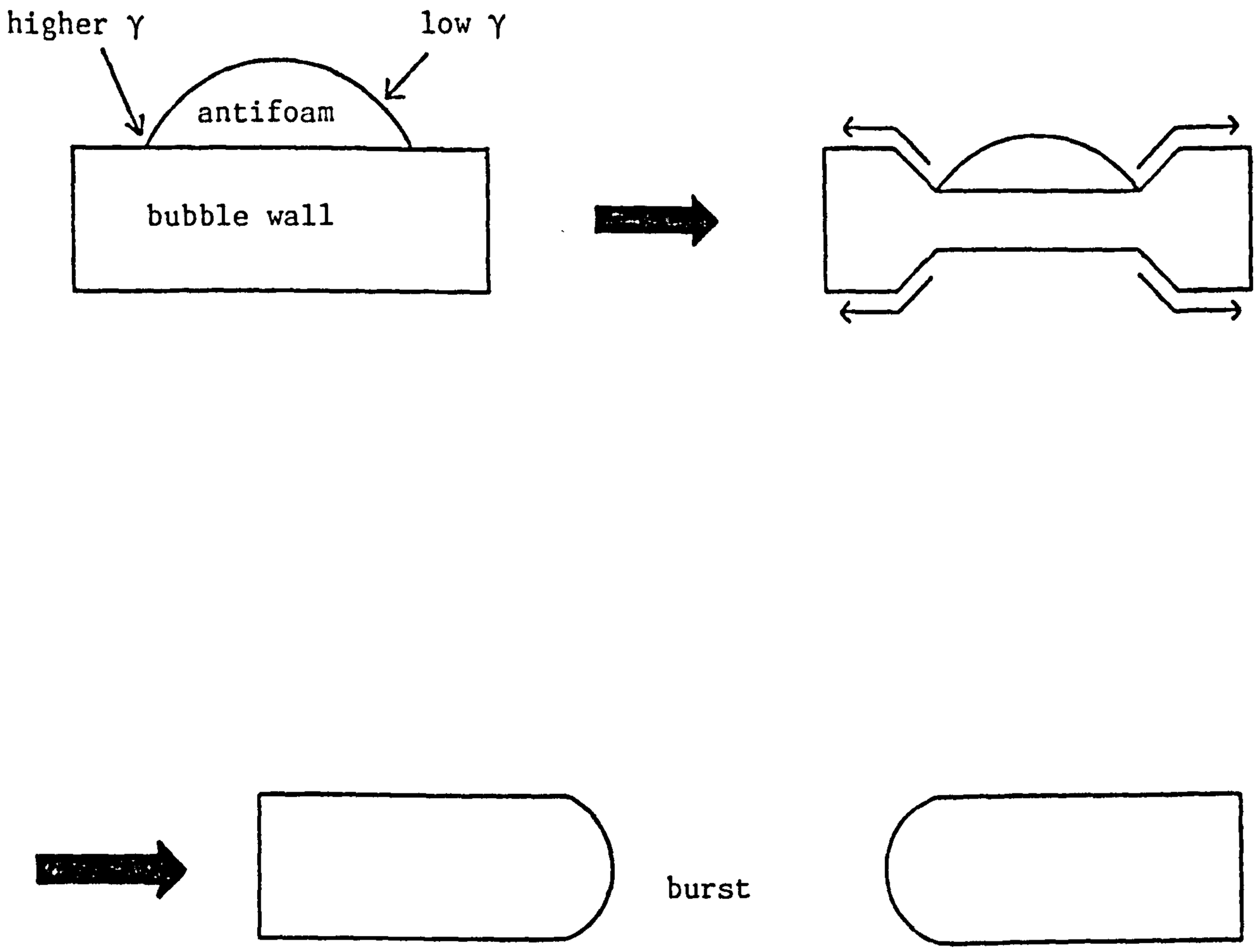

FIGURE 4.2: Antifoam mechanism

consistent with Jacoby's[120] theory of antifoam action. That is, the addition of silicone beyond the limit of solubility caused the film to build up to a point where it lost its elasticity, thus causing the foam to collapse.

Hence a silicone antifoamer such as polydimethylsioxane can disrupt the foam-stabilizing mechanisms presented in the previous section. Surface viscosity would be reduced if the foam-stabilizing surfactant was displaced by a silicone that does not exhibit hydrogen bonding. Non-ionic silicones would displace ionic surfactants and destroy electrical double-layer effects. Similarly, displacement of the surfactant by gas-permeable silicone would remove the gas diffusion resistance between bubbles and allow the operation of the bubble-breaking mechanism in Figure 4.2.

4.5 Types of Silicone Antifoams

Silicone antifoams can be divided into three broad classes: fluids, compounds and emulsions. Silicone fluids include all the basic polydimethylsiloxane polymers and any modified polymers in which the methyl groups have been substituted by other organic groups to confer special properties. Antifoam compounds are a combination of silicone fluid and fine particulate silica. An antifoam emulsion is a stabilized dispersion of an antifoam compound in water; this is a convenient product form for delivering the antifoam compound into the application medium.

For non-aqueous non-polar systems, foams can be controlled very efficiently with low levels of a polydimethylsiloxane fluid - since they provide the low surface and interfacial tensions necessary, and moreover can enter and spread in the foam films. They also lack any

direct foam-stabilizing mechanism, such as high surface viscosity.

However, in aqueous systems, it has long been recognized that finely-dispersed hydrophobic solids such as polydimethylsioxane-treated silica are needed for effective antifoam action. The most recent theory attributes the principal antifoam action to the solid by virtue of its ability to adsorb the foam-stabilizing surfactant and transport it from the foaming interface[121].

4.5.1 The Linear Polydimethylsiloxanes

The general formula of the class of compounds known as the linear silicones (though the term 'silicone' is still used, it is gradually being replaced by the term 'siloxane') is shown in Figure 4.3(i), where R_1, R_2 are the substituents on the repeating group $\begin{matrix}R_1\\R_2\end{matrix}\!\!>\!Si\text{—}O$, the end groups are -OZ and -OY (where OZ and OY can both be $SiMe_3$ or C_2H_5), and n can vary from unity to a large number. The formula of an ethoxy end-blocked polydimethylsioxane is shown in Figure 4.3(ii). The formula of a trimethylsiloxy end-blocked linear polydimethylsiloxane or dimethyl silicone, where R_1, R_2 are methyl groups. Structurally, it consists of a polymeric inorganic backbone of alternating silicon and oxygen atoms with methyl groups attached to silicon, and is shown in Figure 4.3(iii).

In the preparation of the polydimethylsiloxane, the Si-O-Si linkage is formed by the condensation of silanol hydroxyl groups on adjacent molecules; compounds containing silicon-alkoxyl and silicon-halogen bonds can be readily hydrolysed to produce the linkage. Hunter *et al*[122] have described the laboratory preparation of the polydimethylsiloxanes from the co-hydrolysis of a mixture of ethoxytrimethylsilane and diethoxydimethylsilane. In the commercial manufacture, however, a mixture of methylchlorosilanes, $(CH_3)_nSiCl_{4-n}$, (n = 0,1,2,3,4), is produced by

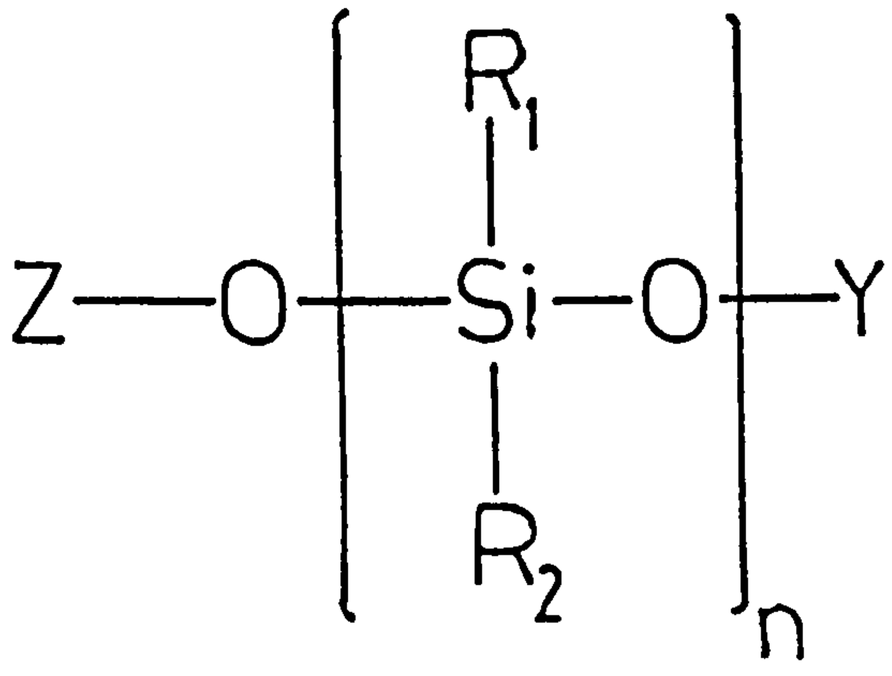

FIGURE 4.3(i): General formula of the linear silicones

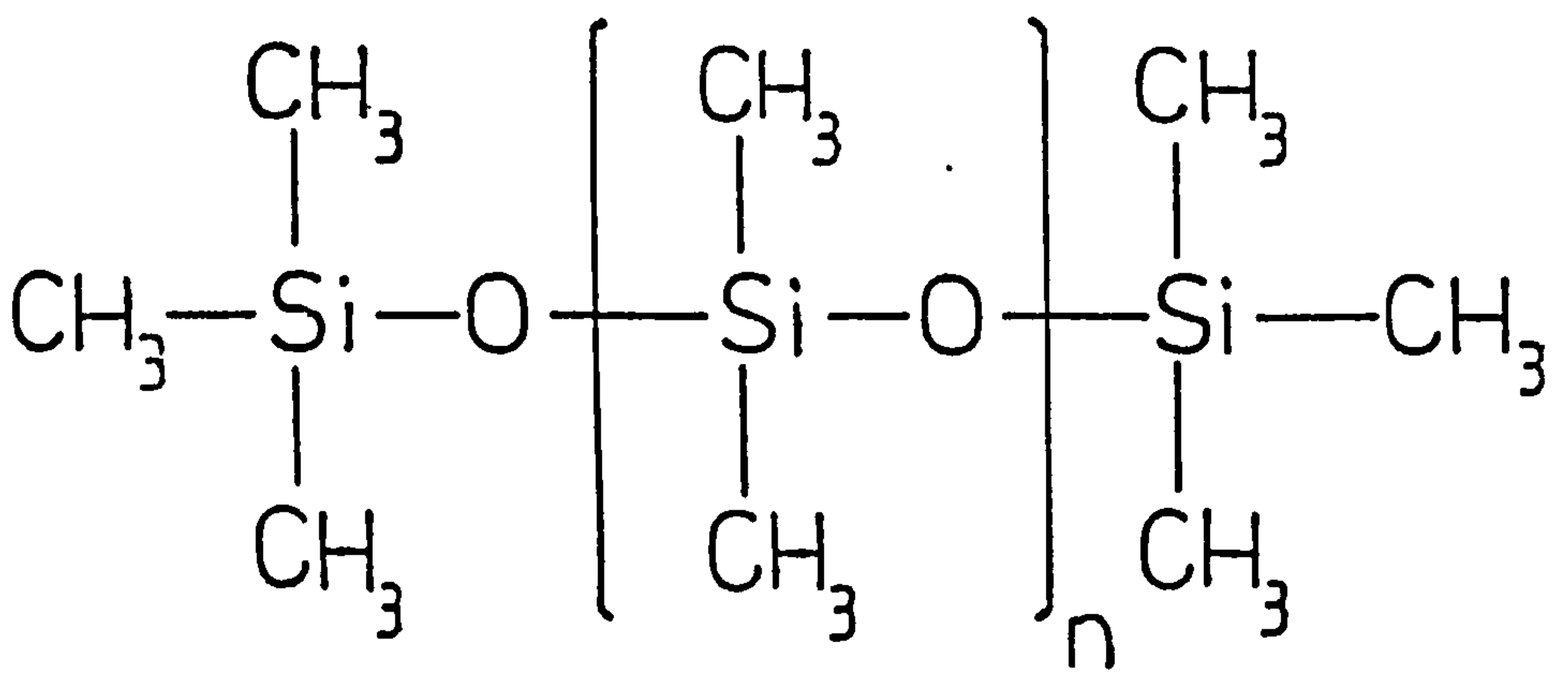

FIGURE 4.3(ii): Trimethylsiloxy end-blocked polydimethylsiloxane

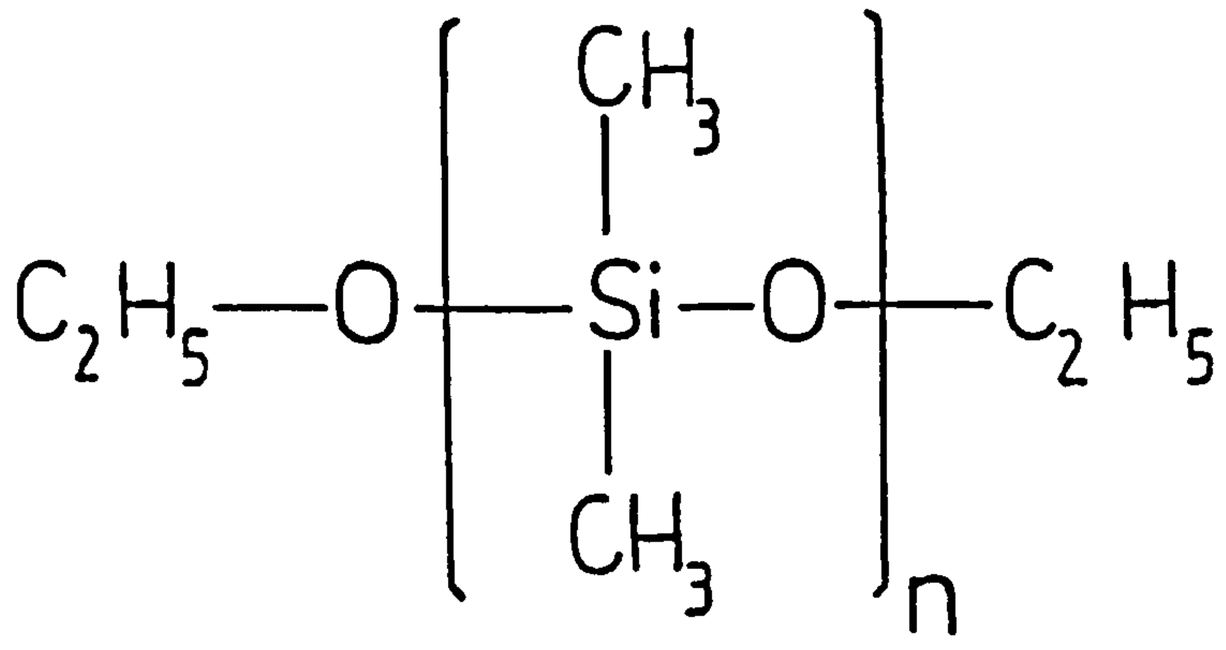

FIGURE 4.3(iii): Ethoxy end-blocked polydimethylsiloxane

passing methylchloride vapour over silicon containing a copper catalyst at high temperature[2,123]. The polydimethylsiloxanes are produced by aqueous hydrolysis of mixtures of methylchlorosilanes, and the chain length of the final product depends on the mole ratio of reactants used.

In a viscometric study of linear polydimethylsiloxanes in toluene solution, Barry[124] found that the viscosity of the polymer, η, expressed in Pas at 25°C, was related to the number-average molecular weight, M, through the equation

$$\log_{10} \eta = 1.00 + 0.0123M^{0.6} \qquad (4.5)$$

for values of M between 2,500 and 200,000.

However, Warwick *et al*[125] deduced from both independent data for low and high-molecular-weight polydimethylsiloxanes, that the intrinsic viscosity measured as an 'initial viscosity' depended on the molecular weight, M, in different ways above and below M = 40,000.

For M < 40,000, the relationship

$$\log_{10} \eta = 1.43 \log M - 5.54 \qquad (4.6)$$

was valid and for M > 40,000, with the viscosity in poise and at the same temperature:

$$\log_{10} \eta = 3.64 \log M - 15.44 \qquad (4.7)$$

The mean molecular weight values and the number of units in the polymer chain obtained using Barry's expression correlated with those obtained by Warwick *et al*[125]

4.5.1.1 Properties of Linear Polydimethylsiloxanes

Unlike hydrocarbons, which become waxes or solids beyond chain lengths of C_{14}, silicones - particularly polydimethylsiloxanes - are colourless liquids or flowable gums, even at very long chain lengths. With the exception of those with very short chain lengths, polydimethyl-

siloxanes can be regarded as non-volatile polymers with very low vapour pressure even at high temperature. The polydimethylsiloxanes are non-polar, non-ionic and are very insoluble in water. Due to their hydrophobic nature, they may also be used as water repellents. However, they are soluble in most common organic solvents such as toluene, petroleum ether, chloroform and n-hexane.

Due to the coupling of a short stable methyl group and the flexibility of the silicone backbone, many useful properties also arise: thermal stability, oxidative stability, weather-resistance and small variation of properties with temperature. Polydimethylsiloxanes, though usually non-toxic and non-irritating, are an essential additive in the petroleum industry as antifoams[126].

4.6 Methods for the Measurement of Antifoaming Efficiency

Once the correct antifoam has been selected, it must be used in the proper manner. The antifoam must be added to the foaming liquid in such a way that will give a good dispersion. Adequate dispersion can be obtained if the antifoam is diluted suitably before addition.

Most of the industrial methods used to investigate the film-breaking and foam-preventing performances of the antifoam are largely dependent on measuring the foam heights with or without the antifoam. Included in these methods are those of Bikerman[109,110,111] (of which a detailed version is given in the experimental section). Ross and Miles[112] measured the foam-preventing ability of the antifoamer as the foam height observed immediately when a volume of the foaming liquid containing the antifoamer was dropped into the same solution in the foaming column, while the foam height after 5 minutes indicated the foam stability. In the pop-test of Ross and Mcbain[105], the performance of

the antifoamer was classified qualitatively in terms of the film-breaking ability, where a platinum wire ring on which the foaming film was formed, and another platinum wire ring that had previously been dipped in the antifoamer, were gently touched. However, the details of making the contact between the two platinum rings were not specified.

The Deutshe Industrie Norm method[127] assessed the performance of the antifoamer by moving a perforated plate 55mm in diameter up and down 30 times continuously during a 30-second period in a measuring cylinder containing a 200ml sample solution. The foam height was measured after 30 seconds. Okasaki and Sasaki[113] employed the 'standard' method of measuring the foam height after the foaming solution and antifoamer were poured into a glass tube and shaken at constant frequency and amplitude; while the film-breaking test involved the addition of the antifoamer drop to the foam formed by bubbled air. However, this method is semi-quantitative in nature.

4.7 Monolayers of Polyorganosiloxanes on Aqueous and Organic Liquid Substrates

Insoluble films of polyorganosiloxanes on aqueous and organic liquid substrates have been investigated. Fox *et al*[11,128] have made a series of studies including the force-area and potential-area relations of linear polyorganosiloxane monolayers on water. Their studies revealed relations between the critical spreading pressure, spreading coefficient and the viscosity. They concluded that the larger diameter of the silicon atom in comparison to the carbon atom was responsible for the greater ability of the polymethylsiloxanes to coil; also that at low pressures each helix uncoiled, and the molecule adsorbed with the long axis in the water.

This spreading behaviour of polyorganosiloxanes on water has also been investigated by Noll *et al*[17,129-133]. Their recent study[12] has determined the molecular orientation obtained in monomolecular films as a function of area on the one hand; and on the other, the substitution, molecular size and molecular structure of the polyorganosiloxanes on the water. They concluded that hydrogen bonding was responsible for the orientation effect of the polyorganosiloxane molecules on the surface of the water, i.e. that the structure of the polyorganosiloxane skeleton appeared not to influence the spreading phenomena.

Arslanov and Ogarev[134] have also studied the properties of films of polydimethylsiloxanes on the surface of water. From surface pressure and surface tension measurements, they tried to determine whether thermodynamic stability was fulfilled for all thicknesses of polydimethylsiloxane films on the water/air interface.

Stable films of a polydimethylsiloxane (MW = 2,000) on substrates including oleic acid, olive oil, tri-acetin and ethylene glycol, were studied by Banks[135,16]. The spreading of the film was followed by the placing of a drop of the polydimethylsiloxane solution in ether on the substrate contained in a trough and measuring ℓ, the distance travelled by lycopodium powder on the liquid surface in time, t; ℓ was directly proportional to $t^{\frac{1}{2}}$, and the constant of proportionality was inversely proportional to the square-root of the viscosity for the different substrates. Ellison and Zisman[15] obtained surface pressure-area per molecule curves for an ethoxy end-blocked polydimethylsiloxane (MW = 8,250) on n-hexadecane and tricreyl phosphate. They also concluded that the defoaming action of the dimethylsiloxanes was due to the displacement of the organic foam-stabilizer by a monolayer of polydi-

methylsiloxane and to the low surface viscosity of the resulting film.

Jarvis[20] measured the surface viscosities of a series of polydimethylsiloxanes at the water/air interface using a canal viscometer as well as a torsional surface viscometer. The polydimethylsiloxane monolayer investigated had molecular weights ranging from 520 to approximately 105,000, and included both the ethoxy and trimethyl end-blocked polymers. He found that the surface viscosity of even the highest molecular weight polydimethylsiloxane monolayer was extremely low - below the limits of sensitivity and detectability of both surface viscometers (though the canal was of the order of 10^{-5} surface poise) used - and was exceptionally low for polymers adsorbed at the water/air interface. He also found that the low surface viscosity of the polydimethylsiloxanes reflected the low intermolecular cohesion that existed between adjacent polydimethylsiloxane chains in a monolayer. This low surface viscosity may, in part, explain the defoaming and antifoaming ability of the polydimethylsiloxane fluids. Jarvis[136] also obtained force-area per molecule curves for a series of polydimethylsiloxanes of various chain lengths on several organic substrates; the curves depended on the molecular weight of the polymer, and on the polarity of the solvent.

Garett and Zisman[137] and Shuler and Zisman[138] have both reported the effect of linear polydimethylsiloxane films on the so-called 'capillary waves' of water and other liquid substrates respectively. They found that these films could be very effective in damping the capillary waves, but only at certain regions of compression of the monolayer. Large 'damping coefficient' peaks were obtained at areas per molecule corresponding to: the initial rapid increase in film pressure with decreasing area; the beginning and inflection point on the plateau region;

and at the approach to closest packing of the adsorbed molecules. It is interesting that surface viscosity has shown no correlation with the structure of the monolayer, or that such a remarkable damping of capillary waves could occur at all in the absence of a measured surface viscosity.

CHAPTER 5

THE FORCES ACTING IN FOAM FILMS

There are four forces described in this section that act in foam films, namely: van der Waals', electrical double layer and steric interaction forces, and capillary and gravitational pressures. A potential energy diagram for the film which may be constructed from the understanding of these forces, assists in giving an insight into the stability of the system.

5.1 Van der Waals' Forces

In 1873, van der Waals introduced two correction terms into the ideal gas equation to help to explain the behaviour of imperfect gases; the terms represented the finite size of the gas molecules, and for the attractive forces between the molecules respectively. Two theories have been developed to interpret the forces between macroscopic bodies. The microscopic approach evaluates the interaction energy by assuming that the forces between the atoms or molecules which make up the body are linearly additive; whereas the macroscopic approach evaluates the interaction energy by knowing the bulk properties of the bodies.

5.1.1 The Microscopic Approach

In the study of the forces between isolated atoms and molecules, Keesom[139] showed that two isolated molecules containing permanent dipole moments, μ_1, μ_2, assumed a relative orientation, giving rise to an attractive intermolecular force. The average interaction energy, V_k, over all configurations was in the region

$$V_k = - \frac{2\mu_1^2\mu_2^2}{3kTr^6} \qquad (5.1)$$

where r is the distance between the molecules, k is the Boltzmann constant, and T is the absolute temperature. At low temperature, the dipoles exhibited a parallel end-to-end configuration.

Debye[140] suggested that if one of two molecules has a permanent dipole moment, then it is possible to obtain an attractive force between two molecules due to the formation of an induced dipole in the other atom. The attractive energy, V_D, is obtained by the interaction of the electric fields of both dipoles, and is given by

$$V_D = - \frac{(\alpha_1 \mu_2^2 + \alpha_2 \mu_1^2)}{r^6} \qquad (5.2)$$

where α_1, α_2 are the molecular polarizabilities.

However, London[141] showed that an attractive force was obtainable between two atoms or molecules even when neither species had a permanent dipole. For two atoms, instantaneous fluctuations in electron density on one atom produce a transient dipole which induces a dipole on a neighbouring atom. The fluctuations were represented as those from a linear harmonic oscillator with a zero point energy $h\nu_0$ (where h and ν_0 are the Planck's constant and characteristic frequency respectively). An attractive force was obtained from the interaction of both dipole fields, and the difference between the coupled system and zero point energies of the isolated atoms gave rise to energy, V_L, expressed for two similar atoms as:

$$V_L = - \frac{3h\nu_0\alpha^2}{4r^6} \qquad (5.3)$$

where α is the static atomic polarizability, r is the distance between atoms, and ν_0 is the ground state frequency of vibration for the electron. The interaction force is given by the first derivative of the energy with respect to distance, i.e.

$$F_L = \frac{\partial V_L}{\partial r} \tag{5.4}$$

The frequency, ν_0, was termed the proper frequency by London, but it is more usually termed the dispersion frequency because the associated wavelength, λ_0, is of the order which produces optical dispersion[142] ($\sim$ 1,000Å). The van der Waals' energy is the sum of V_K, V_D and V_L, and except for polar molecules V_L can be of the same magnitude or greater than V_D and V_K.

5.1.1.1 Retardation

Dispersion forces are electromagnetic in nature, and a finite term is necessary to allow a dipole's electric field to travel and return from a neighbouring atom. When the magnitude of the time is similar to the period of fluctuation for the dipole, the two dipole fields will be out of phase and the force becomes retarded or reduced. Retarded and non-retarded forces occur at distances $r > \lambda_0$ and $r < \lambda_0$ between the atoms respectively.

Casimir and Polder[143] have found that V_L varies as the inverse second power of the distance, v, for retarded dispersion forces, and obtained an expression of

$$V_L = - \frac{3h\nu_0\alpha^2}{4r^6} f(p) \tag{5.5}$$

where $p = 2\pi\nu/\lambda_0$. The functions of p have two ranges:

$$f(p) = 1.01 - 0.14p \text{ for } 0 < p < 3$$

$$f(p) = 2.45/p - 2.04/p^2 \text{ for } 3 < p < \infty$$

5.1.1.2 The London Energy for Macroscopic Bodies

London demonstrated that dispersion forces are essentially independent of the molecular environment, and therefore these forces are not lost in the condensed state, but are actually additive. This property

of additivity initiated Kallman and Willstatter[144] to consider the effects of intermolecular attractive forces on the stability of colloids. Using this as a starting point, Bradley[145] and Hamaker[146] calculated the force between two spheres of unequal radii, while the force between two flat plates was calculated by de Boer[147] and Hamaker[146]; the latter also being responsible for evaluating the force between a sphere and a flat plate. These calculations assumed the forces to be both non-retarded and additive, and also that the macroscopic bodies interacted in a vacuum.

In this microscopic approach, an integral replaces the summation over all integrating pairs, assuming that the separation is large enough, so that the materials appear as continuous media and not as isolated atoms or molecules.

For two identical plane parallel plates with thickness d, separation H in a vacuum, the expression[148] for the van der Waals'-London energy per unit area is given by

$$V_A = - \frac{A}{12\pi} \left[\frac{1}{H_0^2} - \frac{2}{(H_0 + d)^2} + \frac{1}{(H_0 + 2d)^2} \right] \qquad (5.6)$$

where A is the non-retarded Hamaker constant and is defined as

$$A = \pi^2 q_1^2 \lambda \qquad (5.7)$$

where q_1 is the number of molecules per unit volume of material and λ is the coefficient of r^{-6} in equation (5.3).

For semi-infinite plane parallel plates, $d \to \infty$, hence

$$V_A = - \frac{A}{12\pi H_0^2} \qquad (5.8)$$

and the attractive force per unit area, F_A, is expressed as

$$F_A = \frac{A}{6\pi H_0^3} \qquad (5.9)$$

The problem of the attractive interaction between two spheres of arbitrary dimensions, and at an arbitrary distance apart, was resolved by Hamaker[146]. His result for the case of two equal spheres of radius a with a distance, R, between their centres was given as

$$V_A = - \frac{A}{6} \left[\frac{2a^2}{R^2 - 4a^2} + \frac{2a^2}{R^2} + \ell n \frac{R^2 - 4a^2}{R^2} \right] \qquad (5.10)$$

If the smallest distance between the spheres is H_0, then for small values of H_0, equation (5.10) reduces to

$$V_A = - \frac{Aa}{12H_0} \qquad (5.11)$$

In order to allow for the effect of retardation on the van der Waals' attractive energy per unit area, V_A, between two identical plane parallel plates, of infinite thickness, separation H_0 in a vacuum, Overbeek[149] expressed V_A as a product of the non-retarded energy $A/12\pi H_0^2$ and a correction factor (where A is the non-retarded Hamaker constant). The correction factor was observed to decrease continuously as the plate separation increased, reaching a limiting value of 0.98/p (where $p = 2\pi H_0/\lambda_0$; with λ_0 the characteristic wavelength for a plate of material about 100nm).

Typical values for the correction factor are:

(i) 0.77; when $p = 0.5$ ($H_0 \sim 8$nm);

(ii) 0.39; when $p = 2$ ($H_0 \sim 30$nm).

For fully-retarded interactions, V_A was expressed as

$$V_A = \frac{A\lambda_0(0.98)}{24\pi^2 H_0^3} \qquad (5.12)$$

and the corresponding force per unit area, F_A,

$$F_A = \frac{B}{H_0^4} \qquad (5.13)$$

where B is the retarded Hamaker constant and equals $0.0124\lambda_0 A$.

Hunter[150] has extended this approach to the van der Waals' attraction between two identical plane parallel plates of infinite cross-section but finite thickness, d. He allowed for the effect of electromagnetic retardation and calculated V_A for four possible situations:

(i) when $r_0 + 2d \leq \frac{3\lambda_0}{2\pi}$ (small separations);

(ii) when $r_0 + d \leq \frac{3\lambda_0}{2\pi} \leq r + 2d$;

(iii) when $r_0 \leq \frac{3\lambda_0}{2\pi} \leq r + d$;

(iv) when $r_0 \geq \frac{3\lambda_0}{2\pi}$ (large separations).

In each case, r_0 is the plate separation, and the results may be expressed as

$$V_A^R = V_A f(a,b) \qquad (5.14)$$

where V_A^R is the retarded attractive force, $a = 2\pi r_0/\lambda_0$ and $b = 2\pi d/\lambda_0$. The function f(a,b) is an explicit function which may be readily evaluated. Overbeek[149] has given the results of the retarded interaction energy, V_A, of two spheres, while Schenkel and Kitchener[151] have given a similar solution valid for all values of $p > 0.5$. Clayfield *et al*[152] also derived similar expressions for the retarded dispersion force between two spheres of unequal radii and between a sphere and a thick plate.

5.1.1.3 The Hamaker Constant

The presence of a liquid medium 2 has the effect of weakening the interaction between the plates of different material 1 and 3, as the molecules in 2 are attached to the molecules in 1 and 3, producing a smaller net or composite effect. Hence the net or composite Hamaker

constant for a system, A_H, is given by

$$A_H = A_{13} + A_{22} - A_{12} - A_{23} \tag{5.15}$$

For a symmetrical system, i.e. when materials 1 and 3 are identical, $A_{11} = A_{13}$ and $A_{12} = A_{23}$, so that

$$A_H = A_{11} + A_{22} - 2A_{12} \tag{5.16}$$

In the microscopic approach, the Hamaker constant for the interaction in a vacuum of two thick parallel plates of material 1 and 2 is expressed as a geometric mean of the Hamaker constant for the interaction of identical plates A_{11}, A_{12}, namely

$$A_{12} = (A_{11}, A_{22})^{\frac{1}{2}} \tag{5.17}$$

If $\lambda_{11} = 3h\nu_1\alpha_1^2/4$ and $\lambda_{22} = 3h\nu_2\alpha_2^2/4$ for the interaction in a vacuum of two atoms in materials 1 and 2 respectively, then the coefficient λ_{12} for the interaction in a vacuum of an atom of material 1 and an atom of material 2 is defined as

$$\lambda_{12} = \frac{3}{2} h \frac{\nu_1\nu_2}{\nu_1 + \nu_2} \alpha_1\alpha_2 \tag{5.18}$$

where α_1, α_2 are the static polarizabilities and ν_1, ν_2 are the characteristic frequencies for an atom of materials 1 and 2, and the geometric mean identity assumes that

$$\lambda_{12} = (\lambda_{11}, \lambda_{22})^{\frac{1}{2}} \tag{5.19}$$

is valid, then for the symmetrical system

$$A_H = (A_{11}^{\frac{1}{2}} - A_{22}^{\frac{1}{2}})^2 \tag{5.20}$$

Equation (5.20) demonstrates that the potential energy of attraction must always be positive, and thus particles always tend to be mutually attracted. The magnitude of A_H does not change when materials 1 and 2 are interchanged so that, for example, the Hamaker constant for the

interaction of two silicone droplets in a hydrocarbon liquid would be the same as for the interaction of two hydrocarbon droplets in a silicone liquid.

The calculation of the Hamaker constant, A, from atomic and molecular properties has been discussed by Gregory[153] and Visser[154]. For hydrogen-like atoms considered by London, the static polarizability α and characteristic frequency ν_0 are related by the equation

$$\nu_0^2 = \frac{e^2}{4\pi^2 m_e \alpha} \tag{5.21}$$

where m_e and e are the mass and charge of the electron respectively.

The Lorentz-Lorentz equation can be applied to the condensed system in order to relate the static polarizability of an isolated atom to the refractive index of the system, extrapolated from high to zero frequency $n_{v\to 0}$, so that

$$\alpha = \frac{3M}{4\pi N \rho}\left[\frac{n_{v\to 0}^2 - 1}{n_{v\to 0}^2 - 2}\right] \tag{5.22}$$

where N, M and ρ are the Avogradro number, molecular weight and density for the system respectively. A knowledge of α and ν_0 enables a value for λ, as defined in equation (5.3), to be obtained, and hence a value of the Hamaker constant.

For more complex atoms, the interaction between isolated atoms can result from fluctuations due to more than one electron on each atom. A value for λ, the coefficient of r^{-6} in equation (5.3), for identical isolated atoms, was derived by Eisenchitz and London[155] where

$$\lambda = \frac{3he^4 s^2}{64\pi^4 m_e^2 V_\nu} \tag{5.23}$$

where V_ν is a characteristic frequency of the atom and s is the effective

number of dispersion electrons. The variation of $(n^2 + 2)/(n^2 - 1)$ with frequency, where n is the frequency-dependent refractive index for a condensed system yields information on the values of s and V_ν[156].

5.1.1.4 The Modification of van der Waals' Attraction by Adsorbed Layer

Although the most marked effect on interaction caused by the presence of an adsorbed layer is that on the repulsive forces the presence of adsorbed molecules also modifies the van der Waals interaction, Vold[157] predicted that the presence of the adsorbed layers would lead to a reduction in the attraction between the particles - a reduction later termed the 'Vold effect'. Vincent[156] has derived expressions for the interaction of two identical flat plates containing adsorbed layers, and also for the interaction of a sphere of one material containing an adsorbed layer and a flat plate of a different material containing an adsorbed layer.

The non-retarded van der Waals energy, V_A, for two identical flat parallel plates of thickness T, when each plate contained an adsorbed layer of material, thickness ℓ, on both surfaces (Figure 5.1), was given for a separation h between the surfaces of the adsorbed layer by the expression[156]

$$-12V_A = (H_o + H_i - 2H_{oi})(A_\ell^{\frac{1}{2}} - A_m^{\frac{1}{2}})^2 + H_f(A_f^{\frac{1}{2}} - A_m^{\frac{1}{2}})^2 + 2(H_{of} + H_{if})(A_\ell^{\frac{1}{2}} - A_m^{\frac{1}{2}})(A_f^{\frac{1}{2}} - A_m^{\frac{1}{2}}) \quad (5.24)$$

where A_f, A_m, A_ℓ were the Hamaker constants for the materials of the plates, medium and adsorbed layers respectively, and H_o, H_i, H_{oi}, H_f, H_{of}, H_{if} were the geometric functions defined as

$$H(\Delta, t_1, t_2) = \frac{1}{\pi}\left[\frac{1}{\Delta^2} + \frac{1}{(\Delta+t_1+t_2)^2} - \frac{1}{(\Delta+t_1)^2} - \frac{1}{(\Delta+t_2)^2}\right] \quad (5.25)$$

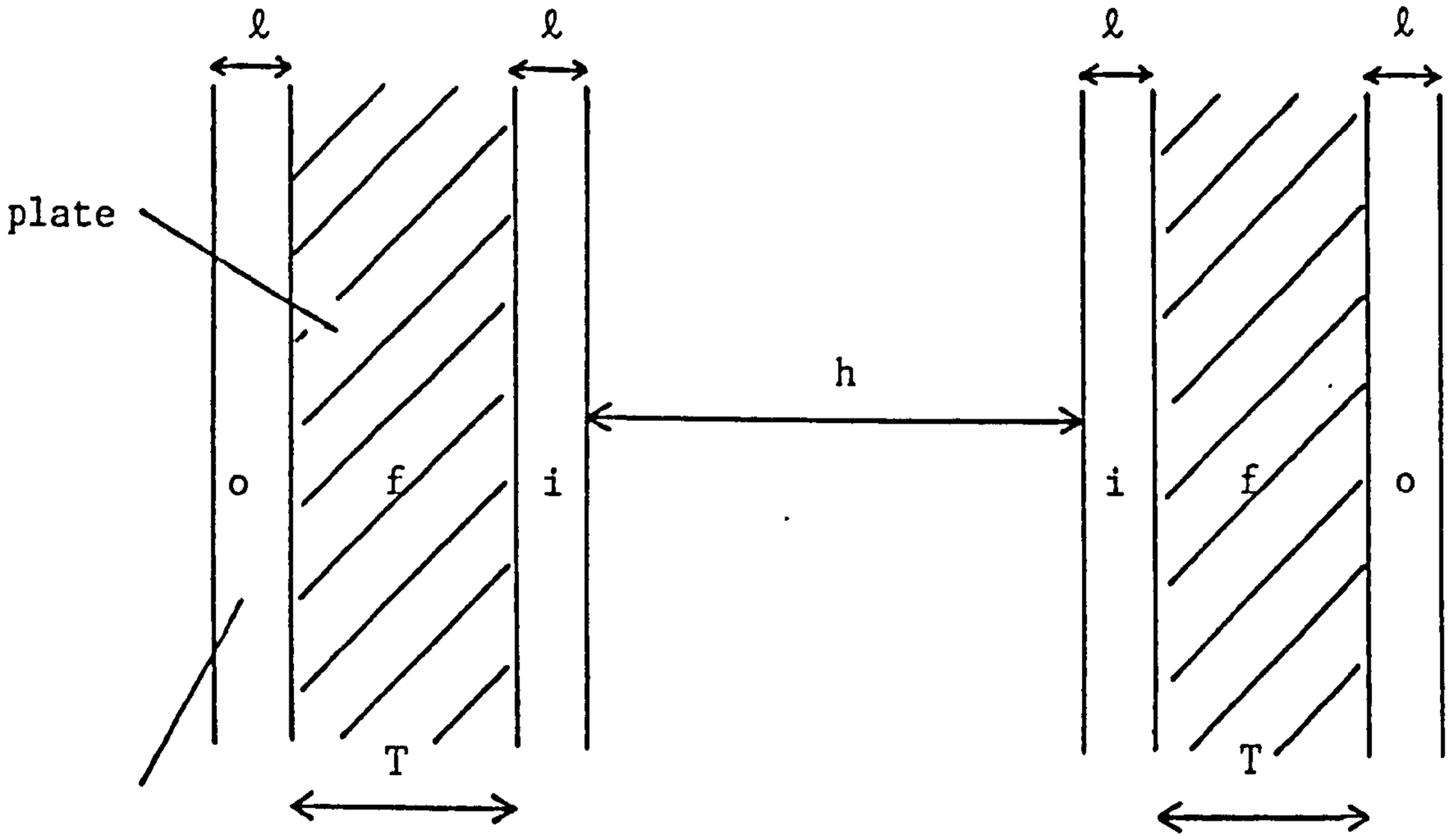

FIGURE 5.1: Interaction of two identical flat plates containing adsorbed layers(183)

where for

H_o , $\Delta = h + 2T + 2\ell$, $t_1 = 1$, $t_2 = 1$,

H_i , $\Delta = h$, $t_1 = 1$, $t_2 = 1$,

H_{oi}, $\Delta = h + T + \ell$, $t_1 = 1$, $t_2 = 1$,

H_f , $\Delta = h + 2\ell$, $t_1 = T$, $t_2 = T$,

H_{of}, $\Delta = h + 2\ell + T$, $t_1 = 1$, $t_2 = T$, H_{if}, $\Delta = h + 1$, $t_1 = 1$, $t_2 = T$.

The subscripts f, o and i referred to the plate, outer adsorbed layer and inner adsorbed layer respectively. For the semi-infinite plates, $T \to \infty$, and

$$-12V_A = H_f(A_f^{\frac{1}{2}} - A_m^{\frac{1}{2}})^2 + H_i(A_\ell^{\frac{1}{2}} - A_m^{\frac{1}{2}})^2 + 2H_{if}(A_\ell^{\frac{1}{2}} - A_m^{\frac{1}{2}})(A_f^{\frac{1}{2}} - A_m^{\frac{1}{2}}) \tag{5.26}$$

5.1.1.5 The Limitations of the Microscopic Approach to van der Waals Forces

The electronic charge fluctuations that occur in a narrow band of frequencies in the ultraviolet part of the spectrum are responsible for the van der Waals-London force and the fluctuations at other frequencies make no contributions to this force. The force between two isolated atoms is assumed to arise from a dipole-dipole interaction only, and dipole-quadripole and quadripole-quadripole interactions are neglected (these give rise to contributions to the energy which vary at r^{-8} and r^{-10} respectively, where r is the distance between the atoms compared to r^{-6} for dipole-dipole interactions). At separations of macroscopic bodies of the order of atomic dimensions, molecular orbital overlap can occur to produce a repulsive force, and the London treatment does not apply for this area.

The calculation of forces between isolated atoms in a dilute gas are assumed to be additive when summed in a condensed system such as liquid or solid. However, the charge fluctuations in these systems

can cause the force between the two atoms to be perturbed due to the close proximity of neighbouring atoms, and the assumption that forces are additive is no longer applicable. The London theory was initially derived for non-retarded interactions in a vacuum, and has been modified to allow for electromagnetic retardation and the dielectric medium on the transmission of the force.

5.1.2 The Macroscopic Approach

The most fundamental problem based on this approach is that the parameters α and ν_0 in equations (5.3) and (5.5) have different values in the gaseous and condensed states. Thus, it is difficult to decide whether, in using the macroscopic formulae to deal with the interaction between the bodies in their condensed state, it is better to use gaseous or condensed state values of α and ν_0. The situation arises whereby one must choose between using 'condensed parameters' in 'gaseous equations' applied to condensed systems, or using 'gaseous parameters' in 'gaseous equations' applied to condensed systems.

In an attempt to avoid all these difficulties, Lifshitz[158] derived general equations for which the van der Waals forces between macroscopic bodies were derived from a knowledge of the bulk properties of the materials, namely: the optical properties over the complete electromagnetic spectrum. Hence the Lifshitz theory is restricted to materials for which electromagnetic data are available.

The Lifshitz equations give the attractive force as a function of the complex dielectric permeability of the bodies, which in turn is a function of the circular frequency of the electromagnetic field. The equations automatically take retardation into account and reduce to those of Casimir and Polder[143] under the appropriate conditions. The

transition to the case when both bodies are gaseous reduces the Lifshitz equations to those given by the microscopic theory[159]. However, although the Lifshitz equations are exact and require no correction terms, the collection of the experimental data required to use the equations is not an easy task, even for the simplest systems[160].

In trying to reduce the differences between the microscopic and macroscopic theories (which are really not as large as their difference of derivation might suggest), Njiboer and Renne[161,162] have recently developed the microscopic approach by introducing the complex dielectric constant into their expression for the interaction of one atom at a distance from a semi-infinite wall of the same kind of atoms. They show the same resulting expression as that given by Lifshitz under the appropriate conditions. McLachlan[163] has also derived the Lifshitz equations in a different way.

Due to the magnitude of van der Waals forces being small, their measurement has been confined to macroscopic bodies. Many attempts have been made[159,164-170] in recent years to make a direct determination of this attractive force.

5.2 Electrical Double Layer Forces

In non-aqueous foam films, the assumption that any repulsive force arising from the overlap of electrical double layers (depends on the value of the dielectric constant and water contaminants etc.) in the film is negligible, is employed; however, this force, which occurs in aqueous foam films, will be discussed in this section.

When a flat charge is immersed in a solution of an electrolyte, the ionic concentration in the neighbourhood of the surface of the plate

differs from the bulk, and the concentration of ions of opposite charge to the plate is greater in this region than in the bulk solution. The electrical potential decreases, moving away from the surface from a value ψ_0 at the surface to the value of the bulk solution. The region where this potential decay occurs is known as the 'electrical double layer'.

The first quantitative treatment of the electrical double layer was advanced by Gouy[171,172] and Chapman[173], based on the theory that ions were point charges and were free to migrate throughout the diffuse double layer, proposed by Debye and Huckel[174,175]. The potential decay, ψ, can be expressed as a function of the distance, x, from the charged plane surface (Figure 5.2),

$$\psi = \psi_0 \exp(-k'x) \qquad (5.27$$

where ψ is the potential at a distance x from the surface, and k' is the Debye-Huckel reciprocal length, defined for a symmetrical electrolyte as

$$k' = \left(\frac{2e^2 n_0 z^2}{\varepsilon_r \varepsilon_0 kT}\right)^{\frac{1}{2}} \qquad (5.28)$$

where n_0 is the number of cations and anions per cm^3 of solution, e is the electronic charge, z is the ionic valency, ε_r is the relative permittivity of the medium, ε_0 is the permittivity of free space, k is the Boltzmann constant, and T is the absolute temperature. Equation (5.28) is applicable for the limiting case of low potentials, such that $ze\psi_0/2kT \ll 1$. The quantity $1/k'$ describes the distance at which the surface potential has fallen to ψ_0/exp; it is often referred to as 'thickness of the electrical double layer'[176].

The Gouy-Chapman approach was modified by Stern[177], who took into account the finite dimensions of the ions. The ions were not able

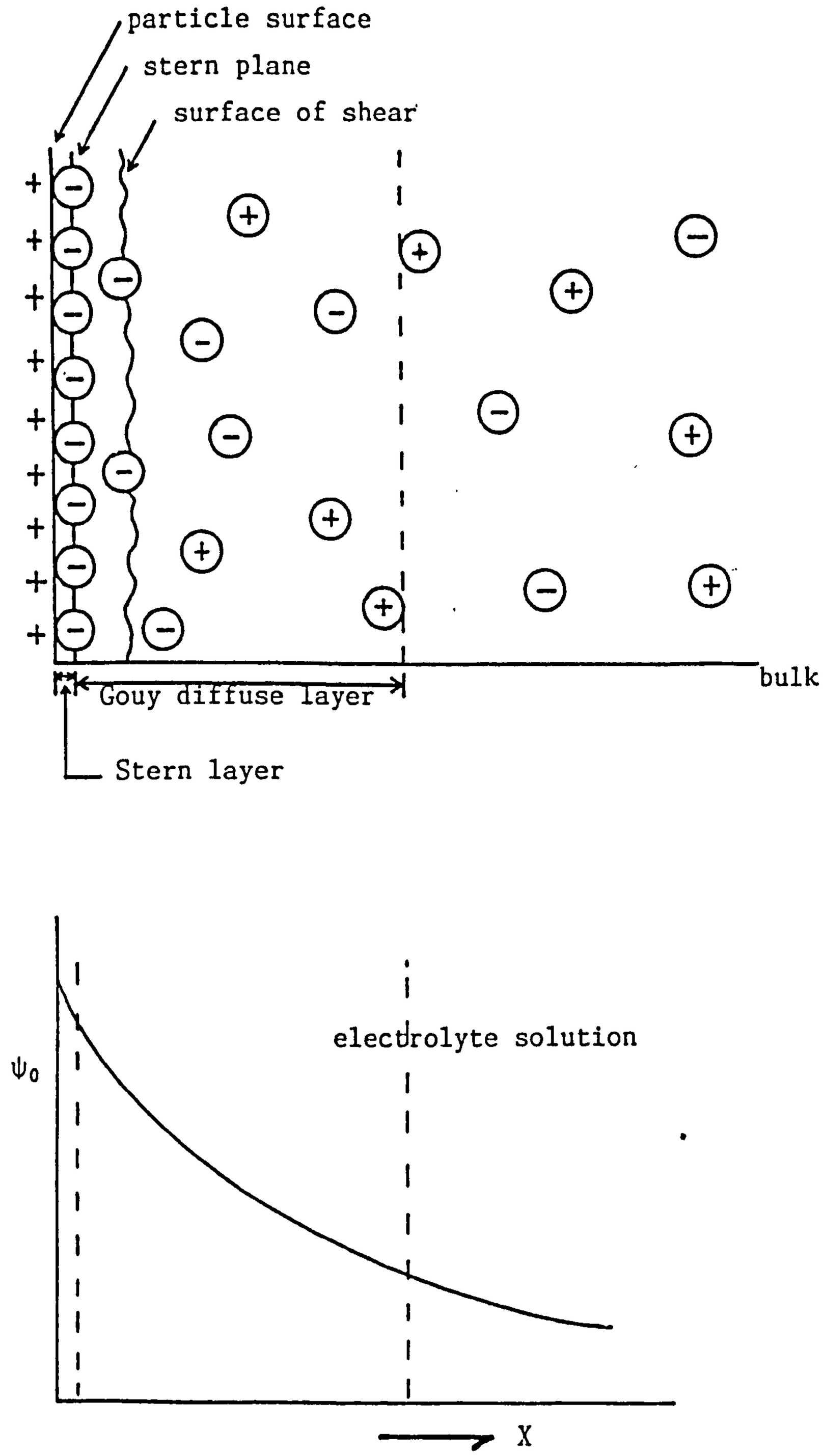

FIGURE 5.2: Schematic representation of the structure of the electrical double layer according to Stern's theory and the corresponding potential decay diagram

to approach closer to the surface than to some plane, the Stern plane. The region between the plane and the interface, and consisting of a compact layer of ions, was termed the 'inner part or Stern layer'; whereas the outer part extending from this plane to the bulk solution was a 'diffuse or Gouy layer'.

More recently[178], the Stern layer has been referred to as the 'outer Helmholtz plane', to indicate the closest distance of approach of hydrated ions in solution to the charged interface, while the 'inner Helmholtz plane' indicates the locus of the centres of ions which were specifically adsorbed onto the interface; the region from the 'outer Helmholtz plane' to the bulk solution also consists of a diffuse double layer.

Langmuir[179] derived an expression for the repulsive force, based on the Gouy-Chapman model of diffuse double layers, by considering the overlap of the double layers on each plate between two approaching yet identical flat charged plates. The repulsive force per unit area on each plate, F_R, can be expressed as

$$F_R = 2n_0kT(\cosh u - 1) \qquad (5.29)$$

where $u = ze\psi_h/2kT$, ψ_h is the midpoint potential when the plate separation is 2h (see Figure 5.3). The force, F_R, remained a repulsion for all values of u.

Lyklema[180] has recently considered the nature of the electrical double layer in non-aqueous systems. In a non-aqueous system, the values of ε_r and n_0, defined in equation (5.28), can differ considerably from that of an aqueous system whereby the decay of ψ is affected by the parameter k.' The interaction energy, V_R, for the repulsive force of two spheres of equal radius, a, and equal potentials, $\psi_0 < 25$ milli-

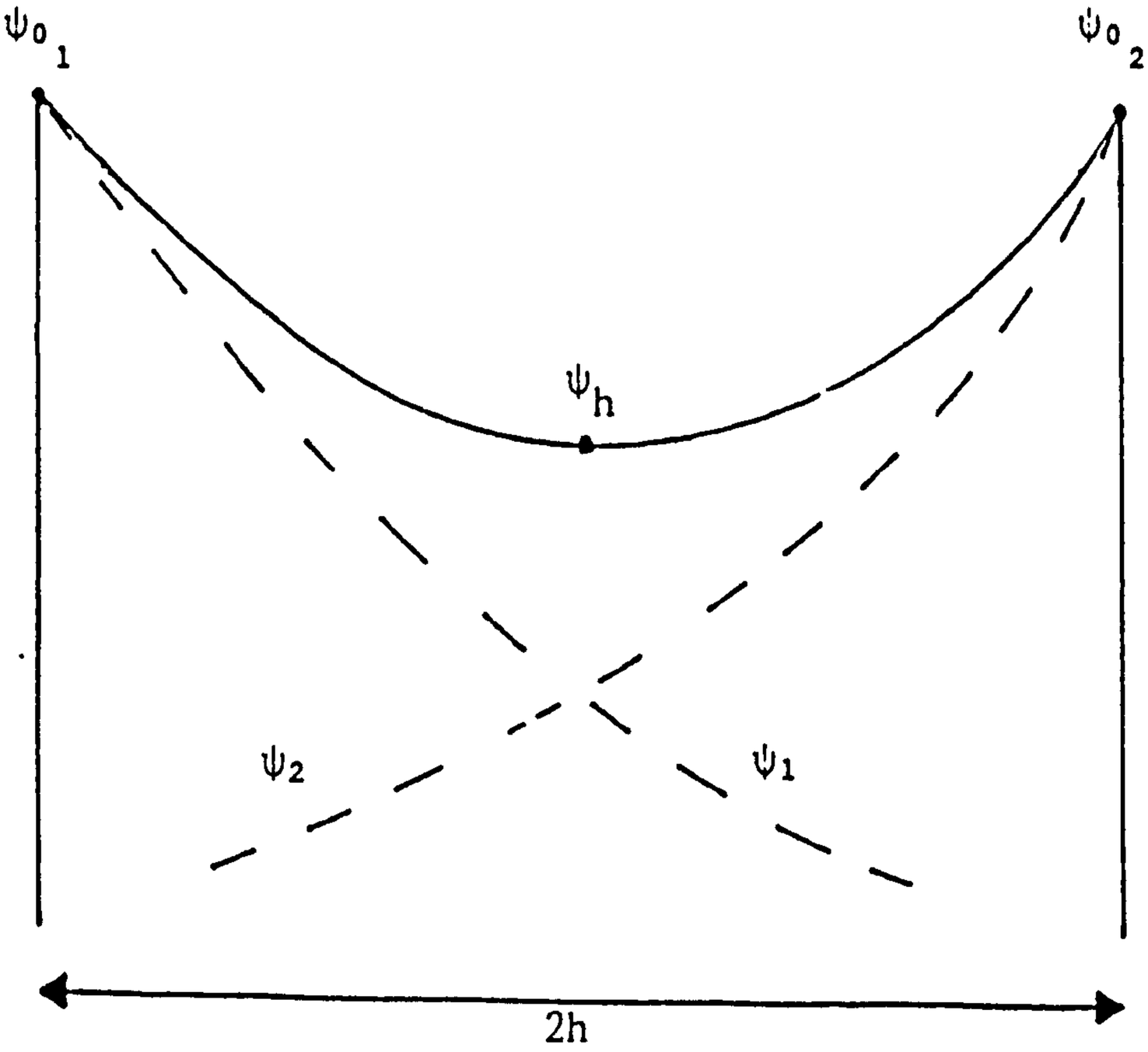

FIGURE 5.3: Interaction of two diffuse double layers

volts, separation of closest approach H_o and for small particles $\kappa a' < 3$, is given by

$$V_R = \frac{4\pi\varepsilon_r\varepsilon_0 a\psi_0^2}{H_o + 2a} \exp(-\kappa H_o) \qquad (5.30)$$

and for large particles with $\kappa a > 10$,

$$V_R = 2\pi\varepsilon_r\varepsilon_0 a\psi_0^2 \ln(1 + \exp(-\kappa H_o) \qquad (5.31)$$

5.3 Steric Stabilization

The energy change of a system when interaction of adsorbed layers on two particles in a dispersion occurs, and the interaction of adsorbed layers which may occur during liquid drainage from certain types of foam film, are both discussed in this section.

The interaction of two flat parallel plates containing adsorbed molecules that were represented by rigid rods, which were secured to the plates by freely-hinged joints, has been considered by Mackor[181]. The number of configurations which the rods could have was proportional to the area swept out by the free ends of the rods, and there was a reduction in this number as the plate separation was reduced below the length of the rods. This resulted in a decrease in the configurational entropy of the system, which gave rise to a repulsive force between the plates. The Mackor-van der Waals model[182] considered the interaction of flat plates whose surfaces were divided into lattice sites occupied by solvent molecules (represented as spheres, or adsorbate represented as dumb-bells), and is applicable for a high surface coverage of rod-shaped molecules.

The overlap of adsorbed layers on two spherical particles of equal radius is depicted schematically in Figures 5.4(i) and 5.4(ii)[183].

(i) Overlap without compression

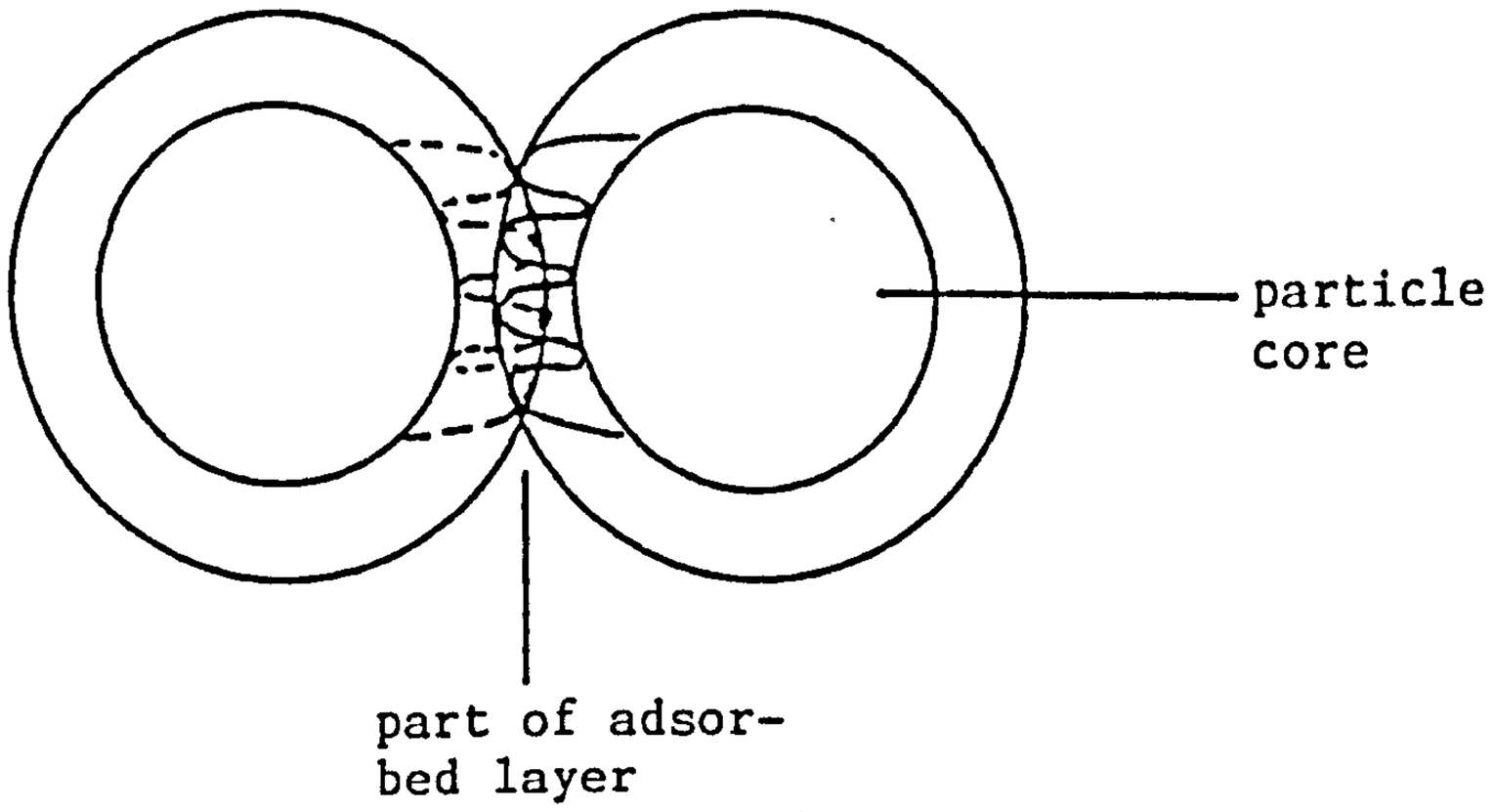

(ii) Compression without overlap

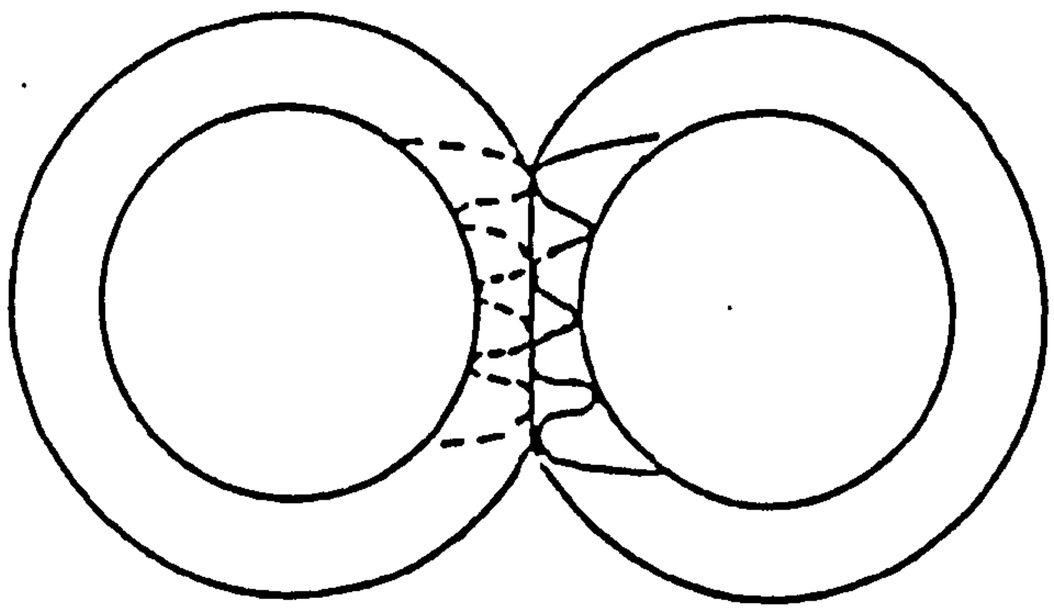

FIGURE 5.4: Types of overlap for adsorbed layers on identical spherical particles

In Figure 5.4(i), interpenetration of the layers occurs without compression, hence loss of configurational entropy of the material in the layers; whilst in Figure 5.4(ii), compression of the layers occurs without interpenetration. The Mackor[181] and Mackor-van der Waáls[182] models use the decrease in configurational entropy which arose for the material in the adsorbed layers on the approach of the particles, as the only contribution to the increase in free energy of the system, and hence the reuplsive force between the particles.

An expression for the free energy change, ΔG_M, produced by the mixture of the adsorbed layers on two spherical particles, was derived by Fischer[184]. This model assumed that interpenetration occurred without compression of the adsorbed layers, and that the concentration of adsorbed material in the overlapping region was greater than in the layers of the isolated particles. The excess osmotic pressure, π_E, in this region was expressed in terms of the second virial coefficient of the adsorbate, B,

$$\pi_E = RTBc_s^2 \qquad (5.32)$$

where c_s is the concentration of material in the layer. A relationship was obtained for the free energy of mixing for the adsorbed layers, ΔG_M, after integration of π_E with respect to the overlapping volume in the form

$$\Delta G_M = \frac{4}{3}\pi RTBc_s^2\left(d - \frac{H_o}{2}\right)^2\left(3a + 2d + \frac{H_o}{2}\right) \qquad (5.33)$$

where d, a, H_o are the layer thickness, particle radius and separation between the surfaces of the core of the particles respectively. When $B > 0$, ΔG_M was positive, and a repulsion occurred between the particles.

Three contributions to the total free energy change, ΔG, for the

overlap of adsorbed layers has been suggested by Ottewill[185]. Thus

$$\Delta G = \Delta G_s + \Delta G_M + \Delta G_c \qquad (5.34)$$

where free energies; ΔG_s was contributed due to a change in configurational entropy of the adsorbed material; ΔG_M, was produced by mixing of the adsorbed layers and ΔG_c, produced from the different state of compression of adsorbed material in the isolated particles and overlap region (elastic energy stored on compression of the molecules produced a repulsion between the particles) respectively.

Ottewill and Walker[186] developed Fischer's model by deriving an expression for the free energy of interaction of adsorbed layers from isolated spherical particles which allowed for changes in the solvation of the layer that could occur on overlap. They allowed for the enthalpy term that could contribute to the stability of the system in the expression

$$\Delta G_M = \frac{4\pi c_s^{\,2} kT}{3 v_1 \rho_2^{\,2}} (\psi_1 - \chi_1)\left(d - \frac{H_o}{2}\right)^2 \left(3a + 2d + \frac{H_o}{2}\right) \qquad (5.35)$$

The terms c_s, ρ_2, v_1 are the concentration, density and volume fraction for the adsorbed material respectively. The quantity χ_1 was a dimensionless quantity divided by kT which characterized the interaction energy of the adsorbed layer material per solvent molecule, and ψ_1 was an entropy parameter for the mixing of the layers. The Fischer-Ottewill-Walker model for overlap is shown schematically in Figure 5.5, where the volume for the combined layers $\delta v = \delta v_i = \delta v_j$, where δv_i, δv_j were the volume elements in the separate particles.

When a collision occurs in a dispersion between two identical particles, each containing an adsorbed layer, the distance between the surfaces is increased by twice the adsorbed layer thickness relative to when a collision occurs between two bare particles, i.e. those which do

(i) Before overlap

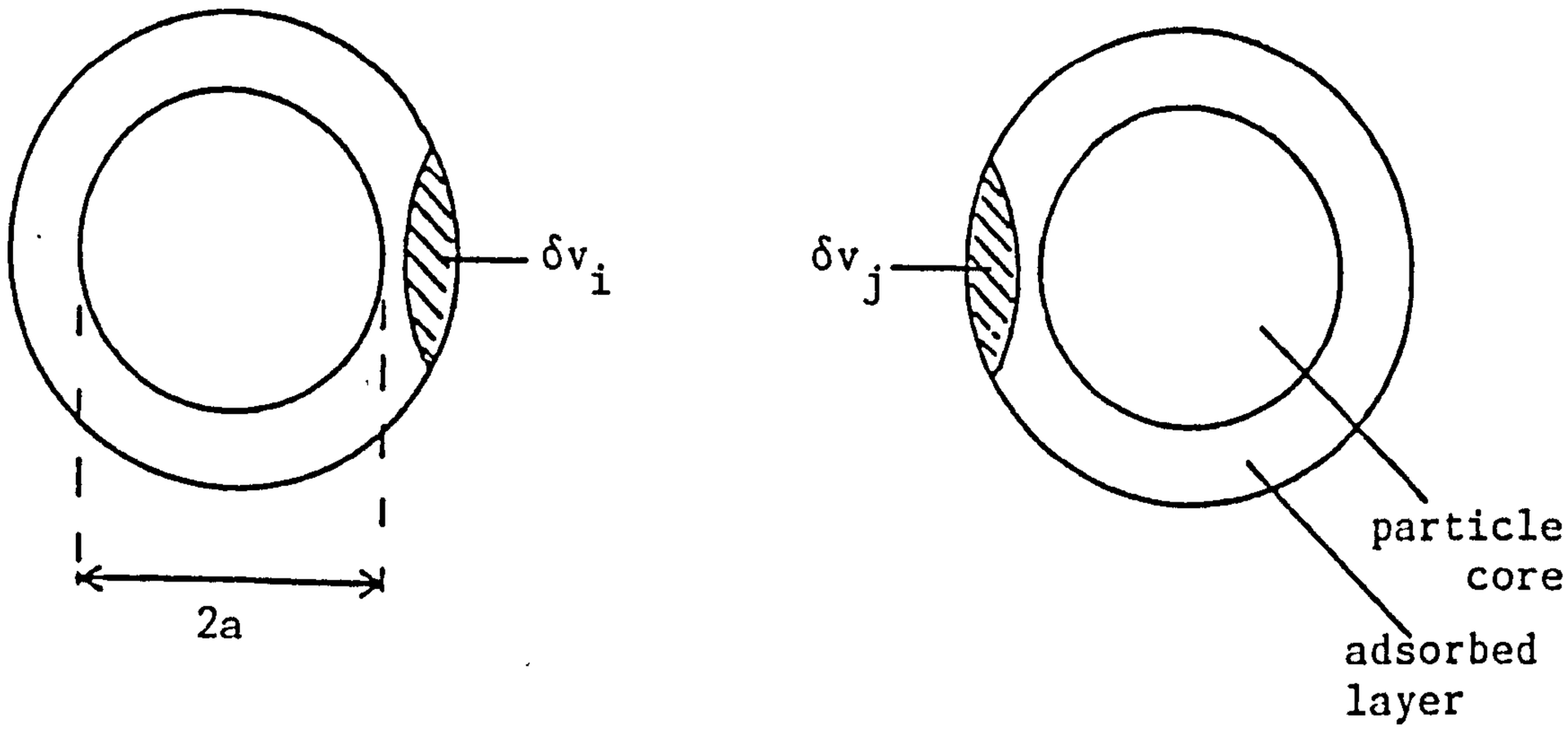

(ii) After overlap

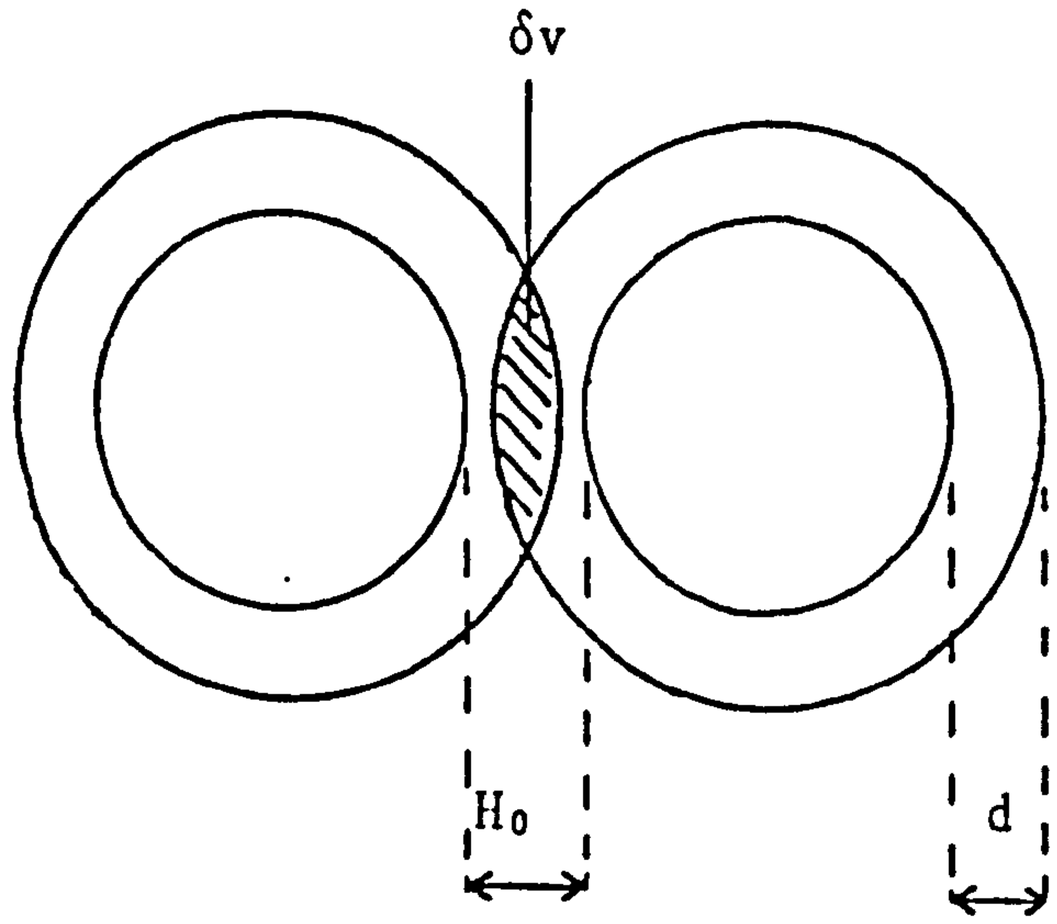

FIGURE 5.5: Overlap of adsorbed layers on identical spherical particles

not contain an adsorbed layer. As the separation decreases further due to the van der Waals attraction between the particles, assuming that electrostatic repulsion between the particles is zero, overlap of the layers occurs and a Gibbs free energy for the mixing of the layers, ΔG_R, is expressed using the Gibbs-Helmholtz equation[187]

$$\Delta G_R = \Delta H_R - T\Delta S_R \qquad (5.36)$$

where ΔH_R is the enthalpy change, ΔS_R is the entropy change of the mixing process, and T is the absolute temperature. When $\Delta G_R < 0$, overlap of the layers is thermodynamically (i.e. energetically) favourable, and flocculation of the individual particles can take place. When $\Delta G_R = 0$, flocculation can occur as if the adsorbed layers were present; however, when $\Delta G_R > 0$, the particles can be stabilized against flocculation, as overlap of the layers is an energetically unfavourable process. The stability of colloidal particles against flocculation due to the presence of an adsorbed layer of material on the particles is known as 'steric stabilization'.

Three types of steric stabilization that can occur when $\Delta G_R > 0$ have been discussed by Napper[188]. These are the entropic stabilisation, which occurred when the entropy term $T\Delta S_R$ was greater than the enthalpy term ΔH_R in equation (5.36) and both terms were negative; the enthalpic stabilization, with $\Delta H_R > T\Delta S_R$ and both terms positive; and the enthalpic-entropic stabilization, with ΔH_R positive and $T\Delta S_R$ negative and both contributing to a positive ΔG_R.

Clayfield and Lumb[189] have determined the configurational energy change produced by compression of a terminally-adsorbed polymer molecule containing up to 100 links using a Monte Carlo technique. Two types of interaction were considered: a sphere-sphere and a sphere-plate; and for

each particle the molecule was irreversibly adsorbed at one end to the surface. Their model assumed that the solvent did not interact with the unadsorbed part of the polymer, and that no interpenetration of the adsorbed layers occurred as the particle separation decreased. Meier[190] has also considered the free energy change that occurred when two flat parallel plates containing adsorbed polymer molecules approached each other, and the polymer was assumed to be of sufficient length and flexibility that random flight statistics could be applied to it. The molecules were anchored at one end to the surface and there were two free energy contributions; the first due to a decrease in configurational entropy of the polymer molecules, and the second due to a free energy of mixing of polymer and solvent molecules as the density of chain segments changed during the approach of the surfaces. The entropy term dominated the free energy for low surface coverages, whereas the mixing term dominated for higher surface coverages.

5.3.1 Steric Repulsion

A steric repulsion can occur due to the interaction of adsorbed layers in certain types of foam film. Single foam films have been formed from solutions of long chain surface-active materials in a hydrocarbon solvent, with an aqueous medium on both sides of the film; the formation of films from solutions of glycerol mono-oleate in n-decane[191] is a typical example. The hydrocarbon chains of the surface-active molecules are sandwiched between the head groups which are in contact with the aqueous electrolyte solution. The structure of this type of foam film is schematically illustrated in Figure 5.6[192]. When liquid drainage proceeds from the film, a repulsion arises due to the interaction of the hydrocarbon chains of the surfactant that are adsorbed on either side of the film, when the film thickness is approximately twice the length of

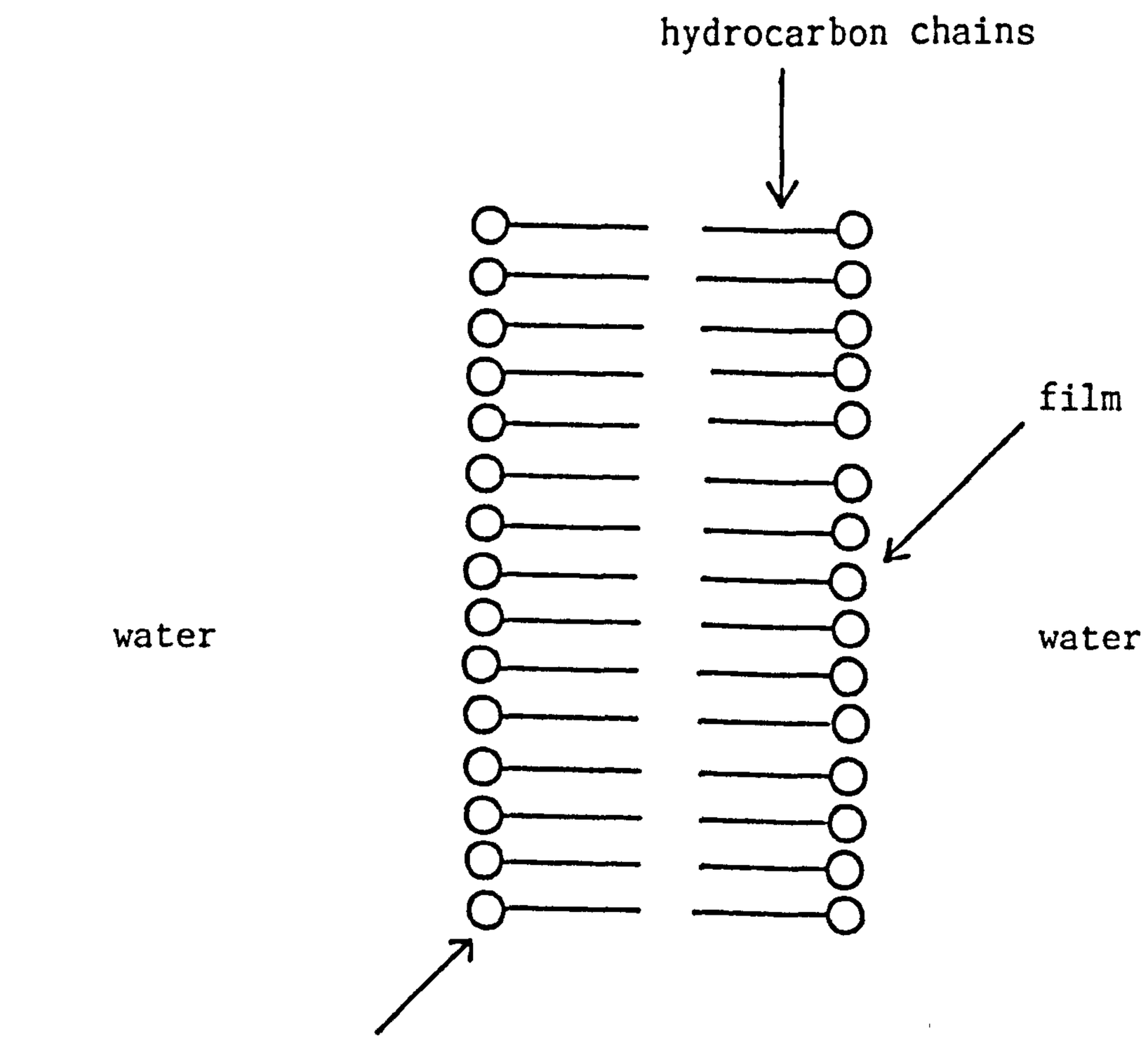

FIGURE 5.6: Schematic illustration of the structure of a bimolecular lipid film[192]

the hydrocarbon chains. Equilibrium black films are formed from these systems, i.e. liquid drainage proceeds until a constant thickness is attained less than 10nm, whereupon the film appears black in reflected light.

It is thought that the steric repulsive solvation force which may arise in thin free aqueous foam films (due to the steric interaction of water, adsorbed layer of surfactant and ions) may play a vital role in the determination of the stability of Newton black films[196]. The thickness of Newton black films (less than 10nm) is independent of electrolyte concentration which indicates that the repulsive force due to overlap of electrical double layers on opposing sides of the film is not important in determining its stability.

5.4 Capillary Pressure

The plateau border is known as the curved transition region, where a film meets the bulk solution. The radius of curvature of the surface changes in going from the film to the bulk solution, and a capillary suction or Laplace pressure exists at the border and is expressed by the Young-Laplace equation[53]

$$P_{\hat{\gamma}} = - \hat{\gamma}\left(\frac{1}{R_1} + \frac{1}{R_2}\right) \qquad (5.37)$$

where R_1, R_2 are the principal radii of curvature at the border and $\hat{\gamma}$ is the bulk interfacial tension. Hence $P_{\hat{\gamma}}$ is independent of film thickness and acts to thin the film.

Exerowa *et al*[193] have expressed the capillary pressure, $P_{\hat{\gamma}}$, for a horizontal film, radius R, with biconcave geometry formed in a vertical tube radius r

$$P_{\hat{\gamma}} = \frac{2\hat{\gamma}r}{r^2 - R^2} \qquad (5.38)$$

when $r \gg R$, equation (5.38) becomes

$$P_{\hat{\gamma}} = \frac{2\hat{\gamma}}{r} \tag{5.39}$$

which is independent of the radius of the film.

5.5 Gravitational Pressure

When a vertical foam film is in contact with the bulk solution, the gravitational pressure, P_G, acting at any part on the film can be expressed as

$$P_G = - \Delta\rho G z' \tag{5.40}$$

where $\Delta\rho$ is the difference in density between the liquid in the film and the surrounding medium, G is the gravitational constant, and z' is the height difference between the point on the film and the bulk solution with which the film is in contact at its lower plateau border. Equation (5.40) is applicable only if the film consists of a fluid of uniform and similar composition as the bulk solution[194].

5.6 Total Interaction Energy and Disjoining Pressure for a Foam Film

The total interaction energy, V_T, for a foam film may be written as a linear sum of the van der Waals energy, V_A, the electrical double layer repulsion, V_R, and a steric interaction energy, V_G. Thus for a foam film

$$V_T = V_A + V_R + V_G \tag{5.41}$$

and for each component of V_T in equation (5.41), an interaction force can be related to the interaction energy by the equations

$$F_A = \frac{\partial V_A}{\partial H_o}, \; F_R = \frac{\partial V_R}{\partial H_o}, \; F_S = \frac{\partial V_G}{\partial H_o}, \; F_T = \frac{\partial V_T}{\partial H_o} \tag{5.42}$$

where H_o is the film thickness, F_A, F_R, F_S and F_T are the forces corres-

ponding to the van der Waals energy, double layer repulsion, steric interaction energy and the total interaction energy in the film. Thus

$$F_T = F_A + F_R + F_S \tag{5.43}$$

In a foam film, the component forces in equation (5.43) act normal to the film and can be expressed as a pressure, so that, in general, there is a van der Waals interaction pressure, π_A, an electrostatic pressure, π_{el}, and a steric interaction pressure, π_s. These pressures act in a direction normal to the film, and their sum, π_D, has been termed the disjoining pressure by Derjaguin and Kussakov[195], hence

$$\pi_D = \pi_A + \pi_{el} + \pi_s \tag{5.44}$$

The sign of π_D is assumed to be negative when film thinning is aided, and positive when film thinning is hindered. Film drainage is affected by the gravitational pressure, P_G, and the capillary suction, $P_{\hat{\gamma}}$, (both are not normal forces). Their sum is termed the hydrostatic pressure, P_H,

$$P_H = P_G + P_{\hat{\gamma}} \tag{5.45}$$

when $P_H + P_D = 0$, a single free foam film is in equilibrium.

Schematic representations of the variation of the total potential energy for interaction V_T, with film thickness h, are shown in Figures 5.7(i)-(iv) for several types of foam film. The term V_H in Figures 5.7(iii) and (iv) refers to the interaction energy corresponding to the gravitational pressure, P_G, when the film thickness is h. Equilibrium foam films are thought to be at separations corresponding to the energy minima in these diagrams; the common black film corresponds to the secondary minimum, and is analogous to the flocculated state; whereas the Newton black film corresponds to the primary minimum and is analogous to the

(i) Uncharged horizontal film with steric cut-off

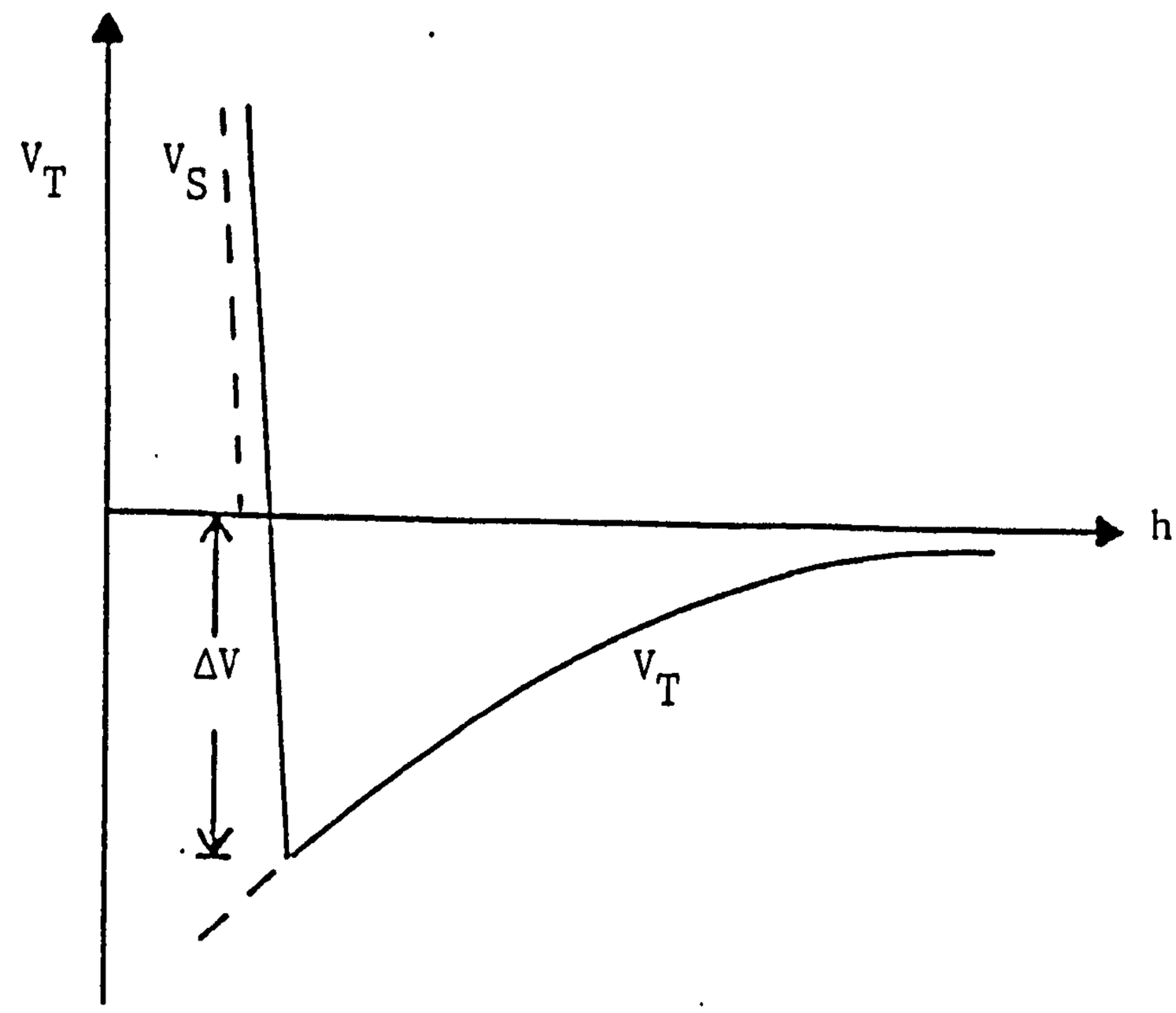

(ii) Charged horizontal film

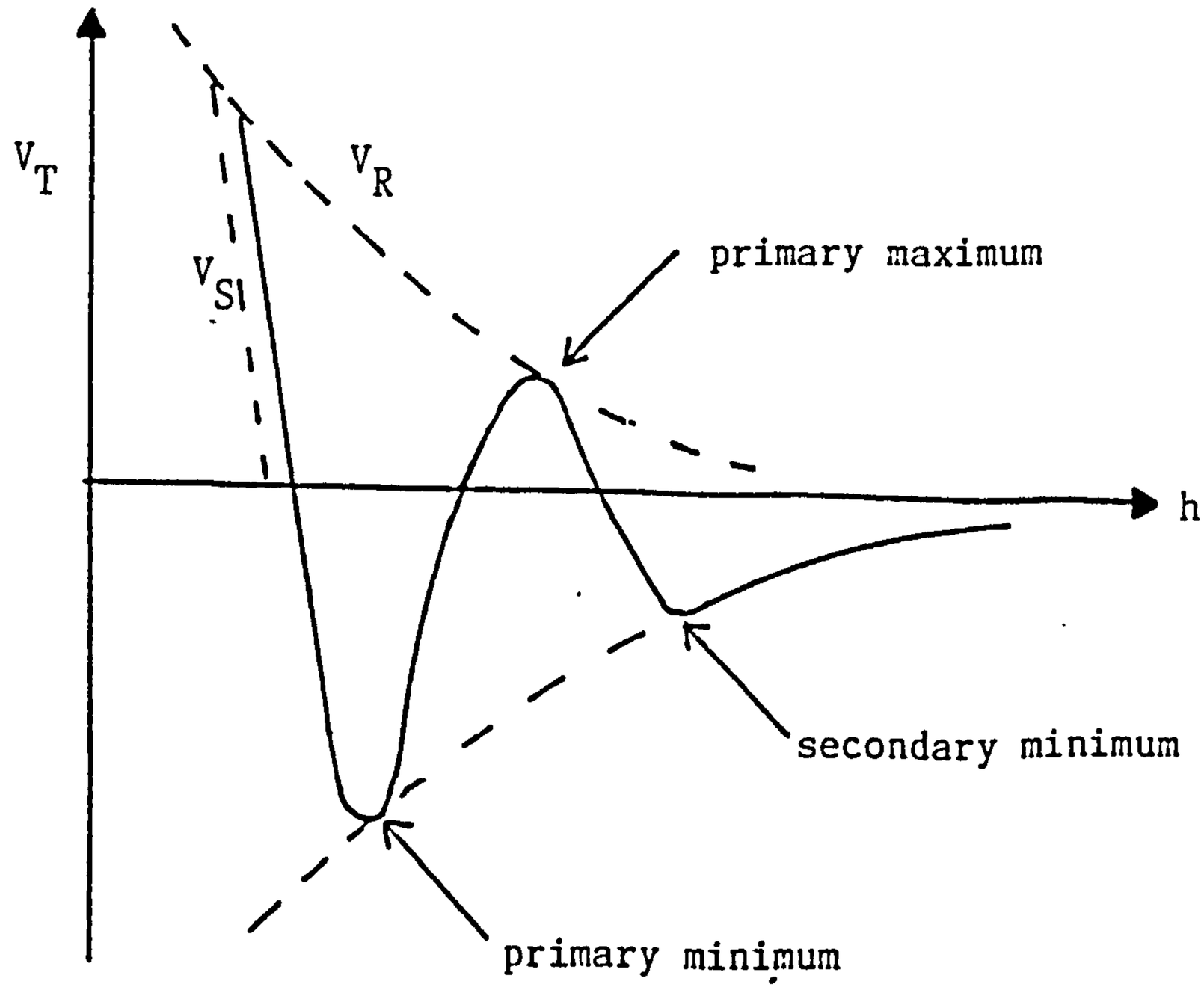

(iii) Charged vertical film

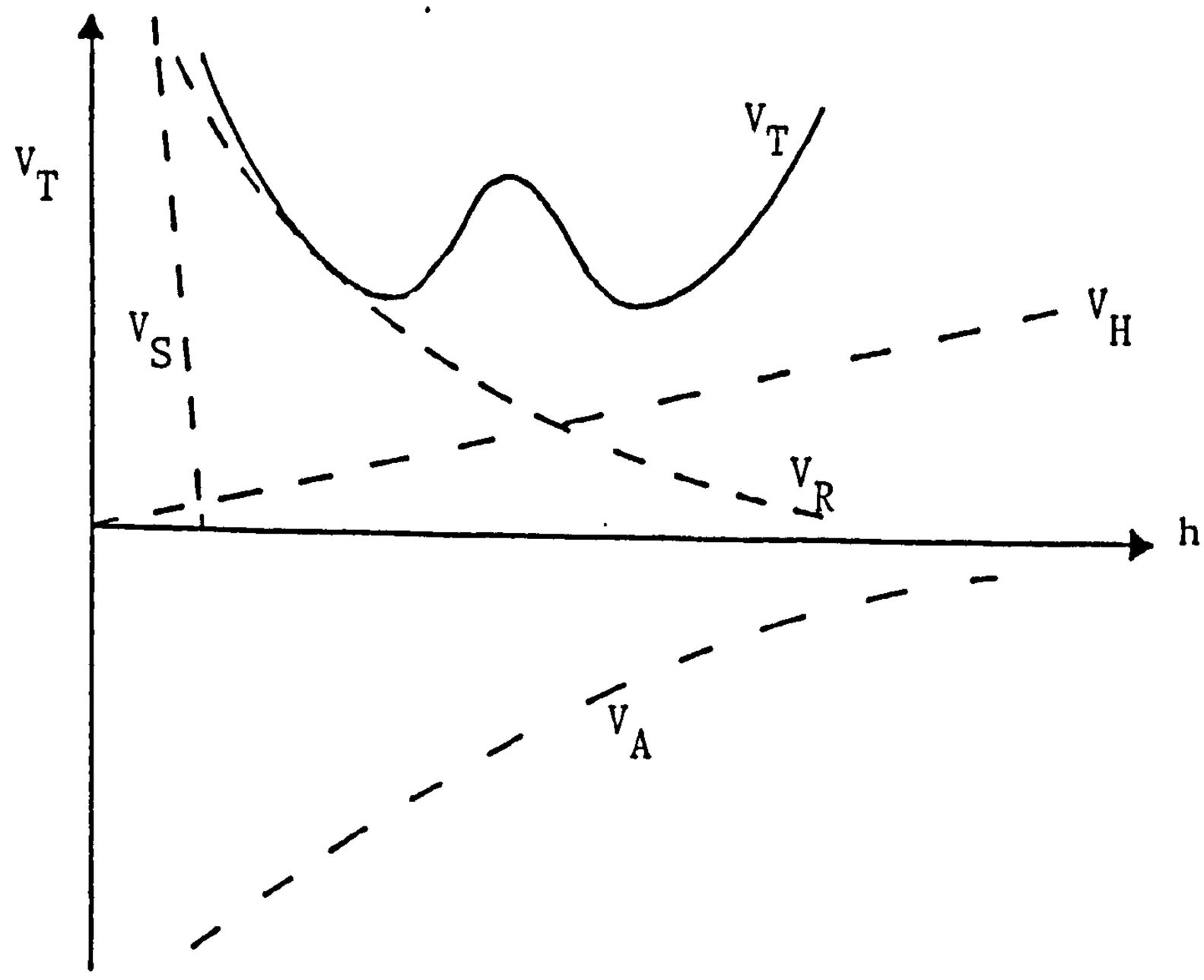

(iv) Uncharged vertical film with steric cut-off

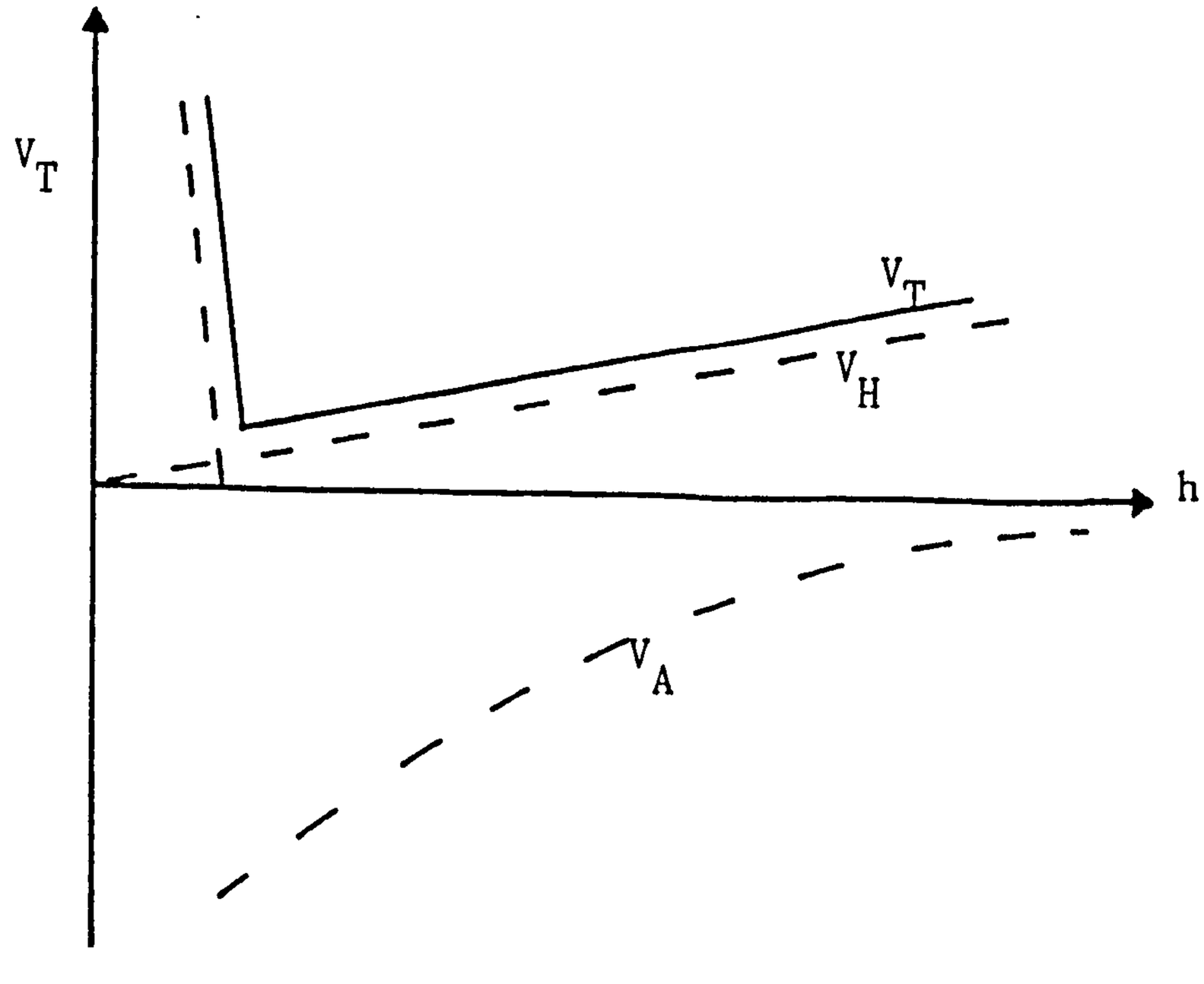

FIGURE 5.7: Schematic illustration of the variation of potential energy, V_T, with separation, h, for a foam film

coagulated state of lyophobic colloidal systems.

A relationship between the disjoining pressure, π_D, and the difference in potential energy between molecules in the film and bulk solution may be derived as follows[196]. The hydrostatic pressure in a bulk liquid is an isotropic quantity, but due to the asymmetric nature of the liquid film/vapour interface, the pressure in the film is anisotropic and can be represented as a normal component, P_N (of equal pressure as in vapour phase) and P_T, a tangential component responsible for the surface tension. The pressure in the film is represented as $\bar{p}$, and is generally a tensor quantity of magnitude $\frac{1}{3}(2P_T + P_N)$. The transfer of an amount of material from the bulk to the film for a one-component system (with the stress kept constant at the bulk liquid value), results in a change in chemical potential, $\Delta\mu$, due to the element interacting with a smaller number of molecules.

$$\mu_I^f - \mu^b_{(p^b,T)} = \Delta\mu \qquad (5.46)$$

where μ_I^f is the chemical potential of the element in the film and $\mu^b_{(p^b,T)}$ is the chemical potential of the element at an isotropic pressure, p, and bulk temperature, T.

The chemical potential change that occurs when the steady state of stress of the element changes from p^b to the midpoint plane value of the film, p^{-f}, is

$$\mu_{II}^f - \mu_I^f = \int_{p^b}^{p^{-f}} \left(\frac{\partial\mu}{\partial p}\right)_T dp \qquad (5.47)$$

When the liquid in the bulk solution and film is incompressible, then

$$\left(\frac{\partial\mu}{\partial p}\right) = v \qquad (5.48)$$

where v is the partial molar volume of the liquid. Combining equations (5.47) and (5.48) gives

$$\mu_{II}^{f} - \mu_{I}^{f} = (p^{-f} - p^{b})v \tag{5.49}$$

The chemical potential of the element in the film is μ_{II}^{f} where

$$\mu_{II}^{f} = \mu^{f}_{(p^{-f},T)} \tag{5.50}$$

hence, combining equations (5.46), (5.49) and (5.50) gives

$$\mu^{f}_{(p^{-f},T)} - \mu^{b}_{(p^{b},T)} = (p^{-f} - p^{b})v + \Delta\mu \tag{5.51}$$

For equilibrium between film and bulk solution

$$\mu^{f}_{(p^{-f},T)} = \mu^{b}_{(p^{b},T)} \tag{5.52}$$

substituting this into equation (5.51) gives

$$\frac{\Delta\mu}{v} = -(p^{-f} - p^{b}) \tag{5.53}$$

Derjaguin[197] has predicted that the disjoining pressure is the pressure difference that existed at the boundary of the film and the bulk phase necessary for the hydrostatic and capillary equilibrium of the system to be maintained. So, from equation (5.53), the disjoining pressure is equal in magnitude to the difference in potential energy per unit volume between the film and the bulk liquid molecules.

A relation between the contact angle that exists at the boundary of a foam film and bulk solution, and the depth of the energy minimum in which an equilibrium film resides, can be obtained likewise[197].

CHAPTER 6

THE DRAINAGE OF LIQUID FROM FOAM FILMS

The initial thinning that occurs when a foam film is formed is due to the action of capillary and vertical film gravitational pressures. Thinning is aided by the components of the disjoining pressure in the film. The drainage of liquid from the film to the bulk solution will continue until an equilibrium film thickness is attained, or film rupture occurs. The theories that have been developed to explain spontaneous rupture of foam films, and a brief description of the kinetics of thinning of single foam films, are described below.

6.1 Films, Plateau Borders and Foams

Initially, it is necessary to understand that in a foam individual films are separated from one another by liquid channels known as Plateau borders. These borders play a unique and important role in the behaviour of foams, both under static and dynamic conditions. All stresses on the foam film are exerted by, or transmitted through, the Plateau borders, and the liquid draining through the film has got to flow through them. More or less violent turbulent processes take place in the transition region between film and border during drainage, and these processes can greatly speed-up flow of liquid out of films.

6.2 Navier-Stokes Equation

In the motion of a fluid, the rate of accumulation of mass in a volume element bounded by a surface is equal to the rate of mass inflow minus the rate of mass outflow across the surface. This is expressed by the continuity equation[198]:

$$\frac{\partial \rho}{\partial t} + \text{div}(\rho v) = 0 \tag{6.1}$$

where ρ is the fluid density, t is the time, and v is the velocity of the fluid.

The divergence of a vector quantity, v, is defined for rectangular coordinates as

$$\text{div } v = \frac{\partial v_x}{\partial x} + \frac{\partial v_y}{\partial y} + \frac{\partial v_z}{\partial z} \tag{6.2}$$

where v_x, v_y and v_z are the components of v parallel to the x,y,z axes respectively. When the flow is steady and the fluid is incompressible (ρ is constant), equation (6.1) can be written as

$$\text{div } v = 0 \tag{6.3}$$

The Navier-Stokes equation describes the variation of pressure, p, and velocity vector, v, of a viscous Newtonian fluid (viscosity η) as a function of space and time coordinates. A viscous Newtonian fluid is one in which the components of shearing stress and rate of strain on an element are linearly related. The Navier-Stokes equation can be written in the form[198]

$$\rho\left[\frac{\partial v}{\partial t} + (v \text{ grad})v\right] = - \text{grad } p + \eta\nabla^2 v + pf + \frac{\eta}{3} \text{grad div } v \tag{6.4}$$

div v = 0 from the continuity equation for an incompressible fluid, hence the above equation reduces to

$$\rho\left[\frac{\partial v}{\partial t} + (v \text{ grad})v\right] = - \text{grad } p + \eta\nabla^2 v + pf \tag{6.5}$$

where the operators are defined as

$$\nabla^2 = \frac{\partial^2}{\partial x^2} + \frac{\partial^2}{\partial y^2} + \frac{\partial^2}{\partial z^2} \tag{6.6}$$

$$\text{grad } \phi = i \frac{\partial \phi}{x} + j \frac{\partial \phi}{y} + k \frac{\partial \phi}{z} \tag{6.7}$$

where ϕ is a scalar quantity and i, j, k are the unit vectors parallel

to the x, y, z axes. The two terms on the left-hand side of equation (6.5) are inertia terms and represent the product of mass and acceleration for a volume element. The Navier-Stokes equation is a non-linear differential equation because of the convective term, quantity (v grad)v, and this can be neglected for low liquid velocities. The first term on the right-hand side of equation (6.5) represents any force due to the change in hydrostatic pressure in the fluid, the term $\eta\nabla^2 v$ represents the viscous force due to momentum transferred between fluid layers moving with different velocity, and the term f represents external flow per unit mass of fluid acting on the body such as gravity. The x-component of the non-linear Navier-Stokes equation for an incompressible viscous Newtonian fluid can be written as

$$\frac{\partial v_x}{\partial t} + v_x \frac{\partial v_x}{\partial x} + v_y \frac{\partial v_x}{\partial y} + v_z \frac{\partial v_x}{\partial z} = - \frac{1}{\rho} \frac{\partial \rho}{\partial x} + \frac{\eta}{\rho}\left(\frac{\partial^2 v_x}{\partial x^2} + \frac{\partial^2 v_x}{\partial y^2} + \frac{\partial^2 v_x}{\partial z^2}\right) + f_x \qquad (6.8)$$

where η/ρ is the kinematic viscosity of the fluid and f_x is the x-component of the external force f. Similar equations apply to the y- and z-components of equation (6.8).

6.3 Radial Flow of Liquid Between Circular Plates

The application of Navier-Stokes equation (6.5) to the radial outflow of an incompressible liquid between two circular horizontal parallel plates, radius R, separation h, at time t when an external pressure is applied to the upper plate while the lower plate is fixed (Figure 6.1).

If the inertia and gravitational terms in equation (6.5) are assumed to be negligible, the Navier-Stokes equation can be written in cylindrical coordinates in the form[199]:

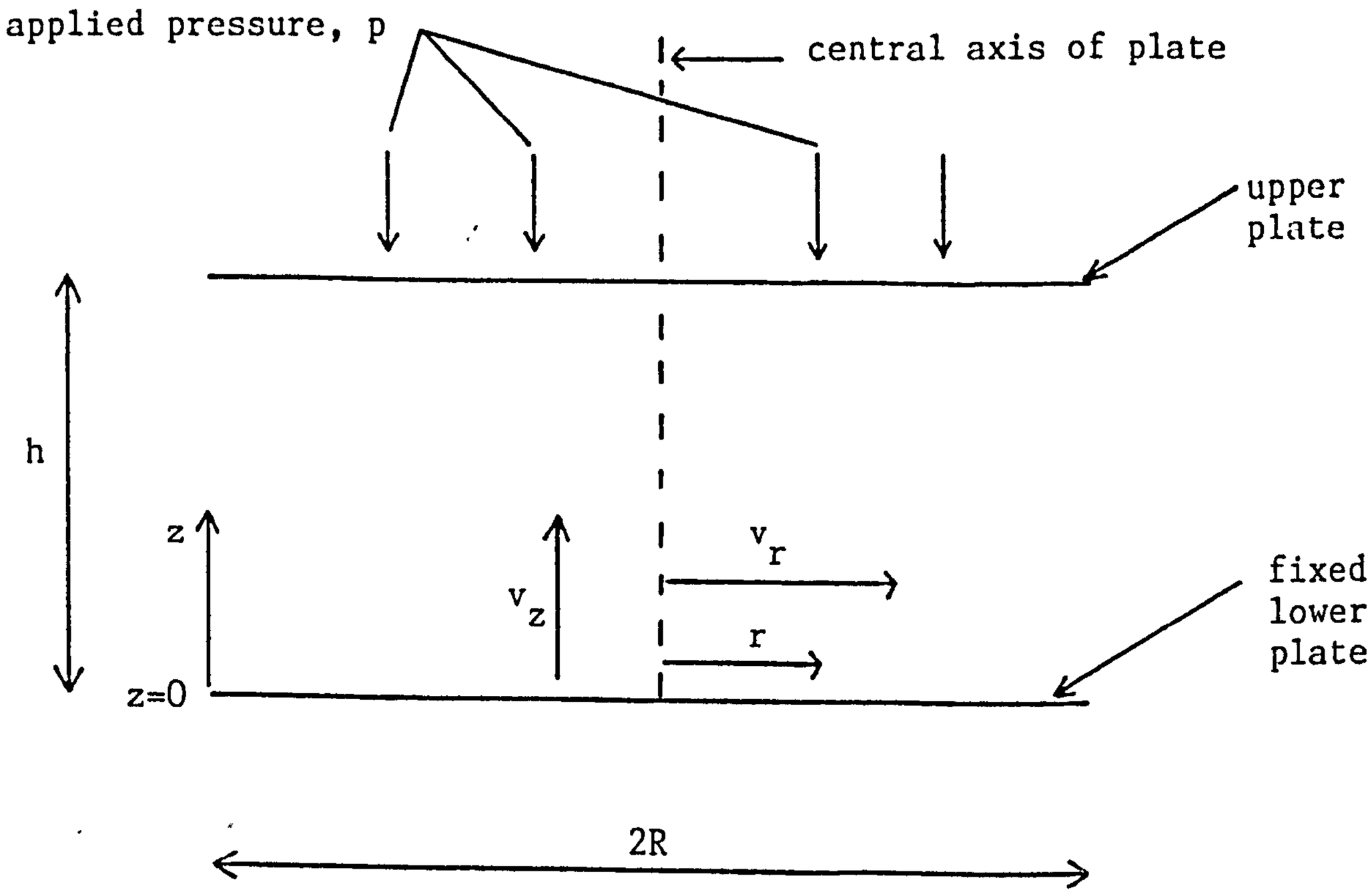

FIGURE 6.1: Co-ordinate system for radial flow of liquid between horizontal circular parallel plates

$$\frac{\partial^2 v_r}{\partial z} = \frac{1}{\eta}\frac{\partial p}{\partial v} \tag{6.9}$$

$$\frac{\partial p}{\partial z} = 0 \tag{6.10}$$

$$\frac{1}{r}\frac{\partial (r v_r)}{\partial v} + \frac{\partial v_z}{\partial z} = 0 \tag{6.11}$$

where v_r is the liquid velocity in the radial direction r, v_z is the velocity in the direction z measured up from the lower plate. The viscosity of the liquid, η, is assumed to remain constant during the outflow and p is the pressure acting downwards from the upper plate. If it is further assumed that no tangential motion of liquid occurs at the surface of the plates, then the following boundary conditions apply for equations (6.9), (6.10) and (6.11) when the lower of the two circular plates is fixed:

(i) at $z = 0$, $v_z = 0$ and $v_r = 0$;

(ii) at $z = h$, $v_z = dh/dt$ and $v_r = 0$;

(iii) at $r = R$, $p_v = 0$ where p_v is the viscous pressure in the liquid.

Reynolds[200] was able to show that the solutions of equations (6.9), (6.10) and (6.11), subject to the boundary conditions could (assuming only viscous forces acted in the system) be written as

$$\frac{d(1/h^2)}{dt} = \frac{4p}{3\eta R^2} \tag{6.12}$$

where p was the external pressure acting on the upper plate.

6.4 The Application of the Reynolds Equation to Foam Films

It is possible to apply Reynolds equation (6.12) to the liquid outflow from foam films. Here, the pressure, p (in equation (6.12)) can be written as

$$p = p_0 - \pi_D \tag{6.13}$$

where p_0 is the total external pressure acting on the film and π_D is the disjoining pressure in the film. Substituting equation (6.13) into equation (6.12) and integrating, one obtains,

$$\frac{1}{h^2} - \frac{1}{h_0^2} = \frac{4}{3\eta R^2}(p_0 - \pi_D)(t - t_0) \qquad (6.14)$$

where h_0 and h are the thickness at time t_0 and t respectively; R is the film radius and η is the viscosity of the material in the film. The variation of π_D with film thickness can be determined from the slope of the graph $(1/h^2 - 1/h_0^2)$ versus $(t - t_0)$ and hence determine whether the forces acting in the film are attractive or repulsive. With a thick film ($h \to \infty$, $\pi_D \to 0$), then true Reynolds flow occurs and the slope is linear[196] (see Figure 6.2). At equilibrium, when drainage has stopped, the following conditions can be applied:

$$\frac{dh}{dt} = 0 \text{ and } p_0 = \pi_D \qquad (6.15)$$

Thus, in order to produce an equilibrium film thickness, π_D must be sufficiently positive to counteract the capillary pressure effect, i.e. a repulsive force of sufficient magnitude must act on the film. So far, the analysis has assumed that transfer of liquid from film to bulk solution only occurs by viscous flow. However, transfer can also occur by the evaporation of liquid from the film followed by condensation onto the bulk liquid.

6.5 Drainage of Stationary Vertical Films

The drainage of an inextensible free vertical rigid foam film where the tangential velocity of liquid at the air/film interface is zero, and the disjoining pressure in the film, π_D, was assumed to be zero, has been discussed by Mysels *et al*[201]. The assumptions that the film was protected from evaporation, and that the flow was steady,

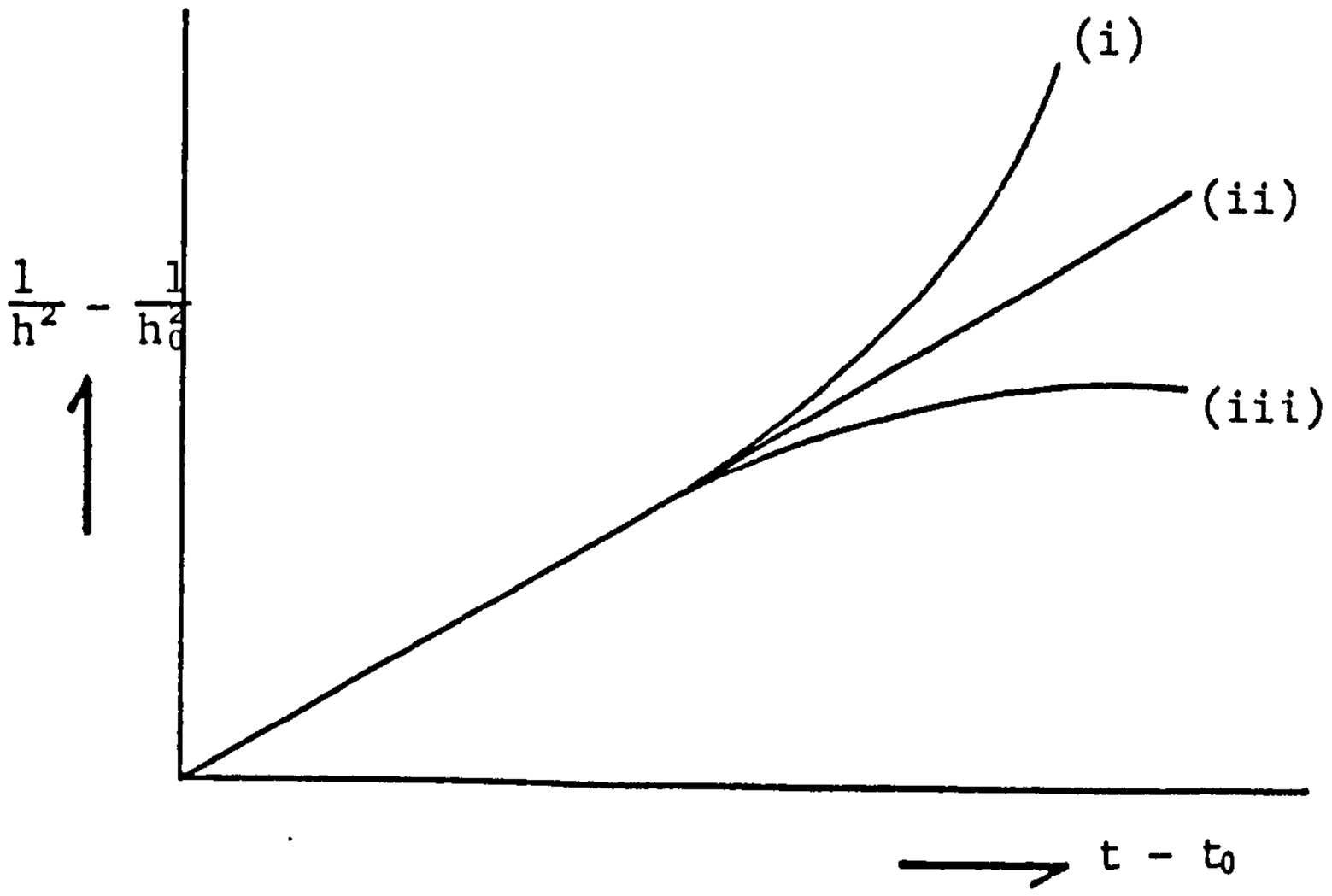

(i) With attractive normal forces between the film surfaces;

(ii) Reynolds flow;

(iii) With repulsive normal forces between the film surfaces.

FIGURE 6.2: Schematic illustrations of $1/h^2 - 1/h_0^2$ against $t - t_0$ for a circular horizontal parallel-sided foam film[196]

which enabled the weight of an element of liquid to be balanced by the viscous forces acting on the element, were also made. The volume flow rate per unit film width, Q, was given by

$$Q = \frac{\rho g h^3}{12\eta} \tag{6.16}$$

where ρ, η, h and g are the liquid density, liquid viscosity, film thickness and gravitational constant respectively. The term ρg in the equation has dimensions of a pressure gradient. The thickness, h, at a distance z, measured downwards from the top of the film, was related to the draining time, t, through the equation

$$h^2 = \frac{4\eta z}{\rho g t} \tag{6.17}$$

which, when differentiating h with respect to r at constant z followed by the elimination of t, gives

$$\frac{d(1/h^2)}{dt} = \frac{\rho g}{4\eta z} \tag{6.18}$$

Johannes and Whitaker[202] have analysed both the effects of surface shear and dilational viscosities on the gravitational drainage ($\pi_D = 0$) of a surfactant stabilized foam film; while the rigid films investigated by Mysels *et al*[201] corresponded to an infinite surface viscosity.

6.6 Drainage of a Moving Vertical Foam Film

Mysels *et al*[201] have analysed the effect of withdrawing a vertical film with velocity v from a solution on the film thickness, h. The hydrostatic pressure in the flat film is greater than in the Plateau border, and changes in the transition region connecting the film to the border. The pressure in this region is determined by the curvature of the film surface and the pressure difference between the film and border

causes a viscous laminar flow of liquid into the border.

In a steady state, the volume of flow per unit width of film, V_h, is given by

$$V_h = 2V_y + \left(\frac{2y^3}{3\eta}\right)\hat{\gamma}\,\frac{d^3y}{dx^3} \qquad (6.19)$$

where $\hat{\gamma}$ and η are the liquid surface tension and viscosity respectively, x is a coordinate measured in the direction of drawing, and y is a ordinate measured perpendicular to x.

The line y = 0 was placed symmetrically in the film, and the term ($\hat{\gamma}\ d^3y/dx^3$) represented the pressure responsible for the drainage.

Overbeek[203] has allowed for the presence of a van der Waals force and electrical double layer forces acting in the film on the drainage of a moving vertical film. These forces vary in the transition region due to the variation in thickness in that region, and give rise to pressure gradients in the film which aid or hinder drainage.

6.7 Marginal Regeneration

Due to the curvature at the Plateau border, a capillary suction exists whereby there is a rapid downward flow of liquid from the film through the border to the bulk solution. Mysels *et al*[201] have suggested that there is a much stronger suction action on a thick film than on a thin film; hence, the thick film tends to be drawn into the border while the thin film is drawn out of the border. The thick film that is drawn into the vertical border flows downwards under gravity while, simultaneously, the thinner film pulled from the border rises through the film until it reaches a level of the same density and thickness. This process is known as marginal regeneration, and was considered to be an important mechanism by which mobile films become thinner.

6.8 Film Rupture and Surface Fluctuations

The drainage in a foam film stops when either an equilibrium thickness is reached or spontaneous film rupture occurs. A foam film is a thermodynamically unstable system due to the surface energy it possesses, and if a hole is formed in a film it will grow to release the surface energy of the system. Some films similar to those formed from aqueous solutions of surface-active agents can form kinetically metastable equilibrium states that require an external agent, such as vibrations, to cause rupture.

De Vries[204] has analysed the change in surface area when a circular hole was formed in a plane parallel film, assuming that the inner surface of the hole remained circular during expansion, after the hole was formed.

The surface tension tends to make the air/film interface as flat as possible, but thermal motions cause surface ripples or corrugations in a macroscopically plane parallel foam film.

Vrij[205] has shown that values of the second derivative of the potential energy, v, with respect to film thickness, d^2v/dh^2, can be obtained from measurement of the mean intensity of light scattered from a foam film. For a free liquid film there are two possible, but different, modes for surface corrugations: the first is a stretching mode (symmetric wave) in which both surfaces moved parallel to each other; and the second is a squeezing mode (antisymmetric wave) where both surfaces moved anti-parallel to each other.

Scheludko[206] assumed that the corrugations on the surface of a foam film were cylindrical, with radius r and wavelength λ (see Figure 6.3). A capillary pressure, $\pi_{\hat{\gamma}}$, acting normal to the film, tended to

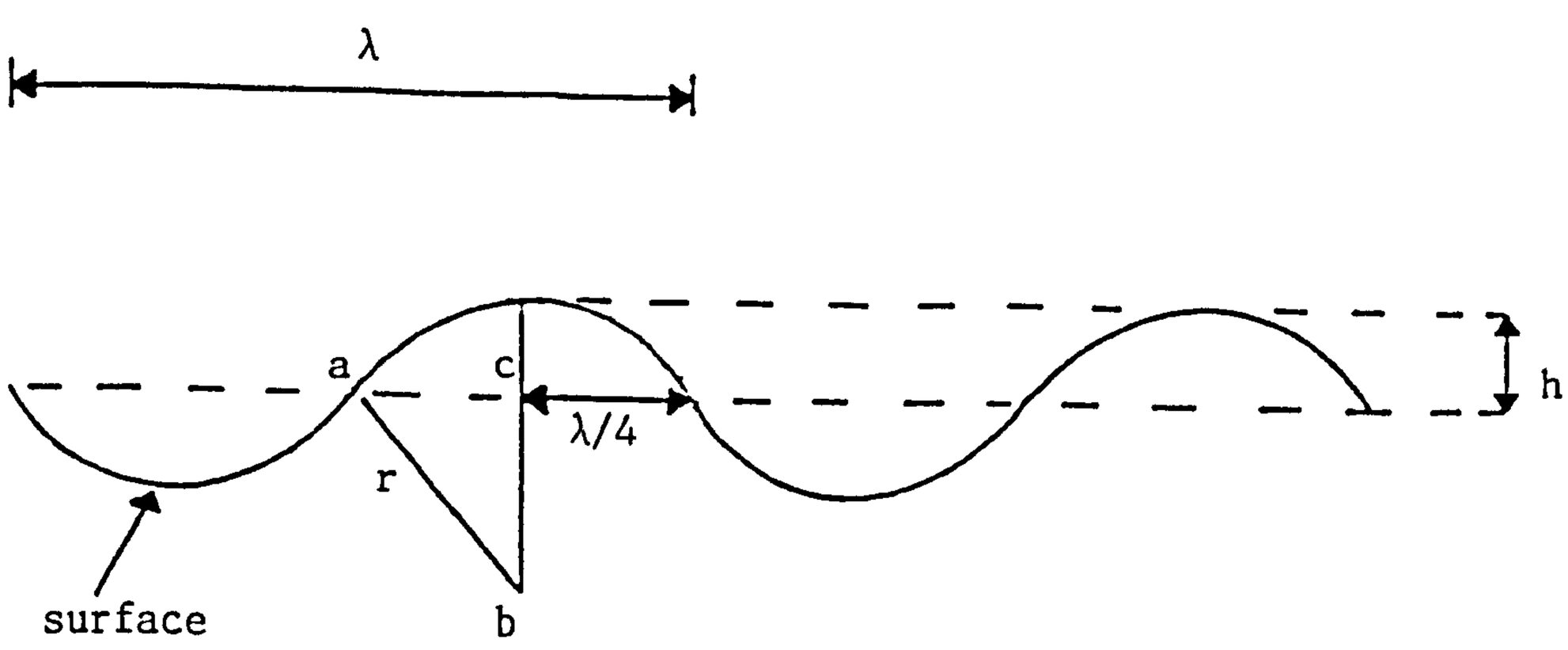

FIGURE 6.3: Schematic diagram for sinusoidal surface corrugation on a foam film

cause film thickening and its magnitude, given by the Young-Laplace[93] equation was

$$\pi_{\hat{\gamma}} = \frac{2\hat{\gamma}}{r} \tag{6.20}$$

where $\hat{\gamma}$ was the interfacial tension and r was the radius of the surface corrugations. The van der Waals disjoining pressure, π_A, was assumed to be the only component of the disjoining pressure π_D and π_A acted in the opposite direction to $\pi_{\hat{\gamma}}$. Film rupture occurred when

$$\frac{d\pi_A}{dh} > \frac{d\pi_{\hat{\gamma}}}{dh} \tag{6.21}$$

where h is the thickness of the film, and a critical thickness at which rupture occurred, h_{cr}, was taken as the thickness when

$$\frac{d\pi_A}{dh} = \frac{d\pi_{\hat{\gamma}}}{dh} \tag{6.22}$$

Scheludko[206] calculated the critical thickness of rupture to be independent of the viscosity of the film but dependent on the surface tension of the bulk solution from which the film was formed.

The free energy of a foam film can be affected by fluctuations in the film thickness in two ways; firstly, the component due to interaction forces, π_D, is altered; and secondly, the change in surface area due to fluctuations leads to a perturbed value of the interfacial energy of the system. Vrij[207] and Vrij and Overbeek[208] have represented the surface corrugations as independent standing waves whose amplitudes were represented by time-dependent exponential functions. This enabled them to derive a value summed over two energy terms for the critical thickness of rupture, h_{cr}, given by the expression

$$h_{cr} = \left(\frac{A\lambda_{cr}^2}{4\pi^2\hat{\gamma}}\right)^{\frac{1}{4}} \tag{6.23}$$

It was assumed that non-retarded van der Waals forces acted on the film and that $\pi_A = \pi_D$. It was also assumed that during the growth of the corrugations tangential motion of any surfactant present on the surface did not occur. Vrij's[207] theory has a distinct advantage over that of Scheludko[206], for the values for the critical thickness of rupture can be evaluated from experimental quantities.

6.9 The Effect of Surfactant on the Drainage of Single Free Foam Film

The application of Reynolds' equation (6.12) to the drainage of a foam film assumes that no tangential motion of liquid occurs at the air/film interface. However, when surface-active material is present in a film, diffusion of surfactant molecules from the bulk to the surface, the adsorption there, and surface diffusion may occur and affect the drainage of liquid from the film.

The normal and tangential stresses are continuous across the air/film interface when the latter is subjected to periodic disturbance; the normal stress depends on the curvature and the surface tension at the surface, while the tangential stress depends on the surface tension gradient at the surface. When a surfactant is present as a monolayer on the surface, the surface concentration of surfactant changes continuously from its value on the unperturbed surface, as the wave undergoes a periodic motion; there is a point in the surface at which the surface tension changes continuously. If the surfactant is soluble, there is an exchange between the bulk and the surface molecules; and if the wave motion is sufficiently low, the molecules in the bulk and surface phases can remain in chemical equilibrium. But if this wave motion occurs too rapidly for the equilibrium to be maintained, then exchange will not take place.

A general approach used for the determination of the surfactant effect on liquid drainage from and rupture of foam films has been to solve the Navier-Stokes equation for the viscous flow of liquid in the film subjected to a periodic disturbance at the air/film interface, in conjunction with the equations describing the conservation of mass in the transfer of surfactant to the surface. Film rupture occurs when a solution to the equations in which the amplitude of the surface wave grows with time can be found. Ruckenstein and Jain[209,210] considered the stability of a liquid film on a solid surface, and the distance was represented as a time-dependent exponential function. Gumerman and Hormsy[211] have expressed the critical thickness of rupture, h_{cr} (when $\pi_D = \pi_A$) as a dimensional critical aspect ratio h_{cr}/R, where R is the radius of the film.

Ivanov *et al*[212,213] analysed h_{cr} for a foam film in terms of the film radius, surface tension and disjoining pressure using the Navier-Stokes equation; the calculated value for h_{cr} was not a function of surfactant concentration. When the effect of surface diffusion on the drainage of single foam films was allowed for (this was neglected by Radoev *et al*[214]), the drainage rate, V (= dh/dt) of a film stabilized with soluble surfactant was found[215] to be greater than the drainage rate V_{Re}, calculated according to the Reynolds equation. An expression for the ratio V/V_{Re} was derived in the form

$$\frac{V}{V_{Re}} = 1 - \left(1 + \frac{2D_s}{D_b h}\frac{\partial \Gamma_0}{\partial c_0}\right)\frac{3D_b \eta}{\Gamma_0\ \partial \hat{\gamma}_0/\partial c_0} \qquad (6.24)$$

where D_s, D_b, η and h were the coefficients of surface and bulk diffusion, bulk liquid viscosity and film thickness respectively. The terms Γ_0 and $\hat{\gamma}_0$ referred to the surface concentration and surface tension when no perturbation of the surface occurred, and c_0 referred to the concen-

tration of surfactant in the interior of the film which was taken as the bulk surfactant concentration when no surface perturbation occurred.

Ivanov and Dimitrov[216] have also considered the effect of a constant shear viscosity, η_s, on the drainage of the foam films, and have obtained a value for V/V_{Re} as defined in equation (6.24); this transformed into equation (6.24) when $\eta_s = 0$ and the Reynolds equation when $\eta_s = \infty$.

Lucassen *et al*[217] and Vrij *et al*[218] analysed the effect of a surface elasticity, ε, of an adsorbed layer on the growth of fluctuations in a film surrounded by a liquid medium, and extended their analysis to free liquid films. The surface elasticity was defined by equation (4.1)

$$\varepsilon = \frac{d\hat{\gamma}}{d\ \ell n\ A}$$

where $\hat{\gamma}$ is the surface tension and A is the surface area. When $\varepsilon = 0$, the interfaces are mobile and when $\varepsilon = \infty$, as was assumed by authors (207) and (208), the interfaces were rigid and no tangential motion occurred. Vincent[219] has reviewed the similarity of drainage in foams and emulsions. He suggested that the liquid films of continuous phase formed in an emulsion or foam experienced two stages in their lifetimes before catastrophic breakdown could occur leading to coalescence. That in the early stages, whilst the films were thick, gravitational forces were primariliy responsible for their drainage, since steady drainage in a film requires a high dilational elastic modulus, ε, for the two interfaces concerned, which has to be provided by adsorbed surfactant molecules, then the solvent flow in the boundary regions of the film (i.e. close to the two interfaces) was impeded by the tendency for interfacial tension gradients to be created. Hence a velocity profile across the

film resulted (i.e. similar to capillary flow). If ε was too low, on the other hand, drainage was too rapid, resulting in film collapse and rupture. For thick films undergoing steady drainage, some idea of the drainage rate could be obtained from the arguments presented by Mysels *et al*[201] for a single soap film. Clearly, in a foam or emulsion consisting of a series of interconnecting liquid films, further drainage was governed by the capillary forces and took place through the interconnected Plateau border channels.

CHAPTER 7

EXPERIMENTAL DETAILS

Two separate Langmuir film balances were used; one was manually operative, with the trough made of fluon-coated duralumin, while the other was fully-automatic with the trough made of glass.

Initially, a brief description of the experimental procedures when using the manually-operated trough will be outlined, followed by a description for the fully-automated trough. The latter trough was particularly useful in helping with partial characterization of some polydimethylsiloxane polymers.

Experiments using a torsion pendulum surface viscometer and an oscillating ring surface rheometer are also outlined, and the foaming experiments used to determine the antifoaming abilities of polydimethylsiloxanes are finally described.

7.1 Materials

7.1.1 Used on the Fluon-Coated Trough

Double-distilled water was used in all the experiments.

Alkanoic acids such as myristic and stearic acids used on this trough were obtained fromBDH Chemicals Ltd., and had melting points of 53.5-55^{o}C and 70-71^{o}C respectively. The spreading solutions of both acids were prepared by dissolving known amounts in petroleum ether (bp. 60-80^{o}C), the concentrations being of the order of 1mg cm^{-3}. For the time-dependence experiments, the myristic acid solution was delivered to the water surface via a micropipette syringe (Scientific Glass Engineering Property Ltd.), whilst in the other experiments the acids were

delivered from an Agla micrometer syringe, capable of adding volumes as small as 0.01cm^3 to an accuracy of within $\pm$0.00005cm^3. The purity of the spreading solvent was tested by performing blank experiments where the solvent alone was added to the water surface. No reduction of the surface tension was observed, thus demonstrating the absence of any amphiphilic contaminants in the solvent. 2.5×10^{-4}M cadmium sulphate was present in the subphase for the viscosity measurements.

7.1.2 Used on the Joyce-Loebl (Glass) Trough

All experimental work was carried out using an aqueous subphase based on water from a 'milli-Q' system. The pH of the subphase was conveniently adjusted by the addition of hydrochloric acid or ammonium hydroxide solutions of AR purity. Sodium and copper (II) ions were added to the subphase from sodium chloride and copper (II) chloride solutions respectively. The long-chain alkanoic acids of $C_{17}H_{35}COOH$ (stearic) to $C_{19}H_{39}COOH$ (arachidic) were obtained from BDH Biochemicals and of 99% minimum assay (GLC). The alkanoic acids $C_{13}H_{27}COOH$ (myristic) to $C_{16}H_{33}COOH$ (heptadecanoic) were obtained from fluka AG, and of >99% GC. The polydimethylsiloxanes were supplied by BP Research Centre, Sunbury-on-Thames, and had weight-average molecular weights ranging from 6610-110000. Mixtures of these polymers were also prepared and used.

The spreading solvents were 'Analar' chloroform for the fatty acids and re-distilled n-hexane for the polydimethylsiloxane polymers respectively.

7.1.3 Used on the Torsion Pendulum Surface Viscometer

The bob and the trough were cleaned with 'Analar' ethanol, chloroform and then double-distilled water. The alkanoic acids and polydimethylsiloxanes were obtained from BDH Biochemicals and BP Research Centre,

Sunbury-on-Thames respectively.

The acids $C_{17}H_{35}COOH$ (stearic) to $C_{19}H_{39}COOH$ (arachidic) were spread from 'Analar' chloroform, while the polydimethylsiloxanes of weight-average molecular weights 6610, 31000 and 110000 were spread from re-distilled hexane on triple-distilled water. The aqueous subphase at pH ∿2 was prepared from dilute hydrochloric acid.

7.1.4 Used on the Oscillating Ring Surface Rheometer

The acids $C_{13}H_{27}COOOH$, $C_{17}H_{35}COOH$-$C_{19}H_{39}COOH$, and $C_{22}H_{45}COOH$ (tricosanoic) were spread from 'Analar' chloroform, while the polydimethylsiloxanes of weight-average molecular weights 6610, 31000, 110000 and a mixture M_{3C} (containing a 3:1 molar proportion of 31000+48150) were spread from re-distilled hexane on 'milli-Q' water. The aqueous subphase was pH ∿2.

7.1.5 Used for Measuring Antifoaming Ability

1. Aerosol OT (dioctyl ester of sodium sulphosuccinic acid); this is an anionic surfactant, and ethanediol were BDH reagent and analar grade respectively.
2. Offshore Magnus and Ninian Crude Oils ('stabilised' and kept under a jacket of nitrogen), were obtained from BP Research Centre, Sunbury-on-Thames.

Silicone Antifoams

Dow Corning Ltd. 200 series silicone oils. These oils were polydimethylsiloxanes of the general formula:

$$(CH_3)_3Si\left[(CH_3)_2SiO\right]_n Si(CH_3)_3$$

Molecular weights used were 6610, 14420, 19100, 31000, 48150 and 110000, and the mixtures were varying molar proportions of the (6610+19100) and

(31000+48150) polydimethylsiloxanes.

Profoamer

3M Co. Ltd. fluorocarbon surfactant FC740 is a non-ionic surfactant belonging to the chemical class of perfluoroalkyl polymeric esters. However, the molecular weight was unknown.

The model crude oil was a 3% (w/v) solution of aerosol OT in ethanediol, and polydimethylsiloxane concentrations of 10% (w/v) in distilled petroleum ether(in the boiling point range 60-80^{o}C) were used.

7.2 The Fluon-Coated Duralumin Trough (Plate 7.1)

The apparatus consisted of a trough with two compartments separated by a barrier containing a canal of adjustable width. The flow of material at the air/water interface depended upon a difference in surface pressure, $\Delta\pi$, between the ends of the canal of length ℓ (1.26cm) and width 2a (0.03cm). The depth (1.68cm) of the canal was very large compared to the width.

The measurements consisted of the determination of the surface flux, i.e. the area of film per unit time, Δs, which, under a constant pressure drop, flows from compartment I into compartment II. The surface pressure in compartment I, π_1, was maintained by the simultaneous movement of the teflon barrier. Occasionally it was found that compartment II was sufficiently large that the surface pressure in this section, π_2, was always very much smaller than π_1, i.e. $\Delta\pi = \pi_1 - \pi_2 \simeq \pi_1$.

The surface pressure, π_1, was obtained from the pressure-area isotherms of the acids.

PLATE 7.1: The duralumin Langmuir trough

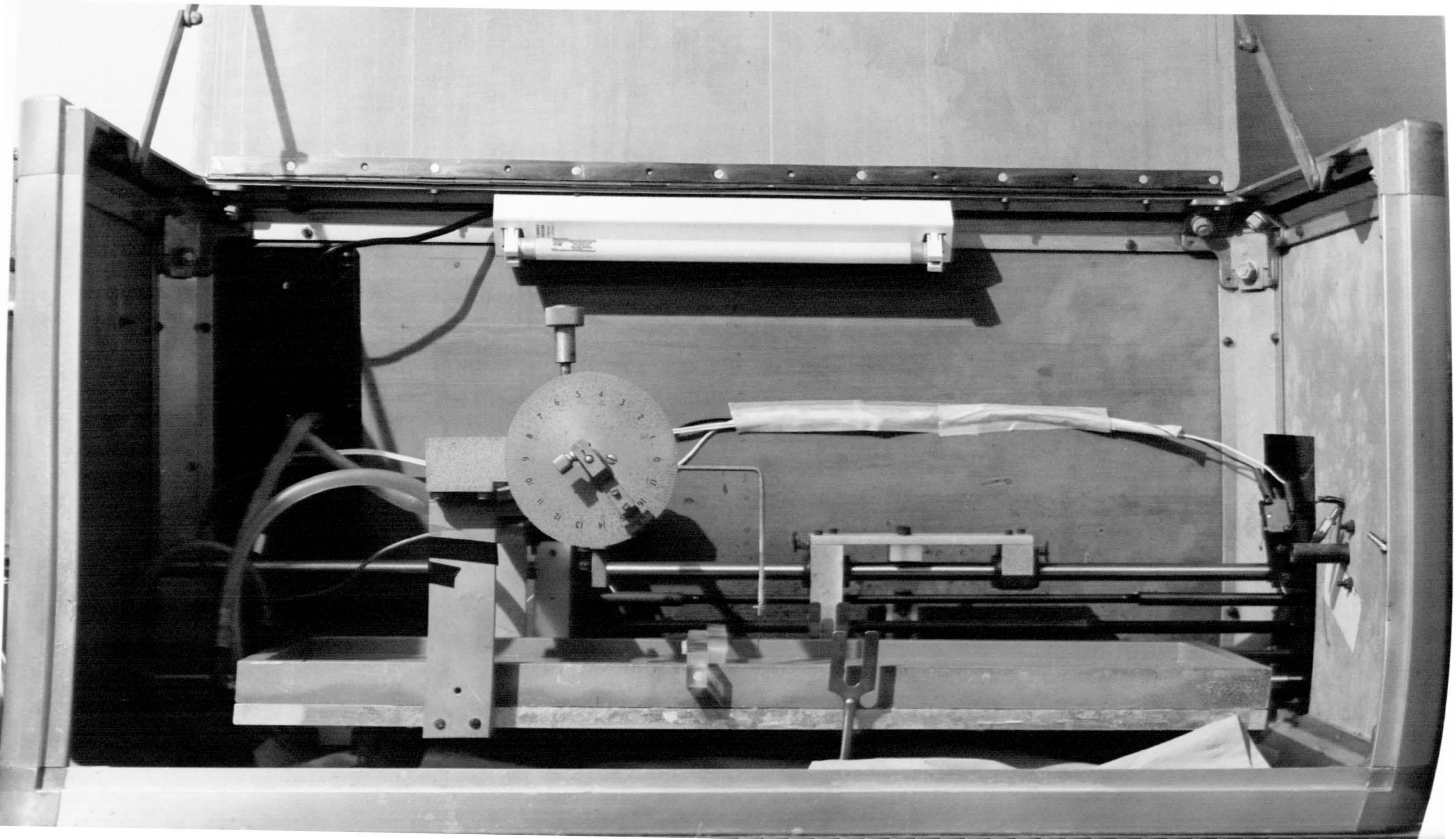

7.2.1 Analysis of Data

The experimental data were obtained as the area of compartment I, A_1, as a function of time, t, at a constant surface pressure, π_1. A logarithm-logarithm plot was used to give A = f(t) as smoothed data. The area lost or transferred was calculated using the slope of the A = f(t) plot.

The surface flux, Δs, was obtained from the differential of the area lost, A_1, i.e.

$$\Delta s = \frac{dA_1}{dt} \qquad (7.1)$$

The surface concentration of material on compartment II was calculated in order to correct for the back pressure, π_2, and this was used to calculate the pressure drop,

$$\pi_1 - \pi_2 = \Delta\pi.$$

7.2.1.1 Calculation of the Surface Shear Viscosity, η_s

For very narrow canals, Poiseuille's formula in two-dimensions gives a very good description of the flow[220,223]:

$$\eta_s = \frac{2a^3}{3q} \qquad (7.2)$$

where the reduced flux, $q = \Delta s.\ell/\Delta\pi$ and $\Delta s = dA_1/dt$. Therefore equation (7.2) becomes

$$\eta_s = \frac{2a^3}{3\ell} \frac{\Delta\pi}{dA_1/dt} \qquad (7.3)$$

7.2.2 Description of Apparatus

The arrangement of the instrument is shown in Figure 7.1. It is a shallow rectangular tray made of fluon-coated duralumin. The top edge of the trough was coated with paraffin wax to make it hydrophobic. This enabled the trough to be filled to the brim, so that sweeping with the

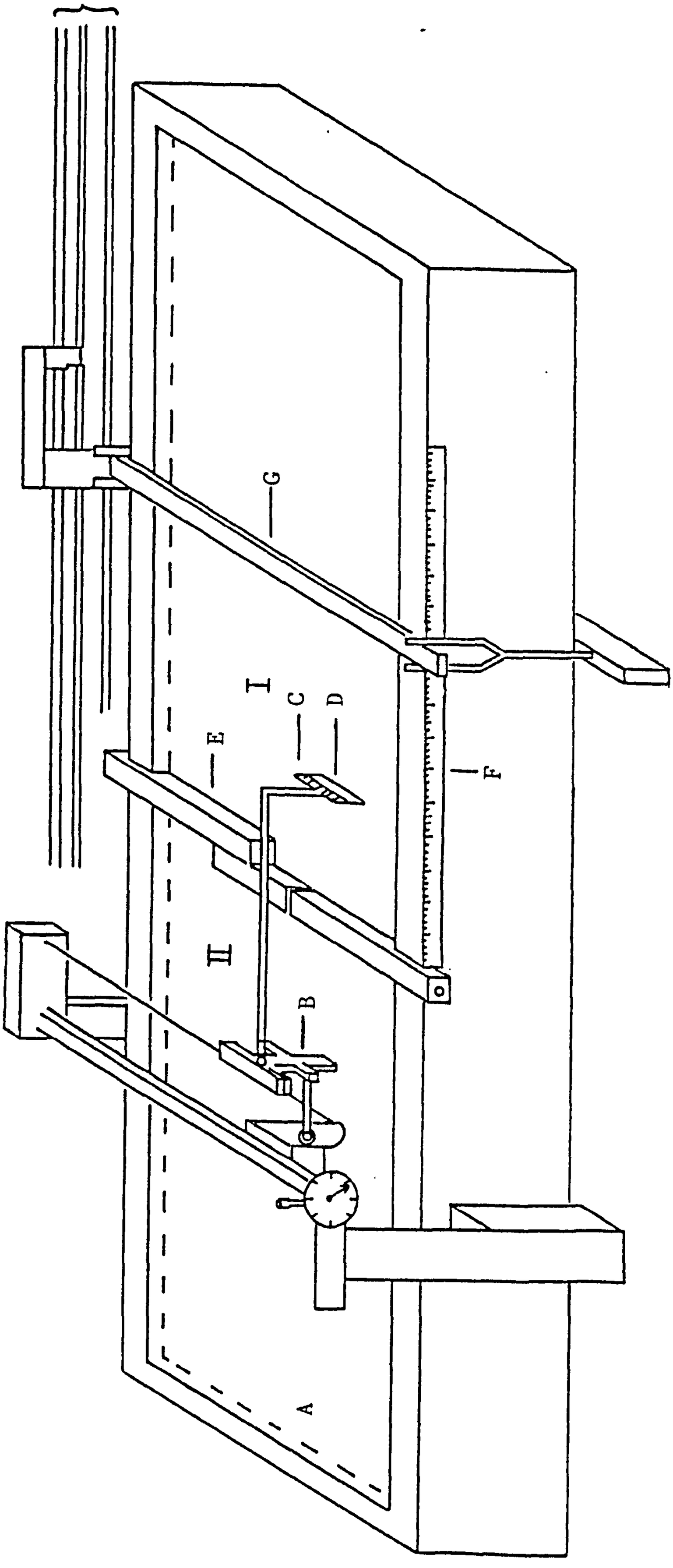

FIGURE 7.1: The Duroalumin Langmuir Trough. A = fluon-coated duralumin trough; B = transducer; C = mica; D = Wilhelmy plate; E = perspex block; F = ruler; G = PTFE barrier

barriers would be effective.

The moveable barriers were normally controlled by a sweep device which was driven by a controlled motor (this was situated outside the box in which the trough itself was placed). The box was used so that a controlled atmosphere could be maintained over the film. The motor was removed because its vibrations caused surface waves when used to drive the barrier, and this produced an unacceptable uncertainty in the Wilhelmy plate readings. Hence, the sweep was controlled by turning the rod connection to the barrier manually.

The trough was divided by two separate blocks of perspex inter-joined to give a very narrow canal. It was found that unless the inner surfaces of the canal were hydrophobic, the level of the liquid in the canal was higher than that on either side due to capillary rise, thereby obstructing the flow of the film. The nature of the canal was in fact quite critical, for the more hydrophobic the surfaces the greater the flux of film through it. Therefore, a light coating of paraffin wax was applied and then allowed to harden thoroughly before commencing any experiment.

The surface tension was monitored by way of a Wilhelmy plate tensiometer constructed from a microscope cover-slip (48x22mm) situated in front of the canal and dipping into the solution. The Wilhelmy plate was suspended from a torsion balance arm and pivoted against a pressure transducer. The transducer output was connected to an X-T chart recorder, where the surface tension could be read easily. A constant transducer output was maintained during flow by using the barrier to reduce the area gradually. The accuracy of the chart recorder was $\pm 0.2 mNm^{-1}$.

7.2.3 Time-Dependence of Surface Shear Viscosity

By using this apparatus, it was possible to observe and monitor the time-dependence of the shear viscosity of various surface concentrations of fatty acid monolayers (myristic acid taken as an example) uninfluenced by evaporation of the solution and contamination from the surrounding atmosphere.

Experiments were performed where various quantities of the fatty acid were added to both sides of the canal. The aim of these experiments was two-fold. Firstly, a check on the flow onto a surface already occupied was required; and secondly, to monitor the dependence of the viscosity on applied stress.

The experiments consisted of adding a constant volume of myristic acid solution to compartment II and measuring the flow rate with various surface concentrations on compartment I. The surface pressure-area isotherm of myristic acid was used to convert the area per molecule into surface pressures where possible, and the surface pressure on compartment II was maintained at a constant level. The surface shear viscosities were obtained using equation (7.3).

7.2.4 Experimental Procedures

7.2.4.1 Calibration of the Wilhelmy Plate and Chart Recorder

To calibrate the instrument, known weights, w, were suspended from the plate and the deflections, α, recorded. The deflections against weights produced a straight-line plot, and therefore the following equation was used:

$$\alpha = kw \qquad (7.4)$$

where w is the weight hung from the Wilhelmy plate and k is a constant.

The downward force on the Wilhelmy plate of the water was 7.2mN,

since the surface tension of water, γ_0, was $72mNm^{-1}$ and the length of the Wilhelmy plate in contact with the water was 0.1m. When the long-chain fatty acid was added to the surface, the surface tension was lowered and therefore the force on the plate decreased. The change in deflection of the chart recorder could be related to the decrease in force by

$$\frac{\Delta\alpha}{k} = \Delta w \qquad (7.5)$$

Also

$$\frac{\Delta w}{2\ell} = \hat{\gamma}_0 - \hat{\gamma} \qquad (7.6)$$

where ℓ is the length of Wilhelmy plate and $\hat{\gamma}$ is the surface tension of the film-covered surface.

The surface pressure, π (mNm^{-1}) of a surface is given by

$$\pi = \hat{\gamma}_0 - \hat{\gamma} \qquad (7.7)$$

Therefore

$$\pi = \frac{\Delta\alpha}{k.2\ell} \qquad (7.8)$$

7.2.4.2 Measurement of the Surface Pressure-Area Isotherms

During this experiment, the canal was temporarily sealed with a microscope cover-slip which had been lightly greased on the two vertical edges using silicone grease. The water surface was swept clean using the moveable teflon barriers. Beginning near a perspex barrier, a teflon rod was drawn across the surface to the end of the trough, thus clearing the surface of contaminants. This procedure was repeated three to four times. The subphase used for the experiment was ~0.01M hydrochloric acid solution at pH 2.2.

The fatty acids were applied to the surface of compartment II at low surface concentration, so that the surface pressure was very small

and no surface tension change could be detected by the Wilhelmy plate tensiometer. 0.06cm^3 of spreading solution was found to be adequate with the teflon barrier about 20cm from the central perspex divide. After allowing a few minutes for the evaporation of the spreading solvent, the monolayer was compressed by moving the teflon barrier. The increase in surface pressure was observed directly from the chart recorder. The surface pressure was recorded as a function of distance moved by the teflon barrier.

7.2.4.3 Measurement of the Time-Dependence of Surface Shear Viscosity

In order to determine surface viscosity using a canal viscometer, it is necessary to measure the area of film passing through the canal in unit time, with a given pressure differential across the ends of the canal.

Initially, the trough was filled with 0.01M hydrochloric acid and the water surface on both sides of the fixed perspex canal was swept clean using the moveable teflon barrier. With the Wilhelmy plate dipping into clean water, the deflection on the chart recorder was taken as zero surface pressure.

The canal was then covered with the microscope cover-slip, which had been lightly smeared with silicone grease along its vertical edges to give a seal between the sides of the canal. A known volume of the spreading solution was applied to the surface of compartment I at low surface concentration. If the surface concentration was too high, unsuitable spreading of the film occurred, leading to lenses of the solution being formed. A 30cm-rule had been attached to one of the sides of the trough, enabling the distance moved by the barriers at selected time intervals to be measured. After allowing a time period for the spreading

solvent to evaporate, the film was compressed using the moveable barrier to the required surface pressure. When the canal was opened (by removing the cover-slip), the film flowed from compartment I to compartment II and a stopwatch was started simultaneously. Consequently, the surface pressure in compartment I dropped, so the barrier was moved slowly to maintain a constant reading from the Wilhelmy plate. The distance travelled by the barrier at 30-second intervals was recorded, a process continued for over 12 minutes.

The surface was then swept to remove any existing film or contaminants and the procedure was repeated for various surface concentrations. The following concentrations were used: 10, 15, 20, 25 and 30 microlitres of a $4x10^{-3}$M myristic acid solution.

Experiments in which 20 microlitres were added to compartment I while various amounts were added to compartment II were also carried out. The following concentrations were delivered on compartment II: 5, 10, 44 and 46 microlitres of myristic acid solution.

7.3 The Joyce-Loebl Glass Trough

The apparatus was a fully-automatic Langmuir trough. The principal modes of operation carried out on this trough were: isotherm plotting, surface potential and viscosity measurements, and relaxation profiles of surface films.

A twin-channel chart recorder (Recorder 314, Scientific Instruments, Switzerland) with X-Y and Y-t modes was used to monitor and record the surface characteristics of the monolayers. The unit was housed in a purpose-built clean cabinet, which was in turn supported on a balance column, the whole apparatus being housed in a dust-free tent (see Plate 7.2 and Figure 7.3).

PLATE 7.2: The experimental set-up used to monitor and record the surface characteristics of monolayers

(a)

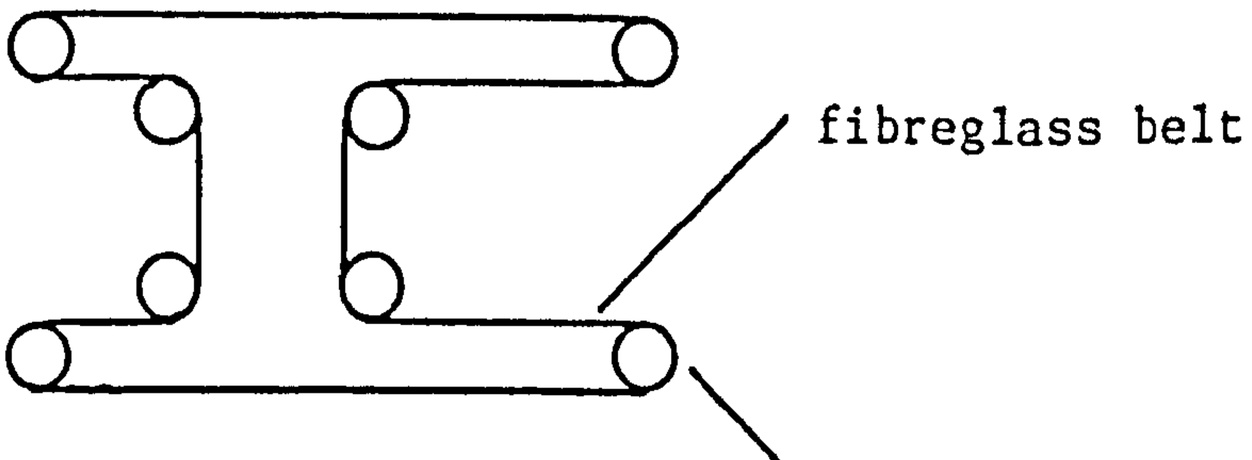

(b)

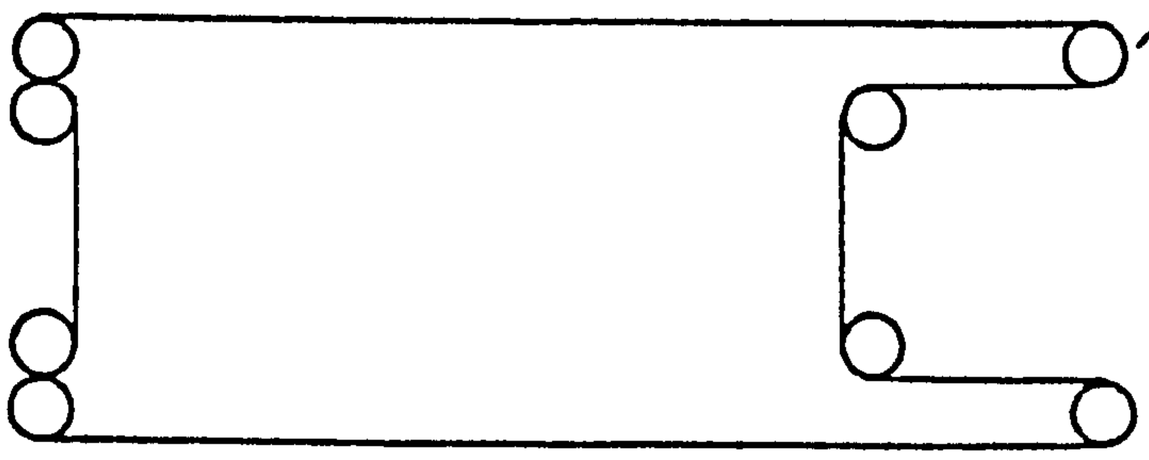

FIGURE 7.2: Molecules are deposited in the area defined by the PTFE tape.
(a) minimum area
(b) maximum area

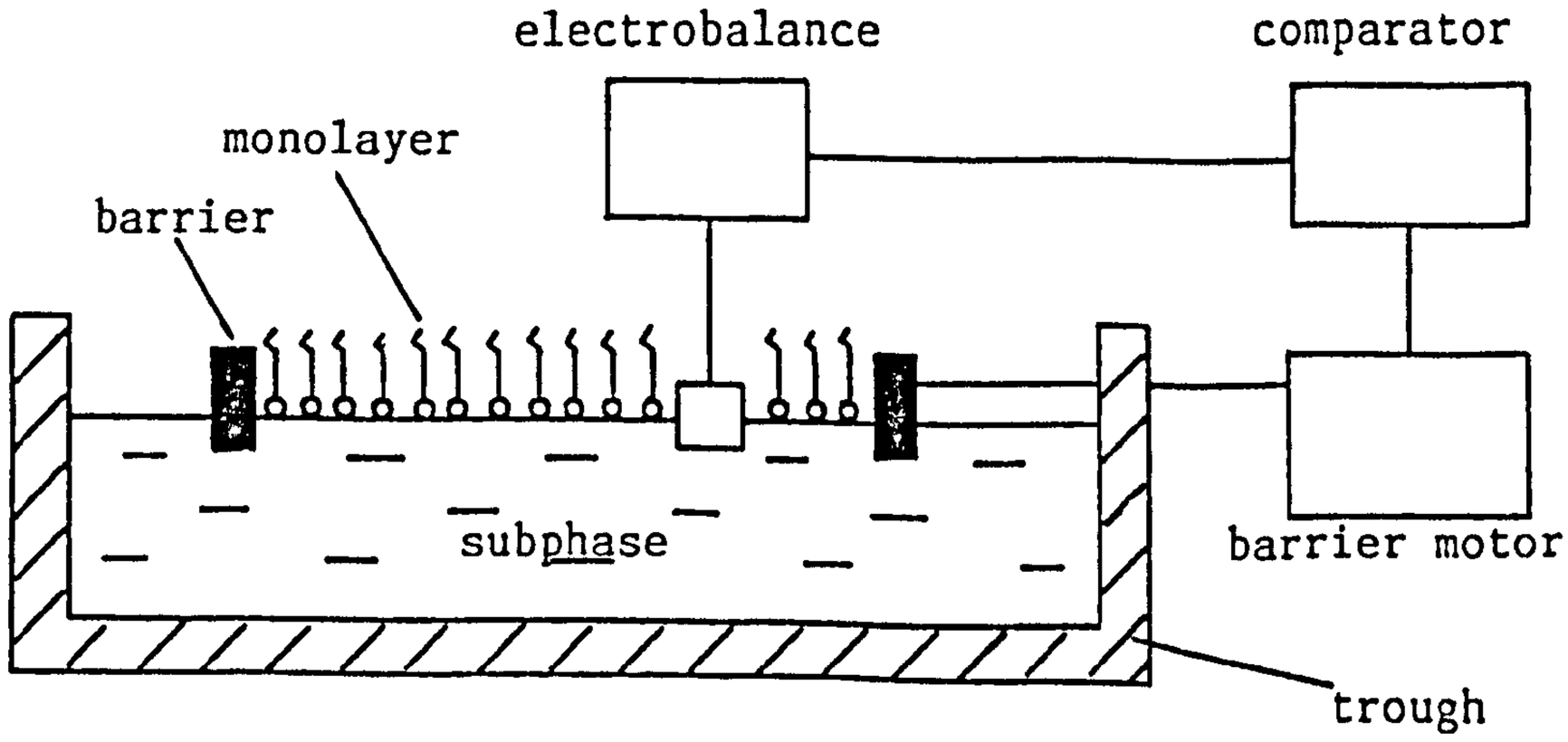

FIGURE 7.3: Schematic diagram of a monolayer under study in the trough.

7.3.1 Compression System (see Figure 7.2)

In traditional troughs (similar to the one described earlier in this chapter), the container which holds the liquid subphase upon which the monolayer flats forms an integral part of the boundary of the compression system. However, an important feature of this trough was the constant perimeter PTFE-coated fibreglass barrier which defined the working area on the liquid surface. Enclosing the monolayer within a continuous band avoided the familiar problems of contamination and film leakage. The liquid container was made of glass and rested on a metal frame which could be raised or lowered by means of a lifting mechanism.

The size of the film-covered area was carefully controlled by means of a highly-geared motor which moved two overarms (secured to 8 PTFE rollers) symmetrically inwards or outwards, thus keeping the barrier taut at all times. . The overarms were located and suspended by concave vee-section rollers running smoothly along circular cross-section stainless steel rails. A range of speeds was available when using the instrument in a compression or relaxation mode.

7.3.2 Wilhelmy Plate Analysis

The Wilhelmy plate technique in which a sensitive microbalance with sensor in the liquid surface monitored the differential surface tension was again employed. The barrier drive was linked to the microbalance by an electronic feedback system, enabling the working area to be compressed until a monomolecular film was formed.

The Wilhelmy balance was based on a thin plate which was semi-immersed in the subphase and attached to a microbalance vertically above it. Values of weight could be related directly to surface pressure, provided the contact angle of the plate with the liquid was zero. In this

case, the material used for the Wilhelmy plate was a 1cm-wide piece of filter paper attached to the balance head by a length of fine cotton thread.

The forces acting on the plate consist of gravity and surface tension downwards, and buoyancy due to the displaced water upwards. Consider a rectangular plate of dimensions ℓ, w, t and of density ρ_p, immersed in water to a depth, h. The net downward force is given by:

$$F = \rho_p g\ell wt - \rho_o gtwh + 2\hat{\gamma}(t + w)\cos\theta \qquad (7.9)$$

where $\hat{\gamma}$ is the liquid surface tension, θ is the contact angle (normally zero and therefore $\cos\theta = 1$), g is the gravitational constant and ρ_o is the subphase density. The surface pressure, π, is again considered to be equal to the reduction of the pure liquid surface tension by the film, i.e.

$$\pi = \hat{\gamma}_o - \hat{\gamma} = \Delta\gamma \qquad (7.10)$$

The depth h and the plate dimensions remain constant, and thus the first two terms remain unchanged. Therefore:

$$\Delta F = 2(\hat{\gamma}_o - \hat{\gamma})(t + w) \qquad (7.11)$$

As the plate had negligible thickness and width 1cm, then:

$$\Delta F = 2\Delta\gamma \qquad (7.12)$$

so that the weight measured (500mg) was equal to twice the surface tension measured in mNm^{-1}.

An essential feature of this trough was the feedback system to control the surface pressure. A voltage corresponding to surface pressure was derived from the microbalance control unit. The output was +1V for a 100mg load, and it was also used to drive the barrier control mechanism. A voltage corresponding to the area of the monolayer was derived from a 10-turn potentiometer connected to the barrier motor.

7.3.3 Experimental Procedures

7.3.3.1 Instrument Calibration

In order to calibrate the abscissae of the X-Y mode of the chart recorder, a knowledge of the maximum and minimum areas contained within the constant perimeter barrier was necessary. These were measured as accurately as possible at a specific barrier speed, this speed value being the one commonly used for barrier compression.

The maximum area of the enclosed trough surface was 298.23cm^2 and the minimum area attainable without disturbing the filter paper sensor was 104.46cm^2. The voltage across the potentiometer when the area was at a maximum was 0.0299V, and the voltage corresponding to the minimum area 1.6672V. Hence the area enclosed at any particular value of the voltage was calculated using the equation

$$A = A_{max} - \left(\frac{V - 0.0299}{1.6672 - 0.0299}\right)(A_{max} - A_{min}) \qquad (7.13)$$

The voltage, V, was calculated from the chart recording in that: V = $x \times 0.0125$, where x was the distance in centimetres from the zero position (i.e. trough at maximum area) along the X-axis of an X-Y recording. From the area enclosed, and knowing how many molecules were spread on the surface, it was possible to calculate at any particular point the area per headgroup for a particular surface pressure of an insoluble adsorbate, hence allowing accurate pressure-area isotherms to be plotted.

The microbalance was calibrated using standard weights so that the surface pressure was simply related to the microbalance reading via the dimensions of the Wilhelmy plate; i.e. 2mg measured on the microbalance corresponded to a surface pressure of 1mNm^{-1}. The ordinate of the X-Y mode of the recorder was conveniently calibrated by the addition of known weights (i.e. 100mg ≡ 50cm) to the left pan of the microbalance.

7.3.3.2 Cleaning of the Trough

The cleaning of the glass trough took approximately 30 minutes to complete. It began by initially emptying and draining the trough, followed by a thorough washing and cleaning process using paper tissue with 'Analar' grade chloroform (this was to remove organic contaminants). The trough was then washed with water, followed by a repeat process using isopropyl alcohol. This was to remove inorganic contaminants. Finally, chloroform was used once again. In between each process, separate gloves were worn and the trough was washed with water. Finally, the trough was washed with purified water from the 'milli-Q' system and wiped and dried with a tissue partly-soaked in chloroform.

The barrier and rollers were placed in a 600cm^3 beaker, approximately 10cm^3 of decon-90 was added, then filled up with purified water and followed by ultrasonic cleaning in a water bath for approximately 5 minutes. The next step was to rinse them three times in purified water, and then finally under reflux using isopropyl alcohol for one hour.

7.3.3.3 Plotting of Monolayer Isotherms

Once the trough had been cleaned, it was filled with purified water until it reached half-way up the fibreglass belt. The pH and temperature electrodes were then inserted into the subphase via leads connected to a pH-meter (Model PTL 15) and the pH was cautiously altered to the required value. The surface of the subphase was cleaned; this was conveniently done with the aid of a glass teat pipette attached to a water pump, surface cleaning being more easily accomplished with the barrier set to minimum area. The effectiveness of the cleaning procedure was being monitored by opening the barrier to maximum area, compressing at a slow speed and observing any change in the surface pressure.

The Wilhelmy plate was gently lowered into the subphase (this was balanced by a weight situated on top of the draught-proof box). The surface was once again swept clean, thus enabling the Wilhelmy plate sufficient time to get completely wetted.

The surface was then checked for contamination by advancing the barrier from its initial rest position to one corresponding to one-tenth of the initial area. A known quantity of a fatty acid in chloroform or a polydimethylsiloxane in n-hexane was spread on the surface of the subphase using an 'agla' micrometer syringe. The spreading solution was added from just above the surface, one drop at a time, allowing the drop time to spread out onto the surface. When the correct quantity had been applied to the surface, 5 to 10 minutes was allowed for the solvent to evaporate.

The compression was performed very slowly by means of the forward movement of the barriers. Once the main features of the isotherm had been observed and plotted on the X-Y mode of the recorder, the barriers were returned to the maximum area position, thus avoiding the possible collapse of the film if compressed too far. The barrier reverse mode enabled relaxation and any evident hysteresis of the film to be observed.

Calculation of Area/Molecule From the Monolayer Isotherm

If R_1 and R_2 are the initial and final readings on the micrometer dial when a quantity of solution has been applied to the surface, the volume of solution in microlitres is $(R_2 - R_1) \times 20 = c$, therefore:

$$\text{number of molecules per microlitre} = \frac{6.023 \times 10^{23}}{m^*} = N_1 \qquad (7.14)$$

Hence

$$\text{area per molecule} = \frac{298.23 \text{ (max area)}}{N_1 \times c} \qquad (7.15)$$

where m^* = number of moles of surfactant x volume of flask.

The calculation of the area at any particular point on the profile is described below (see Figure 7.4). If E is chosen as the point at a distance x/cm from the starting point, then the voltage at that point is calculated from the equation

$$V = x/cm \times 0.0125 \qquad (7.16)$$

where 0.0125 is the scaling factor of the chart recorder. Therefore, area/molecule at this point is given by:

$$\frac{298.23 - 655.658(V - V_0)}{N_1 \times c} \qquad (7.17)$$

where V_0 is the initial voltage. The estimated errors were $\pm 0.1 mNm^{-1}$ for the surface pressure, π, and $\pm 0.01 Å^2$ for the area.

7.3.3.4 Measurement of the Surface Potential

These measurements were made with an electrode bearing an americum-241 source of approximately 5 microcuries, protected by an aluminium foil window in its tip. Figure 7.5 illustrates the set-up of the circuit.

The reference electrode was platinum and this was usually cleaned with concentrated nitric acid, then high-purity water, and then finally immersed in the 0.01M sodium chloride subphase at the far left of the trough in an area not used for surface film formation.

A Vibron electrometer (Model 335, Electron Instruments Ltd.) was used to register the potentials set up by the system. A screened cable connected the platinum electrode to the electrometer, the screen cable being earthed. In fact, it was found that all the metal contacts in the trough cabinet needed to be earthed. The perspex box containing the trough was surrounded by aluminium foil which was also earthed and so provided a Faraday cage.

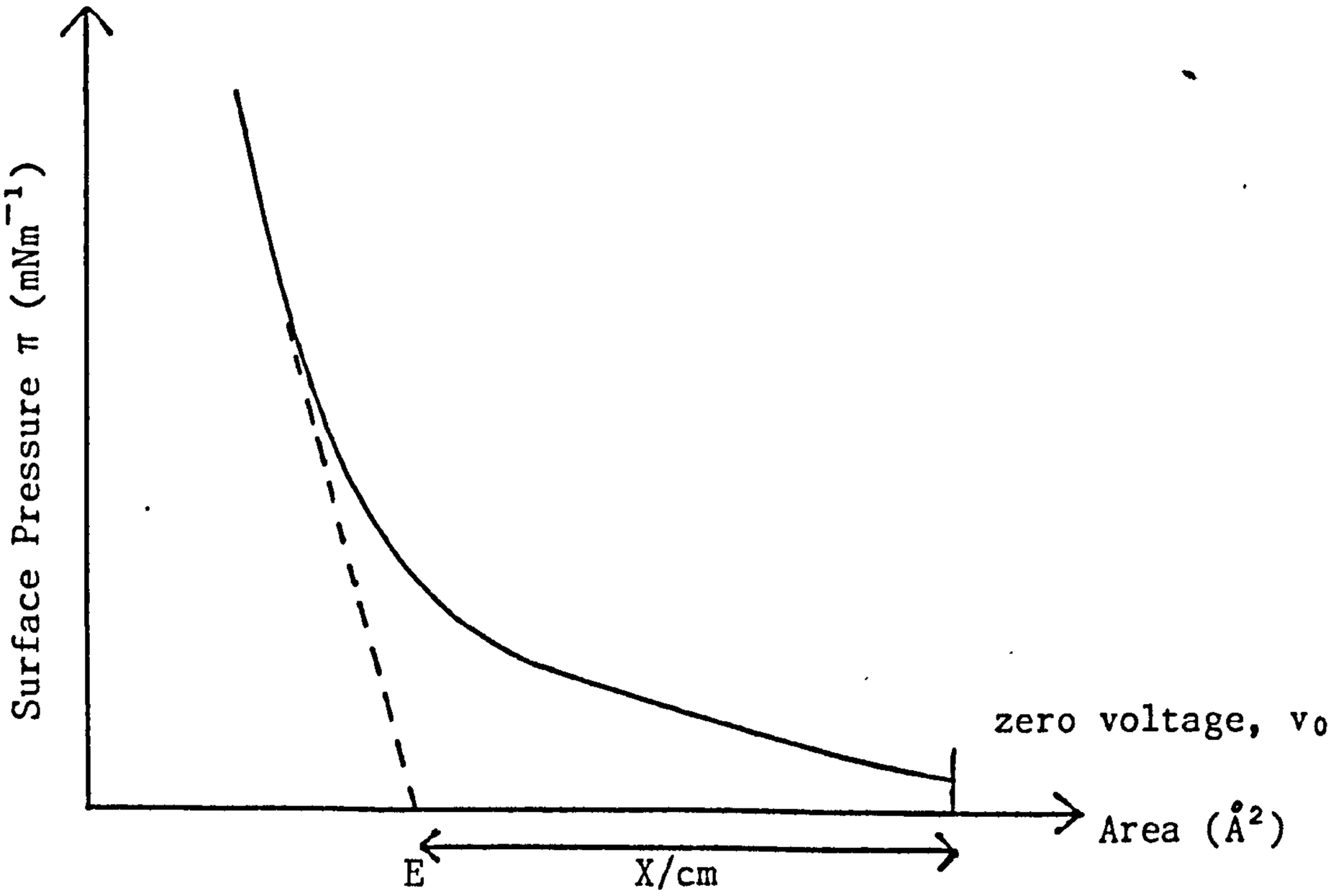

FIGURE 7.4: Schematic diagram of a π(A) profile of a fatty acid obtained from the trough.

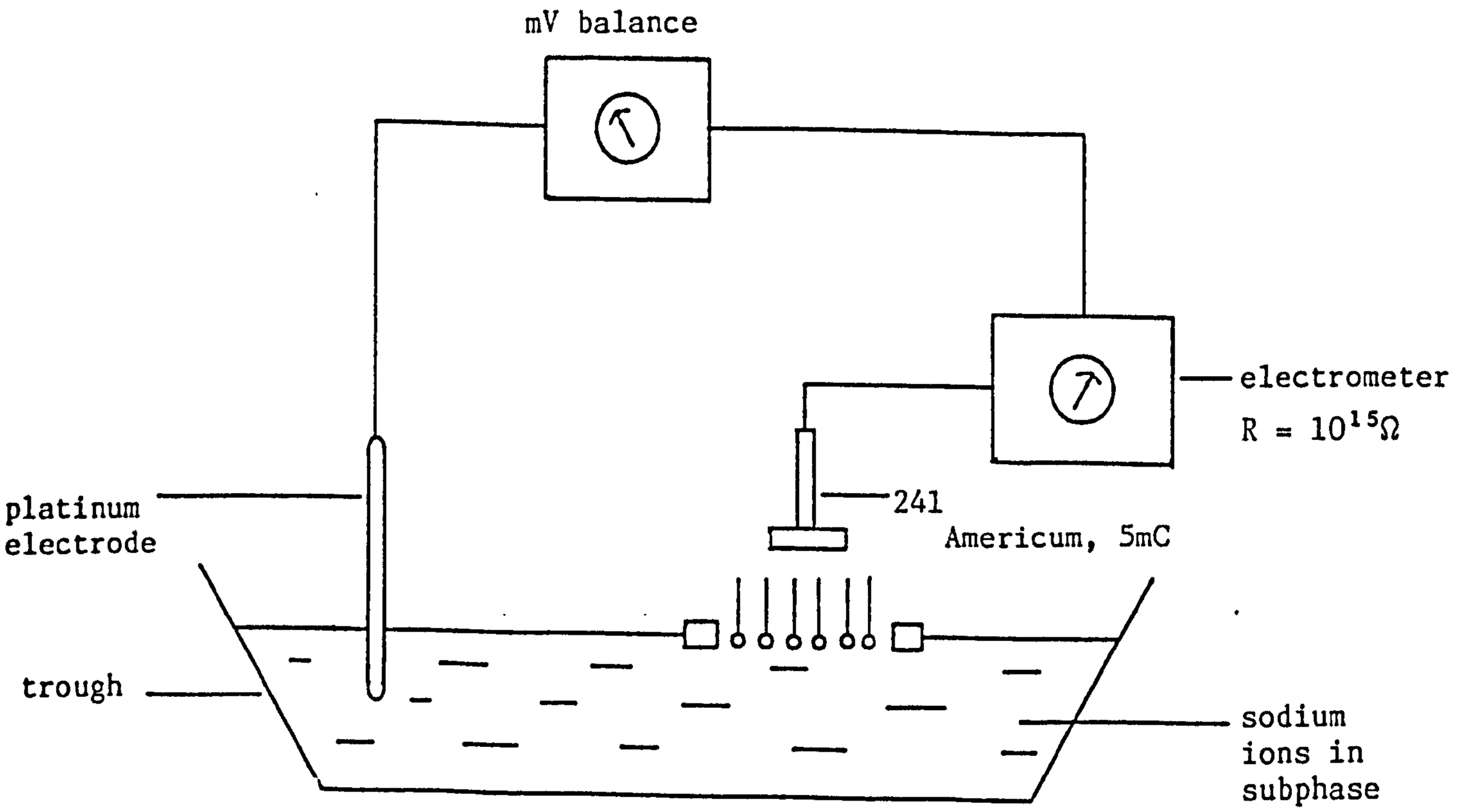

FIGURE 7.5: The circuit for surface potential measurements.

The detection of an adequate response from the electrometer confirmed that the apparatus was operational. No input resistor was used, since the resistance of the air-gap between the americum-241 electrode and the subphase surface was already very high. Full use was made of the back-off facility provided on the electrometer, so that potentials would normally be read to $\pm$0.5mV over a 700mV range. The output from the Vibron electrometer was connected to an X-Y chart recorder (Bryands, Model 28000) on which any rise or lowering of the surface potential, V, could be detected.

Once all connections and earthings had been secured, the americum-241 electrode was connected to a micrometer dipping arm and lowered to a position as close as possible to the surface without touching it. The surface potential, V, of the clean surface was measured for approximately 1 hour in order to obtain a stabilized potential reading for the surface.

The americum-241 electrode was then raised and disconnected so that a monolayer could be spread. After spreading, the electrode was reconnected and the potential changes resulting from alterations in the compression of the spread monolayer were read off the electrometer.

The difference between the potentials of the clean surface and that with a spread monolayer gave the surface potential of the monolayer, ΔV, which enabled the dipole moment, $\mu_\perp$, to be calculated using equation (3.68):

$$\mu_\perp = \frac{\varepsilon_0 . \Delta V}{n}$$

where all the parameters have already been defined in Section 3.2.5.

7.3.3.5 Measurement of Surface Shear Viscosity

A simple canal-type viscometer was constructed to measure the rate of flow of a surface film through a 'canal' at a known shear stress.

The viscometer (see Figure 7.6) comprised a polytetrafluoroethylene (PTFE) frame intersecting the water/air interface with an opening (canal) of variable width in one side. The fibreglass barrier was used to control the monolayer at a given surface pressure (π_2) outside the PTFE frame, which was supported by four PTFE legs standing on the trough base. The canal viscometer was usually soaked in decon-90 for about 30 minutes, washed with 'milli-Q' water and dried with pressurized air. The viscometer was twice cleaned with isopropyl alcohol and then dried using filtered pressured air prior to each measurement. This was an hydrophobic canal, and the canal depth of approximately 9mm was ensured before commencing each experiment.

The surface was swept clean and a base-line run carried out. Then the transducer measuring the pressure in the viscometer was calibrated. The canal viscometer was then placed in the middle of the area enclosed within the barriers and the surface swept again. The surface pressure at the canal exit, π_1, was reduced to zero before proceeding with any measurements by using a suction pipette. Once this had been achieved, the 'agla' microsyringe was thoroughly cleaned in chloroform or n-hexane (spreading solvents for the fatty acids and polydimethylsiloxane polymers respectively). Two Wilhelmy plate sensors were in use here; one monitored the surface pressure outside the canal, while the other monitored the surface pressure of the monolayer as it passed through the canal.

The monolayer was spread from the respective spreading solvent and an evaporation time of at least 60 seconds was allowed prior to taking measurements. After compressing the monolayer-to-surface pressure, π_2, the canal (width 0.065cm and length 1.3cm) was opened and the surface flux, q, through the canal was recorded. The flow was stopped as soon as the pressures (both inside and outside) had equilibrated, which tended

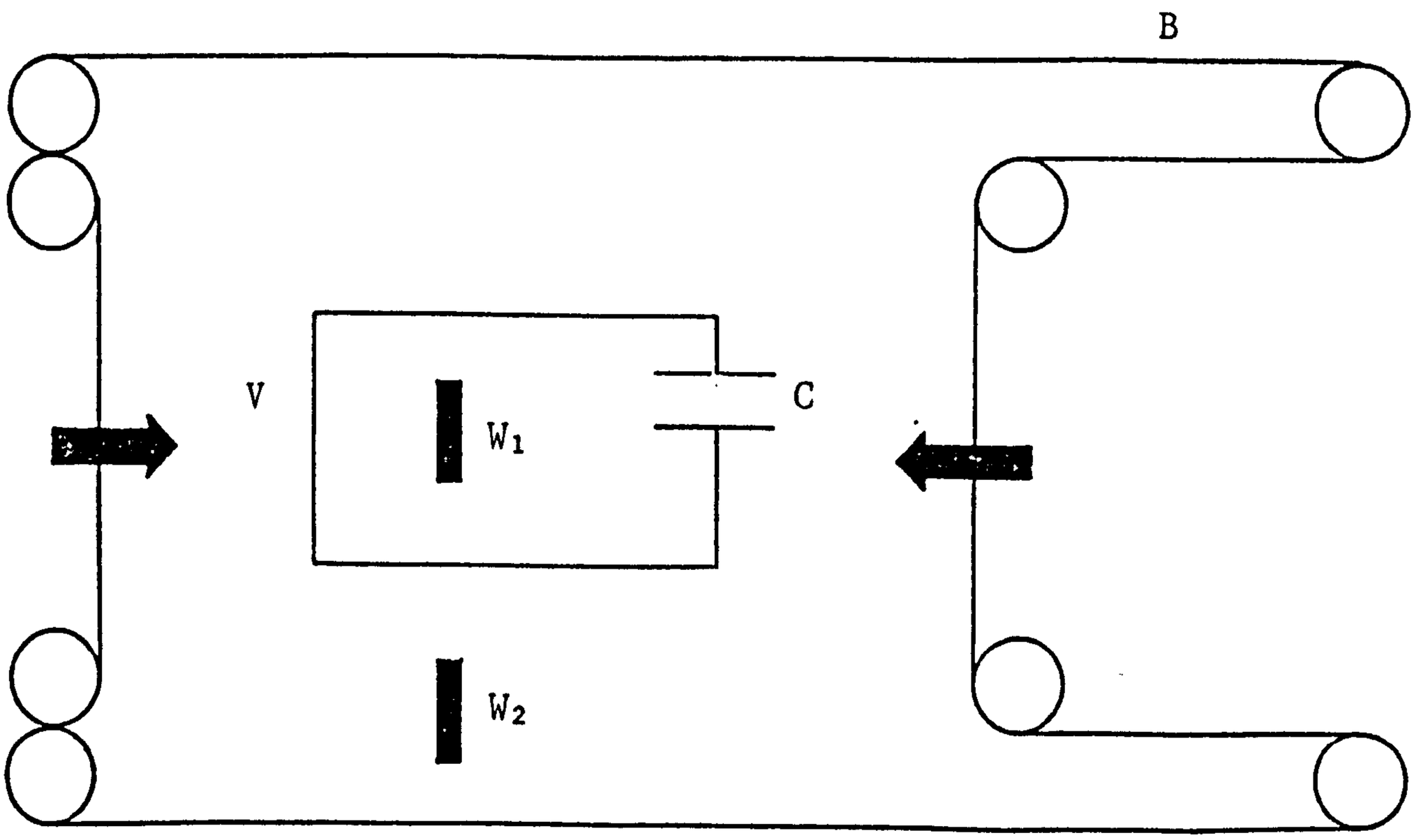

FIGURE 7.6[230]: Schematic plan view of the trough and viscometer used to measure in-plane shear viscosity. B = belt positioned by 8 PTFE rollers; W_1 and W_2 are Wilhelmy plates to monitor surface pressures inside (π_1) and outside (π_2) the viscometer, V, with variable width canal, C.

to coincide with the barriers almost touching the canal viscometer .

A seemingly identical formula to equation (7.2), but including a correction term for the viscous drag due to the subphase being pulled through the canal with the monolayer, and for a deep canal ($h \gg a$) due to Harkins and Kirkwood[220], was used to calculate the surface viscosity, η_s:

$$\eta_s = \frac{2}{3} \frac{\pi_2 - \pi_1}{\ell} \frac{a^3}{q} - \frac{2a\eta_0}{\pi} \qquad (7.18)$$

where η_0 is the bulk subphase viscosity, h is the height of the subphase in the canal, and all other parameters have been defined in Section 3.2.3. The major source of experimental uncertainty was the ill-defined meniscus shape in the canal (caused by the turbulence of the subphase on the edges of the polytetrafluoroethylene frame), which could lead to an uncertainty in its effective width. Also, the Harkins and Kirkwood formula assumes that the shape of the meniscus in the canal is flat with a contact angle of 90^o, when in practice it was found to be closer to 110^o.

7.3.3.6 Relaxation Profiles

It was necessary to convert the arbitrary figures of the forward and reverse speeds available on the Langmuir trough control unit. A relationship was thus obtained which related the arbitrary speed settings of the barriers to their real speed values in centimetres per second.

For the relaxation experiments, the monolayers of the fatty acids and polydimethylsiloxanes were spread on the surface, the the forward sweep set to zero speed while the reverse speed was set to speeds ranging from 25 (0.0317cm s^{-1}) to 400 (0.556cm s^{-1}). The barriers were now held at chosen surface pressures and then relaxed back to the maximum surface film area, which correlated to zero surface pressures.

PLATE 7.3: The bob and trough used on the torsion pendulum surface viscometer

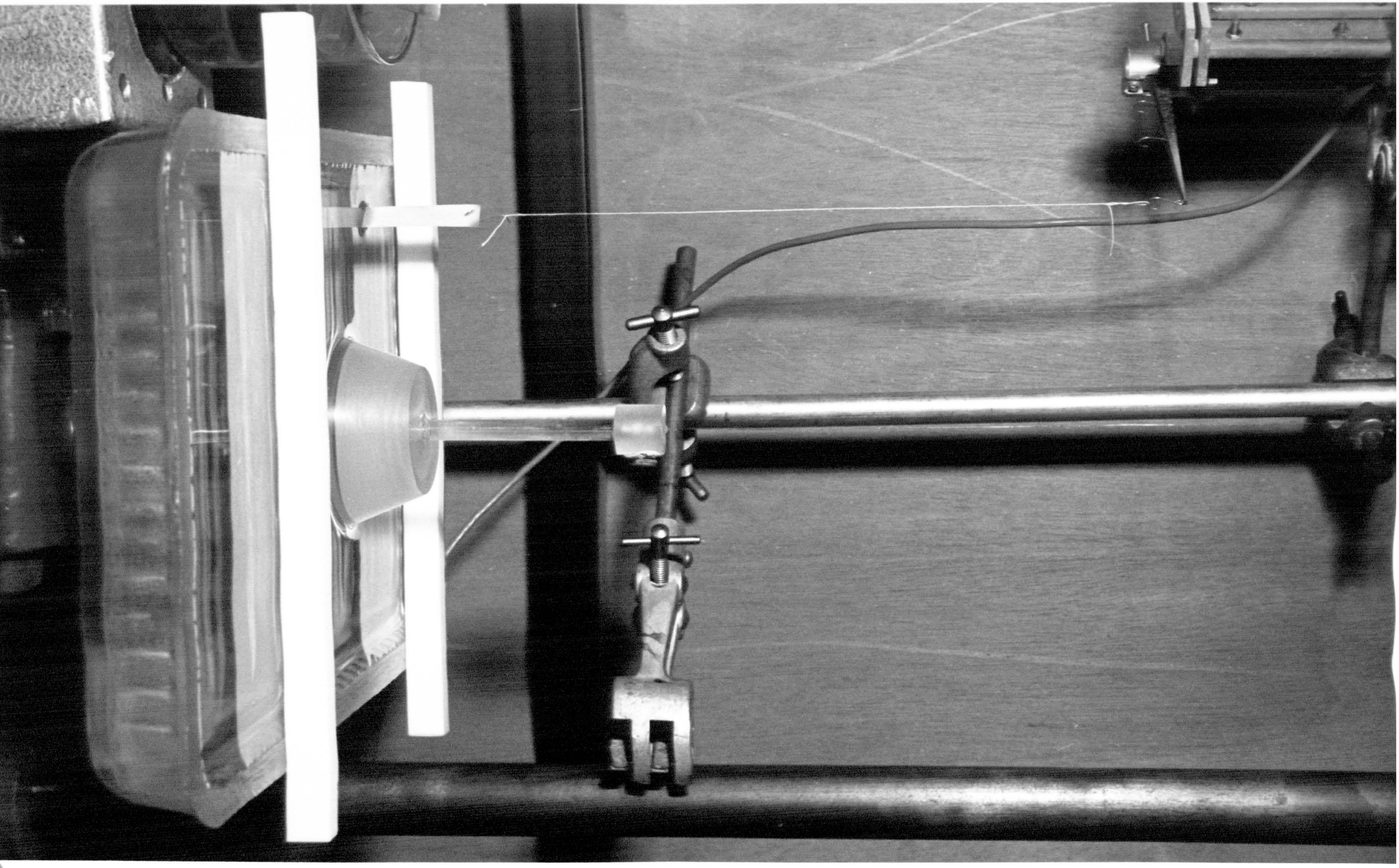

7.3.3.7 Stability of Polydimethylsiloxane Monolayers

To observe the behaviour of collapse of these films, experiments were performed whereby a monolayer was spread on a surface and the area was rapidly compressed and held at a surface pressure of 7.5mNm^{-1} for approximately 2 hours. The criterion of collapse was taken as some measurable change in film area and was indicative of the stability of these films.

7.4 The Torsion Pendulum Surface Viscometer

This viscometer was similar to many that have been reported in the literature[22,221,222]. A schematic representation of the apparatus is shown in Figure 7.7. Plate 7.3 shows the bob and trough.

The bob, A, was suspended from support, B, by a torsion wire, C. The small glass Langmuir trough containing the subphase was placed on the turntable, F, which could be raised to bring the liquid surface into contact with the oscillating bob. The surface pressure was measured by a Wilhelmy plate, and could be adjusted by moving the teflon barriers across the surface.

7.4.1 Calibration

The calibration of the wire, C, was performed as follows. Firstly, the wire had been preheated by suspending a 0.5kg weight from one end and then passing a bunsen flame up and down the wire at a speed of 1cm s^{-1} and at a distance of about 2cm from the wire; a process necessary to anneal the wire.

Secondly, the wire was then calibrated with known weights using the Langmuir trough, and torque was applied to bring the light spot on the scale back to its original position. The angle through which the pointer on the trough turned was recorded as θ.

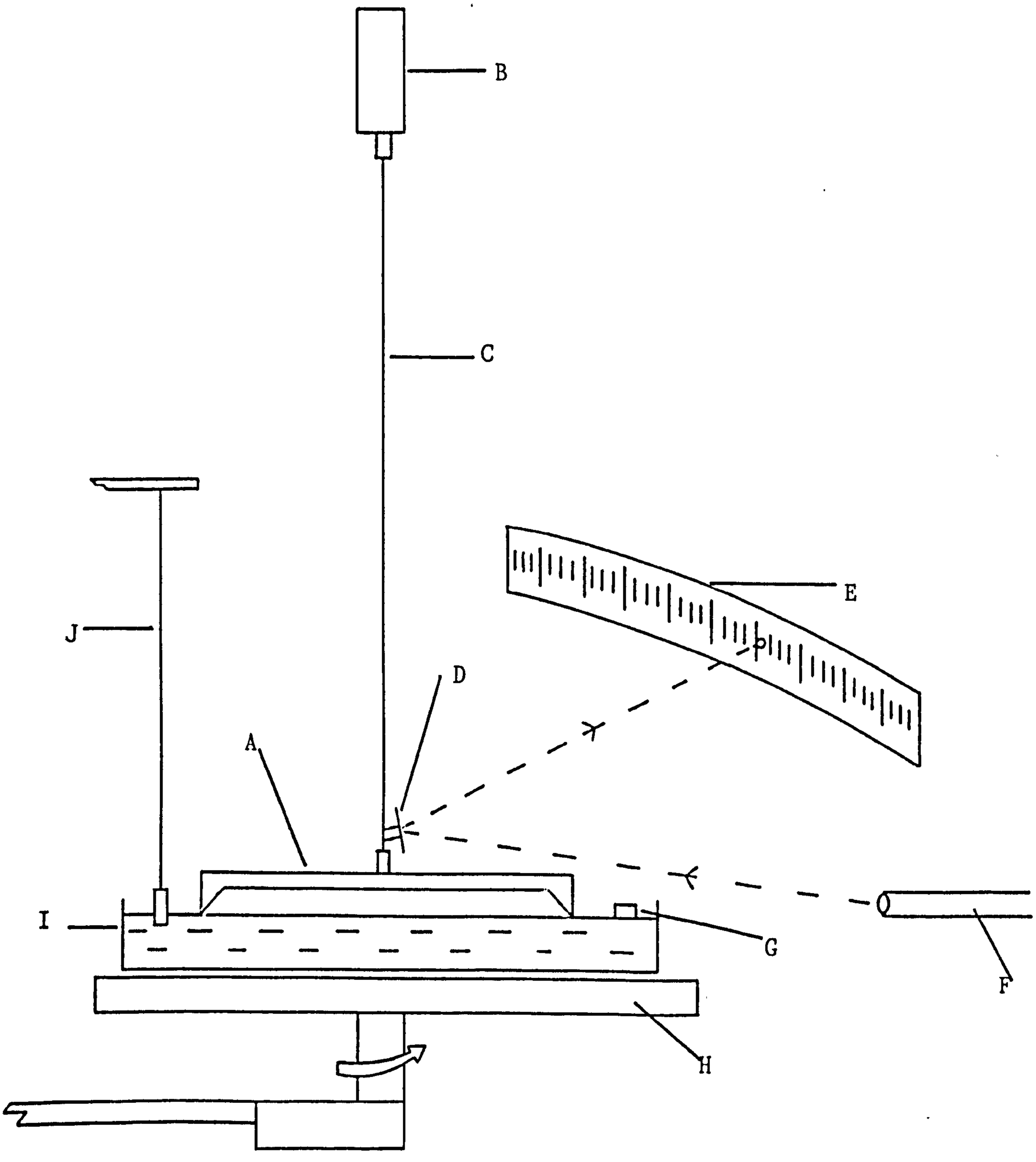

FIGURE 7.7: The rotational surface viscometer. A = bob; B = support; C = torsion wire; D = mirror; E = scale; F = light source; G = PTFE barrier; H = turntable; I = glass trough; J = Wilhelmy plate.

Finally, the linear plot of θ against weight in the pan, m, gave the torsional constant, k, for the wire using the equation

$$\theta = km \tag{7.19}$$

7.4.2 Measurement of Surface Viscosity

The monolayer was initially spread on the maximum surface area of the trough. After allowing the spreading solvent to evaporate, the area was compressed to the required surface pressure. The bob (a poly-tetralfuoroethylene ring) which was in contact with the surface was given an initial rotational impulse and the angular amplitudes of successive swings using a light lever were recorded. The surface viscosity was determined by measuring the logarithmic decrement of the torsional oscillation of the ring at a clean surface and comparing it with a similar measurement for the monolayer-covered surfaces. The surface viscosity was calculated using the equation[73]:

$$\eta_s = \frac{\sqrt{CI}}{2\pi}\left(\frac{1}{R_1^2} - \frac{1}{R_2^2}\right)\left[\frac{\lambda}{\sqrt{4\pi^2 + \lambda^2}} - \frac{\lambda_0}{\sqrt{4\pi^2 + \lambda_0^2}}\right] \tag{7.20}$$

where C is the torsional constant of the wire (260g cm^2s^{-1}), I is the moment of inertia of the bob (71g cm^2), R_1 is the radius of the bob (3.7cm), R_2 is the radius of the trough (measured by inserting glass rings of different radii, and being equal to 8cm), and λ, λ_0 are the logarithm of the amplitude of successive swings with and without the spread monolayer. Five periodic oscillations were plotted for each natural logarithmic decrement.

The subtraction of the term for the subphase surface obtained in the absence of a spread monolayer should correct for the damping of the oscillations by the subphase, if there were complete slippage of the monolayer over the subphase. However, this is highly unlikely. When the monolayer is present, its drag on the ring is greatly enhanced by

the subphase drag on the monolayers[22]. The surface viscosity by this technique is sometimes referred to as the apparent surface viscosity.

7.5 The Oscillating Ring Surface Rheometer

This surface rheometer is an improved model of the one first used by Wibberley[281], and later by Warburton[282]. The advantage of this rheometer is its versatility, which enables it to be used to measure surface viscosity and viscoelasticity without having to change the measuring system.

The Mk. 2 surface rheometer operates by conveying a small surface shear stress to the surface or interface by means of a sinusoidally-varying torque (TmNm) applied to a small platinum ring, R, sitting at the interface (see Figure 7.8). The ring then executes a sinusoidal angular displacement about an axis perpendicular to the plane of the ring and through the centre of the circle of the ring (for further information on description, operation and theory, see Colston's paper[283] and operational manual).

7.5.1 Preparation of the Glassware and the Ring

The glass trough was thoroughly cleaned with chloroform, isopropyl alcohol and then chloroform - while the ring was cleaned by lowering it into a very small petri-dish filled with acetone or ethanol prior to taking any measurement.

7.5.2 Procedure For Measurement

Prior to any measurement, the zero and attenuation settings for the displacement transducer were checked. Then a resonant frequency and amplitude were obtained for the ring in air. This was followed by levelling the trough and filling it with 'milli-Q' water; the surface was

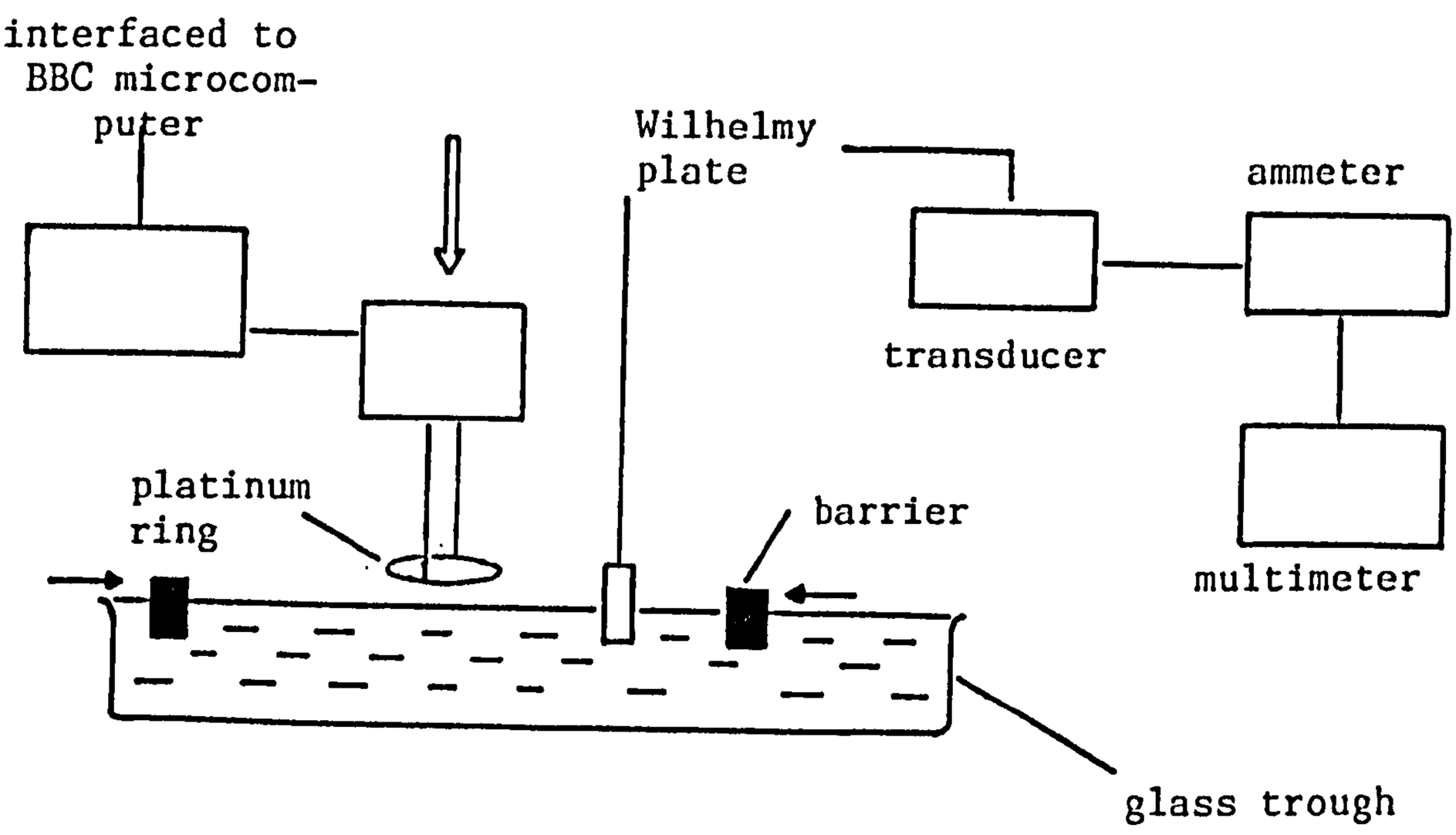

FIGURE 7.8: Schematic diagram for the dynamic surface shear measurements using the oscillating ring surface rheometer.

swept clean using a vacuum pipette. The ring was lowered into the water for good 'grip', and then raised very slightly so that it was sitting in the plane of the water. Once again, a resonant frequency and amplitude were needed for the air/water interface. The ring was then lowered back into the water to enable the spreading of a monolayer. Surface pressure was measured using the Wilhelmy plate technique.

Further measurements were continued by repeatedly lowering the ring and raising it to the surface, until a resonant frequency and amplitude were obtained at the air/water-with-monolayer interface for various surface pressures.

The final results were obtained from a BBC microcomputer system interfaced to the power supply unit of the rheometer. These results were given in the form of the dynamic surface shear viscosity, η_s', and the dynamic surface shear modulus, G_s^*; from which the real and imaginary components G_s' and G_s'' could be deduced as follows:

$$\eta_s' = gf \times I_r \times KO \times KON/1000 \qquad (7.21)$$

$$G_s' = gf \times Min \times 4\pi^2 \times (F^2 - F\phi^2) \qquad (7.22)$$

$$G_s'' = 2\pi \times \eta_s' \times \text{frequency} \qquad (7.23)$$

where gf is the geometric factor ($0.196 cm^{-2}$), I_r is the moment of inertia of the ring ($0.2548 g\ cm^{-2}$), KO is the input amplitude, KON is the final or resonant amplitude, F is the resonant frequency of the ring at the air/water-with-monolayer interface, and $F\phi$ is the resonant frequency at the air/water interface.

7.6 Measurement of the Antifoaming Ability of Polydimethylsiloxane Polymers

The objective of these measurements was, in part, to try to corr-

elate the rheological properties of polydimethylsiloxane polymers with their unique defoaming and antifoaming ability.

A modified foaming method by Bikerman[110] has been used to try to examine their foam-preventing action. A comprehensive study was made of the antifoaming ability of the polydimethylsiloxane polymers in Magnus, Ninian and 'Model' crude oils. Also observed were the synergistic effect of mixtures of two polydimethylsiloxanes of varying mole fractions and antifoamers; and the effect of a fluorocarbon surfactant, FC740, as a profoamer.

7.6.1 The Modified Bikerman Method

A schematic representation of the experimental set-up for the antifoaming tests is given in Figure 7.9. (See also Plate 7.4)

The column, F, was made of a graduated glass tube of about 30cm in length, with two fine sintered glass discs (number two) placed about 1cm apart and situated at the base of the tube, just above the gas inlet/two-way tap, D.

The gas, B, used to create the foam was admitted into the column via the flowmeter assembly, A. The flow rate was controlled by a valve, C. The froth was let out by way of the two-way tap, D, using a vacuum suction, G. A flow rate of 25cm s^{-1} for the Magnus crude oil and 12.5cm s^{-1} for both the Ninian and 'Model' crude oils, was established and maintained prior to any measurements. The quantities of mixtures (containing polydimethylsiloxanes in various crude oils) used for the study are listed in Table 7.1.

7.6.2 Procedure For Measurement

The measurements were initiated by pipetting the appropriate

PLATE 7.4: The Foaming Apparatus

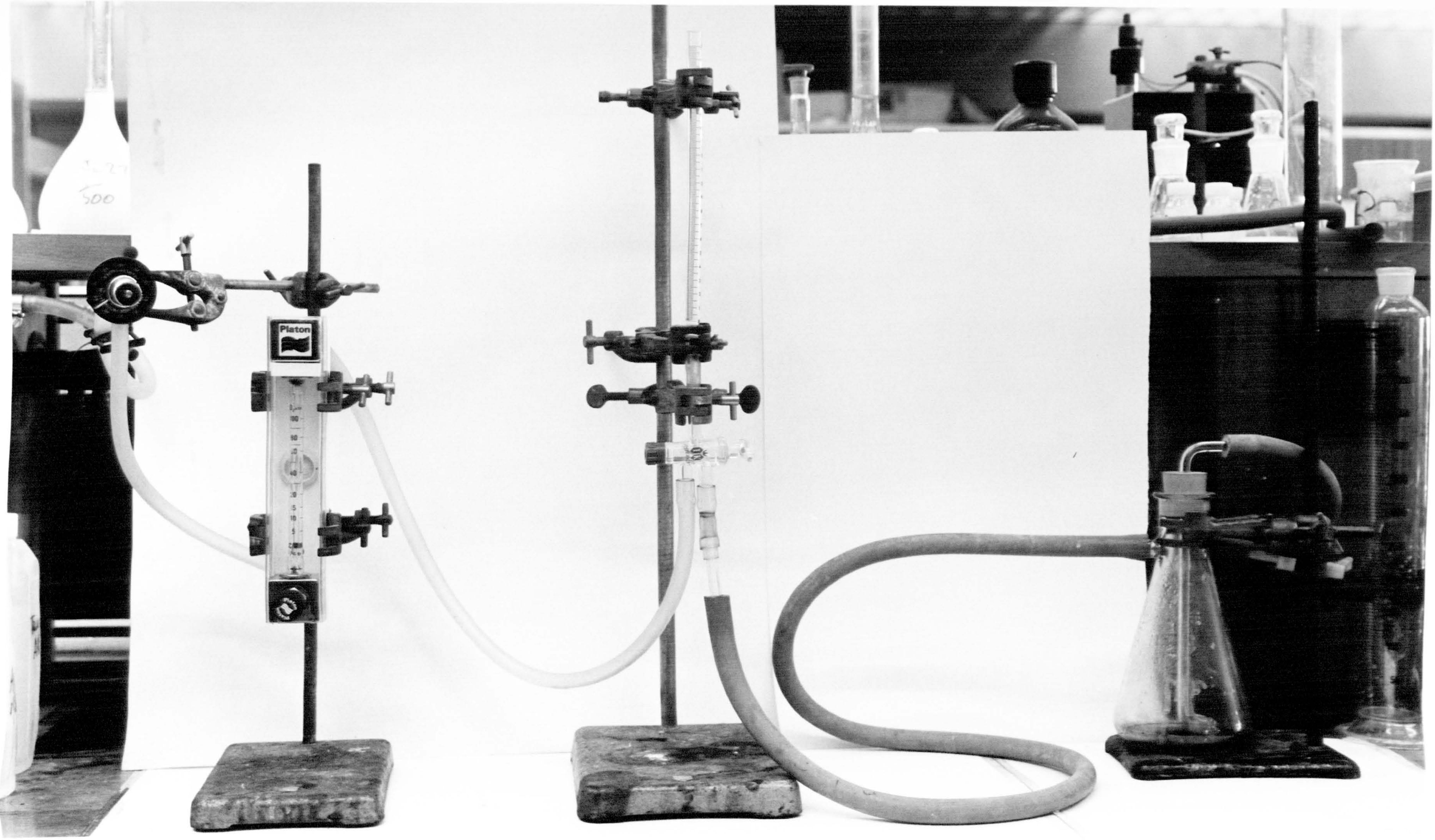

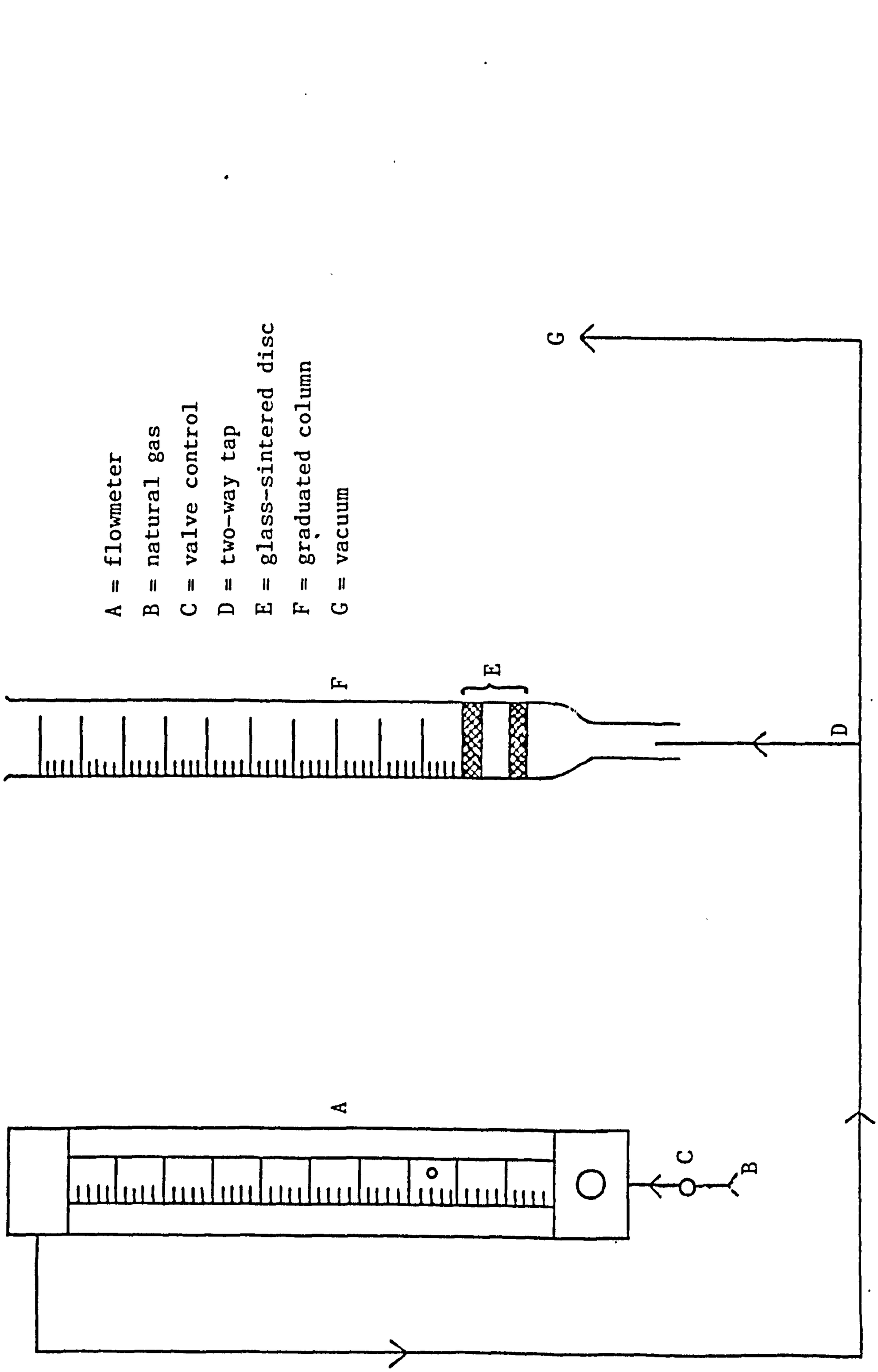

FIGURE 7.9: Schematic diagram of the foaming apparatus.

Antifoaming Agent	Crude Oil	Volume Needed (ml)
Diluted polydimethylsiloxane	Magnus	1.5
Undiluted " " "	Model	3.0
Diluted " " "	Model	2.0
Diluted " " "	Ninian	1.5
Diluted mixtures of polydi-methylsiloxanes	Model	2.0

TABLE 7.1: Data showing the various quantities of polydimethylsiloxane/crude oil needed for measuring the antifoaming efficiency

aliquot of a polydimethylsiloxane in Offshore/Model crude oil (using a micropipette, Model RTM 880D, Payne Clapham), sufficient to cover the upper sintered disc in the column.

The polydimethylsiloxane/crude oil mixture was allowed to spread over the disc and nitrogen gas (flowing at the chosen rate) was then admitted and the polydimethylsiloxane/crude oil mixture was taken up into the froth. The bubbling continued until all the liquid had been taken up into the foam.

When an homogeneous foam had been achieved, an average height of the upper foam/air interface was recorded. The foam was flushed out initially with toluene solvent, 'analar grade' toluene, then acetone, and finally with 'analar grade' acetone. These procedures were repeated at least four times on each concentration of polydimethylsiloxane/crude oil mixture.

7.6.3 Preparation of a Polydimethylsiloxane Dispersion in Petroleum Ether (bp 60-80^{0}C)

A solution of each polydimethylsiloxane (and the fluorocarbon FC740) was made up in petroleum ether and a volume of this solution was added to 10cm^3 of a chosen crude oil contained in cylindrical containers.

The mixtures were thoroughly shaken using a mechanical 'shaker' for about 15 minutes. Dispersions were prepared with the concentration of the polydimethylsiloxane (and fluorocarbon FC740) in the range 20ppm-300ppm and the antifoaming efficiency measured using the foaming apparatus.

Individual values of the Antifoaming Index (AFI) were obtained from four height measurements for a particular concentration of each polydimethylsiloxane and fluorocarbon FC740. The difference between the individual values of the AFI and the average AFI for a particular concentration were calculated. The average of these differences was taken as a measure of the error for the overall antifoaming ability.

7.6.4 Calculation of the Antifoaming Index (AFI)

The antifoaming efficiency of an antifoaming agent at a concentration of x ppm/gdm^{-3} is characterized by an antifoaming index, AFI(x ppm/gdm^{-3}), which is defined as

$$AFI(x\ ppm/gdm^{-3}) = \frac{FH(0\ ppm/gdm^{-3}) - FH(x\ ppm/gdm^{-3})}{FH(0\ ppm/gdm^{-3})} \qquad (7.24)$$

where FH(0 ppm/gdm^{-3}) is the foam height given by crude oil and FH(x ppm/gdm^{-3}) is the foam height after the addition of x ppm/gdm^{-3} of antifoaming agent. Hence: an antifoaming agent with no antifoaming action gives AFI(x pppm/gdm^{-3}) = 0; an antifoaming agent with complete antifoaming action gives AFI(x ppm/gdm^{-3}) = 1; and an antifoaming agent with profoaming action gives AFI(x ppm/gdm^{-3}) < 0.

CHAPTER 8

THE DEER RHEOMETER

8.1 Introduction

The Deer Rheometer (Rheometer Marketing Ltd., Leeds) is capable of operating in both the continuous and oscillatory modes if it has been successfully modified into a rotational torsion surface viscometer. In its role as a surface viscometer, it was used to measure the surface viscosities of a myristic acid monolayer at low shear rates.

With this instrument, the shear rate is measured as a function of applied shear stress, where the applied shear stress can be as low as $1 \times 10^{-4} mNm^{-1}$. However, further experiments could not be performed because of the inertia problems developed by the instrument, since surface work needed to be carried out at low frequencies, amplitudes and masses.

8.2 Instrumentation

The instrument used was a constant stress Deer Rheometer (Series III); the control console and measured assemblies are shown in Plate 8.1. It was calibrated using a cone and plate geometry (see Figure 8.1)

A characteristic of bearings that are lubricated by compressed air is a preferential rotation or 'windmill' of the spindle, caused by the flow of air as it passes through the bearing. In the Series III model, this effect was adjusted so as to cause rotation in an anticlockwise direction when viewed from above with no electric drive applied to the motor. This effect was corrected by means of an automatic bias system. Compressed air, maintained at 60psi, was fed into the air-bearing. In order to maintain free spindle rotation, it was found to be important

PLATE 8.1: The Deer Rheometer

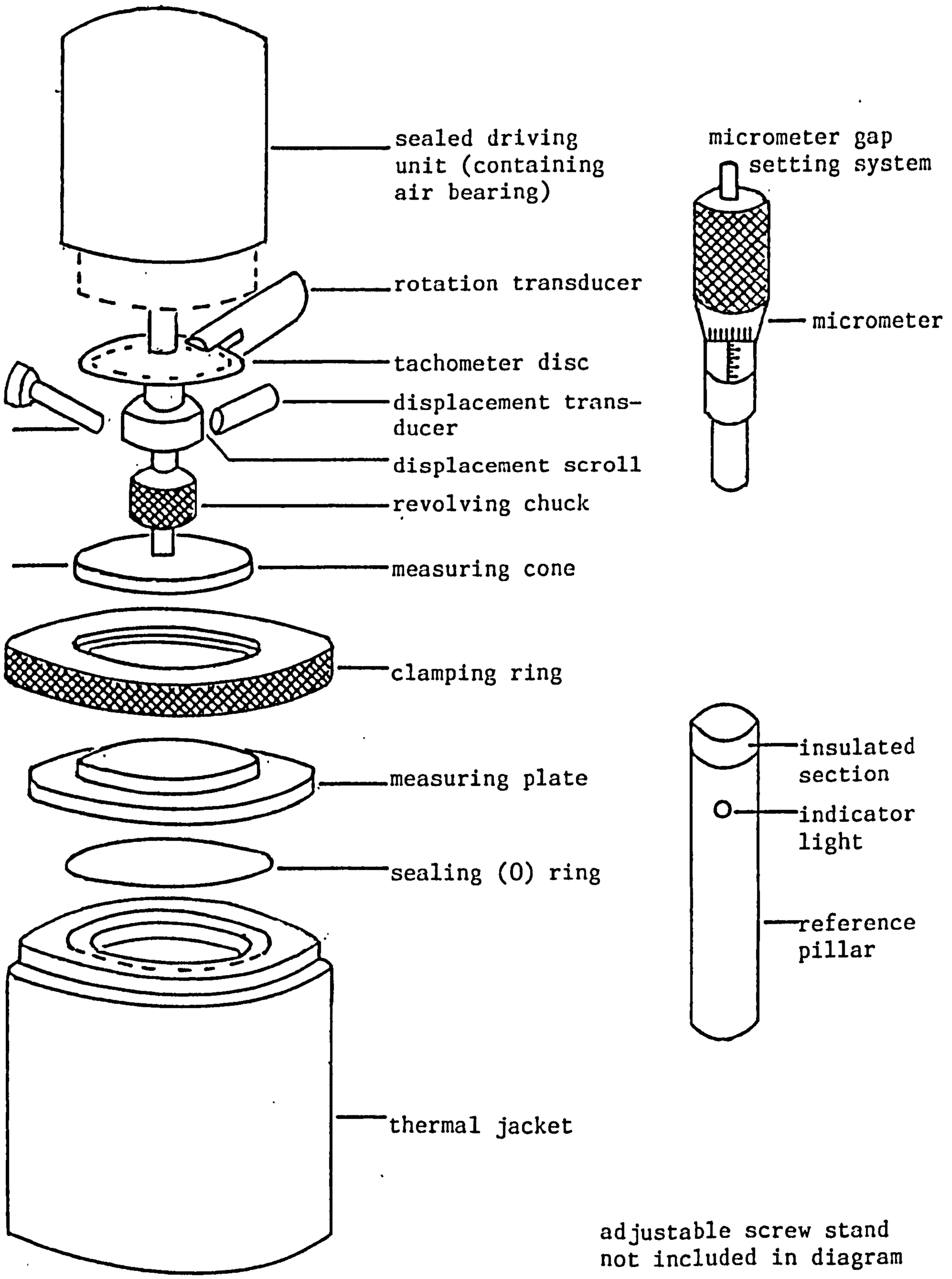

FIGURE 8.1: Schematic representation of the rheometer assembly with cone and plate system

that the air was free of contaminants. For this purpose, a set of four filters (Norgren, Shipston-on-Stour, Warwickshire) was inserted into the air circuit.

The gap-setting micrometer and an electrical indicator ensures the correct separation of 0.026mm between the cone and plate assembly.

As the spindle was also the main shaft of a servo-motor rotor, a constant torque was supplied, regardless of the spindle rotation rate. The torsional force was selected by adjustment of the five-digit thumb-wheel switches located on the control console. The torque control allowed operation over the range 1-99,999 $\times 10^{-7}$Nm. The torque was converted to the shear stress by means of a calibration (or instrument) constant discussed in Section 8.2.2.

Angular velocities were obtained directly from a display unit on the console. The velocities were converted from an oscillating electrical signal generated by a tachometer disc and a photoelectric cell on the rheometer.

The combined sweep and oscillatory unit was designed to be used as an optional accessory to the Series III model. It provides alternative and automatic torque profiles not available from the basic control console, to repeat these accurately if required, and finally to increase the dynamic investigation of viscoelastic properties. The torque profiles are generated when the unit is in the sweep generator mode, while the dynamic capability is exploited in the oscillatory mode.

8.2.1 Analysis of the Instrument

Continuous Rotation

In a cone-and-plate viscometer, the sample is contained between the cone and the plate, as shown in Figure 8.2. The angle between the

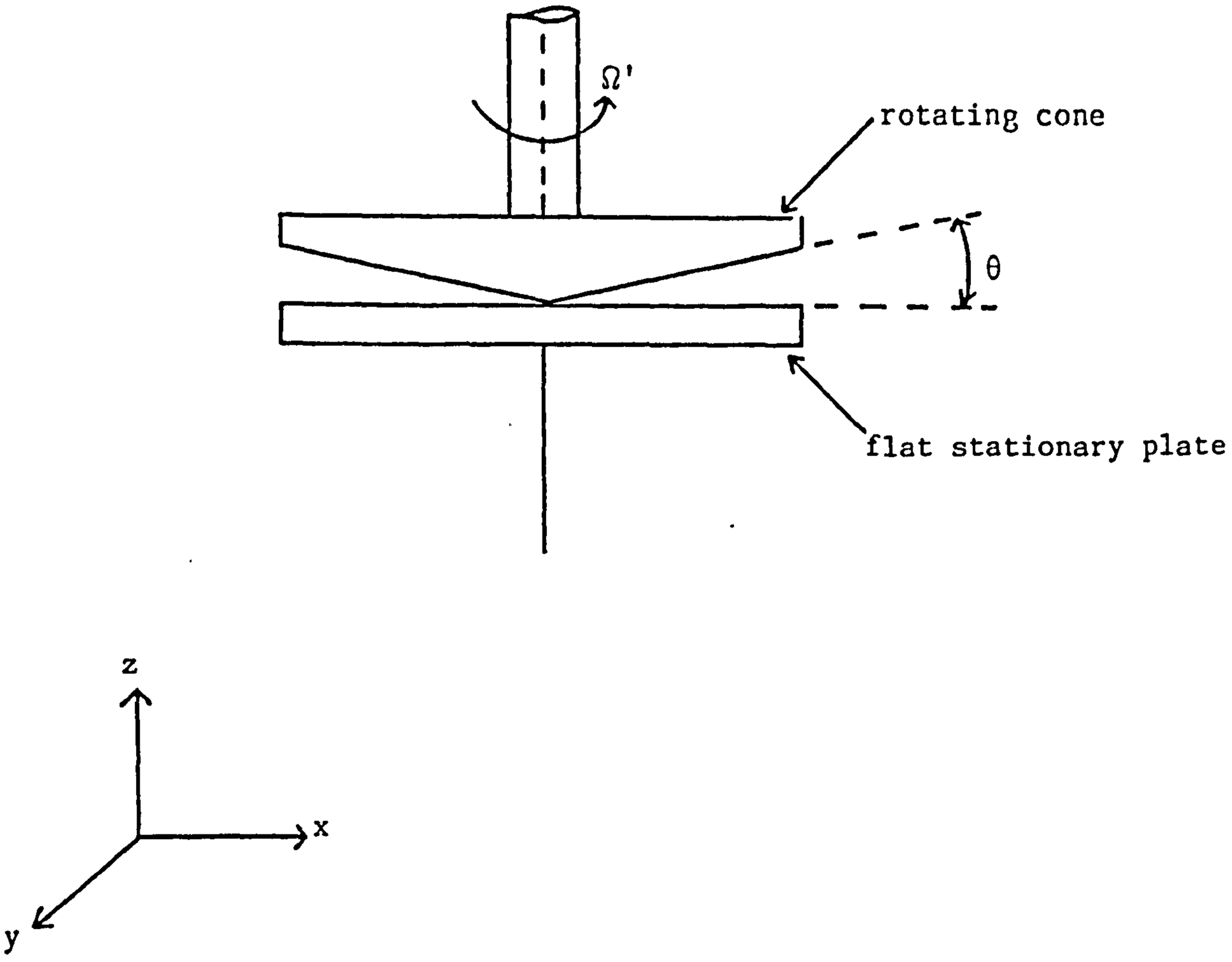

FIGURE 8.2: Diagram showing the geometry for the basic cone and plate

cone and the plate, α, is small (usually less than 3^{o}). The main feature of this type of viscometer is that, provided the angle between the cone and plate is small, the rate of shear is uniform throughout the sample.

The velocity gradient or rate of shear is

$$\dot{\gamma} = r \frac{d\Omega'}{dz} \tag{8.1}$$

and for small z the velocity gradient is constant, so

$$\dot{\gamma} = r \frac{\Omega'}{z} \tag{8.2}$$

where Ω' is the angular velocity of the cone and r is the distance from the y-axis in the x-y plane. By making use of the conical gap, as shown in Figure 8.2, then

$$\frac{z}{r} = \tan \alpha \tag{8.3}$$

where α is in radians. Hence,

$$\dot{\gamma} = \frac{\Omega'}{\tan \alpha} \tag{8.4}$$

and

$$\dot{\gamma} = \frac{\Omega'}{\alpha} \tag{8.5}$$

for small values of α; i.e. $\dot{\gamma}$ is independent of r.

The moment of the tangential frictional force is

$$M = \int_{o}^{R_1} \frac{\Omega'}{\alpha} \eta \; r2\pi r.dr \tag{8.6}$$

or

$$M = \frac{\Omega'}{\alpha} 2\pi\eta \int_{o}^{R_1} r^2.dr \tag{8.7}$$

where η is the viscosity of the sample under test.

On integration, η is given as

$$\eta = \frac{3M\alpha}{2\pi\Omega' R_1^3} \qquad (8.8)$$

8.2.2 Calibration of the Instrument

Two calibration constants had to be determined for the cone-and-plate assembly, one to convert the angular velocity, Ω, to the shear rate, γ, and the other to convert the torque, T, to the shear stress, τ_c.

The shear rate may be given by

$$\dot{\gamma} = \frac{\Omega'}{\theta} = \Omega'\alpha_c \qquad (8.9)$$

where θ, the cone angle = 0.013rad , and α_c, the calibration constant = 76.9.

The shear stress may be given by

$$\tau_c = \beta_c T \qquad (8.10)$$

The calibration constant, $\beta_c = 3/2\pi R_1^3$ (where $R_1(2.5\times10^{-2}m)$ is the radius of the cone) determined using 20% w/w, 40%w/w and 60%w/w sucrose solutions of known viscosity[259]. In all cases, the angular velocity, and hence the shear rate, was measured as a function of applied torque and plots made of torque against shear rate. The gradient of the shear stress against shear rate plot was the viscosity of the solutions, η. However, inaccurate values were obtained for these known viscosity solutions. So the torque, T, of the instrument had to be re-calibrated to obtain a correction factor necessary for the determination of accurate values for the sucrose solutions at 25^oC.

The torque of the instrument was re-calibrated and a correction factor obtained by a method illustrated schematically in Figure 8.3. Different weights were hung at the centre of the thread length (which

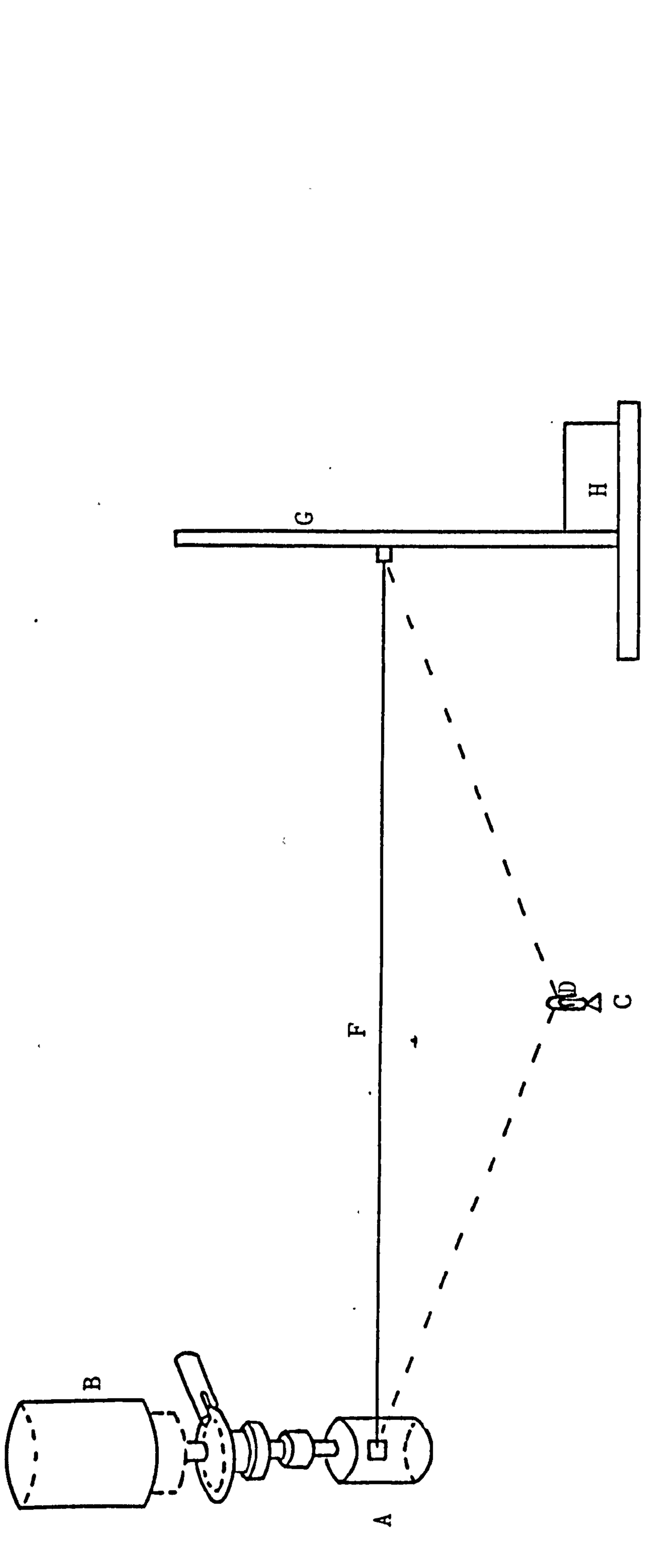

FIGURE 8.3: Schematic diagram of the recalibration method. A = measuring element (concentric cylinder);
B = driving unit; C = plasticine; D = paper clip; E = Travelling microscope; F = cotton thread;
G = retort stand; H = brick

simultaneously lowered the thread). Then, different torques were used to return the thread instantly to its original position. The thread was wound round the rotating element (of a concentric cylinder assembly) in the opposite direction to that in which the upper cylinder would windmill freely.

Hence, the correct torque was applied to counterbalance the effect of the weights. The heights with and without weights were determined using a travelling microscope.

8.2.2.1 Analysis of the Correction Factor

Let us assume that C_1 and C_2 are the resultant force components as shown in Figure 8.4. Therefore

$$A = B \sin \gamma \tag{8.11}$$

$$B = \frac{C_1}{\sin \gamma}, \text{ therefore } C_1 = B \sin \gamma \tag{8.12}$$

$$A = C_1 \frac{\cos \gamma}{\sin \gamma} = C_1 \frac{a/b}{c/b} \tag{8.13}$$

therefore

$$T_1 = C_1 \frac{a}{c} \tag{8.14}$$

Similarly,

$$T_2 = C_2 \frac{d}{c} \tag{8.15}$$

therefore

$$\frac{T_1}{T_2} = \frac{C_1}{C_2} \frac{a}{d} \tag{8.16}$$

as $T_1 = T_2$, then $C_1 = \frac{d}{a} C_2$

$$mg = C_1 + C_2 = C_1\left(1 + \frac{d}{a}\right) \tag{8.17}$$

therefore

$$C_1 = mg\left(\frac{a}{a + d}\right) \tag{8.18}$$

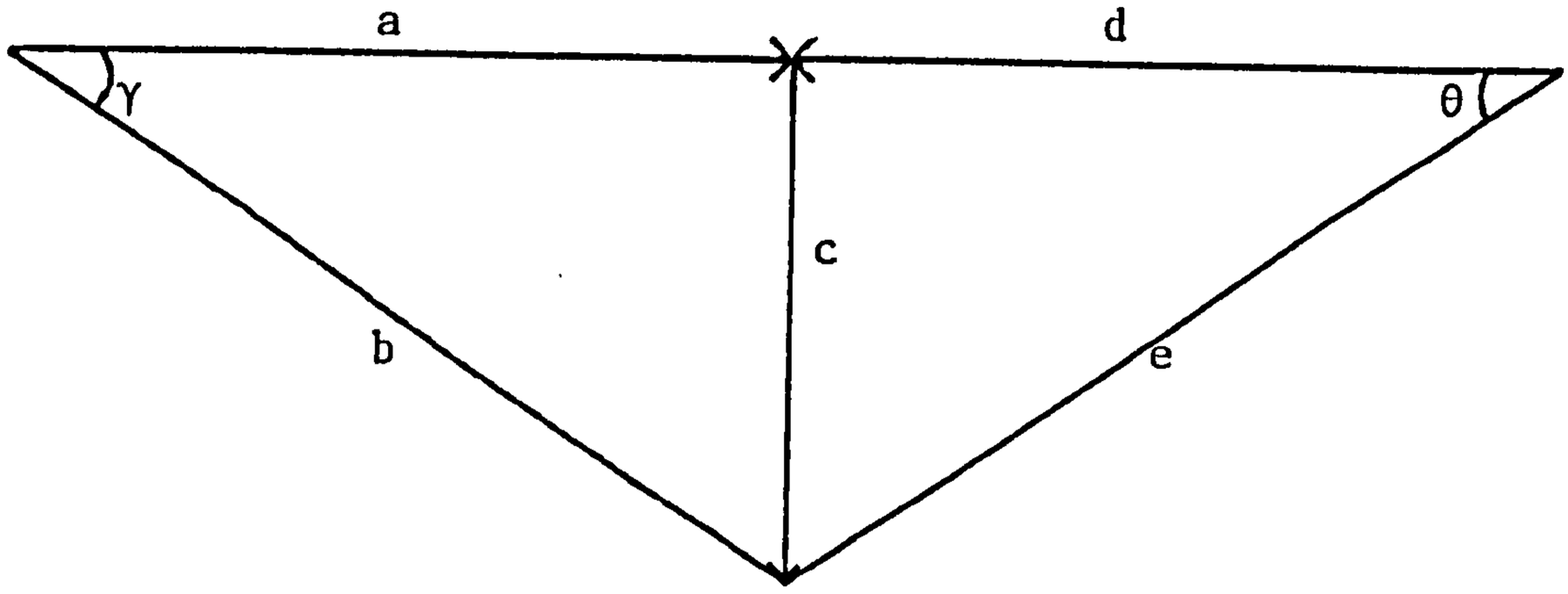

Force Components

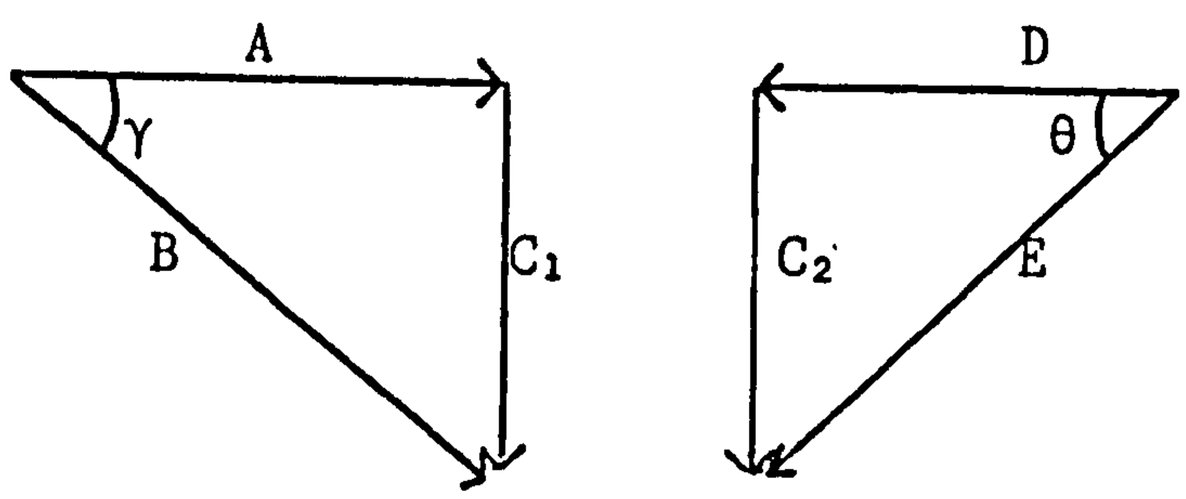

FIGURE 8.4: Schematic diagram for analysis

Substituting equation (8.18) into (8.14), we have

$$T_1 = mg\left(\frac{a}{a + c}\right)\frac{a}{c} \qquad (8.19)$$

therefore

$$T = mg\,\frac{a^2}{c(a + d)} \qquad (8.20)$$

where m is the mass of the weight, r is the radius of the rotating element, and g is the acceleration due to gravity ($9.81 ms^{-2}$). The length (a + d) remained constant throughout the experiment.

The values determined for the 20% w/w, 40% w/w and 60% w/w sucrose solutions were $1.437 \times 10^{-3} Nsm^{-2}$, $4.47 \times 10^{-3} Nsm^{-2}$ and $5.02 \times 10^{-2} Nsm^{-2}$ respectively.

The correction factor determined for the torque was 0.6909, and the calibration constant for the instrument taken as 2.111×10^4.

Therefore

$$\dot{\gamma} = 76.9\Omega' \qquad (8.21)$$

$$\tau_c = 2.111 \times 10^4 T \qquad (8.22)$$

8.3 Modification of the Rheometer Into a Rotational Torsion Surface Viscometer

8.3.1 Introduction

Rotational methods[284-286] where the surface layer is sheared in an annular space between the two concentric boundaries are not as likely to suffer from artefacts introduced by dissolution of the surface-active material as the canal method, where there is a variable surface pressure. However, both methods do suffer from drag penetration into the layers of the solution below the shearing planes. If the surface viscosity of the film is high, however, the contribution to the stress from the bulk material will be low.

Here, the essential elements are three concentric perspex rings, of which one pair is stationary and fixed, while the other ring turns about its axis with a constant rotational velocity. The resistance of a film entrained between the fixed rings opposes this motion. A certain section of the surface is separated by bringing up the stationary (lower) element of the rings to just break through the surface, and hence isolate a region which can be rotated or oscillated.

8.3.2 Description of the Apparatus

This couette-type viscometer is illustrated schematically in Figure 8.5. The trough was made of perspex and was screwed down to the base of the adjustable screw stand. It was necessary to sweep the surfaces and to contain the film, so that the subphase stood above the rim of the trough. The surface pressure was measured by a Wilhelmy plate, and it could be adjusted by moving teflon booms across the liquid surface. The pair of stationary concentric rings could be raised or lowered by way of a micrometer. The upper rotating element was connected to the sealed driving motor of the rheometer.

8.3.3 Analysis of the Apparatus

For a purely elastic planar membrane sheared between concentric circular boundaries of radius r_2 and r_1, and arbitrary radius r such that $r_2 > r > r_1$, the shear rate and shear stress for a small annular element in the surface distance r from the axis may be written explicitly for a small relative motion. The geometrical arrangement of the surface viscometer is shown in Figure 8.6.

The surface shear stress is given by

$$\tau_s = \frac{\text{peripheral force}}{\text{circumference}} = \frac{T}{2\pi r^2} \qquad (8.23)$$

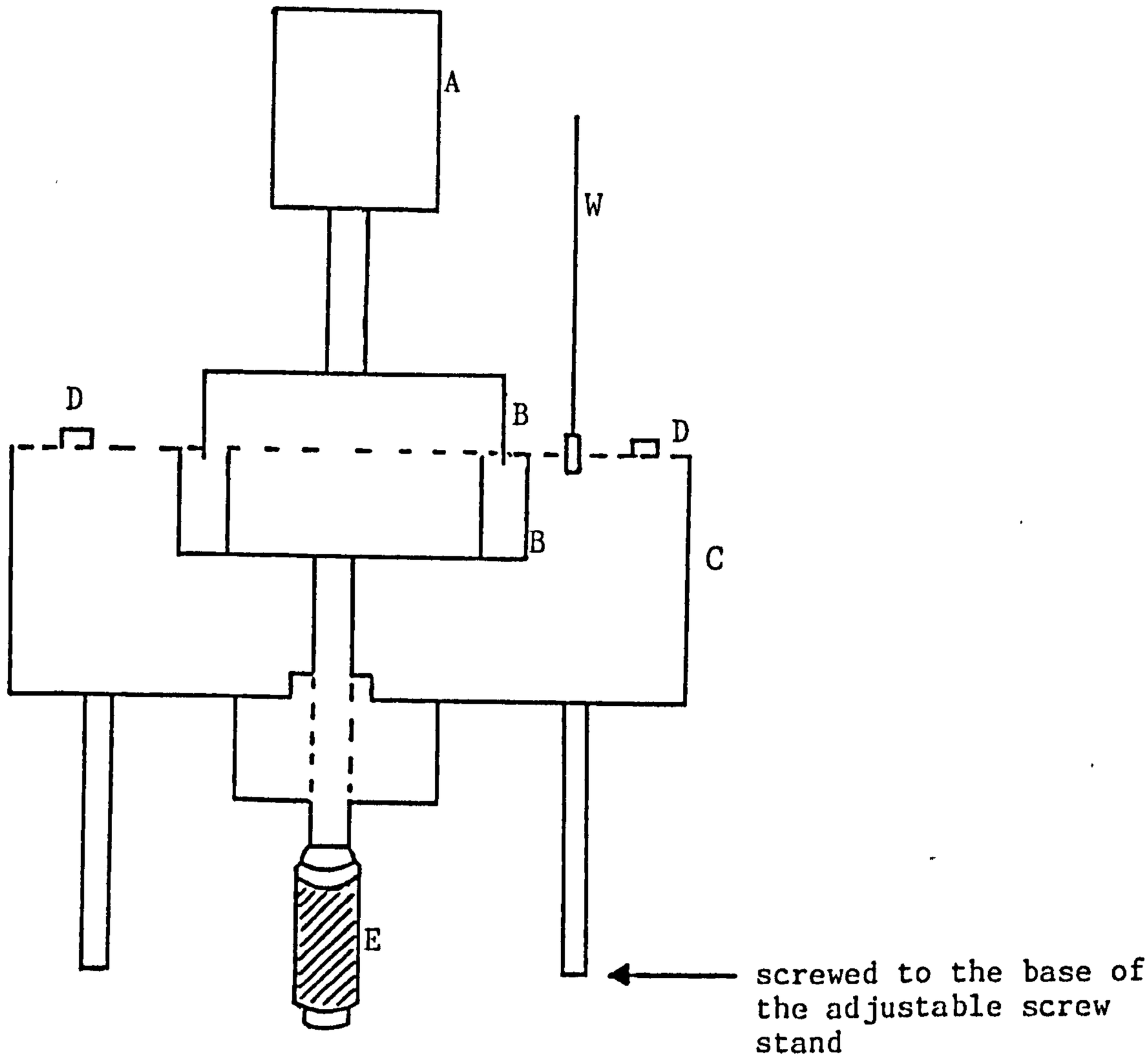

FIGURE 8.5: Cross-sectional diagram of the Deer rheometer as a rotational torsion surface viscometer. A = sealed driving unit; B = measuring elements (perspex); C = perspex trough; D = teflon barrier; E = micrometer; F = Wilhelmy plate

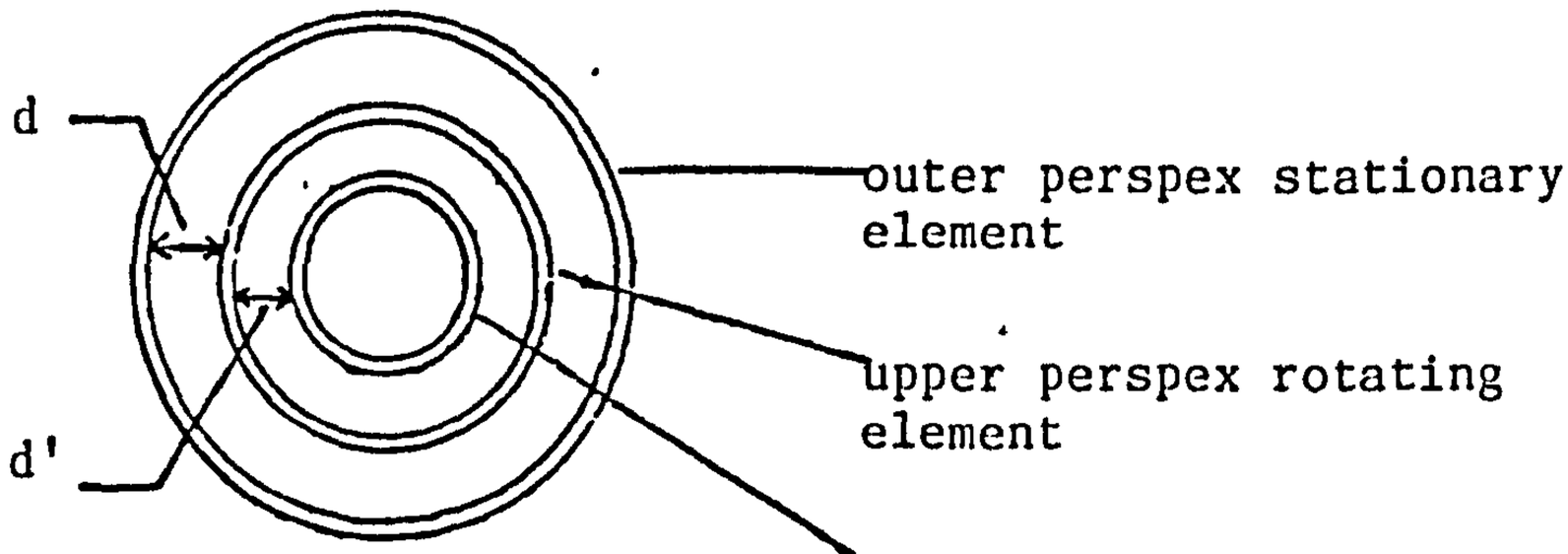

d' = 1.75mm

d = 1.15mm

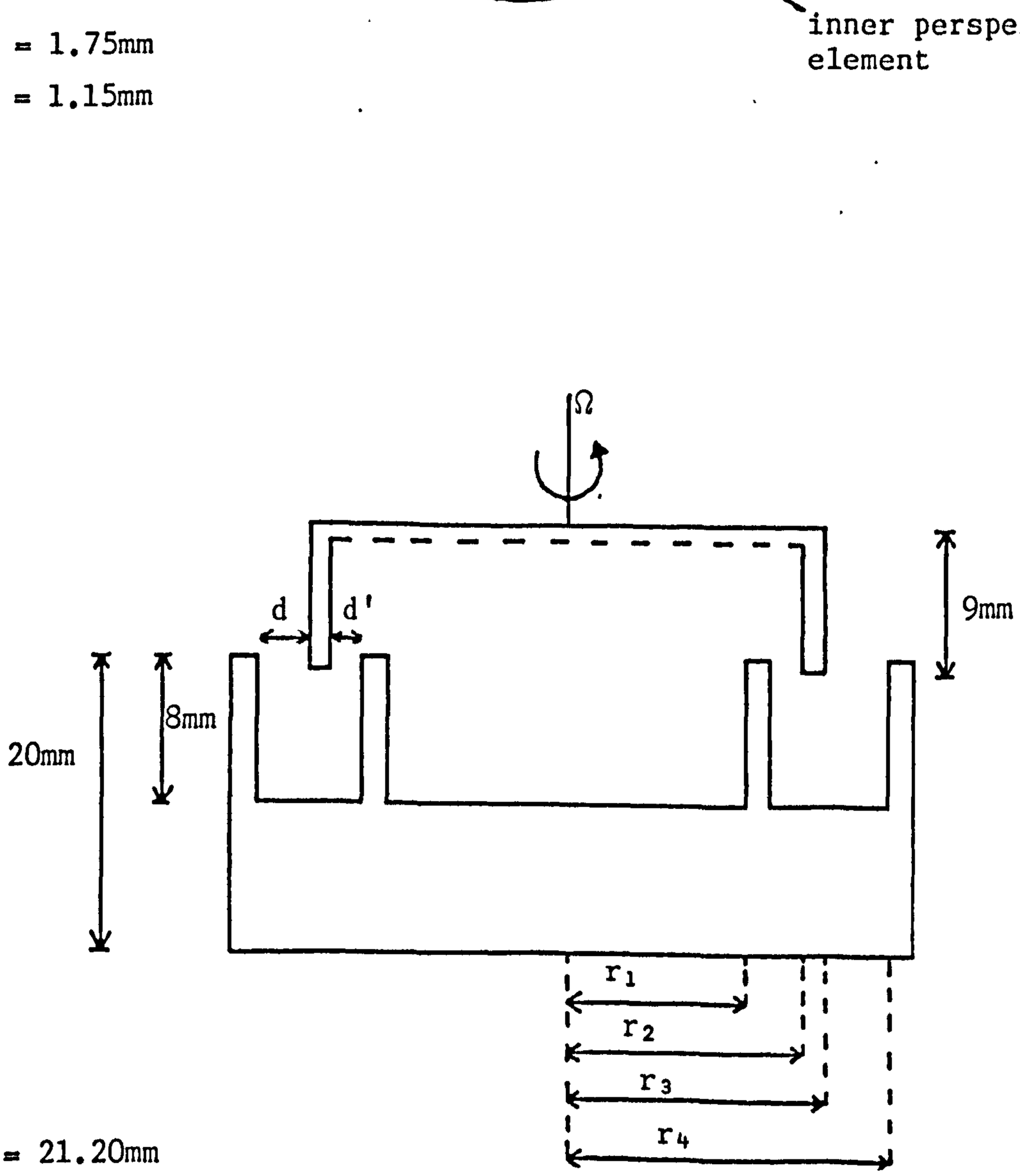

r_1 = 21.20mm

r_2 = 22.95mm

r_3 = 23.40mm

r_4 = 24.55mm

FIGURE 8.6: Diagram showing dimensions of the rotational torsion surface geometry of the Deer rheometer (not drawn to scale)

where T is the applied torque.

The surface shear rate can be written as the velocity gradient, i.e.

$$\dot{\gamma} = \frac{du}{dr} = \frac{r d\Omega}{dr} \qquad (8.24)$$

where Ω is the angular rotation.

The surface shear viscosity, η_s, is then given by equation (8.23) and equation (8.24)

$$\eta_s = \frac{\tau_s}{\dot{\gamma}} = \frac{T\ dr}{2\pi r^3 d\Omega} \qquad (8.25)$$

It is then necessary to integrate over the limits $r = r_1$ and $r = r_2$ and $\Omega = {}'\Omega$ and $\Omega = \Omega_0$ and by rearranging

$$\eta_s = \frac{T}{4\pi}\left(\frac{1}{r_1^2} - \frac{1}{r_2^2}\right)\frac{1}{{}'\Omega - \Omega_0} \qquad (8.26)$$

where ${}'\Omega$, Ω_0 are the angular rotations in the absence and presence of the film.

This method assumes that the rotating element is of zero thickness and makes a line contact with a plane, semi-infinite, liquid surface; that there is no slip between the rotating element and its line contact with the liquid surface; also, that there is no swelling of the perspex trough, which might alter the day-to-day value of the instrument constant, α_D.

8.3.4 Instrument Constants

Figure 8.6 shows the dimensions of the gaps d and d' between the upper rotating element and the inner and outer stationary elements respectively.

The shear rate may be given as

$$\dot{\gamma} = \frac{r_2\Omega}{\delta} = \alpha_D\Omega \qquad (8.27)$$

where r_2 is the radius of the rotating element, δ is the gap (d or d'), Ω is the angular velocity of the rotating element, and α_D is the calibration constant. The value of α_D was found to be 16.73.

For any given applied torque, the shear stress may be given by

$$\tau = \beta_D T \qquad (8.28)$$

The value of β_D was found to be 2.713×10^4.

The viscosity of 20% w/w, 40% w/w and 60% w/w sucrose solution at 22°C has been accurately determined to be $2.12 \times 10^{-3} Nsm^{-2}$, $5.67 \times 10^{-3} Nsm^{-2}$ and $5.587 \times 10^{-2} Nsm^{-2}$ respectively.

8.3.5 Experimental

The trough was filled with a subphase of 0.01M hydrochloric acid, and the surface was swept clean using a vacuum pipette. A micropipette syringe was used to spread a known quantity of myristic acid dissolved in petroleum ether (bp 60-80°) onto the available surface area. The lower stationary element was raised to a position which just broke the surface, and the upper rotating element was lowered until it was just in contact with the surface also.

Different torques were then applied to the upper rotating element and the resultant angular velocities noted. A similar procedure had earlier been performed on the clean surface without the monolayer.

8.3.6 Result and Discussion

The result obtained for a myristic acid monolayer was plotted as the surface shear viscosity as a function of shear rate. The plot shows a shear thickening behaviour, as described in Section 3.1.1.1. This shows a marked similarity to the viscosity-time plots of myristic acid, obtained from the fluon-coated Langmuir trough. There is no known ref-

erence to this feature in the literature. Figure 8.7 shows an increase in viscosity with shear rate. Table 8.1 presents values for the difference in the angular rotation in the absence and presence of a film, viscosity, shear stress and the shear rate.

Because of the necessity to work at very low frequencies for surface rheology, this apparatus would not have been sensitive enough for the detection of polydimethylsiloxane monolayers. However, further work may include the use of a glass trough (to avoid the swelling problem of perspex) to study the viscosities of fatty acid monolayers as a function of solubility.

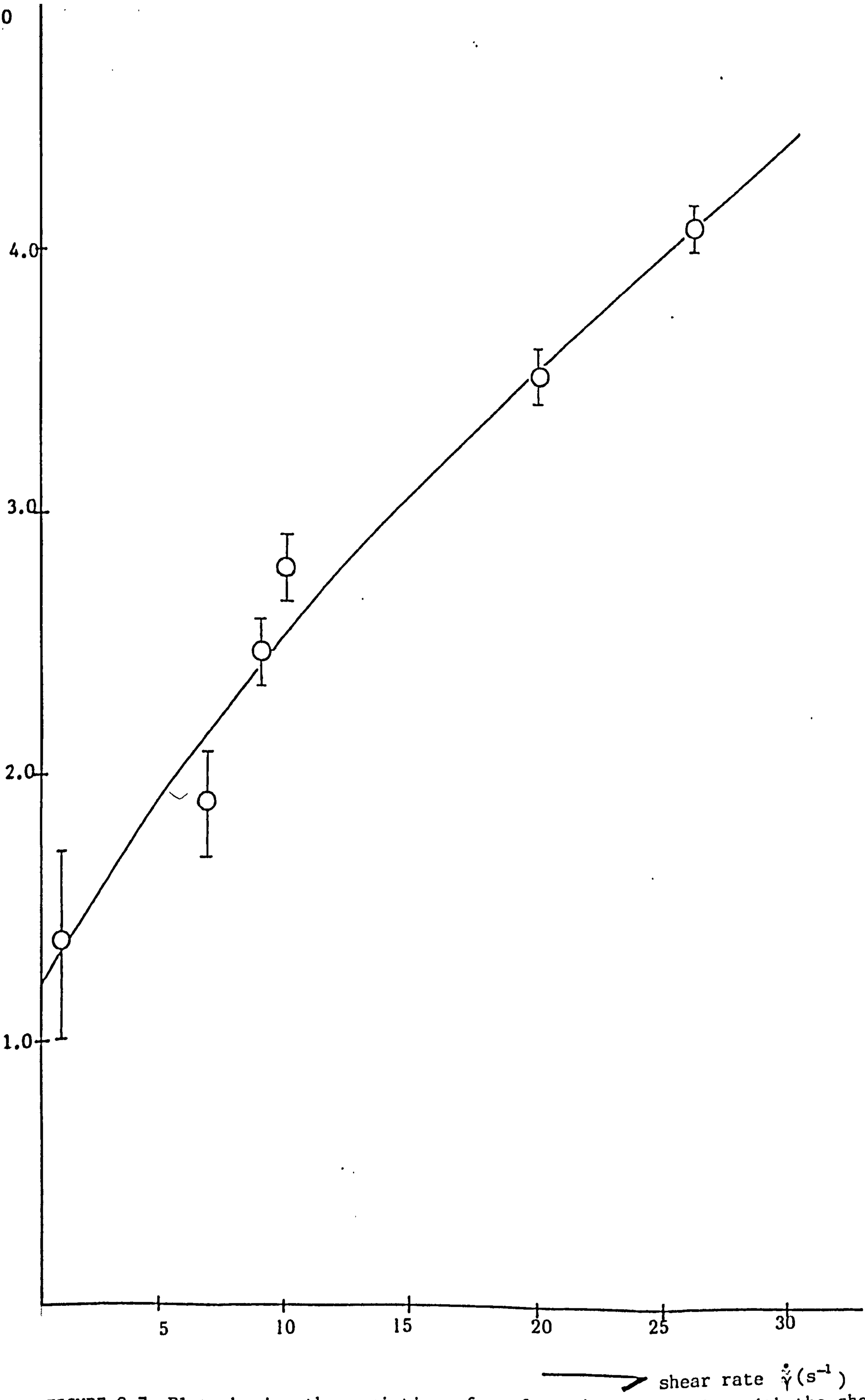

FIGURE 8.7: Plot showing the variation of surface shear viscosity with the shear rate for myristic acid on an 0.01M hydrochloric acid subphase. pH = 2.3 ± 0.02, T_r = 20.5 ± 0.1°C

$'\Omega-\Omega_0$ (s^{-1})	Surface Viscosity (sP)	Shear Rate, γ (s^{-1})	Surface Shear Stress (mNm^{-1})
0.05	1.41×10^{-5}	0.8365	1.18×10^{-5}
0.4	1.88×10^{-5}	6.692	1.258×10^{-4}
0.55	2.47×10^{-5}	9.201	2.27×10^{-4}
0.6	2.83×10^{-5}	10.04	2.84×10^{-4}
1.2	3.53×10^{-5}	20.08	7.088×10^{-4}
1.7	4.02×10^{-5}	28.44	1.00×10^{-3}

$'\Omega,\Omega_0$ = angular rotation in the absence and presence of the monolayer

TABLE 8.1: Data obtained from the rotational torsion surface viscometer of the surface shear rate, shear stress and viscosity of myristic acid on an 0.01M hydrochloric acid subphase

$T_6 = 20.5 \pm 0.1^{o}C$

pH = 2.3 ± 0.02

surface pressure = $10mNm^{-1}$

volume of myristic acid added = 43µl

CHAPTER 9

THE PULSED DROP TENSIOMETER

9.1 Introduction

The method used to measure the interfacial dilational parameters of a crude oil/aqueous phase involved the propagation of longitudinal waves of known frequency, and measuring changes of interfacial tension with a Wilhelmy plate using an interfacial film balance[225]. However, this technique suffered from a number of disadvantages.

A new technique was developed, capable of measuring dynamic interfacial tensions of crude oil/aqueous systems by Clint *et al*[226], and recently modified by Goodall[227] at the BP Research Centre, Sunbury-on-Thames.

So, the aim of this work was to develop and improve the performance of the instrument's capability to measure the pressure drop of a bubble formed in an air/water interface. This method involved the pressure inside a bubble being forced to undergo a pulsed surface area change. The relaxation of the pressure was recorded and subsequently used to calculate the surface dilational elasticity (or modulus), ε_d, and dilational viscosity, η_d, at a range of frequencies via the Fourier transformation of temporal interfacial tension data

$$\varepsilon = \frac{d\gamma}{d\ \ell n\ a} = \frac{A\ d\gamma}{dA} \qquad (9.1)$$

where ε is the pure elasticity and A is the surface area.

9.2 Relaxation Processes Within Interfaces

For an interface to exhibit viscoelastic behaviour, it must undergo some relaxation process on either compression or dilation. For this

behaviour to be observed, the time-scale of at least one of the relaxation processes must fall within the time-scale of the experiment.

A few possible relaxation mechanisms with their time-scale on dilation are:

(i) The equilibration of surface tension via the Marangoni effect $\sim 10^{-3}$sec. The time-scale of this process depends largely on both the chain cohesion of the surface-active material and on the bulk viscosity of the adjoining liquids. The process would take longer with high chain cohesion and bulk viscosity.

(ii) The rapid adsorption of material from the immediate sublayer region $\sim 10^{-2}$sec. Here, the time-scale would be dependent on the bulk concentration of the surfactant; if micelles were present, then rapid adsorption from the sublayer could be determined by the time for micellar breakdown.

(iii) The diffusion of material to the interface from the bulk liquid phases ≥ 1 sec. The rate of diffusion to the interface depends on the bulk viscosity, the concentration and size of the species, the temperature and any enhancement by eddy or convection currents.

(iv) The adsorption of and displacement by competing material ≥ 1 sec. This may occur where the rate of adsorption at an interface of one component was more rapid than another; however, if the component adsorbing more slowly was more surface-active, then it would eventually displace the rapidly-adsorbed material from the interface.

On compression of an interface, in the absence of even film collapse, the number of possible relaxation mechanisms would appear to be fewer.

(i) The reorientation of surface material to more constrained positions.

(ii) The re-equilibration of surface tension gradients via the Marangoni effect.

(iii) The rapid desorption of material into the immediate subsurface regions followed by slower diffusion into the bulk liquids.

The type of relaxation mechanism that occurs upon dilation or compression is largely dependent on the type of interface being examined. Interfaces can be divided into four types when discussing their dilational rheological properties:

(i) pure interfaces;

(ii) insoluble material spread at the interface;

(iii) soluble material adsorbed at the interface;

(iv) a mixture of soluble and insoluble material at the interface.

Pure interfaces only exhibit rheology on compression or dilation at short times. Soluble monolayers are examined over a time-scale of 1-1000 seconds, the measured modulus $|\varepsilon|$ at high frequencies determines the surface properties after rearrangements and Marangoni effects have taken place, but before the occurrence of any adsorption or desorption by diffusion. Here, the interfacial layer acts as if it were insoluble and the viscosity falls to zero, $|\varepsilon| \rightarrow \varepsilon = d\gamma/d\ \ell n\ A$ (only if the area also falls to zero).

Insoluble monolayers will exhibit elastic behaviour when observed over time-scales greater than the time taken for Marangoni and orientational effects to occur, i.e. $\geq 10^{-3}$ seconds. In this case, $|\varepsilon| = \varepsilon_d$, $\eta_d \approx 0$, $\varepsilon_d = \varepsilon = d\gamma/d\ \ell n\ A$ (only if the area change is small).

In the case of soluble/insoluble monolayers, the amount of insoluble material is fixed or has very little effect on the experimental time-scale, so the relaxation processes observed over times $\geq 10^{-3}$ seconds include the adsorption or desorption of the soluble component of the film, as well as reorientational effects.

9.3 Analysis of the Instrument

The area changes were calculated from a knowledge of the bubble and tip diameters, and interfacial tension changes determined by measuring the Laplace pressure over the bubble using a sensitive pressure transducer.

The equilibrium pressure after the experiment was lower than that at the beginning because the bubble radius was larger. The pressure change, after the rapid rise, was assumed to take place at a constant bubble radius, the final radius r_2.

The interfacial tension at any time $\gamma(t)$ is given by

$$\Delta p(t) = \frac{2\gamma(t)}{r_2} \tag{9.2}$$

The interfacial modulus is usually written as

$$\varepsilon^* = d\gamma/d\ \ell n\ A = \varepsilon' + i\varepsilon'' \tag{9.3}$$

Taking Fourier transforms of the numerator and denominator converts the perturbation time function $\Delta A(t)/A$ and the response time function $\gamma(t)$ to the frequency function. Thus:

$$\varepsilon^*(\omega) = \frac{\int_{-\infty}^{\infty} \Delta\gamma(t)\ e^{-i\omega t}\ dt}{\int_{-\infty}^{\infty} \frac{\Delta A}{A}(t)\ e^{-i\omega t}\ dt} \tag{9.4}$$

For a perfect step function (instantaneous area change),

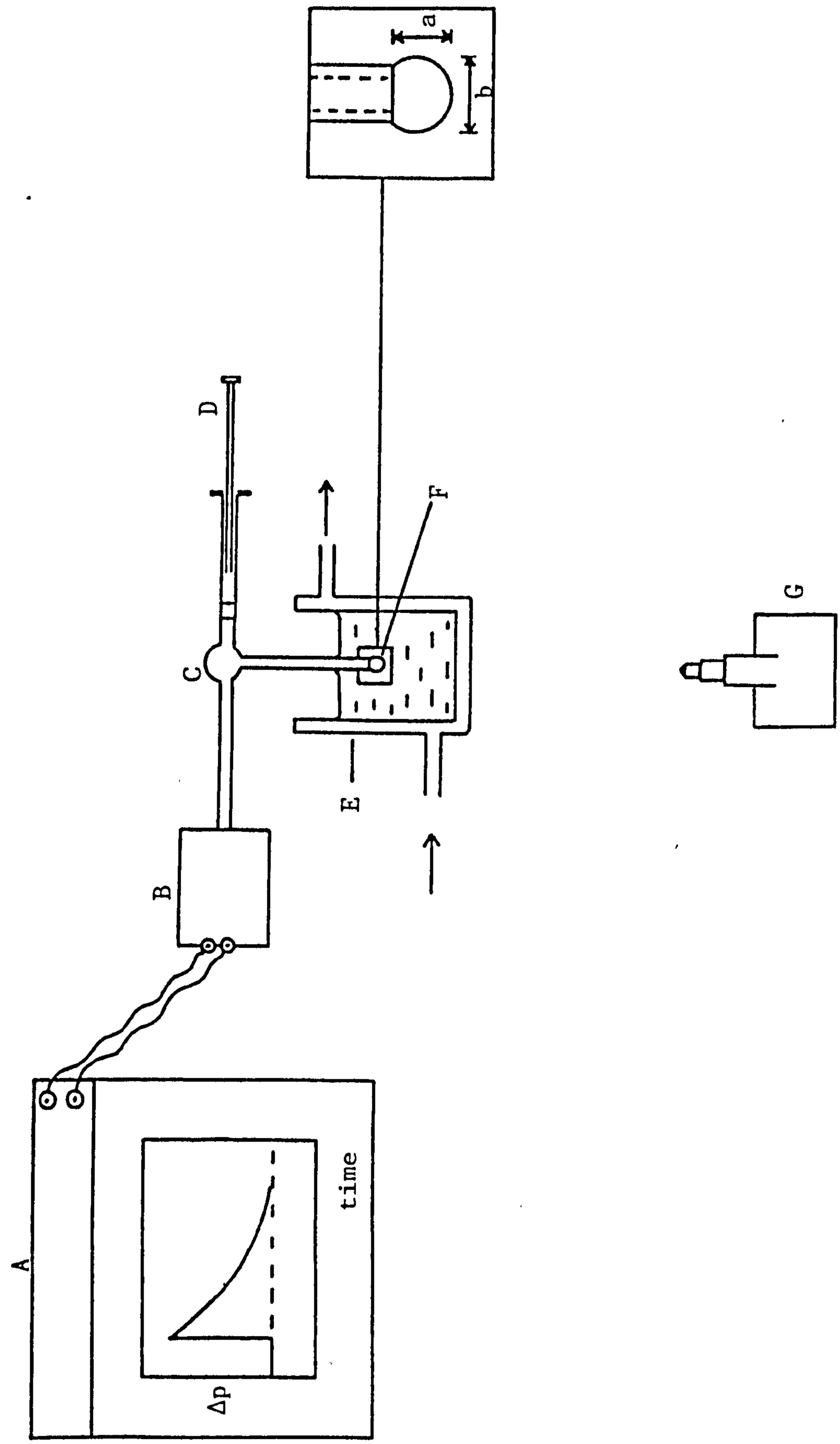

FIGURE 9.1: Schematic diagram of the pulsed-drop tensiometer. A = chart recorder; B = sensitive pressure transducer; C = three-way 'cheminert' adaptor; D = 1000µl syringe; E = thermostatted glass vessel; F = air bubble; G = travelling microscope

$$\int_{-\infty}^{\infty} \frac{\Delta A}{A}(t)\, e^{-i\omega t}\, dt = \frac{\Delta A/A}{i\omega} \tag{9.5}$$

Therefore:

$$\varepsilon^*(\omega) = \frac{i\omega}{\Delta A/A} \int_{o}^{\infty} \Delta\gamma(t)[\cos \omega t - i \sin \omega t]dt \tag{9.6}$$

The real part gives the dilational elasticity

$$\varepsilon' = \varepsilon_d(\omega) = \frac{\omega}{\Delta A/A} \int_{o}^{\infty} \Delta\gamma(t) \sin \omega t\, dt \tag{9.7}$$

The imaginary part gives the dilational viscosity

$$\varepsilon'' = \omega\eta_d(\omega) = \frac{\omega}{\Delta A/A} \int_{o}^{\infty} \Delta\gamma(t) \cos \omega t\, dt \tag{9.8}$$

where ω is the angular frequency (radians per second).

9.4 Experimental Details

The pulsed-drop apparatus is schematically illustrated in Figure 9.1. It consists of a gas-tight syringe connected via a three-way 'cheminert' fitting to a narrow-bore needle with a flattened end (at which the bubble of air was formed), and a sensitive pressure transducer (SE Lab Ltd., Type No. SE 1150/D5964, 25WG).

The narrow-bore needle was immersed in a thermostatted temperature bath containing sodium lauryl sulphate (0.01M) solution. In a typical experiment, a bubble of known size (measured using a travelling microscope) was formed at the needle tip and allowed to age for a known period of time, was then made to undergo an instantaneous area deformation; the interfacial tension change was indirectly measured from the varying output of the transducer, observed on a chart recorder. When equilibrium

was re-established, the bubble size was adjusted or a new bubble formed.

Discussion of Instrument Artefacts

A number of problems were encountered while determining the performance of the instrument in its new mode. One of the main problems was due to a leak in the pressure transducer; this resulted initially in an evident reduction in bubble size and then later in an enlargement of the bubble, when a constant size was needed for ageing before undergoing an instantaneous area deformation. To overcome this leak problem, the earlier method by Clint *et al*[226] was referred to, where the membrane of the transducer was completely filled with fluid for a liquid/liquid interface. Using this method, the membrane (and transducer as a whole) needed to be rid of all solvent. This task was performed by dismantling and thoroughly cleaning all parts of the transducer, then drying, before sealing it back so that it was air-tight. However, the leak problems persisted, and so all connections to and away from the three-way 'chemin-ert' valve were also made air-tight.

Some of the traces presented were obtained with a micromanometer MDC-FC004 (Furness Controls Ltd., England), which appeared to be a more sensitive pressure transducer than that from SE Lab Ltd.

9.5 Results and Discussion

It was not the aim of an examination of this system to obtain absolute values for rates of adsorption from solution; rather, it was to determine the workability of the pulsed-drop tensiometer in a new modified form. However, there is an evident proportionality between the measured pressure and the surface tension at constant radius, with the surface tension being related to the area per surface-active molecule[228] (a non-linear relationship). Also, if the area change of the bubble is

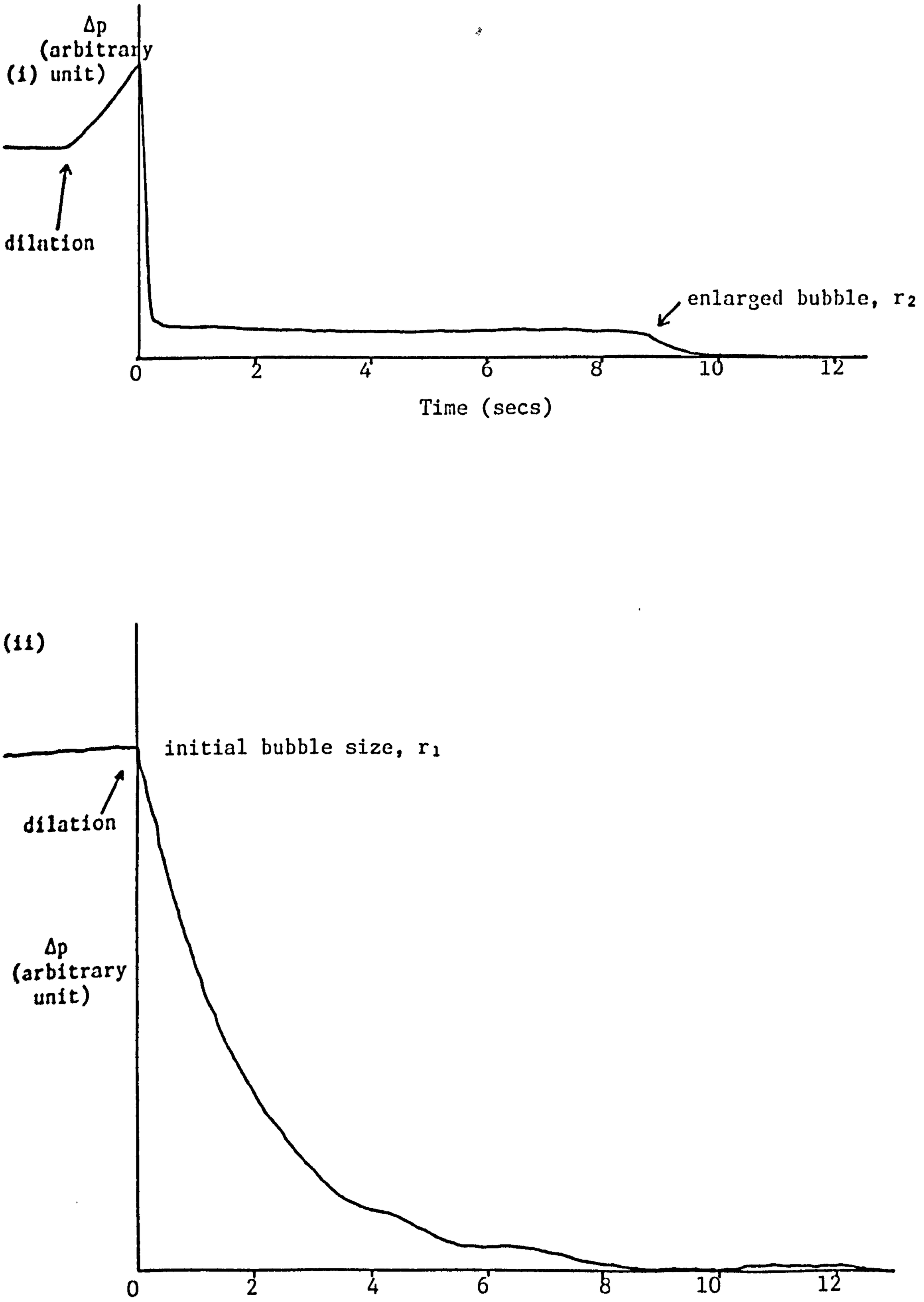

FIGURE 9.2(i)-(ii): Typical chart recorder output for dilation of an air bubble in 10^{-2}M sodium lauryl sulphate solution

(iii)

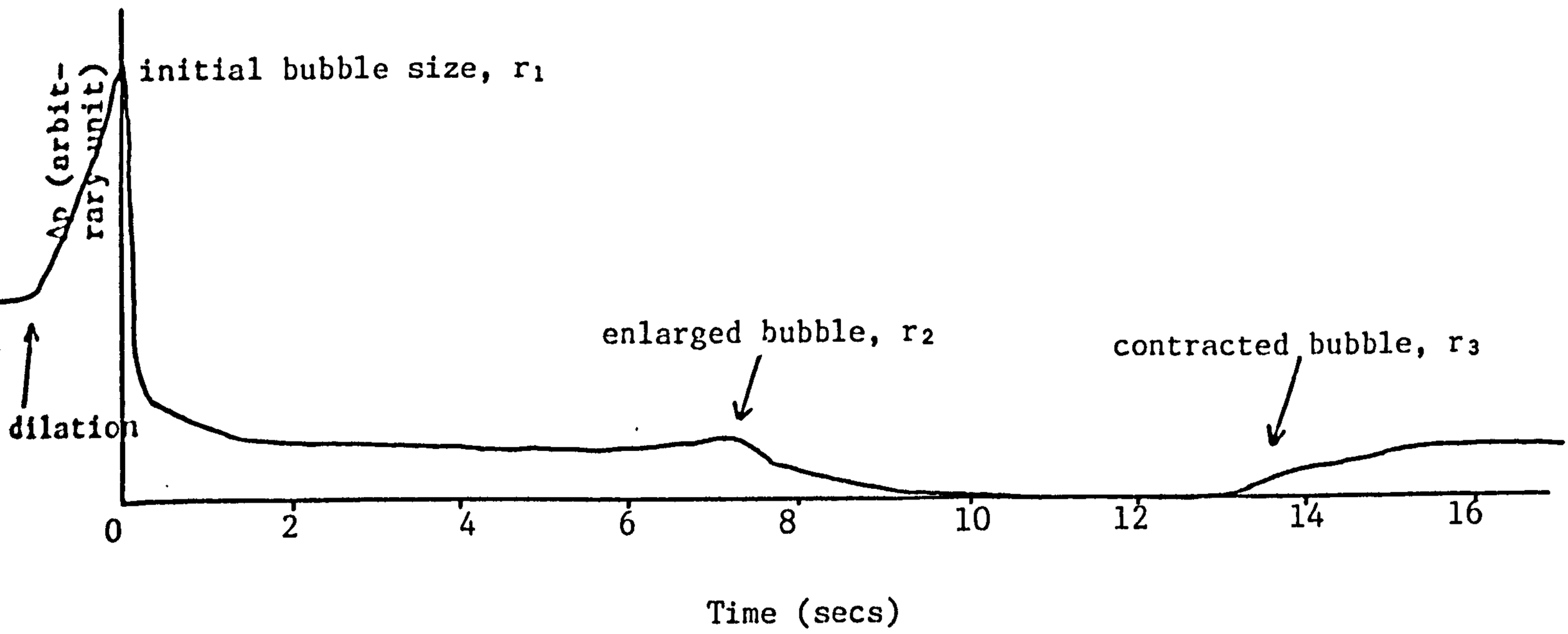

(iv)

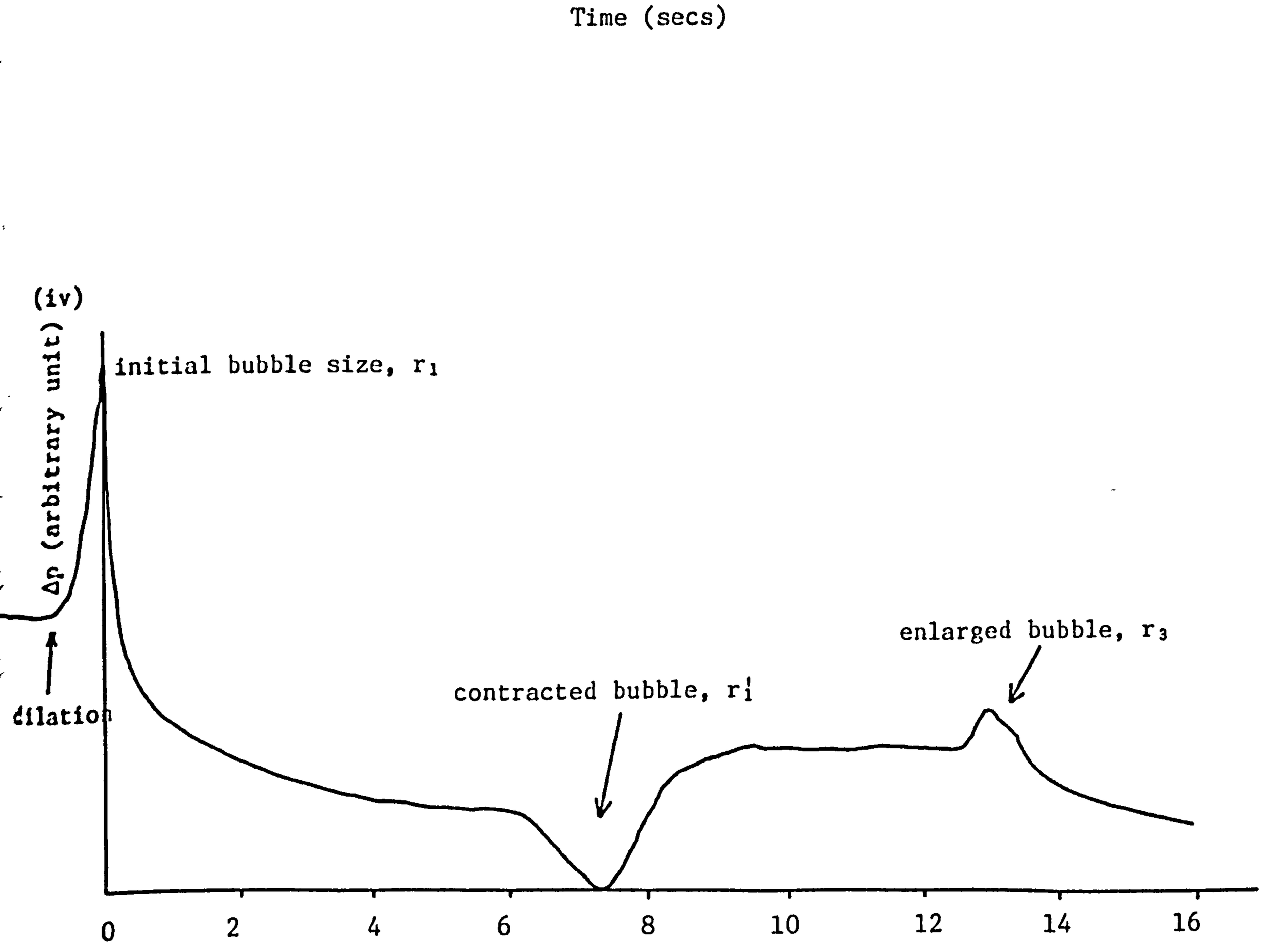

FIGURE 9.2(iii)-(iv): Typical chart recorder output for the dilation of an air bubble in 10^{-3} M sodium lauryl sulphate solution

(v)

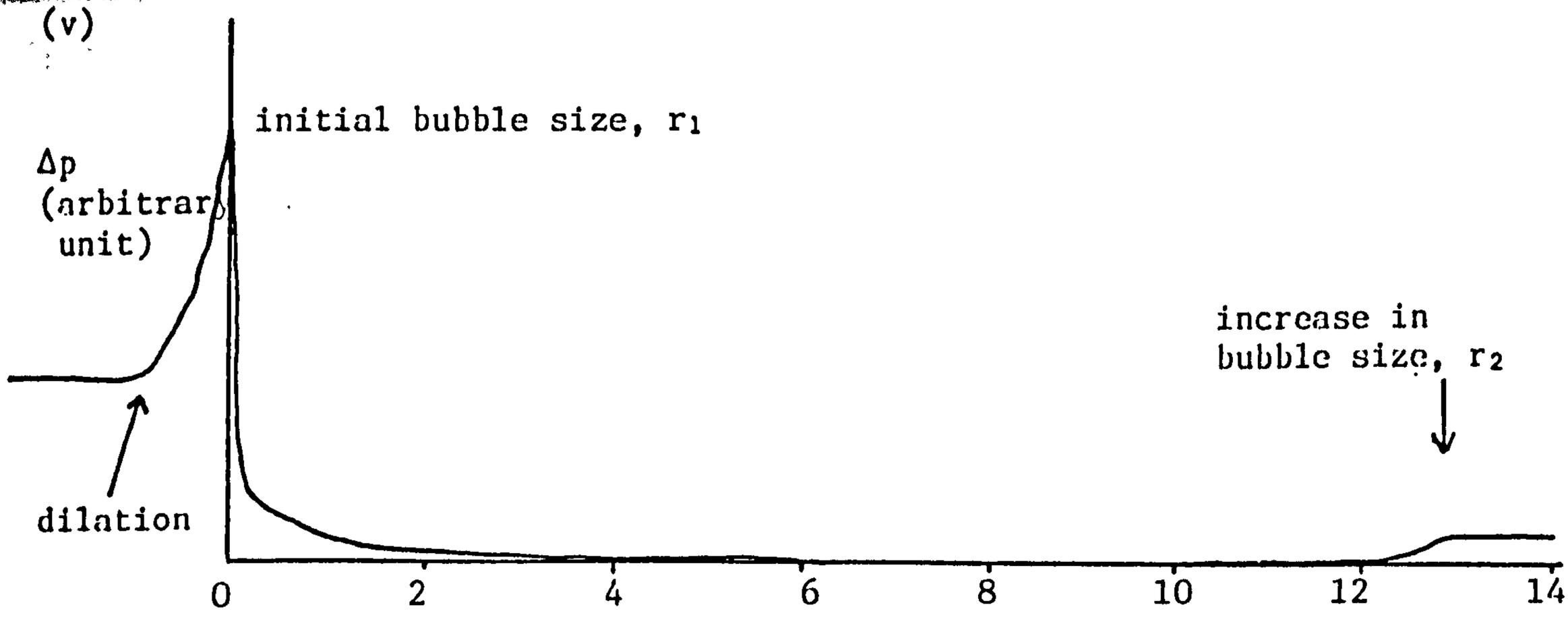

(vi)

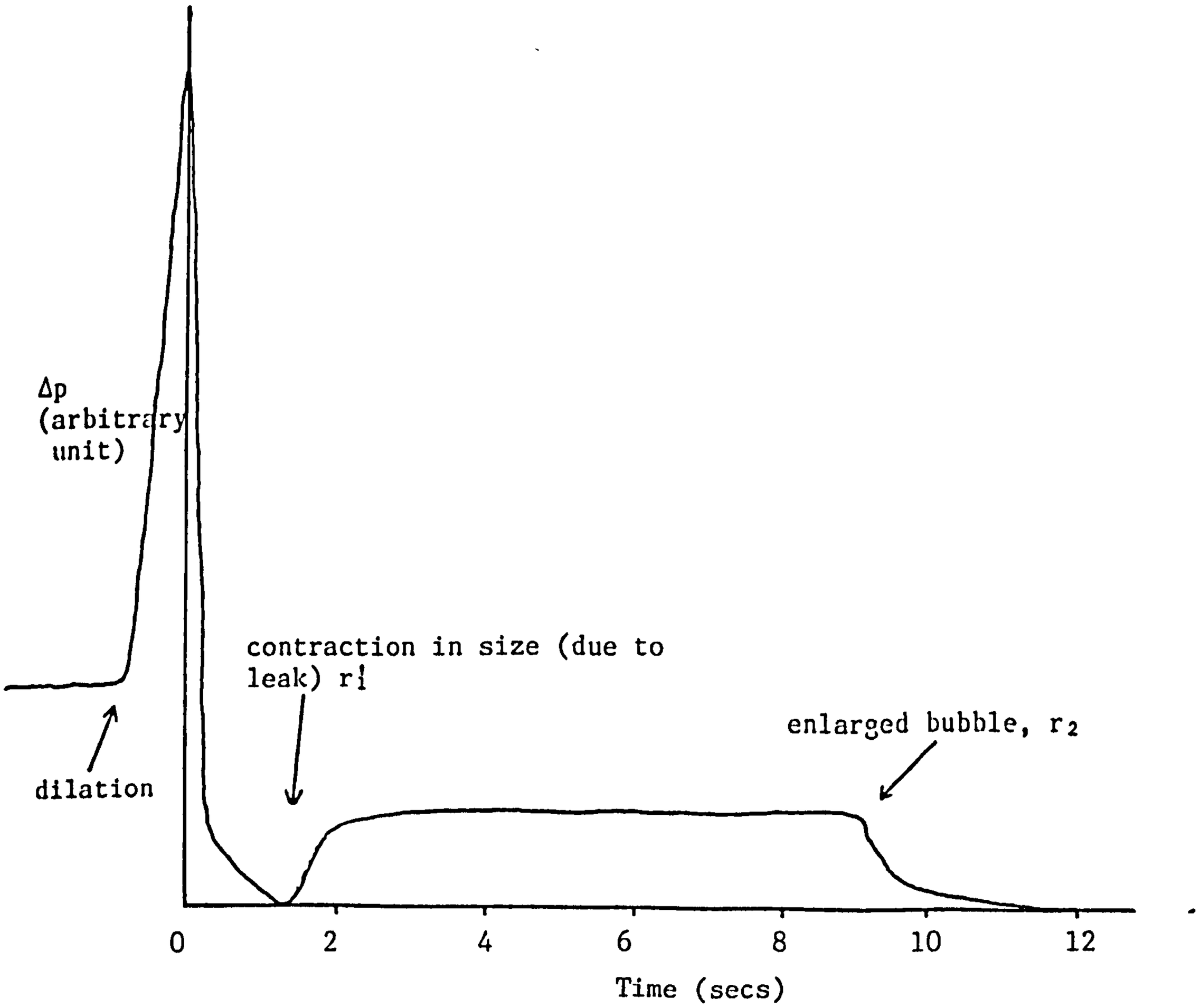

FIGURE 9.2(v)-(vi): Typical chart recorder output for the dilation of an air bubble in 10^{-4}M sodium lauryl sulphate solution

vanishingly small, then there is a similar effect from the adsorbing molecules on the interfacial tension with the adsorption process being reflected in the pressure change. This is not necessarily the case if the area change is large and/or covers a phase change in the pressure-area curve for the particular surfactant present.

Typical traces from a chart recorded of the changing pressure within the bubble with time during a dilation and re-equilibration are shown in Figures 9.2(i)-(vi). It was necessary to alter the zero point of the differential pressure transducer to suit the particular chart recorder's sensitivity being used - hence absolute rather than relative pressure was measured.

If P_1 is the pressure over the bubble at radius r_1, and P_2 is the pressure after dilation to r_2 and re-equilibration, then the interfacial tension is determined from

$$P_1 = \frac{2\gamma}{r_1}, \quad P_2 = \frac{2\gamma}{r_2}$$

hence

$$P_1 - P_2 = 2\gamma\frac{1}{r_1} - \frac{1}{r_2} \qquad (9.9)$$

All the traces show very fast relaxation times (t secs). However, the object of this work was not to study the adsorption of sodium lauryl sulphate solution in detail.

The initial assumption related the increase in area (~10%) to a similar increase in radius (~0.5%), so that the surface tension increased as the area increased, therefore the pressure would increase simultaneously, as shown in the traces. This pressure could not be transmitted into voltage because of the differential transducer's leak problem. These problems are shown by the contraction troughs in the traces, and

also by the bubble size stability test, especially evident on the SE1150 transducer when connected to a Hewlett-Packard microcomputer which gave a digital pressure drop readout (in millivolts); this is shown in Figure 9.3. The computer program for the test is given in Appendix C.

The effect of the surfactant concentration as a stabilizing factor shows that at lower concentration the relaxation is slightly slower. This is probably due to the molecules taking a longer time to diffuse from the bulk to the interface, and so perhaps the only occurrence is the re-arrangement or re-alignment of molecules at the interface alone. Traces on Figures 9.2(iii)-(vi) show the initial formation of the bubble, followed by contraction and finally enlargement. This was the only way in which a bubble could be held long enough without losing it. The initial relaxation is rapid, followed by a slower one. As the area is increased initially, the surface potential at the interface is higher than that of the bulk, hence the rapid diffusion to the interface; but as the area is later increased, the diffusion is slower and therefore a slower relaxation time is apparent (~0.5 seconds).

Conclusion

It appears that a very sensitive and stable differential pressure transducer would show that the pulsed-drop tensiometer can be used under certain circumstances to obtain values of surface and interfacial tension, and to follow the relaxation processes occurring within a dilated interface in a reasonable and reproducible manner, yielding data which are well fitted by existing theory.

FIGURE 9.3: STABILITY TEST OF BUBBLE SIZE INCREASE

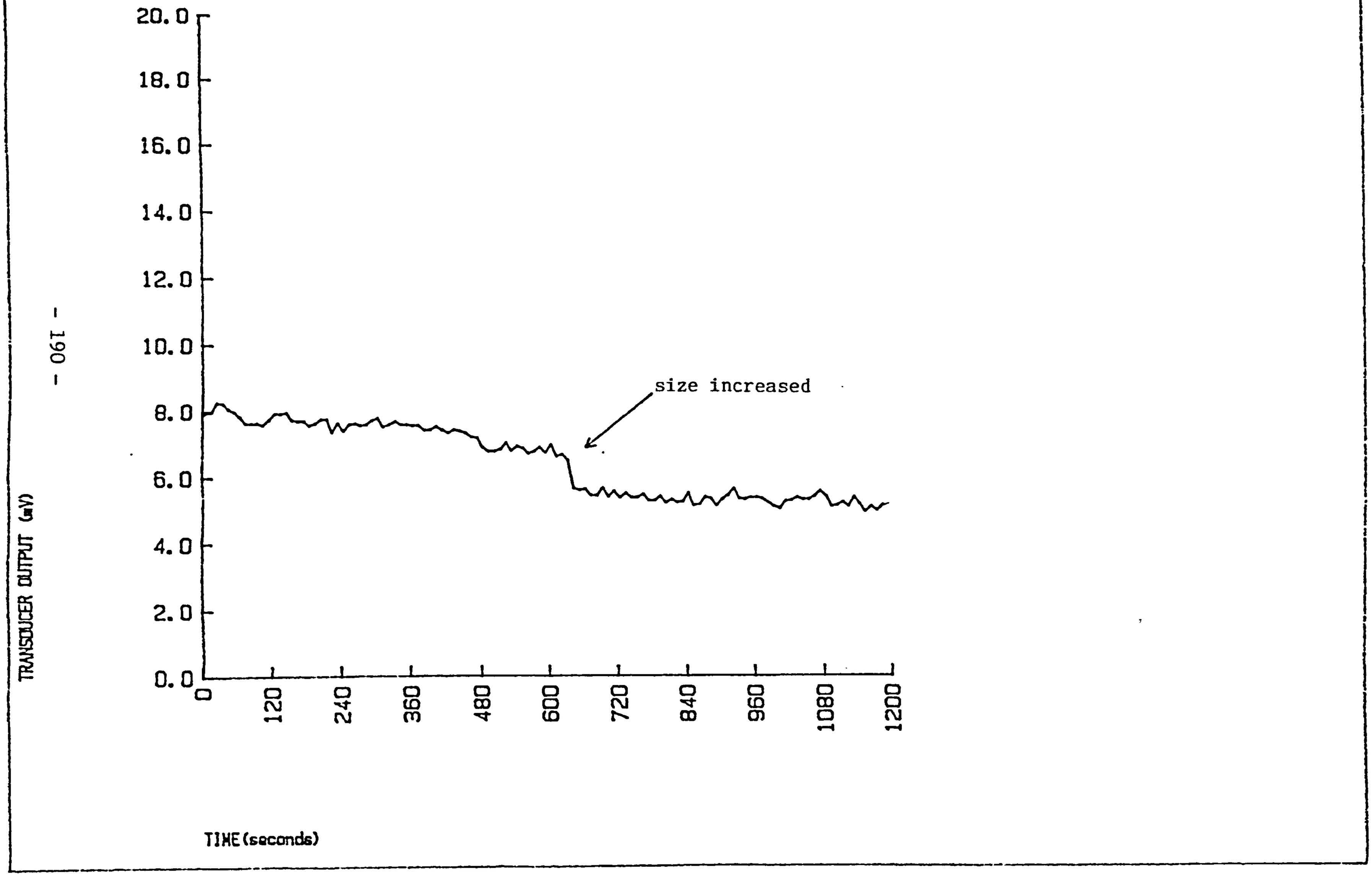

CHAPTER 10

RESULTS AND DISCUSSION

10.1 Fluon-Coated Trough Measurements

10.1.1 Results

The data obtained from this Langmuir trough apparatus for myristic and stearic acid monolayers were analysed as described in Chapters 3 and 7.

Figure 10.1 shows the straight line plot obtained for the calibration of the Wilhelmy plate and the chart recorder, and from the slope a value of 9.57mm/mN was found for the constant, k.

The dependence of surface pressure with the molecular area for both myristic and stearic acid monolayers is shown in Figures 10.2 and 10.3. The π-A isotherms showed a sharp discontinuity at surface pressures of approximately $12mNm^{-1}$ and $25mNm^{-1}$ for myristic and stearic acid respectively, indicating a phase change. The curves when extrapolated to zero surface pressures give molecular areas of 27.8Å^2 and 19.6Å^2 respectively, showing that the π-A isotherm of myristic acid is shallower. The compression moduli for various molecular areas from these acids are listed in Tables 10.1 and 10.2, and represented graphically in Figures 10.4 and 10.5. In both cases, the compression modulus falls to a minimum where the π-A isotherm exhibits a transition region. Myristic acid gave lower compression modulus values than stearic acid, even though the rate of change with surface pressure was higher.

(i) Canal Viscometer

The variation of flux, viscosity and activation energy of flow with the surface pressure across the canal were observed for the stearic

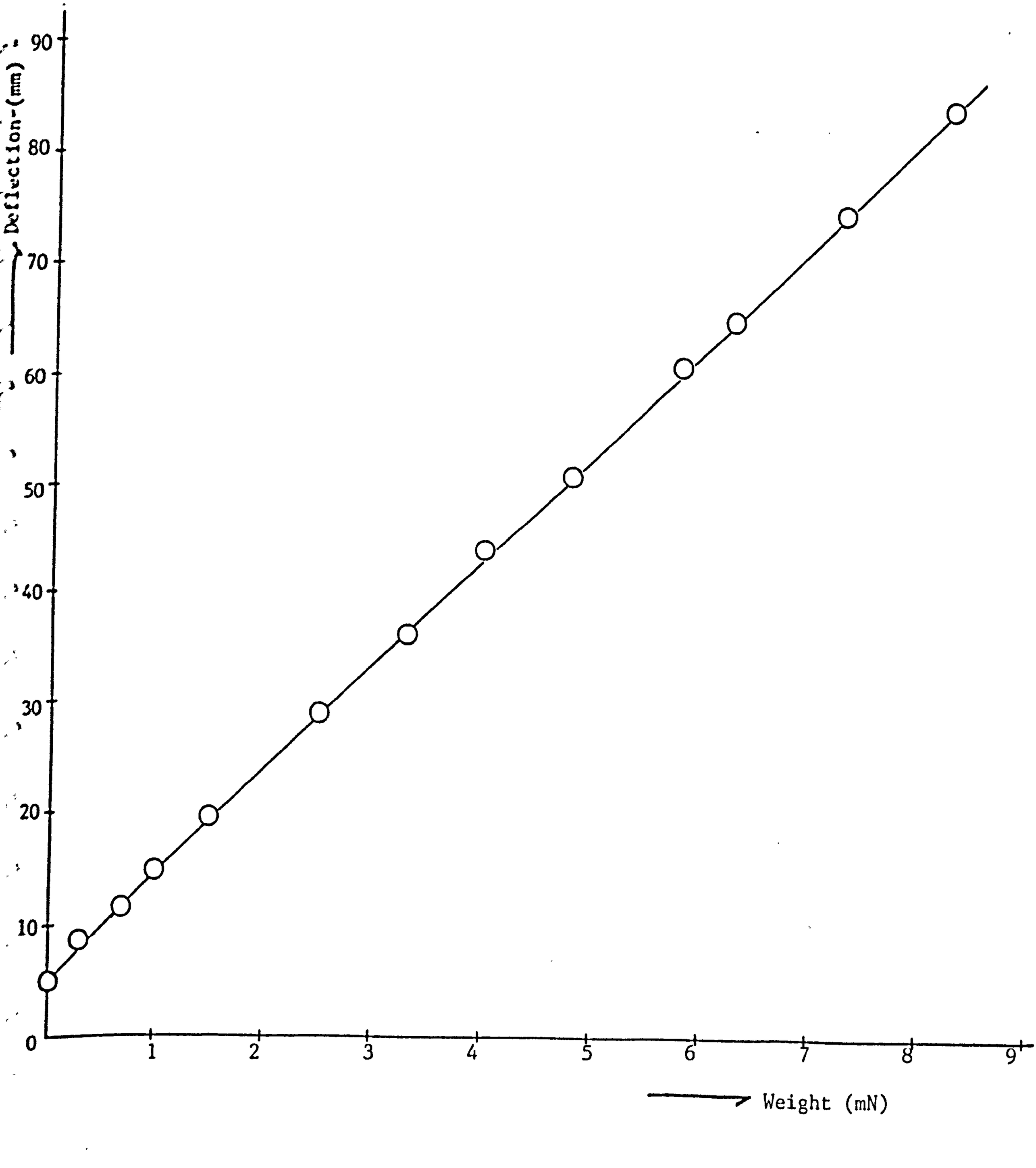

FIGURE 10.1: Plot showing the calibration of the Wilhelmy plate

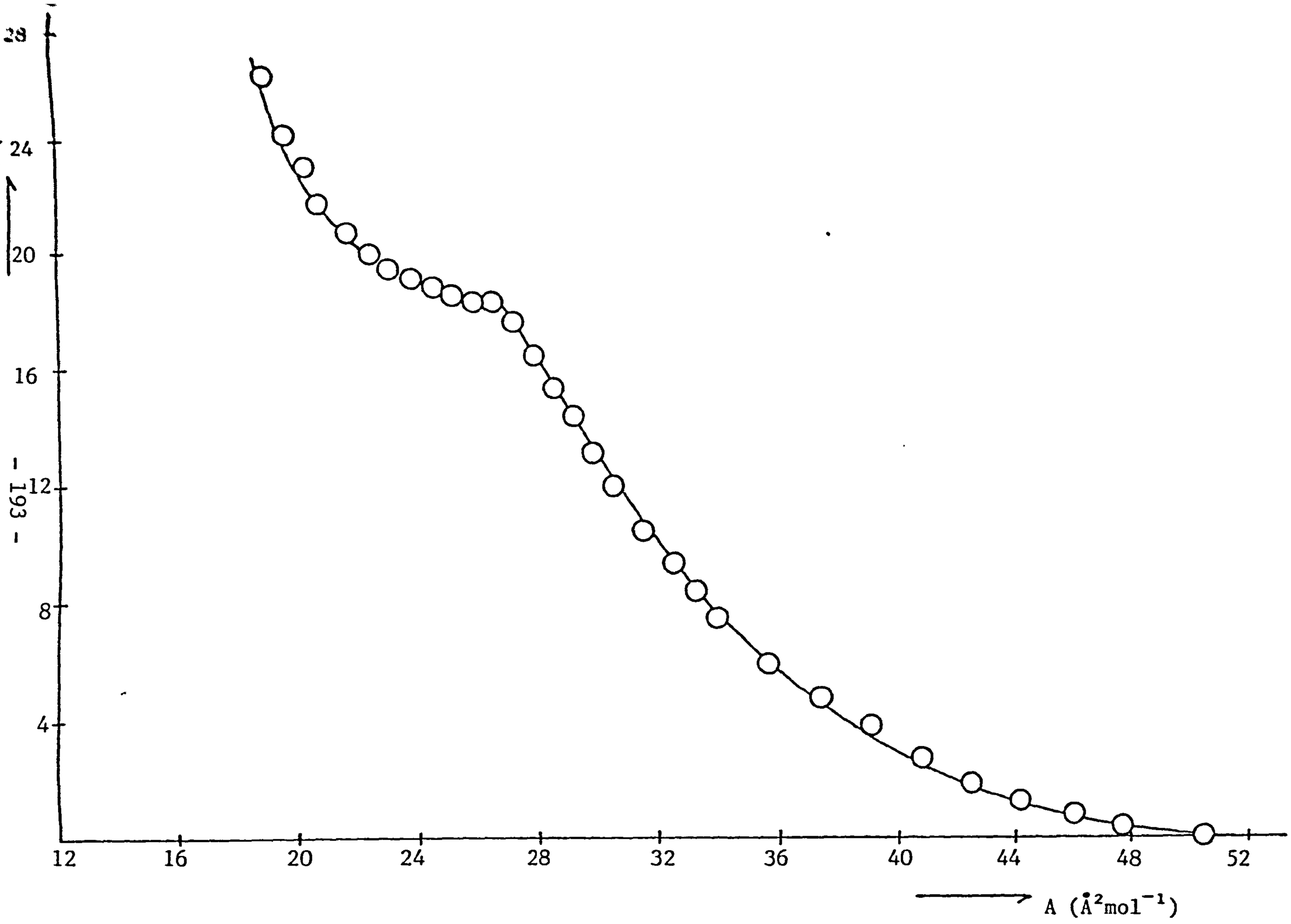

FIGURE 10.2: Plot of surface pressure against molecular area for myristic acid on an 0.01M hydrochloric acid subphase. T = 20.5 ± 0.5°C

TEXT BOUND INTO

THE SPINE

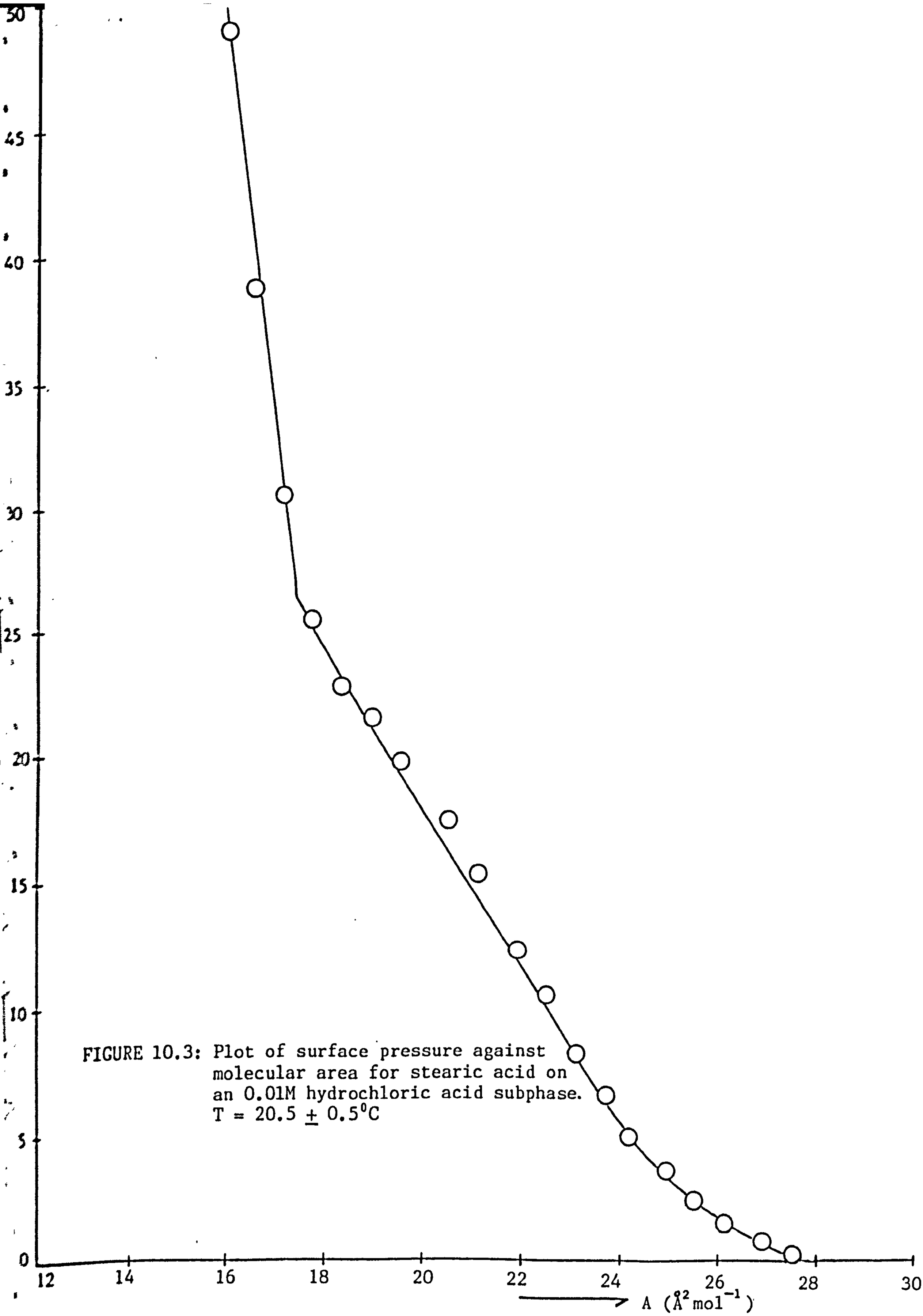

FIGURE 10.3: Plot of surface pressure against molecular area for stearic acid on an 0.01M hydrochloric acid subphase. T = 20.5 ± 0.5°C

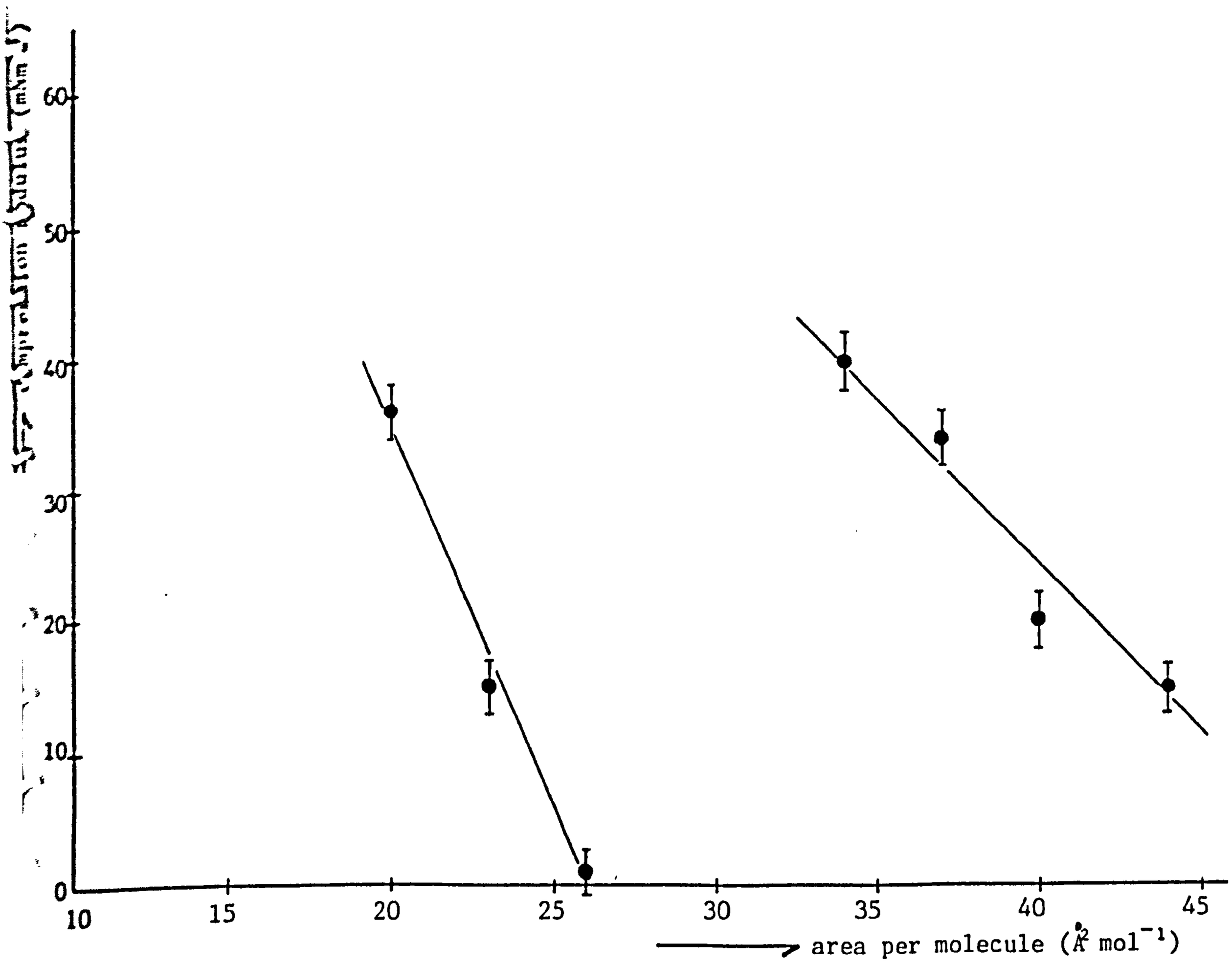

FIGURE 10.4: Plot showing the variation of compression modulus with area per molecule of myristic acid on an 0.01M hydrochloric acid subphase.

$T = 20.5 \pm 0.5^{o}C$

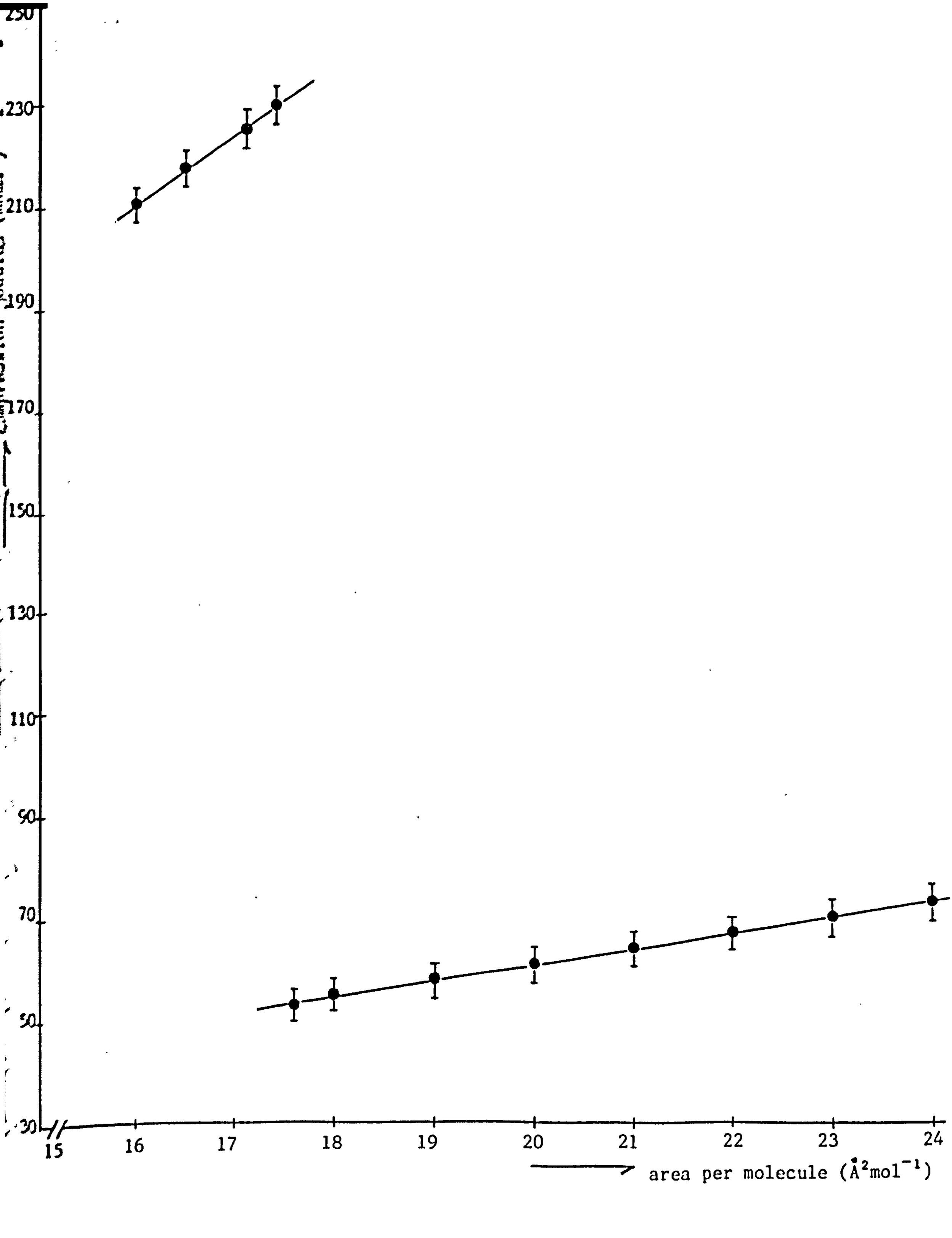

FIGURE 10.5: Plot showing the variation of compression modulus with area per molecule of stearic acid on a 0.01M hydrochloric acid subphase. T = 20.5 ± 0.5°C

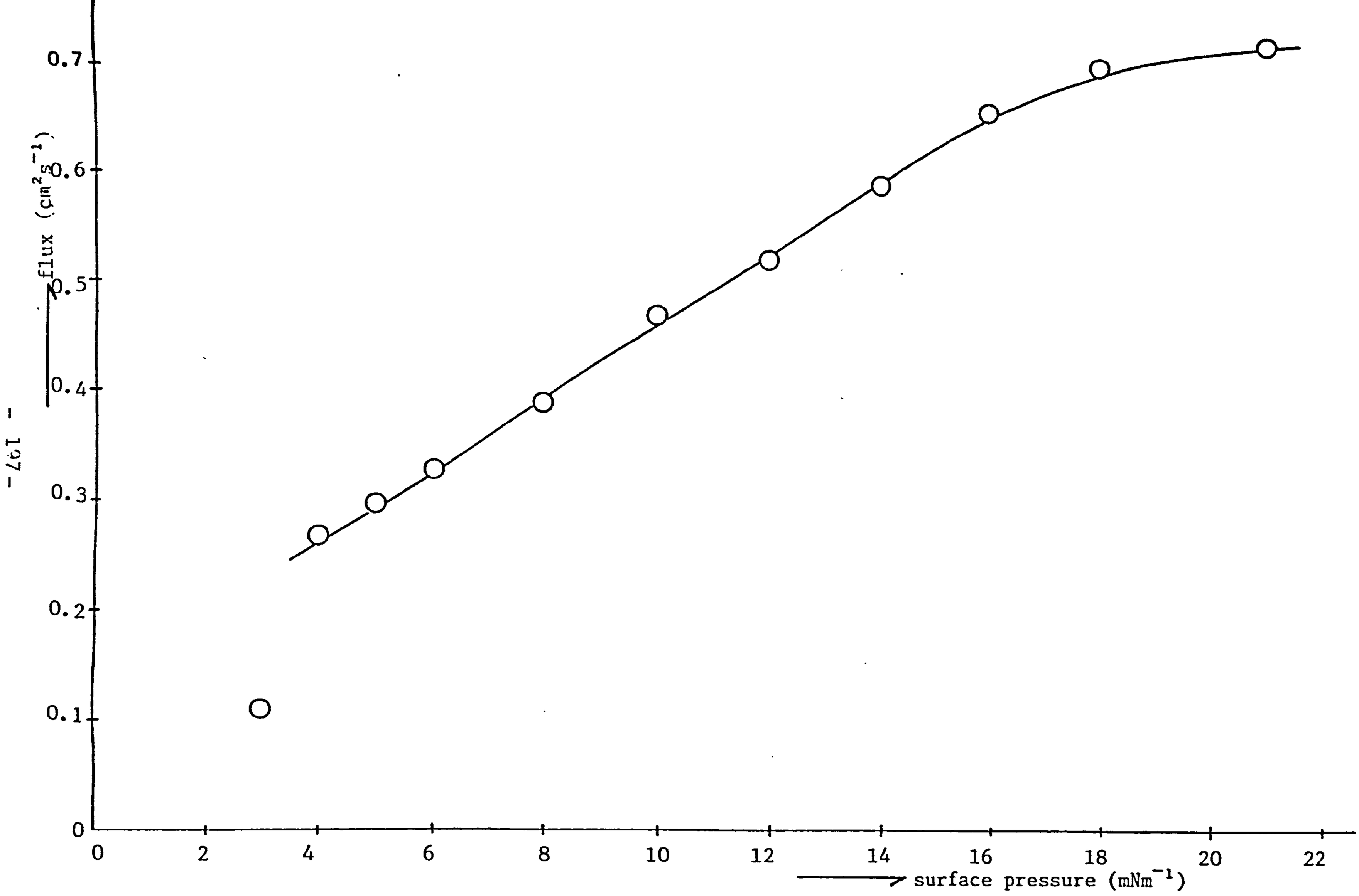

FIGURE 10.6: Plot of flux against surface pressure for stearic acid on an 0.01M hydrochloric acid subphase
$T = 20.5 \pm 0.5^{o}C$

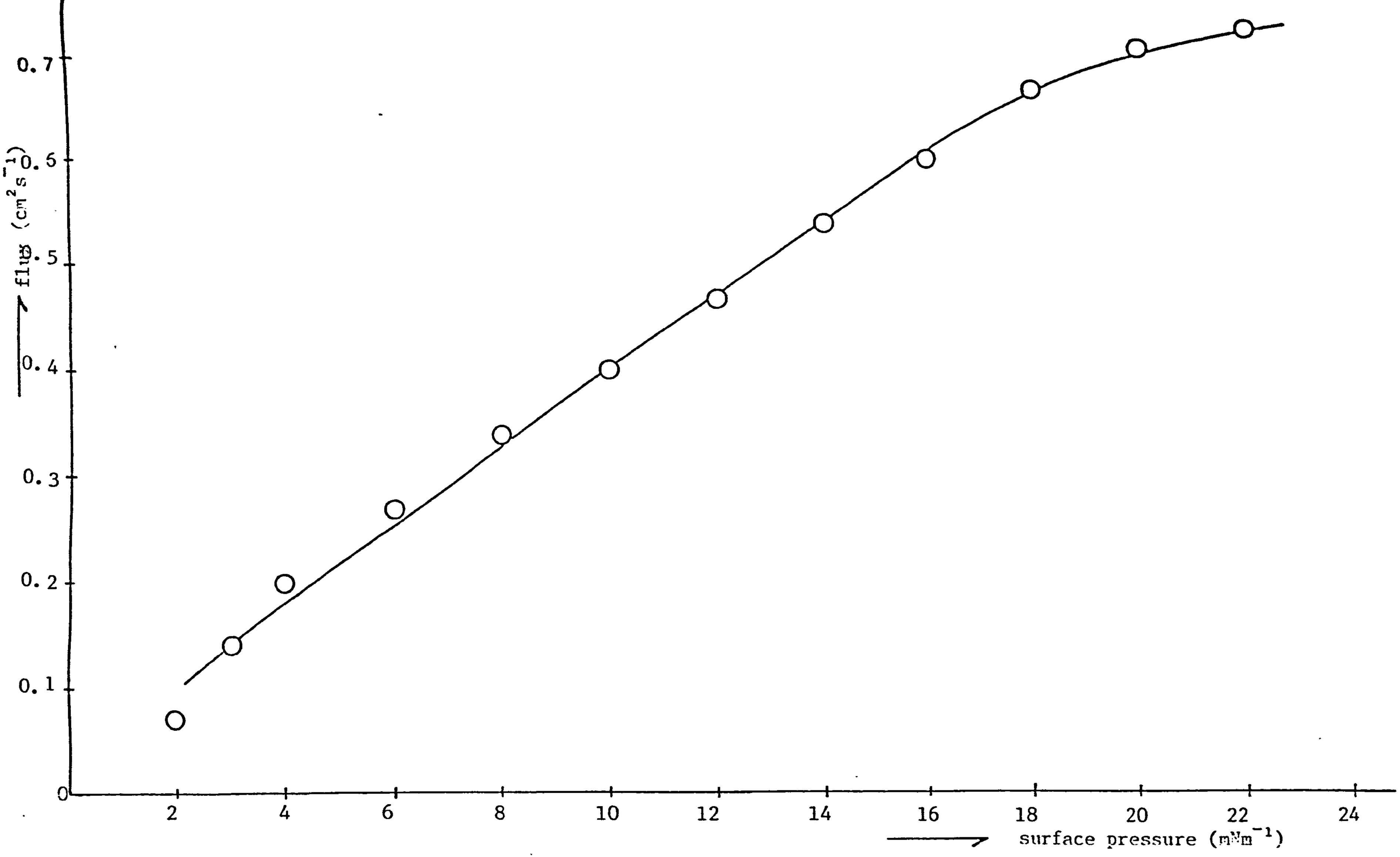

FIGURE 10.8: Plot of surface flux against surface pressure for stearic acid on a 2.5×10^{-4}M cadmium chloride subphase. T = $20.5 \pm 0.5^{o}C$

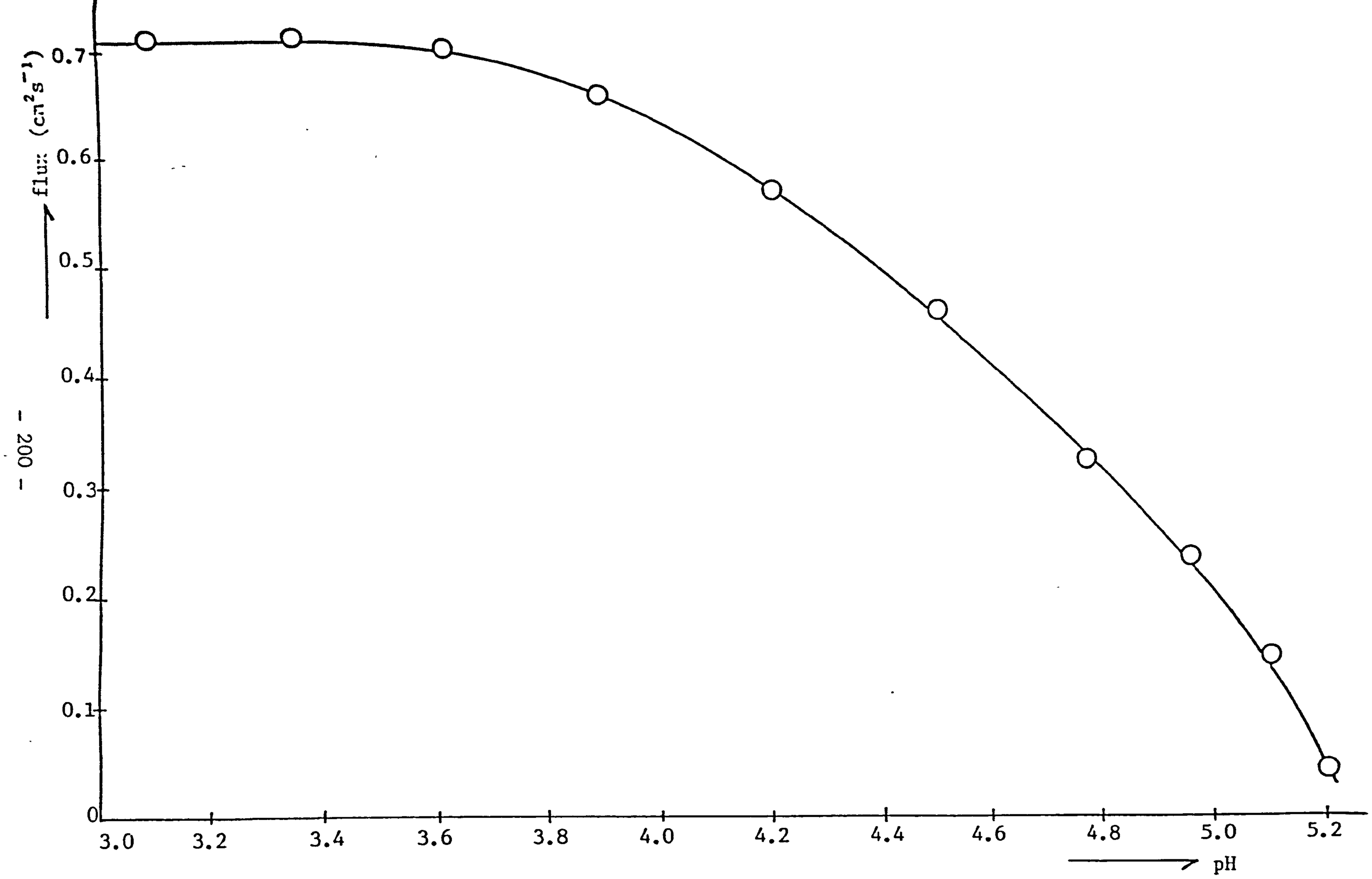

FIGURE 10.9: Plot showing the variation of surface flux with pH at a surface pressure of $15mNm^{-1}$ for stearic acid on a 2.5×10^{-4}M cadmium chloride subphase. T = $20.5 \pm 0.5^{o}C$

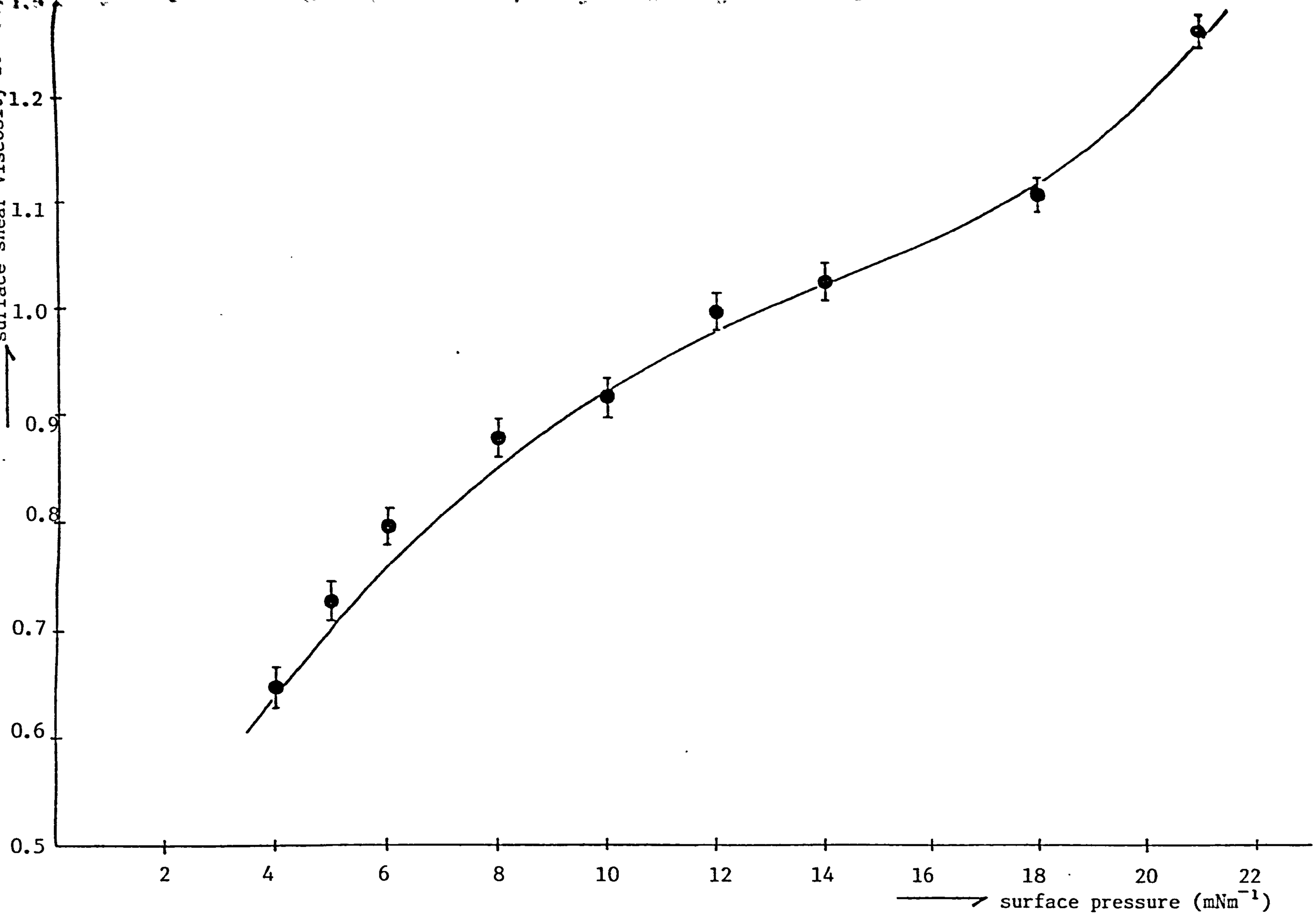

FIGURE 10.10: Plot showing the variation of surface viscosity with surface pressure for stearic acid on an 0.01M hydrochloric acid subphase. pH ~ 2.2; T = 20.5 ± 0.5°C

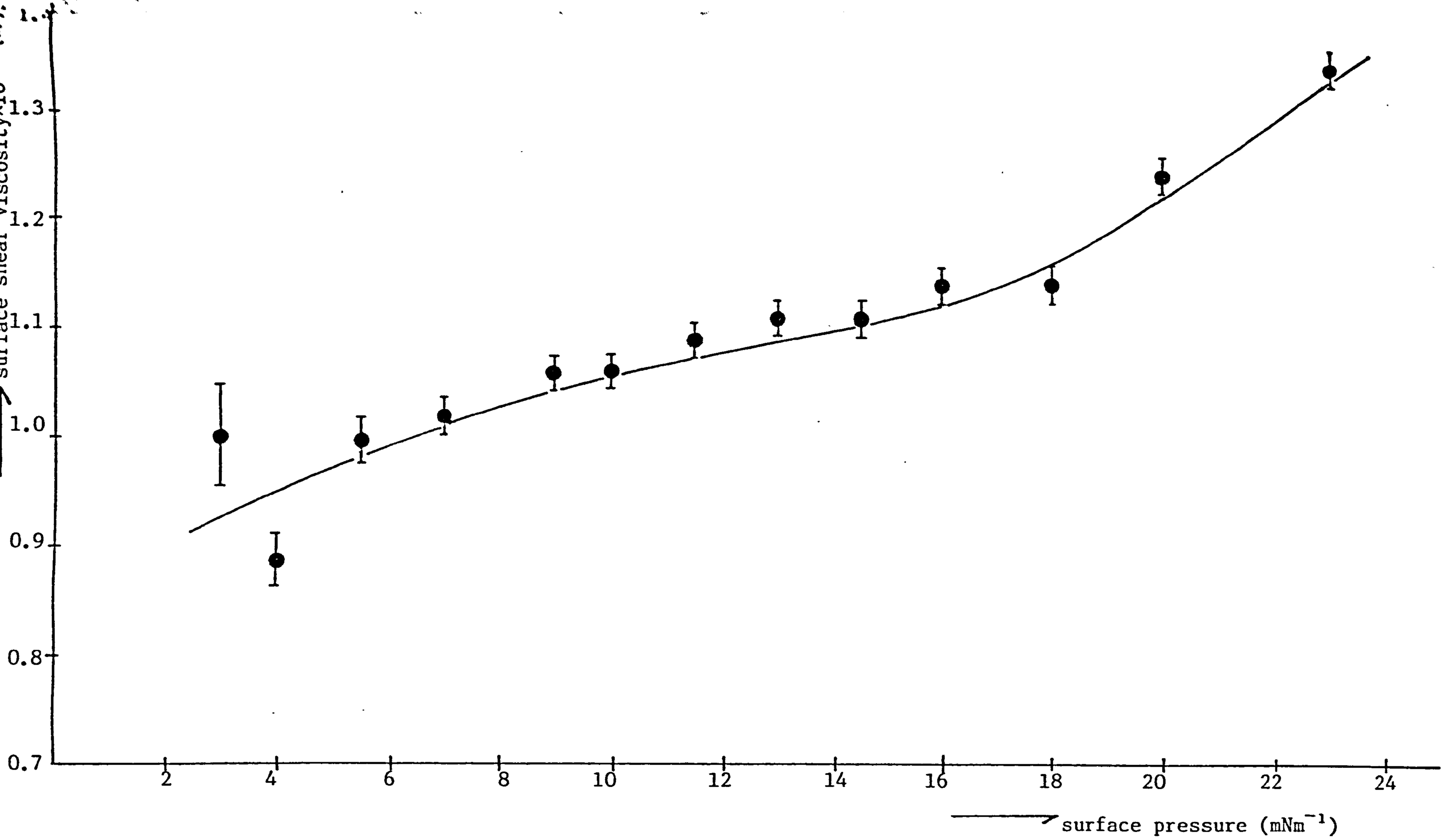

FIGURE 10.11: Plot showing the variation of surface viscosity with surface pressure for stearic acid on a 2.5×10^{-4}M cadmium sulphate subphase. pH ~ 2.2; T = 20.5 ± 0.5°C

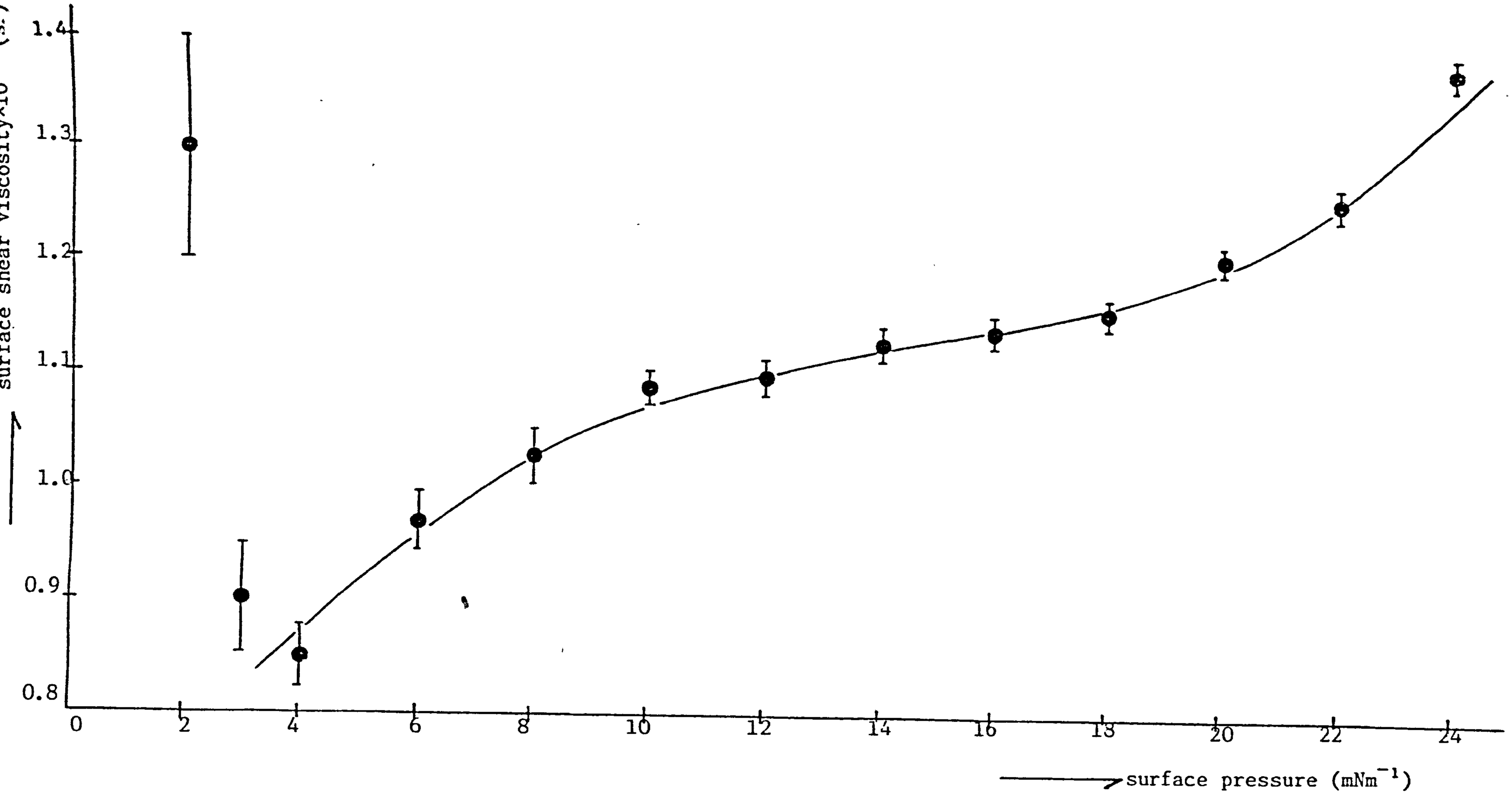

FIGURE 10.12: Plot showing the variation of surface viscosity with surface pressure for stearic acid on a 2.5×10^{-4}M cadmium chloride subphase. pH $\sim$ 2.2; T = 20.5 $\pm$ 0.5°C

acid monolayers on three subphases, and the data obtained are summarized in Tables 10.3, 10.4 and 10.5. Figures 10.6, 10.7 and 10.8 show the plots of flux against surface pressure, and a linear relationship was found for a wide range of surface pressures, with the flux becoming constant at pressures of greater than about $18mNm^{-1}$. Figures 10.10, 10.11 and 10.12 illustrate the variation of shear viscosity with surface pressure. These plots show an increase in viscosity at very low surface pressures ($\leq 4mNm^{-1}$) and at high pressures ($\geq 18mNm^{-1}$). Between these pressures, a smooth curve was obtained with viscosity increasing with surface pressure. Table 10.6 summarizes the relationship between pH, flux, viscosity and activation energy of flow at a surface pressure of $15mNm^{-1}$. Figure 10.9 shows that the flux does not vary at pH values of less than 3.4. As the acidity of the subphase was decreased, the flux also decreased until it almost reached zero at pH 5.2. Figures 10.13 and 10.14 both show that the viscosity and activation energy of flow increased with pH.

(ii) Time-Dependence Measurements

These measurements were performed on myristic acid, to study the variation of surface viscosity with applied stress. The experimental data were obtained in the form of the area of compartment I, as a function of time at a constant surface pressure, π_1. The surface flux was obtained from the differential of the area of film lost or transferred, and the surface concentration of material in compartment II was calculated in order to correct for the back pressure, π_2. The surface shear viscosity was obtained using equation (7.3)

$$\eta_s = \frac{2}{3} \times \frac{a^3}{\ell} \frac{\pi_1 - \pi_2}{q}$$

where $\pi_1 - \pi_2 = \Delta\pi$ the pressure drop, q the time surface flux = ds/dt,

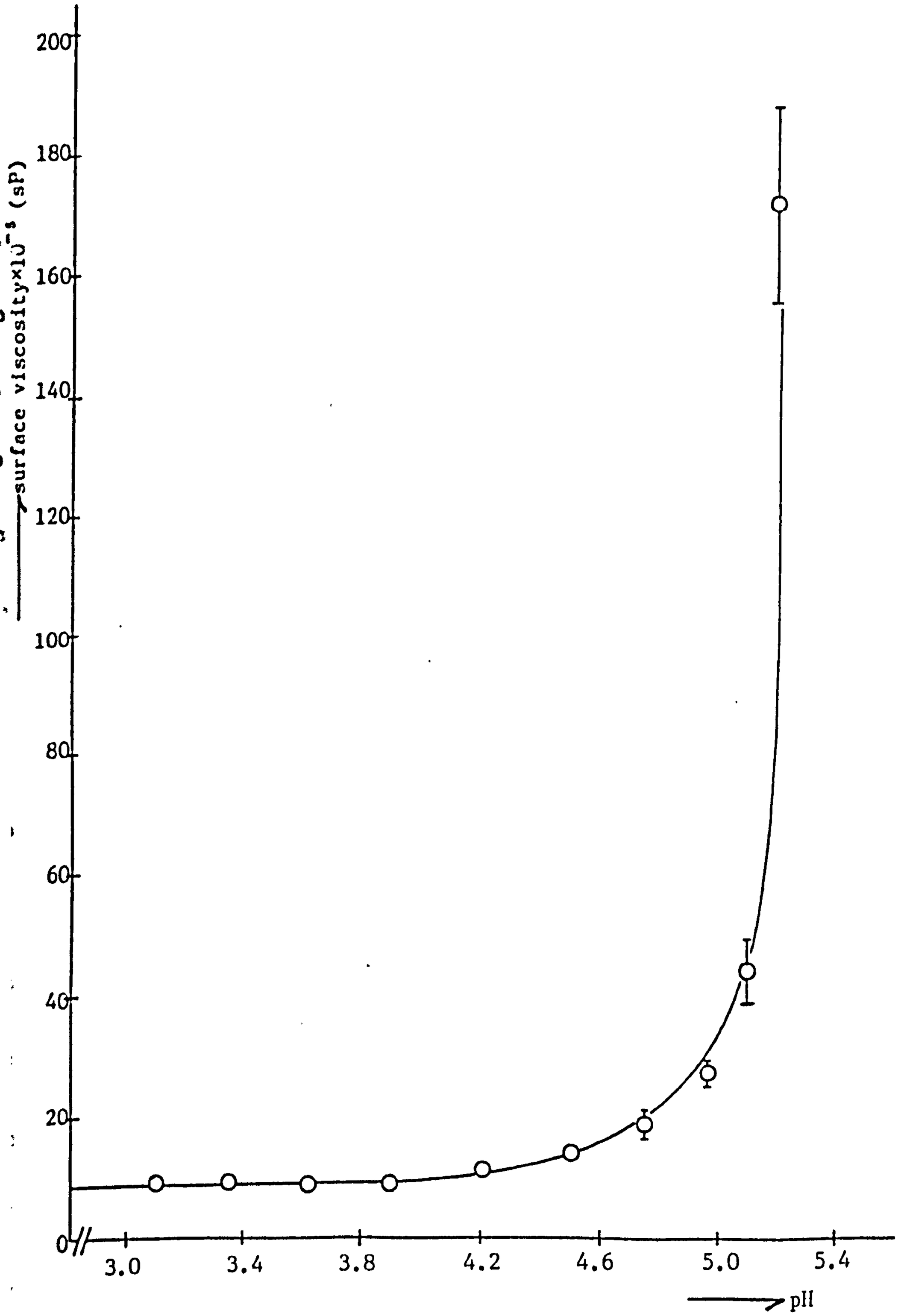

FIGURE 10.13: Plot showing the variation of surface viscosity with pH at a surface pressure of $15 mNm^{-1}$ for stearic acid on a $2.5 \times 10^{-4} M$ cadmium chloride subphase. $T = 20.5 \pm 0.5^{\circ}C$

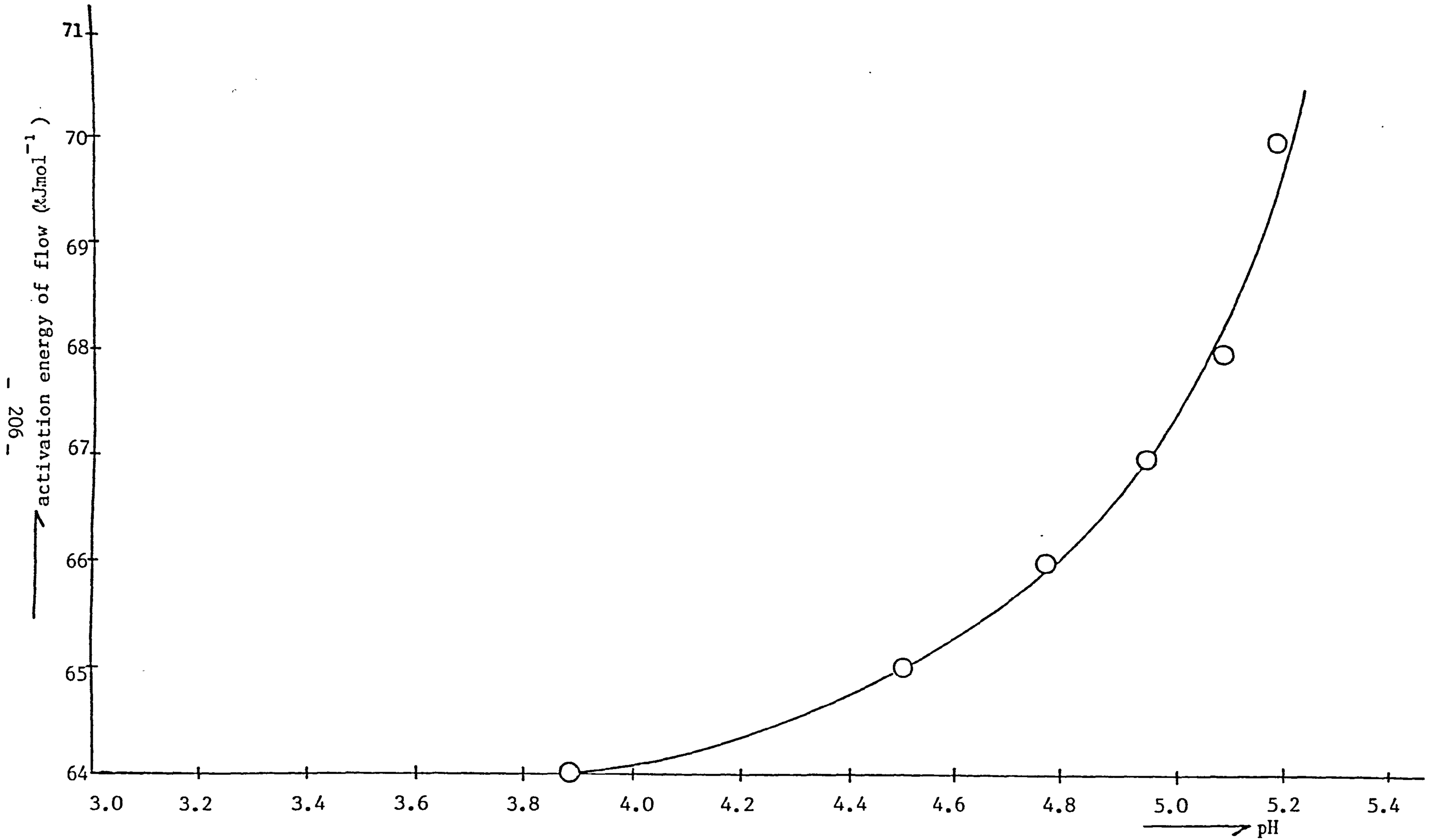

FIGURE 10.14: Plot showing the variation of activation energy of flow with pH at a surface pressure of 15mNm^{-1} for stearic acid on a 2.5×10^{-4}M cadmium chloride subphase. T = 20.5 $\pm$ 0.5°C

ℓ and a are the length and width of the canal respectively (Appendix D shows a calculated example). Tables 10.7 and 10.8 summarize the typical set of data that were obtained. .Five runs were performed for each volume of myristic acid added to compartmentII of the trough, and a mean surface shear viscosity value taken after 400 seconds. The viscosity values obtained for the various surface concentrations are summarized in Table 10.9 and represented graphically in Figure 10.15. Figure 10.16[223] shows the results obtained for myristic acid on 0.01M hydrochloric acid. A striking feature of this plot is that surface viscosity reduces as the film is compressed.

Experiments were also performed to ascertain whether addition of a measured volume of myristic acid to compartment I would result in a change in surface viscosity with applied stress. The data obtained are summarized in Table 10.10 and represented graphically in Figure 10.17.

10.1.2 Discussion

The π-A isotherm plots of myristic and stearic acid monolayers shown in Figure 10.2 and 10.3 are types of liquid films which indicate the presence of some degree of co-operative interaction. When myristic and stearic acids are spread on a slightly acidified subphase, they form fluid films when the molecular area exceeds 26.6$\mathring{A}^2$ and 17.5$\mathring{A}^2$, and solid films when it is less than 26.6$\mathring{A}^2$ and 17.5$\mathring{A}^2$ respectively. The plots extrapolate to zero surface pressure at areas larger than that corresponding to a molecular cross-section, indicating some looseness or disorganization in the structures. Myristic acid occurs as a liquid-expanded film with a shallow isotherm and a limiting area of about 50$\mathring{A}^2$, whilst stearic acid occurs as a liquid-condensed film with a much steeper isotherm and a limiting area of about 28$\mathring{A}^2$.

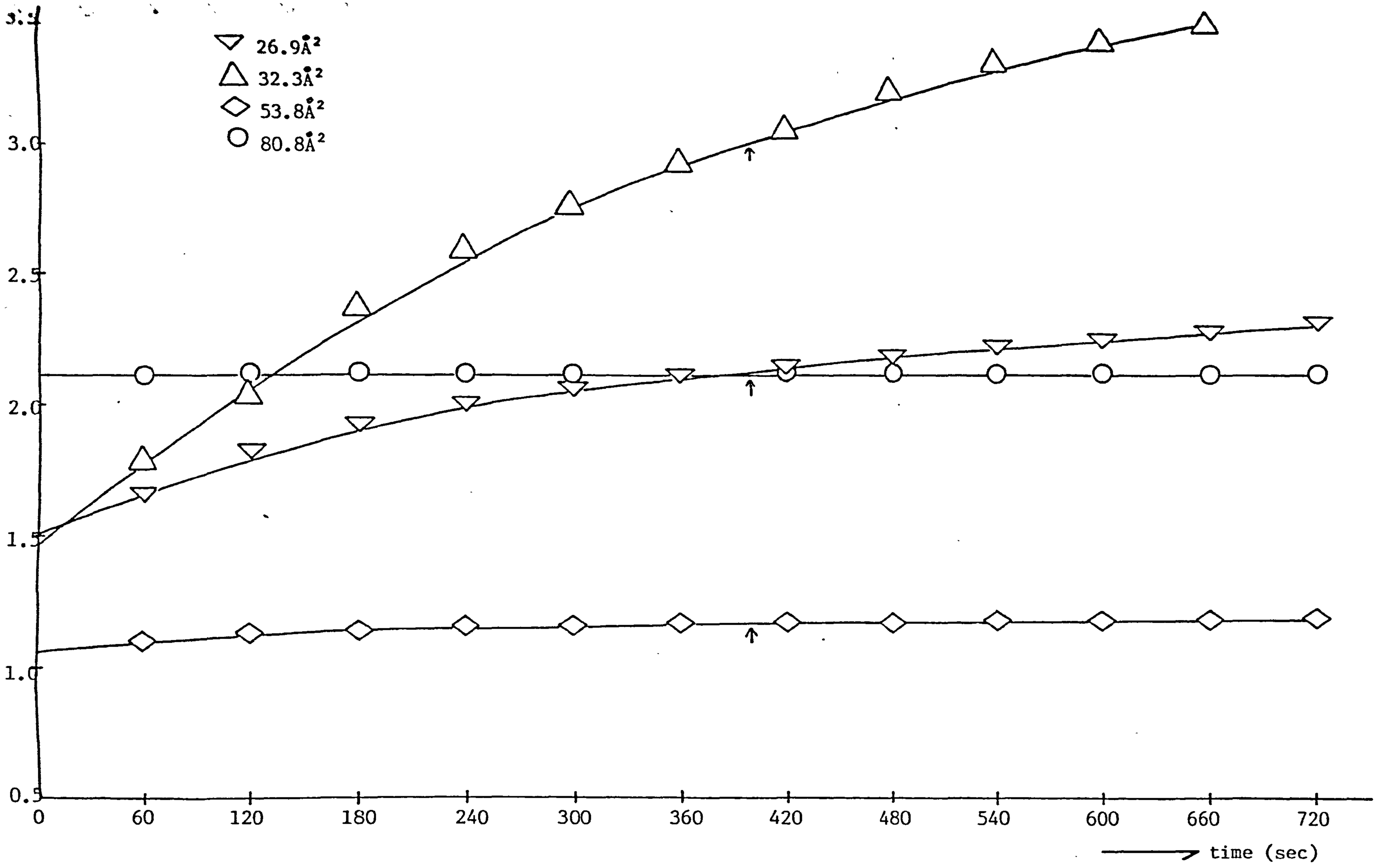

FIGURE 10.15: Plot showing the variation of surface viscosity with time for a slightly condensed film of myristic acid on an 0.01M hydrochloric acid subphase. ↑ = 400 sec; $\Delta\pi$ = 14.1mNm^{-1}; T = 20.5 $\pm$ 0.5^{o}C

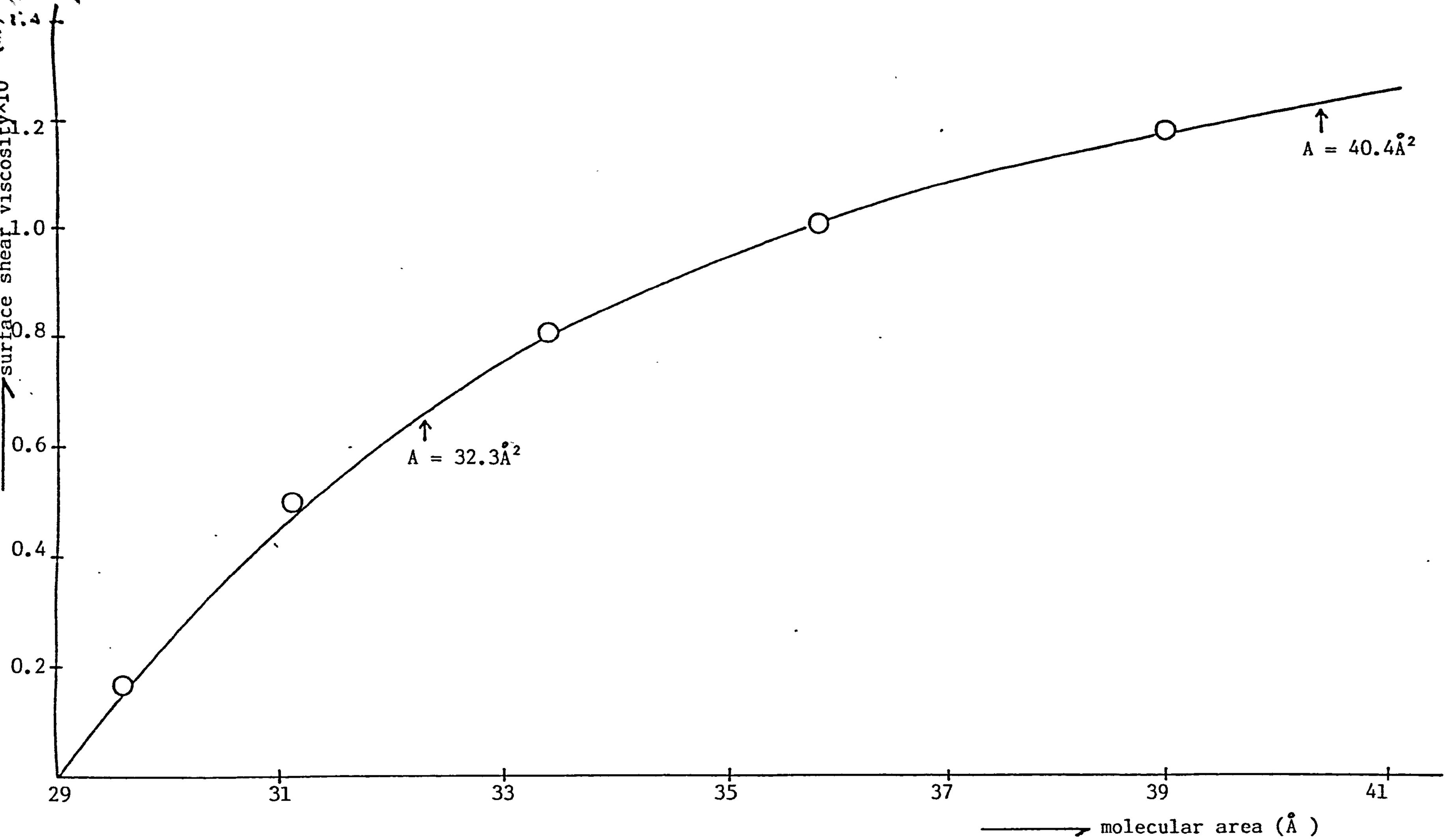

FIGURE 10.16[223]: Plot showing the variation of surface viscosity of a slightly condensed film of myristic acid on an 0.01M hydrochloric acid subphase. T = 22°C

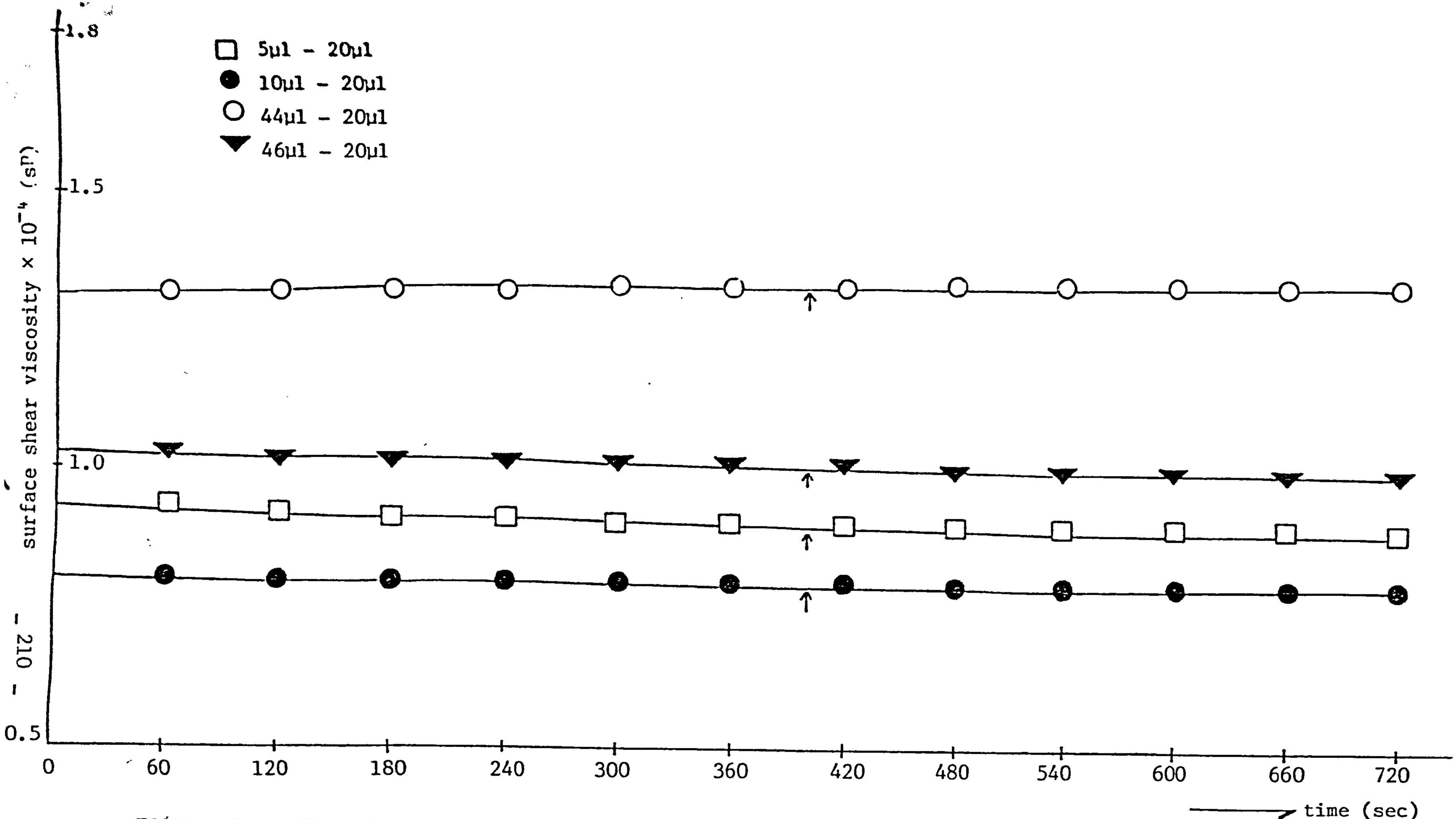

FIGURE 10.17: Plot showing the variation of surface viscosity with time for a slightly condensed film of myristic acid when added to both compartments. Area per molecule = 40.4Å^2; ↑ = 400 sec; $\Delta\pi$ = 3.5mNm^{-1}; T = 20.5 $\pm$ 0.5^{o}C.

The plots of compression modulus as a function of molecular area in Figures 10.4 and 10.5 show that the compression modulus falls to a minimum at the transition point between the fluid and solid film, i.e. at areas per molecule of 26.6$\AA^2$ and 17.5$\AA^2$ for the myristic and stearic acids respectively. The values obtained at this point for both acids agree favourably with those obtained by Adam[29]. With stearic acid, it was observed that a gradual compression of the film resulted in the film collapsing shortly after the transition into the condensed phase, hence surface pressures above 26mNm^{-1} could not be attained. However, a rapid compression of the film enabled the highly-condensed phase to be obtained with surface pressures in excess of 50mNm^{-1} being attained before collapse occurred.

The relationship between surface shear viscosity and surface pressure for stearic acid on 0.01M hydrochloric acid (Figure 10.10) shows that the viscosity depends on the orientation and closeness of the molecules in the film. Figure 10.6 shows distinctly that Newtonian behaviour occurs between the surface pressures of 4mNm^{-1} and 18mNm^{-1}, and that the flux through the canal is directly proportional to the pressure difference across the canal. The values obtained for stearic acid on a 0.01M hydrochloric acid subphase agree with the values of Nutting and Hawkins[234], but are about five times smaller in magnitude than those obtained by Jarvis[248]. The insensitivity of this experimental technique for measuring viscosities of extremely fluid films may explain the increase in viscosity at very low surface pressures (< 4mNm^{-1}). No measurements were carried out at surface pressures greater than 23mNm^{-1} because at these pressures the film became solid, fragile and prone to collapse.

The presence of a small concentration of divalent ions (Cd^{2+}) in the subphase resulted in a minimal increase in the activation energy of

flow, and consequently the viscosity. This is well supported by the explanation that at pH 2.2 (this is well below the pk_a of stearic acid, which occurs at pH 4.8-4.9), the stearic acid molecules are associated and uncharged, and therefore will not bind to the Cd^{2+} ion. Also, at pH 2.2, the concentration of H^+ ions will be about $10^{-2}M$, whereas the concentration of Cd^{2+} ions is only $10^{-4}M$. Therefore, the binding of H^+ ions will be statistically favoured. So the presence or absence of divalent ions in the subphase does not affect the activation energy of flow. However, at high pH (above the pk_a of stearic acid), the stearic acid molecules are ionized and therefore the divalent ions in the subphase can bind them together, thus giving a more condensed film with increased viscosity. The pk_a of stearic acid in the bulk phase is between 4.8 and 4.9, but in the monomolecular film the pk_a should be increased slightly due to interactions between the molecules. The pk_a should also be expected to rise with surface concentration, as these inter-molecular interactions will be greater at higher surface concentrations. The pH at which there is a marked increase in the activation energy of flow and the viscosity should be a measure of the approximate pk_a of the film, i.e. the pH at which the molecules become predominantly ionized. This was found to be about pH 5.0-5.1.

In the absence of divalent ions in the subphase, the viscosity of stearic acid monolayer may be expected to decrease with increasing pH, because the stearic acid molecules will be ionized and will therefore tend to repel one another. An expanded rather than a condensed film will be formed, and consequently the viscosity will be lower. However, the situation may not be as simple as this, since electrostatic repulsions between the head groups may, on the other hand, increase the viscosity.

From the plots of surface shear viscosity as a function of time (shown in Figures 10.15 and 10.17), the surface viscosities show a time-dependence with a reduction in the rate of shear thickening behaviour. The time-dependence fell with decreasing concentration and was completely lost at the lowest concentration used. However, no reference has been made to the presence of a shear thickening behaviour in long-chain carboxylic acids such as myristic acid on 0.01M hydrochloric acid.

The plot of Figure 10.16 shows a decrease in surface shear viscosity with molecular area - a behaviour due to the structure of the kinetic units in the film which, as has been indicated in Section 2.5, are the ensemble of an amphiphilic molecule, together with those molecules of the subphase with which it is associated[223]. For a given length of chain and molecular spacing, the contribution to the surface viscosity of the chain-chain interaction increases less rapidly with compression than does the decrease in the contribution from the associated subphase molecules. It follows that $\partial\eta/\partial A$ is positive for such a domain of surface concentration.

The addition of different amounts of myristic acid to compartment II of the trough resulted in no noticeable change in the viscosity with the various surface concentrations used. Figure 10.17 shows that the viscosity is not dependent on the applied stress, and is therefore Newtonian.

Discussion of Errors

The following errors were obtained in the calculation of the surface shear viscosity: weighings $\sim$ 0.5%, volumes $\sim$ 0.1%, molecular area $\sim$ 1% and the compression modulus, k_s, $\sim$ 3%. The contact made by the Wilhelmy plate with the subphase could be measured to within 1mm, i.e. an error of >1%. Since the calculated viscosity is a function of the

flow rate of the film through the canal, the error incurred measuring the surface pressure may be quite large. The teflon barrier movements were measured to within 0.5mm - an error of ±15% for small distances and ±3% for large. For small fluxes of $0.15cm^2s^{-1}$ the error was ±8%, whilst for large fluxes of $0.7cm^2s^{-1}$ it was 1.5%. Also, as the calculated surface viscosity is a function of the cube of the canal width, then the largest error in the calculation was due to the uncertainty involved in measuring the canal width. An overall error of ∿18% was calculated for all measurements

10.1.3 Summary

Using a canal viscometer, the surface shear viscosities of a monomolecular film of stearic acid were determined - the viscosity being calculated from the rate of flow of the film material through a narrow and relatively deep canal. The surface viscosities were measured as a function of film pressure for a number of subphases: 0.01M hydrochloric acid, 2.5×10^{-4}M cadmium chloride, and cadmium sulphate at pH 2.2.

The time-dependence of the surface shear viscosities of various surface concentrations of myristic acid monolayers have also been investigated.

10.2 Joyce-Loebl Glass Trough Measurements

10.2.1 Results For Fatty Acids

In order to gain further and better understanding of the surface monomolecular layer, a variety of surface properties were studied with this instrument - initially using a number of straight chain n-alkanoic acids (where c_n is shorthand for $c_{n-1}H_{2n+1}COOH$) - before proceeding with the polydimethylsiloxane polymers.

The data obtained from this trough for n-alkanoic acids and poly-

dimethylsiloxane polymers were analysed as described in Chapter 3 and 7. Isotherms of surface pressure as a function of the molecular area were obtained for the acids C_{14}-C_{20}, though further experiments were only performed on C_{14}, C_{18}-C_{20}. These acids were all used without further purification. However, mass spectrometry was performed on C_{14} and C_{18} simply to provide a measure of their purities.

The dependence of the surface pressure with molecular area for the acids when spread on high-purity water (pH 5.5; conductivity $\leq 15 Sm^{-1}$) are shown in the isotherms plotted in Figure 10.18. From these plots, and with the added knowledge of the maximum area available to the film and the number of molecules per microlitre spread on the surface, the area per molecule of each acid monolayer can be obtained.

The acids are shown to exhibit essentially similar behaviour with respect to the compressibility of their films. The isotherms also show that beyond the molecular areas of 25Å^2, only the expanded films of C_{14} and C_{15} show any measurable resistance to pressure. A summary of the area per molecule and related data obtained from the monomolecular film measurements is given in Table 10.11. The monolayer compression modulus, k_s, is calculated from the definition

$$k_s = - A\left(\frac{\partial \pi}{\partial A}\right)_T \qquad (10.1)$$

The $(\partial \pi/\partial A)_T$ was obtained from the liquid phase of the films at a surface pressure of $10 mNm^{-1}$. The values obtained for both myristic (C_{14}) and stearic (C_{18}) acids compare favourably with those obtained earlier from the fluon-coated duralumin trough. The compression modulus, k_s^{10}, given in Table 10.12, is represented graphically as a function of the number, n, of carbon atoms in chain for monolayers of various fatty acids measured at a surface pressure of $10 mNm^{-1}$ in Figure 10.19. The plot shows that

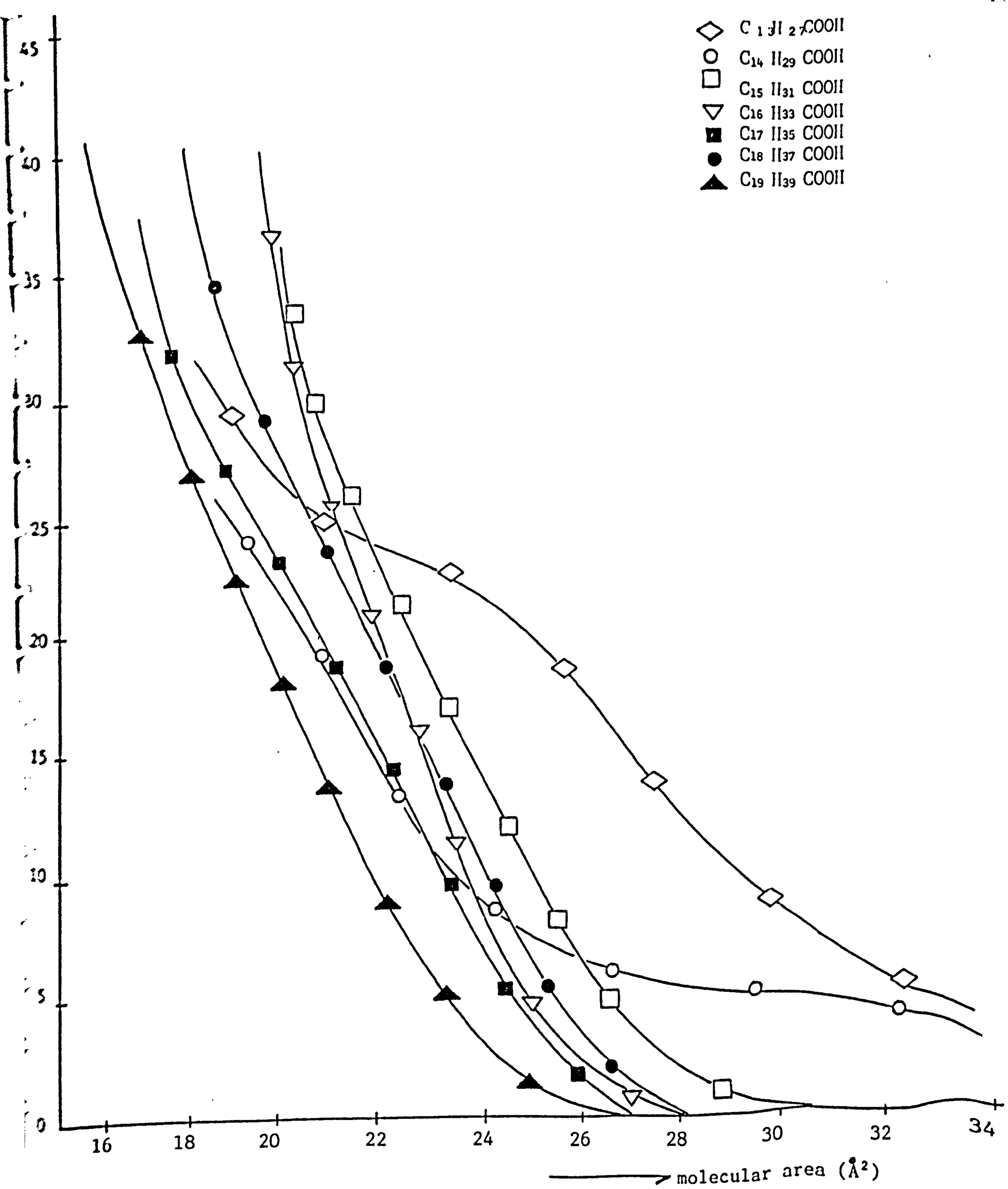

FIGURE 10.18: Plot showing the surface pressure-surface area isotherms for long-chain alkanoic acids on acidic subphases with no added salt. pH = 3.0 ± 0.03; T_b = 21 ± 0.5°C

Fatty Acid	Molecular Weight	Number of Molecules On Surface	Area Per Molecule, $\tilde{A}_{extr}$ ($Å^2$)	Surface Pressure at Transition Change (mNm^{-1})
$C_{13}H_{27}COOH$	228.36	5.596×10^{16}	26.79	20
$C_{14}H_{29}COOH$	242.20	5.1313×10^{16}	26.23	24
$C_{15}H_{31}COOH$	256.43	6.353×10^{16}	23.85	28
$C_{16}H_{33}COOH$	270.46	6.978×10^{16}	23.14	28
$C_{17}H_{35}COOH$	284.49	1.182×10^{16}	21.50	29
$C_{18}H_{37}COOH$	298.18	1.06×10^{16}	22.46	30
$C_{19}H_{39}COOH$	310.20	1.131×10^{16}	21.06	31

TABLE 10.11: Surface pressure-surface area and related data from monomolecular film measurements on the Joyce-Loebl trough for long-chain n-alkanoic acids.

Subphase = acidic pH = 3.05 ± 0.03

Temperature = $21 \pm 0.5^{o}C$ Compression/Expansion rate = $9.6 Å^2 min^{-1}$

$\tilde{A}_{extr}$ = extrapolated area per molecule from the condensed phase to zero surface pressure

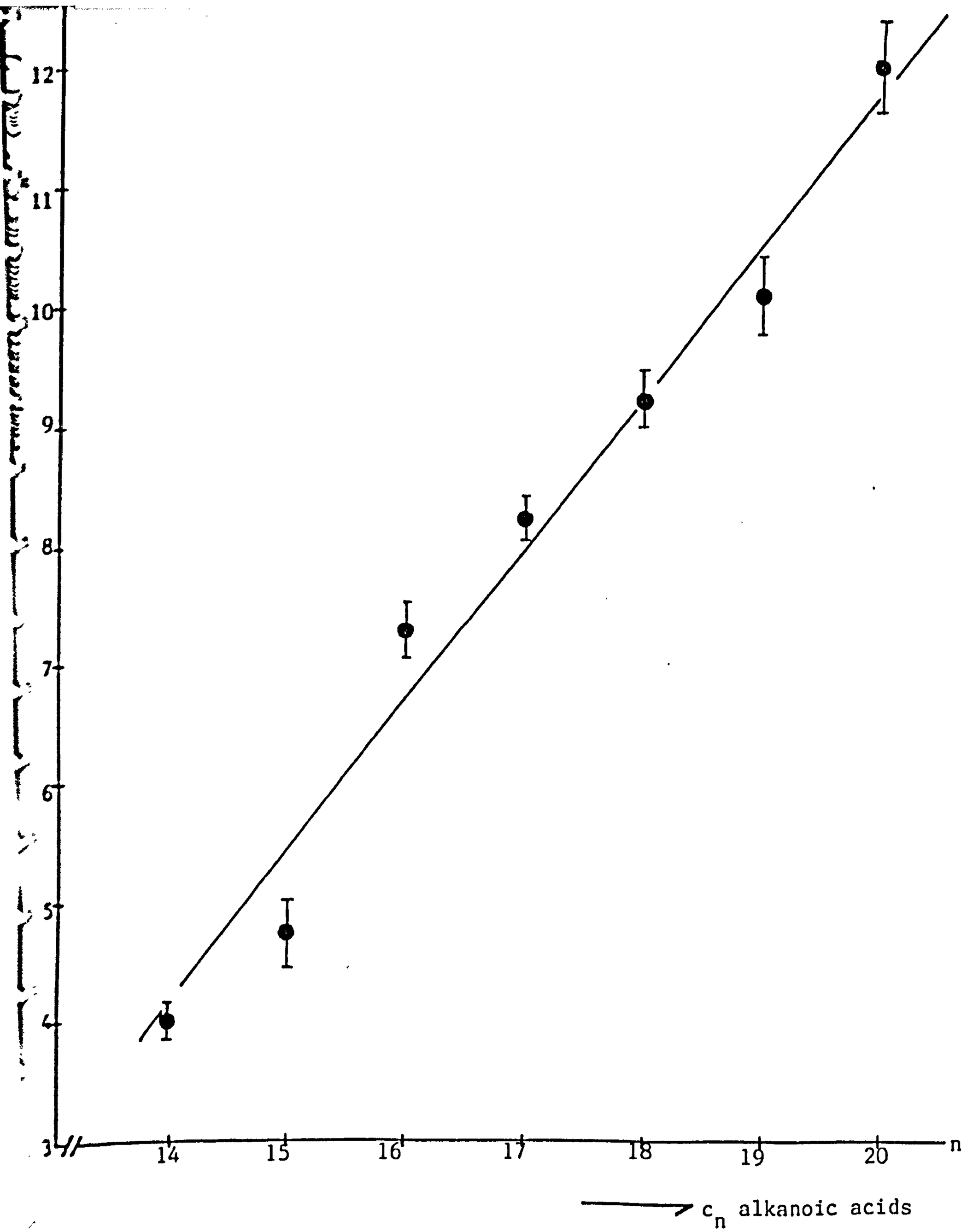

FIGURE 10.19: Plot showing the variation of compression modulus with number, n, of carbon atoms in fatty acid chain.

Surface pressure = $10mNm^{-1}$

Slope = 1.3

Intercept = -10.5

the repulsive intermolecular interactions do increase with chain length, and so a rapid increase in viscosity is to be expected.

Most of the literature work using long-chain fatty acids concludes that there appears to be no ionization if the subphase pH is at least 6, and that the properties of fatty acid monolayers are relatively insensitive to pH or the presence of salts in the acidic subphase. Small quantities of a divalent ion (Cu^{2+}) were added to the subphase and the resulting π-A curves for C_{14}, C_{18} and C_{20} acids are shown in Figures 10.20-10.22. These curves show that the more compressible linear region of the π-A curve becomes shorter with increasing pH.

The variation of pH on the collapse pressures of myristic and stearic acid monolayers on a pure water subphase are shown in π-A isotherms of Figures 10.23 and 10.24. These curves also show the compressible linear region becoming shorter and a reduction in collapse pressure with increasing pH.

Both Figure 10.25 and Figure 10.26 show interesting features apparent with myristic and stearic acid monolayers on a subphase of copper (II) chloride, in that there is a progressive steeping of the π-A isotherms on repeated compressions and expansions 5 minutes apart. There is a shift of the compressible region to smaller molecular areas, with a small indication of a change in slope in the solid phase region of the isotherms.

Canal Viscometer

A canal-type viscometer was used to measure the rate of flow of a surface film through a 'canal' at a known shear stress (see Chapter 7). Harkins and Kirkwood's[220] formula (which takes into account the viscous drag due to the subphase being pulled through the canal with the monolayer)

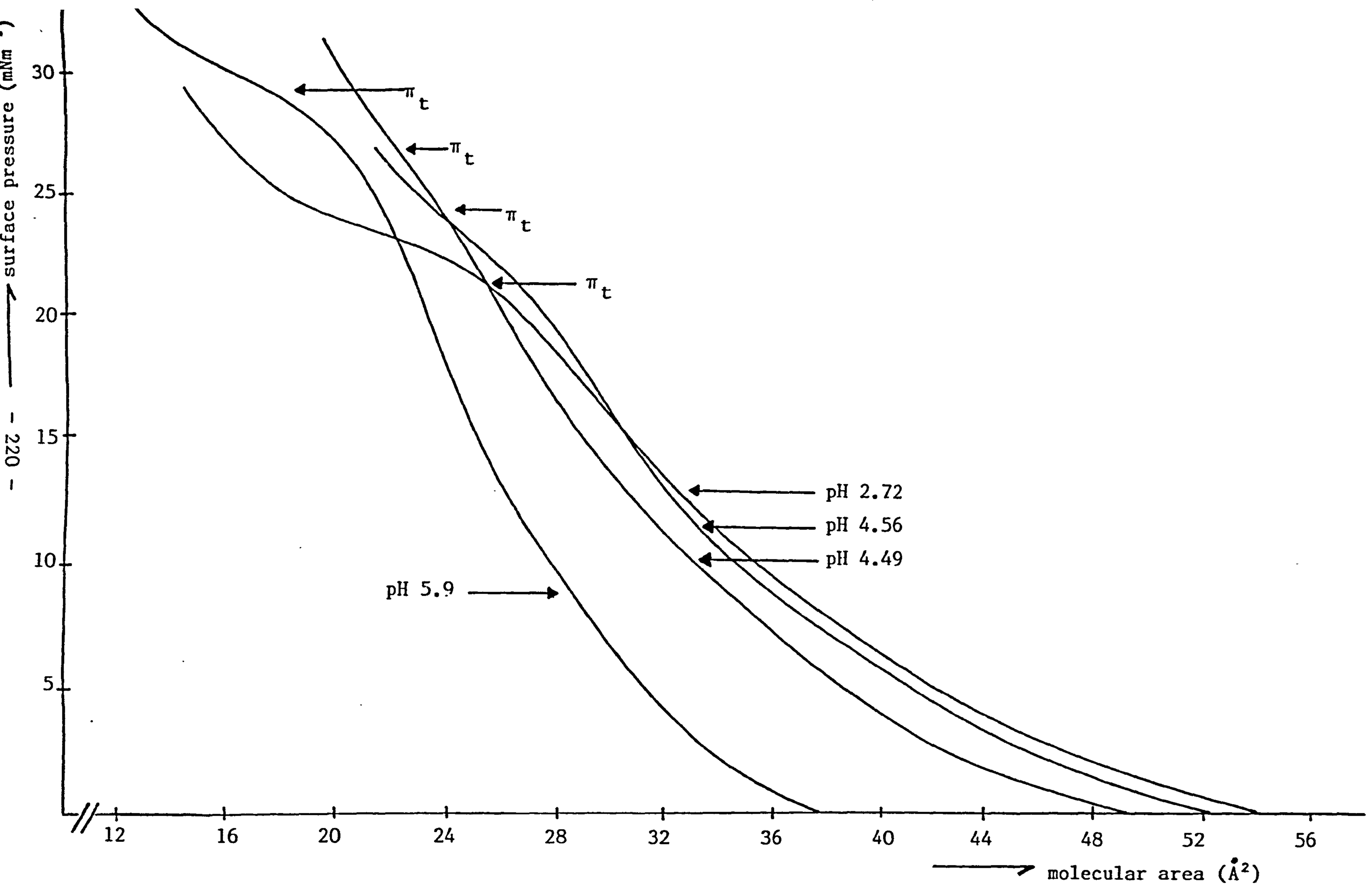

FIGURE 10.20: Plot showing the variation of pH on the surface film and transition pressures and molecular area for $C_{13}H_{27}COOH$ monolayer on a 2×10^{-4}M copper (II) chloride subphase. $T_b = 21 \pm 0.5^oC$

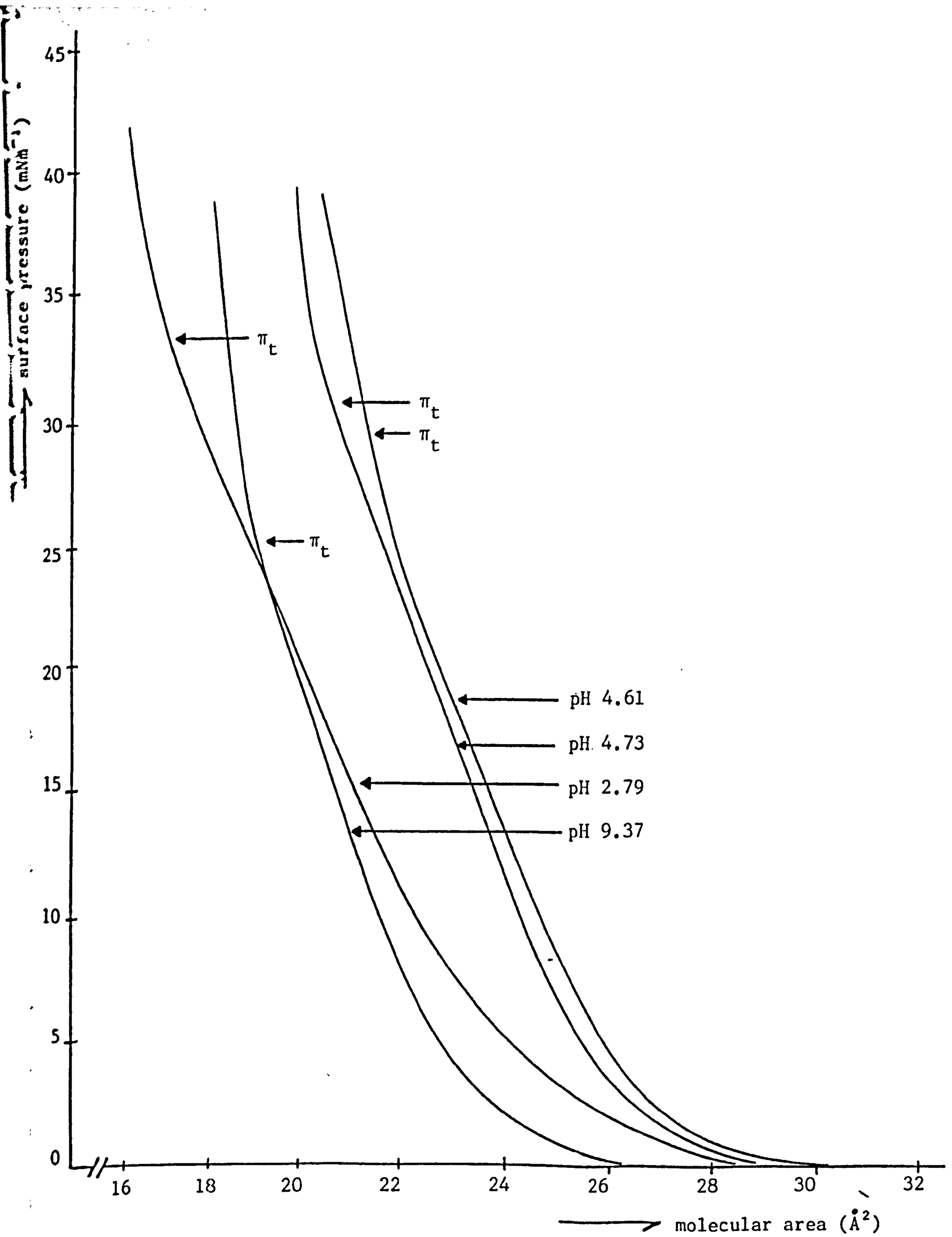

FIGURE 10.21: Plot showing the variation of pH on the surface film and transition pressures, and the molecular area of $C_{17}H_{35}COOH$ monolayer on a 2×10^{-4}M copper (II) chloride subphase. $T_b = 20.6 \pm 0.2^oC$

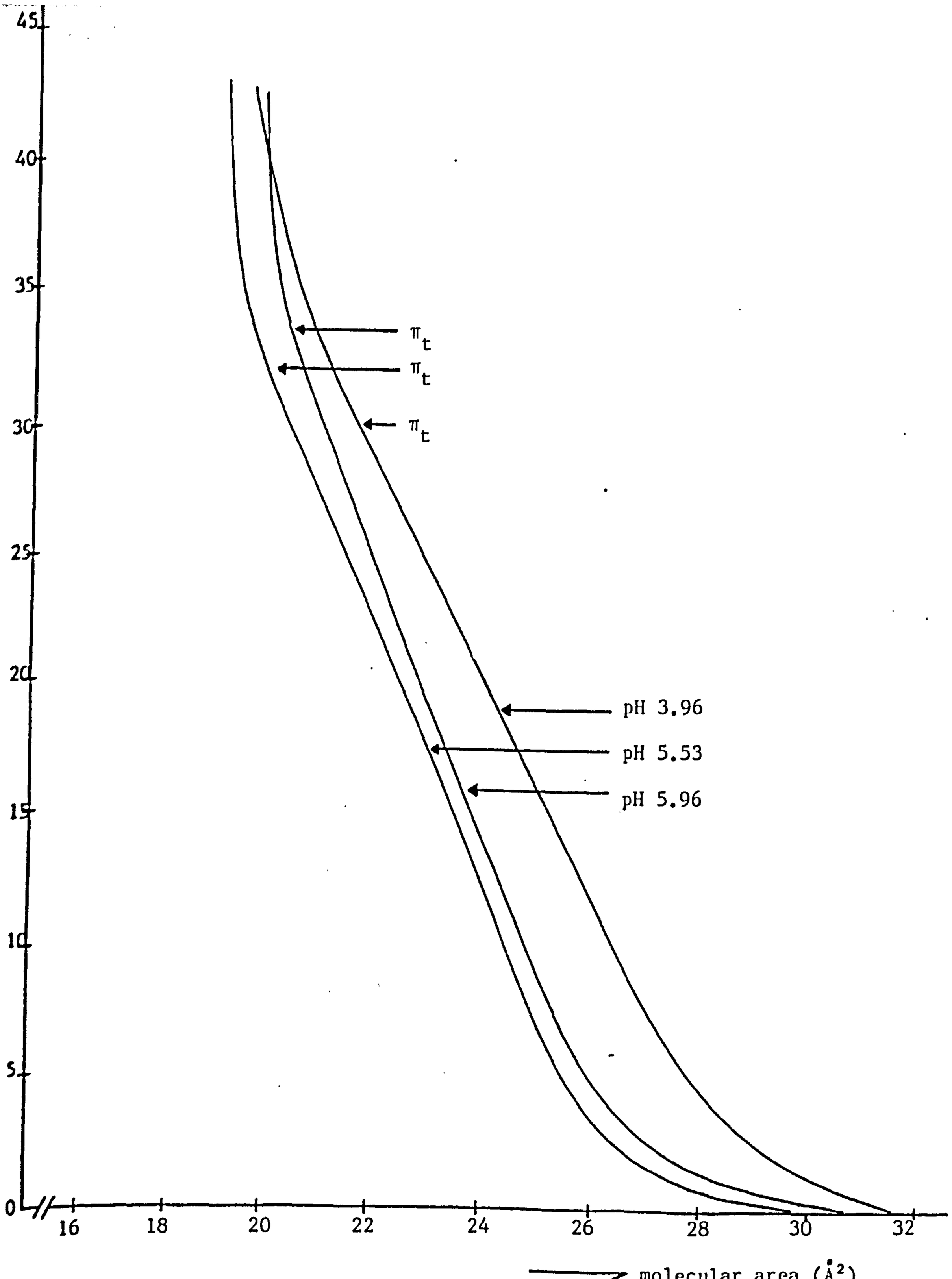

FIGURE 10.22: Plot showing the variation of pH on surface film and transition pressures, and molecular area for $C_{19}H_{39}COOH$ monolayer on a 2×10^{-4}M copper (II) chloride subphase.

$T_b = 20.5 \pm 0.2^oC$

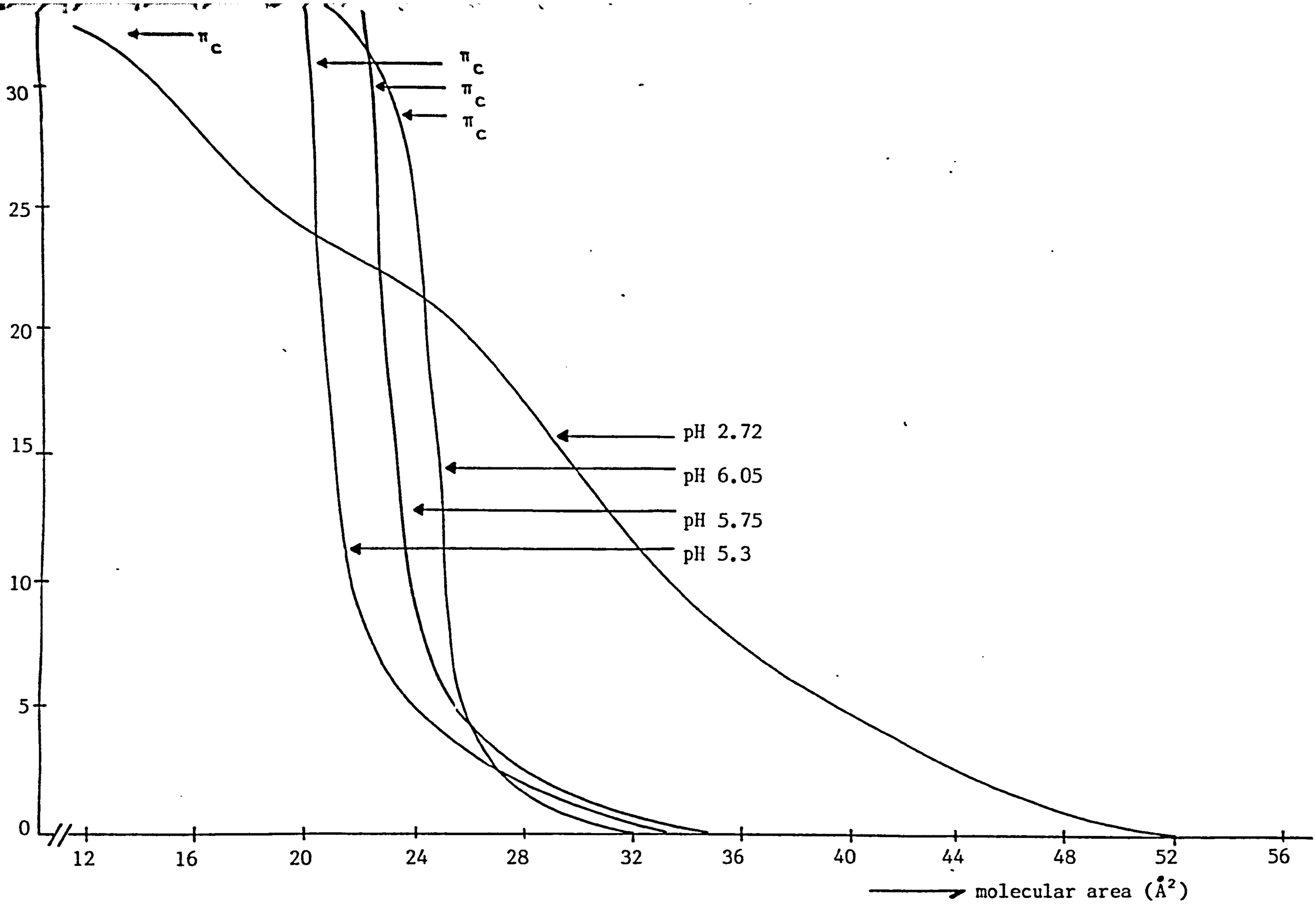

FIGURE 10.23: Plot showing the collapse profiles of $C_{13}H_{27}COOH$ monolayer with varying pH on pure water subphases.
$T_b = 21 \pm 0.5^oC$

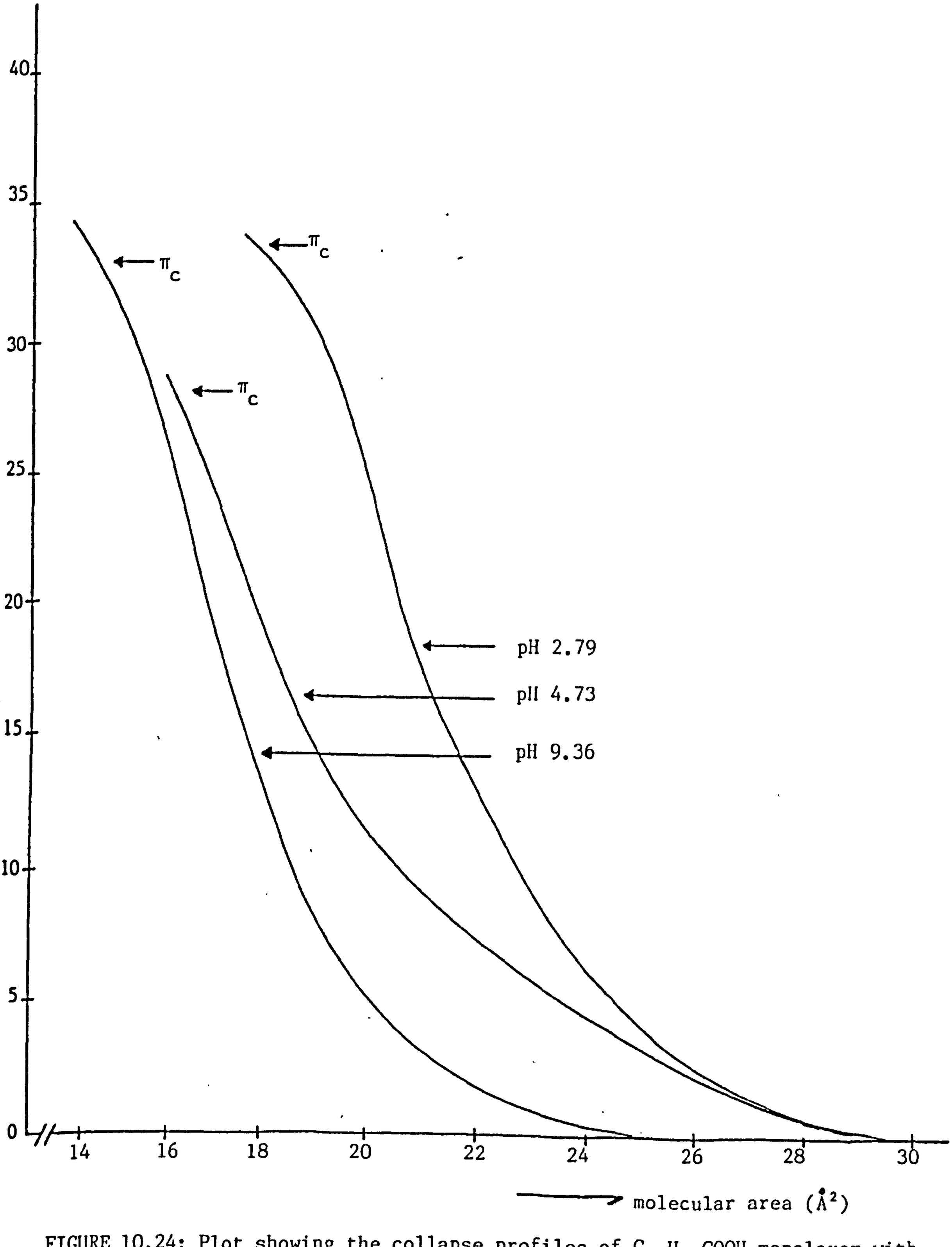

FIGURE 10.24: Plot showing the collapse profiles of $C_{17}H_{35}COOH$ monolayer with varying pH on pure water subphases.

$T_b = 20.6 \pm 0.5^oC$

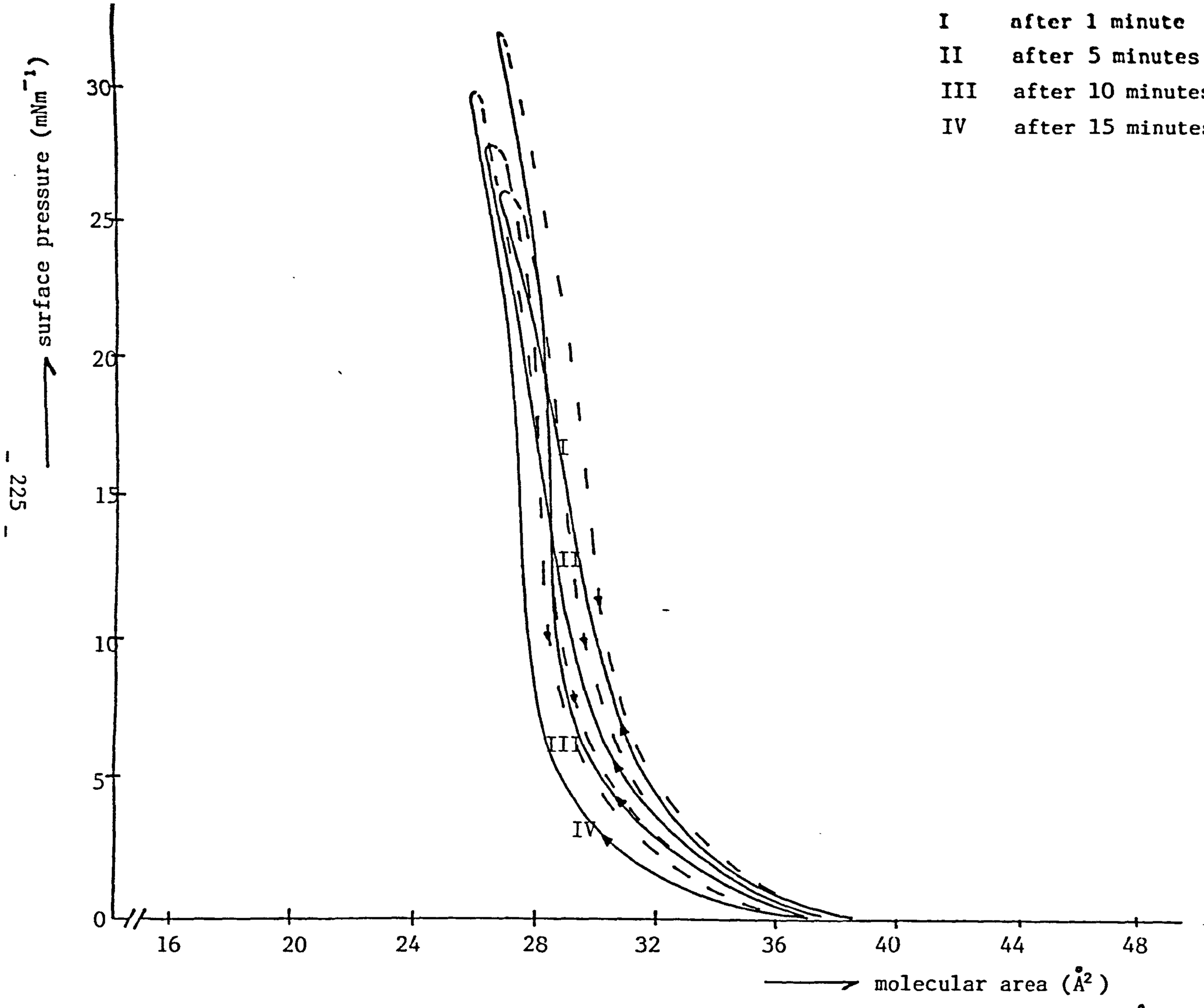

FIGURE 10.25: Plot showing the variation of surface film pressure-molecular area (Å^2) with time for $C_{13}H_{27}COOH$ monolayer on a 2×10^{-4}M copper (II) chloride subphase. pH = 5.84 $\pm$ 0.02; T = 21 $\pm$ 0.5^{o}C

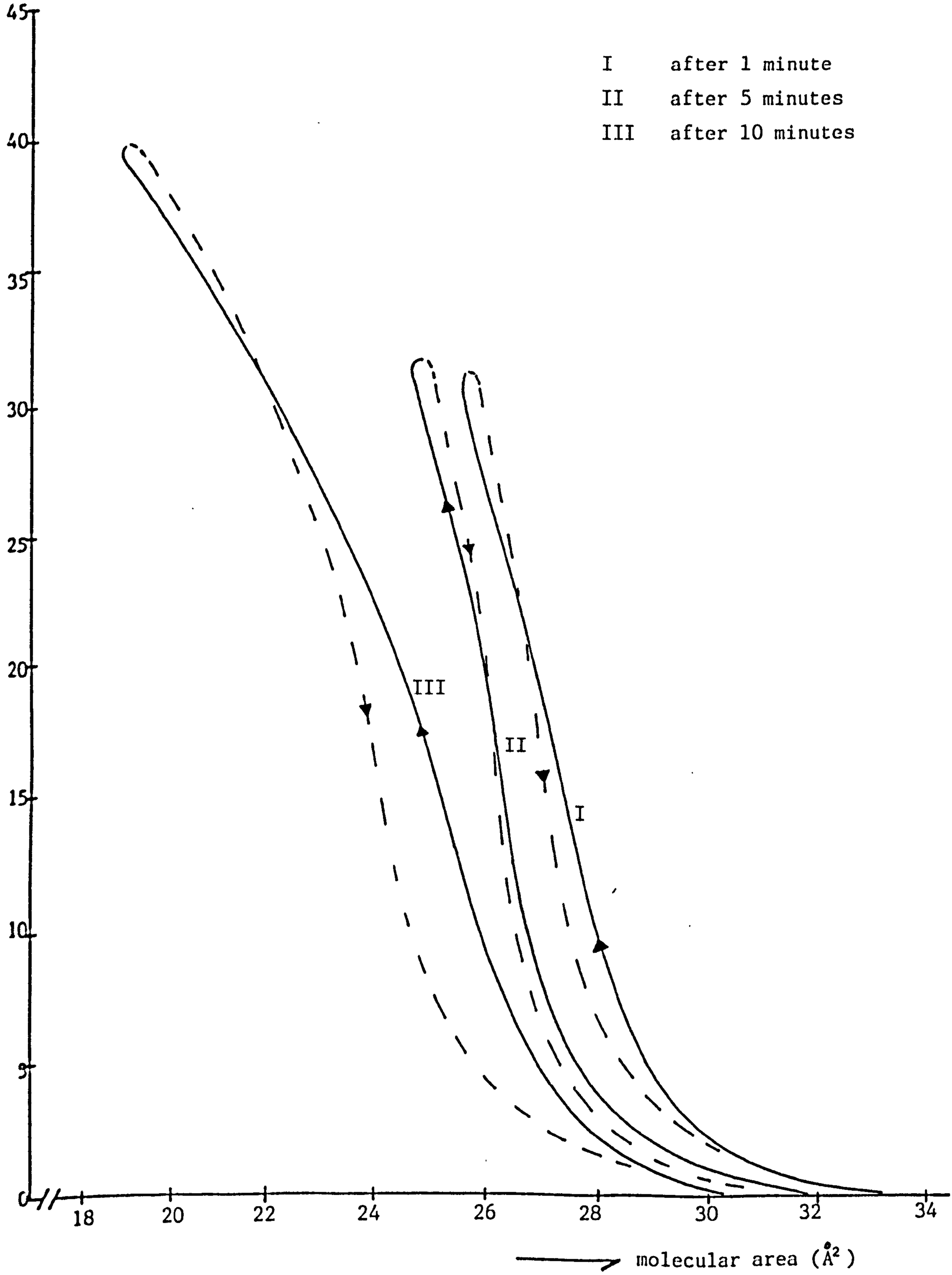

FIGURE 10.26: Plot showing the variation of surface film pressure-molecular area isotherms with time for $C_{17}H_{35}COOH$ monolayer on a 2×10^{-4} M copper (II) chloride subphase.

pH = 5.8 ± 0.01 $T_b = 21 \pm 0.5^{o}C$

was used to calculate the reduced flux, q, and consequently the surface shear viscosity, η_s, for the C_{18}-C_{20} acid monolayers.

$$\eta_s = \frac{2}{3}\frac{\pi_2 - \pi_1}{\ell}\frac{a^3}{q} - \frac{2a\eta_0}{\pi}\coth\frac{\pi h}{2a} \qquad (10.2)$$

where η_0 is the bulk subphase viscosity and h is the height of the subphase in the canal. If $h \gg 2a$, then $\coth \pi h/2a \to 1$, so the formula for a deep canal becomes

$$\eta_s = \frac{2}{3}\frac{\pi_2 - \pi_1}{\ell}\frac{a^3}{q} - \frac{2a\eta_0}{\pi} \qquad (10.3)$$

The data obtained are given in Table 10.13 and represented graphically in Figure 10.27.

Torsion Pendulum Surface Viscometer

Using this viscometer, the surface viscosity was measured by recording the angular amplitudes of successive swings (see Chapter 7). The surface shear viscosity, η_s, was calculated using the formula[73]:

$$\eta_s = \frac{\mu_I}{P_A}\left(\frac{1}{R_1^2} - \frac{1}{R_2^2}\right)\left[\frac{\lambda}{\sqrt{4\pi^2 + \lambda^2}} - \frac{\lambda_0}{\sqrt{4\pi^2 + \lambda^2}}\right] \qquad (10.4)$$

where μ_I is the moment of inertia of the bob ($71 g cm^2$), P_A is the period of bob in air, and the other parameters have been defined in Section 7.4.2. Also, it must be noted that

$$\frac{1}{P_A} = \frac{1}{2\pi}\sqrt{\frac{C}{\mu_I}} \qquad (10.5)$$

where C is the torsion constant of the wire ($260 g\ cm^2 s^{-1}$). The viscosity measurements of the acids were taken at a surface pressure of about $10 mNm^{-1}$ and are summarized in Table 10.13. Figure 10.27 shows the plot of the logarithm of surface shear viscosity ($\log \eta_s$) as a function of the number, n, of carbon atoms in the chain for the fatty acid monolayers spread on acidic subphases using the torsion pendulum (0; pH ~ 2) and canal (□; pH ~ 3) viscometers. The plots show that viscosity increases with increasing

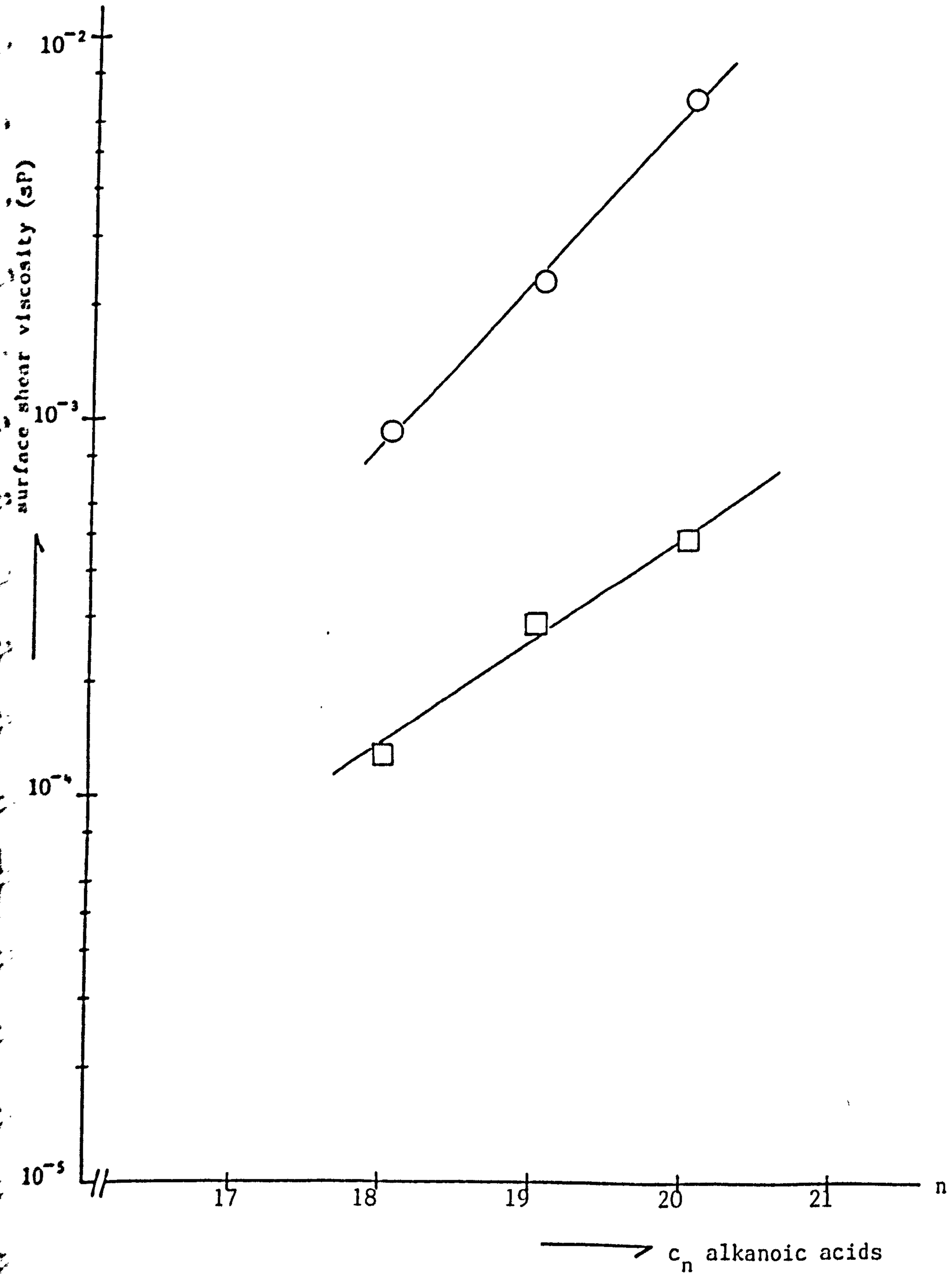

FIGURE 10.27: Plot showing the variation of the canal (□) and torsion pendulum (○) viscosities with C_{18}, C_{19} and C_{20} acid monolayers on acidic subphases.

chain length, hence indicating that at 'low pressures' the viscosity of fatty acid monolayers is low and Newtonian. The viscosity value obtained for C_{18} (stearic acid) using this canal viscometer compares favourably with that obtained from the canal viscometer used on the duralumin trough.

Surface Potential

The ionizing electrode method (see Chapters 3 and 7) was used to investigate the surface potential and dipole moment of the various monolayers. Surface pressure-molecular area and surface potential-molecular area data were obtained for C_{14} and C_{18}-C_{20} acid monolayers at pH $\sim$ 3.0 at the air/water interface.

The apparent vertical dipole moments, $\mu_\perp$, were calculated from the surface potentials, ΔV, using the Helmholtz formula

$$\Delta V = 4\pi n\mu_\perp \qquad \text{(cgs units)} \qquad (10.6)$$

In SI units

$$\Delta V = \frac{4\pi n\mu_\perp}{4\pi\varepsilon_0} = \frac{n\mu_\perp}{\varepsilon_0} \qquad (10.7)$$

or

$$\mu_\perp = \frac{\varepsilon_0 \Delta V}{n} \qquad (10.8)$$

where n is the number of molecules per metre^2 in the monolayer and ε_0 is assumed to be the permittivity of air (and equal to $8.8541 \times 10^{-12} J^{-1} c^2 m^{-1}$). From equation (10.8), $\mu_\perp$ has units of cm mol^{-1}, therefore for $\mu_\perp$ to be expressed in Debyes we have

$$1D = 3.336 \times 10^{-30} cm$$

For conversion of cgs to SI units, see Appendix B.

A summary of the surface pressures, surface dipole moments and related data for each acid is given in Tables 10.14 to 10.17, and repre-

sented graphically in Figures 10.28 and 10.29. The other fatty acid monolayers besides C_{14} give a near horizontal ΔV-π plot, indicating no real change between phases. However, the $\mu_\perp \propto 1/n$ relationship suggests that $\mu_\perp$ should fall as shown in the $\mu_\perp$-π plots. But once again, C_{14} confounds this suggestion and relationship. The C_{14} acid monolayer shows a change in the slope of the $\mu_\perp$-π plot at transition points, going from an increase to a decrease in magnitude.

Relaxation Curves

An important feature of the Langmuir control unit (see Chapter 7) constructed here in Bristol is its ability in enabling pressure-area relaxation curves to be plotted directly by the operation of the PTFE barriers initially in the forward mode (compression) and later in the reverse mode (expansion), without collapsing the film - so that the barriers can be 'relaxed' for a monolayer from various surface pressures to a position of zero surface pressure. However, the forward and reverse speeds of these barriers had arbitrary units - hence a linear relationship needed to be obtained between the arbitrary forward and reverse speeds and their actual speeds. The plots are shown in Figures 10.30 and 10.31, and the following relationships were obtained from the slopes:

(i) for the forward mode:

$$\text{actual speed } (mms^{-1}) = 1.388 \times 10^{-2}\ (mms^{-1}) \times \text{forward speed unit;}$$

(ii) for the reverse mode:

$$\text{actual speed } (mms^{-1}) = 1.395 \times 10^{-2}\ (mms^{-1}) \times \text{reverse speed unit.}$$

The above relationships enabled the actual speed travelled by the PTFE barriers to be known if and when required. Figures 10.32(i)-(iv) show the effect of the 'relaxation' of a monolayer from different 'held surface pressures' to positions of zero surface pressure at various reverse barrier speed units. The profiles exhibit a normal isotherm

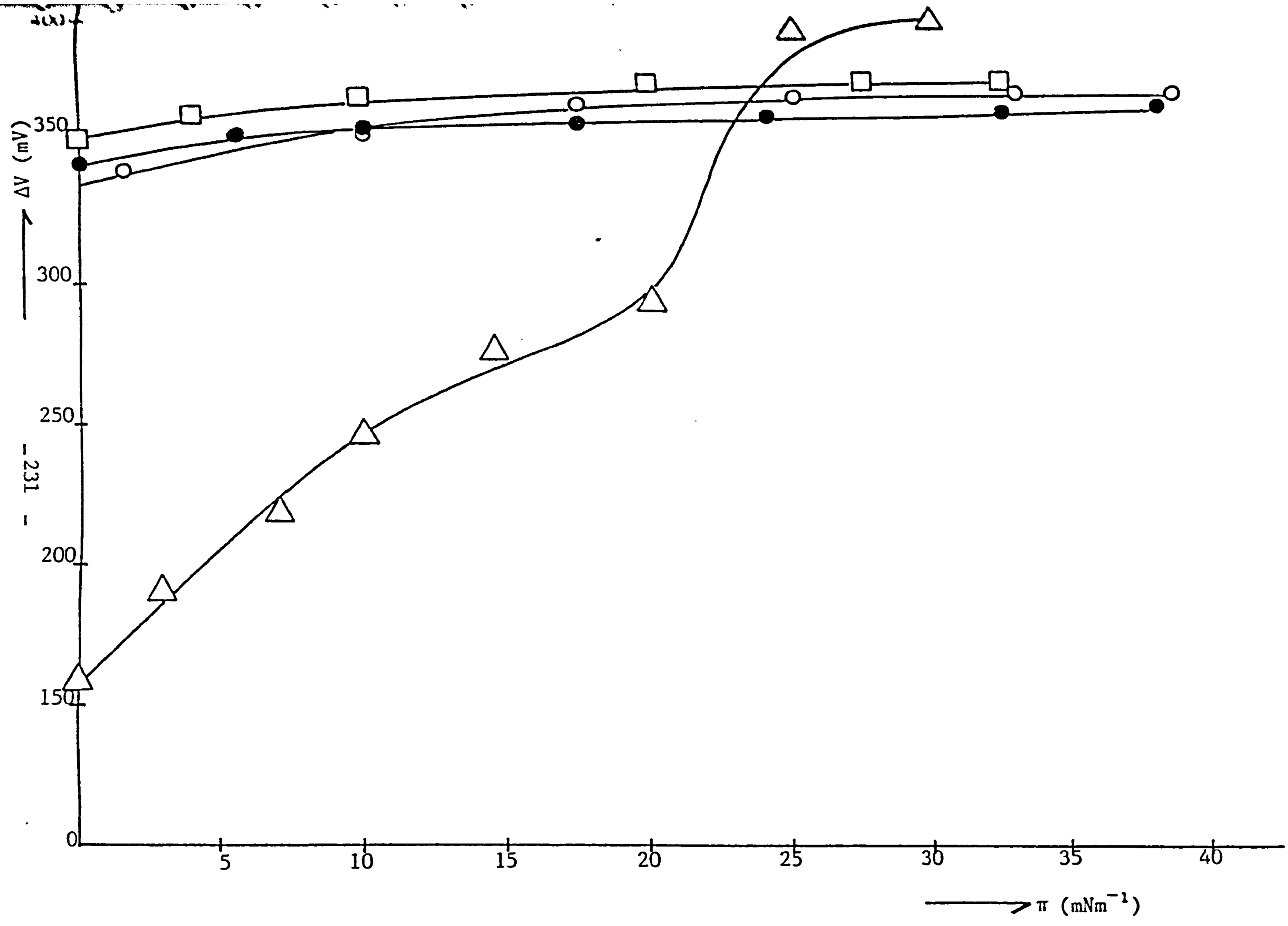

FIGURE 10.28: Plot showing the variation of surface potential with surface pressure for the various fatty acid monolayers

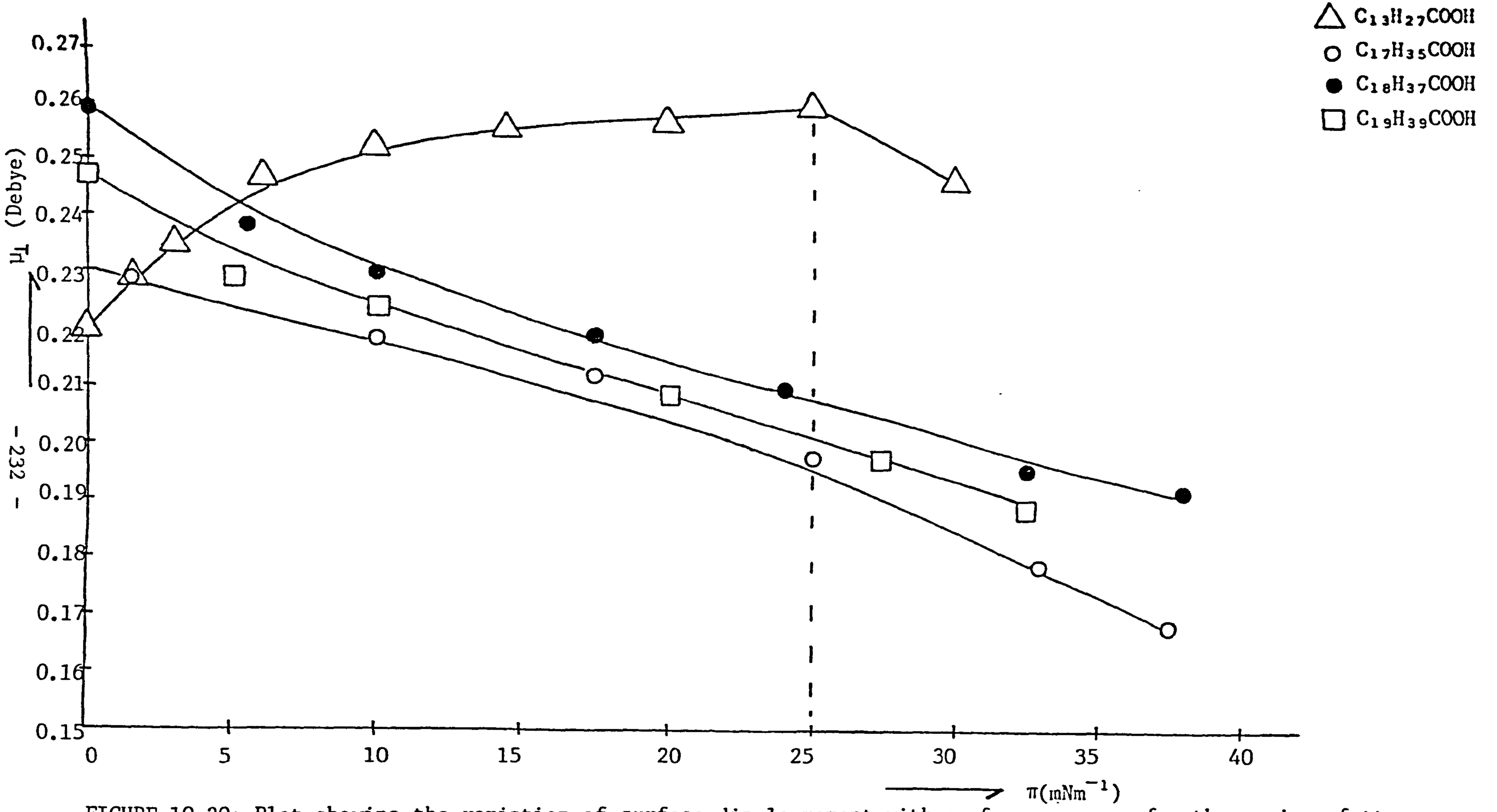

FIGURE 10.29: Plot showing the variation of surface dipole moment with surface pressure for the various fatty acid monolayers

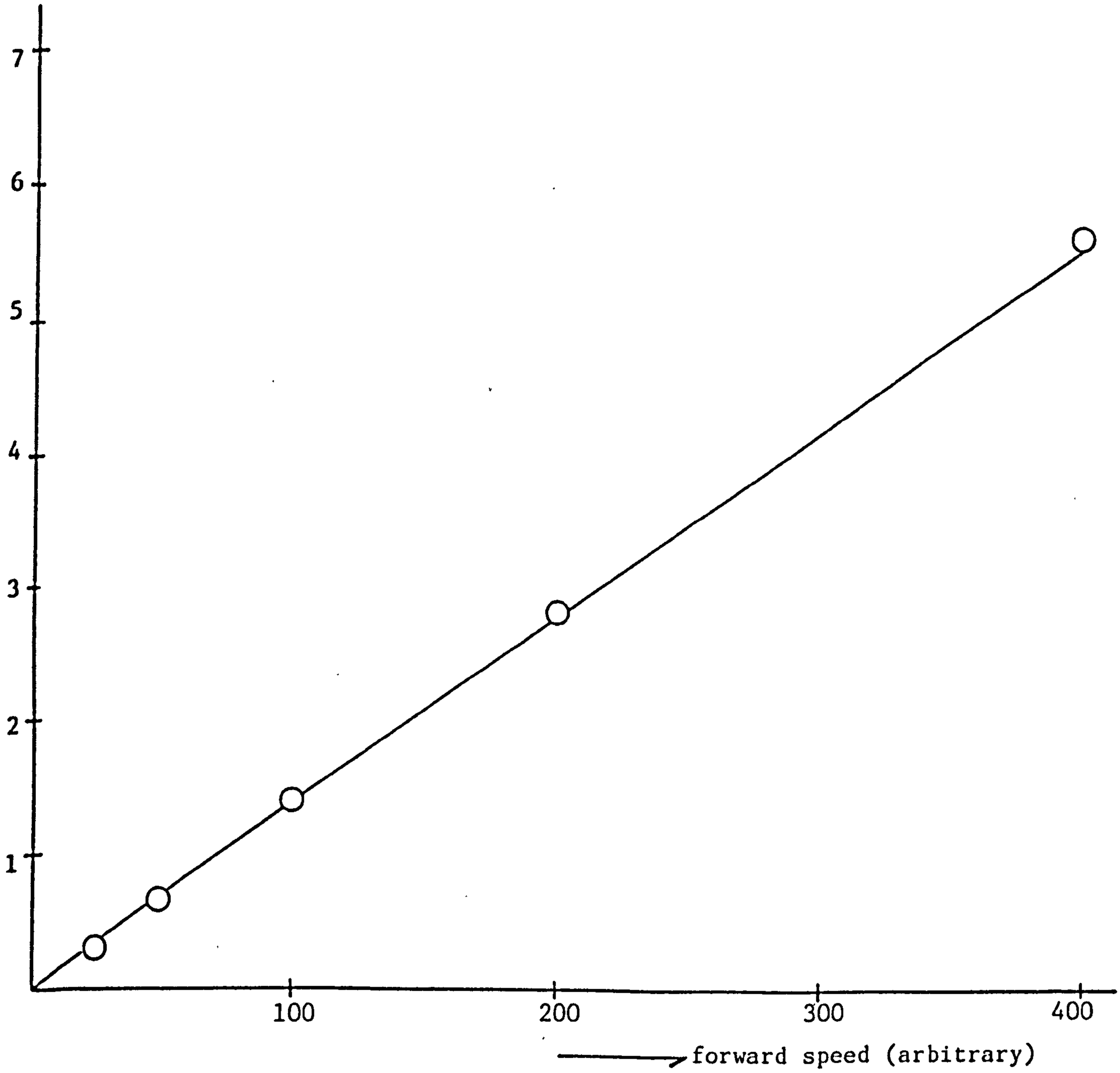

FIGURE 10.30: Plot showing the relationship between the actual speed and the arbitrary forward speed of the PTFE barriers

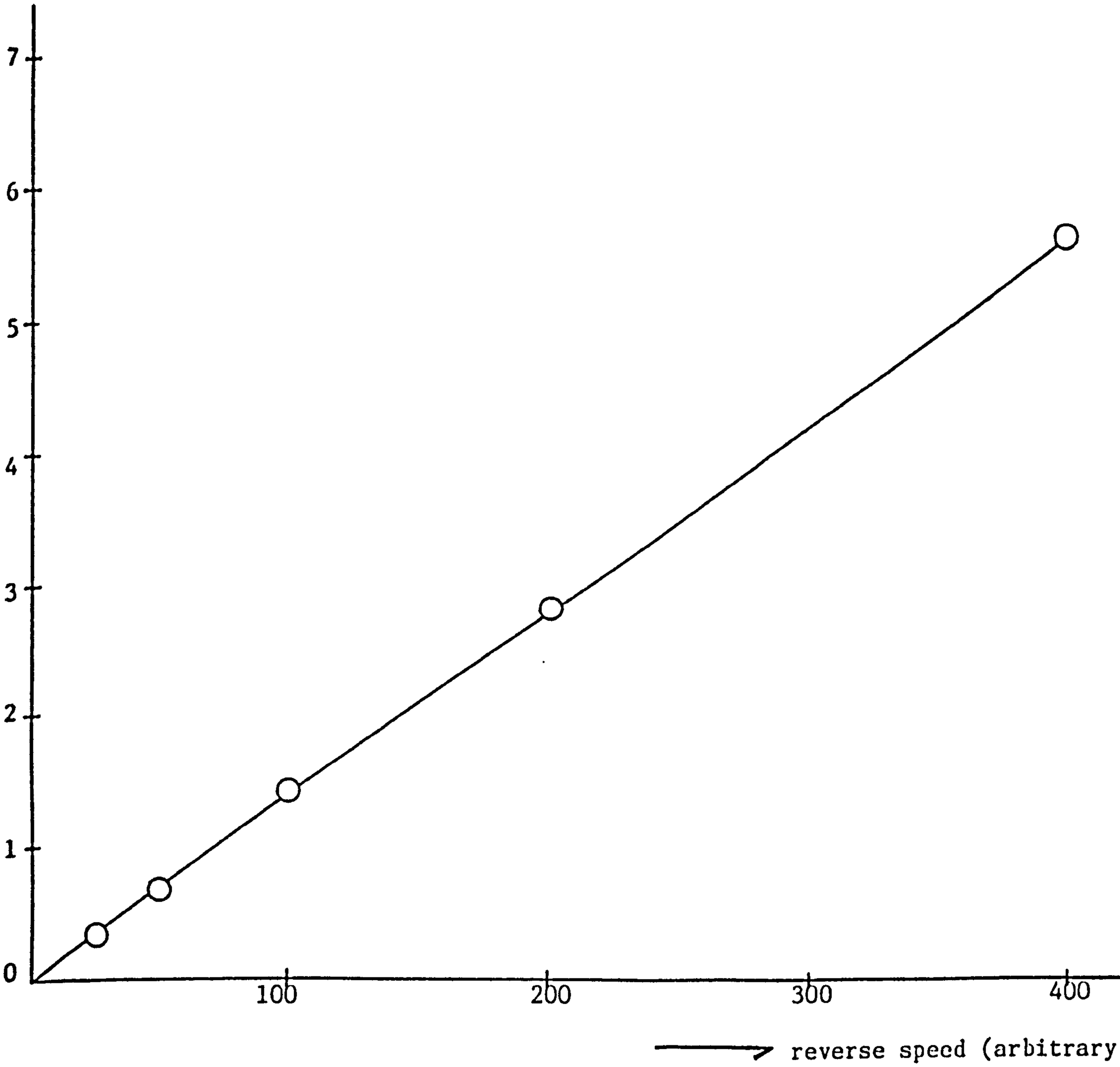

FIGURE 10.31: Plot showing the relationship between the actual speed and the arbitrary reverse speed of the PTFE barriers

(i) Surface pressure held at $5mNm^{-1}$

Reverse Speed	
I	25
II	50
III	100
IV	200
V	400

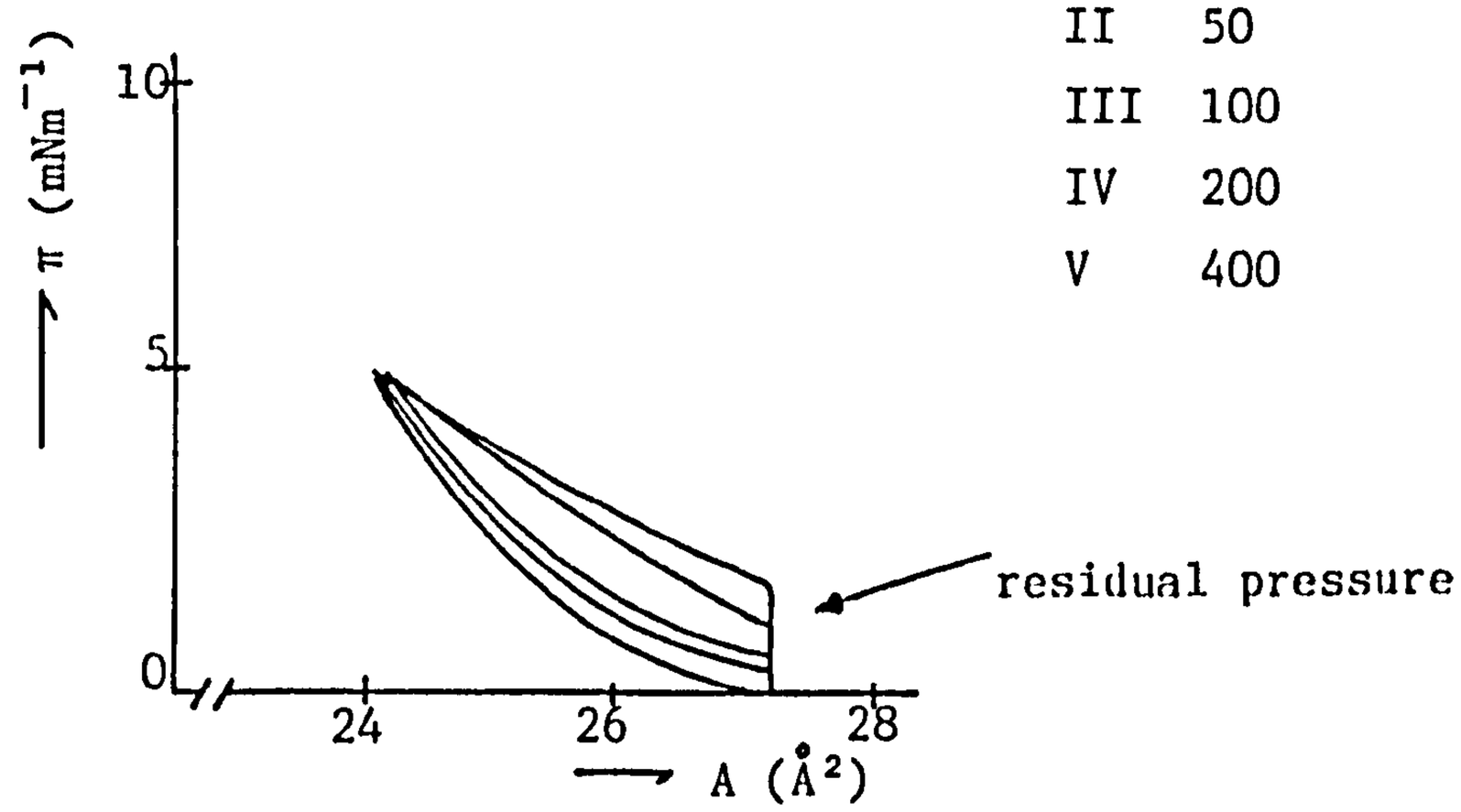

(ii) Surface pressure held at $10mNm^{-1}$

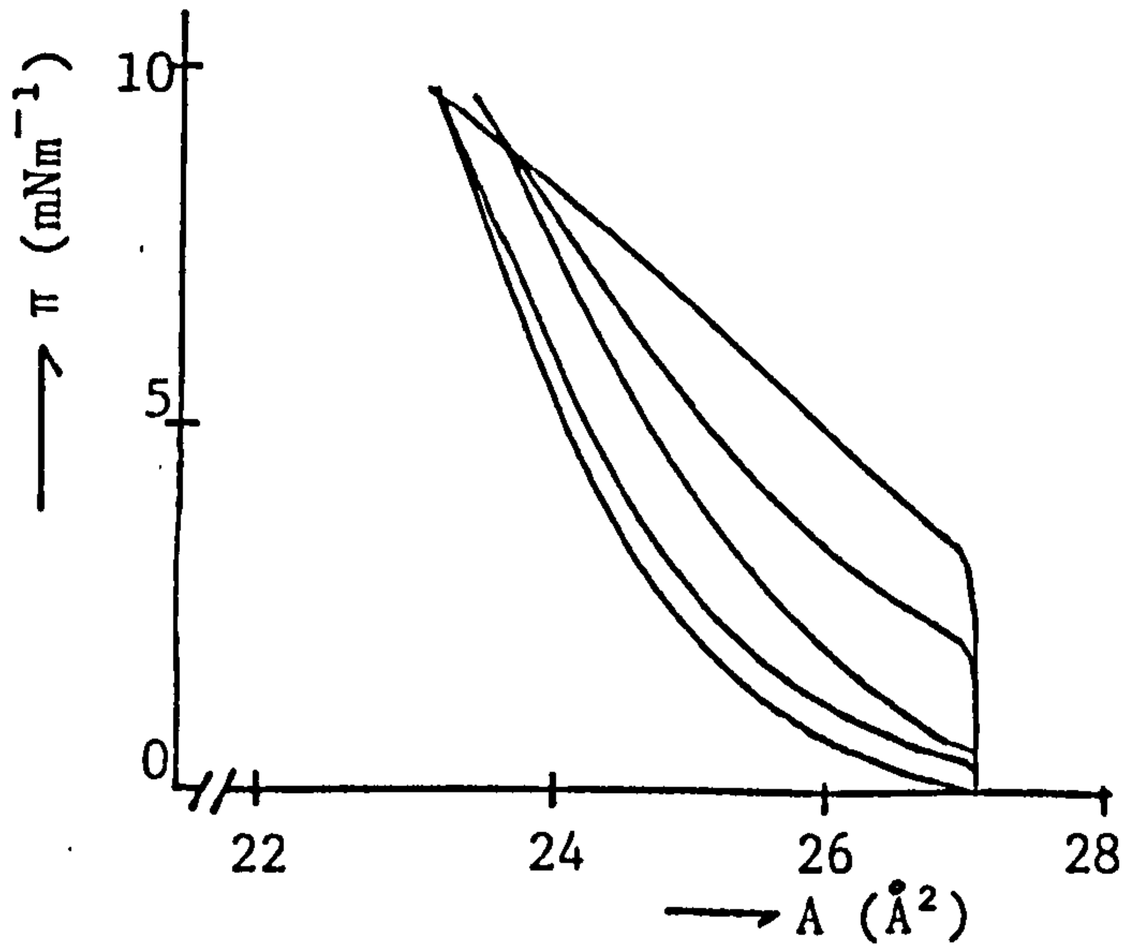

FIGURE 10.32(i)-(iv): Traces of relaxation profiles of $C_{17}H_{35}COOH$ monolayer showing the measure of the residual pressure as a function of the reverse barrier speed.

pH = 4.25 ± 0.03

T_b = 20.4 ± 0.2°C

No salt added to subphase

(iii) Surface pressure held at $25mNm^{-1}$

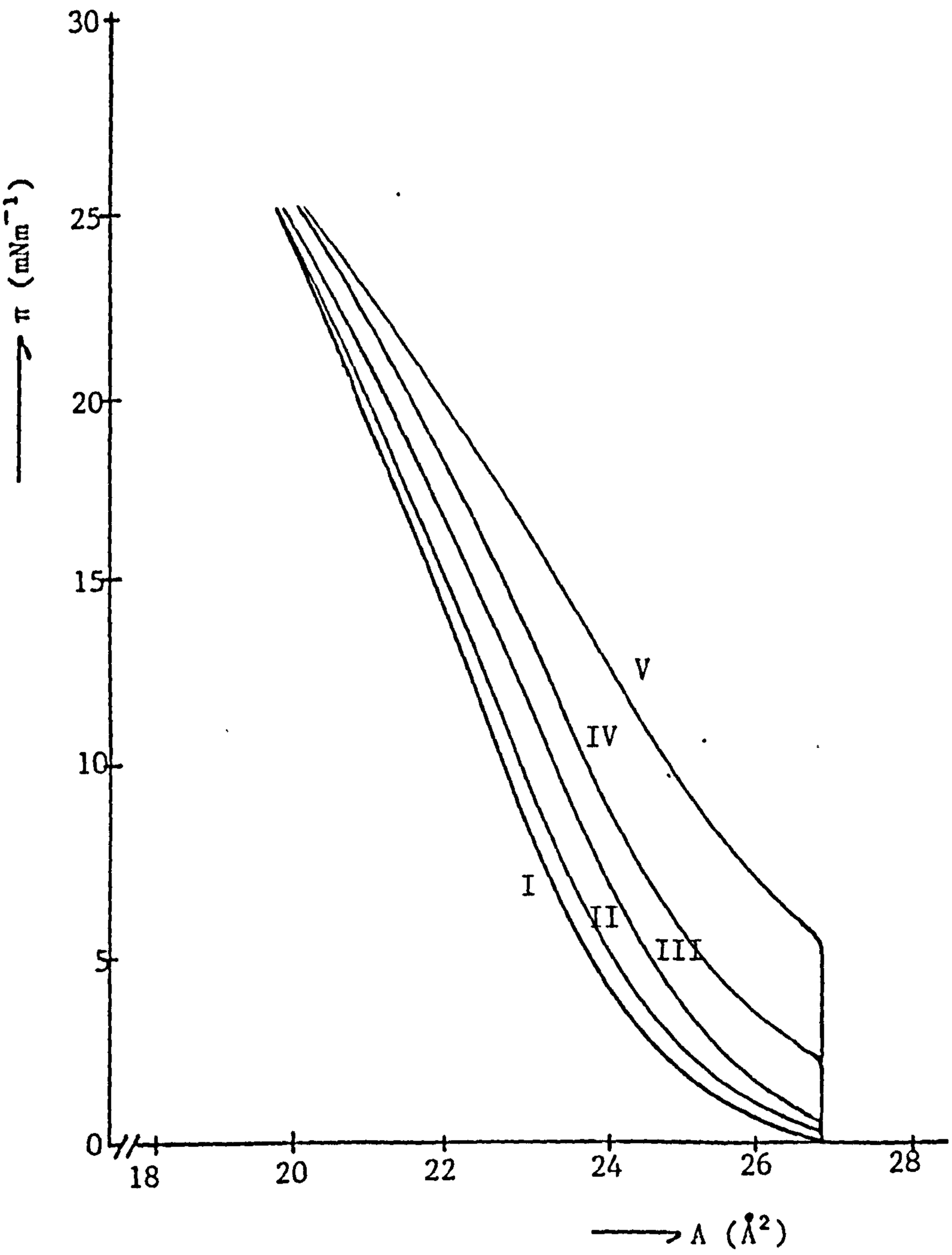

(iv) Surface pressure held at $35 mNm^{-1}$

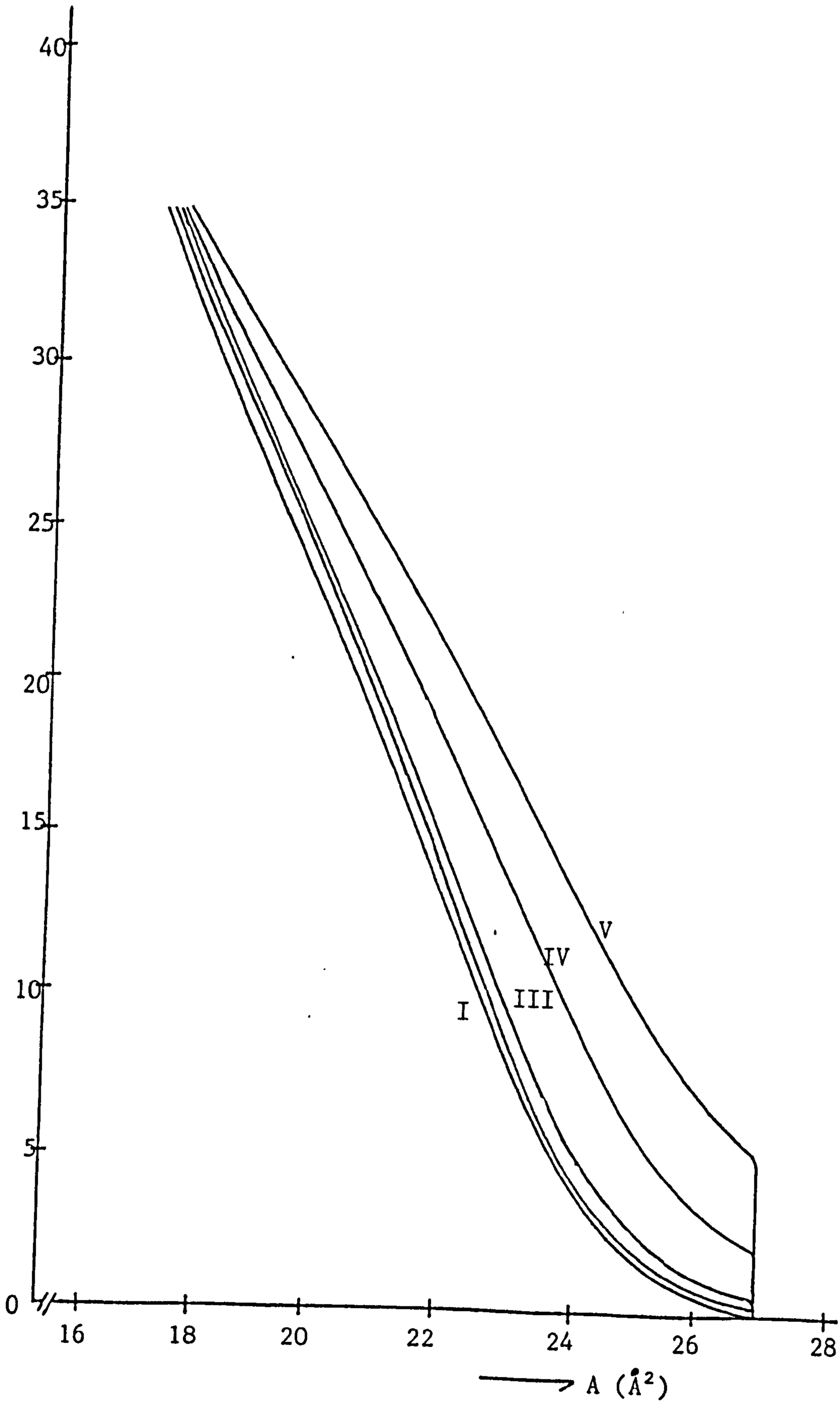

behaviour at low speeds, but gradually increase in residual pressure as both the 'held surface pressures' and reverse barrier speeds increase. This is probably due to the fact that the barriers are relaxing faster than the film molecules.

The mass spectra of C_{14} and C_{18} acids shown in Figures 10.33 and 10.34 provide added information on the purity of two of the acid samples used.

10.2.2 Discussion

A thorough study of the surface pressure-area behaviour of fatty acid monolayers from C_{14} to C_{22} has been made by Adam and his co-workers [42,229-231], and also by Nutting and Harkins[232]. The surface pressure-area isotherms shown in Figure 10.18 include regions where the monolayers are under pressures considerably above the equilibrium spreading pressure.

The isotherms of C_{14} and C_{15} exhibit well-defined transition regions between the expanded and condensed states at low pressures. But this feature has completely disappeared for C_{16} and the larger acid isotherms, where it appears that as the area appropriate to the condensed monolayer is approached, the isotherm turns upwards more steeply with generally no readily-observed discontinuity of slope as the fully-condensed region is reached.

It can also be observed that there is a gradual decrease in the area per molecule of about 27Å^2 for C_{14} to 21Å^2 for C_{20}, indicating that larger chains lead to better packing in the condensed state. This is in good agreement with the observation made by Nutting and Harkins[232] that the condensed film π-A curves shifted to slightly smaller areas as the fatty acid chain length increased.

PC022 0
CAL: C6K7LM

MYRISTIC ACID

12-SEP-
1:12

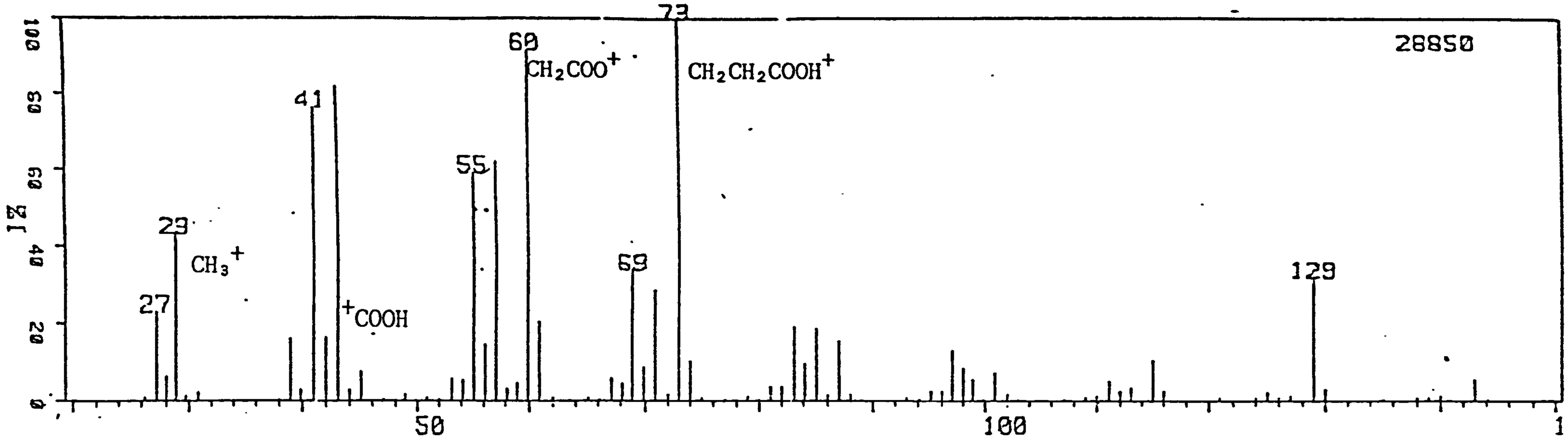

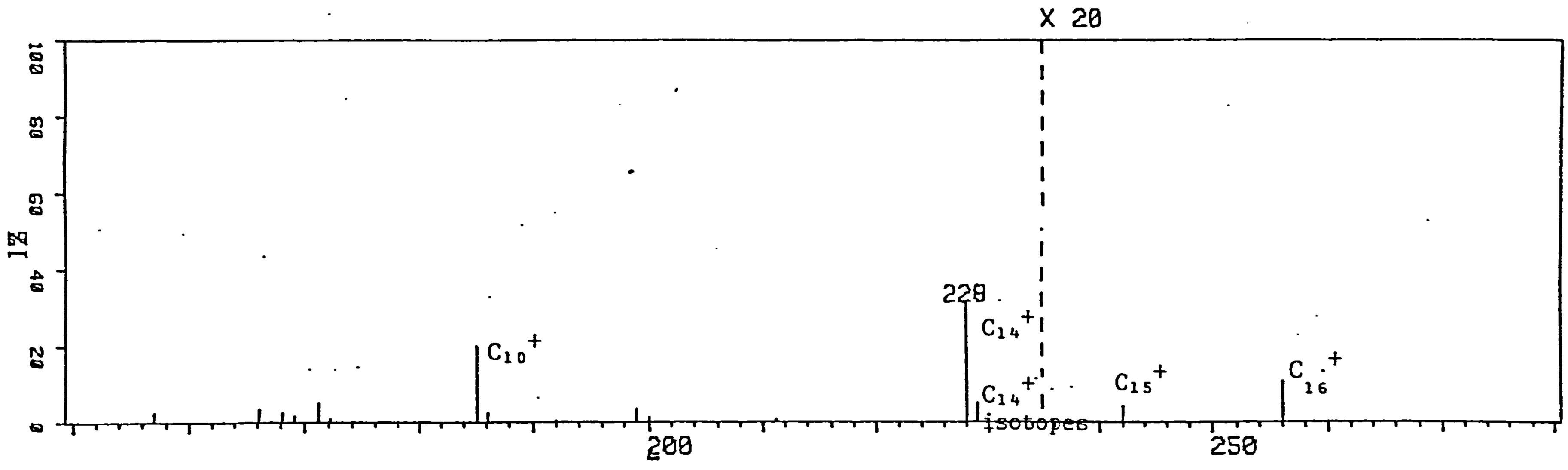

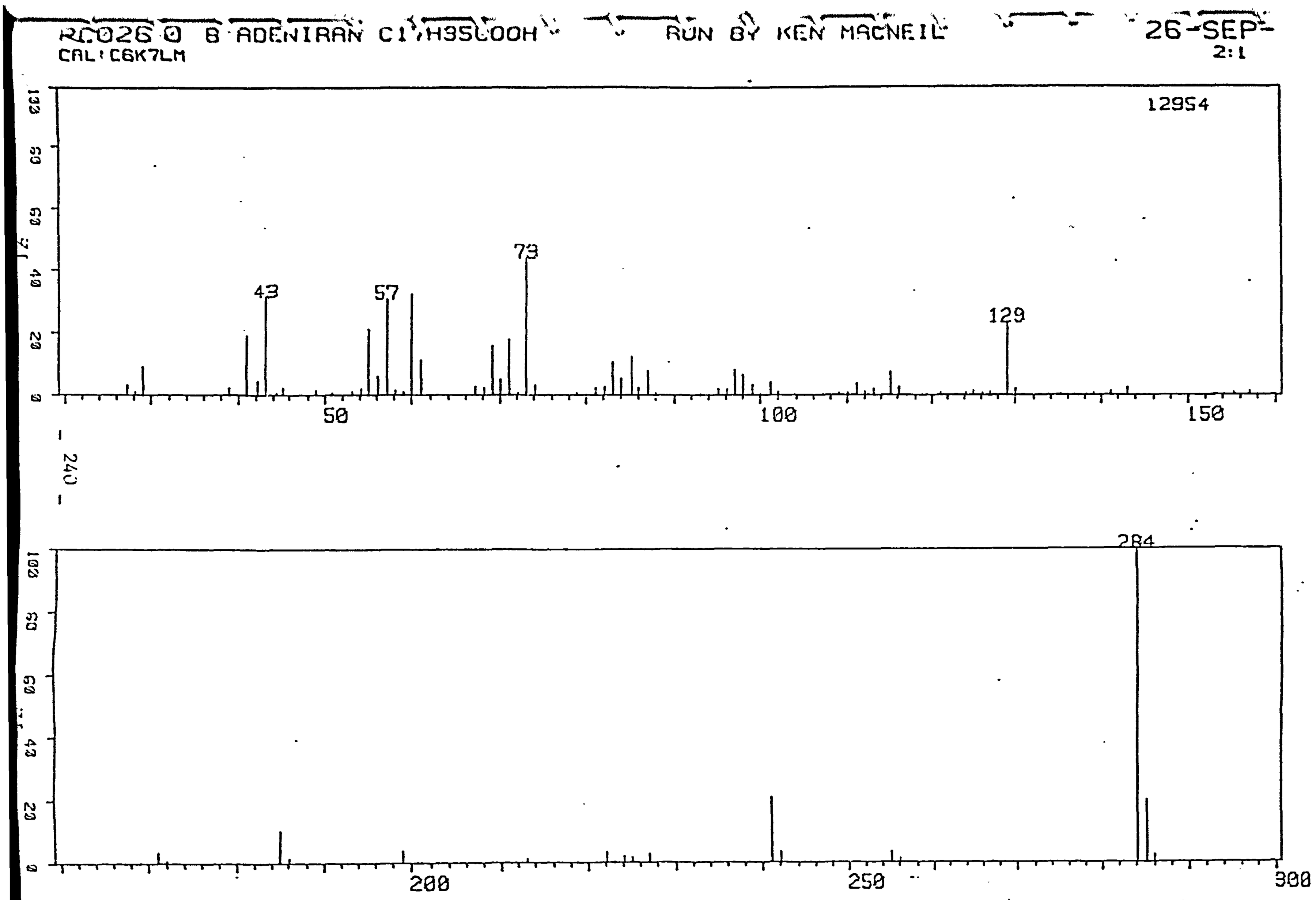

FIGURE 10.34: Mass spectrum of stearic acid, $C_{17}H_{35}COOH$

Several theories have been proposed to account for the behaviour of monolayers in the transition region. However, Langmuir's[43] assumption that the beginning of the transition occurred because some of the molecules in the liquid-like expanded film become organized into clusters or two-dimensional 'micelles', still has the greatest intuitive appeal. That the observed surface pressure was the sum of contributions from both single molecules and 'micellar'-type aggregates, and that molecules in aggregates occupied the area characteristic of the condensed film, while the area of single molecules was that found at the upper pressure limit of the expanded monolayer.

If this were so, then it might be expected that on slow compression, the course of the pressure-area curve would, for a time, be parallel to the area axis. In actuality, the curves obtained in Figure 10.18 are similar to those obtained by Adam and Jessop[231] and also Nutting and Harkins[232].

The compression modulus, k_s, depends on both the physical state and molecular packing of the film, and is defined by the formula

$$k_s = \frac{1}{c_s^*} = A\left(\frac{\partial \pi}{\partial A}\right)_{T,\pi=10 mNm^{-1}} \qquad (10.9)$$

where c_s^* is the coefficient of compressibility. The sequence of increasing compression moduli (i.e. decreasing compressibility) is also the sequence of decreasing area per molecule. Figure 10.19 shows that the van der Waals inter-molecular interactions do increase with the fatty acid chain length.

The results obtained by Spink[233] showed that π-A characteristics of all fatty acids were sensitive to pH, that the C_{14}-C_{17} acids began to dissolve at pH values $\leq$10, and that increases in head-group attraction

resulting from their partial ionization have little effect. On high pH subphases, when most of the carboxyls are ionized (e.g. 75% at pH 9-10), head-group repulsion partially overcomes inter-chain cohesion and film expansion occurs. On the other hand, with the shorter chain acids the attractive forces set up through partial ionization are sufficient to augment intermolecular cohesion, so that expanded monolayers contract a little. However, at high subphase pH these too finally expand by repulsion of more-or-less fully-ionized carboxyls. Figures 10.23 and 10.24 compare favourably with similar results obtained by Spink[233], and only the C_{18} acid could be studied above pH 9-10. Spink's summary of the pH, together with the associated behaviour of the acids (the area per molecule was assumed to be about 21Å^2) is given in Table 10.18.

Spink noted that C_{20} (arachidic) and C_{22} (behenic) acid monolayers also expand at high pH values. Goddard *et al*[234] also observed a small contraction for behenic acid monolayers over the pH range 3-10, followed by expansion at higher pH values. Spink's interpretation of the list in Table 10.18 is that homologues having less than 15 carbon atoms in their paraffinic chains have lower interchain cohesive forces than those of longer-chain members, resulting in expanded monolayers on low pH subphases. However, at intermediate pH values, the -COOH groups begin to ionize, so that the layer of polar head-groups in the surface comprises a mixture of ionized and unionized carboxyls. He proposed that in a sheet of partially-ionized groups, there would be increased ion-dipole interaction and/or increased hydrogen bonding, and that either effect led to intermolecular attractive forces. With longer-chain acids, the interchain cohesion is already so strong that condensed monolayers result.

The remarkable sensitivity of the properties of insoluble mono-

Acid	Behaviour	pH Range	α
Myristic (C_{14})	contracts	2.0 - 5.0	0 - 0.05
Pentadecanoic (C_{15})	contracts	2.0 - 7.2	0 - 0.20
Palmitic (C_{16})	contracts	6.4 - 8.0	0.12 - 0.35
Heptadecanoic (C_{17})	expands	9.0 - 10.0	ca. 0.75
Stearic (C_{18})	contracts slightly	9.0 - 10.0	ca. 0.75
" " "	expands	10.0 - 12.0	near 1

α is the degree of dissociation of the -COOH groups

TABLE 10.18 : Summary of the monolayer behaviour and estimated degree of dissociation of aliphatic long-chain fatty acids

layers to the presence of metallic ions in the subphase has been demonstrated by several authors[235-241]. More recently, it has been shown that metallic ions in the subphase can exert a profound influence on the pressure-area curves of acid monolayers[242-244]. It is also well-known that counter-ion effects with divalent cations such as Ca^{2+}, Ba^{2+} or Cu^{2+} render the film more closely-packed and insoluble.

Figures 10.20-1Q22, 10.25 and 10.26 show the variation of pH, transition and collapse pressures on the pressure-area characteristics of C_{14} (myristic) and C_{18} (stearic) acids on copper (II) chloride subphase. The plots of stearic acid are in good agreement with similar results obtained by Spink and Saunders[245]. Figure 10.26 shows the collapse isotherms of stearic acid at pH 5.8, and with $\pi_t \sim 30 mNm^{-1}$ and $\tilde{A}_m \sim 30 Å^2$ (common with that obtained by Spink and Saunders) and indicates that a sharp transition occurs at pH $\sim$ 5.75 from extremely condensed to expanded-type monolayer which may be due to copper ion attachment.

Spink and Saunders[245] have suggested that for stearic acid with copper ions in the subphase, it is the distearate soap that is formed with the copper ions because:

(i) copper ions cause a condensation of the film which is expected if the stearate chains are bonded in pairs through single copper ions;

(ii) a rapid increase in the molecular area rise value, A_0, occurs at a pH value which depends upon the concentration of copper in the subphase (i.e. the mono-stearate → di-stearate reaction).

The probable sequence of events may be:

subphase: precipitation of Cu^{2+} as $Cu(OH)_2$ at pH 6.3

$$CuCl_2 \xrightarrow{pH\ 5.7} Cu(OH)_x\ Cly \xrightarrow{pH\ 6.3} Cu(OH)_2$$

monolayer: $Cust_2 \xrightarrow{pH\ 5.5} Cu(OH)st$

The basic soap is formed by the equation:

$$Cust_2 + Cu^{2+} + 2OH \rightleftharpoons 2Cu(OH)st$$

The di-soap is formed up to pH 5.5, which then reacts to give the basic soap. Beyond pH 6.3 after the precipitation of $Cu(OH)_2$, the ratio

$$\text{basic soap} \rightleftharpoons \text{di-soap}$$

remains constant.

Surface Viscosity

The surface shear viscosity for three fatty acids was measured using the variable-width canal and torsion pendulum surface viscometers. The pressure of about $10mNm^{-1}$ was chosen simply to check correctness of procedures, and also to verify the literature prediction that at low surface pressures, the viscosity of fatty acid monolayers is low and Newtonian, and that it increases with increased chain length.

One limitation of the deep canal viscometer is that it is only sensitive to surface viscosity when the correction term is small (i.e. $\eta_s \gg a\eta_0$); hence, the Harkins and Kirkwood formula becomes:

$$\eta_s = \frac{2}{3} \times \frac{\pi_2}{q} \times \frac{a^3}{\ell} - \frac{2a\eta_0}{\pi} \qquad (10.10)$$

where $\pi_2 - \pi_1 = \pi_2$ (if π_1 is zero). Provided the above condition is fulfilled, it does provide an absolute measurement of the surface viscosity. A light coating of paraffin wax was applied to the inner surfaces of the canal so that a flat meniscus was obtained with the width of the canal better defined.

For the torsional pendulum viscometer, a hydrodynamic theory has been reported[246], but it does not yield a simple correction factor for the experimentally-measured surface viscosity. This theory has not

been used since a relative value of surface viscosity was sufficient for the present purpose, but an estimation has been made[247] of the magnitude of the amplification by assuming a correction factor of the same dimensional form as that used for the canal viscometer. Equation (10.10) can be rewritten as

$$\eta_s = \eta_s \text{ (apparent)} \left(1 + \frac{2a\eta_0}{\eta_s}\right)^{-1} \qquad (10.11)$$

where

$$\eta_s \text{ (apparent)} = \frac{2}{3} \times \frac{\pi^2}{q} \times \frac{a^3}{\ell} \qquad (10.12)$$

so the correction factor for the torsional pendulum will have the form

$$\text{correction factor} \simeq \left(1 + \frac{\kappa a \eta_0}{\eta_s}\right) \qquad (10.13)$$

where κ is the numerical coefficient of the order of unity. This would indicate a correction factor of between 10^{-1} and 10^{-2}.

The data plotted in Figure 10.27 show that the torsion pendulum measurements are several times higher than those from the canal. There was no evidence of non-Newtonian behaviour in the decay of the pendulum oscillations. Both sets of data show an exponential rise in surface viscosity with increasing number of carbon atoms in the chain. The increase in viscosity with chain length is consistent with the Eyring theory of viscosity in liquids, which predicts an exponential dependence of viscosity on some effective energy barrier, E, to molecules moving past each other:

$$\eta \propto e^{E/RT}$$

The values obtained are typical for fatty acids, and compare favourably with values at $\pi \sim 10 mNm^{-1}$ by Jarvis[248] and Boyd and Harkins[249], using the canal and torsion pendulum surface viscometers respectively.

Surface Potential

Condensed fatty films have been known to have surface potentials near 400mV. Most workers[89,90,250,251] agree that ΔV rises by approx. 20mV as the film is compressed from 25Å^2 mol^{-1} to the minimum area.

Harkins and Fischer[90] and Adam and Harding[89] both agreed that the ΔV-A curves showed a small progressive increase in surface potential with chain length, and that the increment amounted to about 15mV for each additional two carbons in the chain from C_{16} to C_{20}. Mizuno and Yamaguchi[252] and Goddard *et al*[253] have also reported similar observations. Their values are consistent with those found experimentally.

Typical expanded films such as myristic acid at room temperature have yielded ambiguous surface potential results. Yet most workers[250,89] have generally agreed that at the lowest pressures where the film is about 45Å^2, the surface potential, ΔV, is about 160-180mV. Then, as the film is compressed towards the minimum area, ΔV rises and the maximum surface potential measured is close to that observed for condensed fatty acids of about 400mV. This behaviour and these values are consistent with those obtained for myristic acid experimentally.

Addink[254] has suggested that this behaviour may be partly due to the solubility of the monolayer , that such solution led to the establishment of an acid-rich zone in the subphase just under the film, and that the dissolved fatty acid molecules contributed in some way to the observed surface potential.

In monolayers of fatty acids on aqueous subphases, the dipole is directed in such a way that the negative end is downwards, with the resultant dipole moment, $\mu_\perp$, being positive - as is ΔV. Estimates of the

exact orientation have been made for some situations, e.g. Dreher and Sears[255] deduced that in a monolayer of stearic acid at 20Å^2 mol^{-1}, where the 'tails' are vertical and the C-COOH bond is at 38° to the vertical, the carboxyl group contributed -0.670D to $\mu_\perp$; the orientated water dipoles in the vicinity of the -COOH group contributed +0.900D, giving a net $\mu_\perp$ value of +0.230D - consistent with the value (0.229D) obtained in Table 10.15. The work of Dreher and Sears compared ΔV values for monolayers on H_2O and D_2O subphases, and appears to support previous proposals that orientated layers[256] of water or 'soft ice'[28] are associated with polar head-groups in monolayers on aqueous subphases.

When the -COOH group ionizes, counter-ions in the subphase assume a statistical distribution about it, and the resultant dipole is then the sum of the $-COO^-$ moment and the moment of the system of cations about this anion. The latter normally outweighs the former, so that the resultant $\mu_\perp$ is negative. There must be changes in the orientation of water dipoles attending ionization of the carboxyl, but no analysis comparable to that of Dreher and Sears is known to this author.

The myristic acid $\mu_\perp$-π plot of Figure 10.29 shows a sharp discontinuity from the gradual increase in $\mu_\perp$, to a fall in magnitude at a transition point. This indicates that there is a defined condensed state beyond the transition pressure, π_t, when compared to higher fatty acid analogues. It is likely that the reduction in $\mu_\perp$ on compression (which must be a head-group phenomenon) would be due to:

(i) damping out of the head-group by ions or water molecules;

(ii) tilting of the head-group.

The increase of dipole in the liquid-expanded state may be related to the number of molecules, n, in equation (10.8):

$$\mu_{\perp} = \varepsilon_0 \times \frac{\Delta V}{n}$$

When n is small and slowly-changing, ΔV rises and so $\mu_{\perp}$ goes through a maximum.

Relaxation Curves

The profiles shown in Figure 10.32(i)-(iv) for stearic and monolayer indicate the existence of intermolecular cohesion as the surface area is relaxed, and that these molecules are still held together and are unable to relax because the barriers are relaxing at a faster rate than the rate of aggregate breakdown. Similar relaxation profiles were also obtained for the higher homologues,of which the residual pressure (a measure of the entanglement occurring between the molecules) increased at high pressures and barrier speeds, with increased fatty acid chain length. Rabinovitch *et al*[257] have studied the relaxation of surface pressure and collapse of stearic acid monolayers..

The mass spectra of both C_{14} and C_{18} acids show the samples used to be reasonably purified, with large mass ion peaks occurring at molecular weights 224 and 284 respectively.

10.2.3 Summary

Surface pressure-area isotherms have been determined for monolayers of $C_{13}H_{27}COOH$-$C_{19}H_{39}COOH$ on acidic subphases. Pressure-area isotherms for myristic and stearic acids on copper (II) chloride subphase indicate that with increasing pH, divalent and basic soaps are successively formed in the monolayer.

The surface viscosities of monomolecular films of long-chain fatty acids were determined using the canal and torsion pendulum viscometers, and the data obtained were in good agreement with those previously reported. The canal surface viscosity values were an order of magnitude

less than the values obtained from the torsion pendulum viscometer.

Under the most favourable conditions, surface potential measurements were obtained for four fatty acids, namely: myristic, stearic, nonadecanoic and arachidic. The surface potential difference attained a maximum or saturation value at a certain definite surface concentration. A value of about 350mV was obtained for most of the saturated fatty acids. The vertical component of the dipole moment was then calculated by applying the Helmholtz's formula.

10.3 Polydimethylsiloxane Film Measurements

10.3.1 Results

The correlation given by Barry[116] was used to characterize the molecular weights of the polydimethylsiloxane polymers used in the experimental work. This correlation predicted that the value of n in the structure

$$(CH_3)_3Si\text{-}O[(CH_3)_2Si\text{-}O]_n - Si(CH_3)_3$$

is ≤87 for a polydimethylsiloxane of weight-average molecular weight 6610. Similarly, a value of n has been evaluated for the remaining polydimethylsiloxanes and these are listed in Table 10.19. A summary of the area per molecule and related data obtained from the monomolecular film measurements is given in Table 10.19.

The plots of surface pressure against molecular area for the polydimethylsiloxanes were independent of the chain length in the range from 87 up to 1482 siloxane units, and were measured with good reproducibility. Isotherms of a similar kind to polydimethylsiloxane <6610> (see Figure 10.35) were obtained for the other polydimethylsiloxanes. The curve which extends up to high area values is characterized by two

Weight-Average Molecular Weight, $\overline{M}_w$	Density, ρ ($g\ cm^{-1}$)	No. of Molecules on Surface	Area per Molecule, $\tilde{A}_m$ at $OmNm^{-1}$ ($\leq Å^2$)	No. of Repeating Units ($\leq$ link)
6610	0.883	2.07×10^{15}	1440	87
14420	0.8571	7.73×10^{14}	3857.3	192.4
19100	0.849	5.72×10^{14}	5068	255.5
31000	0.890	3.25×10^{14}	7841.1	416.1
48150	0.8099	2.34×10^{14}	12167.4	647.5
110000	0.827	8.85×10^{13}	33346.2	1482

TABLE 10.19 : Surface pressure-surface area and related data from monomolecular film measurements on the Joyce-Loebl trough of polydimethylsiloxanes on a pure water subphase.

pH = 4.9 ± 0.02

Temperature of bath, $T_b = 22.5 \pm 0.1^{o}C$

Forward/Reverse barrier speed = 50/50 (arbitrary unit)/$0.75 mms^{-1}$

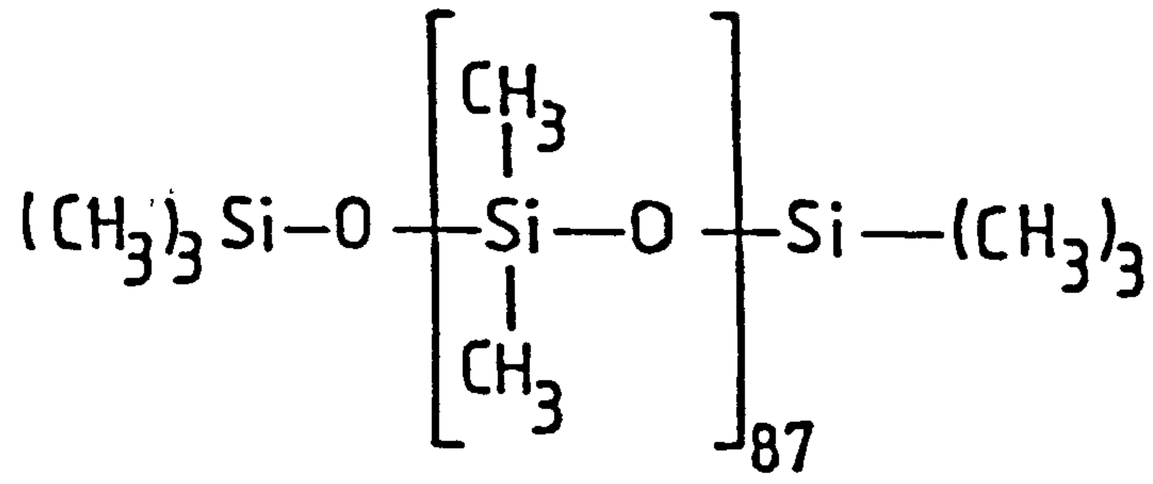

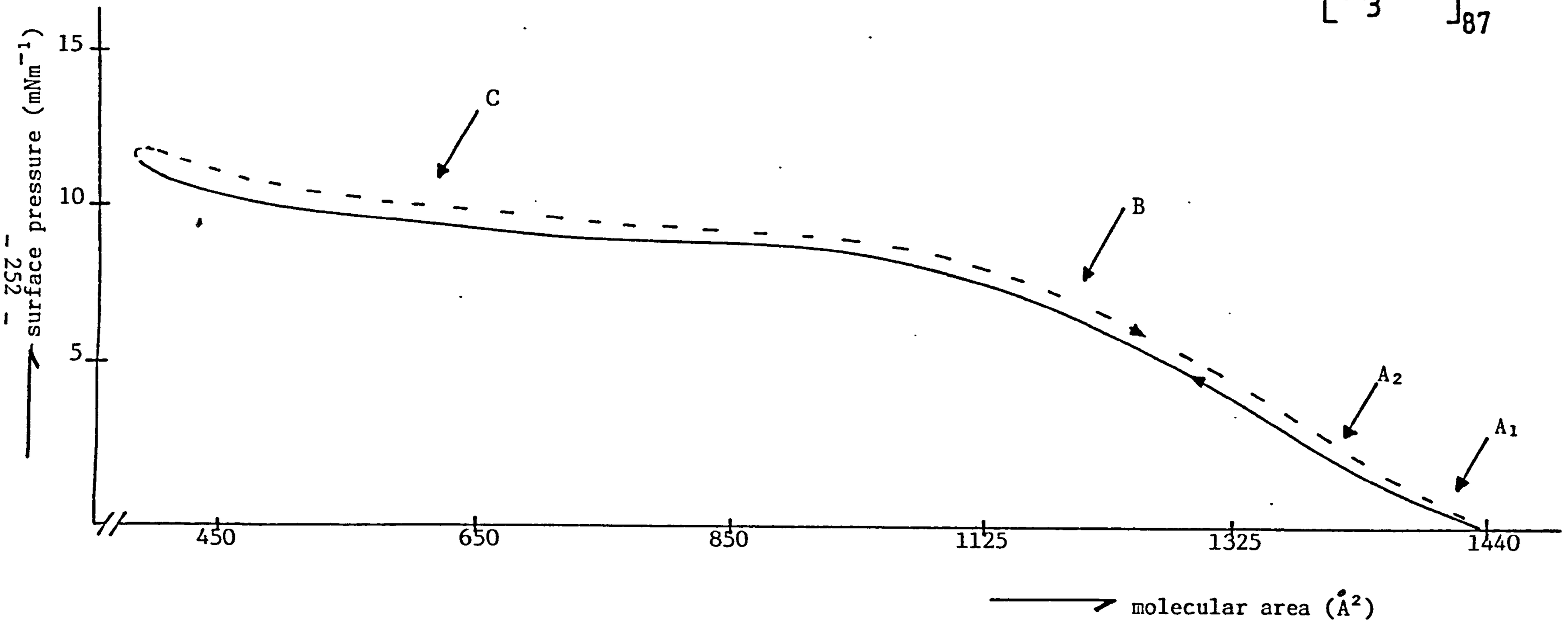

FIGURE 10.35: Plot showing the surface pressure-surface area isotherm for polydimethylsiloxane <6610> monolayer on a pure water subphase. pH = 4.89 $\pm$ 0.02; T_b = 22.7 $\pm$ 0.1°C

pronounced discontinuities at A_2 and B, as well as by two small steps at A_1 and C. These points are very important in the interpretation of the structure of the monolayer.

The area per molecule for each polydimethylsiloxane was calibrated by extrapolating the compression curve back to zero surface pressure; these are given in Table 10.19. Figure 10.36 shows the variation of surface pressure with the area per siloxane monomer for the various polydimethylsiloxane monolayers. Most of the polydimethylsiloxanes give an area per siloxane monomer of about $20\mathring{A}^2$, with only polydimethylsiloxane <6610> giving less than $18\mathring{A}^2$.

A linear relationship was obtained between the molecular weight and the extrapolated area per molecule for the polydimethylsiloxanes, and is shown in the plot of Figure 10.37. The expression holds when

$$\text{molecular weight, } \bar{M}_w = 3.2 \times \text{area per molecule, } \tilde{A}_m$$

or

$$\text{area per molecule, } \tilde{A}_m = 0.313 \times \text{molecular weight, } \bar{M}_w$$

The effect of acid addition to the aqueous subphase was examined on the typical pressure-area isotherm of polydimethylsiloxane <6610> and is depicted in Figure 10.38. When the pH value was reduced to 1.66, the stage C disappeared and the pressure rose more strongly from B onwards. However, when the pH value was finally lowered to 0.41, the curve changed its course entirely from B onwards by rising quickly to high pressure values.

The addition of sodium ions to the subphase also had a distinct effect on the pressure-area isotherms. It seemed that the sodium ions were making the lower part of the isotherms much broader, so that there was an apparent increase in area per molecule at both zero surface

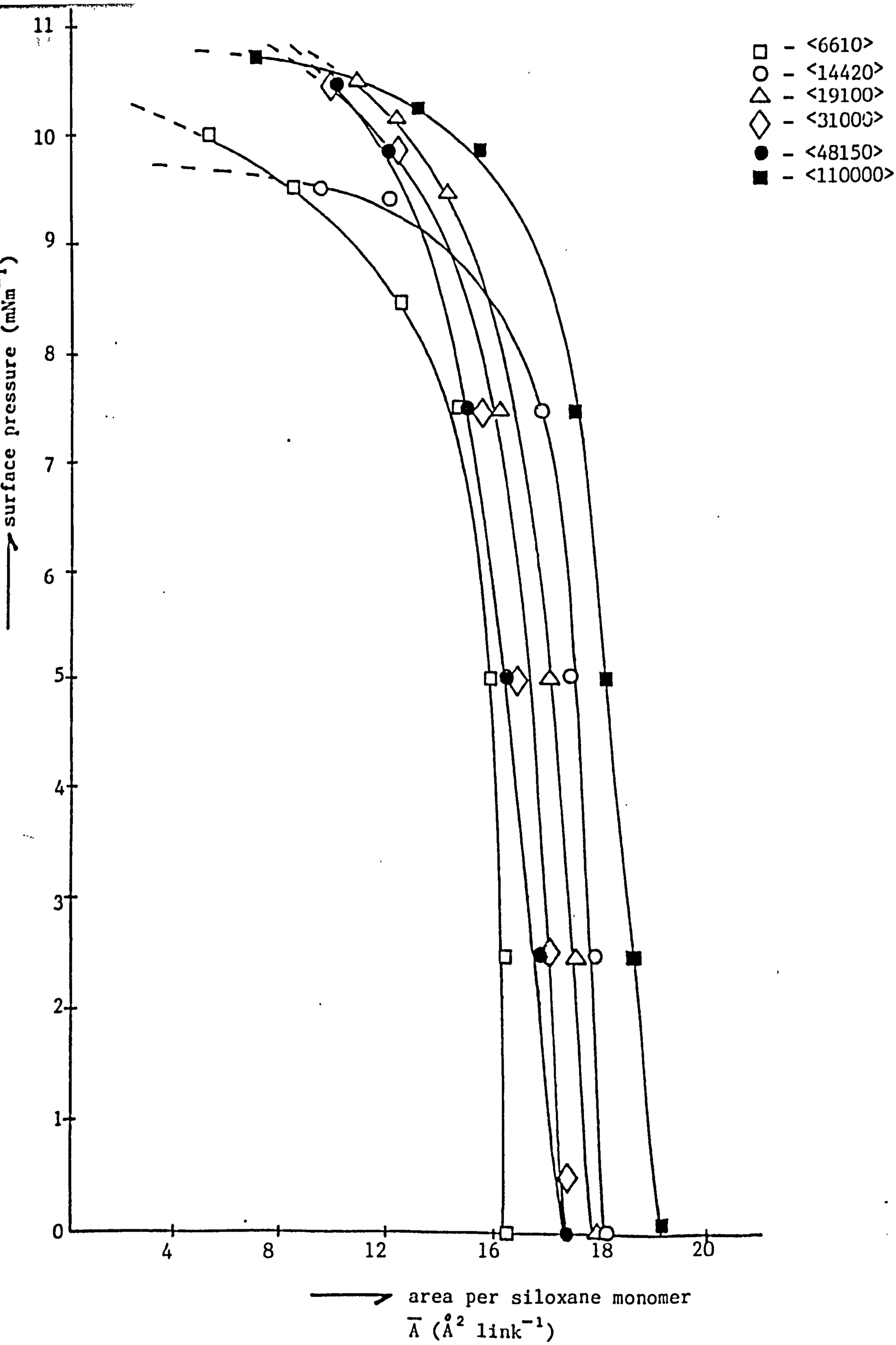

FIGURE 10.36: Plot showing the variation of surface pressure with the area per siloxane monomer for the single polydimethylsiloxanes on a pure water subphase. pH = 4.98 ± 0.02; T_b = 22.5 ± 0.1°C

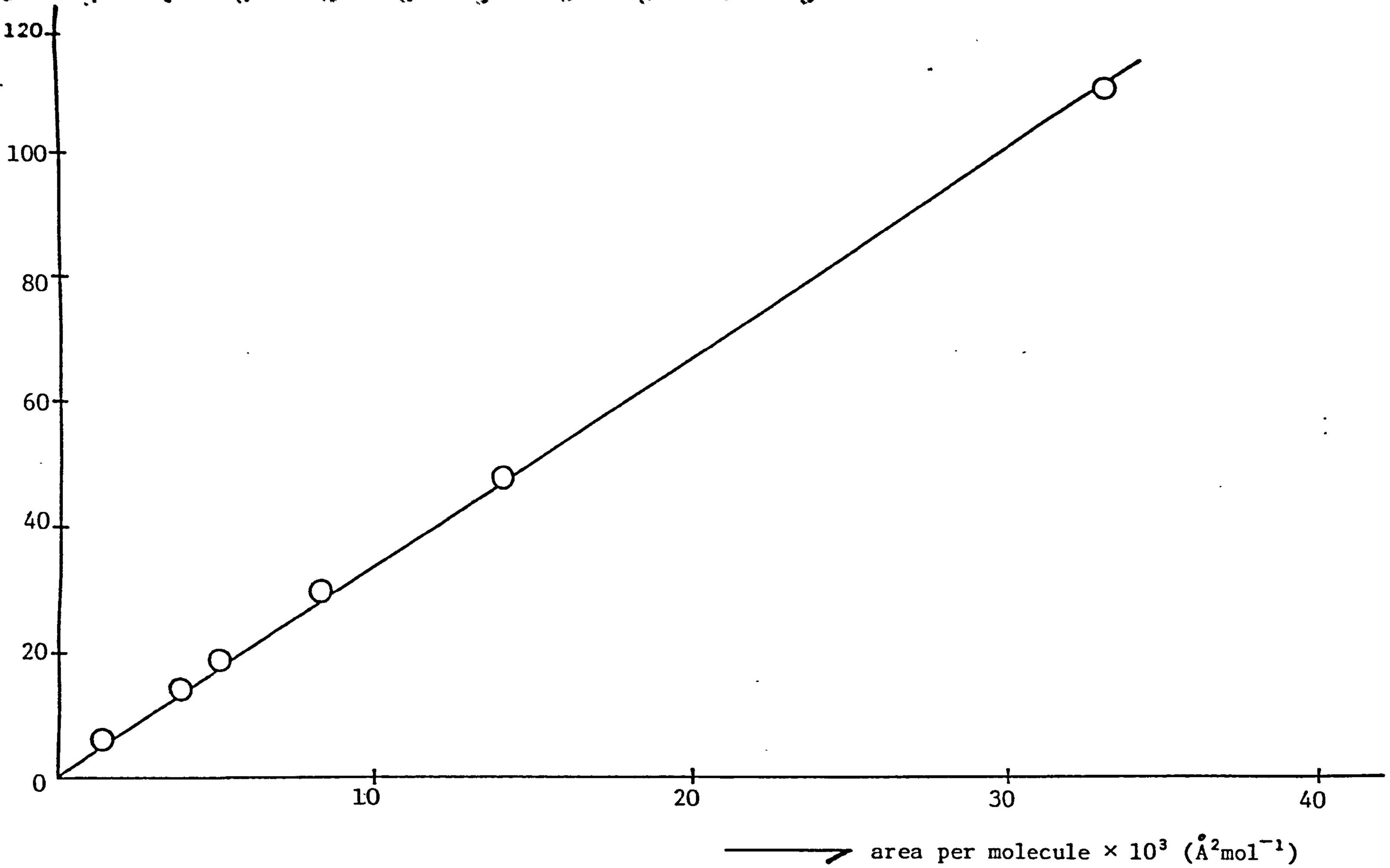

FIGURE 10.37: Plot showing the linear relationship between weight-average molecular weight and the area per molecule for the polydimethylsiloxanes

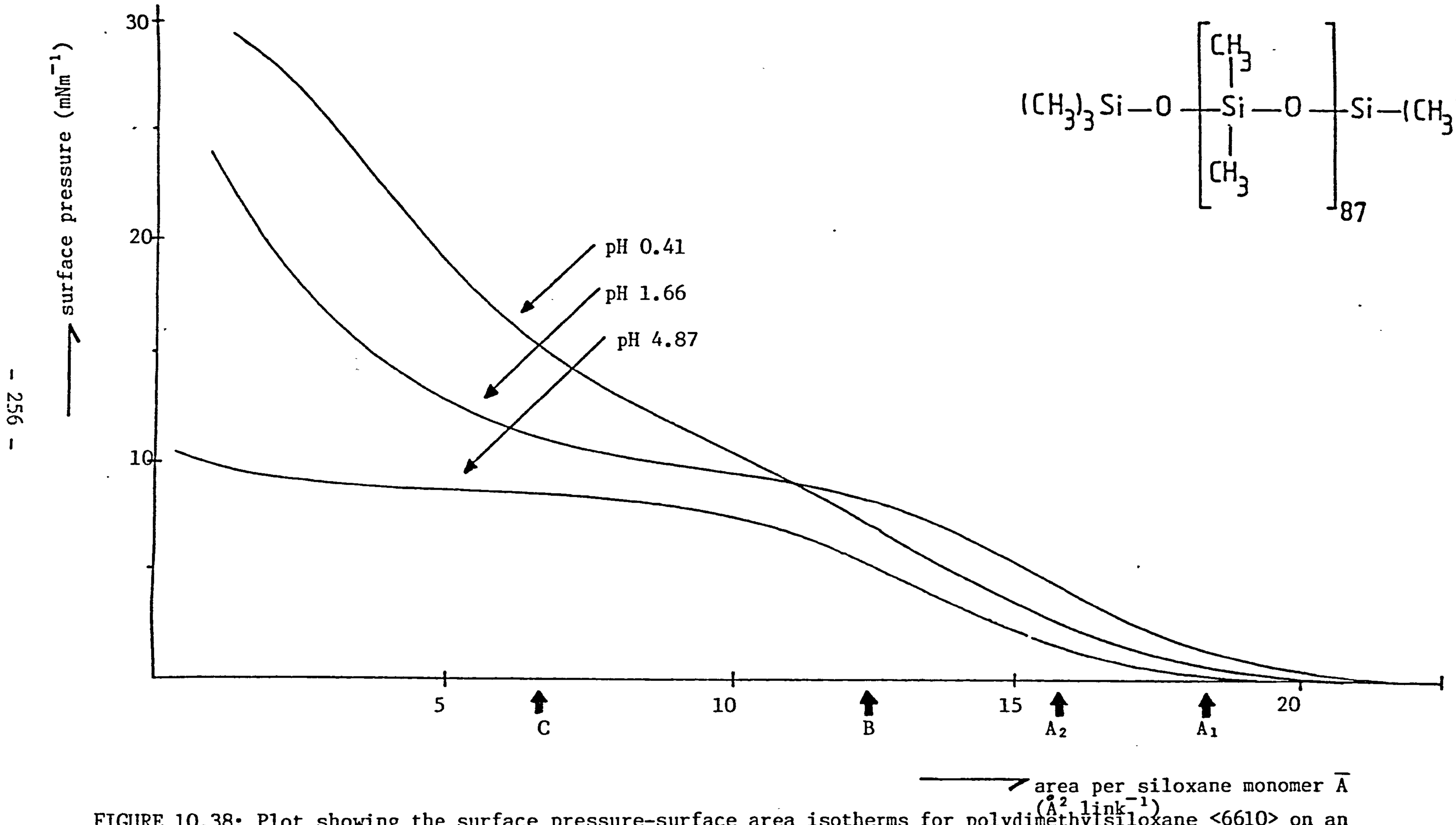

FIGURE 10.38: Plot showing the surface pressure-surface area isotherms for polydimethylsiloxane <6610> on an aqueous hydrochloric acid subphase of different pH values. $T_b = 22.7 \pm 0.1^oC$

pressure, $\tilde{A}_m(0)$, and other surface pressures, $\tilde{A}_m(5)$ and $\tilde{A}_m(10)$, as given in Table 10.20.

Surface Potential

The volta potential difference, ΔV, due to the presence of each polydimethylsiloxane film on the 0.01M sodium chloride subphase, is expressed as a function of the degree of packing, and is tabulated in Tables 10.21, 10.22 and 10.23, and represented graphically in Figures 10.39, 10.40 and 10.41. The apparent vertical dipole moments, $\mu_\perp$, were calculated from the interface potentials, ΔV, by means of the Helmholtz formula

$$\Delta V = 4\pi n\mu_\perp$$

where n is the number of polydimethylsiloxane molecules per unit area of the interface. Values of about 220mV and 0.15 Debyes were obtained for the surface potentials and the vertical dipole moments for the three polydimethylsiloxanes when measured at zero surface pressure respectively. The plots indicate a decrease in vertical dipole moment with increasing interface potential, and as the area occupied by the polydimethylsiloxane molecule decreases.

Surface Viscosity

The surface viscosity measurements obtained for each polydimethylsiloxane monomolecular film was the average of at least 4 measurements, and could normally be reproduced to within $\pm$10% of all viscosities under the experimental conditions. Figure 10.42 shows the traces of the variation of the internal pressure of the canal viscometer with time, as the various molecular weight polydimethylsiloxane monolayers flow through the 'opened' slit of the viscometer. This occurred seconds before the internal and external pressures of the viscometer equilibrated. At the canal width of 0.65mm, the flux, q, was found to be independent of the

$\bar{M}_w$	No. of Repeating Units (link)	Area Per Molecule on Pure Water ($Å^2$)	Area Per Molecule on 0.01M NaCl ($Å^2$)	Surface Pressure (mNm^{-1})	Increase in Area/Link ($Å^2$ $link^{-1}$)	% Increase in Area ($Å^2$)
6610	87	1387	1491	5	1.19	7.4
14420	192	2908	3450	10	2.82	18.6
19100	255	5067.7	5213	0	0.57	2.88
110000	1482	28270	29824	5	1.05	5.55

TABLE 10.20: Data obtained from the Joyce-Loebl trough of the area per molecule of polydimethylsiloxane monolayers on pure water and 0.01M sodium chloride subphases

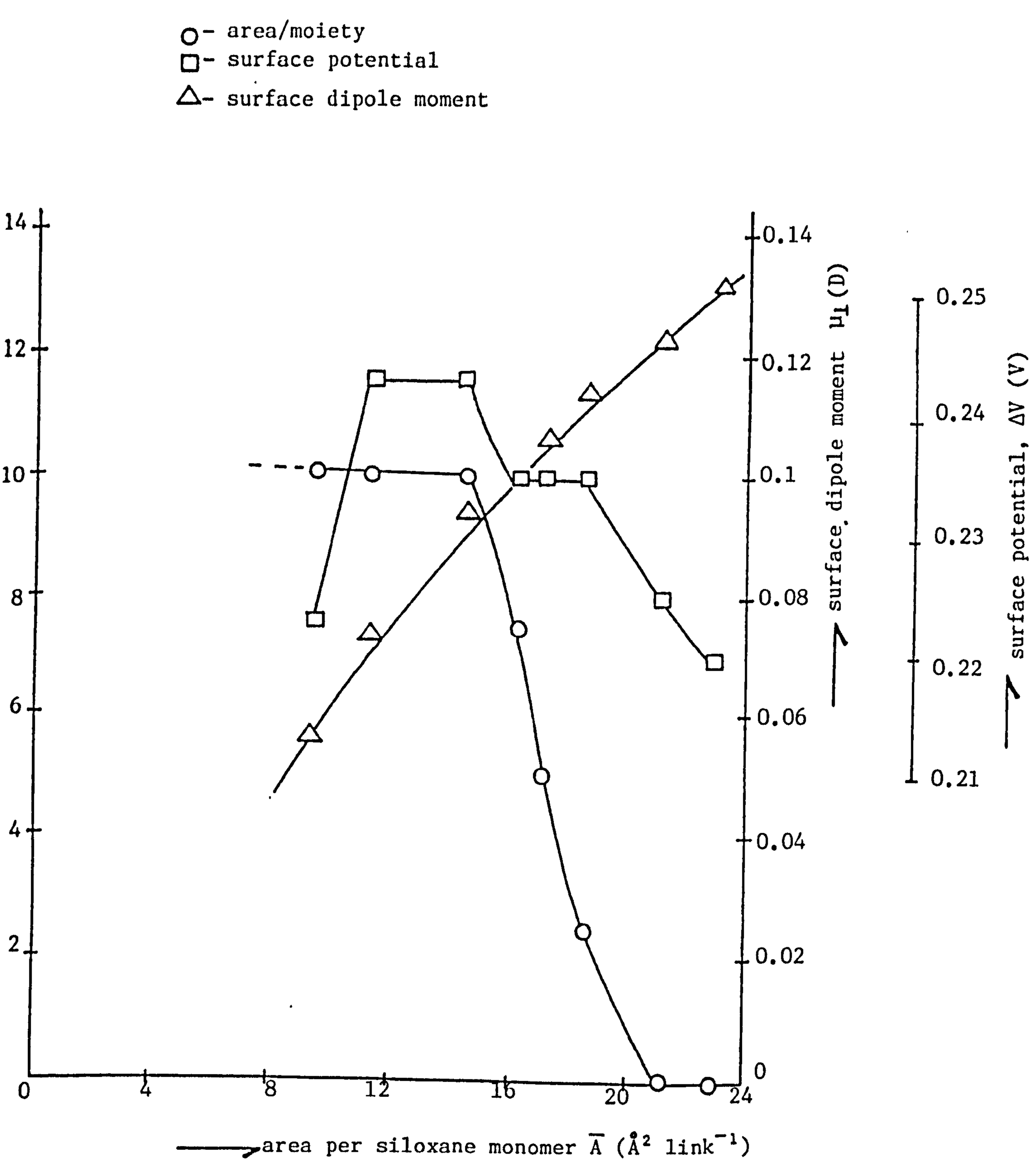

FIGURE 10.39: Plot showing the variation of surface pressure, surface potential and surface dipole moment with the area per siloxane monomer for polydimethylsiloxane <6610>

pH = 5.87 $\pm$ 0.02

T_b = 21.8 $\pm$ 0.1°C

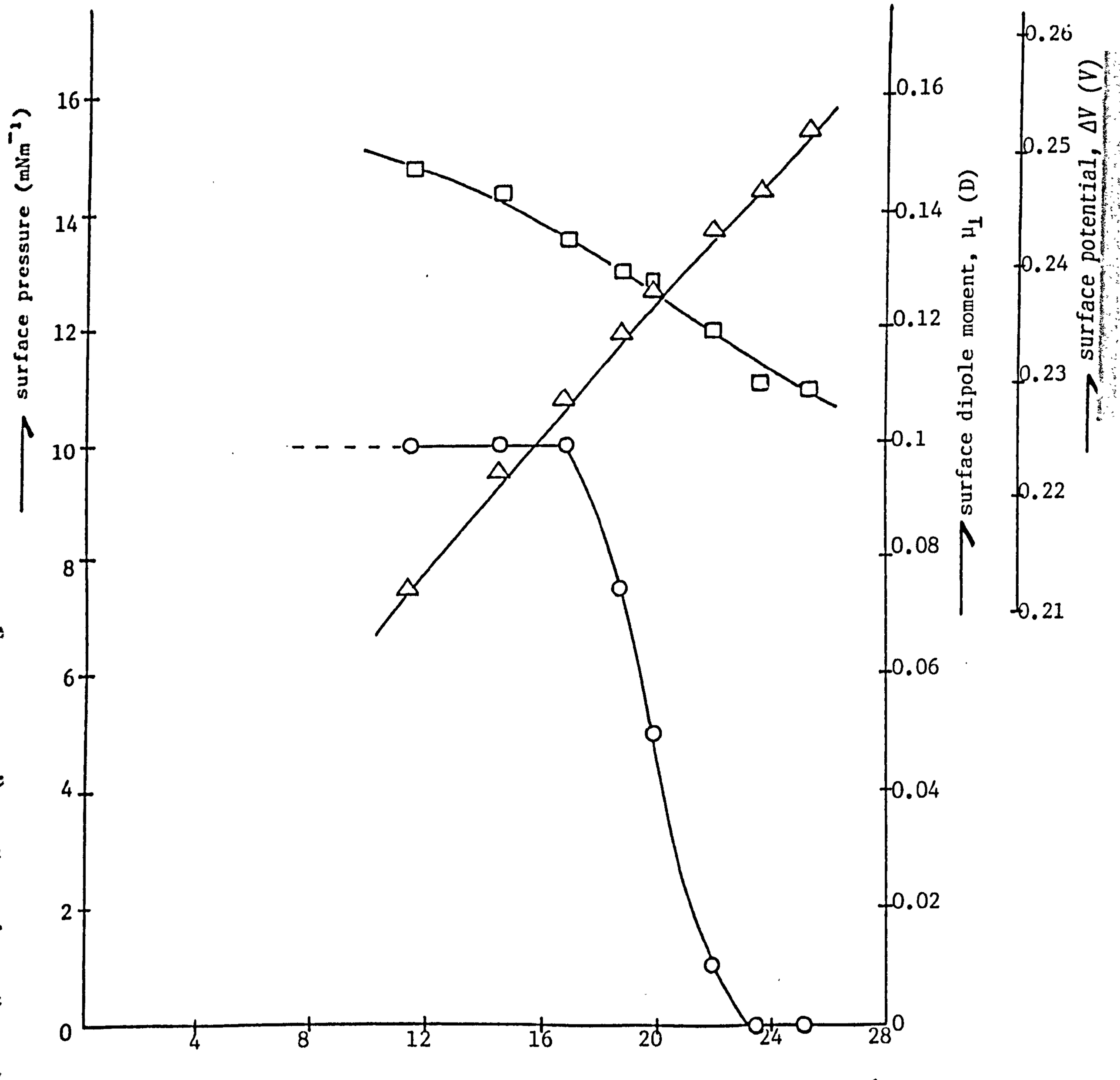

FIGURE 10.40: Plot showing the variation of surface pressure surface potential and surface dipole moment with the area per siloxane monomer for polydimethylsiloxane <14420>

pH 5.81 $\pm$ 0.02

T_b = 21.3 $\pm$ 0.1°C

Text cut off in original

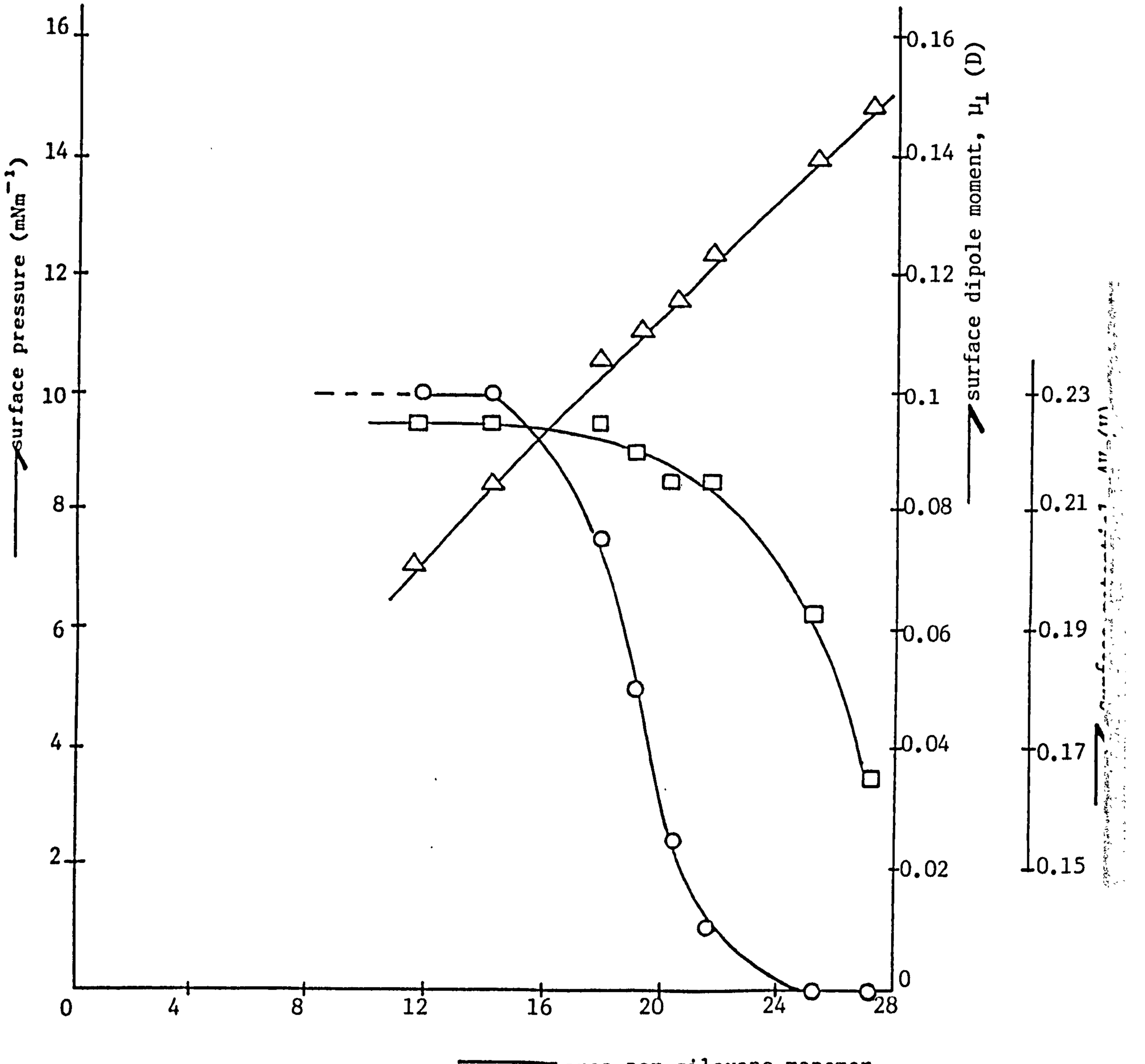

FIGURE 10.41: Plot showing the variation of surface pressure, surface potential and surface dipole moment with the area per siloxane monomer for polydimethylsiloxane <110000>

pH = 5.87 ± 0.02

T_b = 21.8 ± 0.1°C

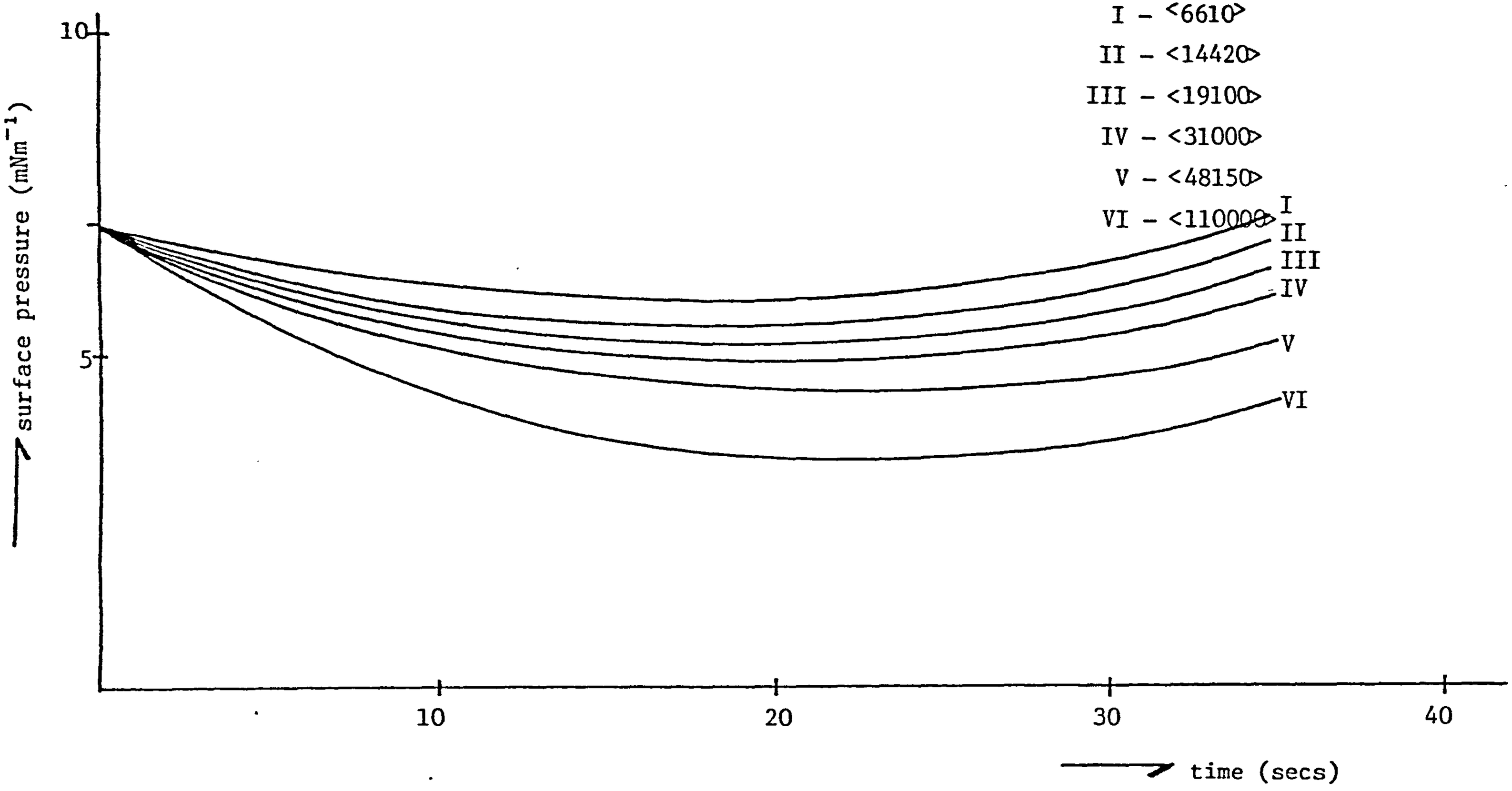

FIGURE 10.42: Traces showing the variation of the pressure inside the canal viscometer with the time taken to flow through the slit for the various polydimethylsiloxanes

molecular weight of the polydimethylsiloxane. The average film flow rates or fluxes and surface shear viscosities are listed in Table 10.24. The surface viscosity, η_s, was calculated using equation (10.2):

$$\eta_s = \frac{\pi_2}{q} \times \frac{2}{3} \times \frac{a^3}{\ell} - \frac{2a\eta_0}{\pi} \coth \frac{\pi h}{2a}$$

where all the various parameters have been defined in Chapter 7.

The surface viscosity of polydimethylsiloxane <6610> is similar to that of $C_{17}H_{35}COOH$ (stearic acid). Figure 10.43 shows a decrease in surface viscosity as the molecular weight of the polydimethylsiloxanes increases.

Relaxation Profiles

Relaxation profiles were obtained for the various polydimethylsiloxanes, whereby the PTFE barriers were held at about $10mNm^{-1}$ and the monolayers were expanded at different speeds. Similar profiles were obtained for all the polydimethylsiloxanes, and Figure 10.44 shows a typical example for polydimethylsiloxane <110000>. These profiles indicate a measure of the residual pressures at different speeds, which may be related to presence of the entanglement of molecules. The residual pressures increase with speed and also with increasing molecular weight. For example, polydimethylsiloxane <31000> shows an increase in residual pressure of about $2mNm^{-1}$, compared to $1mNm^{-1}$ for polydimethylsiloxane <19100> at a high reverse speed of 400. Hence, entanglement of molecules is more pronounced as the molecular weight increases.

The monolayer compression modulus, k_s, at different reverse speeds was calculated from equation (10.1):

$$k_s = - A\left(\frac{\partial \pi}{\partial A}\right)_{T, \pi=7.5mNm^{-1}}$$

The values of $(\partial\pi/\partial A)T$ and k_s were obtained at $\pi = 7.5mNm^{-1}$ and are given

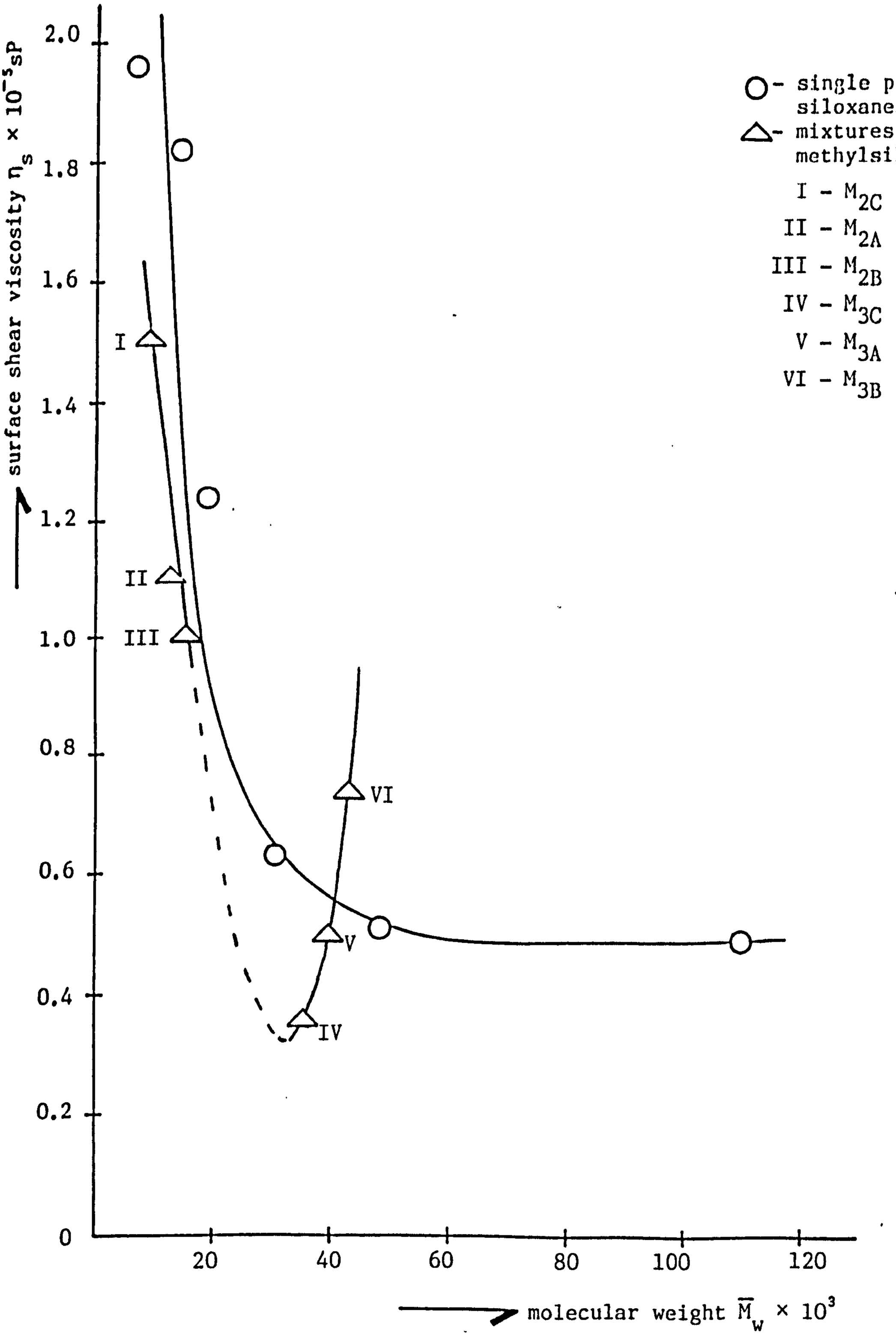

FIGURE 10.43: Plot showing the variation of the surface shear viscosity with the weight-average molecular weight for single and mixtures of polydimethylsiloxanes

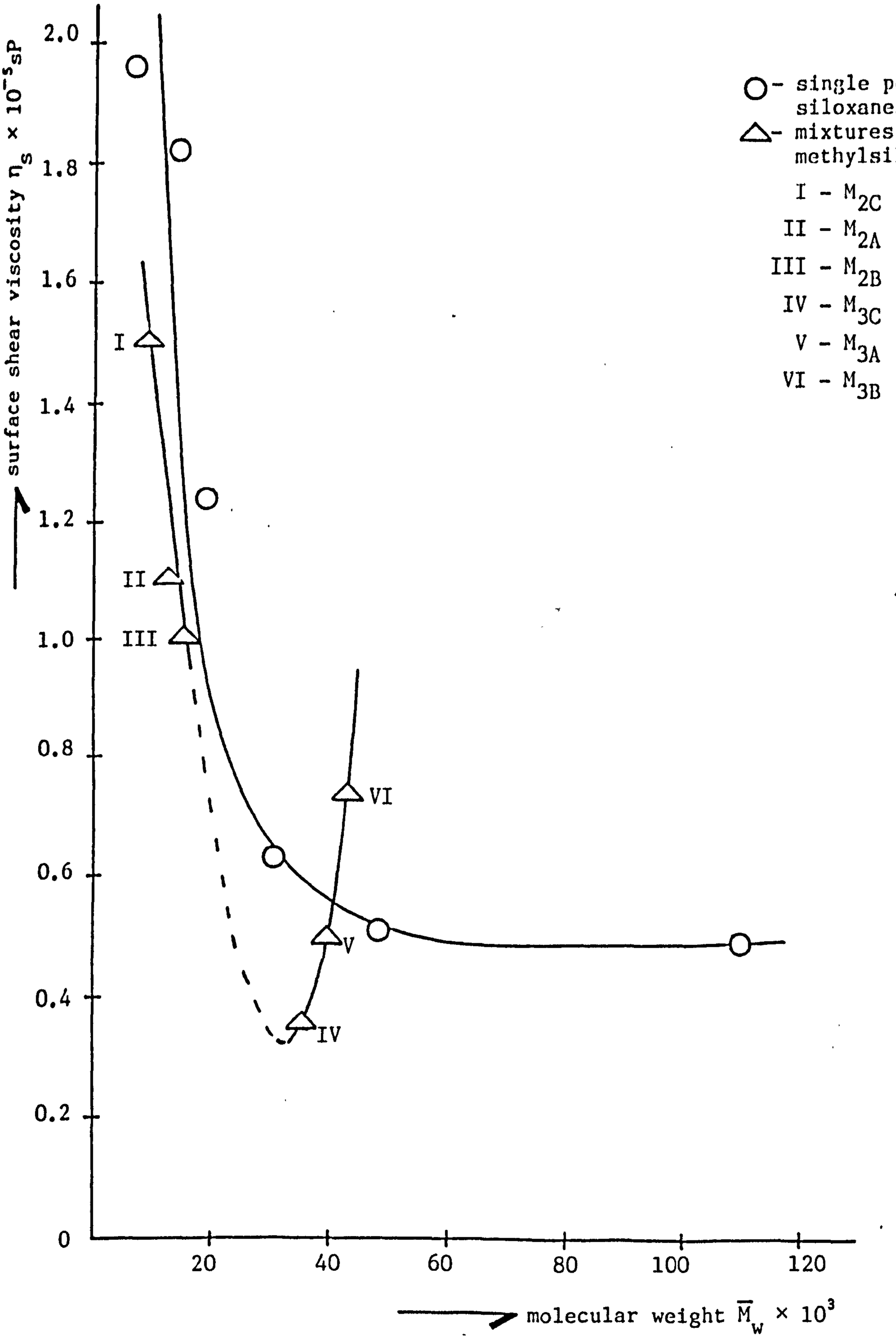

FIGURE 10.43: Plot showing the variation of the surface shear viscosity with the weight-average molecular weight for single and mixtures of polydimethylsiloxanes

Surface pressure held at $10mNm^{-1}$ for 110000

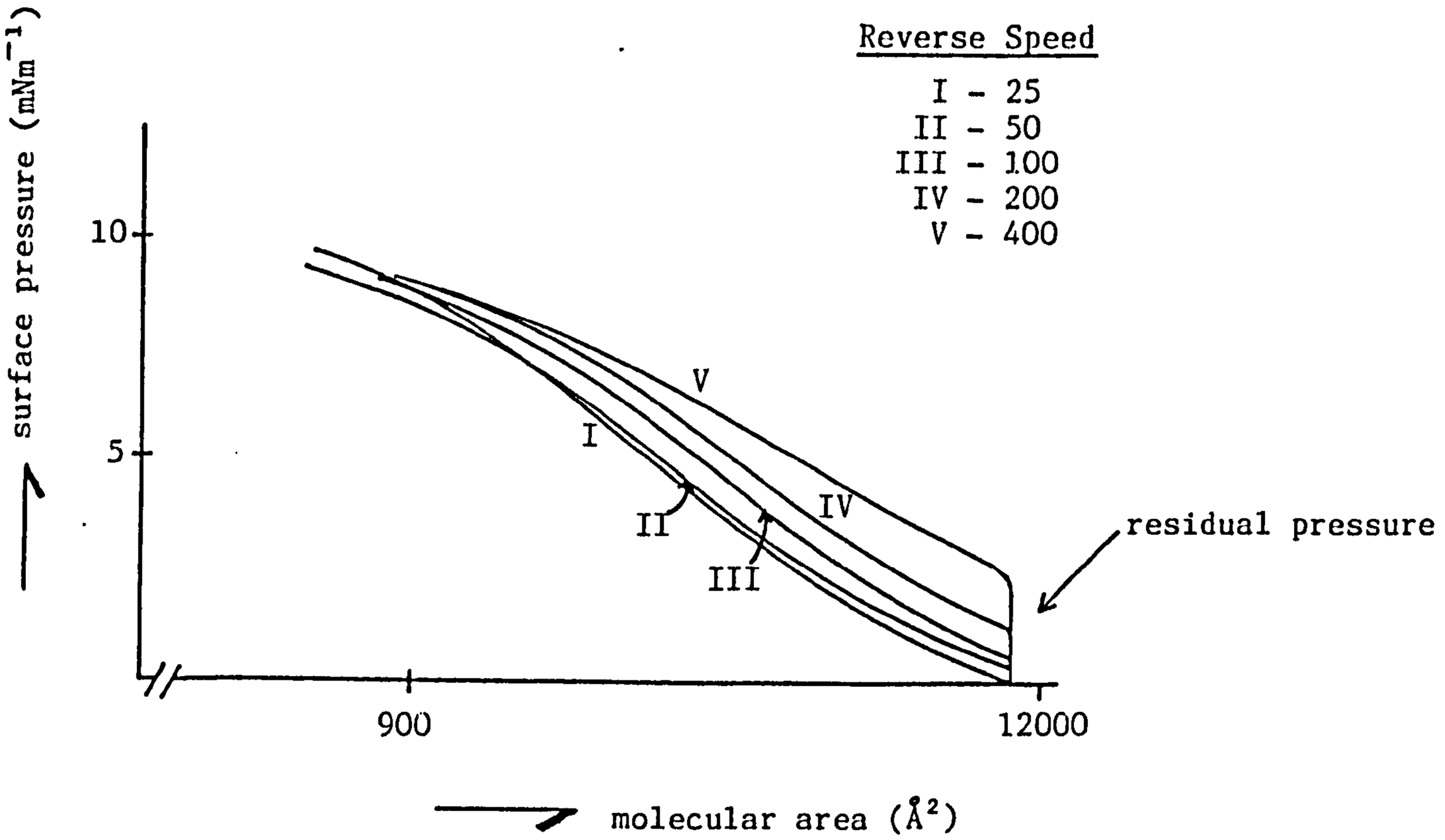

FIGURE 10.44: Surface pressure-surface area curves of polydimethylsiloxane <110000> monolayer showing the variation of the reverse speed of the barriers on the relaxation of the monolayer.

pH = 5.82 ± 0.02

T_b = 22.3 ± 0.1°C

No salt added to subphase

in Tables 10.25(i)-(v) and represented graphically in Figures 10.45 and 10.46. The compression modulus, $k_s^{7.5}$ was found to decrease as the barrier speeds increased, and also as the molecular weight of the polydimethylsiloxanes increased.

Various molar proportions of two polydimethylsiloxanes have been made up into mixtures; these, together with their calculated weight-average molecular weights[258], are listed in Table 10.26. Since the two distinct compounds used had the same chemical structure, and differed only in molecular weight, Barry's correlation was again used to predict the number of repeating siloxane monomer units in the various mixtures of chain lengths. These, together with a summary of the area per molecule and related data obtained from monomolecular film measurements, are given in Table 10.27.

Isotherms similar to those of the single polydimethylsiloxanes were obtained for the variation of surface pressure with molecular area for these mixtures, and a typical curve for mixture $\langle M_{3C} \rangle$ is shown in Figure 10.47. Other mixture surface pressure-surface area isotherms showing identical characteristic features at A_1, A_2, B and C were obtained.

The area per molecule for each mixture was again calculated by extrapolating the compression curve back to zero surface pressure, and is given in Table 10.27. Figure 10.48 shows the variation of the surface pressure with the area, per siloxane monomer, of the (various molar-proportions) mixtures. The mixtures were found to give an area per siloxane monomer of between 22Å^2 and 32Å^2, highly-dependent on the molar-proportion of the individual constituents.

A comparison between the values obtained from the extrapolated

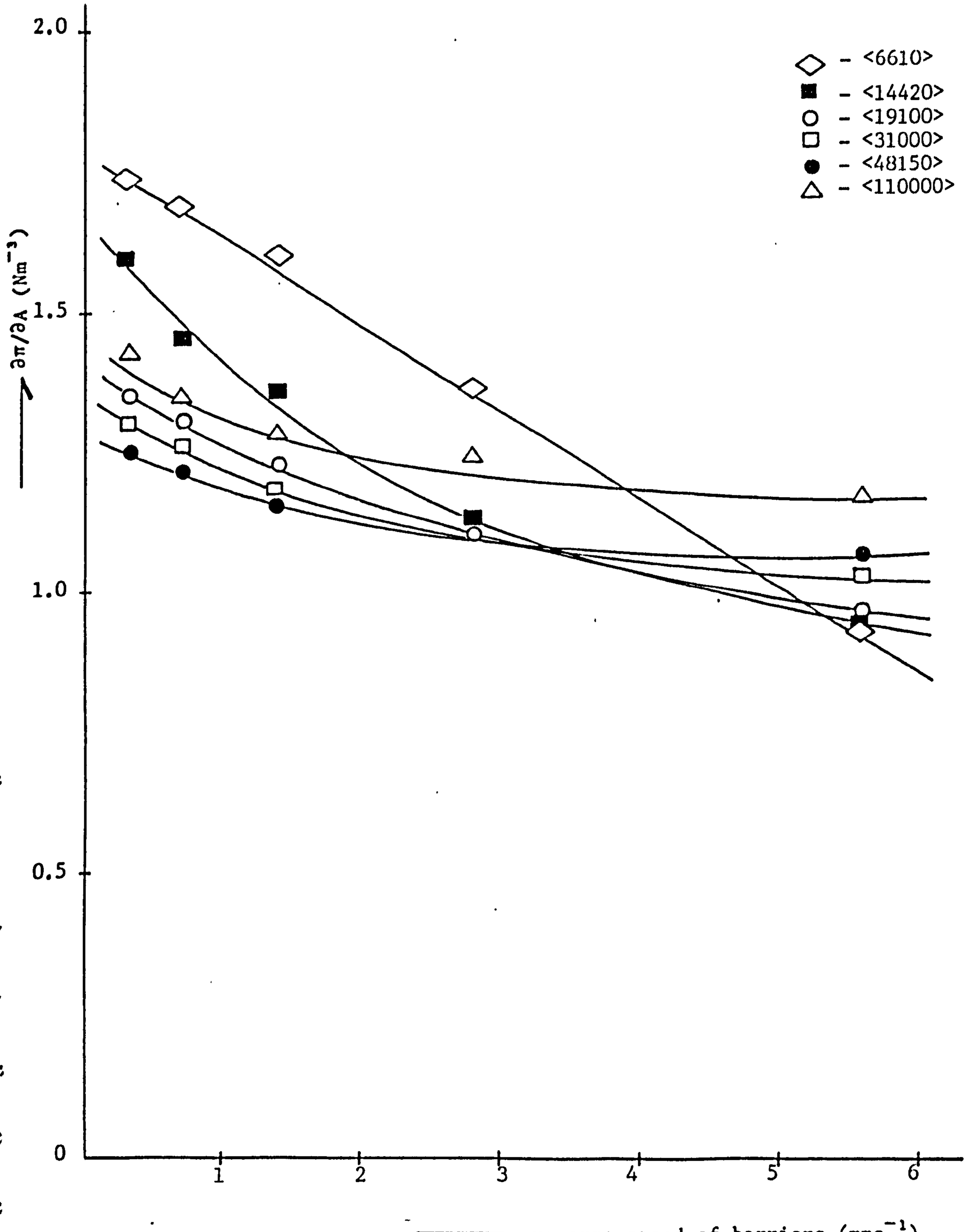

FIGURE 10.45: Plot showing the variation of $\partial\pi/\partial A$ ($\sim 7.5 mNm^{-1}$) with the reverse speeds of the PTFE barriers for the single polydimethyl-siloxanes.

Mixture	Types of Polydimethylsiloxanes	Molar Proportion	Calculated Weight-Average Molecular Weight of Mixture
M_{2A}	6610 + 19100	0.5:0.5	12855
M_{2B}	6610 + 19100	0.25:0.75	15978
M_{2C}	6610 + 19100	0.75:0.25	9733
M_{3A}	31000 + 48150	0.5:0.5	39575
M_{3B}	31000 + 48150	0.25:0.75	43863
M_{3C}	31000 + 48150	0.75:0.25	35288

TABLE 10. 26 data showing the two different polydimethylsiloxanes and their molar proportions present in the various mixtures.

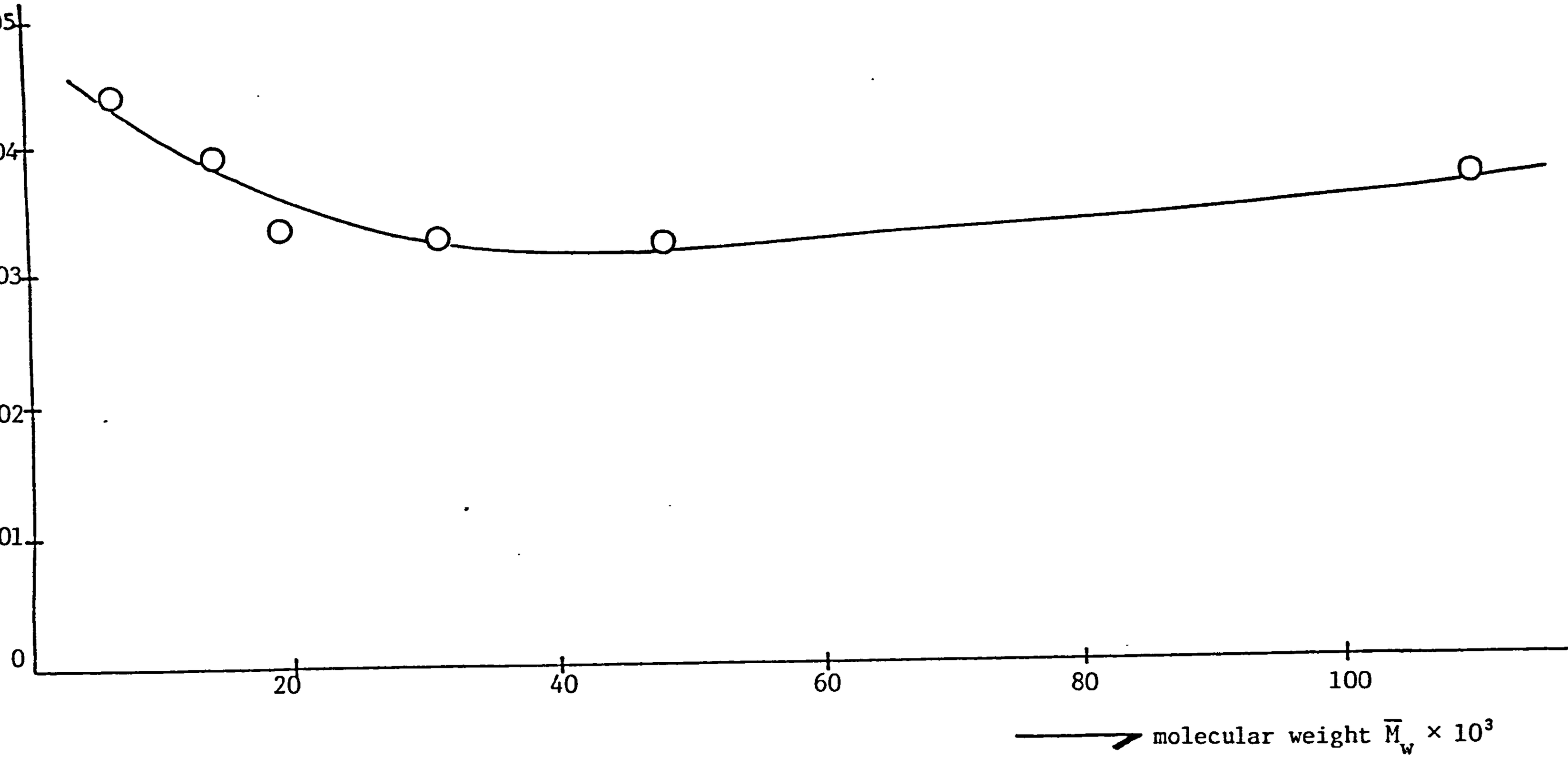

FIGURE 10.46: Plot showing the variation of compression modulus, $k_s^{7.5}$ with the weight-average molecular weight for the single polydimethylsiloxanes obtained at a reverse speed of $0.6972 mms^{-1}$.

Mixture	$\overline{M}_w$	Average Density (gcm^{-3})	No. of Molecules on Surface	Area Per Molecule, A_m at $OmNm^{-1}$ ($\leq Å^2$)	No. of Repeating Units ($\leq$ link)
M_{2C}	9733	0.934	8.32×10^{14}	3583.1	129
M_{2A}	12855	0.866	5.36×10^{14}	5568.2	171
M_{2B}	15978	0.951	4.67×10^{14}	6379.9	213
M_{3C}	35288	0.834	2.48×10^{14}	12003.6	474
M_{3A}	39575	0.827	2.08×10^{14}	14308.5	532
M_{3B}	43863	0.844	2.29×10^{14}	13012.9	590

TABLE 10.27: Surface pressure-surface area and related data from monomolecular film measurements on the Joyce-Loebl trough of various molar proportion mixtures of polydimethylsiloxane monolayers on a pure water subphase.

pH = 4.81 ± 0.02

Temperature of bath, $T_b = 21.3 \pm 0.1^{o}C$

Compression-expansion rate = $9.6 Å^2 min^{-1}$

Mixture $\langle M_{3C} \rangle$ contains a 0.75:0.25 molar proportion of polydimethylsiloxanes <31000> and <48150> respectively

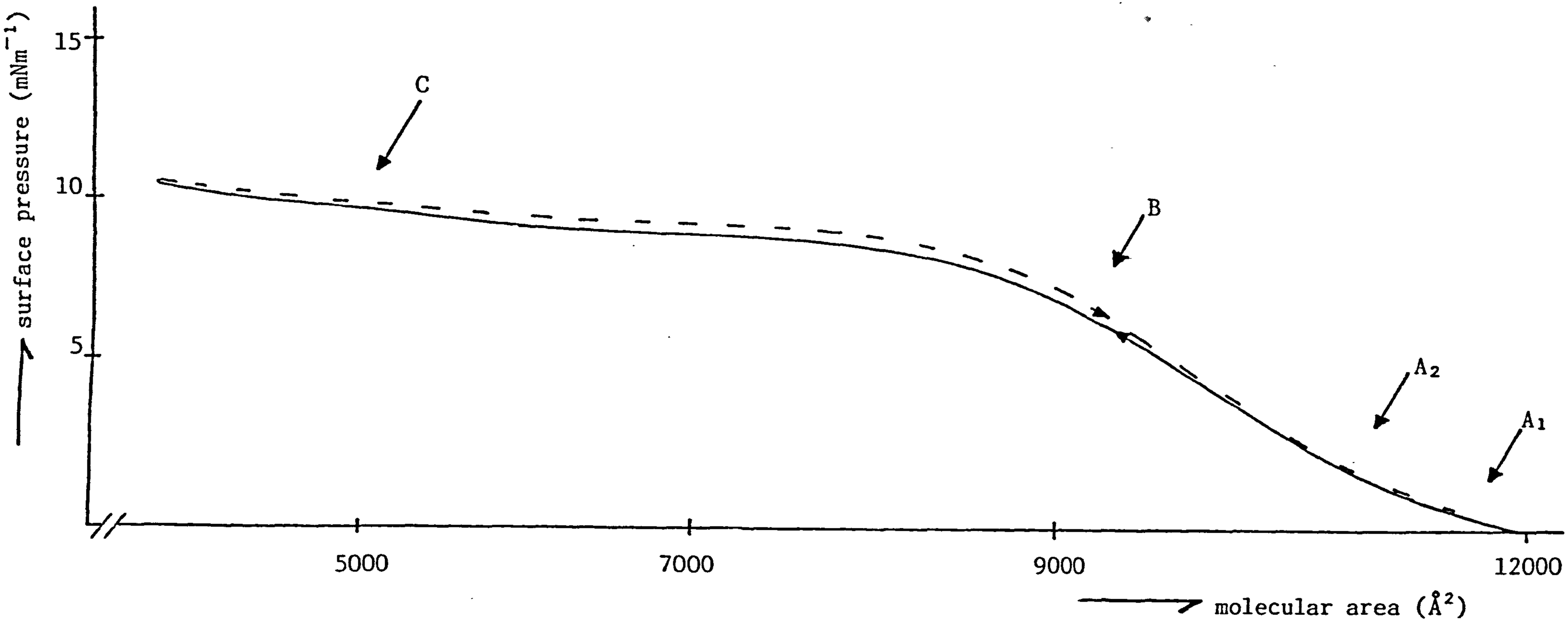

FIGURE 10.47: Plot showing the surface pressure-surface area isotherm of mixture $\langle M_{3C} \rangle$ monolayer on a pure water subphase.

pH = 5.50 ± 0.02

T_b = 21.2 ± 0.1°C

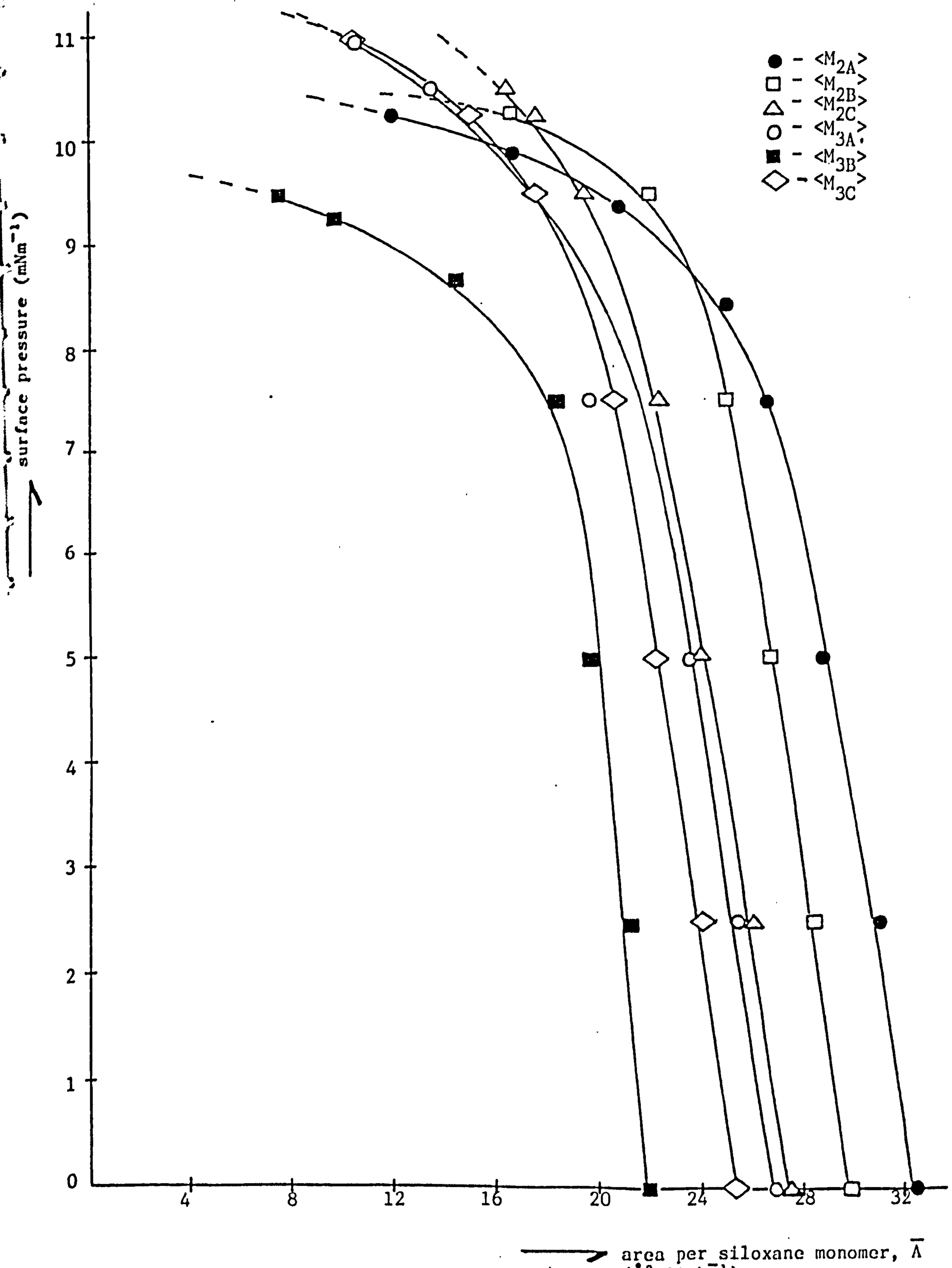

FIGURE 10.48: Plot showing the surface pressure with area per siloxane monomer for the various molar proportion mixtures of polydimethylsiloxanes on a pure water subphase.

pH = 4.8 ± 0.02; T_b = 21.3 ± 0.1°C

and predicted (i.e. from the relationship: area per molecule $\tilde{A}_m$ = 0.313 × molecular weight, $\bar{M}_w$) area per molecule is given in Table 10.28. There is close parity between the values.

The monolayer compression modulus, k_s, at $\pi \sim 7.5 mNm^{-1}$ was calculated and is given in Table 10.29. Linear increases in compression moduli as the molecular weight increased were found. Figure 10.49 illustrates the relationship.

Surface viscosity has once again been studied to provide valuable information about the intermolecular interactions and two-dimensional phase transformations in monolayers by flow. The average film flow rates or fluxes and the surface shear viscosities of the various molar-proportion mixtures of polydimethylsiloxane monolayers are listed in Table 10.30. Figure 10.43 shows the plot of these values, indicating that an increase in molecular weight is accompanied by an increase in flux, and hence a decrease in surface viscosity.

Table 10.31 gives the data on the areas of particular polydimethylsiloxane monolayers that have been compressed and held at a constant surface pressure of $7.5 mNm^{-1}$. After a period of about 2 hours, no appreciable change in area was found, although the measuring system was sensitive to area changes of $0.01 cm^2$, as shown in Figure 10.50. During this period, the film areas corresponded to values of area per molecule typical of the values obtained for the polydimethylsiloxanes in conventional pressure-area measurements.

10.3.2 Discussion

The first research work on surface films of polydimethylsiloxanes at the water/air interface was made in 1947 by Fox *et al*[11]. Further work on the reactions of polyorganosiloxane monolayers with aqueous

Mixture	$\overline{M}_w$	Extrapolated Value ($\leq$ Å^2)	Predicted Value ($\leq$ Å^2)
M_{2C}	9733	3583.1	3046.3
M_{2A}	12855	5568.2	4023.6
M_{2B}	15978	6379.9	5000.9
M_{3C}	35288	12003.6	11044.9
M_{3A}	39575	14308.5	12386.9
M_{3B}	43863	13012.9	13728.9

TABLE 10.28: Data obtained of the extrapolated and predicted (from $\tilde{A}_m = 0.313 \times MW$ relationship) values of the area per molecule at $0 mNm^{-1}$ for the various molar-proportion mixtures of polydimethylsiloxane monolayers

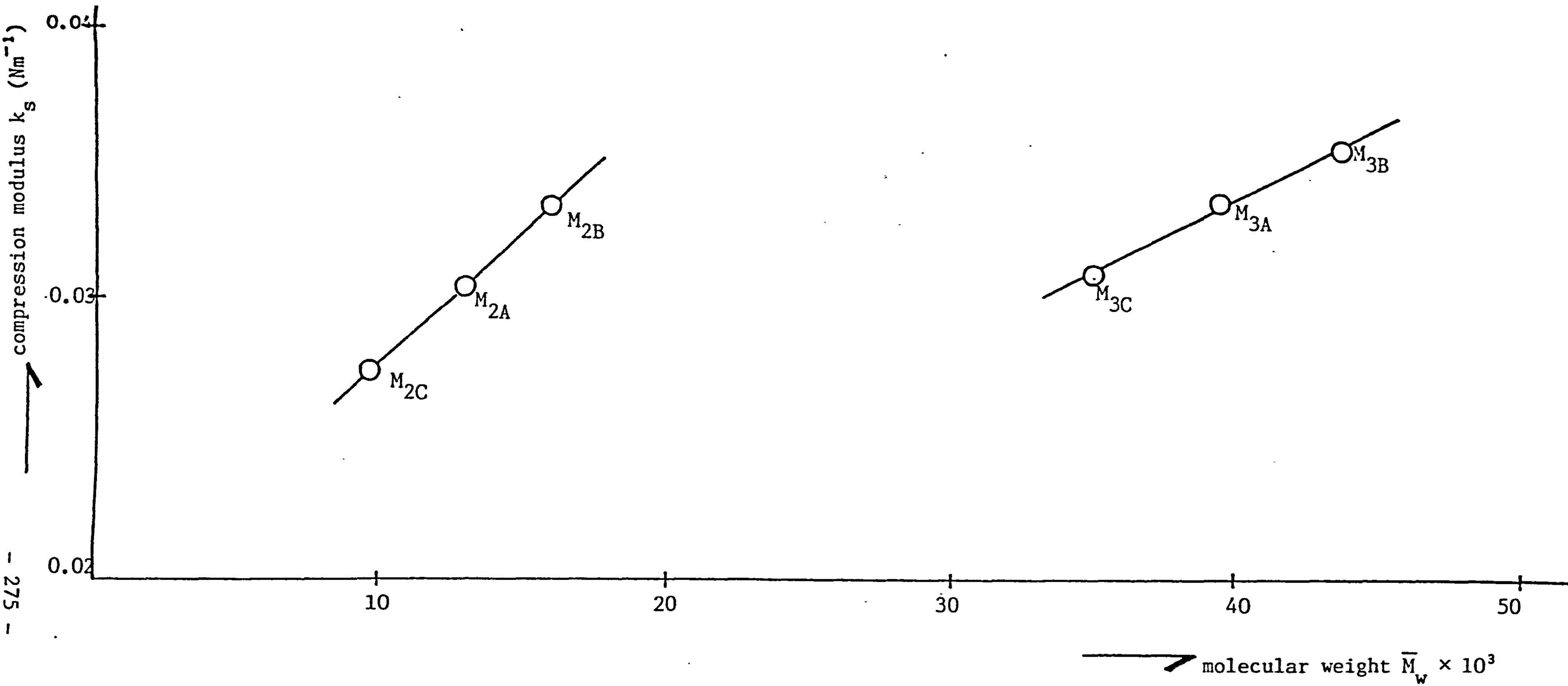

FIGURE 10.49: Plot showing the variation of compression modulus, $k_s^{7.5}$ with the weight-average molecular weight for different mixtures of polydimethylsiloxanes at a reverse speed of $0.6972 mms^{-1}$

$\overline{M}_w$	No. of Molecules on Surface Initially	Area Drop (cm^2)	No. of Molecules on Surface Finally	% Loss	No. of Molecules Remaining in Time Period (mols sec^{-1})
6610	2.07×10^{15}	21.75	1.76×10^{11}	0.0085	2.47×10^{7}
31000	3.25×10^{14}	0.0656	8.37×10^{10}	0.026	1.16×10^{7}
110000	8.85×10^{13}	10.22	3.52×10^{12}	3.98	4.89×10^{8}
M_{2C} (9733)	8.32×10^{14}	-	8.32×10^{14}	-	1.16×10^{11}
M_{3C} (35288)	2.48×10^{14}	-	2.48×10^{14}	-	3.45×10^{10}
M_{3B} (43863)	2.29×10^{14}	6.163	5.39×10^{12}	2.35	7.49×10^{8}

TABLE 10.31: Data obtained from the Joyce-Loebl trough of the area drop and number of molecules lost (due to solution) for single and mixtures of polydimethylsiloxane monolayers when the pressure is held constant at $7.5 mNm^{-1}$ for about 2 hours.

Subphase = pure water

Temperature = $21.8 \pm 0.1^{o}C$

pH = 4.20 ± 0.02

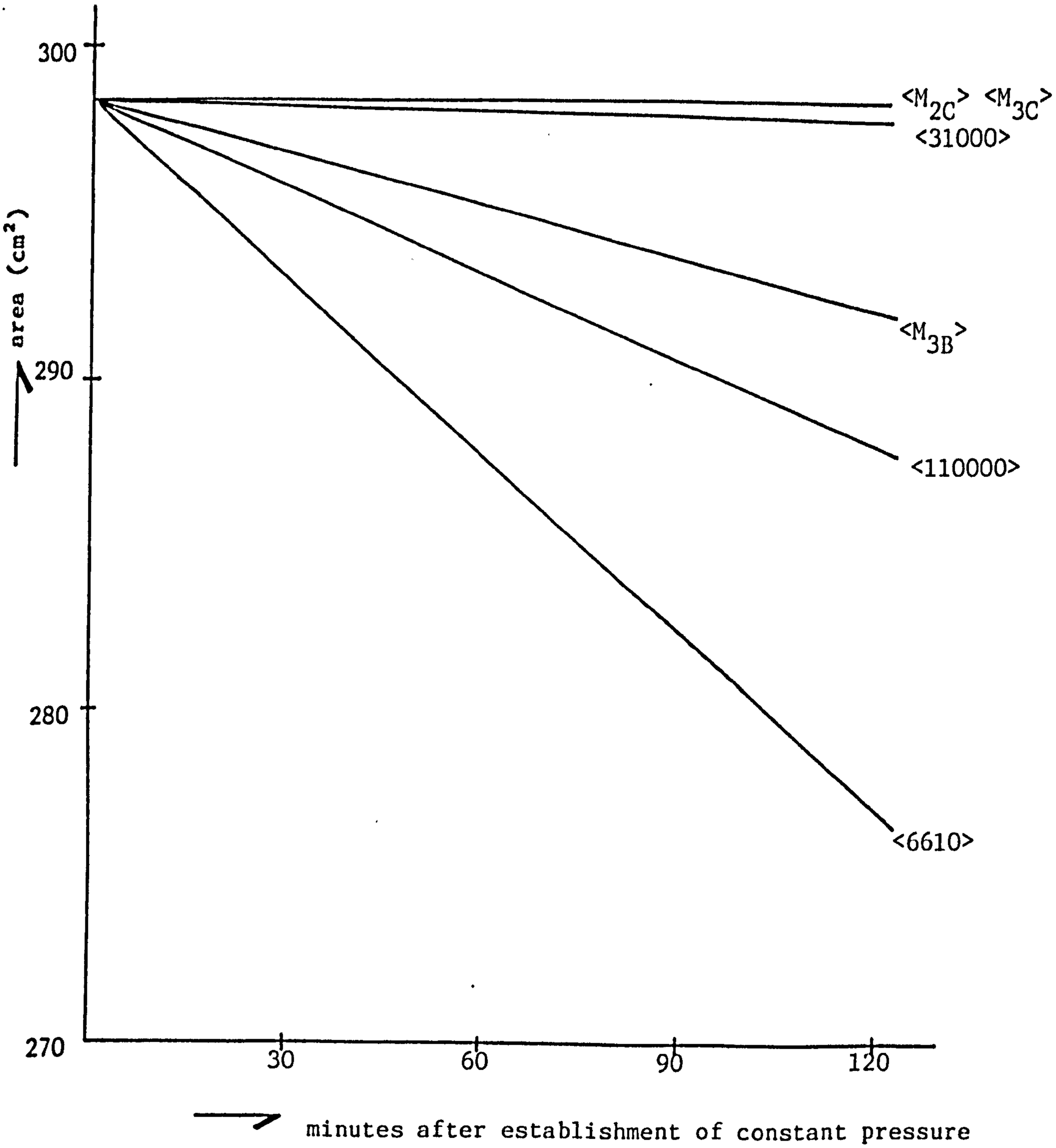

FIGURE 10.50: Plot showing the change of area with time for single and mixtures of polydimethylsiloxane monolayers on a pure water subphase and held at a constant surface pressure of $7.5 mNm^{-1}$

$T_b = 21.8 \pm 0.1^{o}C$

$pH = 4.20 \pm 0.02$

subphases have also been done by Fox *et al*[260] and by Newing[261]. Recently, films of polydimethylsiloxanes have been studied on organic subphases[2,15,16,135]. The basis of this work was also in the pressure-area diagrams, though these have been recorded with a modern, continuously-recording film balance instead of the 'old' point-by-point method. Its essential characteristic was that it worked fully automatically and recorded continuously, so that even fine details of the isotherms could be shown with great reliability.

The isotherms obtained for all linear polydimethylsiloxanes were typical of Figure 10.35, and were very similar to those obtained by the earliest researchers[2,15,16,135,136,260,261] and recently by Noll *et al*[12] The researchers' interpretation of the structure of the monolayer agreed favourably with that of Noll *et al*, but differed in some major points from those of Fox *et al*[11]; e.g. that for all areas greater than B, the 'siloxane' chains lie in a caterpillar-like form on the water surface in such a manner that each Si-O-Si bond is orientated towards the water, while the methyl groups are crowded together and orientated towards the gas phase. The orientation of the 'siloxane' chain towards the water is due to the interaction forces between the 'siloxane' bond and the water molecules, which may be assumed to be dipole forces or hydrogen bridges, as in Figure 10.51[12]. An arrangement like this may result in two possibilities: either the lateral methyl groups may lie in the same plane as the oxygen atoms of the 'siloxane' linkage, resulting in a configuration corresponding to a pyroxene chain in which the oxygen atoms not linking silicon atoms are replaced by methyl groups; or that these methyl groups are lifted out of the common plane with the oxygen atoms, with weak deformation of the valency angle Si-O-Si, so that they lie in one plane with the Si atoms of the 'siloxane' chain. The interpretation

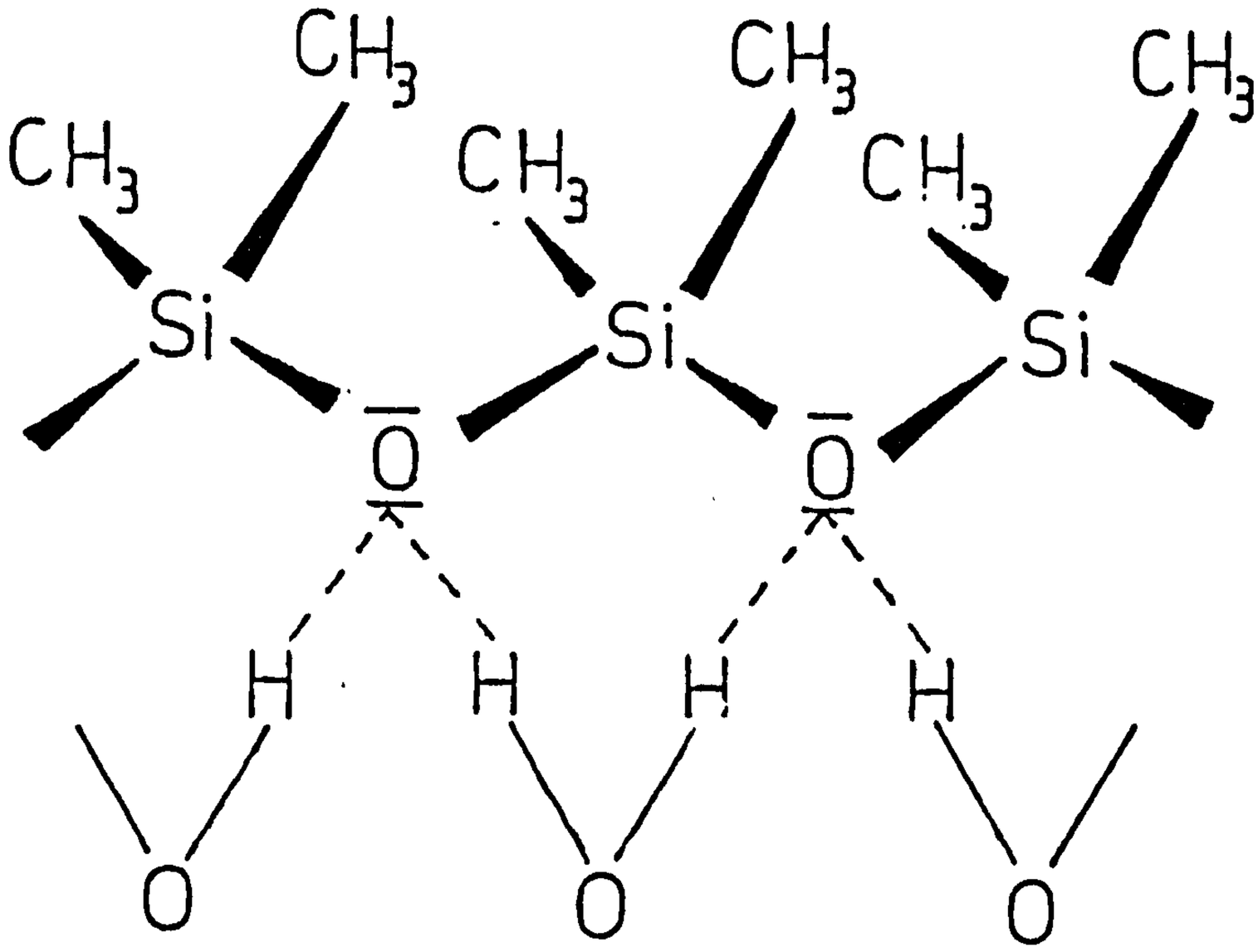

FIGURE 10.51[12]: Orientation of the dimethylsiloxane on the water surface under the influence of hydrogen bridge linkages

made by measuring the specific area of 'siloxane' units in a Stuart ball model in all conceivable conformations and packings suggested that the arrangement was one of a spreading chain that occurs when the polydimethylsiloxanes are spread on water. The spreading chain is also more probable than the pyroxene chain because the hydrophobic methyl groups are removed from the water surface more than in the pyroxene chain.

It must be emphasized that the conformation of the spreading chain is only established at the water/air interface. The physicochemical properties of the polydimethylsiloxanes support the assumption that in a polydimethylsiloxane fluid the molecules are coiled to form helices in which the 'siloxane' bonds are orientated towards the axis of the helix, while the methyl groups are orientated towards the outside. When they are placed on the water surface, this structure thus changes - i.e. the helix opens to form an extended chain.

Returning to figure 10.35, in the range of a larger area $A \gg A_1$, the polydimethylsiloxane molecules move on the water surface with a long free path. As the film is compressed, the mean free path between the molecules is reduced. When point A_1 has been reached, the surface film can be interpreted as a hydrate of the 'siloxane', i.e. the ratio of water/polydimethylsiloxane molecules is sufficient to give a sequence of water molecules between polysiloxane chains. Apart from this, there will be water molecules in the wedges between the methyl groups. On further compression to point A_2, the water molecules between the polydimethylsiloxane molecules are now orientated outwards so that the methyl groups approach each other until they make contact. Only the water molecules bound in the wedges between the methyl groups are maintained in the surface film.

With further compression, these last water molecules are expelled from the monolayer and the polydimethylsiloxane chains enmesh together. This process is connected with a certain amount of steric hindrance and repulsive forces must be overcome. This would explain why there is a pronounced pressure which is terminated after point B has been reached. It is at point B that the spreading film is water-free and gives the closest packing of polydimethylsiloxane chains, with all the 'siloxane' bonds directed towards the liquid subphase and the methyl groups towards the gas phase[12,260,261].

However, if the film is compressed beyond point B, its structure changes considerably. As closer packing than that in B is no longer possible, and whilst still maintaining contact between the polydimethylsiloxane chains and water, chain after chain is now lifted off the surface so the molecules then roll up again to form a helix. After termination of the process at stage C, the film thus consists of the closest packing of polydimethylsiloxane helices, with their axes lying parallel to the water surface. From the measurements of Noll *et al*[12], it appears that one turn of the helix comprises 6 polydimethylsiloxane units. Further compression should have resulted in the collapse of the film, but this was never attained (perhaps due to the small trough area used).

As the films were expanded again after the compression, it was found that the reversal of the process resulted in a pressure/area isotherm that at times did not in all details correspond to the compression curve. Hysteresis occurred in the point B to A_2 range, to the effect that on expansion the pressures corresponding to a given area were larger than in the case of compression (see Figure 10.35). The hysteresis may be attributed to the fact that the disentanglement of the molecules from the most closely packed arrangement according to point B only took place while

overcoming steric hindrance and the process thus moves ahead of the area during expansion.

Polydimethylsiloxanes on Acids

The effect of acid addition to the aqueous phase on the pressure/area isotherm was explained by Noll *et al*[12] by assuming that within a short period of contact between the polydimethylsiloxane film and the water, the chains of the spreading film are hydrated via hydrogen bonds with the degree of hydration increasing with the proton concentration. However, it may not be excluded that in a highly acidic medium, especially if the period of contact is extended, the 'siloxane' bonds are split to form silanol groups[11]. Fox *et al*[260] deduced that every Si-O bond is in contact with an ideal hydrolysing medium at close packing, and that it is reasonable to visualize the mechanism as involving a rupture of the Si-O linkage with the formation of two terminal -OH groups which re-condense only infrequently, thus:

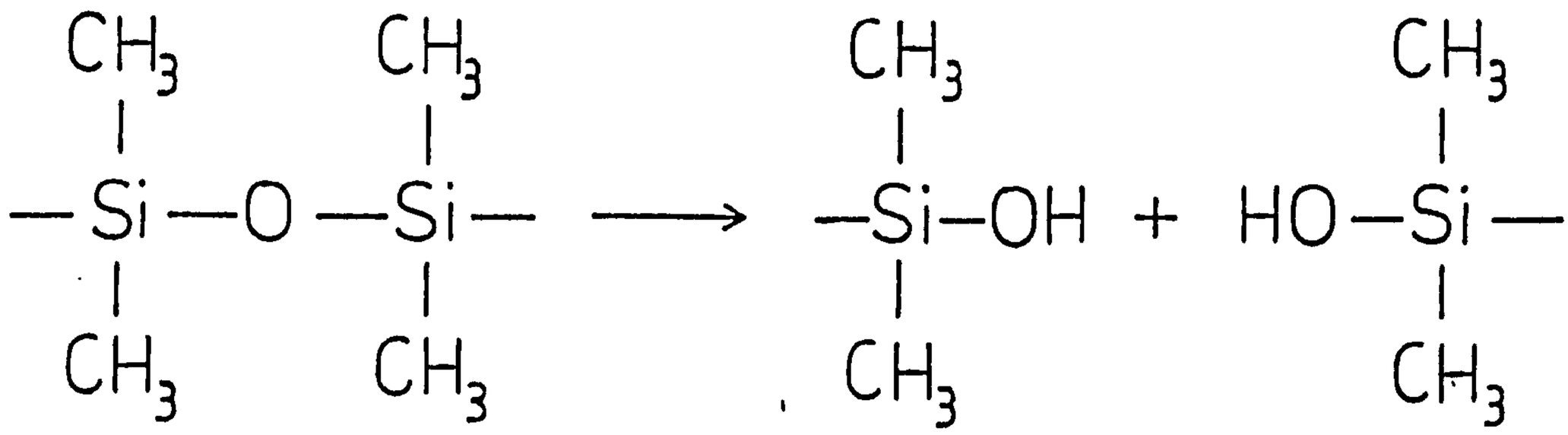

Addition of Sodium Ions to the Subphase

The addition of sodium ions to the subphase resulted in the increase in the limiting area of the various polydimethylsiloxanes. This may suggest that the sodium ions are trapped in the network or they might actually bind the network together, thus expanding the area per molecule. An alternative explanation might be due to double-layer repulsion.

Surface Potential-Surface Dipole Moment

There was apparently no distinct change in the interface potential, ΔV for any of the three polydimethylsiloxanes used. A consistent value of about 220mV was obtained for all three, which compares favourably with values obtained by Fox *et al*[11,260] for polyorganosiloxanes.

Examination of the similar pressure/area, potential/area and the dipole moment/area curves indicates that the maximum value of the dipole moment $\mu_\perp$ corresponds to the area of closest packing of the flat 'caterpillar-shaped' molecules. When the molecules begin to be confined by increasing pressure, each molecule must straighten out into a rod-like shape, so orientated that every oxygen atom is in the water, while the silicon atoms are arranged immediately above in a slight zig-zag alternately on either side of a vertical plane passed through the line formed by the oxygen atoms. This arrangement evidently results in the maximum vertical moment at close packing. Increase in pressure can result only in disorganisation of the dipoles by causing the chains to buckle out of the interface with accompanying decrease in moment.

Surface Viscosity

Monomolecular films of many polymeric materials adsorbed at the water/air interface are known to have high surface viscosities, even at film pressures as low as 1 or $2mNm^{-1}$ [262,263,268]. This is particularly true for protein monolayers, which often become plastic or viscoelastic as the film pressure increases[60,264,265,266,267]. The high surface viscosity or viscoelasticity of these films has been attributed to the strong intermolecular cohesive forces, such as hydrogen bonding, that occur between adjacent molecules in the film. The surface viscosity of even the highest molecular weight polydimethylsiloxane monolayer was extremely low when compared with monolayers of other polymeric materials

that have been studied at the water/air interface.

However, surface viscosity values of about 10^{-5} surface poise are remarkably low for a long-chain polymeric material, particularly one having a molecular weight as high as 110,000. This must reflect on the low intermolecular cohésion that exists between adjacent chains in polydimethylsiloxane films, compared with monolayers of proteins and certain linear synthetic organic polymers[269]. It may therefore be concluded that the ability of polydimethylsiloxane polymers to act as defoaming and antifoaming agents is related to their unusually low surface viscosities and their ability to displace the less strongly adsorbed foam-stabilizing materials.

Jarvis[20] used the formula below to calculate the surface shear viscosity of polydimethylsiloxane monolayers using a canal viscometer:

$$\eta_s = \frac{(F_1 - F_2)a^3}{12\ell Q} - \frac{a\eta_0}{\pi} \qquad (10.14)$$

where F_1 and F_2 are the pressures registered by the film on both sides of the canal, a is the width in centimetres, Q is the flux of the film through the canal in 1 second, ℓ is the length of canal, and η_0 is the bulk viscosity of the aqueous subphase.

Taking an example from his results, where the canal width, a = 0.190cm, and a flow rate or flux, Q = $0.248 cm^2 sec^{-1}$, he obtained a surface viscosity of 2.0×10^{-5}sP with his correction factor (i.e. the second term in equation (10.14)) being larger than the corrected surface viscosity. However, using equation (10.2) with the proper approximation and correction factor, a value of $\eta_s = 1 \times 10^{-4}$ sP is obtained for this example, and this would have been detected by the low sensitivity canal viscometer used by Jarvis. This indicates that the correction factor used by Jarvis is incorrect.

The decrease in the compression modulus with increasing molecular weight of the polydimethylsiloxane polymer at various reverse barrier speeds reveals some information on the intermolecular arrangement of the polymers. It appears that some entanglement of molecules exists at the higher reverse barrier speeds. The polydimethylsiloxane chains appear to slip over one another with the larger polymers exhibiting a larger degree of compressibility.

Mixed Monolayers

Insoluble monolayer mixtures of two polydimethylsiloxane polymers were prepared and then spread from a mixed solution in a spreading solvent (re-distilled n-hexane), with the monolayer of both polydimethylsiloxanes having already been investigated. If the two polydimethylsiloxanes had been immiscible in the surface film, spreading of the mixed solution would have produced patches of one monolayer distributed in the monolayer of the other. Figure 10.52[270] illustrates schematically the behaviour which might be expected from the spreading of a 'mixed' monolayer. Such a distribution is unstable with respect to larger aggregates in the monolayer, but no studies appear to have been made on the tendency to such two-dimensional aggregation.

The properties of a monolayer in which the two components are immiscible will normally reflect those of the two separate single component films. Hence, the area occupied by the combined film will be the sum of the areas of the separate films. Monolayers in which the components are immiscible will obey an equation such as:

$$A_{12} = N_1A_1 + N_2A_2 \qquad (10.15)$$

where A_{12} is the average molecular area in the two-component film, N_1 and N_2 are the mole fractions of the components, and A_1 and A_2 are the

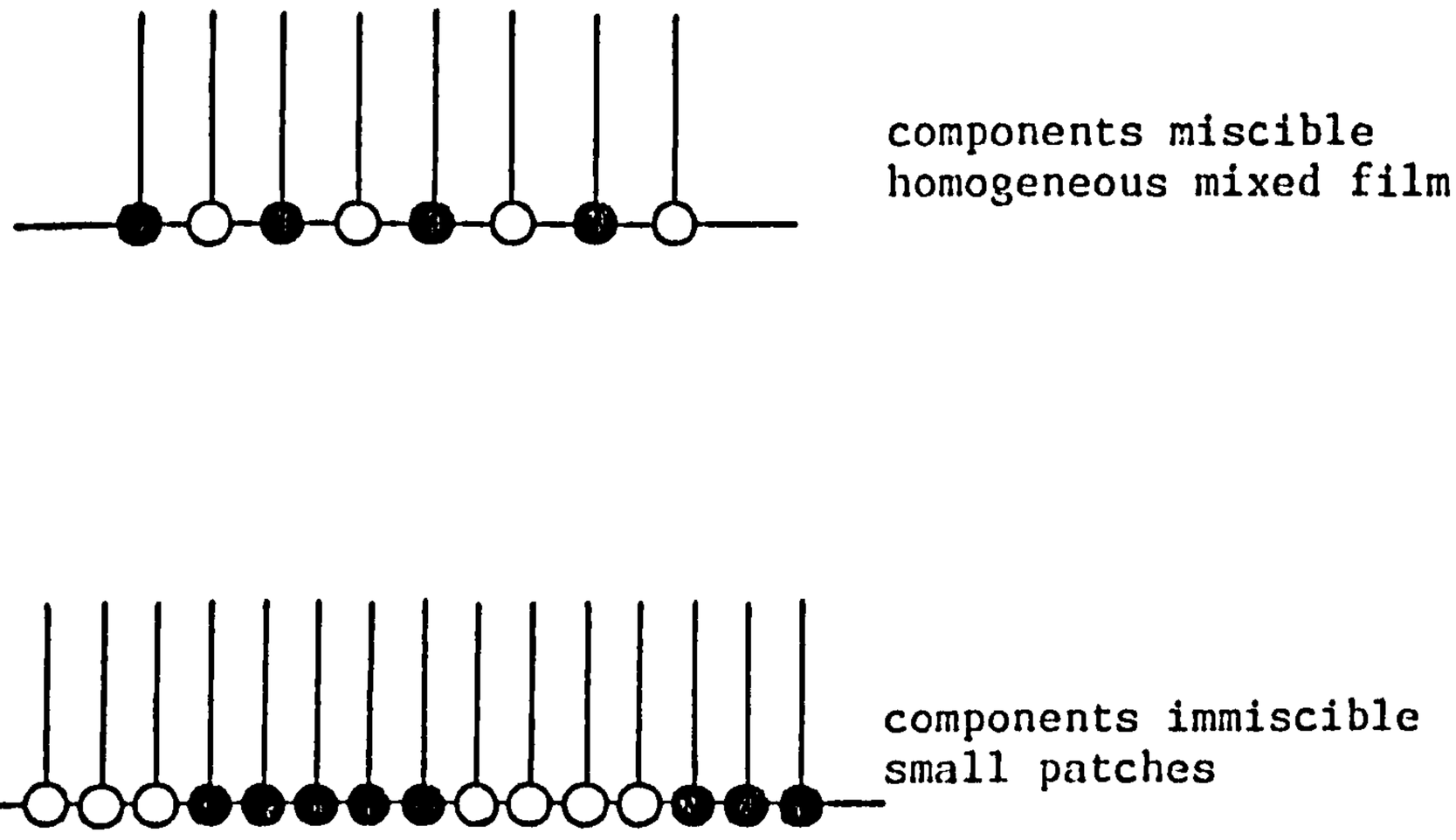

FIGURE 10.52[270]: Possible molecular distributions which may result from the spreading of a 'mixed' monolayer

molecular areas in the two single-component films at the same surface pressure.

With surface viscosity measurements, it is fluidity, $\phi^s = 1/\eta_s$, which is averaged[22] so that

$$\phi^s_{12} = N_1\phi^s_1 + N_2\phi^s_2 \qquad (10.16)$$

(It must be noted that these equations assume every molecule is in an identical environment with that which it would have in its own pure monolayer and therefore neglects the few molecules present at the boundaries between patches. As long as the patches contain more than 10^5 molecules, that is more than about 10^{-4}mm in diameter, the number of molecules situated there will be less than 1% of the total.)

Any deviation of mixed monolayer behaviour from equations (10.15) and (10.16) provides evidence for miscibility in the film. Goodrich[271] has also carried out a thermodynamic analysis of a system, in which the system is truly 'mixed'.

For the various mixtures of polydimethylsiloxanes listed in Table 10.26, the equations (10.15) and (10.16) have been applied to see if there was any evidence of miscibility and the results are given in Tables 10.32-10.34. From the various data, it is evident that the mixtures do not agree with the ideal mixing equations and are probably non-ideal mixtures. It has been assumed that the various mixtures of polydimethylsiloxanes studied formed miscible monolayers.

The surface pressure/surface area isotherms of mixtures of polydimethylsiloxane monolayers have very similar characteristic features typical of the single polydimethylsiloxane monolayers. This may suggest a similarity in the behaviour of the molecular chains with an increase in the repeating 'siloxane' units being accompanied by an increase in the

Mixture	Components	Molar Proportion	$\bar{A}_m$ Obtained From π-A Curve ($Å^2$)	$\bar{A}_m$ Calculated Using Equation (10.15) ($Å^2$)
M_{2C}	6610+19100	0.75:0.25	9732.5	2346.9
M_{2A}	6610+19100	0.5:0.5	5568.2	3253.9
M_{2B}	6610+19100	0.25:0.75	6379.9	4160.8
M_{3C}	31000+48150	0.75:0.25	12003.6	8922.4
M_{3A}	31000+48150	0.5:0.5	14308.5	10003.8
M_{3B}	31000+48150	0.25:0.75	13012.9	11085.2

TABLE 10.32: Data obtained of the average area per molecule, A_m, for the various mixtures of polydimethylsiloxane monolayers all measured at a surface pressure of $OmNm^{-1}$

Mixture	A_m Obtained From π-A Curve ($Å^2$)	Average A_m Calculated Using Equation (10.15) ($Å^2$)
M_{2C}	4128.3	2180.7
M_{2A}	4933.4	2995.5
M_{2B}	5719.1	3810.3
M_{3C}	10567.9	7945.2
M_{3A}	12337.8	8858.2
M_{3B}	11794.0	9771.1

TABLE 10.33: Data obtained of the average area per molecule, A_m, for the various mixtures of polydimethylsiloxane monolayers all measured at a surface pressure of $5mNm^{-1}$

Mixture	η_s Obtained Using Equation (10.2) (sP)	Average η_s Calculated Using Equation (10.16) (sP)
M_{2C}	1.51×10^{-4}	1.006×10^{-4}
M_{2A}	1.093×10^{-4}	1.508×10^{-4}
M_{2B}	1.012×10^{-4}	1.362×10^{-4}
M_{3C}	3.688×10^{-5}	5.898×10^{-5}
M_{3A}	4.677×10^{-5}	5.634×10^{-5}
M_{3B}	7.482×10^{-5}	2.755×10^{-6}

TABLE 10.34: Data obtained of the average surface viscosity, η_s, for the various mixtures of polydimethylsiloxane monolayers all measured at a surface pressure of $6mNm^{-1}$

area per molecule. Comparisons between the extrapolated and predicted values of area per molecule (given in Table 10.28) add support to the earlier views on the behaviour of mixed monolayers. Also supportive are the data obtained for the compression modulus, k_s, at $\pi \sim 7.5 mNm^{-1}$, which are in the range of single polydimethylsiloxane monolayers with similar molecular weights. The surface viscosity data were plotted on the same graph as those for single polydimethylsiloxanes (see Figure 10.43). The plot clearly shows the surface viscosity decreasing with increasing molecular weight. However, the mixtures did give lower surface viscosity values if compared to single polydimehylsiloxanes in a similar molecular weight range.

A fairly common observation of high polymeric materials such as polydimethylsiloxanes is that the monolayer-forming material is extremely insoluble and non-volatile, that no significant amount of it dissolves or evaporates, while at the same time the presence of the interface provides a lower free energy than does the presence of an additional bulk phase. However, this behaviour is less frequently observed with simple non-polymeric species, where the driving force for spreading may often be thought of as an osmotic effect, the free energy of the system being reduced by dilution, in the interface, of subphase liquid molecules by the film-forming substance[272]. Although specific interactions such as hydration of polar functional groups or entropy differences between the bulk and monolayer states may be involved[26].

The collapse pressure is known to be the highest pressure to which a monolayer can be compressed without detectable expulsion of molecules to form a new phase, which implies that a collapse pressure must also specify the criterion of collapse. This is illustrated in Figure 10.53[270],

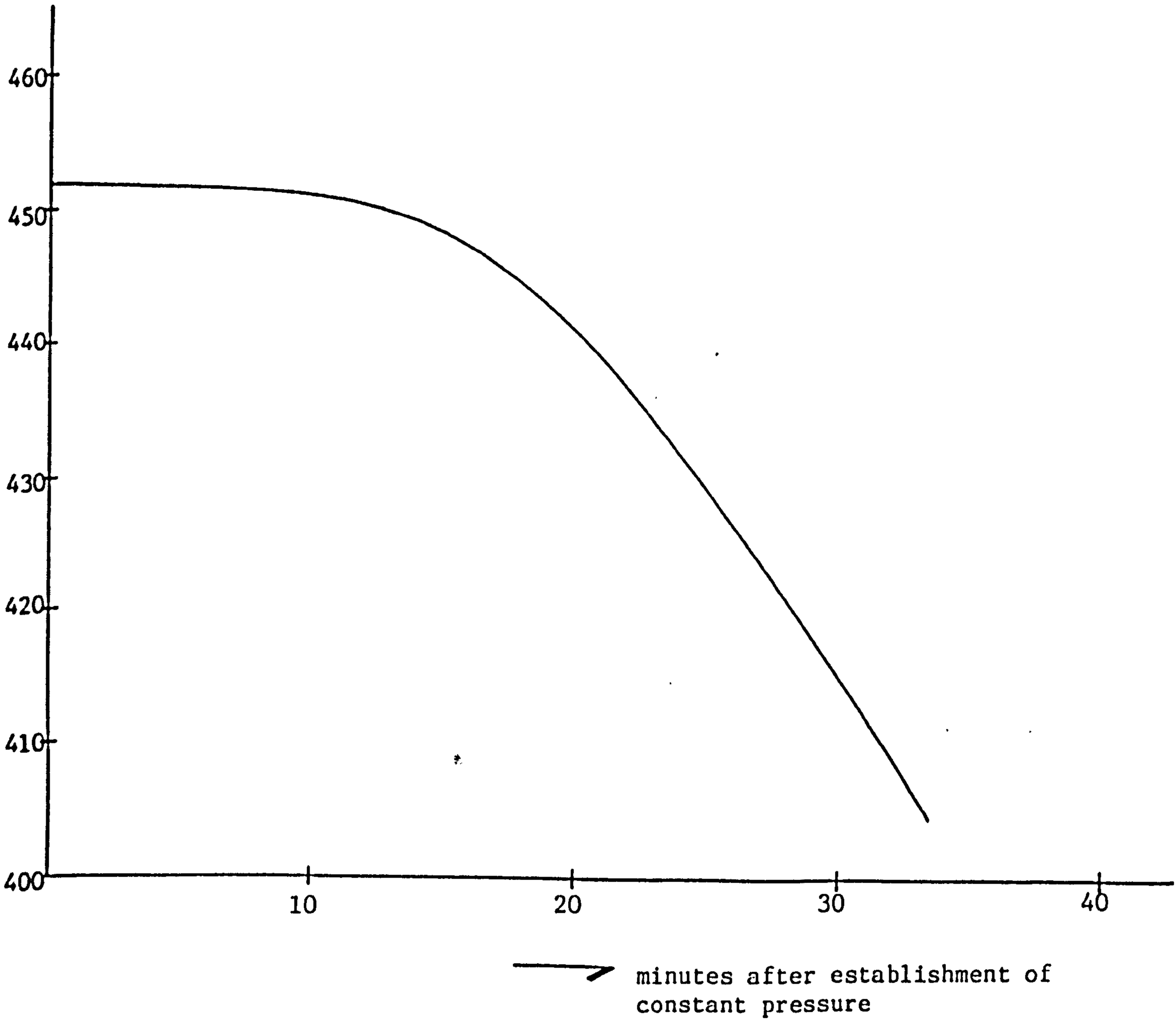

FIGURE 10.53[270]: Change of area with time for a monolayer of stearic acid on 10^{-4}M H_2SO_4 held at constant pressure of 24.8mNm^{-1} (25°C)

which shows the behaviour of the area of a particular stearic acid monolayer rapidly compressed and held at a pressure of 24.8 ($\pm$ 0.1) mNm^{-1}. If Figure 10.50, showing polydimethylsiloxane monolayers, is compared with that for stearic acid, it can be observed that generally over 2 hours the area drop of polydimethylsiloxane monolayers is very small, and yet might be due to dissolution or slow collapse. Therefore, the monolayers would be considered very stable, with the small percentage loss of molecules perhaps indicating a preference of the polydimethylsiloxane molecule to a position whereby the oxygen atoms are sitting in the plane of the surface with the silicon atoms sitting above. Otherwise, the silicon atoms would be dragged into solution.

10.3.3 Summary

Surface pressure/surface area curves were determined for polydimethylsiloxane monolayers ($\overline{M}_w \sim$ 6610-110000). The polydimethylsiloxanes investigated were those in which the molecules, when placed on the surface, were thought to be in an helical form, and then become orientated on the water surface to become 'spreading chains'. It is believed that hydrogen bridging is responsible for the orientational effect.

Pressure/area and surface potential/area isotherms have been obtained and the results interpreted in terms of the molecular packing. The vertical dipole moment per monomer has been obtained, and its significance briefly discussed.

The surface viscosities of these films were studied using a canal viscometer. The surface viscosity data were found to be extremely low, and to decrease with increasing molecular weight. The low surface viscosity ($\sim 10^{-5}$ sP) values of polydimethylsiloxanes reflect the relatively low intermolecular cohesion that exists between adjacent polydimethylsil-

oxane chains in a monolayer. This low surface viscosity may in part explain the defoaming and antifoaming ability of the polydimethylsiloxane fluids.

Surface pressure/surface area isotherms were obtained for mixed monolayers of polydimethylsiloxanes (i.e. of similar chemical structures, but differing only in the average molecular weight). The mixed monolayers were of different molar proportions, and assumed to be miscible. Surface viscosities of these mixed monolayers were determined, and these were also found to be extremely low, like the single polydimethylsiloxanes. The data obtained are of relevance in the antifoaming tests discussed later.

10.4 Oscillating Ring Measurements

10.4.1 Results

The data obtained from the SSE Mk 2 surface rheometer were analysed as described in Chapters 3 and 7. Experiments were performed with polydimethylsiloxanes of molecular weights <6610>, <31000>, <110000> and mixtures $<M_{3C}>$ (containing a 3:1 molar-proportion of <31000> and <48150>), as well as long chain fatty acids $C_{13}H_{27}COOH$, $C_{17}H_{35}COOH$, $C_{18}H_{37}COOH$, $C_{19}H_{39}COOH$ and $C_{22}H_{45}COOH$ on pure water with no added salt.

The data obtained are summarized in Tables 10.35-10.40. The storage (G_s') and loss (G'') moduli were calculated from equations (7.22) and (7.23) respectively. The moment of inertia of the ring, I_r, is related to the natural (phase) resonant frequency by the relation

$$W_o^2 = \frac{k_o}{I_r} \qquad (10.15)$$

where the pulsatance $W_o = 2\pi f_o$ (with f_o being the resonant frequency of the system) and k_o is the spring constant (112g $cm^2 s^{-2}$). The calibration pro-

cedure for the ring given in the operational manual was followed.

Plots of the dynamic surface shear viscosity, η_s', storage (G_s') and loss (G") moduli against surface pressure, π, are shown in Figures 10.54-10.58. The rise in both G_s'' and η_s' at about 20mNm^{-1} of Figure 10.54 might be due to the different orientation of the chains in the transition from the liquid-expanded to the condensed phase. Figures 10.55-10.57 all show an s-shaped behaviour for G_s'' and η_s'. An interesting feature from the data and plots is that the elastic component of the surface shear modulus, G_s', remained zero. However, Figure 10.58 of the longer fatty acid $C_{22}H_{45}COOH$ shows a gradual rise in G_s' at π_t; G_s'', of course, also rises as η_s' rises.

For the polydimethylsiloxane monolayers studied, no data were obtained from the instrument for both the dynamic surface shear viscosity and shear moduli at the various surface pressures of 0, 5 and 10mNm^{-1}. For the long chain fatty acids, the storage modulus remained at zero, even at the higher pressures, while the loss modulus increased minimally. Only $C_{22}H_{45}COOH$ showed more evident characteristics of rigidity at the higher pressures. Here the storage modulus increased from 0mNm^{-1} at zero surface pressure to $\geq$50mNm^{-1} at a pressure of 40mNm^{-1}, while the loss modulus increased to 11.76mNm^{-1} at the higher pressure. The dynamic surface shear viscosity remained at about 10^{-3} sP for most acids except $C_{22}H_{45}COOH$, where it increased from 1.6×10^{-3} sP at zero pressure to 0.26-0.384 sP at 40mNm^{-1}. It appears that the values obtained at the highest pressure were subject to the collapse of the films.

10.4.2 Discussion

No data were obtained for the polydimethylsiloxane monolayers, i.e. the values of the dynamic surface shear viscosity and elasticity at the

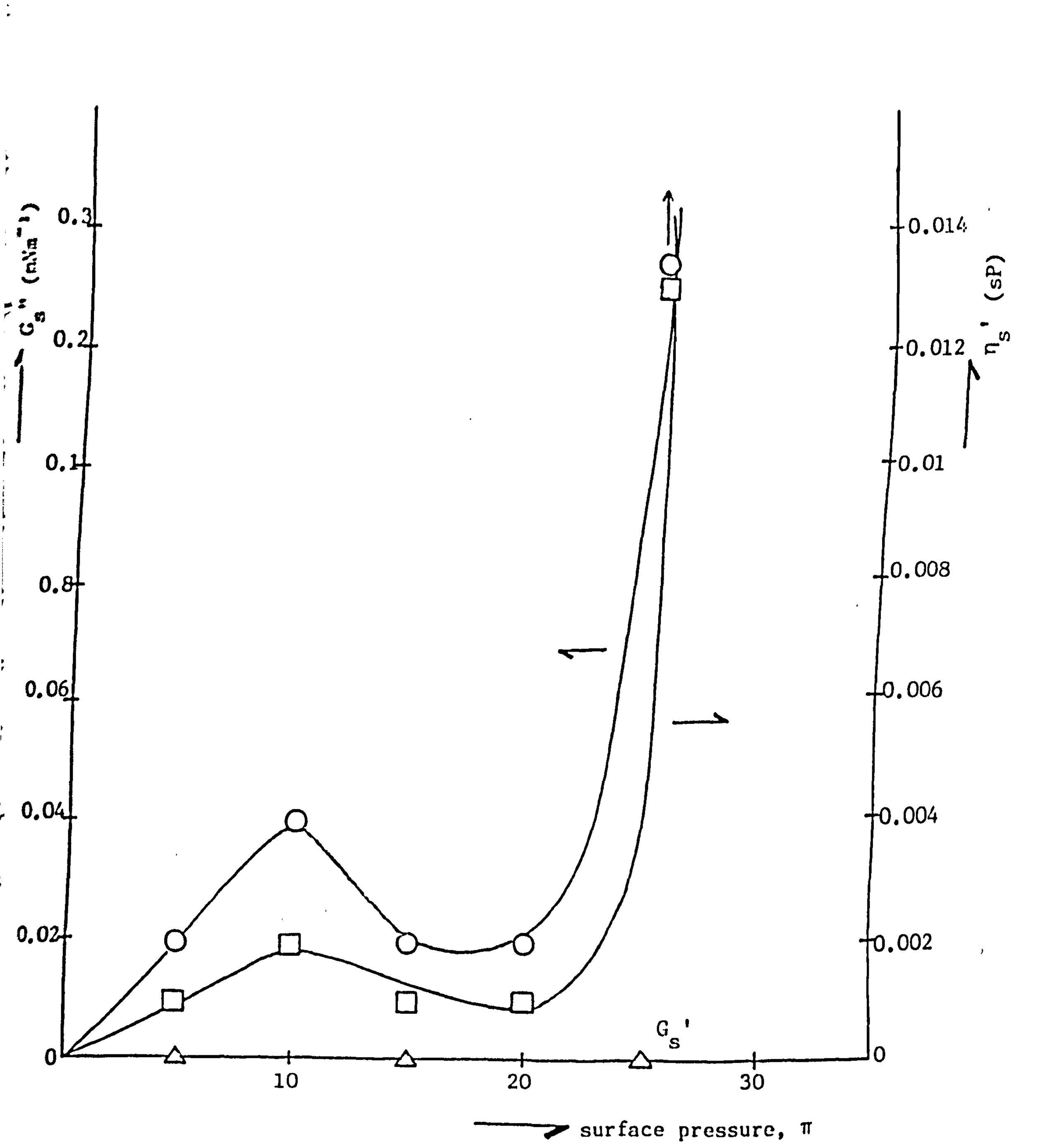

FIGURE 10.54: Plot showing the variation of the dynamic surface shear viscosity, η_s', and shear moduli, G_s', G_s'', with surface pressure, π, for $C_{13}H_{27}COOH$ on a pure water subphase. pH ~ 3.0; T_b = 19.7 ± 0.1°C; resonant frequency, f_o = 3.281Hz.

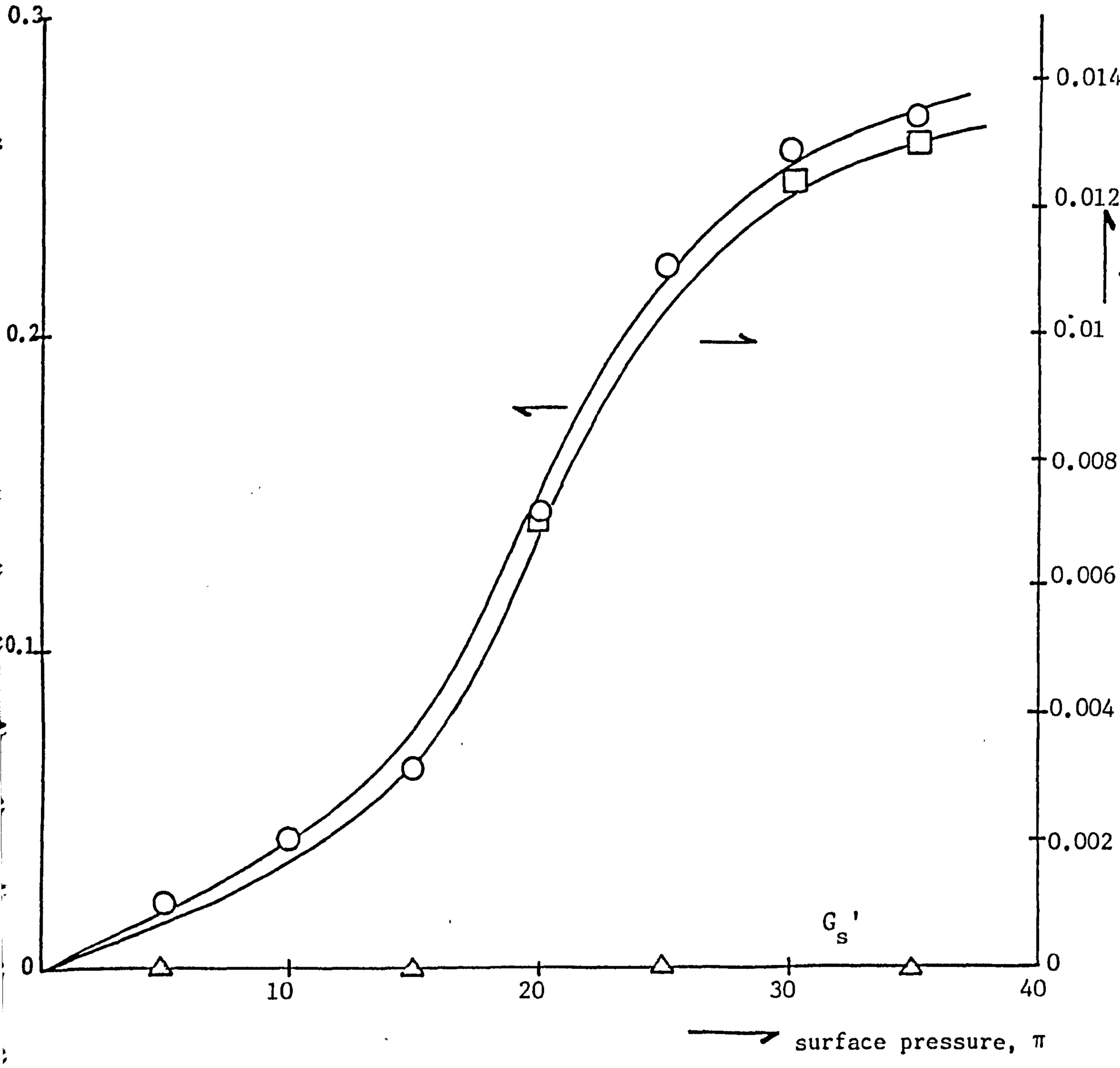

FIGURE 10.55: Plot showing the variation of the dynamic surface shear viscosity, η_s', and shear moduli, G_s', G_s'', with surface pressure, π, for $C_{17}H_{35}COOH$ on a pure water subphase. pH ~ 3.03; $T_b = 19.7 \pm 0.1^{o}C$; $f_o = 3.28$Hz

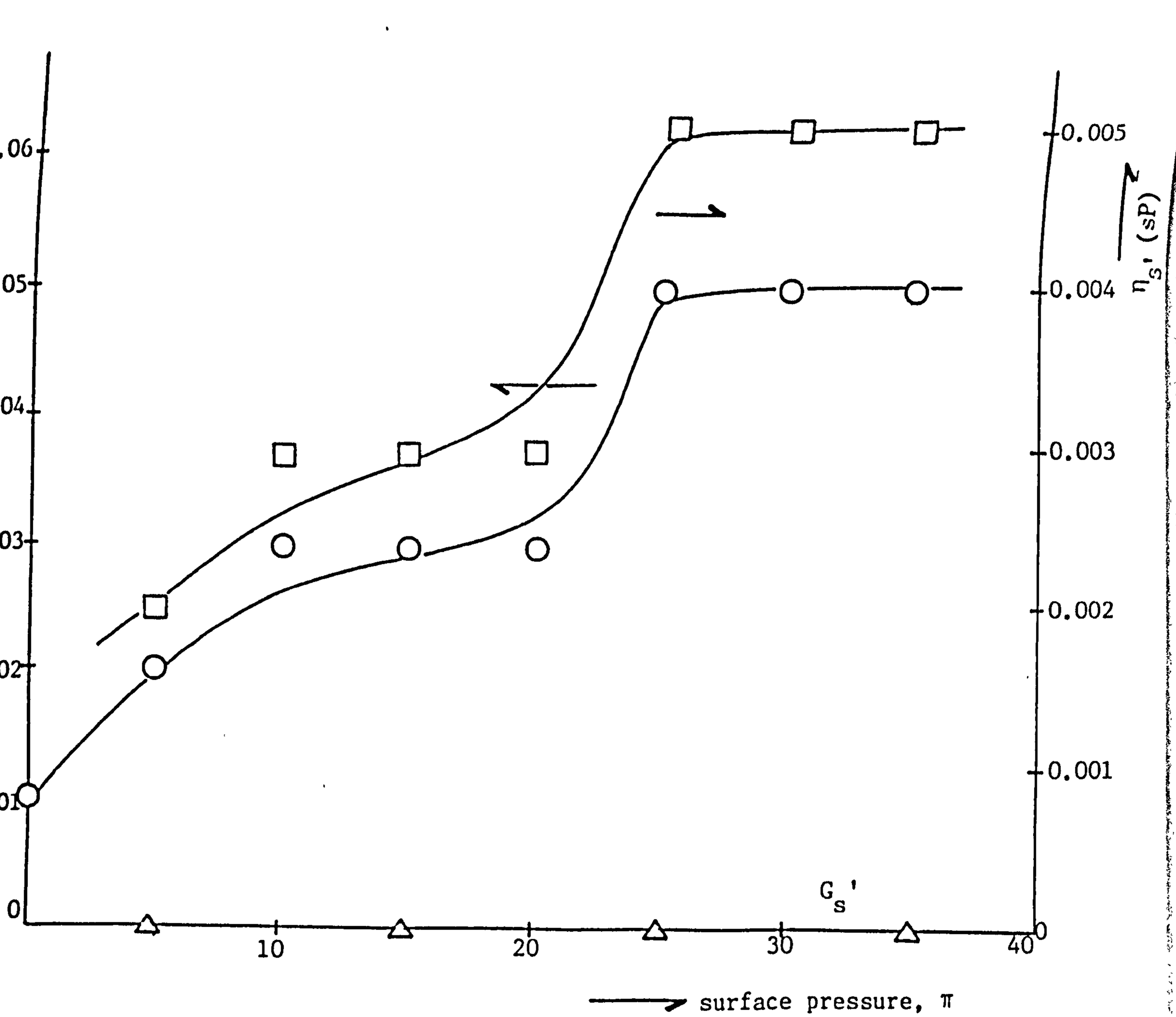

FIGURE 10.56: Plot showing the variation of the dynamic surface shear viscosity, η_s' and shear moduli, G_s', G_s'', with surface pressure, π, for $C_{18}H_{37}COOH$ on a pure water subphase. pH ~ 3.03; $T_b = 20.1 \pm 0.1^oC$; $f_o = 3.309Hz$

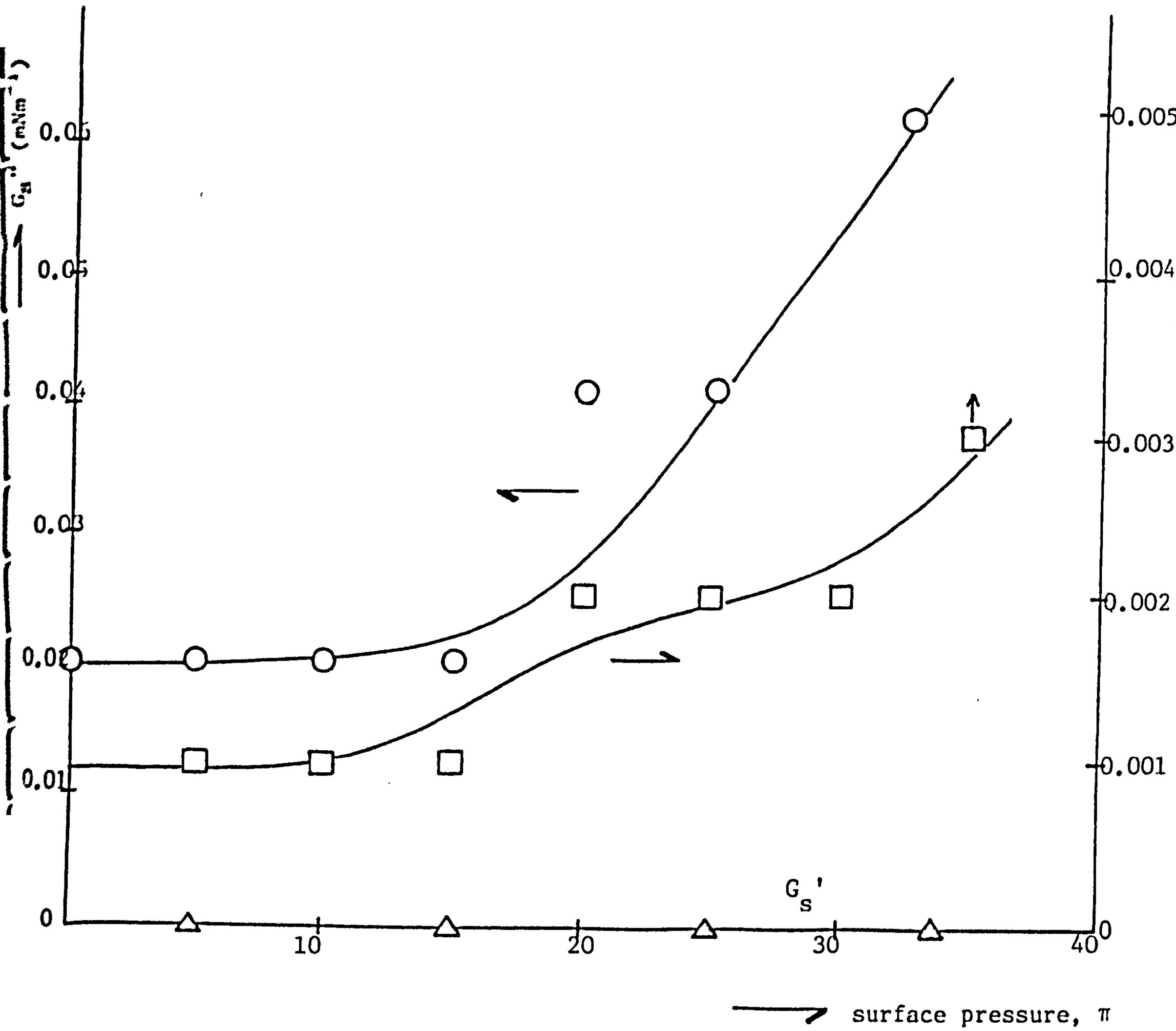

FIGURE 10.57: Plot showing the variation of the dynamic surface shear viscosity, η_s', and shear moduli, G_s', G_s'', with surface pressure, π, for $C_{19}H_{39}COOH$ on a pure water subphase.
pH ~ 3.03; $T_b = 20.1 \pm 0.1^oC$; $f_o = 3.309Hz$

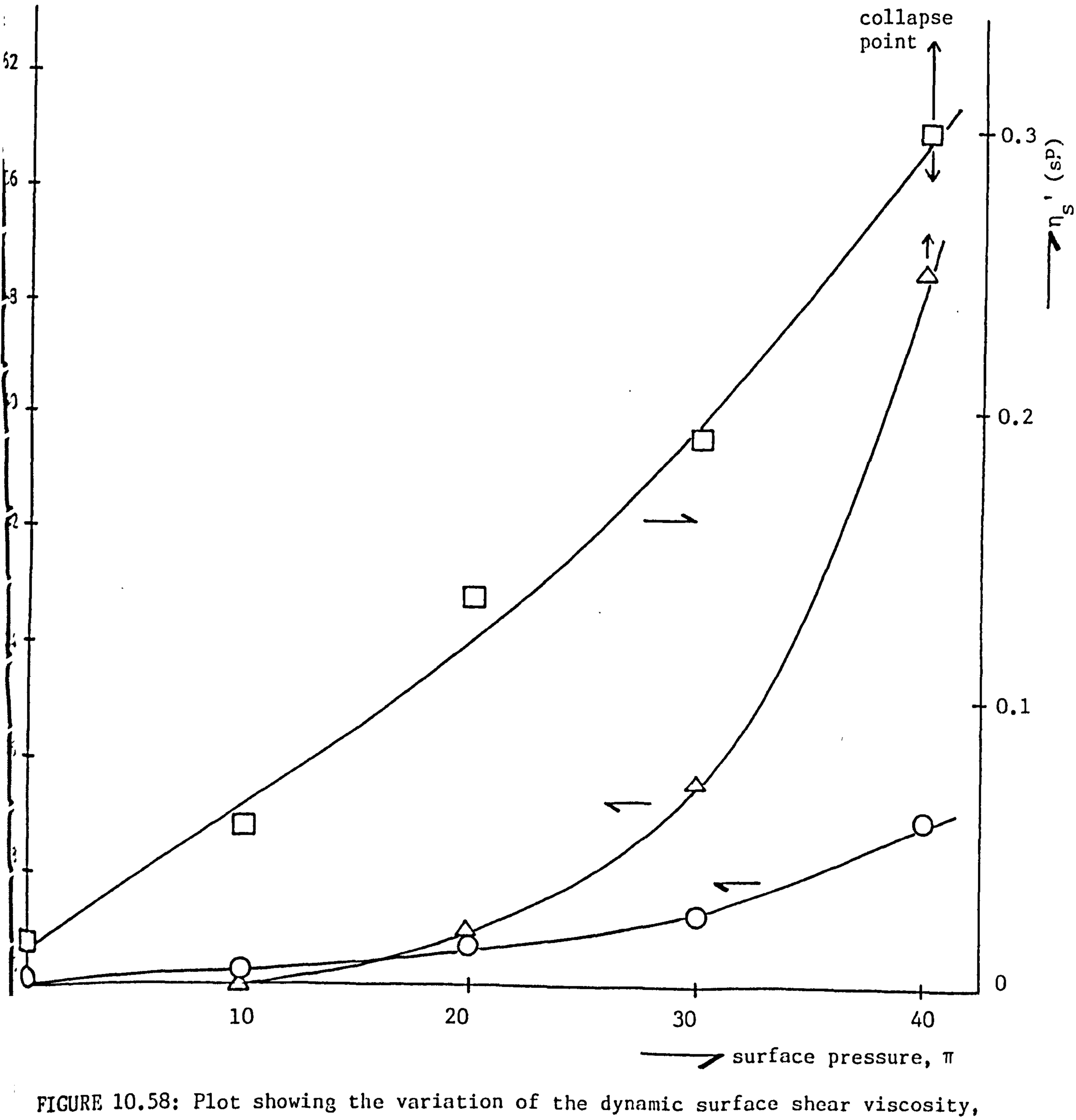

FIGURE 10.58: Plot showing the variation of the dynamic surface shear viscosity, η_s', and shear moduli, G_s', G_s'', with surface pressure, π, for $C_{22}H_{45}COOH$.
pH ~ 3.5; $T_b = 21.5 \pm 0.1^oC$; $f_o = 3.309Hz$

various pressures were lower than the sensitivity of the instrument, which was $10^{-3}mNsm^{-1}$. However, this supports the prediction that, due to the high fluidity of these films, there is negligible rigidity and so all its energy is being lost to the subphase. The molecules can slip over one another, and so no structure is formed, which results in practically no detectable surface viscosity or elasticity.

For the long-chain fatty acids (except $C_{22}H_{45}COOH$) the data obtained showed that all the energy is lost by relaxation of the film rather than being stored, with again very little structure being formed at all. The data obtained for $C_{22}H_{45}COOH$ showed the storage modulus rising at π_t, with the loss modulus also rising, i.e. the dissipation of energy decreases with decreasing molecular area. The gradual rise in the storage modulus G_s' might be due to the packing of the molecules in the condensed phase. The varying η_s' values at the higher pressure were due to the collapse of the film, especially above $30mNm^{-1}$. To summarize, the film showed marked viscoelasticity with the predominant character changing from a fluid-like film at surface pressures below $20mNm^{-1}$ to an elastic or solid-like film when $\pi > 20mNm^{-1}$.

All the fatty acids showed some shear rigidity, but $C_{22}H_{45}COOH$ was chosen because it was least likely to collapse within the experimental timescale. The viscosity value obtained at $10mNm^{-1}$ for $C_{22}H_{45}COOH$ compares favourably with that given by Buhaenko *et al*[247] using a torsion pendulum viscometer.

Abraham *et al*[290] have failed to detect any shear modulus from experiments of $C_{17}H_{35}COOH$ (stearic) on clean water in either of the condensed phases. They give two possibilities as being the reason:

(i) that the threshold for nucleation of dislocations is so low that

it lies below the detection sensitivity of their instrument; and

(ii) that in arriving at the final compressed state, a solid film would exist in such a highly-fractured state as to consist of a large number of small-diameter 2-dimensional platelets which are relatively free to slide around one another.

10.4.3 Summary

No data were obtained on the shear rigidity for the polydimethylsiloxane monolayers. However, some shear rigidity was detected with the long-chain fatty acids, particularly $C_{22}H_{45}COOH$ (tricosanoic), which showed marked viscoelasticity by behaving as a fluid-like film when $\pi < 20mNm^{-1}$ and a solid or elastic film when $\pi > 20mNm^{-1}$.

10.5 Antifoaming Ability Measurements of Polydimethylsiloxane Polymers

10.5.1 Results

The antifoaming tests have been described in detail in Chapter 7. Individual values of the antifoaming index or efficiency, AFI, were obtained from foam heights, and the difference between the individual values of the AFI and the average AFI of a particular concentration for each polymer were calculated. The average of these differences was taken as a measure of the error for the overall antifoaming ability. The expression used to calculate the antifoaming index at a given concentration (equation (7.24)) was:

$$AFI_{(Xppm/gdm^{-3})} = \frac{FH_{(Oppm/gdm^{-3})} - FH_{(Xppm/gdm^{-3})}}{FH_{(Oppm/gdm^{-3})}}$$

where all the parameters have been defined in Section 7.6.4. But with antifoaming agents with no antifoaming, complete antifoaming or profoaming actions,corresponding AFI values of 0, 1 and<0 respectively would have been recorded.

The polymers were all used without further purification. The polymers (diluted in 60-80° petroleum ether) with their respective viscosities, are summarized in Table 10.41. Figure 10.59 shows the variation of viscosity (log η) with the weight-average molecular weight of the polydimethylsiloxanes. Here, a gradual increase in viscosity with increasing molecular weight is obtained as expected.

The effect of concentration on the antifoaming index of five polymers (four of which were polydimethylsiloxanes with different molecular weights and a fluorocarbon surfactant, FC740) dissolved in Offshore Magnus crude oil, is given in Table 10.42 and shown in Figure 10.60. Results have also been obtained from experiments using Offshore Ninian crude oil, and a model crude oil to give a more objective 'picture' of the antifoaming effects of these and other polydimethylsiloxanes over a wider range of concentrations.

Tables 10.43 and 10.44 summarize the effect of concentration on the antifoaming index of the polymers (added as a solution in 60-80° petroleum ether and directly to the oil). These results are presented in Figures 10.61 and 10.62 respectively. The Model crude oil was a solution of aerosol OT in ethanediol (3% w/v).

Both figures show a gradual increase in AFI with concentration, as the molecular weight of the polydimethylsiloxanes increases until a maximum is reached at the molecular weight of <31000>. Antifoaming properties then decrease with further molecular weight increases. The fluorocarbon surfactant, FC740, is clearly a profoamer in all foaming media.

Figures 10.63 and 10.64 show the variation of AFI with the molecular weight at various concentrations of polydimethylsiloxanes added

$\overline{M}_w$	Viscosity (Nsm^{-2})
6610	$7.33 \times 10^{-3} \pm 1.9 \times 10^{-4}$
14420	$1.19 \times 10^{-2} \pm 2.44 \times 10^{-4}$
19100	$2.74 \times 10^{-2} \pm 7.83 \times 10^{-4}$
31000	$6.66 \times 10^{-2} \pm 1.46 \times 10^{-3}$
48150	$1.14 \times 10^{-1} \pm 3.36 \times 10^{-3}$
110000	$1.91 \times 10^{-1} \pm 8.63 \times 10^{-3}$
FC740*	$3.09 \times 10^{-2} \pm 1.67 \times 10^{-3}$

* fluorocarbon surfactant

TABLE 10.41: Data obtained for the viscosities of polydimethylsiloxanes with different weight-average molecular weights.

Temperature = $20.5 \pm 0.2^{o}C$

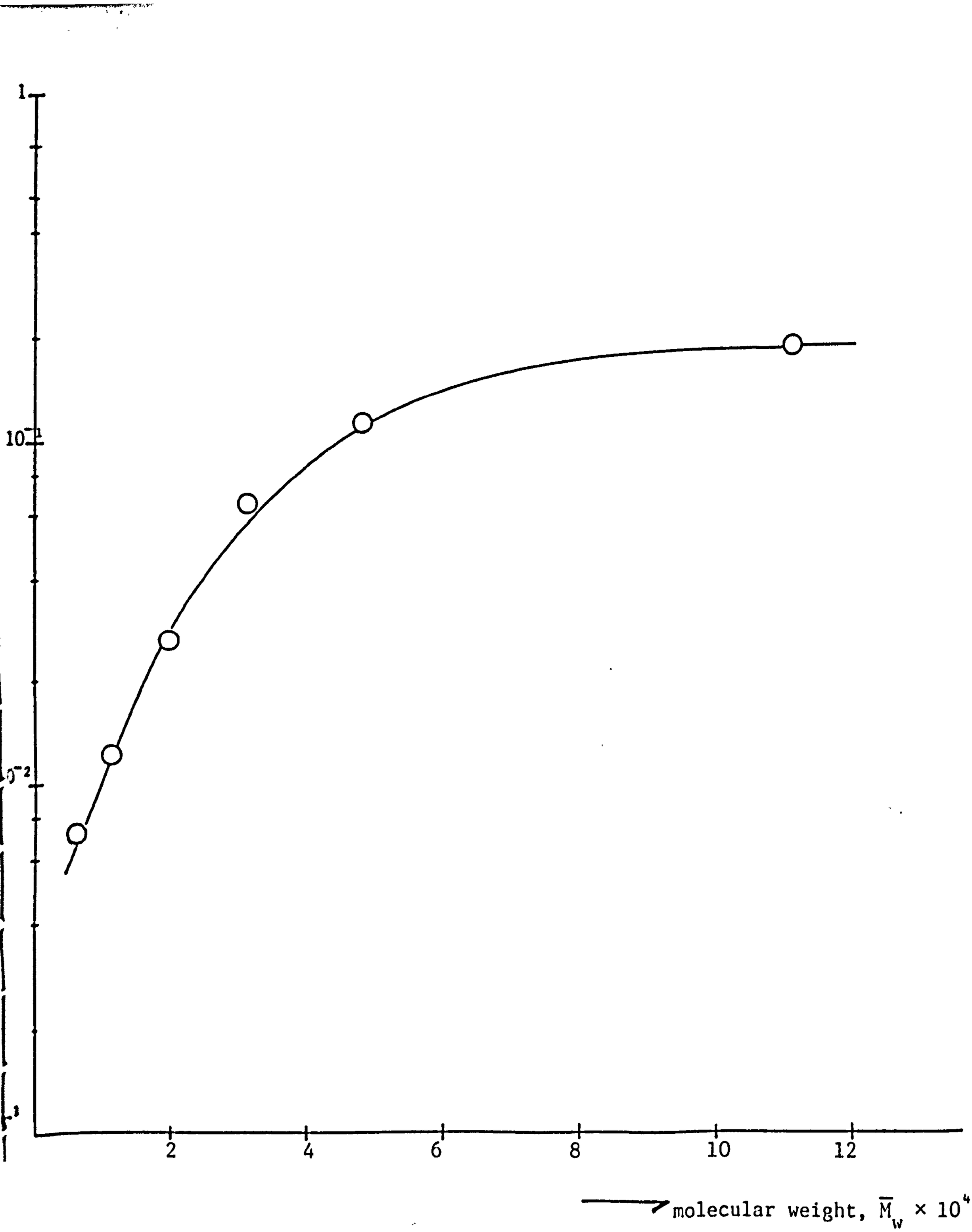

FIGURE 10.59: Plot showing the variation of viscosity with molecular weight of the polydimethylsiloxane polymers

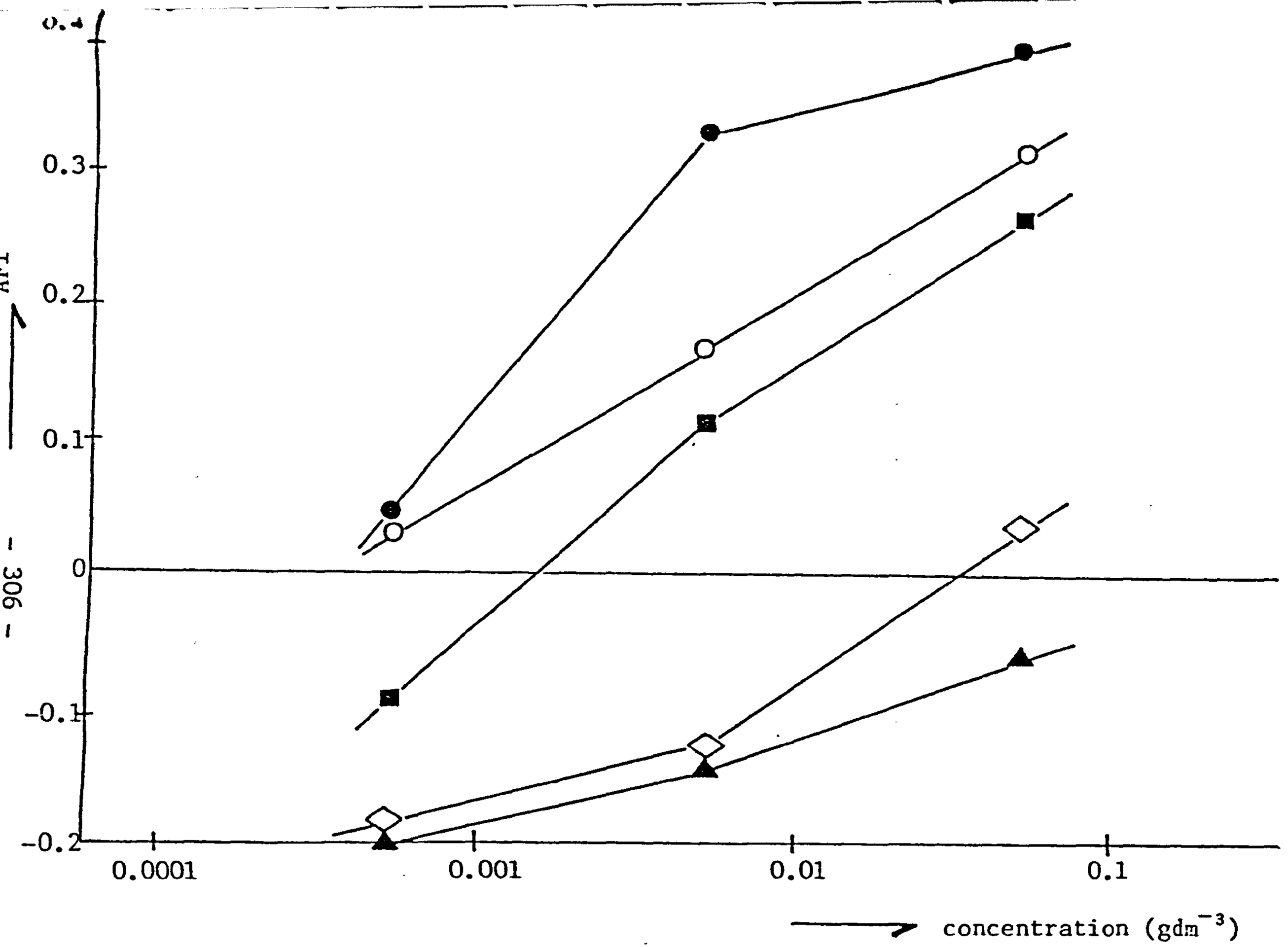

FIGURE 10.60: Plot showing the variation of antifoaming index with the concentration for different polydimethylsiloxanes (added as a solution in petroleum ether) in Offshore Magnus crude oil. $T = 20.1 \pm 0.2^{\circ}C$

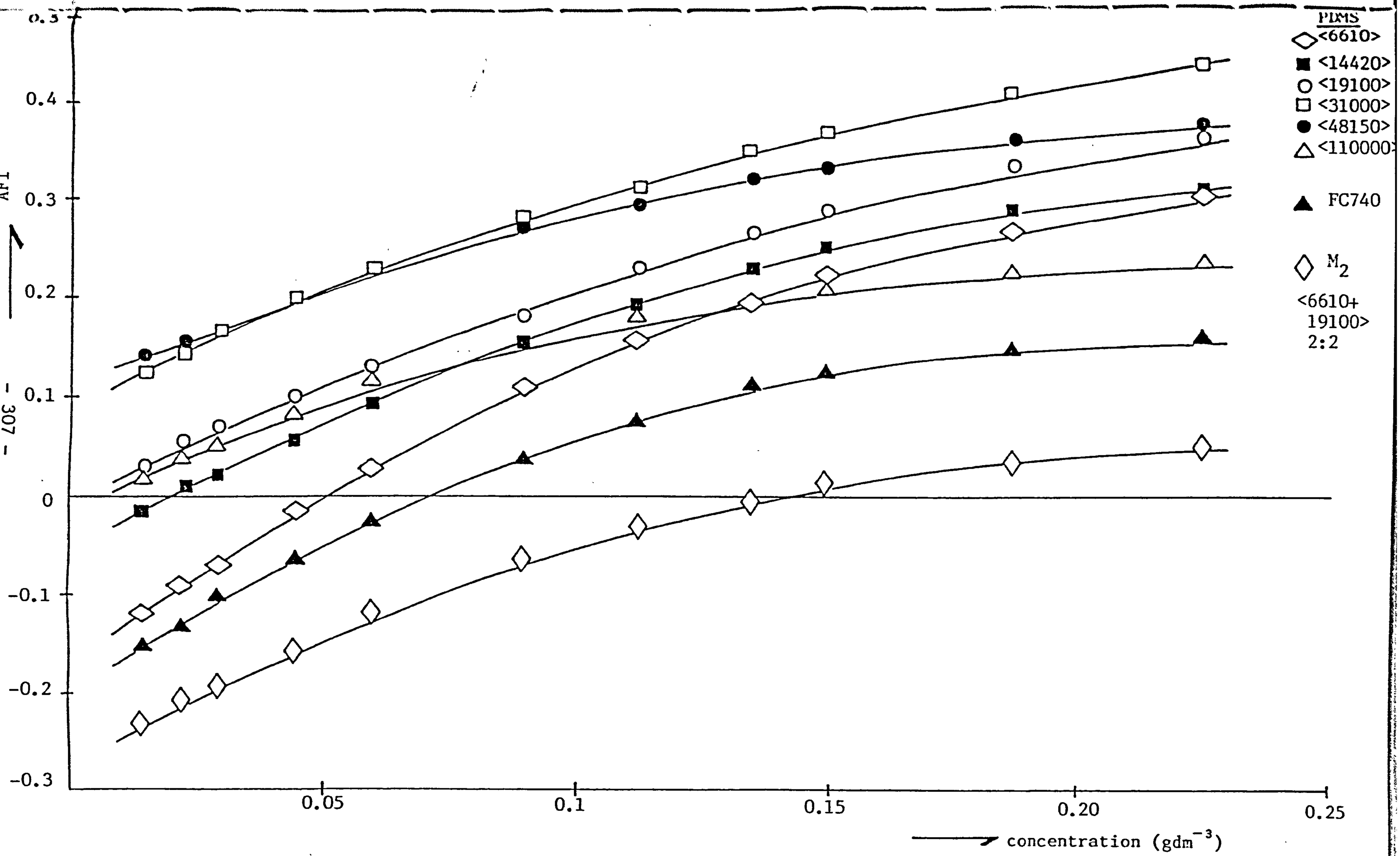

FIGURE 10.61: Plot showing the variation of antifoaming index with the concentration for different polydimethylsiloxanes (direct addition) in Model crude oil. T = 20.3 $\pm$ 0.2^{o}C

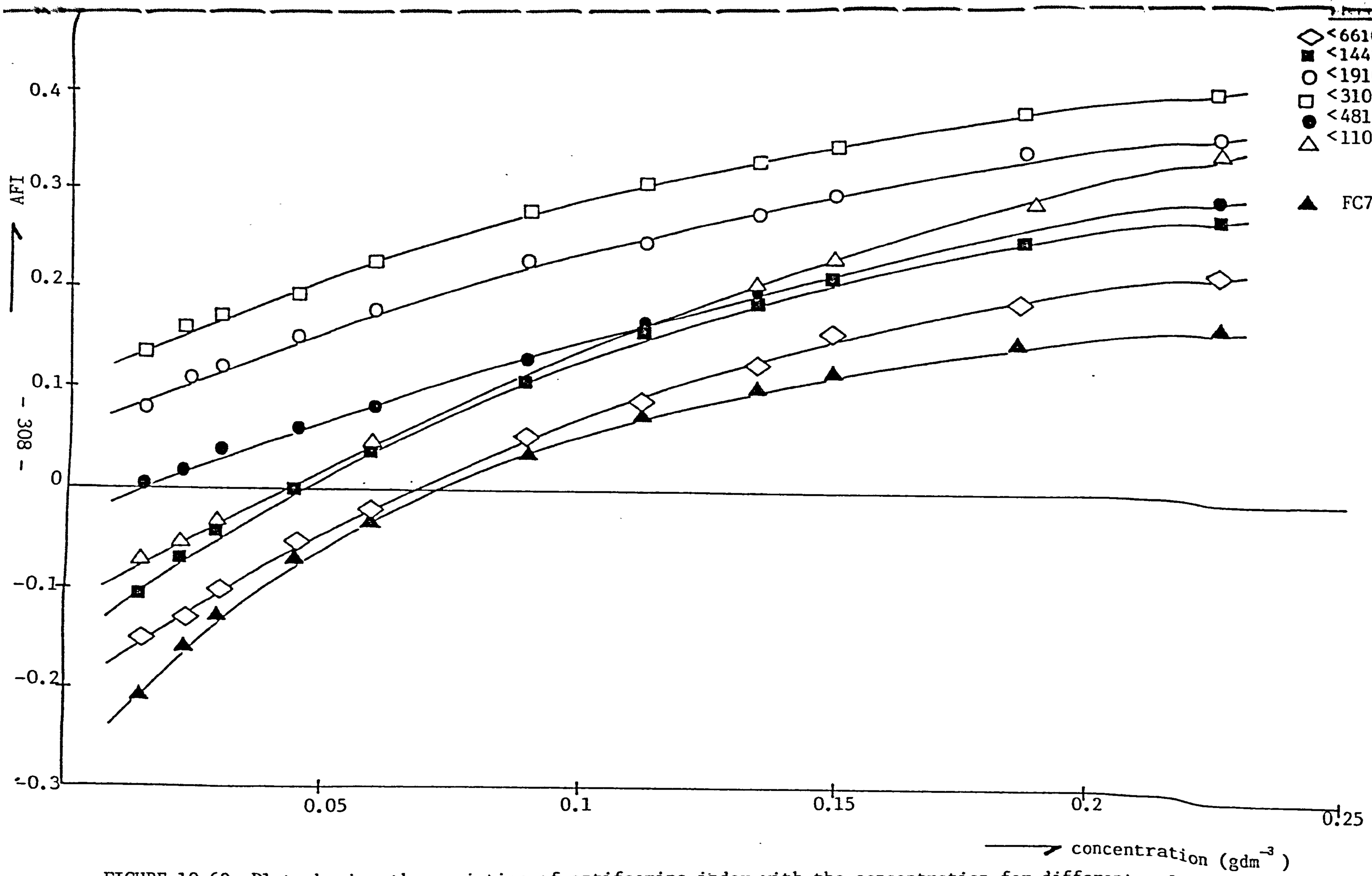

FIGURE 10.62: Plot showing the variation of antifoaming index with the concentration for different polydimethylsiloxanes (added as a solution in petroleum ether) in Model crude oil. T = 20.3 $\pm$ 0.2^{o}C

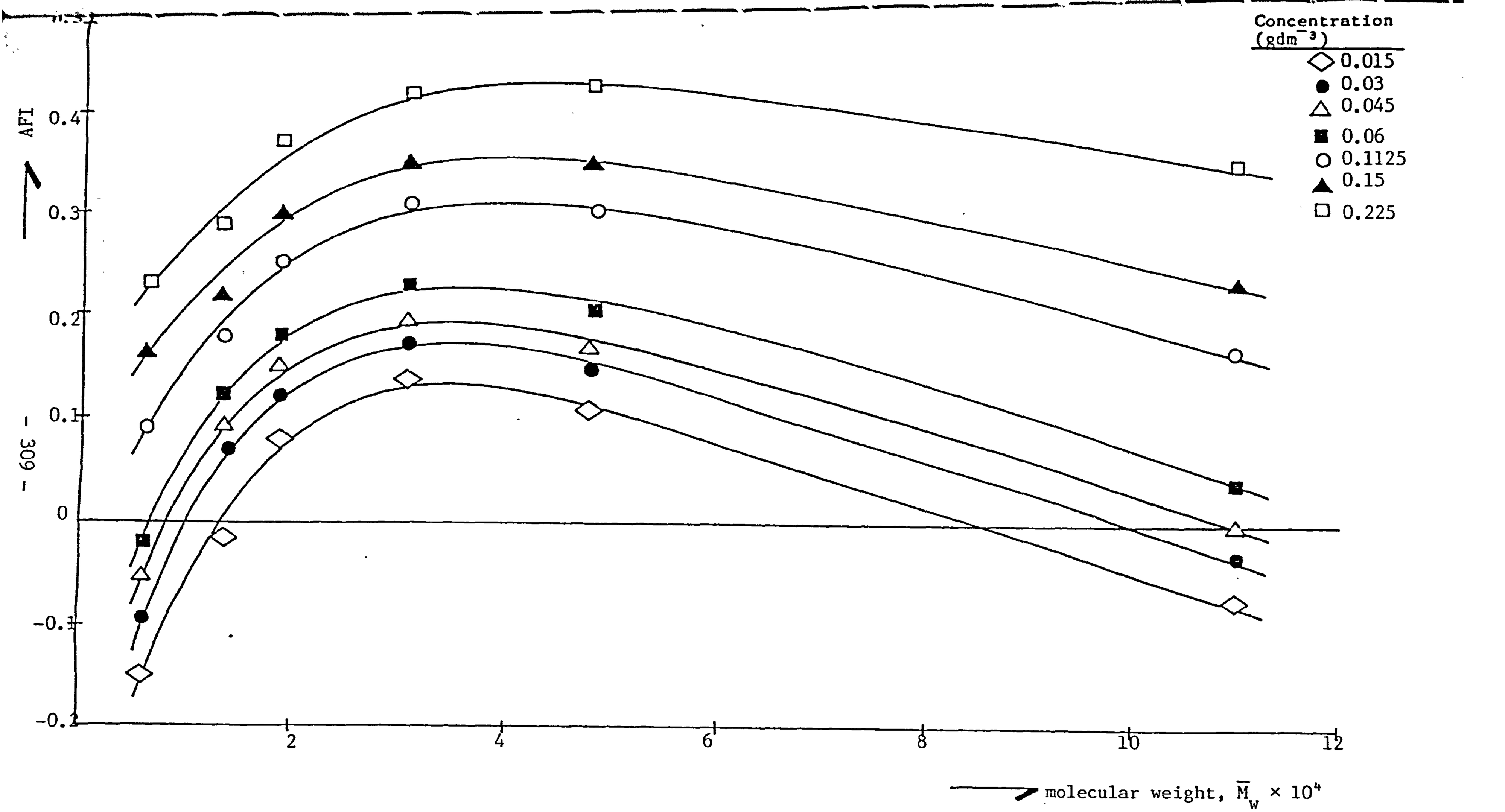

FIGURE 10.63: Plot showing the variation of antifoaming index with the molecular weight for different polydimethylsiloxanes (added as a solution in petroleum ether) in Model crude oil.

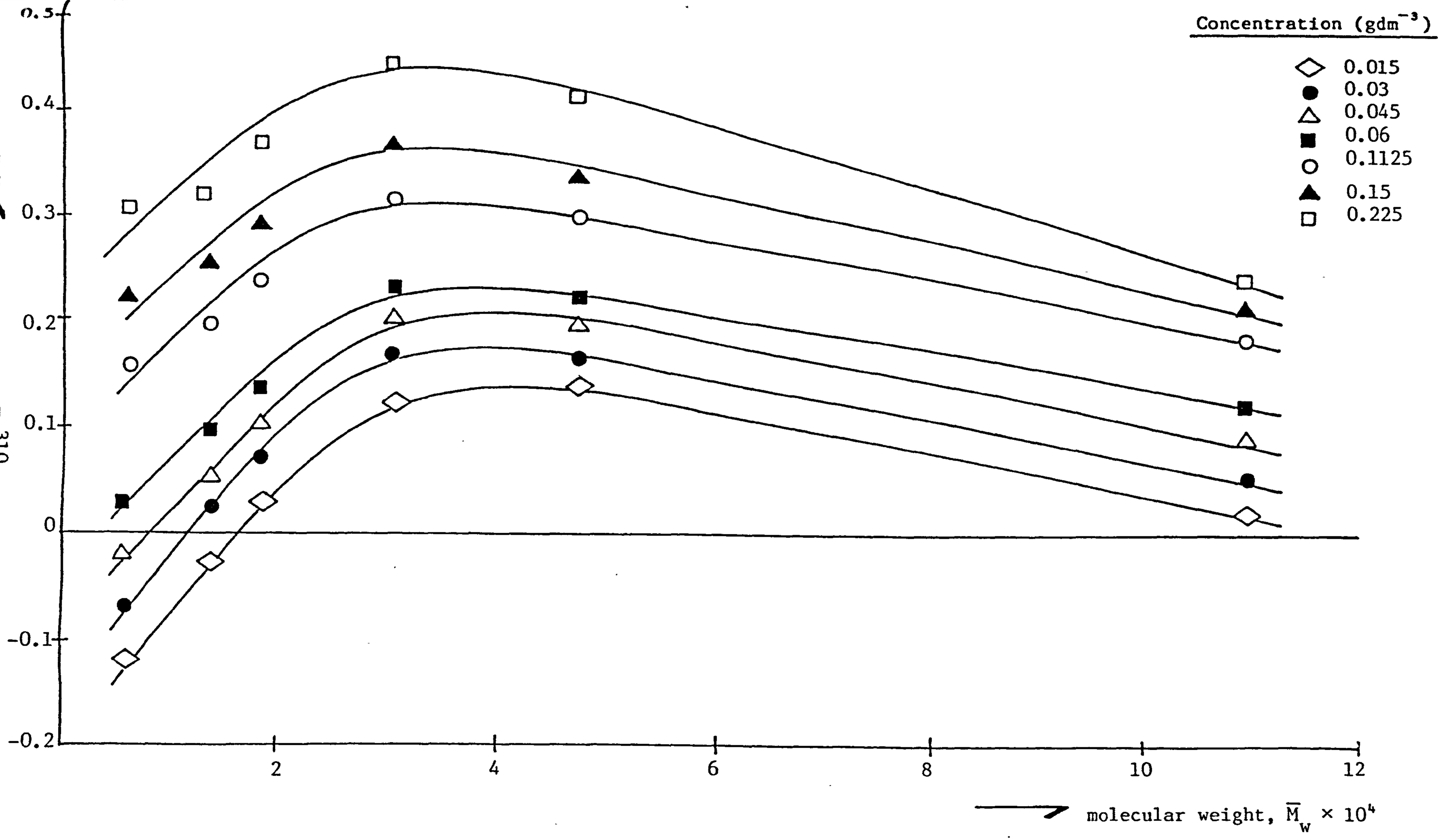

FIGURE 10.64: Plot showing the variation of antifoaming index with the molecular weight for the different polydimethyl-siloxanes (direct addition) in Model crude oil

either with the polymers initially as a solution in petroleum ether, or after direct addition. Here, the AFI increases to a maximum with polydimethylsiloxane <31000> on most concentrations, and then starts to fall with any further increase in molecular weight. This confirms the earlier observations of polydimethylsiloxane <31000>.

However, when these polymers (diluted in petroleum ether) were added to Offshore Ninian crude oil, the results obtained showed polydimethylsiloxane <110000> acting as the best antifoamer. The data are summarized in Table 10.45 and illustrated in Figure 10.65. The plot in Figure 10.66 of AFI against the molecular weight confirms this observation for each concentration of polydimethylsiloxane studied.

Mixtures of two polydimethylsiloxanes with different molecular weights (added as a solution in petroleum ether) were dissolved in the Model crude oil and their antifoaming properties determined. The mixtures with their respective viscosities are summarized in Table 10.46.

The variation of the concentration with the antifoaming index of varying molar-proportions of the mixtures are presented in Tables 10.47 and 10.48 and illustrated in Figures 10.67 and 10.68. The three upper curves are for varying molar-proportions of a mixture of polydimethylsiloxanes <6610> and <19100>, while the lower three are for a mixture of polydimethylsiloxanes <31000> and <48150> respectively. Here, the mixture $<M_{2C}>$ (see Table 10.45) proves to be the best antifoamer mixture.

Tables 10.49 and 10.50 give a comparison between the antifoaming indices of a 'particular' mixture of polydimethylsiloxanes and those of its constituents; this is shown in Figure 10.69. This experiment was performed to observe whether any of the mixtures exhibited synergism, from which any differences in performances of the mixtures from the com-

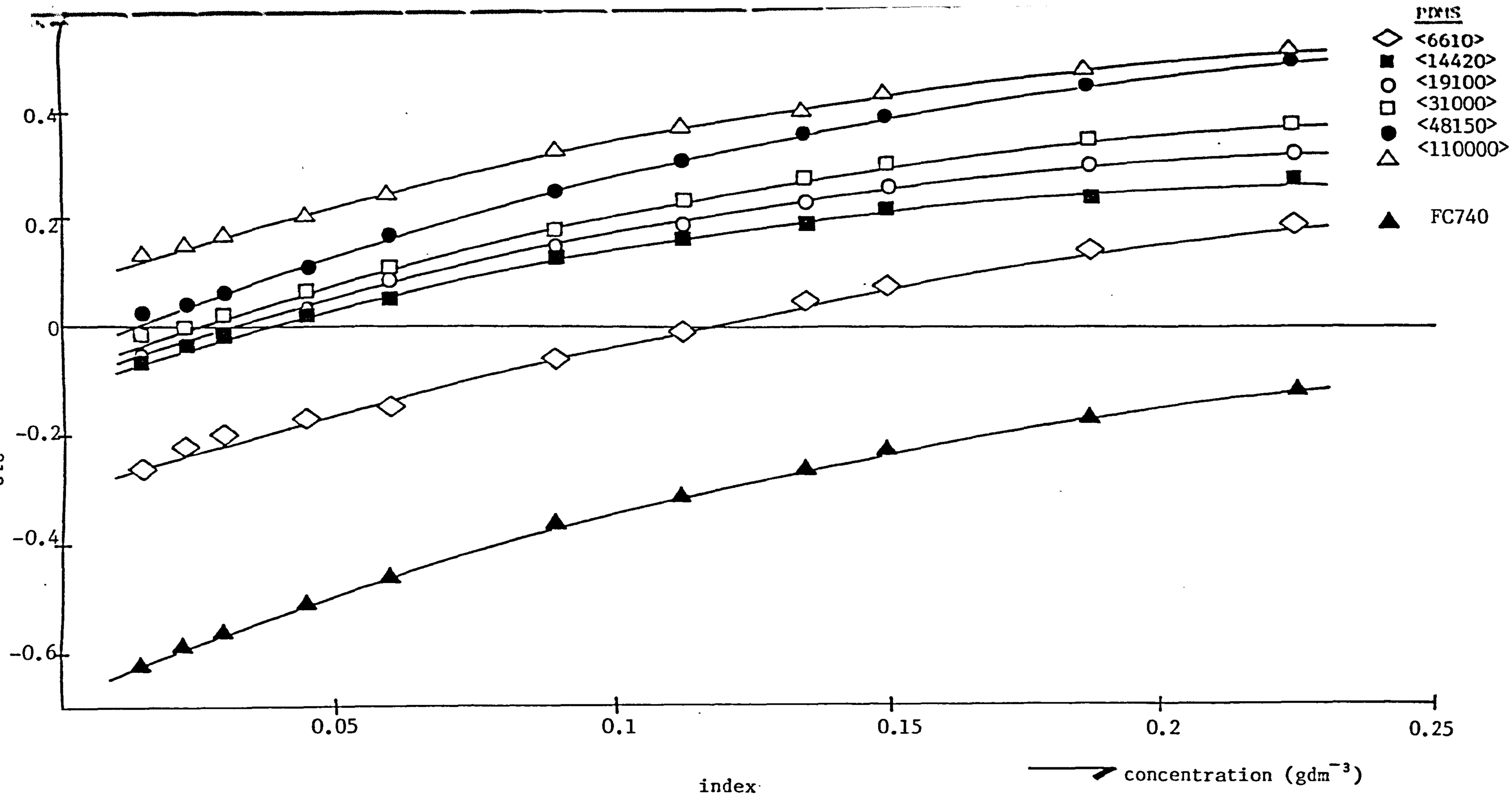

index

FIGURE 10.65: Plot showing the variation of antifoaming with the concentration for different polydimethylsiloxanes (added as a solution in petroleum ether) in offshore Ninian crude oil. $T = 20.4 \pm 0.2^{o}C$

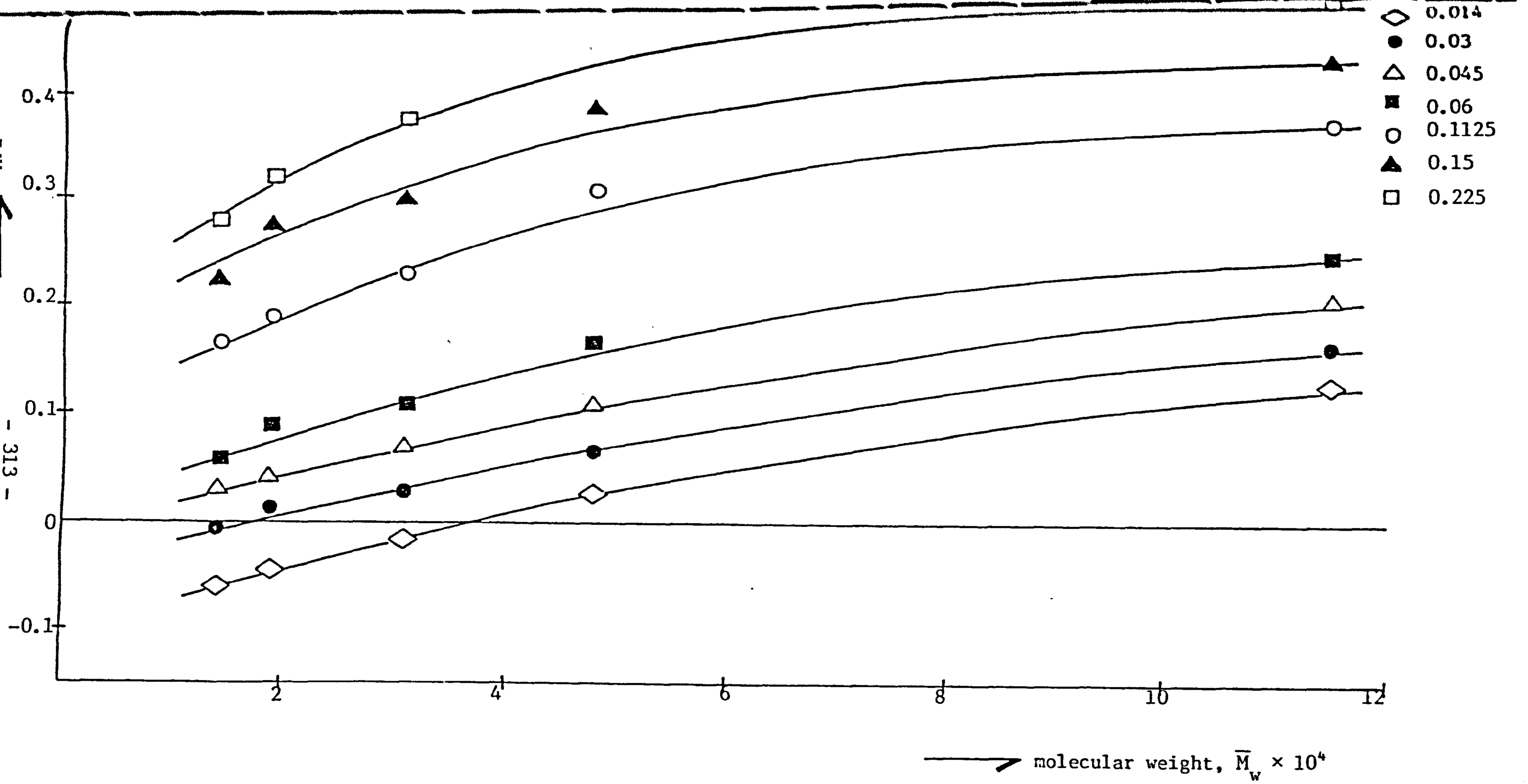

FIGURE 10.66: Plot showing the variation of antifoaming index with the molecular weight for the different polydimethylsiloxanes (added as a solution in petroleum ether) in Offshore Ninian crude oil

Mixture (Molar Proportion) $MW_1 + MW_2$	Viscosity (Nsm^{-2})
M_{2A} (0.5:0.5) <6610 + 19100>	$1.39 \times 10^{-3} \pm 5.1 \times 10^{-5}$
M_{2B} (0.25:0.75) <6610 + 19100>	$3.44 \times 10^{-3} \pm 7.92 \times 10^{-5}$
M_{2C} (0.75:0.25) <6610 + 19100>	$1.129 \times 10^{-3} \pm 2.42 \times 10^{-5}$
M_{3A} (0.5:0.5) <31000 + 48150>	$1.56 \times 10^{-2} \pm 7.95 \times 10^{-4}$
M_{3B} (0.25:0.75) <31000 + 48150>	$2.65 \times 10^{-2} \pm 8.55 \times 10^{-4}$
M_{3C} (0.75:0.25) <31000 + 48150>	$1.22 \times 10^{-2} \pm 4.78 \times 10^{-4}$

TABLE 10.46: Data obtained of the viscosities of the mixtures of polydimethylsiloxanes with varying molar-proportions. Temperature = $20.5 \pm 0.2^{o}C$

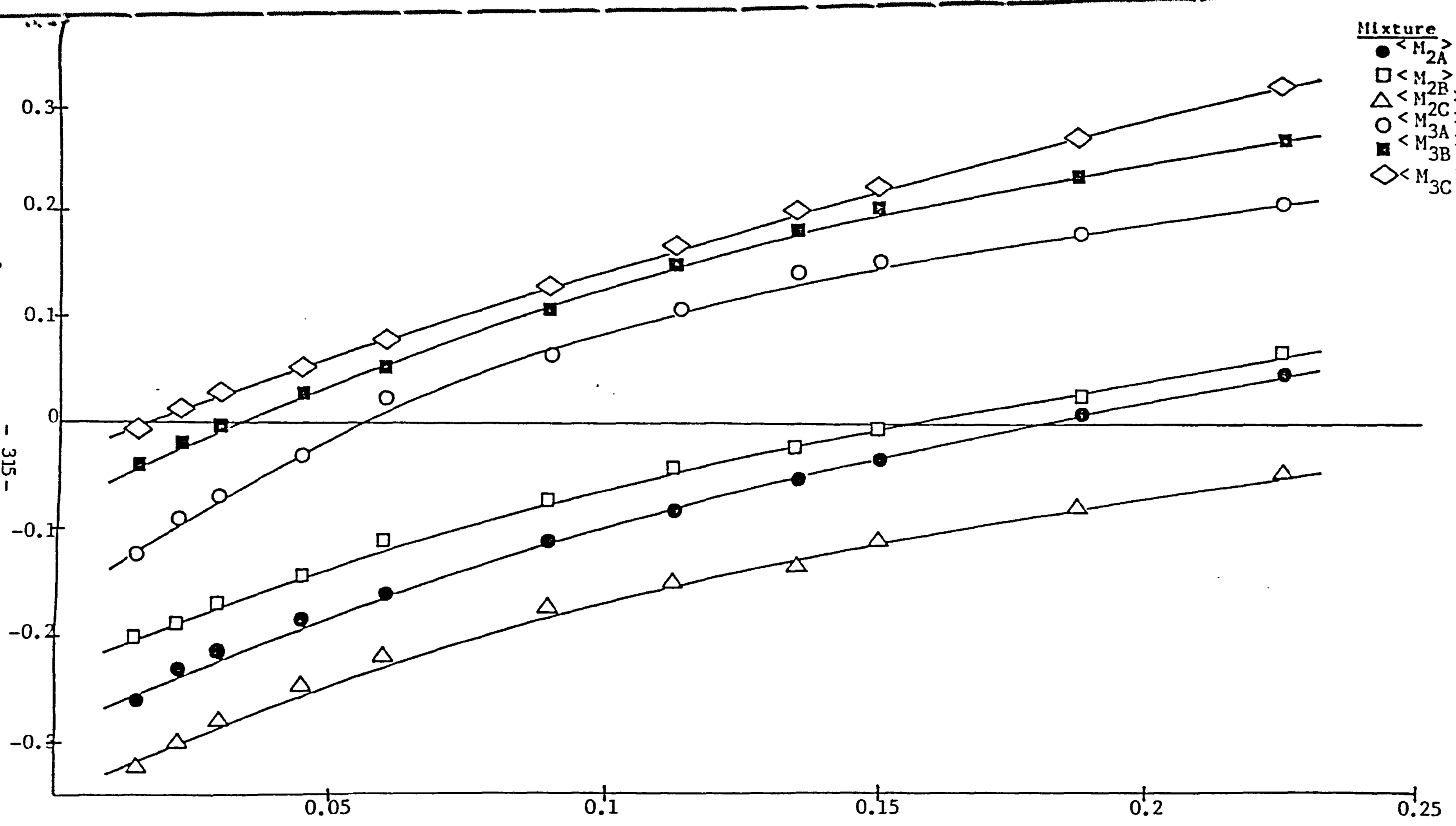

FIGURE 10.67: Plot showing variation of antifoaming index with the concentration for various molar-proportion mixtures of polydimethylsiloxanes (added as a solution in petroleum ether) in Model Crude oil. $T = 20.3 \pm 0.2^{o}C$

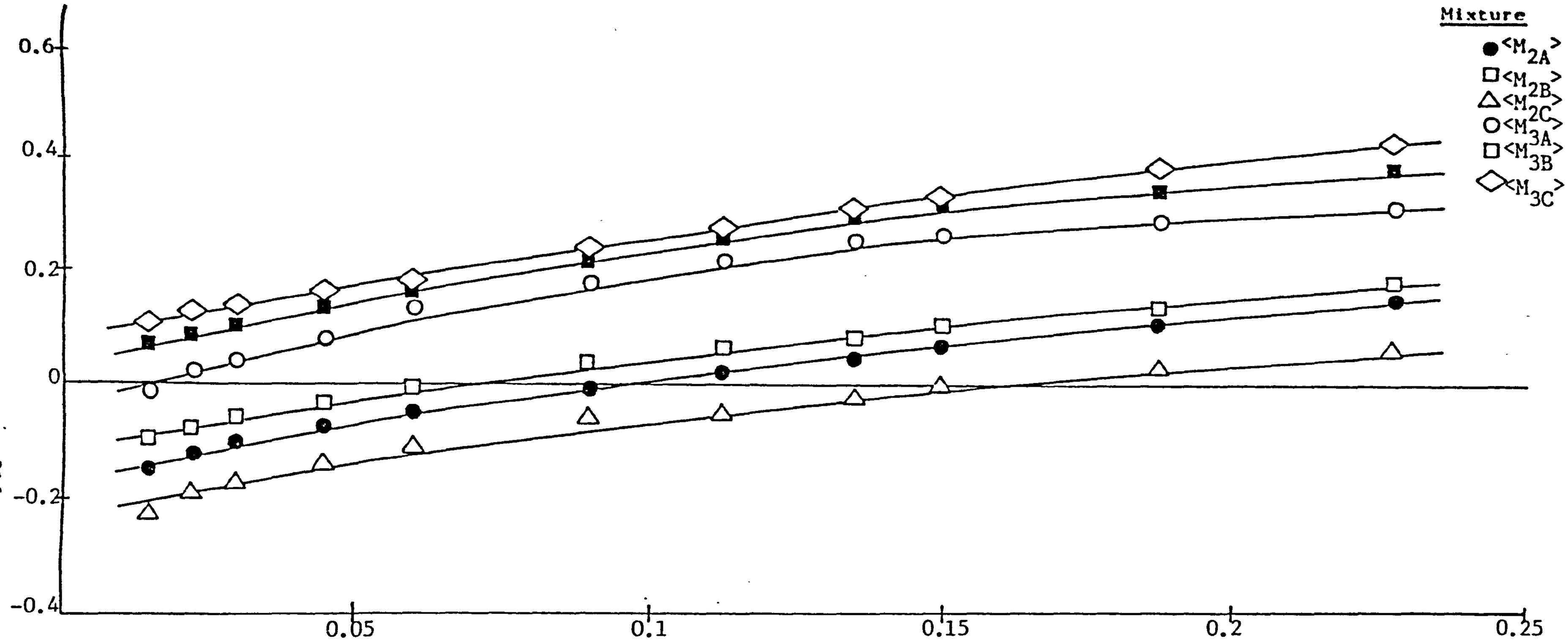

FIGURE 10.68: Plot showing the variation of antifoaming index with concentration for various molar-proportion mixtures of polydimethylsiloxanes (added as a solution in petroleum ether) in Offshore Ninian crude oil. $T = 20.4 \pm 0.2^{o}C$

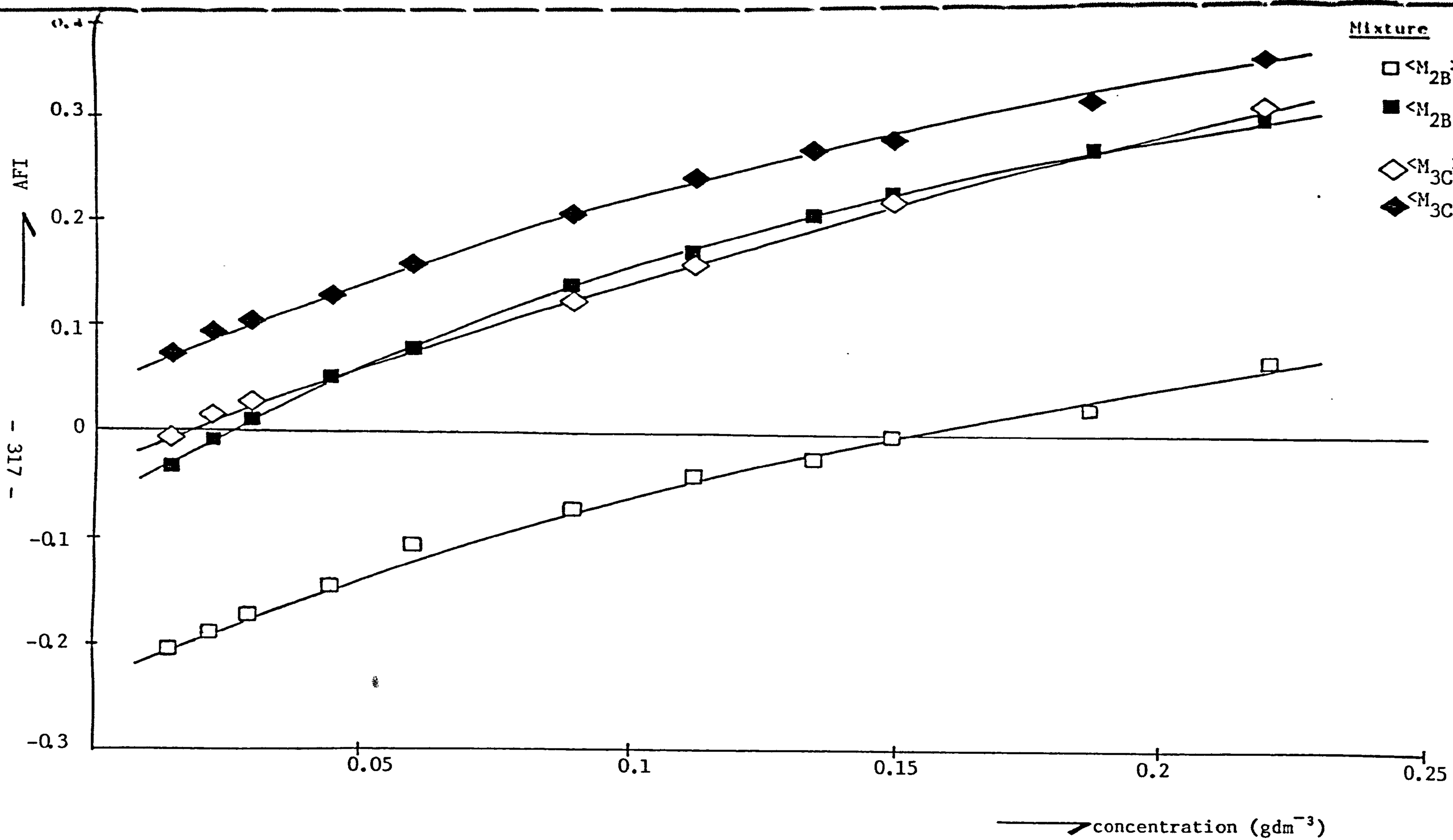

FIGURE 10.69: Plot showing the variation of antifoaming index with the concentration for a particular set of molar-proportion mixtures of polydimethylsiloxanes

bined effect of their individual constituents can be observed.

10.5.2 Discussion

Stable foams such as Offshore crude oils and the Model crude oil are produced from solutions with appreciable surface elasticity[103], and whose liquid lamellae are capable of enduring rapid local surface tension and thickness variations. Effective antifoaming agents such as polydimethylsiloxane function by markedly reducing this surface elasticity. This is brought about by displacing the foam-stabilizing surfactants and maintaining an essentially constant surface tension under conditions of contraction and expansion of the foam lamellae. The polydimethylsiloxane polymers must spread at the interface in order to displace the foam-stabilizing surfactants. This occurs because of their very low intrinsic surface tension, viz. 16-24mNm^{-1}. In the experiments performed, the polydimethylsiloxane was present in a sufficient quantity to maintain a high surface concentration. This was enhanced by the low solubility of the polydimethylsiloxane polymers in all the foaming media. Besides eliminating surface elasticity, the polydimethylsiloxane antifoamers also reduce surface viscosity, thus promoting rapid film drainage. The mechanism here is thought to reflect the low intermolecular cohesion that is present in the polydimethylsiloxane films[9], compared to that in the less-strongly adsorbed foam-stabilizing surfactants.

Profoamers such as the fluorocarbon surfactant FC740 are thought to impart greater surface elasticity to the foam lamellae by forming highly viscoelastic cross-linked surface films, probably via their ester groupings[104]. However, this mechanism is somewhat speculative, and requires further investigation[273]. Kulkarni *et al*[274] have suggested that the foaming surfactant confers a surface charge onto the antifoaming

droplet identical in sign to that of the foam bubble, and that this adsorption becomes significant near the critical micelle concentration of the foaming surfactant.

A comparison between the plots in Figures 10.63 and 10.64 show that there is not a significant change in the respective performances of the polydimethylsiloxanes, and so were independent of the method of addition, when mixed with the model crude oil only. However, polydimethylsiloxane <31000> still proved to be the most effective antifoamer. This observation was also confirmed in Figures 10.61 and 10.62, where the highest antifoaming peak was reached on each concentration with polydimethylsiloxane <31000>. The overall low performance of the higher molecular weight polydimethylsiloxanes may be attributed to the fact that they had not been completely dispersed in the foaming liquid, and so were perhaps performing at a lower level than expected. These plots also exhibited some profoaming behaviour at low concentrations for the smaller molecular weight polydimethylsiloxanes.

However, the plots in Figures 10.60 and 10.65 did show the expected results in the antifoaming behaviour of the various polydimethylsiloxanes in Offshore Magnus and Ninian crude oils. Perhaps the different behaviours of these polydimethylsiloxanes may be due to the viscosity of both foaming liquids. The simple interpretation of the plots indicates that the larger the molecular weight, the better it behaves as an antifoamer. Figures 10.63 and 10.66 also add weight to this observation by showing all the antifoaming indices peaking at the largest molecular weight polydimethylsiloxanes.

Two polydimethylsiloxanes with neighbouring viscosities were blended (with different molar-proportions) together and examined for their

combined antifoaming behaviour in the Model crude oil (aerosol OT in ethanediol). The plots in Figures 10.67 and 10.68 show the mixture $\langle M_{3C} \rangle$ to be the best antifoamer mixture amongst those tested.

These tests for the synergistic effect on the antifoaming ability of a particular mixture of polydimethylsiloxanes, if compared to a combined addition of its constituents' capabilities, revealed that generally the mixtures were not as effective as the combined addition of their constituents, and Figure 10.69 shows the performance of the mixture to be lower than when the effects of its individual constituents are added together. Mixtures are highly dependent on the closeness of the concentration of their constituent polymers.

10.5.3 Summary

It has been shown that the antifoaming ability of polydimethylsiloxanes can be measured quantitatively by a simple modified Bikerman method. A contrast is drawn between the behaviour of antifoamers and a profoamer in different foaming media. It was also shown that the mixtures of polydimethylsiloxanes were not as effective as expected in their ability to act as antifoamers. Perhaps this might be due to the inability of the large molecules to be completely dispersed in the viscous foaming medium of the Model crude oil when compared to the Offshore crude oil.

10.6 General Discussion

On comparing the two sets of data obtained from the manually and fully-operative Langmuir troughs for the surface flux and viscosity of long-chain fatty acids, it will be necessary to concentrate on the results obtained from the latter trough. This is because they were recorded with a modern, continuously-recording film balance instead of the former

point-by-point method, and so even very small details of the curves have been shown with great reliability and reproducibility. Also, the data can be further compared to the results obtained by earlier researchers with more confidence in the experimental procedure.

The use of the Joyce-Loebl (fully-automated) glass trough enabled one to compare the behaviour of a number of long-chain n-alkanoic acids and linear polydimethylsiloxanes at the air/water interface from the two sets of data obtained; it was possible to determine the effect of variations in the length of the hydrocarbon and polymeric chains on the pressure-area isotherms of monolayers (see Tables 10.11 and 10.19, and Figures 10.18 and 10.35). While it was interesting to observe the transition from the liquid-expanded to the condensed phases of the fatty acids, the polydimethylsiloxanes all gave identical expanded films with similar features. The close values of the area per molecule at zero surface pressure for the fatty acids indicated that the van der Waals energy increased with the length of the chain, and drew the molecules closer as the intermolecular attraction increased.

A study of the pressure-area curves revealed that the polydimethylsiloxanes are able to coil reversibly into helices, and this ability is due to the larger diameter of the silicon atom as compared with the carbon atom of analogous linear carbon-based polymers. At low film pressures, each helix uncoils and the molecule adsorbs with the long axis in the water.

Studies on surface viscosity also provide valuable information about the intermolecular interactions and two-dimensional phase transformation in monolayers, when the rate of flow of the film material through a narrow and relatively deep canal of a canal viscometer is

observed. One striking feature from the set of data obtained for the fatty acids and polymeric materials was the similarity in the low order of magnitude of the surface viscosity values using the Harkins and Kirkwood[220] formula, with those of the polymeric materials being remarkably low for such large polymers. This indicates the low intermolecular cohesion that exists between adjacent polydimethylsiloxane chains, and is probably responsible for the similarity in data with smaller fatty acid molecules.

As the values of λ_0 were within the extremes of λ for the monolayer, it was apparent that the logarithmic damping of the oscillating bob on clean water was not significantly different from that on a monolayer-covered surface. Therefore, the surface viscosity of polydimethylsiloxane monolayers was certainly below the sensitivity limit of the torsion pendulum surface viscometer used, even at film pressures corresponding to the collapse pressure of the monolayers.

The viscosity of polydimethylsiloxane monolayers is of particular interest in view of their known proficiency as defoaming and antifoaming agents[136]; however, the mechanism by which the polydimethylsiloxane monolayers act as defoaming agents is still unclear. The role of surface viscosity in determining the ability of many active agents to stabilize foams is also not completely understood, although with foams stabilized by proteins, the high surface viscosity appears to be a dominant stabilizing factor[117,276]. On the other hand, many of the common defoaming agents such as 2-ethylhexanol or methylisobutylcarbinal will have very low surface viscosities. Ellison and Zisman[15] then proposed that the defoaming ability of the polydimethylsiloxanes in both aqueous and non-aqueous systems is due to

(i) the ability of the polydimethylsiloxane monolayers to adsorb at the liquid/gas interface and displace the previously adsorbed foam-stabilizing materials; and

(ii) the inability of the polydimethylsiloxane monolayers to increase the viscosity of the water/air or organic liquid/air interfaces.

Based on the results from the canal viscometer, the viscosities were as low as 10^{-5} surface poise (see Tables 10.24 and 10.30) and as discussed previously, this reflects the low intermolecular cohesion that is present in polydimethylsiloxane films compared with monolayers of proteins and certain linear synthetic organic polymers[269].

No data were obtained for the surface elasticity and viscosity of some smaller fatty acid molecules at pressures up to $25mNm^{-1}$, due to the sensitivity of the instrument. The amplitude of the ring needs to be very low to ensure a linear viscoelastic behaviour, though this may affect the accuracy of the readings as a whole. At surface pressures greater than $25mNm^{-1}$, a resonant frequency could not be attained for the oscillating ring, resulting in the collapse and dissolution of the film. Thus, the films start to collapse before the end of the experimental timescale.

Monquin and Rideal[288] have carried out the determination of the coefficient of rigidity for solid unimolecular films. The value of $4.9 \times 10^{7}mNm^{-1}$ was obtained for palmitic and stearic acids using a rotating disk elastometer. Trapeznikov and Zotova[289] have also obtained G_s^* and η_s measurements for saponin films adsorbed at both water/air and oil/water interfaces.

The surface viscosity values obtained here for $C_{18}H_{37}COOH$ and $C_{19}H_{39}COOH$ using the oscillating ring viscometer compare favourably with

those obtained with the torsion pendulum surface viscometer at $\pi = 10 mNm^{-1}$.

It appears that the difficulty expressed in not obtaining data for polydimethylsiloxane monolayers while using the torsion pendulum surface viscometer is due to its lack of sensitivity. However, it is the fluidity and unstructured nature (i.e. no rigidity) of these polymeric molecules that enables them to move to the foaming interfaces rapidly, whereby their antifoaming properties are exerted. The ability of a polydimethylsiloxane to enter the liquid/gas interface and spread in a developing foam system is determined by a combination of surface and interfacial tensions. If both the entering and spreading coefficients have positive values (see Section 4.4), then the polydimethylsiloxane with low surface tension and interfacial tension with oils is ideally suited to enter and spread in the foam system on a molecular level. When it spreads, it carries with it a quantity of the medium of considerable thickness to increase film drainage, disrupt the Marangoni or 'self-heal' effect, and cause foam rupture.

From the antifoaming tests performed initially on single polydimethylsiloxanes and later on a mixture of two polydimethylsiloxanes with various molar-proportions, dissolved in a variety of crude oils, it was evident that polydimethylsiloxane <31000> (albeit surprisingly) emerged as the best antifoamer in the Model crude oil (see Figures 10.61 and 10.62); whilst, with the Offshore crude oils, a trend of the "larger the polydimethylsiloxane the more effective it is as antifoamer" was followed (see Figures 10.60, 10.65 and 10.66). Looking at the plot of surface viscosity against weight-average molecular weight (see Figure 10.43) for single polydimethylsiloxanes, one can see that the viscosity decreases as the molecular weight increases as far as $\overline{M}_w$ = <31000>, where it then remains fairly constant for the other large polydimethyl-

siloxanes. This may indicate that $\overline{M}_w$: <31000>, <48150> and <110000> all behave quite closely as antifoamers, and this has been partly supported by the antifoaming test results.

The antifoaming tests for the different mixtures of polydimethylsiloxanes showed $<M_{3C}>$ to be the best mixture antifoamer in both the Model and Offshore crude oils (see Figures 10.67 and 10.68). This observation is well supported by the low surface viscosity value observed for that particular mixture. Imposing the plot of the surface viscosity against the calculated weight-average molecular weight[258] of the mixtures on that for the single polydimethylsiloxanes (as shown in Figure 10.43) results in the observation that the surface viscosity follows the decreasing trend with increasing molecular weight of the M_2 mixtures, although it behaves in an opposite fashion with the M_3 mixtures, in which the surface viscosity begins to rise - perhaps indicating a more viscous film, i.e. a non-ideal mixture.

These tests support the earlier conclusion that good antifoamers have unusually low surface viscosities with the larger polydimethylsiloxanes or M_3 mixtures probably not mixing completely[42], and therefore are able to displace the less-strongly adsorbed foam-stabilising materials[20].

An interesting plot of the surface pressure-surface area isotherm of HO-C_{16}-OH (1.16 hexadecanol) showed similar features both in the shape of its isotherm and also its behaviour on the surface of pure water, to polydimethylsiloxane monolayers. Figures 10.70 and 10.71 show the π-A isotherms obtained for 1.16 hexadecanol and a typical long-chain alcohol, 1-hexadecanol. Figure 10.70 shows a similar curve to that of a typical polydimethylsiloxane monolayer (see Figure 2.8), with a plateau-type

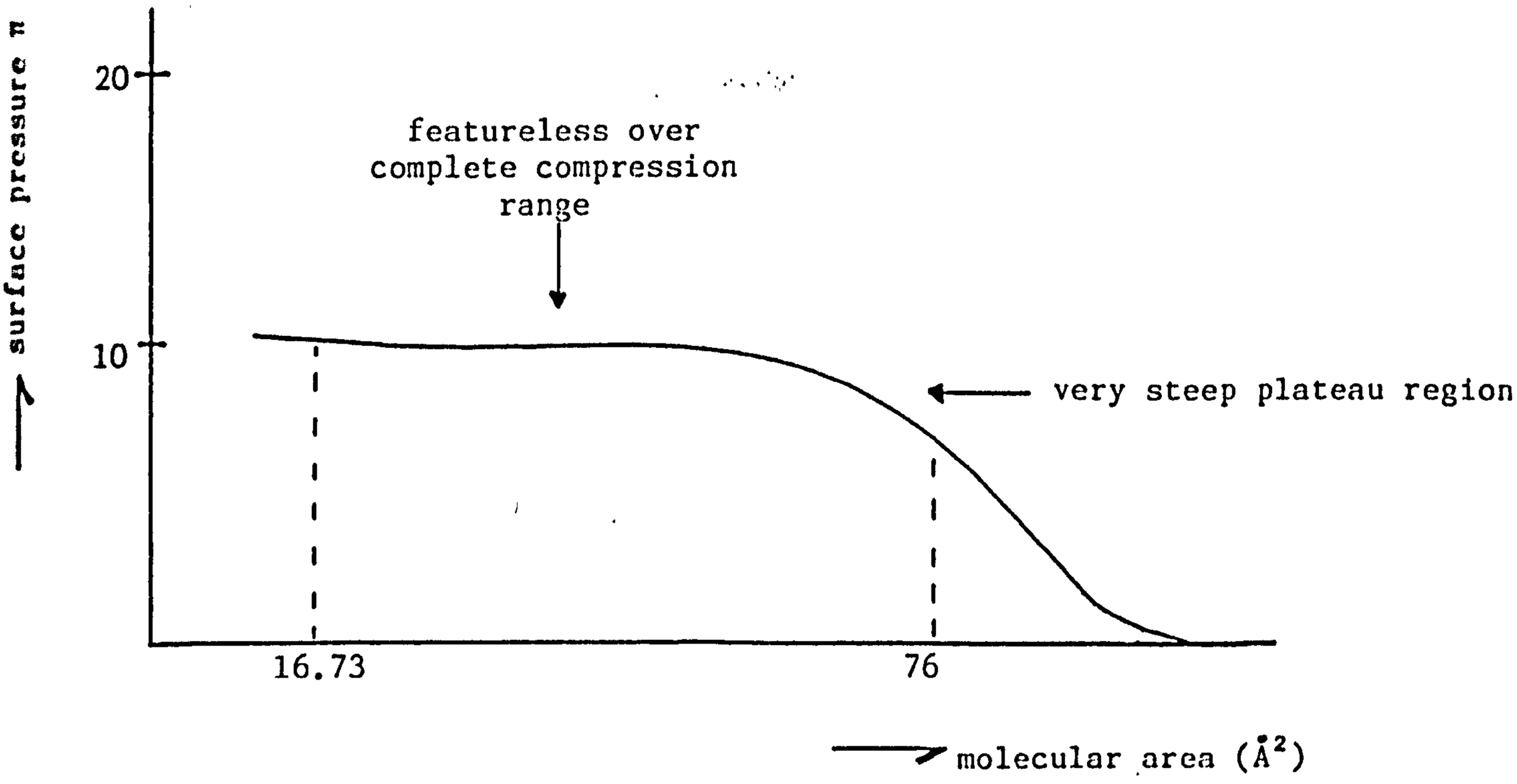

FIGURE 10.70: The π–A isotherm of 1.16 hexadecanol (not drawn to scale)
pH ~ 2.60; T_b = 20.5 ± 0.01°C; subphase = 0.01M HCl

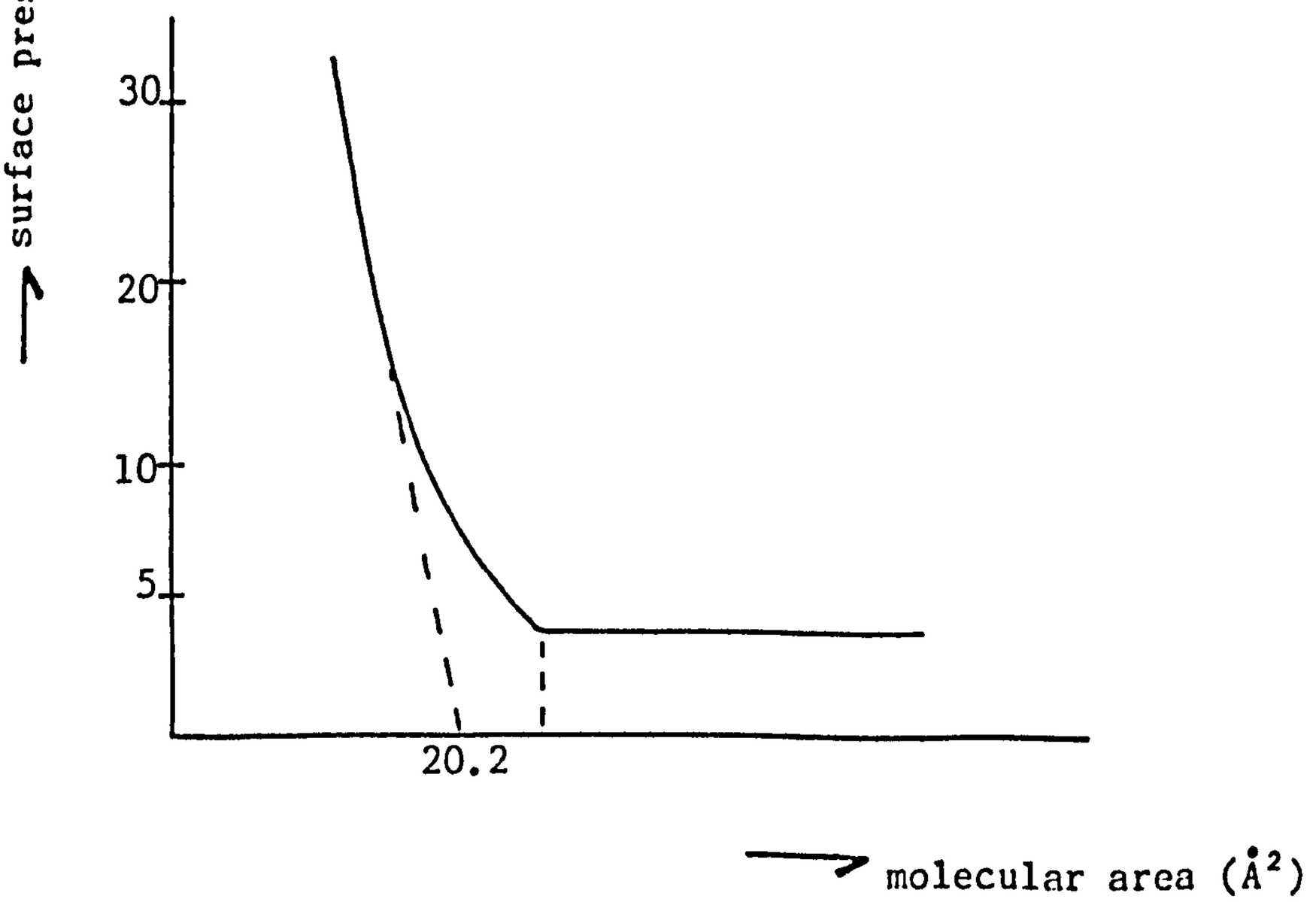

FIGURE 10.71: The π–A isotherm of a typical long-chain alcohol, such as 1-hexadecanol. pH ~ 2.60; T_b = 20.5 ± 0.01°C; subphase = 0.01M HCl

region evident at 10.2mNm^{-1} and then starting to level out at an area per molecule of 76.68Å^2. Here, the 2-OH groups in the molecule anchor to the surface, and coil up with further compression of the film. When the coiled-up structure of the molecule is fully closed, some signs of upturn occur at $\tilde{A}_m$ = 16.73Å^2. Another similar feature of this molecule to those of polydimethylsiloxanes is the absence of collapsed material on the surface. No work has been reported on the surface nature of 1.16 hexadecanol, or of its distinct similarity in behaviour to polydimethyl-siloxanes at the air/water interface.

CHAPTER 11

CONCLUSIONS AND FURTHER WORK

The basis of this work was a study of the surface rheological properties of polydimethylsiloxane monolayers in order to relate these to their unique antifoaming ability.

The film balance developed by Joyce-Loebl had an essential characteristic, in that it worked fully automatically and recorded continuously, so that fine details of the pressure-area curves were easily obtained reproducibly. The measurements were made initially on 'simple fatty acid molecules', to test the workability of the instruments, and later with a series of linear polydimethylsiloxanes. These molecules were measured at the air/water interface, though it had been hoped that studies could be made at the air/oil and oil/water interfaces.

The SSE Mk 2 surface rheometer enabled rheological parameters such as surface shear modulus, creep compliance and viscous relaxation time to be measured. The surface shear modulus gives the surface shear rigidity of the monolayer, whilst a Langmuir trough gives the compressional modulus. A measurement of both the surface shear and compressional moduli gives information on the two fundamental surface parameters, namely: the surface Young's modulus and surface Poisson's ratio[224]. For example, $C_{22}H_{45}COOH$ at $30mNm^{-1}$, and using the equations relating all four parameters (see Section 3.2.2), $k_s \sim 500mNm^{-1}$, $G_s' = 17mNm^{-1}$, $Y = 65.76mNm^{-1}$ and $\mu = +0.934$ ($f_o = 3.3235Hz$). Further work with the instrument may include obtaining the loss and storage components of the surface shear modulus at various frequencies and the evaluation of the relaxation spectra for each monolayer. The relaxation spectra describe the relaxation processes occurring in the monolayer when it is subjected to a shear stress.

Future work may also include a development of a statistical mechanical treatment of the monolayer, of which two fundamental properties are required:

(i) the radial distribution function, g(r), of the monolayer;

(ii) the interaction potential, V(r), between the two molecules at the surface.

Whereas g(r) may be obtained from scattering experiments via the structure factor, S(Q), V(r) has to be modelled theoretically from a consideration of relevant forces operating at the surface, e.g. hydrogen bonding, dispersion and electrostatic forces. The interaction potential may be found by using a perturbation theory[274], V(r) being split up into a reference potential, $V_o(r)$ and a perturbation on that potential dependent on r, $V_p(r)$. The knowledge of both g(r) and V(r) allows the modelling of the monolayer plus the derivation of parameters such as the shear modulus and the zero shear viscosity[275]. Further, any change in subphase conditions, i.e. temperature, ionic strength or pH, would influence V(r) and so predictions made about changes in the isotherm.

The overall performance of the Deer (Series III) rheometer in its role as a surface rheometer proved inconclusive, in that although the instrument had already proved capable of bulk rheological measurements, its use in two-dimensional surface rheology has been beset with electronic problems. In comparison, the pulsed-drop tensiometer only requires an efficient pressure transducer and computational interface to render it capable of measuring dilational properties of surfactants.

However, it must be said that the present investigation does show some conclusive surface rheological measurements of polydimethylsiloxanes, comparable to those reported in the literature[10,11,89], at the air/

water interface for similar polymers, but of varying weight-average molecular weights. These results do indicate that the films were extremely stable and reversible, where no well-defined collapse pressures were observed. It may also be concluded that polydimethylsiloxanes are subject to degradation by water, especially in the presence of dilute or concentrated acid or base. For the rate of degradation to be appreciable, however, there must be a large interface between the polydimethylsiloxane and the water, as is the case on a film balance. Such an interface may be present in an emulsion, aerosol, or porous polymeric form.

The investigation of insoluble monolayers of polydimethylsiloxanes on a variety of organic liquids is likely to give further information on the stability of the films and their effect on the surface tension and solubility in the substrates, whereby a comparison can be made of the difference in behaviour between the monolayers adsorbed on polar and non-polar substrates.

It has been shown that the antifoaming ability of an 'antifoamer' can be measured quantitatively by a simple modified Bikerman method. However, the low performances of the larger polydimethylsiloxane molecules in 'Model' crude oil may have been caused by their inability to disperse in a more viscous oil. Also, the synergistic effect of mixtures of various polydimethylsiloxane monolayers was generally disappointing in their combined effect as 'antifoamers'. Hence, polydimethylsiloxanes form very fluid films in which the molecules slip over one another, whereby no structure is formed. With extremely low surface viscosities and no detectable surface elasticity present at the various surface pressures, these may in part explain their antifoaming and defoaming properties.

Polydimethylsiloxanes may form useful model systems for the investigation of non-aqueous foaming surfaces. It may be possible to correlate surface activity with rupture thickness and foam lifetimes when measured as a function of molecular weight and concentration. Also, if more information can be obtained on the structure of the fluorocarbon FC740, the appropriate study might give an insight into why it behaves as a profoamer.

A broadening of the surface-active applications of polydimethylsiloxanes is expected in the near future. This, combined with their excellent thermal stability, should lead to applications in oil drilling, recovery and processing as wells become deeper and hotter and the push is on to recover more oil from a reservoir.

REFERENCES

1. E.G. Schwarz and W.E. Reid, Ind. Eng. Chem., 56, 26 (1964).

2. R.L. Bass, Chem. Ind. (Lond.), 912 (1959).

3. A.G. Brown, W.C. Thuman and J.C. Mcbain, J. Coll. Sci., 8, 491 (1953).

4. M. Van den Tempel, F. Van Voorst Vader and R.M. Jonkman, 'Foams and Free Liquid Films', ed. by J.A. Kitchener, 1961.

5. B. Stuke, Chem. Eng. Tech., 33, 173 (1961).

6. F.C. Goodrich, Proc. Roy. Soc., A260, 481, 490, 503 (1961).

7. W. Noll, 'Chemistry and Technology of Silicones', Acad. Press Inc., New York, 1968.

8. R.S. Bhute, J. Sci. Ind. Res. (India), 30, 5, 241 (1971).

9. M.J. Owen, Ind. Eng. Chem. Prod. Res. Dev., 19, 97 (1980).

10. P.G. Pape, J. Pet. Tech., 1197 (1983).

11. H.W. Fox, P.W. Taylor and W.A. Zisman, Ind. Eng. Chem., 39, 1401 (1949).

12. W. Noll, H. Steinbach and Chr. Sucker, J. Polymer Sci., C34, 123 (1971).

13. A.V. Tobolsky, 'Properties and Structure of Polymers', John Wiley and Sons, New York, 67 (1960).

14. B. Kanner, W.G. Reid and H. Petersen, Ind. Eng. Chem. Prod. Res. Dev., 6, 8 (1967).

15. A.H. Ellison and W.A. Zisman, J. Phys. Chem., 60, 416 (1956).

16. W.H. Banks, Proc. Int. Cong. Surf. Act. 2nd Lond., 1, 16 (1957).

17. W. Noll, H. Steinbach and Chr. Sucker, Kolloid-z., 204, 94 (1965).

18. H.W. Fox and W.A. Zisman, Rev. Sci. Inst., 19, 274 (1948).

19. A.A. Trapeznikov, T.I. Zatsepma, T.A. Gracheva, R.N. Shcherbakova and V.A. Ogarev., Proc. Acad. Sci. Phys. Chem. Section (USSR), 160, 174 (1965).

20. N.L. Jarvis, J. Phys. Chem., 70, 3027 (1966).

21. G.C. Nutting and W.D. Harkins, J. Am. Chem. Soc., 62, 3155 (1940).

22. G.E. Boyd and F. Vaslow, J. Coll. Sci., 13, 275 (1958).

23. I. Langmuir, J. Am. Chem. Soc., 39, 1848 (1917).

24. F.C. Goodrich, 'The Thermodynamics of Fluid Interfaces', in Surf. Coll. Sci., Vol. I, Wiley-Interscience, New York, 1969, p.1.

25. A. Cary and E.K. Rideal, Proc. Roy. Soc. (Lon.) Ser. A., 109, 318 (1925).

26. G.E. Boyd and J. Schubert, J. Phys. Chem., 61, 1271 (1957).

27. A.E. Alexander and F.C. Goodrich, J. Coll. Sci., 19, 473 (1964).

28. W.D. Harkins, T.F. Young and G.E. Boyd, J. Phys. Chem., 8, 954 (1940).

29. N.K. Adam, 'Physics and Chemistry of Surfaces', Oxford University Press, 1941.

30. L. Ter-Minassian-Saraga, J. Chim. Phys., 52, 80, 99, 181 (1955).

31. A.E. Alexander and T. Teorell, Trans. Far. Soc., 35, 727 (1939).

32. J.T. Davies, Trans. Far. Soc., 48, 1052 (1952).

33. H.D. Cook and H.E. Reis Jr., J. Am. Chem. Soc., 81, 501 (1958).

34. W.D. Harkins, 'The Physical Chemistry of Surface Films', Reinhold Press, New York, 1952, Chapter 2.

35. J. Frenkel, 'Kinetic Theory of Liquids', Oxford University Press, 1946, p.5.

36. R. Merigoux, Compt. Rend., 202, 2049 (1936).

37. R. Merigoux, Compt. Rend., 203, 848 (1936).

38. D.G. Dervichian, J. Chem. Phys., 7, 931 (1939).

39. M. Joly, 'Surface Chemistry', Butterworths, London, 1949, p.37.

40. M. Joly, J. Coll. Sci., 5, 49 (1950).

41. B. Kamiénski, Bull. Acad. Polon. Sci. Ser., 13, 231 (1965).

42. N.K. Adam and G. Jessop, Proc. Roy. Soc. (Lond.)., A110, 423 (1926).

43. I. Langmuir, J. Chem. Phys., 1, 756 (1933).

44. W. Harkins, 'Physical Chemistry of Surface Films', 1941, p.106.

45. W.M. Lee, R.R. Stomberg and J.L. Shereshefsky, J. Res. Natl. Bur. Std., 66A, 439 (1962).

46. H.E. Ries Jr., N. Beredjick and J. Gabor, Nature, 186, 883 (1960).

47. See 'Surface Phenomena in Chemistry and Biology', J.F. Danielli, K.G.A. Pankhurst and A.C. Ruddiford (eds), Pergamon Press, New York, 1958.

48. F.M. Fowkes, J. Phys. Chem., 68, 3515 (1964).

49. M.J. Hunter, M.S. Gordon, A.J. Barry, J.F. Hyde and R.D. Heidenreich, Ind. Eng. Chem., 39, 1389 (1947).

50. M. Reiner and G.W. Scott Blair, 'Rheology, Theory and Applications', Ed. F.R. Eirich, Vol. 4, Academic Press, 1967.

51. J.W. Goodwin, in 'Surfactants', ed. Th. F. Tadvos, Academic Press, 1984.

52. J.W. Goodwin, Lecture Course V, M.Sc. Surface Chemistry and Colloids, Bristol University (1982-83).

53. A.W. Adamson, 'Physical Chemistry of Surfaces', 2nd Ed., Interscience Publishers, New York, 1967.

54. M. Van der Tempel, Trans. Far. Soc., 60, 1170 (1964).

55. D.G. Dervichian and M. Joly, J. Phys. Radium., 10, 375 (1939).

56. V.L. Schneider, R.T. Holman and G.O. Burr, J. Phys. and Coll. Chem., 53, 1016 (1949).

57. M. Reiner, 'Rhéologie Théorique', Dunod, Paris, 1955.

58. N.W. Tschoegl, J. Coll. Sci., 13, 500 (1958).

59. J. Jaffe and J.M. Loutz, J. Poly. Sci., 29, 381 (1958).

60. N.W. Tschoegl and A.E. Alexander, J. Coll. Int. Sci., 15, 168 (1960).

61. F. van Voorst Vader, Th. F. Erkens and M. van den Tempel, Trans. Far. Soc., 60, 1170 (1964).

62. L. Ter-Minassian-Saraga, I. Panaiotov and J.S. Abitboul, J. Coll. Sci., 72, 54 (1979).

63. S.E. Bresler, B.A. Talmund and D.L. Talmund, Physik Z. Sovietunion, 4, 864 (1933).

64. W.D. Harkins and R.J. Myers, Nature, 140, 465 (1937).

65. M. Joly, J. Phys. Radium, 8, 471 (1937).

66. W.E. Ewers and R.A. Sack, Nature, 168, 964 (1951).

67. R.J. Myers and W.D. Harkins, J. Chem. Phys., 5, 601 (1937).

68. W.E. Ewers and R.A. Sack, Austr. J. Chem., 7, 40 (1954).

69. J.T. Davies and G.R. Mayers, Trans. Far. Soc., 56, 691 (1960).

70. M. Joly, J. Phys. Radium, 9, 345 (1938).

71. J.T. Hermans, Physica., 6, 313 (1939).

72. G.L. Gaines Jr., 'Insoluble Monolayers at Liquid-Gas Interface', Interscience, New York, 1966.

73. N.W. Tschoegl, Kolloid-Z., 181, 19 (1962).

74. R.J. Mannheimer and R.S. Schechter, J. Coll. Int.Sci., 32, 225 (1970) and preceding papers.

75. F.C. Goodrich, L.H. Allen and A. Poskanzer, J. Coll. Int. Sci., 52, 201 (1975).

76. F.C. Goodrich and D.W. Goupil, J. Coll. Int. Sci., 75, 590 (1980).

77. D.T. Wasan , A.J. Pinter and A.B. Israel, J. Coll. Int. Sci., 37, 52 (1971).

78. M. Blanck and J.S. Britten, J. Coll. Sci., 20, 789 (1965).

79. R.H. Ewell and H. Eyring, J. Chem. Phys., 5, 726 (1937).

80. W.J. Moore and H. Eyring, J. Chem. Phys., 6, 391 (1938).

81. J. Frenkel, Trans. Far. Soc., 33, 58 (1937).

82. M. Joly, J. Coll. Sci., 11, 519 (1956).

83. M. Joly, J. Coll. Sci., 5, 49 (1950).

84. N.K. Adam, 'The Physics and Chemistry of Surfaces', p.303.

85. J.T. Davies and E.K. Rideal, Can. J. Chem., 33, 947 (1955).

86. J.H. Schulman and E.K. Rideal, Proc. Roy. Soc. (Lond.)., A130, 259 (1931).

87. J.T. Davies, Proc. Roy. Soc. (Lond.)., A208, 224 (1951).

88. J.H. Schulman and A.H. Hughes, Proc. Roy. Soc. (Lond.)., A138, 430 (1932).

89. N.K. Adam and J.B. Harding, Proc. Roy. Soc. (Lond.), A138, 411 (1932).

90. W.D. Harkins and E.K. Fischer, J. Chem. Phys., 1, 852 (1933).

91. A. Volta, Ann. Chem. Phys., 40, 225 (1801), cited by Adam, 'Physics and Chemistry of Surfaces', p.308.

92. Lord Kelvin, Phil. Mag., 46, 91 (1898).

93. H.G. Yasmins and W.A. Zisman, J. Chem. Phys., 1, 656 (1933).

94. E.G. King, J. Phys. Chem., 48, 141 (1944).

95. B.Y. Teitelbaum, Kolloid-nyi-Zhv., 12, 375 (1950).

96. J.V. Robinson and W.W. Woods, J. Phys. & Coll. Chem., 52, 763 (1948).

97. A.P. Brady and S.J. Ross, J. Am. Chem. Soc., 66, 1348 (1944).

98. J.W. Mcbain and J.V. Robinson, Nat. Adv. Comm. Aero. Tech. Note No. 1844 (1949).

99. S.J. Ross and R.M. Haak, J. Phys. Chem., 62, 1260 (1958).

100. R.J. Manheimer and R.S. Schecter, J. Coll. Int. Sci., 32, 212 (1970).

101. A. Scheludko and E. Manev, Trans. Far. Soc., 64, 1123 (1968).

102. R.J. Mannheimer, A. I. Chem. Eng. J., 15, 88 (1969).

103. I.C. Callaghan and E.L. Neustadter, Chem. Ind. p.53 (1981).

104. I.C. Callaghan, C.M. Gould, R.J. Hamilton and E.L. Neustadter, Colloids and Surfaces, 8, 17 (1983).

105. S.J. Ross and J.W. Mcbain, Ind. Eng. Chem., 36, 570 (1944).

106. J.W. Gibbs, Collected Works Vol. 1, Longmans, Green, New York, 1931, pp.287, 301, 307.

107. S.J. Ross, 'Mechanisms of Foam Stabilization and Antifoaming Action', Chem. Eng. Prog., 63, 41 (1967).

108. B.V. Derjaguin and A.S. Titierskaya, 'Status and Kinetic Stability of Free Films and Froths', Proc. 2nd Intl. Cong. on Surface Activity, Butterworth's Scientific Publications, London, 1, 211 (1957).

109. N.A. Aleinikov, Tsetn Metal., 6, 1546 (1931).

110. J.J. Bikerman, Trans. Far. Soc., 34, 638 (1938).

111. G.C. Clark and S.J. Ross, Ind. Eng. Chem., 32, 1594 (1940).

112. S.J. Ross and G.D. Miles, Oil Soap, 18, 99 (1941).

113. S. Okasaki and S. Sasaki, Tenside., 3, 115 (1966).

114. A. Sabiba, Chem. Eng. Prog., 62(5), 112 (1966).

115. J.W. Robinson and W.W. Woods, J. Soc. Chem. Ind., 67, 361 (1948).

116. W.D. Harkins, 'The General Thermodynamic Theory of the Spreading Liquids', J. Chem. Phys., 9, 552 (1941).

117. W.D. Ewers and K.L. Sutherland, 'The Role of Surface Transport in the Stability and Breakdown of Foams', Aust. J. Sci. Res., A5, 697 (1952).

118. L.T. Sheaver and N.W. Akers, J. Phys. Chem., 62, 1264 (1958).

119. C.E. Trautman, Lubricating Eng., 2, 4, 143 (1946).

120. A.L. Jacoby, J. Phys. & Coll. Chem., 52, 689 (1948).

121. R.D. Kulkarni, E.D. Goddard and B. Kanner, Ind. Eng. Chem. Fund., 16, 472 (1977); S.J. Ross and G. Nishioka in 'Emulsions, Latices and Dispersions', P. Becher and Y.N. Yudenfreund (eds), Marcel Dekker, New York, p.237 (1978).

122. M.J. Hunter, E.L. Warwick, J.F. Hyde and C.C. Currie, J. Am. Chem. Soc., 68, 2284 (1946).

123. J.B. Plumb and J.H. Atherton, in 'Block Polymers', D.C. Allport and W.H. Janes (eds), Applied Science, London, 1973.

124. A.J. Barry, J. App. Phys., 17, 1020 (1946).

125. E.L. Warwick, M.J. Hunter and A.J. Barry, Ind. Eng. Chem., 44, 2196 (1952).

126. M.T. Owen, Chem. Tech. (Washington), 11(5), 288 (1981).

127. Deutsche Industrie Norm (DIN), 53902, Teil, 1 (1981).

128. H.W. Fox, E.M. Solomon and W.A. Zisman, J. Phys. & Coll. Chem., 54, 723 (1950).

129. W. Noll, Pure & App. Chem., 13, 101 (1966).

130. W. Noll, Kolloid-z u-z Polymere., 211, 98 (1966).

131. W. Noll, H. Stembach and Chr. Sucker, Ber. Bun. Phys. Chemie., 67, 407 (1965).

132. W. Noll, H. Steinbach and Chr. Sucker, Kolloid-z u-z Polymere., 236, 1 (1970).

133. W. Noll, H. Steinbach and Chr. Sucker, Kolloid-z u-z Polymere., 243, 110 (1971).

134. V.V. Arslanov and V.A. Ogarev, Doklady Academii, Nauk, SSSR, 196(5), 1105 (1971).

135. W.H. Banks, Nature, 174, 365 (1954).

136. N.L. Jarvis, J. Coll & Int. Sci., 29, 647 (1969).

137. W.D. Garett and W.A. Zisman, 'Damping of Capillary Waves by Monomolecular Layers of Linear Polydimethylsiloxanes', presented at the 150th Nat. Meet. Am. Chem. Soc., Coll. & Surf. Chem. Div., New Jersey, September 16, 1965.

138. R.L. Schuler and W.A. Zisman, J. Phys. Chem., 79, 1397 (1973).

139. W.H. Keesom, Z. Physik., 22, 129 (1921).

140. P. Debye, Z. Physik., 21, 178 (1920) and 22, 302 (1921).

141. F. London, Z. Physik., 63, 245 (1930).

142. D. Tabor, 'Gases, Liquids and Solids', Penguin, 1969.

143. H.G.B. Casimir and D. Polder, Physics Review, 73, 360 (1948).

144. H. Kallman and M. Willstatter, Naturwiss., 20, 952 (1932).

145. R.S. Bradley, Phil. Mag., 13, 853 (1932).

146. H.C. Hamaker, Physica., 4, 1058 (1937).

147. J.H. de Boer, Trans. Far. Soc., 32, 10 (1936).

148. E.J.W. Verwey and J. Th. G. Overbeek, 'The Theory of the Stability of Lyophobic Colloids', Elsevier, 1948.

149. J. Th. G. Overbeek, in 'Colloid Science', Vol. 1, ed. R. Kruyt, Elsevier, Amsterdam, 1952.

150. R.J. Hunter, Aust. J. Chem., 16, 774 (1963).

151. J.H. Schenkel and J.A. Kitchener, Trans. Far. Soc., 56, 161 (1960).

152. E.J. Clayfield, E.C. Lumb and P.H. Mackay, J. Coll. & Int. Sci., 37, 382 (1971).

153. J. Gregory, Adv. Coll. & Int. Sci., 2, 396 (1969).

154. J. Visser, Adv. Coll. & Int. Sci., 3, 331 (1972).

155. R. Eisenschitz and F. London, Z. Physick., 60, 491 (1930).

156. B. Vincent, J. Coll. & Int. Sci., 42, 270 (1973).

157. M.J. Vold, J. Coll. Sci., 16, 1 (1961).

158. E.M. Lifshitz, Soviet Phys., JETP, 2, 73 (1956).

159. B.V. Derjaguin, I.I. Abrikossova and E.M. Lifshitz, Quart. Revs., 10, 295 (1956).

160. H. Krupp, Adv. Coll. Int. Sci., 1, 111 (1967).

161. B.R.A. Njiboer and M.J. Renne, Chem. Phys. Lett., 1, 317 (1967).

162. B.R.A. Njiboer and M.J. Renne, Chem. Phys. Lett., 2, 35 (1968).

163. A.D. MacLachlan, Proc. Roy. Soc. (Ser. A), 271, 387 (1963) and 274, 80 (1963).

164. J.A. Kitchener and A.P. Prosser, Proc. Roy. Soc. (Ser. A), 242, 403 (1957).

165. J.Th.G. Overbeek and M.J. Sparnay, Dis. Far. Soc., 18, 12 (1954).

166. W. Black, J.G.V. de Jongh, J.Th.G. Overbeek and M.J. Sparnay, Trans. Far. Soc., 56, 1597 (1960).

167. D. Tabor and R.H.S. Winterton, Proc. Roy. Soc. (Ser. A)., 312, 435 (1969).

168. G.C.J. Rouweler and J.Th.G. Overbeek, Trans. Far. Soc., 67, 2117 (1971).

169. J.N. Israelachvili and D. Tabor, Proc. Roy. Soc. (Ser. A)., 331, 19 (1972).

170. J.N. Israelachvili and D. Tabor, in 'Prog. in Surf. and Mem. Sci.', ed. J.F. Danielli, M.D. Rosenberg and D.A. Cadenhead, Academic Press, Vol. 7, 1973.

171. G. Gouy, J. Physique, 9, 457 (1910).

172. G. Gouy, Ann. Physique, 7, 129 (1917).

173. D.L. Chapman, Phil. Mag., 25, 475 (1913).

174. P. Debye and E. Hückel, Z. Physik., 24, 185 (1923).

175. P. Debye, Z. Physik., 25, 93 (1924).

176. K. Mysels, 'Introduction to Colloid Chemistry', Interscience, 1959.

177. O. Stern, Z. Electrochem., 30, 508 (1924).

178. D.C. Graham, Chem. Revs., 41, 441 (1947).

179. I. Langmuir, J. Chem. Phys., 6, 893 (1938).

180. J. Lyklema, Adv. Coll. Int. Sci., 2, 39 (1968).

181. E.L. Mackor, J. Coll. Sci., 6, 492 (1951).

182. E.L. Mackor and J.H. van der Waals, J. Coll. Sci., 7, 535 (1952).

183. B. Vincent, Adv. Coll. Int. Sci., 4, 193 (1974).

184. E.W. Fischer, Kolloid-z., 160, 120 (1958).

185. R.H. Ottewill, in 'Non-Ionic Surfactants' ed. M. Schick and M. Dekker, New York, 1967, Chapter 19.

186. R.H. Ottewill and T. Walker, Kolloid-z., 227, 108 (1968).

187. e.g. W.J. Moore, 'Physical Chemistry', Longmans (4th Ed.), 1968.

188. D.H. Napper, Ind. Eng. Chem. Prod. Res. Dev., 9, 467 (1970).

189. E.J. Clayfield and E.C. Lumb, J. Coll. Int. Sci., 22, 269 (1966).

190. D.J. Meier, J. Phys. Chem., 71, 1861 (1967).

191. D.A. Haydon, J. Am. Oil. Chem. Soc., 45, 230 (1968).

192. D.A. Haydon and J.L. Taylor, Nature, 217, 739 (1968).

193. D. Exerowa, I.B. Ivanov and A. Scheludko, in 'Research in Surface Forces', ed. B.V. Derjaguin, Consultants Bureau, New York, Vol. 2, p.144.

194. J.S. Clunie, J.F. Goodman and B.T. Ingram, in 'Surface and Colloid Science', ed. E. Matijević, Wiley-Interscience, Vol. 3, 1971.

195. B.V. Derjaguin and M. Kussakov, Acta. Physica Chem., USSR, 10, 25 (1939).

196. R. Buscall and R.H. Ottewill, in 'Colloid Science', ed. D.H. Everett, Specialist Periodical Report of Chemical Society, London, Vol. 2, 1975.

197. B.V. Derjaguin, Coll. J. (USSR), 17, 19 (1955).

198. e.g. J.M. Kay, 'An Introduction to Fluid Mechanics and Heat Transfer', Cambridge University Press, 2nd Edition, 1968.

199. A. Scheludko and D. Platikanov, Kolloid-z., 175, 150 (1961).

200. O. Reynolds, Phil. Trans. Roy. Soc., 177, 157 (1886).

201. K.J. Mysels, K. Shinoda and S. Frankel, 'Soap Films', Pergamon Press (1959).

202. W. Johannes and S. Whitaker, J. Phys. Chem., 69, 1471 (1965).

203. J.Th.G. Overbeek, J. Phys. Chem., 64, 1178 (1960).

204. A.J. de Vries, Rec. Trav. Chem., 77, 383 (1958).

205. A. Vrij, J. Coll. Sci., 19, 1 (1964).

206. A. Scheludko, Prov. Kon. Ned. Akad. Wet., 65B, 87 (1962).

207. A. Vrij, Dis. Far. Soc., 42, 23 (1966).

208. A. Vrij and J.Th.G. Overbeek, J. Am. Chem. Soc., 90, 3074 (1968).

209. E. Ruckenstein and R.K. Jain, J. Chem. Soc. Far., 11, 70, 132 (1974).

210. R.K. Jain and E. Ruckenstein, J. Coll. Int. Sci., 54, 108 (1976).

211. R.J. Gumerman and G.M. Hormsy, Chem. Eng. Commun., 2(1), pp.27-36.

212. I.B. Ivanov, B. Radoev, E. Manev and A. Scheludko, Trans. Far. Soc., 66, 1262 (1970).

213. I.B. Ivanov, B.P. Radoev, E.D. Manev and A.D. Scheludko, God. Sofii, Univ, Khim. Fak., 64, 363 (1969-70).

214. B. Radoev, E. Manev and I. Ivanov, Kolloid-z., 234, 1037 (1969).

215. B. Radoev, D.S. Dimitrov and I.B. Ivanov, Coll. Polym. Sci., 252, 50 (1974).

216. I.B. Ivanov and D.S. Dimitrov, Coll. Polym. Sci., 252, 982 (1974).

217. J. Lucassen, M. van den Tempel, A. Vrij and F.Th. Hesselink, Proc. Kon. Ned. Akad. Wet., 73B, 109 (1970).

218. A. Vrij, F.Th. Hesselink, J. Lucassen and M. van den Tempel, Proc. Kon. Ned. Akad. Wet., 73B, 124 (1970).

219. B. Vincent, in 'Surfactants', ed. Th.F. Tadros, Academic Press, London, 1984, p.175.

220. W. Harkins and J.G. Kirkwood , J. Chem. Phys., 6, 53 (1933) and J. Chem. Phys., 6, 298 (1938).

221. R.J. Myers and W.D. Harkins, ibid., 5, 601 (1937).

222. L. Fourt and W.D. Harkins, J. Phys. Chem., 42, 897 (1938).

223. M. Joly, J. Chim. Phys., 44, 206 (1947).

224. A. Dinsdale and F. Moore, 'Viscosity and Its Measurements', Inst. Phys. and Phys. Soc., (monographs for students).

225. D.E. Graham, T.J. Jones, E.L. Neustadter and K.P. Whittingham, 'Interfacial Rheological Properties of Crude Oil-Water Systems', 3rd Int. Conf. Surf. and Coll. Sci., Stockholm, Plenum Press, 1979.

226. J.H. Clint, E.L. Neustadter and T.J. Jones, Dev. Pet. Sci., 13 (EOR), p.135, 1981.

227. A.P. Goodall, BP Research Centre, Sunbury-on-Thames, Middlesex, 1984.

228. A.F.H. Ward and L. Tordai, J. Chem. Phys., 14, 453 (1946).

229. N.K. Adam, Proc. Roy. Soc. (Lond.)., A101, 452 (1922).

230. N.K. Adam, Proc. Roy. Soc. (Lond.)., A101, 516 (1922).

231. N.K. Adam and G. Jessop, Proc. Roy. Soc. (Lond.)., A112, 362 (1926).

232. G.C. Nutting and W.D. Harkins, J. Am. Chem. Soc., 61, 1180 (1939).

233. J.A. Spink, J. Coll. Sci., 18, 512 (1946).

234. E.D. Goddard, S.R. Smith and O. Kao, J. Coll. Sci., 21, 320 (1966).

235. J. Blodgett, J. Am. Chem. Soc., 57, 1007 (1935).

236. R. Myers and W.D. Harkins, Nature, 139, 367 (1937).

237. J. Mitchell, E.K. Rideal and J.H. Schulman, Nature, 139, 625 (1937).

238. P. Robinson, Nature, 139, 626 (1937).

239. W.D. Harkins and P. Anderson, J. Am. Chem. Soc., 59, 2189 (1937).

240. I. Langmuir and V.J. Schaefer, J. Am. Chem. Soc., 59, 2400 (1937).

241. A. Trapeznikov, Acta. Physicochim., 10, 65 (1939).

242. Wolstenholme and J.H. Schulman, Trans. Far. Soc., 46, 475 (1950) and 47, 788 (1951).

243. T. Sasaki and R. Matuura, Bull. Chem. Soc., (Japan), 24, 274 (1951).

244. J.H. Schulman and M.Z. Dogan, Far. Soc. Dis., 16, 158 (1954).

245. J.A. Spink and J.V. Saunders, Trans. Far. Soc., 51, 1154 (1955).

246. B.M. Abraham, K. Miyano, S.O. Xu and J.B. Ketterson, Rev. Sci. Instr., 54, 213 (1983).

247. M. Buhaenko, M.F. Daniel, J.W. Goodwin and R. Richardson, Thin Solid Films, 134, 217 (1985).

248. N.L. Jarvis, J. Coll. Sci., 69, 1789 (1965).

249. G.E. Boyd and W.D. Harkins, J. Am. Chem. Soc., 61, 1188 (1939).

250. J.H. Schulman and E.K. Rideal, Proc. Roy. Soc. (Lond.), A130, 270 (1931).

251. N.K. Adam, Proc. Roy. Soc. (Lond), A126, 526 (1930).

252. Y. Yamaguchi and S. Mizuno, Bull. Chem. Soc., (Japan), 453, 10 (1933).

253. E.D. Goddard, O. Kao and H.C. Kung, J. Coll. & Int. Sci., 24, 297 (1963).

254. N.W. Addink, J. Chem. Phys., 2, 574 (1934).

255. K.D. Dreher and D.F. Sears, Trans. Far. Soc., 62, 741 (1966).

256. J.T. Davies and E.K. Rideal, 'Interfacial Phenomena', Academic Press, New York, 1963.

257. W. Rabinovitch, R.F. Robertson and S.G. Mason, Can. J. Chem., 38, 1881 (1960).

258. F.N. Billmeyer Jr., 'Textbook of Polymer Science', 2nd Ed., Wiley-Interscience, New York, 1971.

259. International Critical Tables of Numerical Data, Physics, Chemistry and Technology. McGraw-Hill (1933).

260. H.W. Fox, E.M. Solomon and W.A. Zisman, J. Phys. Chem., 54, 723 (1950).

261. M.J. Newing, Trans. Far. Soc., 46, 755 (1950).

263. L. Fourt, J. Phys. Chem., 43, 887 (1939).

264. J. Llopis and A. Albert, Anales. Real. Soc. Espan. Fis. Quim., Ser. B, 55B, 109 (1959).

265. K. Motomura, J. Phys. Chem., 68, 2826 (1964).

266. B. Biswas and D.A. Haydon, Proc. Roy. Soc. (Lond.), A271, 296, 317 (1963).

267. K. Inokuchi, Bull. Chem. Soc. (Japan), 26, 500 (1953); 27, 203 (1954).

268. I. Langmuir and V.J. Schaefer, Chem. Rev., 24, 181 (1939).

269. K. Motomura and R. Matuura, J. Coll. Sci., 18, 295 (1963).

270. G.L. Gaines, Insoluble Films at Air-Water Interface. Wiley-Interscience. New York, p.282, 1966.

271. F. Goodrich, Proc. 2nd Int. Congr. Surf. Act., Vol. 1, ;.85.

272. W.W. Mansfield, Austr. J. Chem., 12, 382 (1959).

273. I.C. Callaghan and C.M. Gould, BP Research Centre, Sunbury-on-Thames, publication in press.

274. R.D. Kulkarni, E.D. Goddard and B. Kanner, J. Coll. Int. Sci., 59, 468 (1977).

275. M. van den Tempel and R.P. van de Riet, J. Chem. Phys., 42, 2769 (1965).

276. J.A. Kitchener and C.F. Cooper, Quart. Rev. (London), 13, 71 (1959).

277. R.W. Zwanzig, J. Chem. Phys., 22, 1420 (1954).

278. S.J. Partridge, Ph.D thesis, University of Bristol (1985).

279. R. Donaldson, Ph.D thesis, University of Bristol (1971).

280. D. Segal, Ph.D thesis, University of Bristol (1977).

281. K.J. Wibberley, Pharm. & Pharmacol., 14, 87T (1962).

282. B. Warburton, Rheo. Acta., 10, 142 (1971).

283. B. Warburton, J. Ions & Macro. Biol. Sys., 29, 273 (1978).

284. J.R. Van Wazer, J. Coll. Sci., 2, 223 (1947).

285. R. Chammadi., D.G. Dervichian and M. Joly, J. Chim. Phys., 47, 883 (1950).

286. S.C. Ellis, A.D. Lanham and K.G.A. Pankhurst, J. Sci. Instr., 32, 70 (1955).

287. M. Buhaenko, Private communication, Bristol University, 1985.

288. H. Monquin and E.K. Rideal, Proc. Roy. Soc. (Lond.), A114, 690 (1927).

289. A.A. Trapeznikov and K.V. Zotova, Kolloidn. Zh., 27, 414 (1965).

290. B.M. Abraham, J.B. Ketterson, K. Miyano and A. Kueny, J. Chem. Phys., 78, 6 (1981).

A P P E N D I C E S

APPENDIX A

The procedure for obtaining the time surface flux, Δs, and surface viscosity, η_s, by a series of approximations, from the Harkins and Kirkwood correction analysis[220] is outlined below:

as $$q = \frac{2a^3}{3\eta}\left[1 + \frac{2a\eta_0}{\pi\eta}\coth\frac{\pi h}{2a}\right]-1$$

(a) If $h \gg 2a$, then $\coth \pi h/2a \to 1$. If $\eta_s \ll 2a\eta_0$, that is, a low viscosity film with

$$\frac{2a\eta_0}{\pi\eta_s} \gg 1 \text{ and } q = \left(\frac{\Delta s}{\Delta\pi}\right)\ell$$

therefore

$$\eta_s = \frac{\Delta\pi}{\Delta s} \times \frac{2}{3} \times \frac{a^3}{\ell} \times \left[\frac{2a\eta_0}{\pi\eta_s}\right]-1$$

or

$$\eta_s = \frac{\Delta\pi}{\Delta s} \times \frac{a^2}{3\ell} \times \frac{\pi\eta_s}{\eta_0}$$

Hence

$$\Delta s = \frac{\pi.\Delta\pi.a^2}{3\ell\eta_0}$$

i.e. flux is independent of η.

(b)

$$\eta_s = \frac{\Delta\pi}{\Delta s} \times \frac{2}{3} \times \frac{a^3}{\ell} \times \left[1 + \frac{2a\eta_0}{\pi\eta_s}\right]-1$$

$$= \frac{\Delta\pi}{\Delta s} \times \frac{2}{3} \times \frac{a^3}{\ell}\left[1 - \frac{2a\eta_0}{\pi\eta_s}\right]$$

To a crude first approximation

$$\eta_s = \frac{\Delta\pi}{\Delta s} \times \frac{2}{3} \times \frac{a^3}{\ell}$$ (Poiseuille formula in two-dimensional - no subphase correction)

therefore

$$\eta_s = \eta_s\left[1 - \frac{2a\eta_0}{\pi\eta_s}\right] = \eta_s - \frac{2a\eta_0}{\pi}$$

resubstituting

$$\eta_s = \frac{\Delta\pi}{\Delta s} \times \frac{2}{3} \times \frac{a^3}{\ell} - \frac{2a\eta_0}{\pi} = 2a\left[\frac{\Delta\pi a^3}{\Delta s.3\ell} - \frac{\eta_0}{\pi}\right]$$

APPENDIX B

Helmholtz

$$\Delta v = 4\pi n \mu_{\perp} \qquad \text{(cgs units)}$$

SI units

$$\Delta v = \frac{4\pi n \mu_{\perp}}{4\pi \varepsilon_0} = \frac{n\mu_{\perp}}{\varepsilon_0}$$

or

$$\mu_{\perp} = \frac{\varepsilon_0 . \Delta v}{n}$$

$$\text{unit} = \frac{m^2}{\text{molecules}} \cdot J^{-1}c^2m^{-1}v$$

$$= \frac{mJ^{-1}c^2v}{\text{molecules}}$$

$1J = 1v \times 1c$, therefore $J^{-1} = v^{-1}c^{-1}$

therefore

$$\mu_{\perp} = \frac{m\ v^{-1}c^{-1}c^2\ v}{\text{molecules}}$$

$$= \underline{\text{cm/molecules}}$$

$1D = 3.3564 \times 10^{-30}$cm

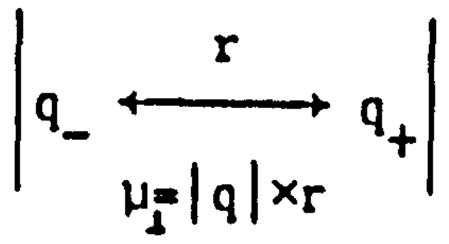

APPENDIX C

COMPUTER PROGRAM FOR THE BUBBLE-SIZE STABILITY TEST

```
 0                    10 DIM A$[3],B$[2],C$[10],D$(10)[2],N(10),V(10),TE(120),P(1
20)
15 PLOTTER IS 1
20 CLEAR
30 DISP USING 210 ; "PROGRAM FOR LOGGING BUBBLE EXPERIMENTS"
40 DISP USING 210 ; "======================================"
50 DISP USING 220 ; "ENTER SURFACTANT,AND CONCENTRATION(%)"
60 INPUT F$,C
70  ! DISP USING 220 ; "ENTER DRIVE FLUID,AND FLOW RATE (CC/MIN)"
80 ! INPUT DF$,Q
90 DISP USING 220 ; "ENTER TIME INTERVAL BETWEEN READINGS(SECS)"
100 INPUT T
110 T=T*1000
120 GOSUB 1190 ! CREATE DATA FILE
130 ON KEY# 1,"START LOG" GOTO 230 ! LOGGING ROUTINE
140 ON KEY# 2,"END LOG" GOTO 1990 ! TERMINATE LOGGING
145 ON KEY# 3,"SET-UP" GOTO 630
150 KEY LABEL
160 A$="    "
170 B$=" "
180 CONTROL 7,16 ; 0
190 L=0
200 GOTO 200
210 IMAGE 25X,K
220 IMAGE /,K
225 GOSUB 630
230 TL0=TIME
240 RESET 7
250 CLEAR 706
260 FOR I=0 TO 9
270 SEND 7 ; MTA UNL LISTEN 6 DATA As
280 ENTER 706 USING "#,B" ; U,S
290 IF S<128 THEN 280
300 SEND 7 ; MTA UNL LISTEN 6 DATA B$
310 IOBUFFER C$
320 TRANSFER 706 TO  C$ FHS ; COUNT 2
330 SEND 7 ; UNT
340 D$(I)=C$
350 NEXT I
360 TL1=TIME
370 IF L=0 THEN GOSUB 450 ! ON TIMER
```

```
400 GOSUB 480 ! CONVERT DATA AND AVERAGE
410 GOSUB 560 ! FILE DUMP
430 GOSUB 850 ! PLOTTING
440 GOTO 440
450 ON TIMER# 1,T-(TL1-TL0) GOTO 230
460 TS=TL0-(TL1-TL0)/2
470 RETURN
480 VT=0
490 FOR I=0 TO 9
500 V(I)=NUM (D$(I)[1])*256+NUM (D$(I)[2])
505 IF V(I)>4095 THEN GOSUB 940
510 VT=VT+V(I)
520 NEXT I
530 VA=VT*.0312
540 P(L)=VA ! *15/1000   TRANDUCER CALIBRATION
550 RETURN
560 ASSIGN# 1 TO  S$
570 PRINT# 1,L ; TE(L),P(L)
620 RETURN
630 GCLEAR
640 GRAPH
650 FRAME
660 SCALE -200,1400,-15,60
670 SETUU
680 XAXIS 0,100,0,1200
690 YAXIS 0,5,0,50
700 FOR I=0 TO 1200 STEP 200
710 MOVE I,-2
720 LORG 5
730 LABEL I
740 NEXT I
750 MOVE 600,-5
760 LABEL "TIME (Secs)"
770 FOR I=0 TO 50 STEP 10
780 MOVE -100,I
790 LABEL I
800 NEXT I
810 MOVE -15,55
920 LORG 2
```

```
950 IF L=1 THEN GOTO 980
960 MOVE TE(L-1),P(L-1)
970 PLOT TE(L),P(L),-1
980 GCLEAR -8
990 MOVE 200,-10
900 LABEL "TIME=";TE(L)
910 MOVE 800,-10
920 LABEL "mV =";P(L)
930 RETURN
940 V(I)=V(I)-32768
950 RETURN
960 MOVE TE(L),P(L)
970 RETURN
1190 DISP USING 220 ; "PLEASE GIVE TITLE FOR DATA FILE"
1200 INPUT S$
1210 DISP USING 220 ; "HAS THE DISC FOR DATA STORAGE BEEN PLACED IN DRIVE#1"
1220 DISP USING 220 ; "PRESS CONT TO CONTINUE AFTER INSERTING DISC"
1230 PAUSE
1240 MASS STORAGE IS ".BODIE"
1250 CREATE S$,120,16
1260 RETURN
1990 OFF TIMER# 1
2000 PRINTER IS 701,80
2010 PRINT CHR$ (27)&"&k1SBUBBLE RELAXATION DATA"
2015 PRINT CHR$ (10)
2020 PRINT "DATA FILE!-";S$
2025 PRINT CHR$ (10)
2030 PRINT CHR$ (27)&"&k0S"
2040 PRINT USING 5000 ; "FOAMING AGENT !-",F$,C,"%"
2050 ! PRINT USING 5000 ; "DRIVE FLUID   !-",DF$,Q,"cc/min"
2060 PRINT CHR$ (10)
2070 PRINT USING 5010 ; "TIME (secs)","OUTPUT (mV)"
2080 PRINT USING 5010 ; "===========","==========="
2090  ! ON ERROR GOTO
2100 FOR I=1 TO L
2110 PRINT USING 5020 ; TE(I),P(I)
2120 NEXT I
2130 PRINT CHR$ (12)
2140 PRINT CHR$ (12)
2150 PAUSE
5000 IMAGE K,K,X,2D.2D,K
5010 IMAGE 10X,11A,5X,14A
5020 IMAGE 12X,4D.2D,11X,2D.3D
```

APPENDIX D

TO CALCULATE THE SURFACE VISCOSITY OF MYRISTIC ACID IN THE DURALUMIN TROUGH

If volume of myristic acid used = 30μℓ

initial surface concentration = 4.063×10^{-3}M (number of moles per litre)

initial trough area = $197.59 cm^2$

$$\text{area per mol in } \mathring{A}^2 = \frac{197.59\ 10}{30\ 10^{-6} \times 4.063 \times 10^{-3} \times 6.02 \times 10^{23}}$$

$$A = 26.9 \mathring{A}^2$$

$$\text{slope} = \frac{1.793 - 0.821}{2.8 - 1.8} = \frac{0.972}{1.0}$$

$$y = mx + c$$

$$\log A = \text{intercept} + 0.972 \log t$$

$$\text{intercept} = -0.929$$

$$\log A = 0.972 \log t - 0.929$$

$$\text{area lost, } A = 0.1178t^{0.972}$$

$$\text{surface flux, } s = \frac{dA}{dr} = 0.1145t^{-0.028}$$

Since area lost or transferred at time t = $0.1178t^{0.972}$

$$\frac{A_1}{\text{start area/mol}} = \text{no. of mole gone out to comp. II at t}$$

$$\text{start area/mol} = \frac{\text{initial area of compartment I}}{\text{volume added} \times \text{concentration of solution} \times N_A}$$

$$A_2 = \frac{\text{area of compartment II}}{\text{number of molecules transferred}} = \frac{\text{area/mol}}{\text{on compartment II}}$$

$$A_2 = \frac{\text{area of compartment II . starting area/mol}}{A_1}$$

Using Poiseuille's formula for 2-D:

$$q = \frac{2a^3}{3\eta_s} = \frac{\Delta s.1}{\Delta \pi} = \frac{dA}{dt} \cdot \frac{1}{\pi_1 - \pi_2}$$

$$\eta = \frac{2a^3}{3\ell} \left(\frac{\pi_1 - \pi_2}{dA/dt} \right)$$

Therefore

$$\eta = \frac{2 \times (0.015)^3 \quad 14.1}{3 \times 1.26 \ dA/dt} = 2.64 \times 10^4 \text{sP}$$

And with experiments with a quantity of myristic acid added to both compartments of the trough, we have:

volume added to compartment I = 20μℓ

volume added to compartment II = 5ℓ

A_1 = area transferred from compartment I → number of molecules transferred

$$A_2 = \frac{\text{area of compartment II}}{\frac{\text{area of compartment II}}{5\mu\ell \times \text{conc} \times N_A} + \text{number of molecular transferred}}$$

π_1 and π_2 can then be obtained from the $\pi(A)$ isotherm of myristic acid.

Molecular Area ($Å^2$)	$-(\partial\pi/\partial A)_T$ (Nm^{-3})	Compression Modulus (mNm^{-1})
20	1.8	36 $\pm$ 1
23	0.7	16.1 $\pm$ 0.5
26.2	0.1	1.62 $\pm$ 0.03
32	1.2	38.4 $\pm$ 1
35	0.9	31.5 $\pm$ 1
40	0.5	20 $\pm$ 0.6
44	0.3	13.2 $\pm$ 0.5

TABLE 10.1: Data obtained from the duralumin trough for the compression modulus of myristic acid on a 0.01M hydrochloric acid sub-phase.

Temperature = 20.5 $\pm$ 0.5°C

pH $\sim$ 2.2

Molecular Area ($\AA^2$)	$-(\partial\pi/\partial A)_T$ (Nm^{-3})	Compression Modulus (mNm^{-1})
16.0	13.8	220.8 $\pm$ 7
16.5	13.8	227.7 $\pm$ 7
17.0	13.8	234.6 $\pm$ 7
17.6	3.0	52.8 $\pm$ 2
18.0	3.0	54 $\pm$ 2
19.0	3.0	57 $\pm$ 2
20.0	3.0	60 $\pm$ 2
21.0	3.0	63 $\pm$ 2
22.0	3.0	66 $\pm$ 2
23.0	3.0	69 $\pm$ 2

TABLE 10.2: Data obtained from the duralumin trough for the compression modulus of stearic acid on a 0.01M hydrochloric acid sub-phase.

Temperature = 20.5 $\pm$ 0.5^{o}C

pH $\sim$ 2.2

Surface Pressure (mNm^{-1})	Flux (cm^2s^{-1})	Viscosity $\times 10^{-4}$ (sP)	Activation Energy of Flow ($kJ\ mol^{-1}$)
4	0.27 ± 0.01	0.65 ± 0.03	63.6 ± 3
5	0.3 ± 0.01	0.73 ± 0.03	
6	0.33 ± 0.01	0.80 ± 0.03	64.0 ± 3
8	0.39 ± 0.01	0.88 ± 0.03	64.2 ± 2
10	0.47 ± 0.01	0.92 ± 0.02	64.3 ± 2
12	0.52 ± 0.01	1.00 ± 0.02	64.4 ± 1
14	0.59 ± 0.01	1.03 ± 0.02	64.4 ± 1
16	0.66 ± 0.01	1.06 ± 0.02	64.4 ± 1
18	0.70 ± 0.01	1.11 ± 0.02	
21	0.72 ± 0.01	1.27 ± 0.02	

TABLE 10.3: Data obtained from the duralumin trough of the dependence viscosity on surface pressure of a monolayer of stearic acid.

Subphase = 0.01M hydrochloric acid at pH 2.2

Temperature = $20.5 \pm 0.5^{o}C$

Width of canal = 0.4mm

Surface Pressure (mNm^{-1})	Flux (cm^2s^{-1})	Viscosity $\times 10^{-4}$ (sP)
3	0.14 ± 0.01	1.0 ± 0.09
4	0.20 ± 0.01	0.88 ± 0.05
5.5	0.25 ± 0.01	0.97 ± 0.04
7	0.30 ± 0.01	1.02 ± 0.04
9	0.37 ± 0.01	1.06 ± 0.03
10	0.41 ± 0.01	1.06 ± 0.03
11.5	0.48 ± 0.01	1.09 ± 0.03
13	0.51 ± 0.01	1.11 ± 0.03
14.5	0.57 ± 0.01	1.11 ± 0.0
16	0.61 ± 0.01	1.14 ± 0.02
18	0.68 ± 0.01	1.14 ± 0.02
20	0.70 ± 0.01	1.24 ± 0.02
22	0.71 ± 0.01	1.34 ± 0.02

TABLE 10.4: Data obtained from the duralumin trough of the dependence of viscosity on surface pressure of a monolayer of stearic acid.

Subphase = 2.5×10^{-4}M cadmium sulphate at pH 2.2

Temperature = $20.5 \pm 0.5^{o}C$

Width of canal = 0.4mm

Surface Pressure (mNm^{-1})	Flux (cm^2s^{-1})	Viscosity $\times 10^{-4}$ (sP)	Activation Energy of Flow ($kJ\ mol^{-1}$)
3	0.14 ± 0.01	0.91 ± 0.08	
4	0.20 ± 0.01	0.85 ± 0.05	64.3 ± 4
6	0.27 ± 0.01	0.97 ± 0.04	64.5 ± 3
8	0.33 ± 0.01	1.03 ± 0.03	64.6 ± 2
10	0.40 ± 0.01	1.09 ± 0.03	64.7 ± 2
12	0.47 ± 0.01	1.10 ± 0.02	64.6 ± 2
14	0.54 ± 0.01	1.13 ± 0.02	
16	0.60 ± 0.01	1.14 ± 0.02	64.6 ± 1
18	0.67 ± 0.01	1.16 ± 0.02	
20	0.71 ± 0.01	1.21 ± 0.02	
22	0.73 ± 0.01	1.31 ± 0.02	
23	0.72 ± 0.02	1.38 ± 0.02	

TABLE 10.5: Data obtained from the duralumin trough of the dependence of viscosity on surface pressure of a monolayer of stearic acid.

Subphase = 2.5×10^{-4}M cadmium chloride at pH 2.2

Temperature = $20.5 \pm 0.5^{o}C$

Width of canal = 0.4mm

pH	Flux ($cm^2 s^{-1}$)	Viscosity $\times 10^{-5}$ (sP)	Activation Energy of Flow ($kJ\ mol^{-1}$)
3.09	0.716 ± 0.01	9.11 ± 0.2	64 ± 1
3.35	0.718 ± 0.01	9.24 ± 0.2	
3.62	0.706 ± 0.01	9.36 ± 0.2	
3.89	0.662 ± 0.01	9.73 ± 0.2	64 ± 1
4.20	0.573 ± 0.01	11.41 ± 0.2	
4.50	0.464 ± 0.01	14.28 ± 0.3	65 ± 1
4.77	0.332 ± 0.01	19.07 ± 1	66 ± 2
4.96	0.241 ± 0.01	27.2 ± 1	67 ± 3
5.10	0.155 ± 0.01	44.3 ± 4	68 ± 5
5.20	0.046 ± 0.01	172 ± 50	70 ± 10

TABLE 10.6: Data obtained from the duralumin trough of the dependence of viscosity on pH, of a monolayer of stearic acid.

Subphase = 2.5×10^{-4}M cadmium chloride at pH 2.2

Temperature 20.5 $\pm$ 0.5°C

Width of canal = 0.4mm

Surface pressure = $15 mNm^{-1}$

t (s)	Area, A (cm^2)	ds/dt ($cm^2 s^{-1}$)	π_1 (mNm^{-1})	Area, A_2 (cm^2)	π_2 (mNm^{-1})	π_2 π_1 (mNm^{-1})	Viscosity $\times 10^{-4}$ (sP)
60	10.4	0.1504	14.1	1229.2	-	14.1	1.674
120	18.99	0.1372	14.1	673.2	-	14.1	1.835
180	26.99	0.1300	14.1	473.6	-	14.1	1.936
240	34.64	0.1251	14.1	369.0	-	14.1	2.01
300	42.04	0.1215	14.1	304.1	-	14.1	2.07
360	49.23	0.1185	14.1	259.7	-	14.1	2.125
420	56.27	0.1162	14.1	227.2	-	14.1	2.167
480	63.18	0.1141	14.1	202.3	-	14.1	2.20
540	69.97	0.1123	14.1	182.7	-	14.1	2.24
600	76.69	0.1107	14.1	166.7	-	14.1	2.275
660	83.27	0.1093	14.1	153.5	-	14.1	2.30
720	89.79	0.1081	14.1	142.4	-	14.1	2.33

TABLE 10.7: Typical data obtained from the duralumin trough to calculate the surface viscosity of myristic acid when added to compartment 1 only.

Temperature $20.5 \pm 0.5^{o}C$

Width of canal = 0.15mm

Volume added = 30µl

Volume Added (µl)	Area Per Molecule ($Å^2$)	Mean Surface Viscosity (sP)
10	80.8	2.1×10^{-4}
15	53.8	1.2×10^{-4}
20	40.4	0.6×10^{-4}
25	32.3	3.2×10^{-4}
30	26.9	2.2×10^{-4}

TABLE 10.9: Summary of the data obtained from the duralumin trough of the mean surface viscosity after 400 seconds, with myristic acid added to compartment 1 only.

Temperature = $20.5 \pm 0.5^{o}C$

Width of canal = 0.15mm

$\Delta\pi = 14.1 mNm^{-1}$

Volume Added to Side 2 (µl)	Volume Added to Side 1 (µl)	Pressure Drop $\pi_1 - \pi_2$ (mNm^{-1})	Mean Surface Viscosity (sP)
5	20	3.5	1.0×10^{-4}
10	20	3.5	0.8×10^{-4}
44	20	1.8	1.45×10^{-4}
46	20	1.1	1.05×10^{-4}

TABLE 10.10: Summary of the data obtained from the duralumin trough of the mean surface viscosity with myristic acid added to both compartments.

Temperature = $20.5 \pm 0.5^{o}C$

Width of canal = 0.15mm

$\Delta\pi = 3.5 mNm^{-1}$

Fatty Acid	$-(\partial\pi/\partial A)_{\pi=10,T}$ (Nm^{-3})	Compression Modulus, k_s^{10} (mNm^{-1})
$C_{13}H_{27}COOH$	1.836	40.7 ± 1.2
$C_{14}H_{29}COOH$	2.524	47.8 ± 1.5
$C_{15}H_{31}COOH$	2.964	73.5 ± 1.9
$C_{16}H_{33}COOH$	3.223	82.1 ± 2.1
$C_{17}H_{35}COOH$	3.460	92.7 ± 3.5
$C_{18}H_{37}COOH$	3.981	101.3 ± 2.0
$C_{19}H_{39}COOH$	4.755	121.2 ± 2.2

Compression rate $\sim 8\text{Å}^2$ molecule^{-1}min^{-1}

TABLE 10.12: Data obtained from the Joyce-Loebl trough for the compression modulus of various fatty acid monolayers measured at $\pi = 10 mNm^{-1}$.

Subphase = pure water

Temperature = $20.5 \pm 0.5^{o}C$

pH = 3.05 ± 0.03

Fatty Acid	Canal Viscosity (sP)	Rotational Viscosity (sP)	Activation Energy From Rotational Viscosity ($E_A \times 10^{-20}$ Jmol^{-1})
$C_{17}H_{35}COOH$	1.287×10^{-4}	9.395×10^{-4}	-
$C_{18}H_{37}COOH$	2.838×10^{-4}	2.315×10^{-3}	5.84
$C_{19}H_{39}COOH$	4.829×10^{-4}	6.944×10^{-3}	18.172

activation energies based on Eyrings Equation: $\ell n\, \eta_s$ = constant - E_A/RT

TABLE 10.13: Summary of the data obtained for the surface shear viscosities of some fatty acid monolayers when spread on acidic subphases using canal (□; pH = 3.0 ± 0.3) and rotational (○; pH = 2.0 ± 0.3) viscometers.

$\pi \sim 10 mNm^{-1}$

$T_b \sim 20.4 \pm 0.1^{o}C$

π (mNm^{-1})	$-V$ (mV)	ΔV (V)	A (cm^2)	$n \times 10^{18}$ (molecules m^{-2})	$\mu_\perp = \Delta V/n \times k$ (Debye)
0	560	0.16	298.23	1.920	0.2210
3	550	0.170	251.18	2.280	0.2234
6	500	0.220	242.24	2.364	0.2469
10	472	0.248	219.78	2.606	0.2525
14.5	440	0.280	196.38	2.916	0.2438
20	424	0.296	187.53	3.054	0.2571
25	325	0.395	143.01	4.005	0.2617
30	320	0.400	133.44	4.292	0.2473

$k = \varepsilon_0/3.336 \times 10^{-30} = 2.653 \times 10^{18} J^{-1} cm^{-2}$

TABLE 10.14: Data obtained from the Joyce-Loebl trough for the calculation of the surface dipole moment of $C_{13}H_{25}COOH$ (myristic). Clean surface potential, $V_0 = -720mV$; area per molecule, $\tilde{A}_m = 26.79\text{Å}^2$; Subphase = 0.01M sodium chloride at pH 3.10 ± 0.03; Temperature of bath, $T_b = 22.6^oC$; Number of molecules put on surface = 5.27×10^{16}; Forward/Reverse barrier speed = 50/50 (arbitrary unit)/$0.075 cms^{-1}$

π (mNm^{-1})	-V (mV)	ΔV (V)	A (cm^2)	$n \times 10^{18}$ (molecules m^{-2})	$\mu_\perp = \Delta V/n \times k$ (Debye)
1.5	382.2	0.3425	298.23	3.963	0.2291
10	370	0.355	274.0	4.313	0.2184
17.5	358	0.367	258.14	4.579	0.2126
25	354.5	0.3705	237.81	4.970	0.1978
33	353.5	0.3715	215.19	5.493	0.1794
37.5	353.5	0.3715	201.85	5.856	0.1683

$k = 2.653 \times 10^{18} J^{-1} cm^{-2}$

TABLE 10.15: Data obtained from the Joyce-Loebl trough for the calculation of the surface dipole moment of $C_{17}H_{33}COOH$ (stearic). Clean surface potential, $V_0 = -725mV$; Area per molecule, $\hat{A}_m = 21.50\text{Å}^2$; Subphase = 0.01M sodium chloride at pH 3.10 ± 0.03; Temperature of bath, $T_b = 22.6^oC$; Number of molecules put on surface = 1.182×10^{17}; Forward/Reverse barrier speed = 50/50 (arbitrary unit)/$0.075 cms^{-1}$

π (mNm^{-1})	-V (mV)	ΔV (V)	A (cm^2)	$n \times 10^{18}$ (molecules m^{-2})	$\mu_\perp = \Delta V/n \times k$ (Debye)
0	350	0.3475	298.23	3.561	0.2589
5.5	341	0.3565	267.42	3.971	0.2382
10	339	0.3585	257.55	4.123	0.2307
17.5	337	0.3605	244.08	4.351	0.2198
24	334	0.3635	230.96	4.598	0.210
32.5	333	0.3645	215.19	4.94	0.1957
38	332.5	0.3650	211.52	5.021	0.1929

$k = 2.653 \times 10^{18} J^{-1} cm^{-2}$

TABLE 10.16: Data obtained from the Joyce-Loebl trough for the calculation of the surface dipole moment of $C_{18}H_{35}COOH$ (nonadecanoic). Clean surface potential, $V_0 = -697.5mV$; Area per molecule, $\tilde{A}_m = 22.46\text{Å}^2$; Subphase = 0.01M sodium chloride at pH 3.10 ± 0.03; Temperature of bath, $T_b = 22.6^oC$; Number of molecules put on surface = 1.062×10^{17}; Forward/Reverse barrier speed = 50/50 (arbitrary unit)/$0.075 cms^{-1}$

π (mNm^{-1})	-V (mV)	ΔV (V)	A (cm^2)	$n \times 10^{18}$ (molecules m^{-2})	$\mu_1 = \Delta V/n \times k$ (Debye)
0	326.5	0.3535	298.23	3.789	0.2475
5	317	0.363	268.43	4.210	0.2287
10	310	0.370	258.07	4.378	0.2242
20	305	0.375	236.76	4.773	0.2084
27.5	304.5	0.3755	223.98	5.045	0.1975
32.5	305	0.375	213.95	5.282	0.1884

$k = 2.653 \times 10^{18} J^{-1} cm^{-2}$

TABLE 10.17: Data obtained from the Joyce-Loebl trough for the calculation of the surface dipole moment of $C_{19}H_{37}COOH$ (arachidic). Clean surface potential, $V_0 = -680mV$; Area per molecule, $\tilde{A}_m = 21.06\text{Å}^2$; Subphase = 0.01M sodium chloride at pH 3.10 $\pm$0.03; Temperature of bath, $T_b = 22.6^oC$; Number of molecules put on surface = 1.13×10^{17}; Forward/Reverse barrier speed = 50/50 (arbitrary unit)/$0.075 cms^{-1}$

π (mNm^{-1})	-V (mV)	ΔV (V)	$\bar{A}$/Moiety ($Å^2 link^{-1}$)	A (cm^2)	n × 10^{16} (molecules m^{-2})	$\mu_\perp = \Delta V/n \times k$ (Debye)
0	465	0.220	22.5	298.2	5.11	0.1312
$0^{(1)}$	460	0.225	20.6	273.8	5.57	0.1233
2.5	450	0.235	18.3	242.7	6.28	0.1142
5	450	0.235	17.2	228.0	6.69	0.1072
7.5	450	0.235	16.3	216.5	7.04	0.1018
$10^{(1)}$	442	0.243	14.5	192.0	7.94	0.0934
$10^{(2)}$	442	0.243	11.4	150.6	10.12	0.0732
$10^{(3)}$	462	0.223	9.5	126.5	12.05	0.0565

$k = 3.0506 \times 10^{16} Jc^{-1}m^{-2}$ Number of links ≤ 87

TABLE 10.21: Data obtained from the Joyce-Loebl trough for the calculation of the surface dipole moment of polydimethylsiloxane <6610>.

Clean surface potential, $V_0 = -685mV$; Area per molecule, $\tilde{A}_m = 1954.9Å^2$;

Subphase = 0.01M sodium chloride at pH 5.87 $\pm$ 0.02; Temperature of bath, $T_b = 21.8^oC$;

Forward/Reverse barrier speed = 50/50 (arbitrary unit)/$0.75mms^{-1}$.

π (mNm^{-1})	$-V$ (mV)	ΔV (V)	$\bar{A}$/Moiety ($Å^2$ $link^{-1}$)	A (cm^2)	$n \times 10^{16}$ (molecules m^{-2})	$\mu_\perp = \Delta V/n \times k$ (Debye)
0	540	0.230	25.3	298.2	2.06	0.1367
$0^{(1)}$	540	0.230	23.6	278.3	2.21	0.1440
1	535	0.235	21.9	258.6	2.38	0.1367
5	530	0.240	19.9	234.1	2.62	0.1264
7.5	530	0.240	18.7	221.0	2.78	0.1194
$10^{(1)}$	527	0.243	16.8	198.1	3.10	0.1083
$10^{(2)}$	523	0.247	14.6	171.9	3.57	0.0955
$10^{(3)}$	521	0.249	11.4	134.3	4.58	0.0752

$k = 1.3823 \times 10^{16} Jc^{-1}m^{-2}$; Number of links ≤ 192.4

TABLE 10.22 : Data obtained from the Joyce-Loebl trough for the calculation of the surface dipole moment of polydimethylsiloxane <14420>.

Clean surface potential, $V_0 = -770mV$; Area per molecule, $\tilde{A}_m = 4855.6Å^2$;

Subphase = 0.01M sodium chloride at pH 5.81 $\pm$ 0.02; Temperature of bath, $T_b = 21.6^oC$;

Forward/Reverse barrier speed = 50/50 (arbitrary unit)/$0.75mms^{-1}$).

π (mNm^{-1})	-V (mV)	ΔV (V)	$\bar{A}$/Moiety ($Å^2$ $link^{-1}$)	A (cm^2)	$n \times 10^{15}$ (molecules m^{-2})	$\mu_\perp = \Delta V/n \times k$ (Debye)
0	460	0.205	27.3	298.2	2.47	0.1484
$0^{(1)}$	450	0.209	25.4	277.2	2.66	0.1408
1	450	0.215	21.6	236.6	3.12	0.1234
2.5	450	0.215	20.4	223.2	3.30	0.1166
5	445	0.220	19.1	223.2	3.54	0.1114
7.5	440	0.225	17.9	208.5	3.77	0.1068
$10^{(1)}$	440	0.225	14.1	195.4	4.77	0.0844
$10^{(2)}$	440	0.225	11.9	154.4	5.68	0.0709

$k = 1.7908 \times 10^{15} Jc^{-1}m^{-2}$; Number of links $\leq$ 1482.1

TABLE 10.23: Data obtained from the Joyce-Loebl trough for the calculation of the surface dipole moment of polydimethylsiloxane <110000>.

Clean surface potential, $V_0 = -665mV$; Area per molecule, $\tilde{A}_m = 3751Å^2$;

Subphase = 0.01M sodium chloride at pH 5.87 $\pm$ 0.02; Temperature of bath, $T_b = 21.8^oC$;

Forward/Reverse barrier speed = 50/50 (arbitrary unit)/$0.75mms^{-1}$

$\overline{M}_w$	Flux, q ($cm^2 s^{-1}$)	Surface Shear Viscosity, η_s (sP)
6610	0.337	1.92×10^{-4}
14420	0.345	1.82×10^{-4}
19100	0.415	1.24×10^{-4}
31000	0.427	6.19×10^{-5}
48150	0.464	5.17×10^{-5}
110000	0.508	4.92×10^{-5}

TABLE 10.24: Data obtained from the Joyce-Loebl trough of the surface shear viscosity for the single polydimethyl-siloxanes on a pure water subphase of pH 5.50 $\pm$ 0.02

Temperature of bath, $T_b = 21.5 \pm 0.1^{o}C$

Width of canal, 2a = 0.65mm

$\pi \sim 7 mNm^{-1}$

Length of canal, l = 1.3cm

Height of water in canal = 9mm

(i) Reverse barrier speed = 25 (arbitrary unit)/0.317mms^{-1}

$\overline{M}_w$	$(-\partial\pi/\partial A)_T$ (Nm^{-3})	Compression Modulus, k_s (Nm^{-1})
6610	1.74	0.0457
14420	1.60	0.0429
19100	1.356	0.0344
31000	1.307	0.0339
48150	1.256	0.0331
110000	1.44	0.0394

TABLE 10.25(i)-(v): This table consists of data obtained from the Joyce-Loebl trough for the compression modulus of various polydimethylsiloxane monolayers measured at $\pi \sim 7.5 mNm^{-1}$ and obtained from different reverse barrier speeds.

Subphase = pure water

Temperature = $21.8 \pm 0.1^{o}C$

pH = 5.92 ± 0.02

(ii) Reverse barrier speed = 50 (arbitrary unit)/0.682mms^{-1}

$\overline{M}_w$	$(-\partial\pi/\partial A)_T$ (Nm^{-3})	Compression Modulus, k_s (Nm^{-1})
6610	1.69	0.0443
14420	1.459	0.0390
19100	1.307	0.0331
31000	1.271	0.033
48150	1.220	0.0321
110000	1.356	0.0373

(iii) Reverse barrier speed = 100 (arbitrary unit)/1.401mms^{-1}

$\overline{M}_w$	$(-\partial\pi/\partial A)_T$ (Nm^{-3})	Compression Modulus, k_s (Nm^{-1})
6610	1.606	0.0421
14420	1.37	0.0366
19100	1.194	0.0303
31000	1.198	0.0311
48150	1.194	0.0314
110000	1.285	0.0353

(iv) Reverse barrier speed = 200 (arbitrary unit)/2.810mms^{-1}

$\overline{M}_w$	$-(\partial\pi/\partial A)_T$ (Nm^{-3})	Compression Modulus, k_s (Nm^{-2})
6610	1.373	0.0360
14420	1.243	0.0332
19100	1.13	0.0287
31000	1.144	0.0297
48150	1.144	0.0301
110000	1.248	0.0343

(v) Reverse barrier speed = 400 (arbitrary unit)/5.585mms^{-1}

$\overline{M}_w$	$-(\partial\pi/\partial A)_T$ (Nm^{-3})	Compression Modulus, k_s (Nm^{-1})
6610	0.928	0.0244
14420	0.947	0.0253
19100	0.963	0.0244
31000	1.031	0.0267
48150	1.070	0.0282
110000	1.174	0.0322

Mixture	$\overline{M}_w$	$-(\partial\pi/\partial A)_T$ (Nm^{-3})	Compression Modulus, k_s (Nm^{-1})
M_{2C}	9733	1.12	0.0275
M_{2A}	12855	1.22	0.0305
M_{2B}	15978	1.13	0.0334
M_{3C}	35288	1.25	0.0312
M_{3A}	39575	1.34	0.0335
M_{3B}	43863	1.42	0.0353

TABLE 10.29: Data obtained from the Joyce-Loebl trough for the compression modulus of various molar-proportion mixtures of polydimethylsiloxane monolayers measured at $\pi \backsim 7.5 mNm^{-1}$.

Subphase = pure water

Temperature = $21.2 \pm 0.1^{o}C$

pH = 5.50 ± 0.02

Reverse speed = 50 (arbitrary unit)/$0.697 mms^{-1}$

Mixture	$\overline{M}_w$	Flux, q ($cm^2 s^{-1}$)	Surface Shear Viscosity, η_s (sP)
M_{2C}	9733	0.350	1.51×10^{-4}
M_{2A}	12855	0.416	1.09×10^{-4}
M_{2B}	15978	0.445	1.01×10^{-4}
M_{3C}	35288	0.496	3.69×10^{-5}
M_{3A}	39575	0.474	4.68×10^{-5}
M_{3B}	43863	0.421	7.48×10^{-5}

TABLE 10.30: Data obtained from the Joyce-Loebl trough of the surface shear viscosity for the various molar-proportion mixtures of polydimethylsiloxane monolayers on a pure water subphase of pH 5.54 $\pm$ 0.02

Temperature of bath, $T_b = 22.1 \pm 0.1^{o}C$

Width of canal, 2a = 0.65mm

$\pi \sim 6 mNm^{-1}$

Length of canal, l = 1.3cm

Height of water in canal = 9mm

π (mNm^{-1})	G_s' (mNm^{-1})	η_s' (sP)	G_s' (mNm^{-1})
0	0	0	0
5	0	0	0
10	0	0	0

TABLE 10.35: Data obtained from the oscillating ring surface rheometer showing the dynamic surface shear viscosity, η_s', and shear moduli, G_s' and G_s'' for a typical polydimethylsiloxane when spread on pure water. Experimental timescale = 2 minutes; pH = 5.90; subphase temperature, T_b = 21.5 $\pm$ 0.1^{o}C; resonant frequency, f_o = 3.3094Hz

π (mNm^{-1})	G_s' (mNm^{-1})	η_s' (sP)	G_s'' (mNm^{-1})
0	0	0	0
5	0	1×10^{-3}	0.0206
10	0	2×10^{-3}	0.0412
15	0	1×10^{-3}	0.0206
20	0	1×10^{-3}	0.0206
25	0	9×10^{-3}-1.3×10^{-2}	0.2680

TABLE 10.36: Data obtained from the oscillating ring surface rheometer showing the dynamic surface shear viscosity, η_s' and shear moduli, G_s' and G_s'' for $C_{13}H_{27}COOH$ (myristic) when spread on pure water with no added salt.

Experimental timescale = 3 minutes

pH ~ 3.0

Subphase temperature, $T_b = 19.7 \pm 0.1^oC$

Resonant frequency, f_o = 3.281Hz

π (mNm^{-1})	G_s' (mNm^{-1})	η_s' (sP)	G_s'' (mNm^{-1})
0	0	0	0
5	0	1×10^{-3}	0.0206
10	0	2×10^{-3}	0.0412
15	0	3×10^{-3}	0.0618
20	0	7×10^{-3}	0.1443
25	0	1.1×10^{-2}	0.2268
30	0	1.254×10^{-2}	0.2585
35	0	1.3×10^{-2}	0.2680

TABLE 10.37: Data obtained from the oscillating ring surface rheometer showing the dynamic surface shear viscosity, η_s', and shear moduli, G_s' and G_s'', for $C_{17}H_{35}COOH$ (stearic) when spread on pure water with no added salt.

Experimental timescale = 3 minutes

pH ~ 3.03

Subphase temperature, $T_b = 19.7 \pm 0.1^{o}C$

Resonant frequency, $f_o = 3.281Hz$

π (mNm^{-1})	G_s' (mNm^{-1})	η_s' (sP)	G_s'' (mNm^{-1})
0	0	1×10^{-3}	0.0206
5	0	2×10^{-3}	0.0412
10	0	3×10^{-3}	0.0618
15	0	3×10^{-3}	0.0618
20	0	3×10^{-3}	0.0618
25	0	5×10^{-3}	0.1031
30	0	5×10^{-3}	0.1031
35	0	5×10^{-3}	0.1031

TABLE 10.38: Data obtained from the oscillating ring surface rheometer showing the dynamic surface shear viscosity, η_s', and shear moduli, G_s' and G_s'', for $C_{18}H_{37}COOH$ (nonadecanoic), when spread on pure water with no added salt.
Experimental timescale = 3 minutes
pH ~ 3.02
Subphase Temperature, $T_b = 20.0 \pm 0.1^{o}C$
Resonant frequency, $f_o = 3.281Hz$

π (mNm^{-1})	G_s' (mNm^{-1})	η_s' (sP)	G_s'' (mNm^{-1})
0	0	1×10^{-3}	0.0206
5	0	1×10^{-3}	0.0206
10	0	1×10^{-3}	0.0206
15	0	1×10^{-3}	0.0206
20	0	2×10^{-3}	0.0412
25	0	2×10^{-3}	0.0412
30	0	2×10^{-3}	0.0412
35	0	3×10^{-3}	0.0618

TABLE 10.39: Data obtained from the oscillating ring surface rheometer showing the dynamic surface shear viscosity, η_s', and shear moduli, G_s' and G_s'', for $C_{19}H_{39}COOH$ (arachidic), when spread on pure water with no added salt.
Experimental timescale = 3 minutes
pH ~ 3.03
Subphase temperature, $T_b = 20.1 \pm 0.1^{o}C$
Resonant frequency, $f_o = 3.309Hz$

π (mNm^{-1})	G_s' (mNm^{-1})	η_s' (sP)	G_s'' (mNm^{-1})
0	0	1.6×10^{-3}	0.3312
10	0	5.5×10^{-2}	1.135
20	4.29	0.135	3.026
30	14.04	0.191	5.08
40	$\geq$50	0.26-0.384	11.763

TABLE 10.40: Data obtained from the oscillating ring surface rheometer showing the dynamic surface shear viscosity, η_s', and shear moduli, G_s' and G_s'', for $C_{22}H_{45}COOH$ (tricosanoic) when spread on pure water.
Experimental timescale = 3 minutes
pH $\sim$ 3.5
Subphase temperature, T_b = 21.5 $\pm$ 0.1°C
Resonant frequency, f_o = 3.309Hz

$\overline{M}_w$ \ Concentration	1 0.00075	10 0.0075	100 0.075 ppm gdm^{-3}
6610	-0.1733	-0.12	0.04
14420	-0.08	0.12	0.273
19100	0.04	0.1733	0.32
48150	0.0533	0.333	0.393
FC740*	-0.1867	-0.134	-0.0533

* fluorocarbon surfactant

TABLE 10.42: Data obtained for the antifoaming indices, AFI, of the polydimethylsiloxanes (dissolved in petroleum ether) in Offshore Magnus crude oil as a function of concentration.
Temperature = 20.1 $\pm$ 0.2°C

$\bar{M}_w$ (gdm^{-3}) \ Concentration (ppm)	20 0.015	30 0.0225	40 0.03	60 0.045	80 0.06	120 0.09	150 0.1125	180 0.135	200 0.15	250 0.1875	300 0.225
6610	-0.149	-0.127	-0.0963	-0.0525	-0.0208	0.0566	0.0905	0.13	0.164	0.198	0.232
14420	-0.104	-0.070	-0.0395	0.00	0.0407	0.1102	0.1610	0.1937	0.218	0.2542	0.2881
19100	0.0815	0.1106	0.1241	0.1530	0.1807	0.232	0.2508	0.2847	0.3	0.3474	0.3728
31000	0.1386	0.1639	0.173	0.1978	0.237	0.2825	0.3108	0.3389	0.3503	0.3898	0.4186
48150	0.00576	0.0212	0.0424	0.0622	0.082	0.1344	0.1695	0.2034	0.2147	0.2572	0.3079
110000	-0.0725	-0.0535	-0.0307	0.00358	0.0496	0.1143	0.1708	0.213	0.238	0.2978	0.3563
FC740	-0.0227	-0.1535	-0.1248	-0.0627	-0.0251	0.0407	0.0754	0.1075	0.1227	0.1502	0.1811

Model Crude Oil = Aerosol OT in ethanediol (3% w/v)

TABLE 10.43: Data obtained for the AFI of the polydimethylsiloxanes (added as a solution in petroleum ether) in Model Crude oil, as a function of concentration. Temperature = $20.3 \pm 0.2^{o}C$

$\bar{M}_w$ (gdm^{-3}) \ Concentration (ppm)	20 0.015	30 0.0225	40 0.03	60 0.04	80 0.06	120 0.09	150 0.1125	180 0.135	200 0.15	250 0.1875	300 0.225
6610	-0.1185	-0.0897	-0.0718	-0.0187	0.0257	0.1137	0.1586	0.1975	0.2269	0.2729	0.3088
14420	-0.0128	0.0105	0.024	0.0569	0.0969	0.1566	0.1967	0.233	0.2549	0.2944	0.3142
19100	0.0308	0.054	0.0707	0.1034	0.1346	0.1847	0.2365	0.2675	0.2905	0.3393	0.3662
31000	0.1231	0.1449	0.1687	0.2003	0.233	0.2872	0.3142	0.3536	0.3732	0.4129	0.4470
48150	0.1403	0.1529	0.1616	0.196	0.223	0.274	0.2998	0.3273	0.3355	0.3629	0.3780
110000	0.02	0.0395	0.0545	0.0933	0.1238	0.1576	0.1855	0.2066	0.2144	0.2316	0.2406
FC740	-0.1502	-0.1346	-0.1002	-0.0641	-0.0252	0.0367	0.07687	0.1157	0.1257	0.1514	0.1622
M_2	-0.2344	-0.2082	-0.195	-0.1679	-0.1167	-0.064	-0.0323	-0.00107	0.0179	0.036	0.0521

M_2 = 6610 + 19100 (2:2 weight ratio)

TABLE 10.44: Data obtained for the AFI of the polydimethylsiloxanes (direct addition) in Model Crude oil, as a function of concentration. Temperature = 20.2 $\pm$ 0.2^{o}C

$\bar{M}_w$ (gdm^{-3}) \ Concentration (ppm)	20 0.015	30 0.0225	40 0.03	60 0.45	80 0.06	120 0.09	150 0.1125	180 0.135	200 0.15	250 0.1875	300 0.225
6510	-0.260	-0.2183	-0.1976	-0.1701	-0.1447	-0.0545	-0.0014	0.0539	0.0794	0.1491	0.1967
14420	-0.06	-0.0211	-0.0012	0.031	0.05774	0.1324	0.1694	0.1948	0.2252	0.2481	0.2805
19100	-0.045	-0.011	0.013	0.042	0.0934	0.1543	0.1903	0.234	0.278	0.304	0.322
31000	-0.015	0.002	0.0277	0.073	0.1117	0.1854	0.2335	0.2779	0.3020	0.349	0.3756
48150	0.0295	0.0432	0.0659	0.1107	0.1700	0.2543	0.3124	0.3629	0.3898	0.4518	0.4949
110000	0.1358	0.1524	0.1722	0.2127	0.2529	0.3301	0.3756	0.4023	0.4365	0.4874	0.5241
FC740	-0.6218	-0.5875	-0.5635	-0.5146	-0.4607	-0.3654	-0.3108	-0.2649	-0.2258	-0.1678	-0.1117

TABLE 10.45: Data obtained for the AFI of the polydimethylsiloxanes (added as a solution in petroleum ether) in Offshore Ninian crude oil, as a function of concentration. Temperature = $20.3 \pm 0.2^{o}C$

Concentration (ppm) / Mixture (gdm^{-3})	20 0.015	30 0.0225	40 0.03	60 0.045	80 0.06	120 0.09	150 0.1125	180 0.135	200 0.15	250 0.1875	300 0.225
M_{2A}	-0.2618	-0.2338	-0.2155	-0.1873	-0.1619	-0.1171	-0.0878	-0.0652	-0.0435	-0.0033	0.0510
M_{2B}	-0.2031	-0.1906	-0.1712	-0.1441	-0.1085	-0.0743	-0.0452	-0.0265	-0.00412	0.0262	0.0705
M_{2C}	-0.3397	-0.2989	-0.2790	-0.2479	-0.2201	-0.1729	-0.1504	-0.1359	-0.1108	-0.0788	-0.0489
M_{3A}	-0.1231	-0.0897	-0.0706	-0.0326	0.0239	0.0670	0.1095	0.1439	0.1526	0.1802	0.2092
M_{3B}	-0.0403	-0.0236	-0.0054	0.0298	0.0552	0.1093	0.1521	0.1834	0.2087	0.2333	0.2794
M_{3C}	-0.005	0.0152	0.0267	0.0542	0.0797	0.1272	0.1543	0.2023	0.2255	0.2743	0.3165

TABLE 10.47: Data obtained for the AFI of the various molar-proportion mixtures (added as a solution in petroleum ether) in Model crude oil, as a function of concentration. Temperature = 20.3 $\pm$ 0.2^{o}C

Mixture \ Concentration (ppm) (gdm^{-3})	20 0.015	30 0.0225	40 0.03	60 0.045	80 0.06	120 0.09	150 0.1125	180 0.135	200 0.15	250 0.1875	300 0.225
M_{2A}	-0.1507	-0.1227	-0.1044	-0.0762	-0.0508	-0.006	0.0233	0.0459	0.0676	0.1078	0.1529
M_{2B}	-0.1020	-0.05	-0.0601	-0.0330	0.0026	0.0368	0.0659	0.0846	0.1069	0.1373	0.1817
M_{2C}	-0.2286	-0.1878	-0.1689	-0.1368	-0.1190	-0.0618	-0.0493	-0.0248	-0.0097	0.0323	0.0622
M_{3A}	-0.0120	0.0214	0.0405	0.0785	0.1340	0.1781	0.2106	0.2540	0.2637	0.2913	0.3103
M_{3B}	0.0708	0.0875	0.1057	0.1309	0.1663	0.2104	0.2632	0.2945	0.3198	0.3444	0.3805
M_{3C}	0.1061	0.1263	0.1378	0.1653	0.1808	0.2383	0.2754	0.3134	0.3366	0.3854	0.4276

TABLE 10.48: Data obtained for the AFI of the various molar-proportion mixtures (added as a solution in petroleum ether) in Offshore Ninian crude oil, as a function of concentration.
Temperature = $20.4 \pm 0.2^{o}C$

Concentration		$AFI_{(M2B)<6610+19100>}$ 0.25:0.75	$\frac{AFI_{<6610>}+AFI_{<19100>}}{2}(M_{2B'})$
ppm	gdm^{-3}		
20	0.015	-0.2031	-0.03375
30	0.0225	-0.1906	-0.0082
40	0.03	-0.1712	0.0139
60	0.045	-0.1441	0.05025
80	0.06	-0.1085	0.0799
120	0.09	-0.0743	0.1443
150	0.1125	-0.0452	0.1706
180	0.135	-0.0265	0.2074
200	0.15	-0.00412	0.232
250	0.1875	0.02625	0.2727
300	0.225	0.0706	0.3024

TABLE 10.49: Data calculated to examine the synergistic effect of a particular mixture of polydimethylsiloxanes <6610> and <19100>

$$AFI_{<MW_1+MW_2>} > \text{or} = \text{or} < \frac{AFI_{<MW_1>} + AFI_{<MW_2>}}{2}$$

Concentration		$AFI_{(M_{3C})<31000+48150>}$ 0.75:0.25	$\frac{AFI_{<31000>}+AFI_{<48150>}}{2}$ (M_{3C}')
ppm	gdm^{-3}		
20	0.015	-0.005	0.07218
30	0.0225	0.0152	0.0925
40	0.03	0.0267	0.1077
60	0.045	0.0542	0.13
80	0.06	0.0797	0.1595
120	0.09	0.1272	0.2085
150	0.1125	0.1643	0.2401
180	0.135	0.2023	0.2711
200	0.15	0.2255	0.2825
250	0.1875	0.2743	0.3235
300	0.225	0.3165	0.3633

TABLE 10.50: Data calculated to examine the synergistic effect of a particular mixture of polydimethylsiloxanes <31000> and <48150>

$AFI_{<31000>,<48150>(M_{3C})}$ and $AFI_{<31000>} + AFI_{<48150>} = M_{3C}'$